frontiers | Research Topics

Innovative tools to support the elimination of neglected tropical diseases (NTDs)

Edited by
Jian Li, Mohamed R. Habib and Wei Wang

Published in
Frontiers in Microbiology

ISSN 1664-8714
ISBN 978-2-8325-2311-7
DOI 10.3389/978-2-8325-2311-7

About Frontiers

Frontiers is more than just an open access publisher of scholarly articles: it is a pioneering approach to the world of academia, radically improving the way scholarly research is managed. The grand vision of Frontiers is a world where all people have an equal opportunity to seek, share and generate knowledge. Frontiers provides immediate and permanent online open access to all its publications, but this alone is not enough to realize our grand goals.

Frontiers journal series

The Frontiers journal series is a multi-tier and interdisciplinary set of open-access, online journals, promising a paradigm shift from the current review, selection and dissemination processes in academic publishing. All Frontiers journals are driven by researchers for researchers; therefore, they constitute a service to the scholarly community. At the same time, the *Frontiers journal series* operates on a revolutionary invention, the tiered publishing system, initially addressing specific communities of scholars, and gradually climbing up to broader public understanding, thus serving the interests of the lay society, too.

Dedication to quality

Each Frontiers article is a landmark of the highest quality, thanks to genuinely collaborative interactions between authors and review editors, who include some of the world's best academicians. Research must be certified by peers before entering a stream of knowledge that may eventually reach the public - and shape society; therefore, Frontiers only applies the most rigorous and unbiased reviews. Frontiers revolutionizes research publishing by freely delivering the most outstanding research, evaluated with no bias from both the academic and social point of view. By applying the most advanced information technologies, Frontiers is catapulting scholarly publishing into a new generation.

What are Frontiers Research Topics?

Frontiers Research Topics are very popular trademarks of the *Frontiers journals series*: they are collections of at least ten articles, all centered on a particular subject. With their unique mix of varied contributions from Original Research to Review Articles, Frontiers Research Topics unify the most influential researchers, the latest key findings and historical advances in a hot research area.

Find out more on how to host your own Frontiers Research Topic or contribute to one as an author by contacting the Frontiers editorial office: frontiersin.org/about/contact

Innovative tools to support the elimination of neglected tropical diseases (NTDs)

Topic editors

Jian Li — Hubei University of Medicine, China

Mohamed R. Habib — Theodor Bilharz Research Institute, Egypt

Wei Wang — Jiangsu Institute of Parasitic Diseases (JIPD), China

Citation

Li, J., Habib, M. R., Wang, W., eds. (2023). *Innovative tools to support the elimination of neglected tropical diseases (NTDs)*. Lausanne: Frontiers Media SA. doi: 10.3389/978-2-8325-2311-7

Table of contents

frontiers | Frontiers in Microbiology

TYPE Editorial
PUBLISHED 10 May 2023
DOI 10.3389/fmicb.2023.1208113

OPEN ACCESS

EDITED AND REVIEWED BY
Axel Cloeckaert,
Institut National de recherche pour l'agriculture, l'alimentation et l'environnement (INRAE), France

*CORRESPONDENCE
Wei Wang
✉ wangweijipd@163.com

RECEIVED 18 April 2023
ACCEPTED 25 April 2023
PUBLISHED 10 May 2023

CITATION
Wang W, Li J and Habib MR (2023) Editorial: Innovative tools to support the elimination of neglected tropical diseases (NTDs). *Front. Microbiol.* 14:1208113. doi: 10.3389/fmicb.2023.1208113

Editorial: Innovative tools to support the elimination of neglected tropical diseases (NTDs)

Wei Wang[1]*, Jian Li[2] and Mohamed R. Habib[3]

[1]National Health Commission Key Laboratory of Parasitic Disease Prevention and Control, Jiangsu Provincial Key Laboratory of Parasite and Vector Control Technology, Jiangsu Institute of Parasitic Diseases, Wuxi, Jiangsu, China, [2]Department of Human Parasitology, School of Basic Medical Science, Hubei University of Medicine, Shiyan, Hubei, China, [3]Medical Malacology Department, Theodor Bilharz Research Institute, Giza, Egypt

KEYWORDS

neglected tropical diseases (NTDs), diagnosis, epidemiology, vaccine, elimination, immunology

Editorial on the Research Topic
Innovative tools to support the elimination of neglected tropical diseases (NTDs)

Neglected tropical diseases (NTDs) are a heterogeneous group of 20 diseases of parasitic, bacterial, viral, fungal, and non-communicable origin that affect approximately one billion impoverished communities around the world. The global age-standardized incidence and number of incident NTDs cases increased between 1990 and 2019, indicating that NTDs remain a substantial public health problem worldwide (Lin et al., 2022). Urged by two road maps for the prevention, control and elimination of NTDs by the World Health Organization (WHO, 2012; Malecela and Ducker, 2021), significant progress has been made in the management of NTDs. The current Research Topic consists of 13 publications covering biology, immunology, epidemiology, diagnosis, and vaccines for NTDs, with the goal of introducing innovative tools implemented to support global elimination of NTDs and facilitating translation of these tools into disease-affected regions.

Epidemiological studies are critical for developing and evaluating disease control strategies, as well as serving as a guide for the management of patients who have already developed illness (Bannister-Tyrrell and Meiqari, 2020). Visceral leishmaniasis has recently reemerged in China (Zheng et al., 2020). Based on data captured from the Infectious Disease Reporting Information Management System of the Chinese Center for Disease Control and Prevention, Li et al. investigated the epidemiological features and spatial-temporal clusters of visceral leishmaniasis in mainland China from 2019 to 2021. The authors identified mountain-type zoonotic visceral leishmaniasis as the predominant type, with peasants and infants as the dominant high-risk populations. The highest peak incidence was recorded between March and May, with 69.57% of cases representing individuals aged 15 years and older. In addition, spatial clustering analysis demonstrated the high-incidence areas of visceral leishmaniasis had shifted to central China, notably in Shanxi and Shaanxi provinces. In the present Research Topic, Yao et al. explored the epidemiology and genetic diversity of the Gram-negative bacterium *Bartonella* spp., the causative agent of bartonellosis in

mammals (Chomel and Kasten, 2010). The authors reported a 6.4% prevalence rate of *Bartonella* in rodents in Guangzhou, southern China, in 2020. Molecular analyses based on the *rrs*, *gltA*, and *rpoB* genes characterized six *Bartonella* species in captured rodents, including *B. queenslandensis*, *B. mastomydis*, *B. tribocorum*, *B. rattimassiliensis*, *Bartonella* sp. AA86HXZ, and *Bartonella* sp. Fuji 12-1.

Ticks are regarded as the second most important vectors of human disease in the world after mosquitoes (de la Fuente et al., 2008). One of the infections carried by ticks is *Anaplasma* spp., the causative agent of anaplasmosis. It is a severe threat to public health and causes huge economic losses on cattle farms. Qi et al. investigated the co-infections and co-existence of several *Anaplasma* spp. and variants in hedgehogs and ticks feeding on hedgehogs and cattle collected in Jiangsu province, Eastern China. They discovered important pathogenic *Anaplasma* spp., such as *A. phagocytophilum*, *A. marginale*, three *A. platys* variants, and two *A. bovis* variants, as well as a novel Candidatus *Cryptoplasma* sp., with varying prevalence in ticks and hedgehogs, and different co-existence combinations were observed only in ticks rather than hedgehogs. Hedgehogs may be more important reservoirs for *A. bovis* than *A. platys*, and *Anaplasma* spp. may be transmitted horizontally between tick species via common hosts. In the current study, the coexistence of several *Anaplasma* spp. or variants may accelerate the creation of novel variants, represent significant hazards to public health as well as economic losses from animal farming, and raise detection and diagnosis issues in the investigated area. With the identification of key pathogenic *Anaplasma* spp. and their co-infections/co-existence in ticks, the current study presented epidemiological data that could be critical for developing strategies for early warning, prevention, and management of possible *Anaplasma.* spp. infections. In addition, Zhang et al. detected a 2.53% prevalence rate of Meihua Mountain virus, a novel member of Nairobi sheep disease orthonairovirus, in ticks captured from cattle and wild boars in Fujian province, Southeastern China from 2019 to 2020.

NTDs control efforts require precise diagnosis (Souza et al., 2021). Jiao et al. developed a convenient, rapid, specific, and sensitive assay combining recombinase-aided amplification and lateral flow strip assay (RAA-LFA) that targeted the *CPSIT_RS02830* gene of *Chlamydia psittaci* for detection of active *C. psittaci* infection, and the RAA-LFA, which was completed within 15 min at a single temperature of 39°C, showed a diagnostic sensitivity of 1 × 100 copies/μl *C. psittaci* DNA, and no cross-reactivity with DNA samples from other intracellular pathogens. In addition, this RAA-LFA tested positive for *C. psittaci* in all fecal samples from mice infected with *C. psittaci* 1 day post-infection.

Based on four helper T lymphocyte (HTL) epitopes, five cytotoxic T lymphocyte (CTL) epitopes and three B-cell epitopes predicted from five patent tuberculosis infections and *Mycobacterium tuberculosis* region of difference (LTBI-RD)-related antigens, Cheng et al. constructed C543P, a novel polypeptide molecule (PPM), which presented high antigenicity, immunogenicity and stability. This C543P candidate was found to activate T and B lymphocytes, and produce high levels of Th1 cytokines, suggesting that C543P may be a promising biomarker for the diagnosis of latent tuberculosis infection (LTBI). Additionally, Zhong et al. reviews the diagnostic potential of microRNAs in schistosomiasis and Quansah et al. reviews the value of the CRISPR-Cas13 system for diagnosis of malaria.

The interaction between the host, indigenous microbiota, and pathogens has been reported to alter the outcome of infections (Libertucci and Young, 2019). Guan et al. found that *Plasmodium yoelii* infection altered the gut microbiota composition in mice, and Zhao et al. reported that the altered microbiota of *Aedes albopictus* affected its susceptibility to dengue fever virus. Alveolar echinococcosis, caused by the larval stage of the tapeworm *Echinococcus multilocularis*, is known as "parasitic cancer" due to its mortality (Xu and Ahan, 2020). Feng et al. found that the complex of key cell cycle regulators EmCyclinD and EmCDK4/6 contributed to the cell cycle regulation of germinative cells in *E. multilocularis* via the EGFR-ERK-EmCyclinD pathway.

Vaccination is widely acknowledged to be one of the most cost-effective health interventions for both human and animal populations (Ghattas et al., 2021). Liang et al. generated an *L. ivanovii* hemolysin gene deletion strain LIΔ*ilo* and a modified strain LIΔ*ilo:hly* of *L. ivanovii*, and the recombinant strain LIΔ*ilo:hly* was found to exhibit high biosafety and immunogenicity, making it a suitable vector for vaccine production. In another review article, Tang et al. discussed the several types of vaccines available for trichinellosis, a worldwide food-borne zoonotic NTD, examined the factors influencing immunization effectiveness, and provided views and difficulties for future vaccine development.

In conclusion, this Research Topic offers unprecedented insights into and innovative strategies for the management of NTDs. We expect that the topic will help accelerate efforts toward the global elimination of NTDs.

Author contributions

All authors listed have made a substantial, direct, and intellectual contribution to the work and approved it for publication.

Acknowledgments

We want to show our most profound appreciation to all authors who contributed to this Research Topic and the editorial office for their support.

Conflict of interest

The authors declare that the research was conducted in the absence of any commercial or financial relationships that could be construed as a potential conflict of interest.

Publisher's note

References

Bannister-Tyrrell, M., and Meiqari, L. (2020). Qualitative research in epidemiology: theoretical and methodological perspectives. *Ann. Epidemiol.* 49, 27–35. doi: 10.1016/j.annepidem.2020.07.008

Chomel, B. B., and Kasten, R. W. (2010). Bartonellosis, an increasingly recognized zoonosis. *J. Appl. Microbiol.* 109, 743–750. doi: 10.1111/j.1365-2672.2010.04679.x

de la Fuente, J., Estrada-Pena, A., Venzal, J. M., Kocan, K. M., and Sonenshine, D. E. (2008). Overview: Ticks as vectors of pathogens that cause disease in humans and animals. *Front. Biosci.* 13, 6938–6946. doi: 10.2741/3200

Ghattas, M., Dwivedi, G., Lavertu, M., and Alameh, M. G. (2021). Vaccine technologies and platforms for infectious diseases: Current progress, challenges, and opportunities. *Vaccines (Basel).* 9, 1490. doi: 10.3390/vaccines9121490

Libertucci, J., and Young, V. B. (2019). The role of the microbiota in infectious diseases. *Nat. Microbiol.* 4, 35–45. doi: 10.1038/s41564-018-0278-4

Lin, Y., Fang, K., Zheng, Y., Wang, H. L., and Wu, J. (2022). Global burden and trends of neglected tropical diseases from 1990 to 2019. *J. Travel Med.* 29, taac031. doi: 10.1093/jtm/taac031

Malecela, M. N., and Ducker, C. A. (2021). road map for neglected tropical diseases 2021-2030. *Trans. R. Soc. Trop. Med. Hyg.* 115, 121–123. doi: 10.1093/trstmh/trab002

Souza, A. A., Ducker, C., Argaw, D., King, J. D., Solomon, A. W., Biamonte, M. A., et al. (2021). Diagnostics and the neglected tropical diseases roadmap: setting the agenda for 2030. *Trans. R. Soc. Trop. Med. Hyg.* 115, 129–135. doi: 10.1093/trstmh/traa118

WHO. (2012). *Accelerating Work to Overcome the Global Impact of Neglected Tropical Diseases: A Roadmap for Implementation*. Geneva: World Health Organization.

Xu, K., and Ahan, A. (2020). A new dawn in the late stage of alveolar echinococcosis parasite cancer. *Med. Hypotheses.* 142, 109735. doi: 10.1016/j.mehy.2020.109735

Zheng, C., Wang, L., Li, Y., and Zhou, X. N. (2020). Visceral leishmaniasis in northwest China from 2004 to 2018: a spatio-temporal analysis. *Infect. Dis. Poverty.* 9, 165. doi: 10.1186/s40249-020-00782-4

frontiers in Microbiology

REVIEW
published: 23 March 2022
doi: 10.3389/fmicb.2022.857786

Vaccines as a Strategy to Control Trichinellosis

Bin Tang[2†], Jian Li[1†], Tingting Li[3,4,5†], Yiting Xie[1], Wei Guan[1], Yanqing Zhao[1], Shuguo Yang[1], Mingyuan Liu[2] and Daoxiu Xu[1]**

[1] Department of Human Parasitology, School of Basic Medicine, Hubei University of Medicine, Shiyan, China, [2] Key Laboratory of Zoonosis Research, Ministry of Education, Institute of Zoonosis, College of Veterinary Medicine, Jilin University, Changchun, China, [3] Key Laboratory of Tropical Translational Medicine of Ministry of Education, Hainan Medical University, Haikou, China, [4] Hainan Medical University-The University of Hong Kong Joint Laboratory of Tropical Infectious Diseases, Hainan Medical University, Haikou, China, [5] Department of Pathogen Biology, Hainan Medical University, Haikou, China

Trichinellosis caused by *Trichinella spiralis* is a worldwide food-borne parasitic zoonosis. Several approaches have been performed to control *T. spiralis* infection, including veterinary vaccines, which contribute to improving animal health and increasing public health by preventing the transmission of trichinellosis from animals to humans. In the past several decades, many vaccine studies have been performed in effort to control *T. spiralis* infection by reducing the muscle larvae and adult worms burden. Various candidate antigens, selected from excretory-secretory (ES) products and different functional proteins involved in the process of establishing infection have been investigated in rodent or swine models to explore their protective effect against *T. spiralis* infection. Moreover, different types of vaccines have been developed to improve the protective effect against *T. spiralis* infection in rodent or swine models, such as live attenuated vaccines, natural antigen vaccines, recombinant protein vaccines, DNA vaccines, and synthesized epitope vaccines. However, few studies of *T. spiralis* vaccines have been performed in pigs, and future research should focus on exploring the protective effect of different types of vaccines in swine models. Here, we present an overview of the strategies for the development of effective *T. spiralis* vaccines and summarize the factors of influencing the effectiveness of vaccines. We also discuss several propositions in improving the effectiveness of vaccines and may provide a route map for future *T. spiralis* vaccines development.

Keywords: *Trichinella spiralis*, trichinellosis, antigens, vaccines, effectiveness

OPEN ACCESS

Edited by:
Lihua Xiao,
South China Agricultural University, China

Reviewed by:
M. Mabel Ribicich,
University of Buenos Aires, Argentina
Ruo Dan Liu,
Zhengzhou University, China

****Correspondence:***
Mingyuan Liu
liumy@jlu.edu.cn
Daoxiu Xu
xdaoxiu@163.com

[†] These authors have contributed equally to this work

Specialty section:
This article was submitted to Infectious Agents and Disease, a section of the journal Frontiers in Microbiology

Received: *19 January 2022*
Accepted: *16 February 2022*
Published: *23 March 2022*

Citation:
Tang B, Li J, Li T, Xie Y, Guan W, Zhao Y, Yang S, Liu M and Xu D (2022) Vaccines as a Strategy to Control Trichinellosis. Front. Microbiol. 13:857786. doi: 10.3389/fmicb.2022.857786

INTRODUCTION

At present, the *Trichinella* genus comprises nine species and three genotypes that can be divided into encapsulated clade (*Trichinella spiralis*, T1; *Trichinella nativa*, T2; *Trichinella britovi*, T3; *Trichinella murrelli*, T5; *Trichinella nelsoni*, T7; *Trichinella patagoniensis*, T12; and *Trichinella* genotypes T6, T8, and T9) and non-encapsulated clade (*Trichinella pseudospiralis*, T4; *Trichinella papuae*, T10; and *Trichinella zimbabwensis*, T11) (Li et al., 2020; Feng et al., 2021). *T. spiralis* is an intracellular parasitic nematode that can infect a wide variety of mammals (Gottstein et al., 2009). Trichinellosis caused by *T. spiralis* is regarded as an emerging and re-emerging zoonotic

parasitic disease in some parts of the world, such as in Argentina, Eastern Europe, and Asia (Cuperlovic et al., 2005; Devleesschauwer et al., 2017). Human can become infected with *T. spiralis* by ingestion of raw or poorly cooked meat containing the infective larvae of *T. spiralis* (Pozio, 2015). In humans, the clinical symptoms range from diarrhea and abdominal pain (intestinal phase) to fever, myalgia, myocarditis, and allergic reaction (muscular phase); in serious cases, facial edema and encephalitis may develop (Gottstein et al., 2009; Faber et al., 2015). Murrell and Pozio (2011) reported that 261 reports were selected from 494 reports for data extraction after applying strict criteria for relevance and reliability, and there are a total of 65,818 cases and 42 deaths were reported in 41 countries between 1986 and 2009. Although the husbandry condition of animals, meat inspection and public health and safety education have been enhanced to prevent trichinellosis, the International Commission on Trichinellosis (ICT) states that more than 11 million people are chronically infected with *T. spiralis* worldwide (Murrell and Pozio, 2011). China is one of the countries with the higher number of trichinellosis cases in the world. As the main source of human infection is domestic pigs and pork-related products, there is a need to develop an effective strategy to prevent *T. spiralis* transmission from pigs to humans (Cui et al., 2011; Cui et al., 2013a; Jiang et al., 2016). It is well-known that vaccines are among the most important ways to control diseases, and developing a vaccine against *T. spiralis* infection in pigs is a promising strategy to control *T. spiralis* infection.

To date, no effective vaccines are available to control *T. spiralis* infection, and therefore vaccine research should be intensified to prevent *T. spiralis* infection. The lack of progress in vaccine research against *T. spiralis* infection reflects both scientific obstacles, such as the complexity of life cycles and diversity of antigens, and policy deficiencies that have resulted in trichinellosis receiving little attention (Hewitson and Maizels, 2014). The developmental cycles of *T. spiralis* include three major stages: adult worms (AD), newborn larvae (NBL), and muscle larvae (ML) (Gottstein et al., 2009). Various antigenic components are expressed at each stage, and as such, a large number of antigens are available for vaccine research against *T. spiralis* infection. Furthermore, different life cycles of *T. spiralis* often occur in distinct tissues causing different immunological environments and pathological consequence. In general, vaccines should aim to block the development of infected larvae in the intestine, interrupt the growth of infected larvae to AD and expel AD from the intestine. Overall, the selection of adjuvants and the route of vaccination are associated with the effects of vaccines (Sander et al., 2020). Most studies of *T. spiralis* vaccines have been performed in murine models, whereas few studies have been conducted in swine models. Nevertheless, pigs are the natural host of *T. spiralis*, and studies have found that the immune responses induced by the same antigen are likely to differ between pigs and mice (Feng et al., 2013; Habiela et al., 2014; Xu et al., 2021). Feng et al. reported that mice vaccinated with a *T. spiralis* serine protease (rTs-Adsp) induced Th1-Th2 mixed immune response with Th2 predominant. However, Xu et al. reported that a Th1-Th2 mixed immune response with Th1 predominant was induced by rTs-Adsp after vaccination. Consequently, future studies of the development of *T. spiralis* vaccines should focus on pigs instead of mice.

Human trichinellosis is treated with anthelmintic drugs, such as mebendazole or albendazole. These drugs are considered relatively safe, except for pregnant women due to teratogenic effects (Shimoni and Froom, 2015). A vaccine for foodborne infection is the best method to control parasite infection, improve public health, and promote socioeconomic development (Hewitson and Maizels, 2014; McAllister, 2014). Compared with chemical treatment, vaccines have several advantages in the prevention of *T. spiralis* infection (Zhang N. et al., 2018). For example, vaccines provide long-term protection and eliminate the phenomenon of drug resistance of *T. spiralis*. Moreover, vaccines improve food safety by reducing drug residues in meat (Joachim, 2016; Sander et al., 2020). Studies have found that a window period between *T. spiralis* infection and anti-*Trichinella* IgG positivity (Gamble et al., 2004; Cui J.et al., 2015; Wang et al., 2017). There have been great efforts over the past few decades with respect to investigating the protective effect of *T. spiralis* vaccines through different strategies (Zhang N. et al., 2018). Vaccine development for *T. spiralis* infection is mainly divided into live attenuated vaccines, natural antigen vaccines, recombinant protein vaccines, DNA vaccines, and synthetic peptide vaccines. Although live attenuated vaccines elicit a strong immune response and protective immunity, their safety is doubtful. Inactivated vaccines are safe and have high protective effects, but antigen resources are limited due to the requirements of numerous animals. Currently, the development of *T. spiralis* vaccines focuses on recombinant vaccines and DNA vaccines. In this review, we will summarize the advances and future innovations in the development of *T. spiralis* vaccines as a strategy against trichinellosis.

VACCINES AGAINST *T. spiralis* INFECTION

Traditional antigens of *T. spiralis* vaccines are derived from crude extracts of whole worms, excretory-secretory (ES) products. It is well-known that live attenuated vaccines and inactivated vaccines are first generation vaccines. With the development of genetic engineering methods, the strategy of genome, proteome, transcriptome, and immunoproteomics have been used to screen novel candidate antigens of *T. spiralis* vaccines (**Figure 1**). Based on these methods, second and third generation vaccines have been performed in rodent and swine models to evaluate their protective effect, such as recombinant protein vaccines, synthetic peptide vaccines and DNA vaccines. The strategies and protective effect of vaccines candidates against *T. spiralis* infection in different models are provided in **Table 1**.

Live Attenuated Vaccines

Live attenuated vaccines were produced with radiation or drugs to reduce the pathogenicity of *T. spiralis* while maintaining immunogenicity. Experimental animals vaccinated with radiation-attenuated larvae exhibited an exciting reduction

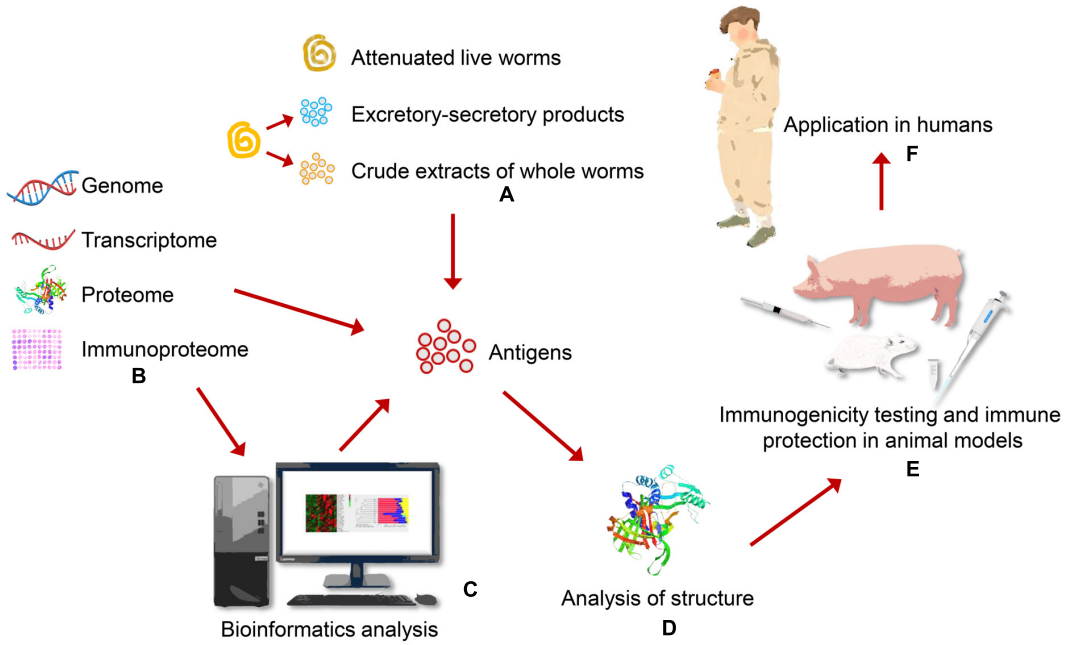

FIGURE 1 | Discovery and identification vaccine candidates through different strategies in animal models. **(A)** Traditional *Trichinella spiralis* vaccines are derived from live attenuated vaccines, crude extracts of whole worms, excretory-secretory (ES) products. **(B)** Vaccine candidates can be screened through different strategies, including genome, transcriptome, proteome, immunoproteome. **(C)** Candidate antigens are selected for *T. spiralis* vaccines through bioinformatics analysis. **(D)** Analyzing structure of antigens contributes to designing effective vaccines in the future. **(E)** Immunogenicity and immune protection of vaccine candidates are identified through vitro and animal experiments. **(F)** High effective vaccines translate to meet people need and are applied in humans.

in muscle larvae burden (Cabrera and Gould, 1964; Agyei-Frempong and Catty, 1983; Hafez et al., 2020). For instance, Hafez et al. (2020) reported that mice vaccinated with radiation-attenuated larvae show a 72.5% reduction in muscle larvae burden, and Nakayama et al. (1998) found significant immunity in mice vaccinated with radiation-attenuated *T. britovi* larvae, with a strong worm reduction. Live attenuated vaccines perform high protective efficacy because they are similar to natural infection, mimicking an approximate microenvironment of *T. spiralis* infection. However, their safety is doubtful due to the potential of pathogenicity. The approach of live attenuated vaccines is gradually abandoned, even though it is associated with strong protective immunity.

Natural Antigens Vaccines

Crude Extracts of Whole Worms

Trichinella spiralis has three major antigenic stages in the same host, namely, AD, NBL, and ML. Mice inoculated with adult worms soluble antigens showed an 89% reduction in adult worms and a 96% reduction in muscle larvae (Gamble, 1985a). Marti et al. (1987) reported that crude *T. spiralis* newborn larvae antigens were treated under freeze-thawing condition resulted in 78% muscle larvae reduction in pigs vaccinated with the antigens. Immunofluorescence results have shown that antibodies from the serum of immunized pigs bind to the surface of newborn larvae. Conversely, it was reported that soluble components of newborn larvae treated by ultrasonication have not protective effect against *T. spiralis* infection (Marti et al., 1987). Eissa et al. (2003) reported that mice vaccinated with the autoclaved *T. spiralis* larvae exhibit a significant reduction in adult worms and muscle larvae. The results of histopathological examination showed degeneration and hyalinization in the *T. spiralis* cyst wall accompanied by pericystic fibrosis. Another study found that the combination of antigens from adult worms and muscle larvae elicited a 73% reduction in *T. spiralis* female fecundity, a 96% reduction in adult worms and an 86% reduction in muscle larvae (Darwish et al., 1996). Although worm antigens from different stages induce a surprising protective effect, antigen resources are limited due to the requirement of numerous animals. Moreover, worm antigens are mainly presented *via* MHC-II pathway and mostly induce humoral immune responses (Aida et al., 2021). High effective vaccines usually induce strong humoral and cell-mediated responses to expel parasites from the host's intestine. With the development of technology, second and third generation vaccines spring up due to these disadvantages of inactivated vaccines.

Excretory-Secretory Products

The major origin of ES antigens are the stichosome and stichocytes (Gamble et al., 1983; Gamble et al., 1988). Here, we summarize the protective effect induced by crude ES products and components of ES products with a defined molecular size. After *T. spiralis* infection, ES antigens are directly exposed to the immune system of the host, and they are

TABLE 1 | The protective effect of different type vaccines against *Trichinella spiralis* infection.

Vaccine type	Animal model	Antigen/Adjuvant	Antigen delivery	Dose	Protection	References
Live attenuated vaccines	Mice	Attenuated larvae	oral	300 attenuated larvae	72.5% reduction in ML	Hafez et al., 2020
Natural antigens vaccines	Pigs	Whole newborn larvae/Freund's complete adjuvant	ip	3.5×10^5 NBL	78% reduction in ML	Marti et al., 1987
	Mice	Larval Excretory-secretory (ES) products/Freund's complete adjuvant	ip	10 μg	65.3% reduction in ML	Gamble, 1985b
	Mice	CTAB antigen/Freund's complete adjuvant	sc	100 μg	50.42% reduction in ML	Grencis et al., 1986
Recombinant protein vaccines	Mice	*T. spiralis* serine protease (rTsSP)/cholera toxin subunit B	in	30 μg	71.10% reduction in Ad and 62.10% reduction in ML	Sun et al., 2019
	Mice	*T. spiralis* serine protease inhibitor (rTsSPI)/Freund's complete adjuvant	sc	20 μg	62.2% reduction in Ad and 57.25% reduction in ML	Song et al., 2018
	Mice	*T. spiralis* adult-specific DNase II-1 (rTsDNase II-1)/Freund's adjuvant	sc	20 μg	40.36% reduction in Ad and 50.43% reduction in ML	Qi et al., 2018
DNA vaccines	Mice	pcDNA3.1(+)-Ts-NBLsp	im	60 μg	77.93% reduction in ML	Xu et al., 2017a
Synthetic peptide vaccines	Mice	A 40-mer synthetic peptide	sc	100 μg	64.3% reduction in Ad	Robinson et al., 1995

ip., intraperitoneal; in., intranasal; sc., subcutaneously; im., intramuscular. Not all antigens appearing in the article are listed in the table. Only representative antigens are listed in the table.

the target antigens that induce an immune response of host (Lightowlers and Rickard, 1988). Thus, ES antigens play a critical role in diagnosing and preventing trichinellosis (Todorova, 2000; Korinkova et al., 2008). According to Isao et al., the main components of ES products in muscle larvae consist of 43 kDa, 53 kDa, and 45 kDa glycoproteins, which are derived from stichosomes (Nagano et al., 2009). Studies on ES products of *T. spiralis* contribute to understanding the interaction between host and parasite, and in developing vaccines against *T. spiralis* infection.

Gamble et al. (1986) reported that pigs vaccinated with the ES antigen of muscle larvae had a significant reduction in female fecundity and a 57% reduction in muscle larvae. Moreover, Gamble (1985b) found significant levels of protection in mice immunized with an antigen isolated from ES products. Although ES antigens keep natural activity and have excellent immunogenicity, ES antigen resources require large numbers of animals. With the development of science and technology, some new strategies have been applied to screen antigens in ES products, such as proteomics and immunoblotting (Liu et al., 2016a,b), and in most studies, the antigen genes screened from ES products are cloned and expressed in a prokaryotic expression system. In the future, more potential immunogenic antigens should be selected from among ES products, and the protective effect of these antigens should be further explored.

Surface Antigens

Trichinella spiralis surface proteins are directly exposed to the immune system of the host and may play an important role in the process of *T. spiralis* invasion (Cui et al., 2013b; Liu R. D.et al., 2014). Grencis et al. (1986) reported that several surface antigens are stripped from the cuticle of *T. spiralis* larvae and that the relative molecular masses of the antigens are 100 kDa, 90 kDa, 69 kDa, 55 kDa, 46 kDa, and 35 kDa. Moreover, mice immunized with surface antigens showed a reduction in adult worms, muscle larvae and female fecundity. In the study of Ortega-Pierres et al. (1989), several antigens extracted from *T. spiralis* larvae displayed the same structural features and surface antigens conferred partial protection against *T. spiralis* infection in mice. Aquaporins (AQPs), also known as water channel proteins, are components of many parasite membranes (Benga, 2009; Faghiri and Skelly, 2009). An aquaporin gene from *T. spiralis* (TsAQP) has been identified, and the TsAQP protein is predicted to contain six

linear B-cell epitopes, suggesting it is a promising antigen for vaccines (Cui J. M.et al., 2015).

Surface antigens of *T. spiralis* are complex, because they may change during the process of worm molting and growth (Bolas-Fernandez and Corral Bezara, 2006). Surface antigens comprise a series of proteins of different biological processes, such as immune reactions, adhesion molecules, and enzyme (Cui et al., 2013b). These antigens are important modulators of the host immune system, and studies of intestinal immunity have revealed that these antigens play a critical role during the process of *T. spiralis* invasion and development. Surface antigens of *T. spiralis* have been identified and characterized by two-dimensional gel electrophoresis (2-DE), mass spectrometry and immunoproteomics (Cui et al., 2013b; Liu R. D.et al., 2014). Research on surface antigens contributes to understanding the host-parasite interaction and identifying target antigens for detection, diagnosis and vaccine development (Bolas-Fernandez and Corral Bezara, 2006; Cui et al., 2013b; Liu R. D.et al., 2014).

Recombinant Protein Vaccines

Certain progress in the development of recombinant protein vaccines against *T. spiralis* infection has been achieved with the rapid development of genetic engineering. Candidate antigens have mainly been screened from ES products, functional proteins and antigens involved in the processes of *T. spiralis* invasion. Protease and protease inhibitor are the most important components of ES products involved in *T. spiralis* infection. In recent years, a large amount of protein vaccine research has been performed on serine proteases, serine proteases inhibitors, cystatins and deoxyribonuclease to control *T. spiralis* infection.

Proteases

Serine proteases from ES products are thought to be key factors in *T. spiralis* invasion of host cells and in processes of immune evasion (Dzik, 2006). Sun et al. (2019) reported that mice vaccinated with recombinant *T. spiralis* serine protease (rTsSP) showed 71.10 and 62.10% reduced worm burdens of AD and ML, and Wang et al. (2013) reported that mice immunized with recombinant *T. spiralis* serine protease (rTspSP-1.2) displayed 34.92 and 52.24% reduced worm burdens of AD and ML. A previous study in our laboratory has found that mice vaccinated with recombinant *T. spiralis* serine protease (rTs-Adsp) exhibited a 46.5% reduction in muscle larvae (Feng et al., 2013). Further research showed a 50.9% reduced worm burden of ML in pigs immunized with rTs-Adsp (Xu et al., 2021). Furthermore, cysteine proteases of parasites are also a focus of attention for parasite vaccines. Cysteine proteases are essential hydrolases present in most organisms, such as viruses and parasites. Cysteine proteases of parasites play an important role in invasion of host tissue and maintenance of parasite survival in the host, rendering them a major target for the development of parasite vaccines (Grote et al., 2018).

Proteases Inhibitor

Serine proteases inhibitors (serpins) are a superfamily of proteins that suppress the activity of serine proteases and play an important role in blood coagulation, inflammation, and complement activation (Molehin et al., 2012). The serpins secreted by worms protect them from the serine proteolysis of the host, and thus, they help parasites overcome defensive barriers and avoid host immune attack (Dzik, 2006). Mice vaccinated with recombinant *T. spiralis* serine protease inhibitor (rTsSPI) exhibited 62.2 and 57.25% reduced worm burdens of AD and ML, in the study by Song et al. (2018), and a 59.95% reduction in adult worms at 10 days post-infection (dpi) and a 46.41% reduction in muscle larvae were detected in mice immunized with recombinant *T. spiralis* serpin (rTs-Serpin) according to Xu et al. (2017b). Cystatins are a superfamily of proteins that specifically inhibit cysteine protease activity (Brown and Dziegielewska, 1997). In nematodes, cystatins play a crucial role in immune evasion and regulate the host immune response during parasite infection (Vray et al., 2002; Hartmann and Lucius, 2003). Tang et al. (2015) reported that mice vaccinated with a cystatin-like protein (Ts-CLP) exhibited a 64.28% reduction in adult worms at 5 dpi and a 61.21% reduction in muscle larvae. Liu X. D.et al. (2014) found that oral administration of a cystatin-like protein to mice resulted in a 91% reduction in the parasite female fecundity.

Deoxyribonuclease II

DNase II mainly exists in lysosomes and nuclei, and plays an important role in pathogen invasion and evasion of the immune response of the host. Compared to DNase II in other species, the DNase II protein family of *T. spiralis* has significantly enlarged. Moreover, studies have found that DNase enzymes of *T. spiralis* may play a key role in parasite-host interactions during infection, suggesting that they can be used as candidate antigens to control and prevent trichinellosis (Liu R. D.et al., 2015; Liu et al., 2016b). Qi et al. (2018) reported that mice subcutaneously vaccinated with rTsDNase II-1 and rTs-DNase II-7 showed 40.36 and 34.86% reductions in adult worms at 5 dpi and 50.43 and 42.33% reductions in muscle larvae, respectively. A previous study by our laboratory found that pigs vaccinated with DNase II-7 recombinant protein showed a 45.7% reduction in muscle larvae (Xu et al., 2020b). Although recombinant protein vaccines have become increasingly popular, the level of immunoprotection is still associated with the antigens, adjuvants, and delivery routes.

DNA Vaccines

DNA vaccines have become more attractive due to their ability to induce a broad immune response and long-lasting immunity (Gu et al., 2014). Additionally, compared to conventional protein vaccines, DNA vaccines are much more stable, cost efficient, simple to produce, and safe for use (Prazeres and Monteiro, 2014; Kumar and Samant, 2016). Compared to protein vaccines, the main disadvantage of DNA vaccines is poor immunogenicity (Li et al., 2012). Furthermore, designing a vaccine suitable for humans is a great challenge for DNA vaccines against parasites. Many studies of DNA vaccines against parasites are focused on murine models, but the results cannot be applied in humans (Kumar and Samant, 2016).

Many DNA vaccines against *T. spiralis* infection have recently been developed in murine models (Gu et al., 2014; Xu et al., 2017a, 2020a). In the study of Wang L.et al. (2016), mice

vaccinated with a *Salmonella*-delivered *TsPmy* DNA vaccine showed 44.8 and 46.6% reduced worm burdens of AD and ML, respectively; Xu et al. (2017a) found a 77.93% reduced worm burden of ML in mice vaccinated with the pcDNA3.1(+)-Ts-NBLsp DNA vaccine. Overall, compared to protein vaccines, the immunogenicity of DNA vaccines is poor due to low levels of antigens expression. Studies have found that DNA plus protein vaccination is an ideal strategy for improving the immune response and protective effect. Gu et al. (2014) reported that mice immunized with Ts87 in a DNA-prime/protein-boost strategy experienced a 46.1% reduced worm burden of ML. In a previous study in our laboratory, mice immunized with pcDNA3.1(+)-Adsp/rTs-Adsp exhibited a 69.50% reduced worm burden of ML (Xu et al., 2020a). With the rapid development of technologies, more methods will be performed to enhance the efficacy of DNA vaccines. The ultimate goal is to develop a DNA vaccine that can be safely applied in humans.

Synthetic Peptide Vaccines

In the past several decades, much research has been carried out to develop vaccines against *T. spiralis* infection, such as crude antigens, recombinant proteins, and DNA vaccines. However, there are only a few studies on controlling *T. spiralis* infection utilizing peptide vaccines. Compared to recombinant protein vaccines, multiepitope peptides have advantages of being easy and fast to produce and may include of multiple protective epitopes (Gu et al., 2020). Robinson et al. (1995) screened a 40-mer synthetic peptide from the glycoprotein of *T. spiralis*, and mice vaccinated with the peptide vaccine exhibited a 64.3% reduction in adult worms, and McGuire et al. (2002) reported a 33.3% reduction in parasite female fecundity in mice immunized with a 30-mer peptide antigen.

In recent years, epitope vaccines against viral, bacterial or even parasitic infection have been rapidly developed. However, epitope vaccines also have some disadvantages: they have poor immunogenicity and need to be conjugated to a large carrier protein. A new strategy of multiple antigenic peptides was developed to improve the immunogenicity of epitope vaccines. Epitope-based vaccines can be constructed as chimeric vaccines by engineering multiple effective epitopes (Gu et al., 2013). Consequently, a chimeric vaccine may improve the level of epitope vaccine protection or prevent parasite immune evasion. Moreover, the life cycle of *T. spiralis* is complex leading to various antigens at different stages. A multiepitope vaccine is an effective way to control *T. spiralis* infection.

FACTORS OF VACCINE EFFECTIVENESS

There are many factors that influence the effectiveness of vaccines, such as the composition of antigens, adjuvants, inoculation doses, delivery routes, infective doses, coinfection, animal species, and vaccination protocol (**Figure 2**). *T. spiralis* has a multistage life cycle, resulting in different antigens at different stages. The composition of antigens determines the effectiveness of vaccines thus identification of excellent antigens is crucial for developing *T. spiralis* vaccines. Different candidate antigens elicit distinct immune response and protective effects. During *Trichinella* infection, Th2-type cytokines are secreted by hosts to promote mast-cell activation and proliferation, which are important for expelling parasite from intestine (Zhang N. et al., 2018). Future studies of the development of *T. spiralis* vaccines should focus on the antigens that could elicit Th2-type immune response. Selecting a suitable adjuvant plays a very important role in vaccine development (Burakova et al., 2018). Adjuvants enhance immune responses induced by parasite antigens, and protect the antigens from being diluted, degraded and eliminated by the host (Stills, 2005). To date, the adjuvants used in experiments include Freund's adjuvant, aluminum hydroxide and emulsions containing water in oil, oil in water, and multiphasic formulations. Freund's adjuvant has been thought to be the gold standard adjuvant and has been used widely in many studies. Nevertheless, the application of Freund's adjuvant is gradually limited due to its toxic effect and specific damage to experimental animals. Although few adjuvants surpass Freund's adjuvant in inducing antibody production, many adjuvants can also induce high antibody responses with less inflammation and tissue destruction. In recent decades, alternative adjuvants have been evaluated against *T. spiralis* infection in murine models, including Montanide ISA series adjuvants and Montanide^{TM} IMS series adjuvants. Montanide^{TM} IMS series adjuvants containing water-dispersed liquid nanoparticles combined with an immunostimulating compound are comparatively non-toxic and have been employed in research on *T. spiralis* vaccines (Jang et al., 2011; Xu et al., 2017b). Yang et al. (2010) reported that recombinant Ts-Pmy formulated with Montanide ISA206 or ISA720 induced similar levels of immune responses and protection, compared to that of Freund's adjuvant formulation group.

Although the adjuvant is very important, the efficiency of immunization also depends on inoculation doses. Regarding dose, Gamble (1985a) reported that mice immunized with 10 μg antigen exhibited a 77% reduction in muscle larvae but that mice immunized with 100 μg antigen displayed a 98% reduction in muscle larvae. In most research, the dose of vaccination in a murine model has varied from 20 to 100 μg. Moreover, few studies have been performed in pig to explore the dose of vaccination and hence there are no standard inoculation doses in pig models. Although mice were immunized with the same antigen formulated with different adjuvants and delivery routes, the immune protection induced differed. At present, vaccine delivery routes include subcutaneous, intradermal, intraperitoneal, intramuscular, intranasal, and oral inoculation. The strategy of encoding *T. spiralis* antigens by the attenuated *Salmonella* and recombinant *Lactobacillus plantarum* has been widely used in the development of *T. spiralis* vaccines, which have been proven to induce mucosal immunity (Liu X. D.et al., 2014; Liu P.et al., 2015; Wang L.et al., 2016; Hu et al., 2021). The model of *T. spiralis* infection involves the intestinal mucosa, and its target is to induce a local immune response. Studies have found that oral or intranasal vaccination can activate systemic and mucosal immune responses. Therefore, vaccination through oral or intranasal routes can be effective, inducing a broad mucosal immune response (Ortega-Pierres et al., 2015).

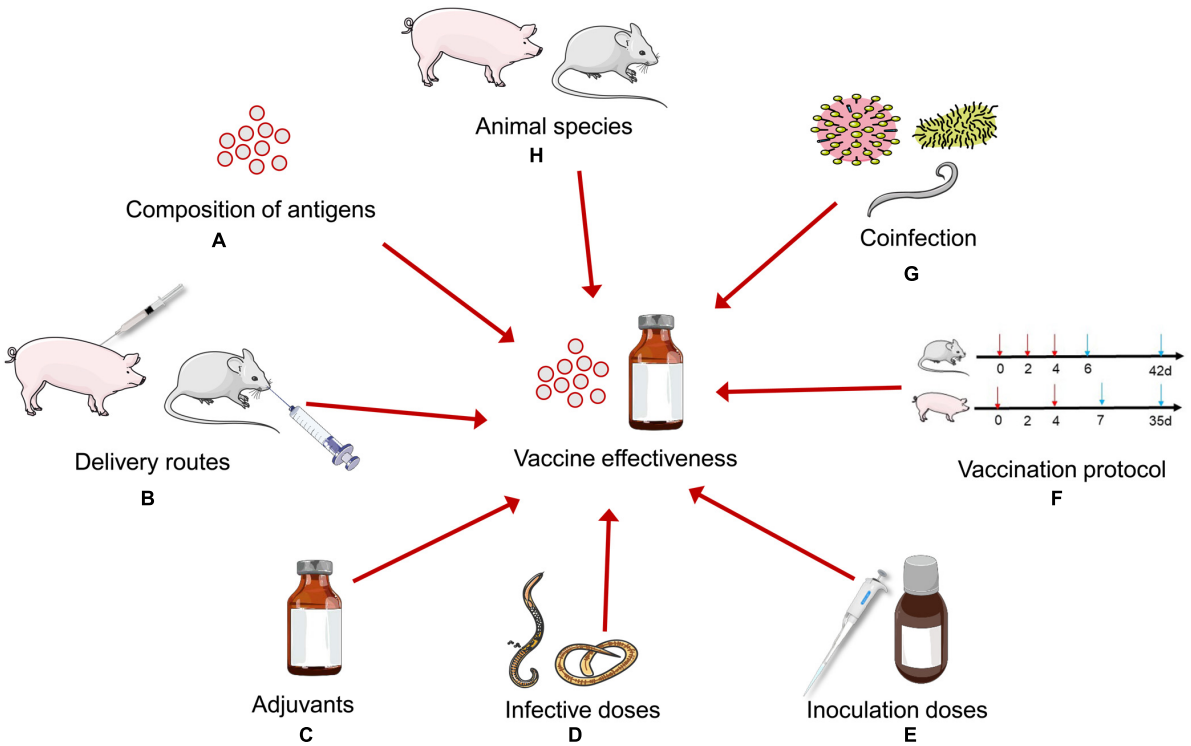

FIGURE 2 | Factors influencing the effectiveness of *Trichinella spiralis* vaccines in animal models. **(A)** Various candidate antigens show different protective effects. **(B)** Several vaccine delivery routes have been used to improve the effectiveness of *T. spiralis* vaccines. **(C)** Suitable adjuvants play a very important role in vaccines effectiveness. **(D)** Infective doses of *T. spiralis* may determine the effectiveness of *T. spiralis* vaccines in animal models. **(E)** The efficiency of immunization also depends on inoculation doses of vaccines. **(F)** There is a lack of a standardized vaccination protocol in animal models. **(G)** Coinfection change the host's immune response to affect the effectiveness of *T. spiralis* vaccines. **(H)** The same antigen may exhibit different protective effects in different animal models.

In most research, the dose of infection in a murine model has varied from 200 to 400 *T. spiralis* ML. In a pig model, Marti et al. (1987) reported that pigs were challenged 2000 *T. spiralis* ML to evaluate the protective effect of antigen. However, Xu et al. (2020b, 2021) reported that pigs were inoculated with 5000 *T. spiralis* ML by oral administration to evaluate the effectiveness of vaccines. The effectiveness of the same candidate antigen may be influenced by infective dose in animal models. Moreover, whether or not the dose of infection is similar to natural infection remains to be explored. In the natural setting, bacteria, viruses and parasites may exist in one host (Wang et al., 2019). Coinfection may change the host's immune response to affect the effectiveness of *T. spiralis* vaccines. Whether or not immune response induced by *T. spiralis* vaccines can be suppressed or neutralized by other pathogens infection remains to be determined. Understanding the immune response induced by multiple pathogens should be a part of *T. spiralis* vaccines development in future. It is well known that animal models play crucial roles in developing vaccines. Most studies on protective effect of vaccines have focused on murine models rather than on pig models. However, the effectiveness of vaccines may vary depending on animal species. Previous studies of our laboratory have found that immune response induced by the same antigen is different between pigs and mice (Feng et al., 2013; Xu et al., 2021). Therefore, high levels of protection induced by candidate antigens in murine models should be further verified in swine models. Considerable efforts have been made to design and verify various vaccination strategies. Although there have been mature vaccination regimens in murine models, they may not be available for pigs or humans. So far, there has been a lack of a standardized protocol in swine models. Consequently, the factors influenced the effectiveness of vaccines should be strongly considered for *T. spiralis* vaccines development in future.

FUTURE PERSPECTIVES AND CHALLENGES

Although substantial efforts and progresses have been made to search for candidate antigens and develop *T. spiralis* vaccines, there is still no effective vaccines to prevent *T. spiralis* infection. With the development of genomics, proteomics, transcriptomics, more immunogenic antigens have been isolated and identified to develop effective *Trichinella* vaccines. More and more strategies have been applied to increase the effectiveness of vaccines. Currently, DNA vaccines are becoming more appealing due to their several advantages, such as cost-effectiveness, stable, long-lasting immunity. Regarding toxoplasmosis vaccines, a DNA multicomponent vaccine showed an 80.22% reduction in the parasite cyst burden (Zhang N. G.et al., 2018). The cocktail DNA

vaccine may be a promising strategy to improve the effectiveness of *T. spiralis* vaccines. Moreover, combination vaccination has been used as a promising approach to improve the effectiveness of *T. spiralis* vaccines in murine models. The strategy of DNA plus protein vaccination exerts the advantages of DNA and protein vaccines to induce high levels of immune response and immune protection. Virus-like particle (VLP) vaccines are one of most popular strategy due to their ability to induce strong immune responses (Pitoiset et al., 2015). The approach has been applied in the field of toxoplasmosis vaccines, and provides a novel idea for the development of *T. spiralis* vaccines. With the development of genetic engineering approaches, the strategy of gene editing has been used to develop live-attenuated toxoplasmosis vaccines (Wang J. L.et al., 2016). Although physiological characters are different between *T. spiralis* and *Toxoplasma gondii*, the strategy can be used as a reference for developing an attenuated *Trichinella* vaccine.

The life cycle of *T. spiralis* in the host is complex, including a diversity of antigens, immune evasion, and regulation of host response. These characteristics make it difficult to achieve the ideal protection with a single *T. spiralis* antigen. The ideal vaccine should promote the process of expelling AD and inhibit the production of NBL and the formation of ML. Moreover, the immune response induced by vaccines should have the ability to disable, degrade, and dislodge the parasites (Maizels et al., 2012). With the development of genetics, new research ideas are being proposed to improve the protection rate of vaccines against *T. spiralis* infection. In-depth research on immunosuppression and immune evasion caused by *T. spiralis* infection will contribute to the design of more effective vaccines against *T. spiralis* infection.

The main source of human *T. spiralis* infection is pork and pork-related products. To date, most research on *T. spiralis* vaccines has been performed in murine models, and more research in pigs should be conducted. The financial and technical issues associated with *T. spiralis* vaccines using swine models make research difficult, but this is a key factor in many vaccinology studies. As the risk of livestock infection with *T. spiralis* is negligible under reasonable management condition, the development of vaccines against *T. spiralis* infection has received little attention. Regardless, vaccines against *T. spiralis* infection are a safe tool that could avoid drug resistance. Therefore, it is crucial to educate the public on the importance of vaccination and its benefit.

CONCLUSION

A successful vaccine for trichinellosis depends on a thorough consideration of immune response caused by *T. spiralis* infection and the factors that influence the effectiveness of vaccines. Finally, research on the protective effect of *T. spiralis* vaccines should focus on pig infection models. To conclude, vaccines are a promising strategy to control trichinellosis.

AUTHOR CONTRIBUTIONS

DX, BT, and TL provided the ideas and wrote the draft manuscript. JL, YX, WG, YZ, and SY contributed to the revising of the manuscript. ML and DX approved the version to be published. All authors read and approved the final manuscript.

FUNDING

This study was supported by Cultivating Project for Young Scholar at Hubei University of Medicine (2021QDJZR012) and the Principle Investigator Program of Hubei University of Medicine (HBMUPI202101).

ACKNOWLEDGMENTS

We thank the staff of the Pathogen biology laboratory. Our thanks are also extended to express our gratitude to all the people who made this work.

REFERENCES

Agyei-Frempong, M., and Catty, D. (1983). The measurement of antigens released by radiation-attenuated *Trichinella spiralis* larvae. *Parasite Immunol.* 5, 289–303. doi: 10.1111/j.1365-3024.1983.tb00745.x

Aida, V., Pliasas, V. C., Neasham, P. J., North, J. F., McWhorter, K. L., Glover, S. R., et al. (2021). Novel vaccine technologies in veterinary medicine: a herald to human medicine vaccines. *Front. Vet. Sci.* 8:654289. doi: 10.3389/fvets.2021.654289

Benga, G. (2009). Water channel proteins (Later Called Aquaporins) and relatives: past, present, and future. *IUBMB Life* 61, 112–133. doi: 10.1002/iub.156

Bolas-Fernandez, F., and Corral Bezara, L. D. (2006). TSL-1 antigens of *Trichinella*: an overview of their potential role in parasite invasion, survival and serodiagnosis of trichinellosis. *Res. Vet. Sci.* 81, 297–303. doi: 10.1016/j.rvsc.2006.01.002

Brown, W. M., and Dziegielewska, K. M. (1997). Friends and relations of the cystatin superfamily–new members and their evolution. *Protein Sci.* 6, 5–12. doi: 10.1002/pro.5560060102

Burakova, Y., Madera, R., McVey, S., Schlup, J. R., and Shi, J. (2018). Adjuvants for Animal Vaccines. *Viral Immunol.* 31, 11–22.

Cabrera, P. B., and Gould, S. E. (1964). Resistance to Trichinosis in Swine Induced by Administration of Irradiated Larvae. *J. Parasitol.* 50, 681–684.

Cui, J. M., Zhang, N. Z., Li, W. H., Yan, H. B., and Fu, B. Q. (2015). Cloning, identification, and bioinformatics analysis of a putative aquaporin TsAQP from *Trichinella spiralis*. *Genet. Mol. Res.* 14, 12699–12709. doi: 10.4238/2015.October.19.14

Cui, J., Jiang, P., Liu, L. N., and Wang, Z. Q. (2013a). Survey of *Trichinella* infections in domestic pigs from northern and eastern Henan, China. *Vet. Parasitol.* 194, 133–135. doi: 10.1016/j.vetpar.2013.01.038

Cui, J., Liu, R. D., Wang, L., Zhang, X., Jiang, P., Liu, M. Y., et al. (2013b). Proteomic analysis of surface proteins of *Trichinella spiralis* muscle larvae by two-dimensional gel electrophoresis and mass spectrometry. *Parasites Vectors* 6:355. doi: 10.1186/1756-3305-6-355

Cui, J., Wang, L., Sun, G. G., Liu, L. N., Zhang, S. B., Liu, R. D., et al. (2015). Characterization of a *Trichinella spiralis* 31 kDa protein and its potential application for the serodiagnosis of trichinellosis. *Acta Trop.* 142, 57–63. doi: 10.1016/j.actatropica.2014.10.017

Cui, J., Wang, Z. Q., and Xu, B. L. (2011). The epidemiology of human trichinellosis in China during 2004-2009. *Acta Trop.* 118, 1–5. doi: 10.1016/j.actatropica.2011.02.005

Cuperlovic, K., Djordjevic, M., and Pavlovic, S. (2005). Re-emergence of trichinellosis in southeastern Europe due to political and economic changes. *Vet. Parasitol.* 132, 159–166. doi: 10.1016/j.vetpar.2005.05.047

Darwish, R. A., Sanad, M. M., and Youssef, S. M. (1996). Immunization against *Trichinella spiralis* using antigens from different life-cycle stages experimental study in mice. *J. Egypt. Soc. Parasitol.* 26, 19–26.

Devleesschauwer, B., Bouwknegt, M., Dorny, P., Gabriel, S., Havelaar, A. H., Quoilin, S., et al. (2017). Risk ranking of foodborne parasites: state of the art. *Food Waterborne Parasitol.* 8–9, 1–13. doi: 10.1016/j.fawpar.2017.11.001

Dzik, J. M. (2006). Molecules released by helminth parasites involved in host colonization. *Acta Biochim. Pol.* 53, 33–64. doi: 10.18388/abp.2006_3361

Eissa, M. M., el-Azzouni, M. Z., Baddour, N. M., and Boulos, L. M. (2003). Vaccination trial against experimental trichrinellosis using autoclaved *Trichinella spiralis* larvae vaccine (ATSLV). *J. Egypt. Soc. Parasitol.* 33, 219–228.

Faber, M., Schink, S., Mayer-Scholl, A., Ziesch, C., Schonfelder, R., Wichmann-Schauer, H., et al. (2015). Outbreak of Trichinellosis due to wild boar meat and evaluation of the effectiveness of post exposure prophylaxis, Germany, 2013. *Clin. Infect. Dis.* 60, E98–E104. doi: 10.1093/cid/civ199

Faghiri, Z., and Skelly, P. J. (2009). The role of tegumental aquaporin from the human parasitic worm, *Schistosoma mansoni*, in osmoregulation and drug uptake. *FASEB J.* 23, 2780–2789. doi: 10.1096/fj.09-130757

Feng, S., Wu, X., Wang, X., Bai, X., Shi, H., Tang, B., et al. (2013). Vaccination of mice with an antigenic serine protease-like protein elicits a protective immune response against *Trichinella spiralis* infection. *J. Parasitol.* 99, 426–432. doi: 10.1645/12-46.1

Feng, Y. Y., Liu, X. L., Liu, Y. Q., Tang, B., Bai, X., Li, C., et al. (2021). Comparative epigenomics reveals host diversity of the *Trichinella* epigenomes and their effects on differential parasitism. *Front. Cell Dev. Biol.* 9:681839. doi: 10.3389/fcell.2021.681839

Gamble, H. R. (1985a). Comparison of immune effects in mice immunized with *Trichinella spiralis* adult and larval antigens. *J. Parasitol.* 71, 680–682. doi: 10.2307/3281444

Gamble, H. R. (1985b). *Trichinella spiralis*: immunization of mice using monoclonal antibody affinity-isolated antigens. *Exp. Parasitol.* 59, 398–404. doi: 10.1016/0014-4894(85)90095-5

Gamble, H. R., Murrell, K. D., and Marti, H. P. (1986). Inoculation of pigs against *Trichinella spiralis*, using larval excretory-secretory antigens. *Am. J. Vet. Res.* 47, 2396–2399.

Gamble, H. R., Pozio, E., Bruschi, F., Nockler, K., Kapel, C. M. O., and Gajadhar, A. A. (2004). International commission on trichinellosis: recommendations on the use of serological tests for the detection of *Trichinella* infection in animals and man. *Parasite* 11, 3–13. doi: 10.1051/parasite/20041113

Gamble, H., Anderson, W., Graham, C., and Murrell, K. D. (1983). Diagnosis of swine trichinosis by enzyme-linked immunosorbent assay (ELISA) using an excretory–secretory antigen. *Vet. Parasitol.* 13, 349–361. doi: 10.1016/0304-4017(83)90051-1

Gamble, H., Rapić, D., Marinculić, A., and Murrell, K. D. (1988). Evaluation of excretory-secretory antigens for the serodiagnosis of swine trichinellosis. *Vet. Parasitol.* 30, 131–137. doi: 10.1016/0304-4017(88)90160-4

Gottstein, B., Pozio, E., and Nockler, K. (2009). Epidemiology, Diagnosis, Treatment, and Control of Trichinellosis. *Clin. Microbiol. Rev.* 22, 127–145. doi: 10.1128/cmr.00026-08

Grencis, R. K., Crawford, C., Pritchard, D. I., Behnke, J. M., and Wakelin, D. (1986). Immunization of mice with surface antigens from the muscle larvae of *Trichinella spiralis*. *Parasite Immunol.* 8, 587–596. doi: 10.1111/j.1365-3024.1986.tb00872.x

Grote, A., Caffrey, C. R., Rebello, K. M., Smith, D., Dalton, J. P., and Lustigman, S. (2018). Cysteine proteases during larval migration and development of helminths in their final host. *PLoS Negl. Trop. Dis.* 12:e0005919. doi: 10.1371/journal.pntd.0005919

Gu, Y., Sun, X., Huang, J., Zhan, B., and Zhu, X. (2020). A multiple antigen peptide vaccine containing CD4(+) T cell epitopes enhances humoral immunity against *Trichinella spiralis* infection in mice. *J. Immunol. Res.* 2020:2074803. doi: 10.1155/2020/2074803

Gu, Y., Wei, J. F., Yang, J., Huang, J. J., Yang, X. D., and Zhu, X. P. (2013). Protective Immunity against *Trichinella spiralis* Infection Induced by a Multi-Epitope Vaccine in a Murine Model. *PLoS One* 8:e77238. doi: 10.1371/journal.pone.0077238

Gu, Y., Zhan, B., Yang, Y., Yang, X., Zhao, X., Wang, L., et al. (2014). Protective effect of a prime-boost strategy with the Ts87 Vaccine against *Trichinella spiralis* infection in mice. *Biomed. Res. Int.* 2014:326860. doi: 10.1155/2014/326860

Habiela, M., Seaga, J., Perez-Martin, E., Waters, R., Windsor, M., Salguero, F. J., et al. (2014). Laboratory animal models to study foot-and-mouth disease: a review with emphasis on natural and vaccine-induced immunity. *J. Gen. Virol.* 95, 2329–2345. doi: 10.1099/vir.0.068270-0

Hafez, E. N., El Kholy, W. A. E. S., and Amin, M. M. (2020). The potential protective role of gamma-irradiated vaccine versus Punica granatum treatment against murine trichinellosis. *J. Radiat. Res. Appl. Sci.* 13, 560–567.

Hartmann, S., and Lucius, R. (2003). Modulation of host immune responses by nematode cystatins. *Int. J. Parasitol.* 33, 1291–1302. doi: 10.1016/s0020-7519(03)00163-2

Hewitson, J. P., and Maizels, R. M. (2014). Vaccination against helminth parasite infections. *Expert. Rev. Vaccines* 13, 473–487. doi: 10.1586/14760584.2014.893195

Hu, C. X., Xu, Y. X. Y., Hao, H. N., Liu, R. D., Jiang, P., Long, S. R., et al. (2021). Oral vaccination with recombinant Lactobacillus plantarum encoding *Trichinella spiralis* inorganic pyrophosphatase elicited a protective immunity in BALB/c mice. *PLoS Negl. Trop. Dis.* 15:e0009865. doi: 10.1371/journal.pntd.0009865

Jang, S. I., Lillehoj, H. S., Lee, S. H., Lee, K. W., Lillehoj, E. P., Bertrand, F., et al. (2011). Montanide IMS 1313 N VG PR nanoparticle adjuvant enhances antigen-specific immune responses to profilin following mucosal vaccination against Eimeria acervulina. *Vet. Parasitol.* 182, 163–170. doi: 10.1016/j.vetpar.2011.05.019

Jiang, P., Zhang, X., Wang, L. A., Han, L. H., Yang, M., Duan, J. Y., et al. (2016). Survey of *Trichinella* infection from domestic pigs in the historical endemic areas of Henan province, central China. *Parasitol. Res.* 115, 4707–4709. doi: 10.1007/s00436-016-5240-x

Joachim, A. (2016). Vaccination against parasites - status quo and the way forward. *Porcine Health Manag.* 2:30. doi: 10.1186/s40813-016-0047-9

Korinkova, K., Kovarcik, K., Pavlickova, Z., Svoboda, M., and Koudela, B. (2008). Serological detection of *Trichinella spiralis* in swine by ELISA (enzyme-linked immunosorbent assay) using an excretory-secretory (E/S) antigen. *Parasitol. Res.* 102, 1317–1320. doi: 10.1007/s00436-008-0911-x

Kumar, A., and Samant, M. (2016). DNA vaccine against visceral leishmaniasis: a promising approach for prevention and control. *Parasite Immunol.* 38, 273–281. doi: 10.1111/pim.12315

Li, L., Saade, F., and Petrovsky, N. (2012). The future of human DNA vaccines. *J. Biotechnol.* 162, 171–182. doi: 10.1016/j.jbiotec.2012.08.012

Li, T. T., Tang, B., Bai, X., Wang, X. L., Luo, X. N., Yan, H. B., et al. (2020). Development of genome-wide polymorphic microsatellite markers for *Trichinella spiralis*. *Parasites Vectors* 13:58. doi: 10.1186/s13071-020-3929-2

Lightowlers, M. W., and Rickard, M. D. (1988). Excretory-secretory products of helminth parasites: effects on host immune responses. *Parasitology* 96, S123–S166. doi: 10.1017/s0031182000086017

Liu, P., Wang, Z. Q., Liu, R. D., Jiang, P., Long, S. R., Liu, L. N., et al. (2015). Oral vaccination of mice with *Trichinella spiralis* nudix hydrolase DNA vaccine delivered by attenuated *Salmonella* elicited protective immunity. *Exp. Parasitol.* 153, 29–38. doi: 10.1016/j.exppara.2015.02.008

Liu, R. D., Cui, J., Liu, X. L., Jiang, P., Sun, G. G., Zhang, X., et al. (2015). Comparative proteomic analysis of surface proteins of *Trichinella spiralis* muscle larvae and intestinal infective larvae. *Acta Trop.* 150, 79–86. doi: 10.1016/j.actatropica.2015.07.002

Liu, R. D., Cui, J., Wang, L., Long, S. R., Zhang, X., Liu, M. Y., et al. (2014). Identification of surface proteins of *Trichinella spiralis* muscle larvae using immunoproteomics. *Trop. Biomed.* 31, 579–591.

Liu, R. D., Jiang, P., Wen, H., Duan, J. Y., Wang, L. A., Li, J. F., et al. (2016a). Screening and characterization of early diagnostic antigens in excretory-secretory proteins from *Trichinella spiralis* intestinal infective larvae by immunoproteomics. *Parasitol. Res.* 115, 615–622. doi: 10.1007/s00436-015-4779-2

Liu, R. D., Qi, X., Sun, G. G., Jiang, P., Zhang, X., Wang, L. A., et al. (2016b). Proteomic analysis of *Trichinella spiralis* adult worm excretory-secretory proteins recognized by early infection sera. *Vet. Parasitol.* 231, 43–46. doi: 10.1016/j.vetpar.2016.10.008

Liu, X. D., Wang, X. L., Bai, X., Liu, X. L., Wu, X. P., Zhao, Y., et al. (2014). Oral administration with attenuated *Salmonella* encoding a *Trichinella* cystatin-like protein elicited host immunity. *Exp. Parasitol.* 141, 1–11. doi: 10.1016/j.exppara.2014.03.015

Maizels, R. M., Hewitson, J. P., and Smith, K. A. (2012). Susceptibility and immunity to helminth parasites. *Curr. Opin. Immunol.* 24, 459–466. doi: 10.1016/j.coi.2012.06.003

Marti, H. P., Murrell, K. D., and Gamble, H. R. (1987). *Trichinella spiralis*: immunization of pigs with newborn larval antigens. *Exp. Parasitol.* 63, 68–73. doi: 10.1016/0014-4894(87)90079-8

McAllister, M. M. (2014). Successful vaccines for naturally occurring protozoal diseases of animals should guide human vaccine research. A review of protozoal vaccines and their designs. *Parasitology* 141, 624–640. doi: 10.1017/S0031182013002060

McGuire, C., Chan, W. C., and Wakelin, D. (2002). Nasal immunization with homogenate and peptide antigens induces protective immunity against *Trichinella spiralis*. *Infect. Immun.* 70, 7149–7152. doi: 10.1128/IAI.70.12.7149-7152.2002

Molehin, A. J., Gobert, G. N., and McManus, D. P. (2012). Serine protease inhibitors of parasitic helminths. *Parasitology* 139, 681–695. doi: 10.1017/S0031182011002435

Murrell, K. D., and Pozio, E. (2011). Worldwide Occurrence and Impact of Human Trichinellosis 1986-2009. *Emerg. Infect. Dis.* 17, 2194–2202. doi: 10.3201/eid1712.110896

Nagano, I., Wu, Z., and Takahashi, Y. (2009). Functional genes and proteins of *Trichinella spp*. *Parasitol. Res.* 104, 197–207. doi: 10.1007/s00436-008-1248-1

Nakayama, H., Inaba, T., Nargis, M., Chisty, M., Ito, M., and Kamiya, H. (1998). Immunization of laboratory animals with ultraviolet-attenuated larvae against homologous challenge infection with *Trichinella britovi*. *Southeast Asian J. Trop. Med. Public Health* 29, 563–566.

Ortega-Pierres, G., Muniz, E., Coral-Vazquez, R., and Parkhouse, R. M. (1989). Protection against *Trichinella spiralis* induced by purified stage-specific surface antigens of infective larvae. *Parasitol. Res.* 75, 563–567. doi: 10.1007/BF00931167

Ortega-Pierres, G., Vaquero-Vera, A., Fonseca-Linan, R., Bermudez-Cruz, R. M., and Argueello-Garcia, R. (2015). Induction of protection in murine experimental models against *Trichinella spiralis*: an up-to-date review. *J. Helminthol.* 89, 526–539. doi: 10.1017/S0022149X15000140

Pitoiset, F., Vazquez, T., and Bellier, B. (2015). Enveloped virus-like particle platforms: vaccines of the future? *Expert. Rev. Vaccines* 14, 913–915. doi: 10.1586/14760584.2015.1046440

Pozio, E. (2015). *Trichinella spp*. imported with live animals and meat. *Vet. Parasitol.* 213, 46–55. doi: 10.1016/j.vetpar.2015.02.017

Prazeres, D. M. F., and Monteiro, G. A. (2014). Plasmid Biopharmaceuticals. *Microbiol. Spectrum* 2:1128. doi: 10.1128/microbiolspec.PLAS-0022-2014

Qi, X., Yue, X., Han, Y., Jiang, P., Yang, F., Lei, J. J., et al. (2018). Characterization of two *Trichinella spiralis* Adult-Specific DNase II and their capacity to induce protective immunity. *Front. Microbiol.* 9:2504. doi: 10.3389/fmicb.2018.02504

Robinson, K., Bellaby, T., Chan, W. C., and Wakelin, D. (1995). High levels of protection induced by a 40-mer synthetic peptide vaccine against the intestinal nematode parasite *Trichinella spiralis*. *Immunology* 86, 495–498.

Sander, V. A., Sanchez Lopez, E. F., Mendoza Morales, L., Ramos Duarte, V. A., Corigliano, M. G., and Clemente, M. (2020). Use of veterinary vaccines for livestock as a strategy to control foodborne parasitic diseases. *Front. Cell. Infect. Microbiol.* 10:288. doi: 10.3389/fcimb.2020.00288

Shimoni, Z., and Froom, P. (2015). Uncertainties in diagnosis, treatment and prevention of trichinellosis. *Expert. Rev. Anti Infect. Ther.* 13, 1279–1288. doi: 10.1586/14787210.2015.1075394

Song, Y. Y., Zhang, Y., Yang, D. Q., Ren, H. N., Sun, G. G., Jiang, P., et al. (2018). The Immune Protection Induced by a Serine Protease Inhibitor From the Foodborne Parasite *Trichinella spiralis*. *Front. Microbiol.* 9:1544. doi: 10.3389/fmicb.2018.01544

Stills, H. F. (2005). Adjuvants and antibody production: dispelling the myths associated with Freund's complete and other adjuvants. *ILAR J.* 46, 280–293. doi: 10.1093/ilar.46.3.280

Sun, G. G., Lei, J. J., Ren, H. N., Zhang, Y., Guo, K. X., Long, S. R., et al. (2019). Intranasal immunization with recombinant *Trichinella spiralis* serine protease elicits protective immunity in BALB/c mice. *Exp. Parasitol.* 201, 1–10. doi: 10.1016/j.exppara.2019.04.006

Tang, B., Liu, M., Wang, L., Yu, S., Shi, H., Boireau, P., et al. (2015). Characterisation of a high-frequency gene encoding a strongly antigenic cystatin-like protein from *Trichinella spiralis* at its early invasion stage. *Parasites Vectors* 8:78. doi: 10.1186/s13071-015-0689-5

Todorova, V. K. (2000). Proteolytic enzymes secreted by larval stage of the parasitic nematode *Trichinella spiralis*. *Folia Parasitol.* 47, 141–145. doi: 10.14411/fp.2000.027

Vray, B., Hartmann, S., and Hoebeke, J. (2002). Immunomodulatory properties of cystatins. *Cell. Mol. Life Sci.* 59, 1503–1512. doi: 10.1007/s00018-002-8525-4

Wang, B., Wang, Z. Q., Jin, J., Ren, H. J., Liu, L. N., and Cui, J. (2013). Cloning, expression and characterization of a *Trichinella spiralis* serine protease gene encoding a 35.5 kDa protein. *Exp. Parasitol.* 134, 148–154. doi: 10.1016/j.exppara.2013.03.004

Wang, J. L., Huang, S. Y., Behnke, M. S., Chen, K., Shen, B., and Zhu, X. Q. (2016). The past, present, and future of genetic manipulation in *Toxoplasma gondii*. *Trends Parasitol.* 32, 542–553. doi: 10.1016/j.pt.2016.04.013

Wang, J. L., Zhang, N. Z., Li, T. T., He, J. J., Elsheikha, H. M., and Zhu, X. Q. (2019). Advances in the development of Anti-*Toxoplasma gondii* vaccines: challenges, opportunities, and perspectives. *Trends Parasitol.* 35, 239–253. doi: 10.1016/j.pt.2019.01.005

Wang, L., Wang, X. H., Bi, K., Sun, X. M., Yang, J., Gu, Y., et al. (2016). Oral Vaccination with Attenuated *Salmonella* typhimurium-Delivered TsPmy DNA Vaccine Elicits Protective Immunity against *Trichinella spiralis* in BALB/c Mice. *PLoS Negl. Trop. Dis.* 10:e0004952. doi: 10.1371/journal.pntd.0004952

Wang, Z. Q., Shi, Y. L., Liu, R. D., Jiang, P., Guan, Y. Y., Chen, Y. D., et al. (2017). New insights on serodiagnosis of trichinellosis during window period: early diagnostic antigens from *Trichinella spiralis* intestinal worms. *Infect. Dis. Poverty* 6:41. doi: 10.1186/s40249-017-0252-z

Xu, D., Bai, X., Xu, J., Wang, X., Dong, Z., Shi, W., et al. (2021). The immune protection induced by a serine protease from the *Trichinella spiralis* adult against *Trichinella spiralis* infection in pigs. *PLoS Negl. Trop. Dis.* 15:e0009408. doi: 10.1371/journal.pntd.0009408

Xu, D., Tang, B., Yang, Y., Cai, X., Jia, W., Luo, X., et al. (2020b). Vaccination with a DNase II recombinant protein against *Trichinella spiralis* infection in pigs. *Vet. Parasitol.* 297:109069. doi: 10.1016/j.vetpar.2020.109069

Xu, D., Tang, B., Wang, Y., Zhang, L., Qu, Z., Shi, W., et al. (2020a). The immune protection induced by a serine protease from the *Trichinella spiralis* adult administered as DNA and protein vaccine. *Acta Tropica* 211, 105622–105622. doi: 10.1016/j.actatropica.2020.105622

Xu, J., Bai, X., Wang, L. B., Shi, H. N., Van Der Giessen, J. W. B., Boireau, P., et al. (2017a). Immune responses in mice vaccinated with a DNA vaccine expressing serine protease-like protein from the new-born larval stage of *Trichinella spiralis*. *Parasitology* 144, 712–719. doi: 10.1017/S0031182016002493

Xu, J., Bai, X., Wang, L. B., Shi, H. N., van der Giessen, J. W. B., Boireau, P., et al. (2017b). Influence of adjuvant formulation on inducing immune response in mice immunized with a recombinant serpin from *Trichinella spiralis*. *Parasite Immunol.* 39:e12437. doi: 10.1111/pim.12437

Yang, J., Gu, Y., Yang, Y., Wei, J., Wang, S., Cui, S., et al. (2010). *Trichinella spiralis*: immune response and protective immunity elicited by recombinant paramyosin formulated with different adjuvants. *Exp. Parasitol.* 124, 403–408. doi: 10.1016/j.exppara.2009.12.010

Zhang, N. G., Gao, Q., Wang, M., Elsheikha, H. M., Wang, B., Wang, J. L., et al. (2018). Immunization with a DNA vaccine cocktail encoding TgPF, TgROP16, TgROP18, TgMIC6, and TgCDPK3 genes protects mice against chronic toxoplasmosis. *Front. Immunol.* 9:1505. doi: 10.3389/fimmu.2018.01505

Zhang, N., Li, W., and Fu, B. (2018). Vaccines against *Trichinella spiralis*: progress, challenges and future prospects. *Transbound Emerg. Dis.* 65, 1447–1458. doi: 10.1111/tbed.12917

Conflict of Interest: The authors declare that the research was conducted in the absence of any commercial or financial relationships that could be construed as a potential conflict of interest.

Publisher's Note: All claims expressed in this article are solely those of the authors and do not necessarily represent those of their affiliated organizations, or those of the publisher, the editors and the reviewers. Any product that may be evaluated in this article, or claim that may be made by its manufacturer, is not guaranteed or endorsed by the publisher.

frontiers in Microbiology

ORIGINAL RESEARCH
published: 31 March 2022
doi: 10.3389/fmicb.2022.858897

Observation of the Gut Microbiota Profile in BALB/c Mice Induced by *Plasmodium yoelii* 17XL Infection

Wei Guan[1†], Xiaonan Song[1†], Shuguo Yang[1], Huiyin Zhu[1], Fang Li[2] and Jian Li[1]**

[1] Department of Human Parasitology, School of Basic Medicine Science, Hubei University of Medicine, Shiyan, China,
[2] Department of Infectious Diseases, Renmin Hospital, Hubei University of Medicine, Shiyan, China

Rodent malaria caused by *Plasmodium yoelii* 17XL (Py 17XL) is an ideal animal model for human malaria studies. Although the gut microbiota plays an important role in the occurrence and development of infectious diseases, the gut microbiota associated with Py 17XL infection remains unclear. In the current study, the gut microbiota composition of infected BALB/c mice was surveyed. Mouse fecal samples were collected at 0, 2, 5 days post-infection (dpi), and the gut microbiota was characterized by 16S rRNA sequencing. Operational taxonomic units (OTUs) were 634 ± 26 on average. *Firmicutes* and *Bacteroidetes* were typically predominant in the gut microbiota composition at the phylum level. Compared with the Ctrl, *Firmicutes* was significantly decreased after infection, while *Bacteroidetes* was notably increased. The most dominant family was *Lactobacillaceae* in all samples. The alpha diversity index showed that compared with that of the Ctrl, the observed OTU number was decreased at 2 dpi and then slightly increased at 5 dpi. LEfSe analysis revealed several bacterial taxa were notably related to Py-infected mice at the phylogenetic level. Several bacterial genera, such as *Lactobacillus*, were overrepresented in the Py-infected fecal microbiota at 2 dpi, while *Muribaculaceae* was overrepresented at 5 dpi. Moreover, *Alistipes and Helicobacter* were overrepresented at 5 dpi compared with 2 dpi. The results indicated Py infection could alter the gut microbiota composition of mice. Besides, biomarkers could serve as direct targets to elucidate their roles in the progression and pathogenesis of malaria and provide insights into studies of antimalarial drugs and malaria vaccines.

Keywords: ***Plasmodium yoelii*, malaria, gut microbiota, 16S rRNA, biomarker**

OPEN ACCESS

Edited by:
George Grant, University of Aberdeen, United Kingdom

Reviewed by:
Rabindra Kumar Mandal, Indiana University, United States
Fátima Brant, Federal University of Minas Gerais, Brazil

****Correspondence:***
Fang Li
sylf2009@sina.com
Jian Li
yxlijian@163.com

† These authors have contributed equally to this work

Specialty section:
This article was submitted to Infectious Agents and Disease, a section of the journal Frontiers in Microbiology

Received: *20 January 2022*
Accepted: *22 February 2022*
Published: *31 March 2022*

Citation:
Guan W, Song X, Yang S, Zhu H, Li F and Li J (2022) Observation of the Gut Microbiota Profile in BALB/c Mice Induced by Plasmodium yoelii 17XL Infection. Front. Microbiol. 13:858897. doi: 10.3389/fmicb.2022.858897

INTRODUCTION

Malaria is an acute infectious disease that threatens the health of approximately half of the world's population and was responsible for an estimated 241 million clinical cases and approximately 627,000 deaths in 2020 (WHO, 2021). Additionally, there were 14 million more cases in 2020 than in 2019 and 69,000 more deaths. Approximately two-thirds of these additional deaths (47,000) were linked to disruptions in the provision of malaria prevention, diagnosis and treatment during the COVID-19 pandemic (WHO, 2021). Malaria is caused by protozoan parasites of the genus *Plasmodium* and is the most prevalent infectious disease in the WHO African Region (De et al., 2016). China, on the other hand, was officially certified as a malaria-free country by the WHO in 2021 (Feng et al., 2021). Malaria confers a large economic burden and disease burden

(Waide and Schmidt, 2020). Five main species of the genus *Plasmodium* can cause human malaria. Fever, chills, headache, muscle aches, and tiredness are the main symptoms of malaria patients. In addition, gastrointestinal symptoms such as vomiting, abdominal pain, and diarrhea develop in *falciparum* malaria patients (Prasad and Virk, 1993). Under laboratory or clinical conditions, different strains or lines of malaria parasites can cause different severities of malaria in their hosts. The rodent malaria parasite *Plasmodium yoelii* is a representative example of parasite lines with significantly different pathogenicity. BALB/c mice infected with the parasite Py 17XL die within 7 dpi (Nair et al., 2017). Rodent malaria caused by Py 17XL is a typical rodent model for studying the pathogenesis of human malaria (Chen et al., 2010). While there is still much to explore before gut microbiota modulation becomes an effective and optimal treatment for preventing fatal malaria, recent evidence in both human studies and rodent models has indicated the gut microbiota composition is a factor in the progression of disease.

Trillions of microbes naturally reside in the human body, especially in the gastrointestinal tract (Gill et al., 2006). The gut microbiota has many important functions in the human body, including resisting pathogens to support protection, enhancing the immune system, and contributing to digestion and metabolism (Gomaa, 2020). The disturbance of the gut microbiota community is associated with several human diseases, such as inflammatory bowel diseases (IBDs) (Nishino et al., 2018), obesity and diabetes (Karlsson et al., 2013), allergies (Bunyavanich et al., 2016), autoimmune diseases (Chu et al., 2017), and cardiovascular diseases (Astudillo and Mayrovitz, 2021). Moreover, there are a lot of methods for modulating the gut microbiota composition and functions, such as the application of probiotics and fecal microbiota transplantation. Previous studies have suggested the gut microbiota could also modulate the pathogenesis of infectious diseases, indicating that gut microbiota variability influences systemic immune responses. For instance, mice colonized with a gut pathobiont could produce antibodies that reacted with *Plasmodium spp.* (Yilmaz et al., 2014). Besides, gastrointestinal environments, especially changes in the gut microbiota, are related to the onset of several diseases.

Malaria infections affect the gastrointestinal tract, and alterations in the intestinal environment appear to influence malaria pathogenesis. Villarino et al. (2016) showed when different vendors' C57BL/6 mice were infected with the non-lethal rodent-specific strain Py 17XNL, the mice presented numerous differences in infection morbidity, severity, and mortality and that these differences in susceptibility were dependent on the gut microbiota. Taniguchi et al. demonstrated that C57BL/6 mice infected with the lethal rodent-specific strain *P. berghei* ANKA developed experimental cerebral malaria. The alterations included intestinal pathology and gut microbiota composition, which were related to the development of ECM. Moreover, Denny et al. verified that proinflammatory cells were increased in the lamina propria and changes in cecal metabolites were observed with differing susceptibility to Py 17XNL (Denny et al., 2019). However, some *Plasmodium* parasites appear to have developed resistance to available antimalarials. Besides, there is no practical or long-term vaccine against malaria. The relationship between human health and disease and gut microbiota has been studied widely in recent years. Hence, gut microbiota modulation may be a potential treatment for malaria (Villarino et al., 2016).

Recent studies have reported that many various diseases can alter the gut microbiota, which led us to hypothesize that the gut microbiota may be affected by malaria infections. BALB/c mice with Py 17XL infection are a lethal malaria model that can be used to clarify the possible role of Py in influencing the gut microbiota of infected BALB/c mice. Therefore, the aims of the study included (1) analyzing the gut microbiota composition obtained from the feces of Py 17XL-infected and -uninfected mice separately by targeting the V4 region of the 16S rRNA through the Illumina HiSeq2500 platform and (2) obtaining biomarkers to offer insight into malaria pathogenesis and antimalarial drugs.

MATERIALS AND METHODS

Mice and Infection With *Plasmodium yoelii* 17XL

Six- and eight-week-old female BALB/c mice (20-25 g weight) were purchased from HNSJA Co., Ltd., Changsha, China, and maintained under specific pathogen-free conditions. The housing and feeding conditions were maintained as per recommended standards (25 ± 3°C). The mice were fed an irradiated diet and pure water. All the mice were allowed to acclimate for one week before starting the experiment.

Donor female BALB/c mice were intraperitoneally infected with Py 17XL by infected red blood cells (iRBCs) prepared from thawed blood. Fresh blood was collected from donor mice at 4 dpi, and the experimental BALB/c mice were intraperitoneally infected with 1×10^6 iRBCs (in 100 μl saline) prepared from the donor mice. Tail blood was collected for thin smears and stained with Giemsa dye at 2 and 5 dpi, respectively. Percent parasitemia assessed as percent iRBCs per total RBCs was evaluated through Giemsa-stained thin blood smears, and parasites versus whole blood cells were counted at 1,000 × magnification under a light microscope.

Sample Collection

The sixteen experimental mice were placed in the cage individually. Fecal pellets were collected at three time points as follows: before infection with Py 17XL (Ctrl), at 2 days post-infection (PyD2), and at 5 days post-infection (PyD5). Mice feces were placed in a sterile centrifuge tube using a sterile tweezer, immediately frozen in liquid nitrogen and stored at −80°C until use.

DNA Extraction, PCR Amplification, and Sequencing

DNA was extracted from the fecal samples using the CTAB or SDS method. PCR amplification and sequencing were performed using the microbial 16S rRNA primers (16S V4: 515F-806R, 392 bp) as well as Phusion® High-Fidelity PCR Master Mix (New England Biolabs). The PCR product mixture was purified using a Qiagen Gel Extraction Kit (Qiagen, Germany).

Sequencing libraries were generated using a TruSeq® DNA PCR-Free Sample Preparation Kit (Illumina, United States). The library quality was evaluated on the Qubit@ 2.0 Fluorometer (Thermo Scientific) and Agilent Bioanalyzer 2100 system. Finally, the library was sequenced on an Illumina HiSeq2500 platform. The 16S rRNA amplicons sequenced in this study were uploaded into the Sequence Read Archive (SRA) in NCBI and registered with the BioProject database (BioProject identification number PRJNA798515).

Data Processing and Statistical Analysis

Data processing and statistical analysis methods followed (Guan et al., 2021). Paired-end reads were merged using FLASH V1.2.7 (Magoč and Salzberg, 2011). Sequence analysis was performed using QIIME (V1.7.0) (Caporaso et al., 2010). The chimera sequences were determined using the UCHIME algorithm (Edgar et al., 2011) and were removed (Haas et al., 2011) to obtain the effective tags. The operational taxonomic units (OTUs) were determined by using Uparse software (Uparse v7.0.1001) (Edgar, 2013) and assigned by sequences with $\geq$ 97% similarity. Representative sequences for each OTU were screened for further annotation. For each representative sequence, the GreenGene Database (DeSantis et al., 2006) was used based on the RDP 3 classifier (Version 2.2) (Wang et al., 2007) algorithm to annotate the taxonomic information. To study the phylogenetic relationships of the different OTUs and the differences among the dominant species in different groups, multiple sequence alignment was conducted using MUSCLE software (Version 3.8.31) (Edgar, 2004).

Operational taxonomic units abundance information was normalized using a standard sequence number corresponding to the sample with the fewest sequences. Statistical analysis was performed by alpha diversity and beta diversity. The alpha diversity was applied to analyze the complexity of the species diversity for a sample based on six indices: Chao1, ACE, Observed-species, Shannon, Simpson, and Goods-coverage. All of these indices in our samples were calculated with QIIME (Version 1.7.0) and displayed with R software (Version 2.15.3).

In contrast, the beta diversity was evaluated by determining the similarity among the microbial communities. Both weighted and unweighted UniFrac calculations were performed by using QIIME software (Version 1.7.0). Principal coordinate analysis (PCoA) was performed to obtain the principal coordinates and visualize the complex, multidimensional data. The WGCNA package, stat packages, and ggplot2 package in R software (Version 2.15.3) were applied for PCoA analysis. The unweighted pair-group method with arithmetic means (UPGMA) clustering and LEfSe were performed to obtain differentially represented microbial taxa at different taxonomic levels.

RESULTS

General Information

On day 0, normal mice (**Figure 1A**) were infected with Py 17XL parasites. At 2 and 5 dpi, the parasites were observed in thin blood smears using microscopy, representing for successful infection (**Figures 1B,C**). The parasitemia of the infected mice at 5 dpi was higher than that of the infected mice at 2 dpi (**Figure 1D**). The feces were collected on day 0, day 2, and day 5 after infection.

Sequencing and Operational Taxonomic Units Clustering

A total of 48 mouse fecal samples were collected and sent for 16S RNA sequencing. In total, 3,805,568 raw sequences were generated from all the samples, and the sequence number varied from 70,216 to 88,910. The mean number of sequences was 79,283 $\pm$ 5,941 (standard deviation, SD) per sample. After a series of experiments, a total of 3,428,267 clean sequences remained, which ranged from 62,444 to 82,917 sequences per sample, with an average of 71,422 $\pm$ 5,514 (**Table 1**). The GC content in all the samples ranged from 51.78% to 53.73%, and the average was 52.68%. The high-quality reads were clustered using $\geq$ 97% sequence similarity into a total of 30,428 microbiota OTUs, ranging from 538 to 686. Each sample had 634 OTUs, 594 observed species, and 71,422 sequences on average (**Table 1**).

In sum, the OTU number was decreased after Py infection compared with that in the control. **Table 1** lists the detailed characteristics of each sample. The Venn diagram and flower diagram were generated to compare the similarities and differences between the communities in the different groups and samples. There were a total of 1,009 OTUs in all three groups, which had 756 common OTUs. There were 39, 29, and 78 OTUs unique to the Ctrl, PyD2, and PyD5 groups, respectively. The PyD2 group had equal OTUs to the Ctrl group. The PyD5 group had 54 more OTUs than the Ctrl group. Meanwhile, the PyD5 group had 54 more OTUs than the PyD2 group (**Figure 2A**). For individual samples, the maximum OTUs were 80 in PyD5.12, the minimum OTUs were 1 in PyD5.2, PyD5.3, and PyD5.10, and the mean number of unique OTUs was 7 (**Figures 2B–D**).

The species accumulation curves represented species richness in all samples that were close to the plateau phase (**Supplementary Figure 1A**). Likewise, the rarefaction curves indicated that species representation in individual samples was close to the saturation number of observed species (**Supplementary Figure 1B**).

Species Annotation and Taxonomic Overview

Figure 3 shows the microbiota community composition of feces in all three groups of BALB/c mice. Each bar represents the average relative abundance of each microbial taxon in the stacked bar chart. The top 10 taxa with high relative abundance, which comprised 97% of the reads, are illustrated.

At the phylum level (**Figure 3A**), *Firmicutes* (55.39%) and *Bacteroidetes* (37.65%) were the major gut microbiota composition in all the samples. Compared with the Ctrl, *Firmicutes* was significantly decreased in post-infection samples, while *Bacteroidetes* was notably increased in post-infection samples.

At the family level (**Figure 3B**), the most dominant family was *Lactobacillaceae* (31.13%) in all the samples. *Muribaculaceae* (17.55%), *Lachnospiraceae* (16.53%), *Bacteroidaceae* (7.20%), *Rikenellaceae* (6.75%), *Helicobacteraceae* (3.11%), *Marinifilaceae* (2.53%), *Prevotellaceae* (2.19%), *Tannerellaceae* (1.43%), and

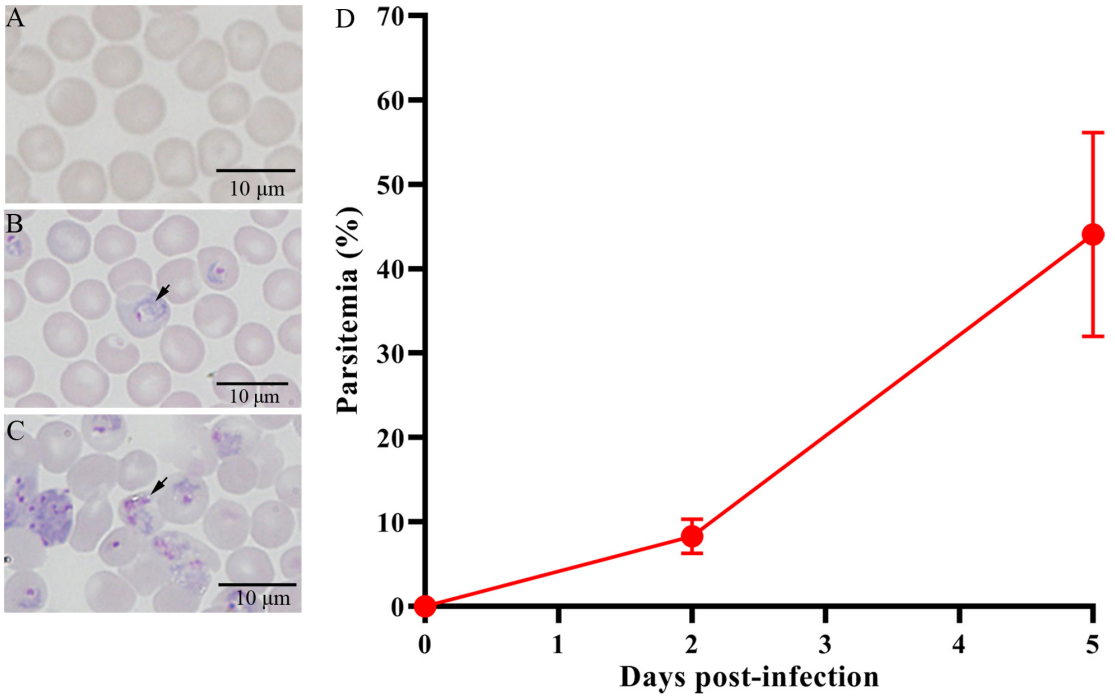

FIGURE 1 | Giemsa's stain to determine the parasitemia of Py 17XL in BALB/c mice. **(A)** The control mice (Ctrl) without parasite infection. **(B)** The PyD2 group with successful parasite infection at 2 dpi. **(C)** The PyD5 group with successful parasite infection at 5 dpi. **(D)** Percent parasitemia was evaluated on the corresponding days. Data are cumulative results (n = 16 mice per group) from two experiments.

Bifidobacteriaceae (0.30%) were the subdominant families. The abundance of *Muribaculaceae*, *Prevotellaceae*, and *Tannerellaceae* was increased in the post-infection samples compared with the Ctrl samples. The abundance of *Lactobacillaceae*, *Bacteroidaceae*, and *Bifidobacteriaceae* was dramatically increased at 2 dpi and then slightly decreased at 5 dpi. At the same time, the abundance of *Lachnospiraceae*, *Rikenellaceae*, *Helicobacteraceae*, and *Marinifilaceae* was slightly decreased at 2 dpi and then slightly increased at 5 dpi.

At the genus level, several taxa displayed significant differences among the three groups. Hierarchical clustering based on the abundance profile of the genera showed the most common genus in each group (**Figure 3C**). The gut microbiota in the samples of infected mice was characterized by higher abundances of *Lactobacillus*, *Muribaculaceae*, *Bacteroides*, *Alistipes*, *Lachnospiraceae_NK4A136_group*, *Helicobacter*, *Odoribacter*, *Alloprevotella*, *Parabacteroides*, and *Bifidobacterium*.

Analysis of the Bacterial Community Within Groups

Alpha diversity analysis was performed to explore the microbiota community diversity in the samples (within-group), reflecting the richness and diversity of the microbiota community. Alpha diversity metrics, including Chao1, Goods-coverage, observed species, Shannon and Simpson diversity index, and phylogenetic diversity values (**Table 1**), revealed a trend that infection with Py transiently changed the richness and evenness among the Ctrl, PyD2 and PyD5 groups. The estimated and observed OTUs in the three groups were different. The OTU number, observed species, and Shannon and Simpson index values were decreased at 2 dpi and then slightly increased at 5 dpi. Outliers were detected in all three groups (**Supplementary Figure 2**).

For Chao1 analysis (**Supplementary Figure 2A**), which represents an index for estimating the number of OTUs in the sample, the Ctrl samples had more estimated OTUs than the PyD2 group (p = 0.0833, t-test; p = 0.0289, Wilcox rank-sum test) and PyD5 group (p = 0.6761, t-test; p = 0.1617, Wilcox rank-sum test), while the PyD2 group had fewer OTUs than PyD5 group (p = 0.377, t-test; p = 0.408, Wilcox rank-sum test).

For observed species analysis (**Supplementary Figure 2B**), which represents the number of species contained in the sample, the Ctrl group samples had higher numbers than the PyD2 group (p = 0.0198, t-test; p = 0.0069, Wilcox rank-sum test) and the PyD5 group (p = 0.6650, t-test; p = 0.2384, Wilcox rank-sum test), and the PyD2 group had fewer observed species than the PyD5 group (p = 0.1388, t-test; p = 0.1084, Wilcox rank-sum test).

For Shannon diversity analysis (**Supplementary Figure 2C**), which assesses the richness and evenness of species composition in the sample, the samples of the Ctrl group had a higher number than the PyD2 group (p = 0.0012, t-test; p = 2.00E-04, Wilcox rank-sum test) but a lower number than the PyD5 group (p = 0.3987, t-test; p = 0.2132, Wilcox rank-sum test), while the PyD2 group had a lower number than the PyD5 group (p = 1.88E-05, t-test; $p < 0.001$, Wilcox rank-sum test).

For phylogenetic diversity analysis (**Supplementary Figure 2D**), which assesses the relationship of species in the microbiota community, samples in the Ctrl group had a

TABLE 1 | Operational taxonomic unit (OTU)-based diversity indexes in mice gut samples during infection.

Sample Name	Group	Raw PE(#)	Nochime (#)	Base(nt)	GC%	Effective%	OTU_ num	Observed_ species	Shannon	Simpson	Chao1	ACE	Goods_ coverage
PyD0.1	Ctrl	70,337	64,174	16,214,197	52.19	91.24	644	606	6.34	0.95	624.32	628.43	0.999
PyD0.2		84,273	73,165	18,487,519	53.14	86.82	674	632	6.87	0.97	658.52	662.18	0.999
PyD0.3		75,412	67,408	17,038,027	52.48	89.39	646	597	6.04	0.94	642.22	632.98	0.999
PyD0.4		84,840	73,283	18,522,540	52.84	86.38	658	613	6.20	0.95	634.36	643.35	0.999
PyD0.5		75,051	65,766	16,619,156	52.82	87.63	614	575	5.37	0.88	616.64	619.24	0.999
PyD0.6		87,986	75,056	18,971,697	53.61	85.3	634	600	6.01	0.93	626.02	625.12	0.999
PyD0.7		83,609	76,237	19,263,197	52.39	91.18	656	611	6.73	0.98	631.57	640.12	0.999
PyD0.8		86,624	79,942	20,204,281	52.46	92.29	643	592	4.75	0.79	614.61	634.14	0.999
PyD0.9		87,613	77,875	19,672,839	53.25	88.89	661	620	6.14	0.93	665.12	662.65	0.999
PyD0.10		75,867	65,990	16,678,473	52.57	86.98	647	601	4.74	0.76	635.88	637.08	0.999
PyD0.11		87,356	78,520	19,832,348	53.07	89.89	674	629	6.99	0.98	648.80	651.66	0.999
PyD0.12		86,098	78,866	19,923,106	52.78	91.6	656	618	6.51	0.96	638.61	652.30	0.999
PyD0.13		76,600	70,510	17,807,037	52.64	92.05	634	589	6.67	0.98	631.14	622.20	0.999
PyD0.14		70,749	64,814	16,363,835	53.43	91.61	636	603	6.68	0.98	631.52	636.62	0.999
PyD0.15		71,469	62,444	15,775,047	53.06	87.37	616	584	6.42	0.96	595.23	602.89	0.999
PyD0.16		78,065	69,093	17,453,274	52.93	88.51	649	602	6.43	0.95	618.72	622.33	0.999
PyD2.1	PyD2	76,928	71,536	18,068,885	52.35	92.99	630	588	6.43	0.97	617.12	615.48	0.999
PyD2.2		71,918	63,493	16,042,265	52.44	88.29	632	599	5.72	0.93	635.40	628.44	0.999
PyD2.3		88,910	81,343	20,519,433	53.64	91.49	627	596	6.38	0.97	618.69	618.30	0.999
PyD2.4		85,378	77,337	19,536,102	52.66	90.58	665	629	5.68	0.91	657.60	667.61	0.999
PyD2.5		84,925	74,679	18,872,116	52.45	87.94	626	593	4.99	0.85	620.02	621.89	0.999
PyD2.6		74,062	70,345	17,767,323	52.45	94.98	578	541	5.71	0.94	569.50	572.46	0.999
PyD2.7		88,829	78,176	19,745,231	52.1	88.01	650	612	6.04	0.94	630.42	639.04	0.999
PyD2.8		79,308	71,996	18,183,311	52.58	90.78	617	577	5.31	0.90	628.94	617.79	0.999
PyD2.9		74,001	64,752	16,364,551	52.35	87.5	612	566	4.62	0.82	596.45	590.92	0.999
PyD2.10		74,817	63,958	16,157,138	52.13	85.49	614	570	5.31	0.91	615.18	609.11	0.999
PyD2.11		80,044	66,995	16,931,900	52.28	83.7	599	550	4.35	0.77	596.47	592.48	0.999
PyD2.12		80,153	70,532	17,827,502	51.84	88	624	580	5.64	0.94	601.28	603.31	0.999
PyD2.13		85,308	76,723	19,379,710	52.46	89.94	678	634	5.78	0.95	668.23	682.08	0.999
PyD2.14		77,261	68,905	17,411,193	52.09	89.18	624	588	5.48	0.91	620.50	627.89	0.999
PyD2.15		72,386	66,325	16,767,584	52.37	91.63	538	501	4.03	0.77	516.11	520.43	0.999
PyD2.16		79,307	72,830	18,401,804	52.58	91.83	622	578	4.73	0.79	608.61	608.17	0.999
PyD5.1	PyD5	79,934	73,460	18,558,327	52.54	91.9	623	586	6.84	0.98	612.73	610.75	0.999
PyD5.2		71,038	65,481	16,539,019	52.47	92.18	637	604	6.95	0.98	630.63	630.28	0.999
PyD5.3		77,717	72,077	18,207,313	52.96	92.74	619	588	6.49	0.97	613.11	615.72	0.999
PyD5.4		88,908	82,917	20,938,956	52.44	93.26	638	601	6.60	0.98	637.85	639.19	0.999
PyD5.5		71,624	66,342	16,759,865	52.75	92.63	624	594	6.52	0.96	614.57	623.67	0.999
PyD5.6		83,105	73,604	18,584,672	53.27	88.57	618	581	5.81	0.93	631.31	621.99	0.999
PyD5.7		84,200	79,036	19,958,270	52.39	93.87	611	569	6.23	0.97	591.64	601.91	0.999
PyD5.8		79,922	73,812	18,642,216	52.71	92.36	647	611	6.64	0.98	645.04	643.89	0.999
PyD5.9		77,161	70,971	17,926,955	52.07	91.98	630	597	6.47	0.97	617.63	620.75	0.999
PyD5.10		77,214	68,398	17,276,058	53.3	88.58	639	608	6.28	0.94	634.56	633.44	0.999
PyD5.11		70,216	63,661	16,078,482	52.69	90.66	618	593	6.60	0.97	616.02	616.95	0.999
PyD5.12		73,293	67,990	17,178,324	51.78	92.76	686	639	6.59	0.97	674.02	676.67	0.999
PyD5.13		84,219	77,320	19,527,987	53.1	91.81	616	569	6.43	0.96	595.91	606.35	0.999
PyD5.14		70,954	64,678	16,331,402	53.73	91.15	659	611	6.81	0.97	623.24	632.25	0.999
PyD5.15		85,073	77,047	19,469,881	52.87	90.57	635	597	6.03	0.93	614.75	625.17	0.999
PyD5.16		75,506	68,405	17,293,772	52.97	90.6	650	610	5.98	0.93	639.50	642.31	0.999
Total		3,805,568	3,428,267	866,074,120			30,428	28,532					
Maximum value		88,910	82,917	20,938,956	53.73	94.98	686	639	6.99	0.98	674	682	0.999
Minimum value		70,216	62,444	15,775,047	51.78	83.70	538	501	4.03	0.76	516	520	0.999
Average		79,283	71,422	18,043,211	52.68	90.11	634	594	6.01	0.93	623	626	0.999
SD		5941	5514	1391042	0.45	2.48	26	25	0.74	0.06	26	27	4E-16

Ctrl, PyD2and PyD5 represent group control and Py 17XL-infected mice at 2 dpi, Py 17XL-infected mice at 5 dpi, respectively.

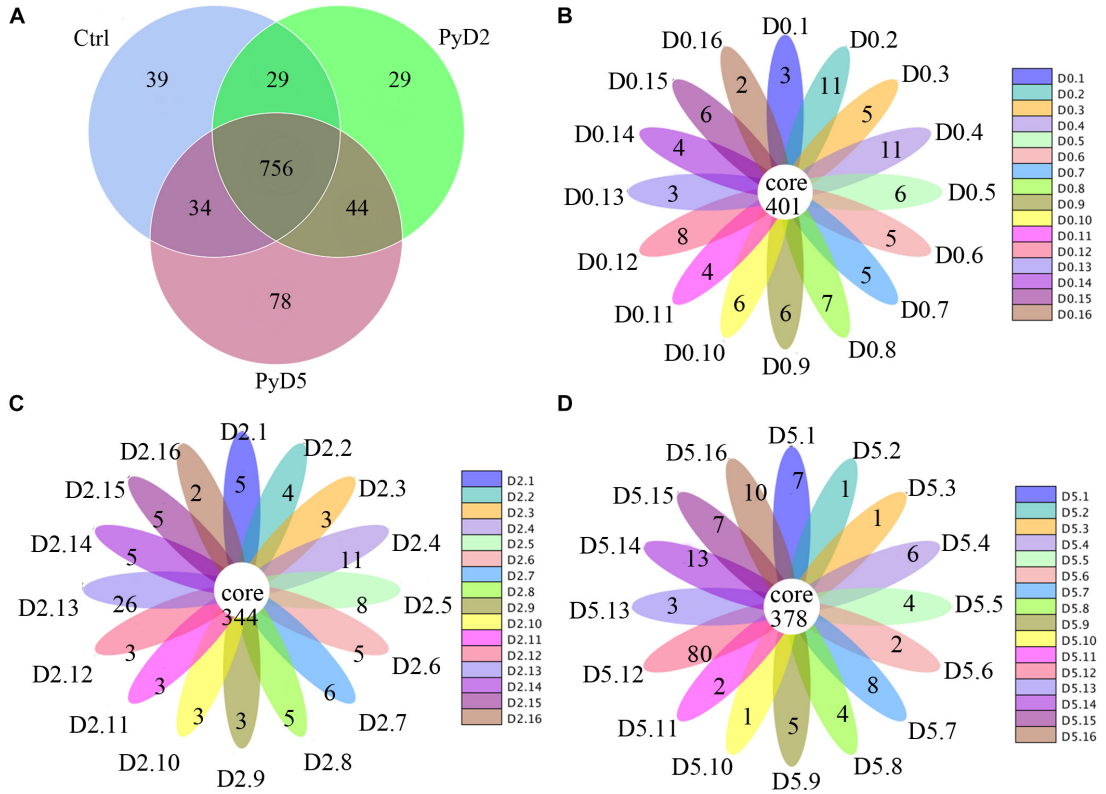

FIGURE 2 | Operational taxonomic unit (OTU) analysis in the different fecal samples. **(A)** Venn diagram showing the unique and shared OTUs in the various groups and communities. **(B)** Flower diagram showing the shared and unique OTUs in the Ctrl samples. **(C)** Flower diagram showing the exclusive and mutual OTUs in the PyD2 samples. **(D)** The flower diagram shows the exclusive and mutual OTUs in the PyD5 samples.

slightly higher number than those in the PyD2 ($p = 0.547$, t-test) and PyD5 groups ($p = 0.959$, t-test), while the PyD2 group had a few lower numbers than the PyD5 group ($p = 0.7182$, t-test).

Analysis of the Bacterial Community Between Groups

For the unweighted UniFrac analysis (**Supplementary Figure 2E**), referring to the presence or absence of alterations in the species, beta diversity analysis was different among the Ctrl, PyD2, and PyD5 groups. The values in the PyD2 samples were increased relative to those in the Ctrl and PyD5 samples, but the values in the PyD5 samples were decreased relative to those in the Ctrl samples. That is, the samples in the PyD2 group had a higher number of OTUs than the Ctrl samples ($p = 0.7244$, t-test; $p = 0.6495$, Wilcoxon rank-sum test) and PyD5 samples ($p = 0.7232$, t-test; $p = 0.0117$, Wilcoxon rank-sum test). Moreover, the samples in the PyD5 group had a lower number of OTUs than the Ctrl group ($p = 0.2843$, t-test; $p = 0.0382$, Wilcoxon rank-sum test). It also demonstrated that the discreteness of the beta diversity increased from Ctrl to PyD2 and then decreased from PyD2 to PyD5. Meanwhile, for the weighted UniFrac analysis concerning both the presence or absence of species and the alterations in species abundance, the values among the Ctrl, PyD2, and PyD5 groups had an obviously similar trend to those of the unweighted UniFrac analysis (**Supplementary Figure 2F**).

The similarity degree between the BALB/c mouse gut microbiota composition in each sample was examined using the principal coordinate analysis (PCoA) based on the unweighted (**Figure 4A**) and weighted (**Figure 4B**) UniFrac distance matrices. The gut microbiota was markedly altered as Py 17XL infection progressed in BALB/c mice. On the PCoA plot, each symbol represents the gut microbiota of one mouse in the relevant stage. The similarity degree between community structures verified by PCoA was examined by comparing within-group unweighted UniFrac distances for the PC1 axis among the Ctrl, PyD2, and PyD5 groups (**Figure 4A**). In contrast, the similarity degree between community structures verified by PCoA was examined by comparing within-group weighted UniFrac distances for the PC2 axis among the Ctrl, PyD2, and PyD5 groups (**Figure 4B**).

Following the PCoA plot, the between-group distances were significantly higher than the within-group distances for each group (ANOSIM, MRPP, $p \leq 0.01$). The R value and P value of the ANOSIM between the Ctrl and PyD2 groups were 0.2386 and 0.002, respectively; the R value and P value of the ANOSIM between the Ctrl and PyD5 groups were 0.1739 and 0.004, respectively, and the R value and P value of the ANOSIM between PyD2 and PyD5 group were 0.3018 and 0.002, respectively. The R value indicated significant differences among the three groups, while the P value indicated statistical significance ($p < 0.05$). MRPP analysis (0.401, 0.384, 0.397; 0.422,

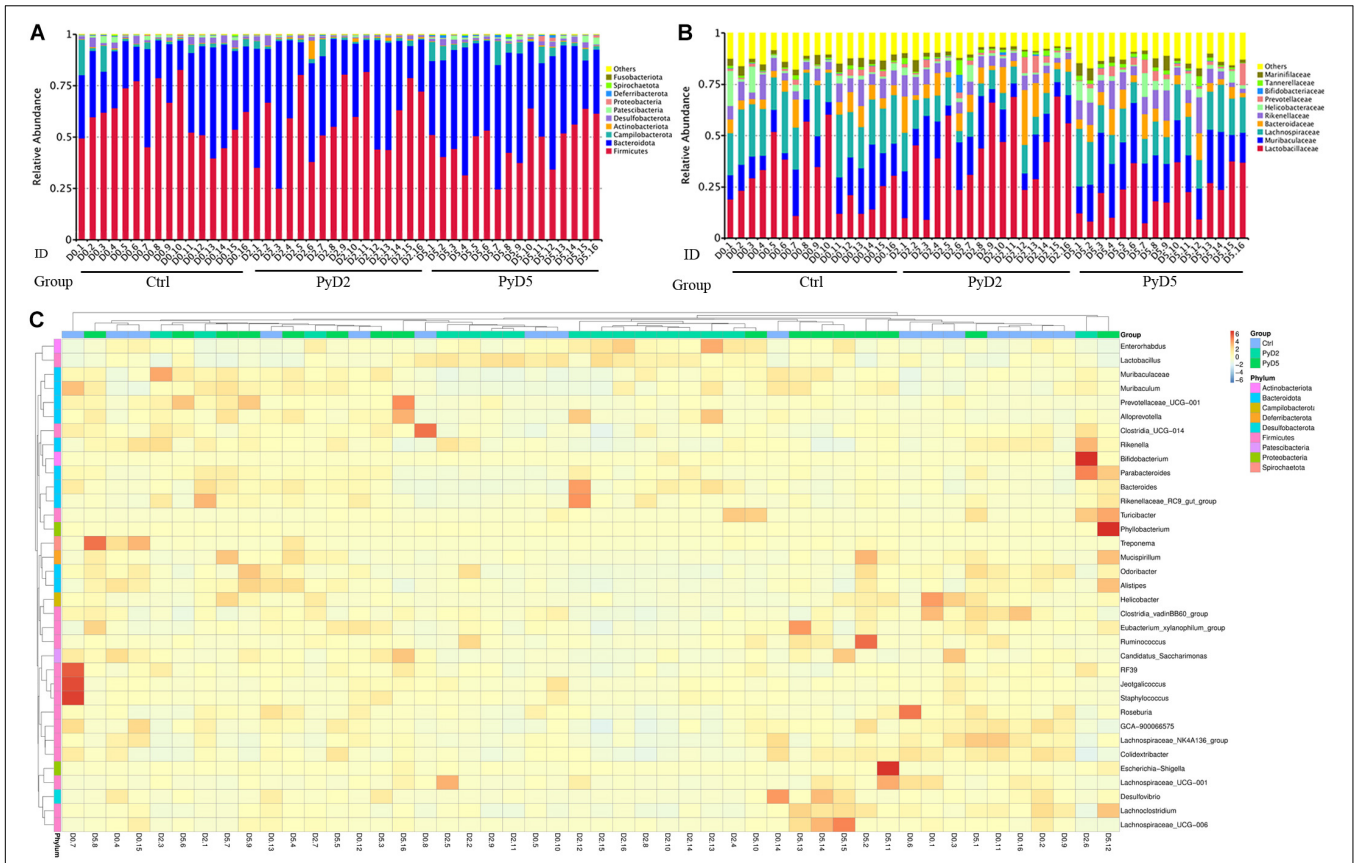

FIGURE 3 | Changes in the gut microbiota composition. Relative abundance of fecal bacterial phyla and families existing in the BALB/c mice. Each bar represents the top 10 abundant phyla and families, whereas "Other" were obtained from low abundant and unclassified OTUs. Sample names represent samples described in **Table 1**. **(A)** Variations in the gut microbiota composition at the phylum level. **(B)** Variations in the gut microbiota composition at the family level; **(C)** Taxonomic heatmap of the three groups at the genus level. Typical relative **g10** abundance of diversified genera present in the Ctrl, PyD2, and PyD5 groups. Each column represents a unique subject.

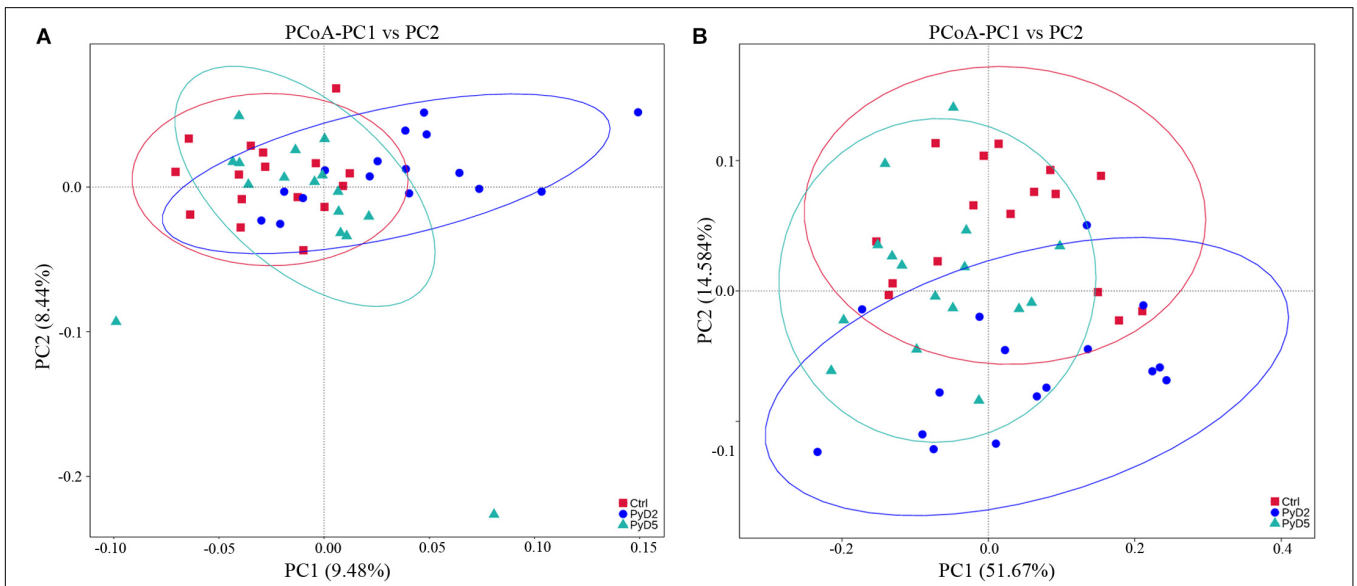

FIGURE 4 | Principal coordinates analysis (PCoA) based on unweighted **(A)** and weighted **(B)** Unifrac distance matrices of fecal samples of BALB/c mice during infection. The fecal bacterial community components of both Py 17XL-infected and -uninfected mice were represented. Sample names are described in **Table 1**.

0.397, 0.423; observed-delta, expected-delta) indicated a lower difference within the groups and a higher difference between the groups. The *A* value of the MRPP was 0.05011, 0.03178, and 0.06291 (representing Ctrl-PyD2, Ctrl-PyD5, and PyD2-PyD5, respectively), demonstrating that the difference between groups was higher than that within groups ($A > 0$). Significance < 0.05 indicated a significant difference. These data demonstrated that the microbiota composition among Ctrl, PyD2 and PyD5 feces was significantly different.

Potential Biomarker Discovery

LEfSe analysis of the top 10 taxa (**Figure 5**) identified the different statistical biomarkers, which were the microbial taxa with significant differences among the three groups. This threshold could obtain as many taxa as possible for significant comparisons and eliminate the rarest taxa in the analysis. The potential biomarkers at different taxonomic levels were determined in all three stages (**Figures 6A-D**). At the genus level, the biomarker with a significant difference between the PyD2 and Ctrl groups was *Lactobacillus* (*Lactobacillus murinus*, which belongs to the *Firmicutes* phylum and *Lactobacillaceae* family) (**Figures 5A,B**). The biomarker with a significant difference between the PyD5 and Ctrl groups was *Muribaculaceae* (belonging to the *Bacteroidetes* phylum and *Muribaculaceae* family) (**Figures 5A,C**). In contrast, the biomarkers with a considerable difference between PyD5 and PyD2 groups were *Muribaculaceae*, *Alistipes* (belonging to the *Bacteroidetes* phylum and *Rikenellaceae* family), and *Helicobacter* (belonging to the *Campilobacterota* phylum and *Helicobacteraceae* family) (**Figures 5A,D**).

Co-genetic network maps (**Supplementary Figures 4, 5**) were generated to identify the OTU co-abundance units and provide new insights for studying complex microbial community compositions and functions. These results presented an OTU co-abundance network approach to successfully generate associations that could generalize empirical data, and therefore, it might become a potential method for identifying microbiota associations. Co-genetic network maps can directly observe the effects on microbiota, the mutual advantage of the dominant species, and the related interactions of species after Py infection. Combined with the LEfSe of the top 10 taxa and networks, they showed that the genus *Lactobacillus* was associated with the genera *Muribaculaceae*, *Bacteroides*, *Alloprevotella*, and *Parabacteroides*. The genus *Alistipes* was correlated with the genera *Rikenella*, *Muribaculum*, *Odoribacter*, *Mucispirillum*, *Bacteroides*, and *Parabacteroides*. The genus *Muribaculaceae* was connected with the genera *Muribaculum*, NK4A214_group, *Clostridia*_UGG_010, and *Rikenellaceae*_RC9_gut_group. In contrast, the genus *Helicobacter* was associated with the genera *Mucispirillum*, *Lactobacillus*, and *Enterococcus*.

DISCUSSION

The rodent and avian *Plasmodium* parasites do not infect humans and are not a threat to public health (Su and Wu, 2021). However, they may have economic impacts (Grim et al., 2008). Therefore, it is meaningful to explore the interactional effect between rodent *Plasmodium* parasites and mice. This study demonstrates that *Plasmodium* rodent species infection can alter the murine gut microbiota composition. Specifically, the gut microbiota compositions in Py 17XL-infected BALB/c mice were altered compared with Py 17XL-uninfected mice. That is, malaria caused by *Plasmodium* might be associated with the alteration of the gut microbiota. Consistent with this thought, a study clarified a meaningful association between the host's microbiota composition and the proleptic risk of *Plasmodium* infection (Yooseph et al., 2015; Waide et al., 2020).

Both species accumulation boxplots and rarefaction curves approached the saturation level, which demonstrated almost full coverage of the whole microbiota diversity. Based on alpha and beta diversity analysis, the diversity and richness of the intestinal microbiota in all fecal samples were altered after Py 17XL infection. In the present study, the gut microbiota at the phylum level was dominated by *Firmicutes* and *Bacteroidetes*, which were consistent with the previous survey (Villarino et al., 2016).

The current data also demonstrate that the relative richness of dominant taxa was altered after infection. The abundance of *Lactobacillaceae* and *Bifidobacteriaceae* was dramatically increased at 2 dpi and then slightly decreased at 5 dpi. A previous study manifested that among differences in the gut flora were increased abundances of *Lactobacillus* (member of the *Lactobacillaceae* family) and *Bifidobacterium* (member of the *Bifidobacteriaceae* family) in resistant mice (Villarino et al., 2016). At the genus level, the gut microbiota in the samples of infected mice was characterized by higher amounts of *Lactobacillus*, *Muribaculaceae*, *Bacteroides*, *Alistipes*, and *Helicobacter*. Meanwhile, LEfSe analysis was performed to obtain biomarkers with significant differences between Py 17XL-infected and -uninfected mice. The biomarker with a considerable difference between the PyD2 and Ctrl groups was *Lactobacillus* (*Lactobacillus murinus*). The genus *Lactobacillus* was indicated to play a role in the stress response in patients (Hemarajata and Versalovic, 2013; Aizawa et al., 2018). That is, the genus *Lactobacillus* in the gut microbiota is related to the disease. Hu et al. verified that IBD induced with DSS caused a decrease in *Lactobacillus* gut microbiota at the genus level (Hu et al., 2020). The biomarker with an obvious difference between the PyD5 and Ctrl groups was *Muribaculaceae*. Moreover, the biomarkers with a noticeable difference between the PyD5 and PyD2 groups were *Muribaculaceae*, *Alistipes*, and *Helicobacter*. Parker et al. (2020) indicated that the genus *Alistipes* in the gut microbiota might have protective effects against some diseases such as colitis, liver fibrosis, and cancer immunotherapy. Other studies have revealed *Alistipes* is pathogenic in colorectal cancer (Moschen et al., 2016), and it is associated with mental signs of depression (Parker et al., 2020). A previous study manifested that the species *Helicobacter pylori* played a potential protective role in IBD (Sjomina et al., 2017). Kubota-Aizawa et al. (2017) performed an epidemiological survey of gastric *Helicobacter* spp. that were related to gastrointestinal disease in dogs.

Meanwhile, co-genetic network maps were generated to identify the OTU co-abundance units. Combined with the LEfSe on top 10 taxa and networks, they indicated

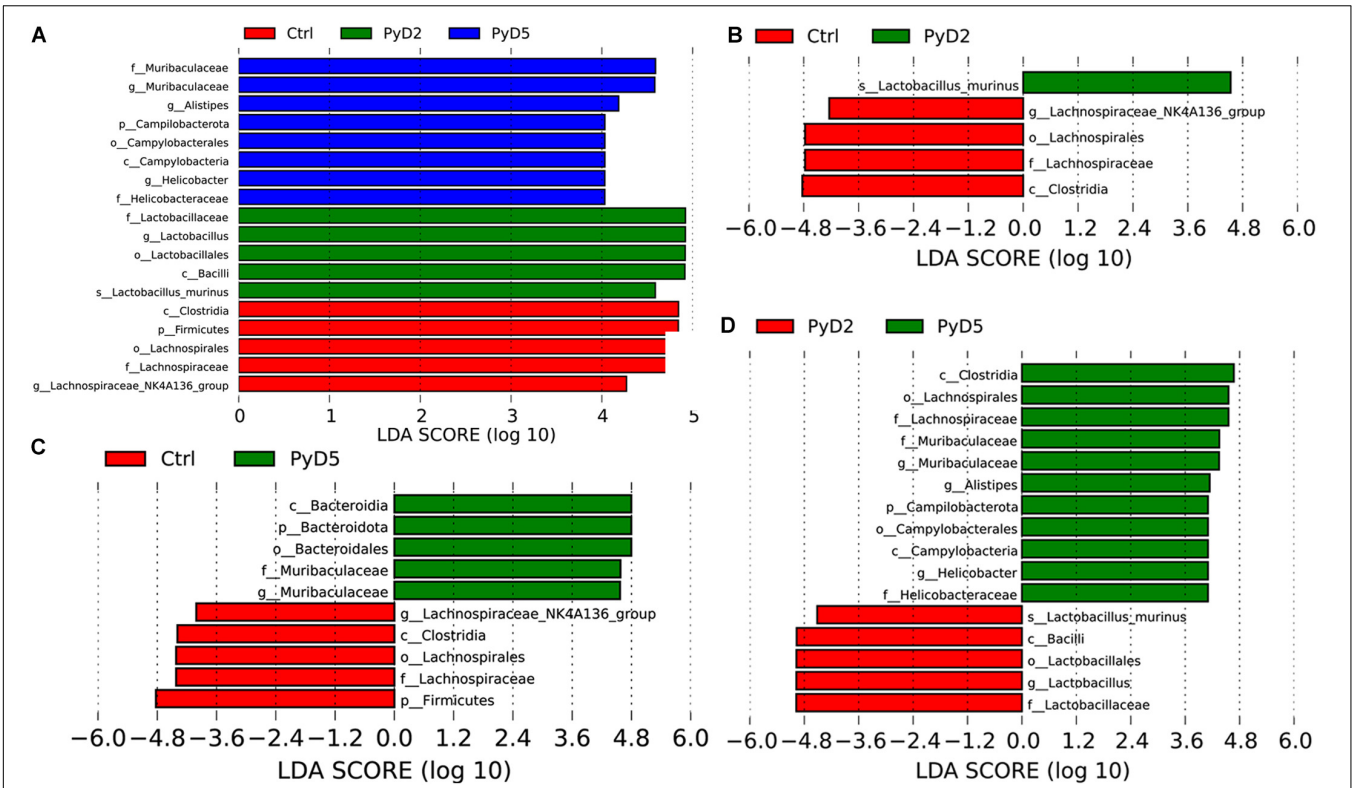

FIGURE 5 | LEfSe identified the bacterial taxa significantly differentiated among different groups. Only taxa with the statistical differences between groups were shown in the figure, which was determined by meeting an LDA significant threshold > 4. **(A)** Histogram of the linear discriminant analysis (LDA) scores distribution among three groups; **(B)** Histogram of LDA score distribution between the Ctrl and PyD2 groups. **(C)** Histogram of LDA score distribution between the Ctrl and PyD5 groups. **(D)** Histogram of LDA score distribution between the PyD2 and PyD5 groups.

that the genus *Lactobacillus* was associated with the genera *Muribaculaceae*, *Bacteroides*, *Alloprevotella*, *Parabacteroides*, and so on. A previous study suggested the attractive probiotic potential of the genus *Bacteroides* (species *B. thetaiotaomicron*) in IBD (Sitkin and Pokrotnieks, 2019). Another study found that genes for *Bacteroides fragilis* toxin encoded secreted oncotoxins correlated with colorectal cancer (Dejea et al., 2018). Chen et al. (2020) discovered that *Bacteroides*, *Alistipes*, *Alloprevotella*, *Odoribacter*, and *Parabacteroides* were closely correlated with short-chain fatty acid (SCFA) production, such as propionate, butyrate, and acetate. Silva et al. (2018) considered that butyrate played an essential protective role in intestinal homeostasis and IBD. In contrast, Chakravarty et al. (2019) demonstrated that the intestinal SCFA composition did not explain the effects of gut microbiota on malaria severity. The genus *Alistipes* was correlated with the genera *Rikenella*, *Muribaculum*, *Odoribacter*, and *Mucispirillum*. The genus *Muribaculaceae* was associated with the genera *Muribaculum* and *Clostridia*_UGG_010. The genus *Helicobacter* was correlated with the genera *Mucispirillum* and *Lactobacillus*. A previous study demonstrated that *Rikenella* or Rikenellaceae had an inverse relationship with body weight or fat mass (Li et al., 2017; Zhou et al., 2018) in mice and humans. Also, a high abundance of *Rikenella* is associated with low chronic non-infective inflammation (Miranda-Ribera et al., 2019). Brugiroux et al. (2016) displayed that *Muribaculum intestinale* was a strictly anaerobic bacterium that inhibited the colonization of pathogenic bacteria and regulated the balance of bacteria. Gomez-Arango et al. (2016) verified that the genus *Odoribacter* was known as a butyrate producer. A previous study reported that *Mucispirillum schaedleri* was abundant in the intestinal mucus layer of mice and humans, and that it played an essential role in inflammation (Loy et al., 2017). Besides, Lin et al. (2019) considered that patients with Parkinson's disease had an increased abundance of *M. schaedleri* in the fecal microbiota. Schönherr-Hellec and Aires (2019) demonstrated that *Clostridia* species were responsible for necrotizing enterocolitis.

A previous study indicated that using probiotics might be a potential method to limit the reproduction of pathogenic microbiota (Pickard et al., 2017). These findings offered more insights into host gut microbiota alterations after Py 17XL infection and showed that microbiota analysis would play an important role in the early diagnosis of fatal malaria and in perceiving the pathogenesis of malaria. LEfSe analysis combined with the co-genetic OTU network showed that the genus *Alistipes* was a potential biomarker that may play a meaningful role in the pathogenesis and progression of Py malaria. The anaerobic bacterium *Alistipes* is found almost in the healthy human gastrointestinal tract (Shkoporov et al., 2015), and it is pathogenic in colorectal cancer (Moschen et al., 2016) and is associated

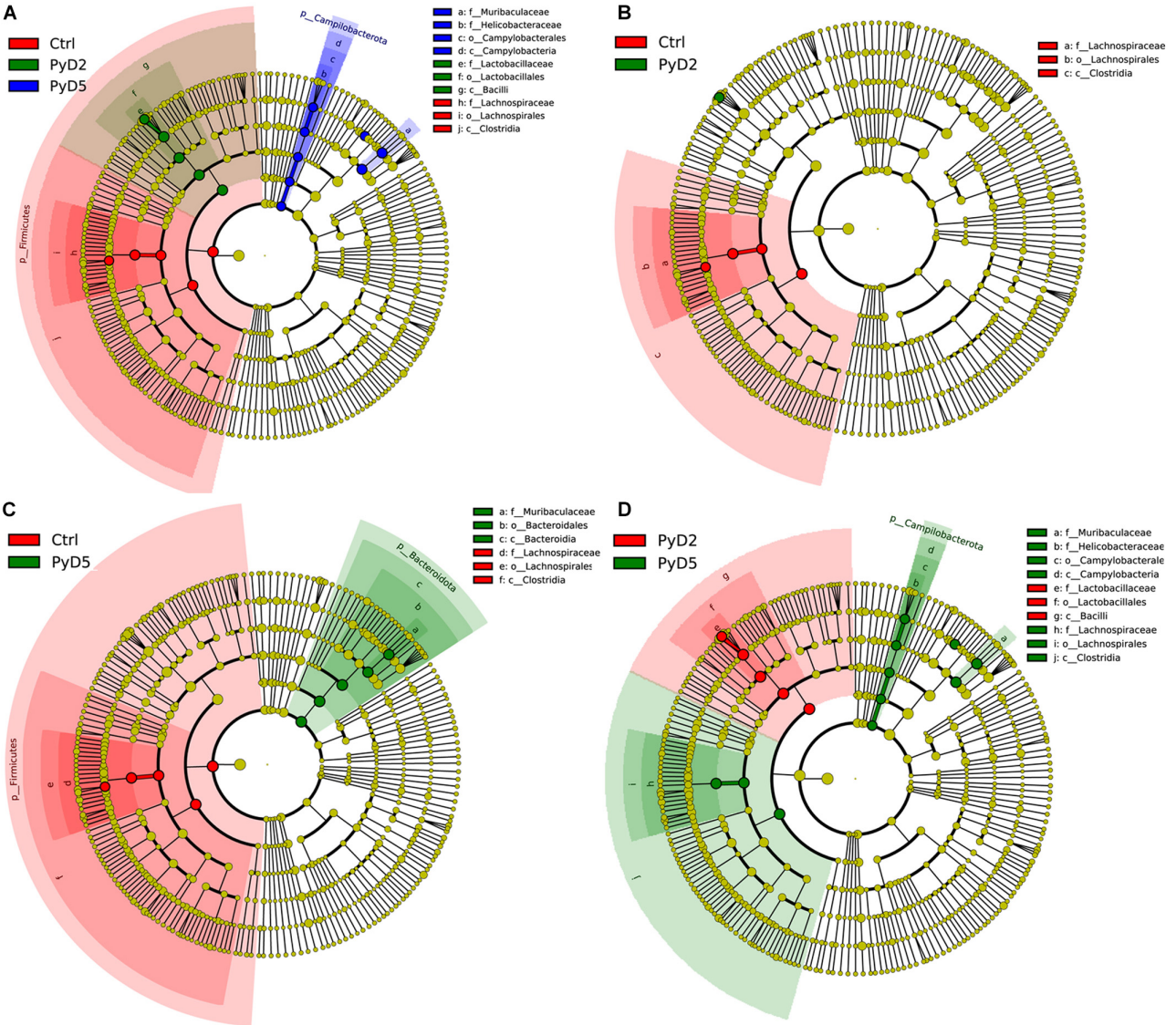

FIGURE 6 | Cladogram of the most differentially abundant bacterial taxa among three groups. The red, green, and blue colors represent the bacterial communities of Ctrl, Py D2, and PyD5 groups, respectively. **(A)** Cladogram of the most differentially abundant bacterial taxa in the Ctrl, PyD2, and PyD5 groups. **(B)** Cladogram of the most differentially abundant bacterial taxa in the Ctrl and PyD2 groups. **(C)** Cladogram of the most differentially abundant bacterial taxa in the Ctrl and PyD5 groups. **(D)** Cladogram of the most differentially abundant bacterial taxa in the PyD2 and PyD5 groups.

with depression (Bangsgaard Bendtsen et al., 2012). These data indicated gut microbiota modulation can regard as a novel method of preventing severe malaria, which is consistent with the insight of Waide (Waide and Schmidt, 2020).

This article studied the alteration of the gut microbiota profile in BALB/c mice induced by Py 17XL infection and obtained potential biomarkers correlated with murine malaria. However, this research also had several limitations. In future studies, it will be important to explore the role of microbiota in the progress of malaria and to evaluate the microbiota modulation interfere with protection and less severity of the disease in a non-lethal infection model as PbA or Py 17XNL in BALB/c mice, and to assess the role of the microbiota more robustly using experimental approaches, such as non-lethal infection models, antimalarial drug therapy, and GF fecal microbiota transplantation.

The gut microbiota in mice before and after Py 17XL infection was characterized, and the overrepresented microbial taxa in infected and uninfected mice were identified. Meanwhile, several potential biomarkers at different taxonomic levels were obtained from this study. These microbiota taxa may serve as direct targets to clarify their roles in the pathogenesis and progression of lethal malaria in future studies. Also, in an association study of Py 17XL infection risk and gut microbiota composition, gut microbiota composition modulation will decrease Py 17XL infection risk and may be regarded as a standard to some antimalarial drugs or malaria vaccines.

DATA AVAILABILITY STATEMENT

The datasets presented in this study can be found in online repositories. The names of the repository/repositories and accession number(s) can be found below website: https://www.ncbi.nlm.nih.gov/sra/PRJNA798515.

ETHICS STATEMENT

The animal study was reviewed and approved by the Institutional Animal Care and Use Committee of the Hubei University of Medicine under permit number HBMU-S20160414.

AUTHOR CONTRIBUTIONS

WG and JL conceived the study, participated in its design, performed the data analysis and interpretation, and drafted the manuscript. WG, SY, and JL carried out the experiments. XS, HZ, and FL participated in analyzing and interpreting the data. All authors contributed to the article and approved the submitted version.

FUNDING

The Initial Project supported this study for the Principle Investigator Program of Hubei University of Medicine (HBMUPI202101), Post-Graduates of Hubei University of Medicine (Grant No. 2016QDJZR04), and the Research Project of the Hubei Provincial Department of Education (Grant No. Q20172102).

SUPPLEMENTARY MATERIAL

The Supplementary Material for this article can be found online at: https://www.frontiersin.org/articles/10.3389/fmicb.2022.858897/full#supplementary-material

REFERENCES

Aizawa, E., Tsuji, H., Asahara, T., Takahashi, T., Teraishi, T., Yoshida, S., et al. (2018). Bifidobacterium and counts in the gut microbiota of patients with bipolar disorder and healthy controls. *Front. Psychiatry* 9:730. doi: 10.3389/fpsyt.2018.00730

Astudillo, A., and Mayrovitz, H. (2021). The gut microbiome and cardiovascular disease. *Cureus* 13:e14519. doi: 10.7759/cureus.14519

Bangsgaard Bendtsen, K. M., Krych, L., Sorensen, D. B., Pang, W., Nielsen, D. S., Josefsen, K., et al. (2012). Gut microbiota composition is correlated to grid floor induced stress and behavior in the BALB/c mouse. *PLoS One* 7:e46231. doi: 10.1371/journal.pone.0046231

Brugiroux, S., Beutler, M., Pfann, C., Garzetti, D., Ruscheweyh, H. J., Ring, D., et al. (2016). Genome-guided design of a defined mouse microbiota that confers colonization resistance against *Salmonella enterica* serovar Typhimurium. *Nat. Microbiol.* 2:16215. doi: 10.1038/nmicrobiol.2016.215

Bunyavanich, S., Shen, N., Grishin, A., Wood, R., Burks, W., Dawson, P., et al. (2016). Early-life gut microbiome composition and milk allergy resolution. *J. Allergy Clin. Immunol.* 138, 1122–1130. doi: 10.1016/j.jaci.2016.03.041

Caporaso, J. G., Kuczynski, J., Stombaugh, J., Bittinger, K., Bushman, F. D., Costello, E. K., et al. (2010). QIIME allows analysis of high-throughput community sequencing data. *Nat. Methods* 7, 335–336. doi: 10.1038/nmeth.f.303

Chakravarty, S., Mandal, R., Duff, M., and Schmidt, N. (2019). Intestinal short-chain fatty acid composition does not explain gut microbiota-mediated effects on malaria severity. *PloS One* 14:e0214449. doi: 10.1371/journal.pone.0214449

Chen, G., Feng, H., Liu, J., Qi, Z. M., Wu, Y., Guo, S. Y., et al. (2010). Characterization of immune responses to single or mixed infections with P. yoelii 17XL and P. chabaudi AS in different strains of mice. *Parasitol. Int.* 59, 400–406. doi: 10.1016/j.parint.2010.05.005

Chen, H., Zhang, F., Zhang, J., Zhang, X., Guo, Y., and Yao, Q. (2020). A holistic view of berberine inhibiting intestinal carcinogenesis in conventional mice based on microbiome-metabolomics analysis. *Front. Immunol.* 11:588079. doi: 10.3389/fimmu.2020.588079

Chu, D., Ma, J., Prince, A., Antony, K., Seferovic, M., and Aagaard, K. (2017). Maturation of the infant microbiome community structure and function across multiple body sites and in relation to mode of delivery. *Nat. Med.* 23, 314–326. doi: 10.1038/nm.4272

De, S. L., Stanisic, D. I., Rivera, F., Batzloff, M. R., Engwerda, C., and Good, M. F. (2016). Plasmodium berghei bio-burden correlates with parasite lactate dehydrogenase: application to murine Plasmodium diagnostics. *Malaria J.* 15:3. doi: 10.1186/s12936-015-1027-2

Dejea, C., Fathi, P., Craig, J., Boleij, A., Taddese, R., Geis, A., et al. (2018). Patients with familial adenomatous polyposis harbor colonic biofilms containing tumorigenic bacteria. *Science* 359, 592–597. doi: 10.1126/science.aah3648

Denny, J., Powers, J., Castro, H., Zhang, J., Joshi-Barve, S., Campagna, S., et al. (2019). Differential sensitivity to plasmodium yoelii infection in C57BL/6 mice impacts gut-liver axis homeostasis. *Sci. Rep.* 9:3472. doi: 10.1038/s41598-019-40266-6

DeSantis, T. Z., Hugenholtz, P., Larsen, N., Rojas, M., Brodie, E. L., Keller, K., et al. (2006). Greengenes, a chimera-checked 16S rRNA gene database and workbench compatible with ARB. *Appl. Environ. Microbiol.* 72, 5069–5072. doi: 10.1128/AEM.03006-05

Edgar, R. C. (2004). MUSCLE: multiple sequence alignment with high accuracy and high throughput. *Nucleic Acids Res.* 32, 1792–1797. doi: 10.1093/nar/gkh340

Edgar, R. C. (2013). UPARSE: highly accurate OTU sequences from microbial amplicon reads. *Nat. Methods* 10, 996–998. doi: 10.1038/nmeth.2604

Edgar, R. C., Haas, B. J., Clemente, J. C., Quince, C., and Knight, R. (2011). UCHIME improves sensitivity and speed of chimera detection. *Bioinformatics* 27, 2194–2200. doi: 10.1093/bioinformatics/btr381

Feng, J., Zhang, L., Xia, Z., Zhou, S., and Xiao, N. (2021). Malaria-free certification in china: achievements and lessons learned from the national malaria elimination programme. *Zoonoses* 1:2. doi: 10.15212/ZOONOSES-2021-1002

Gill, S., Pop, M., Deboy, R., Eckburg, P., Turnbaugh, P., Samuel, B., et al. (2006). Metagenomic analysis of the human distal gut microbiome. *Science* 312, 1355–1359. doi: 10.1126/science.1124234

Gomaa, E. (2020). Human gut microbiota/microbiome in health and diseases: a review. *Antonie van Leeuwenhoek* 113, 2019–2040. doi: 10.1007/s10482-020-01474-7

Gomez-Arango, L. F., Barrett, H. L., McIntyre, H. D., Callaway, L. K., Morrison, M., and Dekker Nitert, M. (2016). Increased systolic and diastolic blood pressure is associated with altered gut microbiota composition and butyrate production in early pregnancy. *Hypertension* 68, 974–981. doi: 10.1161/hypertensionaha.116.07910

Grim, K. C., McCutchan, T., Sullivan, M., and Cranfield, M. R. (2008). Unidentified Plasmodium species in Australian black swans (*Cygnus atratus*) hatched and raised in North America. *J. Zoo. Wildl. Med.* 39, 216–220. doi: 10.1638/2007-0110r.1

Guan, W., Yang, S., Zhao, Y., Cheng, W., Song, X., Yao, Y., et al. (2021). Observation of the Gut Microbiota Profile in C57BL/6 mice induced by plasmodium berghei ANKA Infection. *Front. Cell Infect. Microbiol.* 11:680383. doi: 10.3389/fcimb.2021.680383

Haas, B. J., Gevers, D., Earl, A. M., Feldgarden, M., Ward, D. V., Giannoukos, G., et al. (2011). Chimeric 16S rRNA sequence formation and detection in Sanger and 454-pyrosequenced PCR amplicons. *Genome Res.* 21, 494–504. doi: 10.1101/gr.112730.110

Hemarajata, P., and Versalovic, J. (2013). Effects of probiotics on gut microbiota: mechanisms of intestinal immunomodulation and neuromodulation. *Therapeutic. Adv. Gastroenterol.* 6, 39–51. doi: 10.1177/1756283x12459294

Hu, L., Jin, L., Xia, D., Zhang, Q., Ma, L., Zheng, H., et al. (2020). Nitrate ameliorates dextran sodium sulfate-induced colitis by regulating the homeostasis of the intestinal microbiota. *Free Radic Biol. Med.* 152, 609–621. doi: 10.1016/j.freeradbiomed.2019.12.002

Karlsson, F., Tremaroli, V., Nielsen, J., and Backhed, F. (2013). Assessing the human gut microbiota in metabolic diseases. *Diabetes* 62, 3341–3349. doi: 10.2337/db13-0844

Kubota-Aizawa, S., Ohno, K., Fukushima, K., Kanemoto, H., Nakashima, K., Uchida, K., et al. (2017). Epidemiological study of gastric *Helicobacter* spp. in dogs with gastrointestinal disease in Japan and diversity of *Helicobacter* heilmannii sensu stricto. *Vet. J.* 225, 56–62. doi: 10.1016/j.tvjl.2017.04.004

Li, R., Wang, H., Shi, Q., Wang, N., Zhang, Z., Xiong, C., et al. (2017). Effects of oral florfenicol and azithromycin on gut microbiota and adipogenesis in mice. *PLoS One* 12:e0181690. doi: 10.1371/journal.pone.0181690

Lin, C. H., Chen, C. C., Chiang, H. L., Liou, J. M., Chang, C. M., Lu, T. P., et al. (2019). Altered gut microbiota and inflammatory cytokine responses in patients with Parkinson's disease. *J. Neuroinflamm.* 16:129. doi: 10.1186/s12974-019-1528-y

Loy, A., Pfann, C., Steinberger, M., Hanson, B., Herp, S., Brugiroux, S., et al. (2017). Lifestyle and horizontal gene transfer-mediated evolution of mucispirillum schaedleri, a core member of the murine gut microbiota. *mSystems* 2, e171–e116. doi: 10.1128/mSystems.00171-16

Magoč, T., and Salzberg, S. L. (2011). FLASH: fast length adjustment of short reads to improve genome assemblies. *Bioinformatics* 27, 2957–2963. doi: 10.1093/bioinformatics/btr507

Miranda-Ribera, A., Ennamorati, M., Serena, G., Cetinbas, M., Lan, J., Sadreyev, R. I., et al. (2019). Exploiting the zonulin mouse model to establish the role of primary impaired gut barrier function on microbiota composition and immune profiles. *Front. Immunol.* 10:2233. doi: 10.3389/fimmu.2019.02233

Moschen, A. R., Gerner, R. R., Wang, J., Klepsch, V., Adolph, T. E., Reider, S. J., et al. (2016). Lipocalin 2 protects from inflammation and tumorigenesis associated with gut microbiota alterations. *Cell Host. Microbe.* 19, 455–469. doi: 10.1016/j.chom.2016.03.007

Nair, S., Xu, R., Pattaradilokrat, S., Wu, J., Qi, Y., Zilversmit, M., et al. (2017). A Plasmodium yoelii HECT-like E3 ubiquitin ligase regulates parasite growth and virulence. *Nat. Commun.* 8:223. doi: 10.1038/s41467-017-00267-3

Nishino, K., Nishida, A., Inoue, R., Kawada, Y., Ohno, M., Sakai, S., et al. (2018). Analysis of endoscopic brush samples identified mucosa-associated dysbiosis in inflammatory bowel disease. *J. Gastroenterol.* 53, 95–106. doi: 10.1007/s00535-017-1384-4

Parker, B. J., Wearsch, P. A., Veloo, A. C. M., and Rodriguez-Palacios, A. (2020). The genus alistipes: gut bacteria with emerging implications to inflammation, cancer, and mental health. *Front. Immunol.* 11:906. doi: 10.3389/fimmu.2020.00906

Pickard, J. M., Zeng, M. Y., Caruso, R., and Núñez, G. (2017). Gut microbiota: Role in pathogen colonization, immune responses, and inflammatory disease. *Immunol. Rev.* 279, 70–89. doi: 10.1111/imr.12567

Prasad, R. N., and Virk, K. J. (1993). Malaria as a cause of diarrhoea–a review. *Papua New Guinea Med. J.* 36, 337–341.

Schönherr-Hellec, S., and Aires, J. (2019). Clostridia and necrotizing enterocolitis in preterm neonates. *Anaerobe* 58, 6–12. doi: 10.1016/j.anaerobe.2019.04.005

Shkoporov, A. N., Chaplin, A. V., Khokhlova, E. V., Shcherbakova, V. A., Motuzova, O. V., Bozhenko, V. K., et al. (2015). Alistipes inops sp. nov. and Coprobacter secundus sp. nov., isolated from human faeces. *Int. J. Syst. Evol. Microbiol.* 65, 4580–4588. doi: 10.1099/ijsem.0.000617

Silva, J. P. B., Navegantes-Lima, K. C., Oliveira, A. L. B., Rodrigues, D. V. S., Gaspar, S. L. F., Monteiro, V. V. S., et al. (2018). Protective mechanisms of butyrate on inflammatory bowel disease. *Curr. Pharm. Des.* 24, 4154–4166. doi: 10.2174/1381612824666181001153605

Sitkin, S., and Pokrotnieks, J. (2019). Gut microbiota as a host defender and a foe: the 2 faces of commensal *bacteroides* thetaiotaomicron in inflammatory bowel disease. *Inflamm. Bowel. Dis.* 25:e71. doi: 10.1093/ibd/izy377

Sjomina, O., Heluwaert, F., Moussata, D., and Leja, M. (2017). *Helicobacter* pylori infection and nonmalignant diseases. *Helicobacter* 22:408. doi: 10.1111/hel.12408

Su, X., and Wu, J. (2021). Zoonotic transmission and host switches of malaria parasites. *Zoonoses* 1:11. doi: 10.15212/ZOONOSES-2021-0015

Villarino, N., LeCleir, G., Denny, J., Dearth, S., Harding, C., Sloan, S., et al. (2016). Composition of the gut microbiota modulates the severity of malaria. *Proc. Nat. Acad. Sci. USA* 113, 2235–2240. doi: 10.1073/pnas.1504887113

Waide, M., Polidoro, R., Powell, W., Denny, J., Kos, J., Tieri, D., et al. (2020). Gut microbiota composition modulates the magnitude and quality of germinal centers during plasmodium infections. *Cell Rep.* 33:108503. doi: 10.1016/j.celrep.2020.108503

Waide, M., and Schmidt, N. (2020). The gut microbiome, immunity, and Plasmodium severity. *Curr. Opinion Microbiol.* 58, 56–61. doi: 10.1016/j.mib.2020.08.006

Wang, Q., Garrity, G. M., Tiedje, J. M., and Cole, J. R. (2007). Naive Bayesian classifier for rapid assignment of rRNA sequences into the new bacterial taxonomy. *Appl. Environ. Microbiol.* 73, 5261–5267. doi: 10.1128/AEM.00062-07

WHO (2021). *World Malaria Report 2021*. Geneva: World Health Organization.

Yilmaz, B., Portugal, S., Tran, T., Gozzelino, R., Ramos, S., Gomes, J., et al. (2014). Gut microbiota elicits a protective immune response against malaria transmission. *Cell* 159, 1277–1289. doi: 10.1016/j.cell.2014.10.053

Yooseph, S., Kirkness, E., Tran, T., Harkins, D., Jones, M., Torralba, M., et al. (2015). Stool microbiota composition is associated with the prospective risk of Plasmodium falciparum infection. *BMC Genomics* 16:631. doi: 10.1186/s12864-015-1819-3

Zhou, L., Xiao, X., Zhang, Q., Zheng, J., Li, M., Yu, M., et al. (2018). Improved glucose and lipid metabolism in the early life of female offspring by maternal dietary genistein is associated with alterations in the gut microbiota. *Front. Endocrinol.* 9:516. doi: 10.3389/fendo.2018.00516

Conflict of Interest: The authors declare that the research was conducted in the absence of any commercial or financial relationships that could be construed as a potential conflict of interest.

Publisher's Note: All claims expressed in this article are solely those of the authors and do not necessarily represent those of their affiliated organizations, or those of the publisher, the editors and the reviewers. Any product that may be evaluated in this article, or claim that may be made by its manufacturer, is not guaranteed or endorsed by the publisher.

frontiers | Frontiers in Microbiology

ORIGINAL RESEARCH
published: 11 May 2022
doi: 10.3389/fmicb.2022.891151

Metagenome Sequencing Reveals the Microbiome of *Aedes albopictus* and Its Possible Relationship With Dengue Virus Susceptibility

Teng Zhao[1†], Bo-qi Li[1,2†], He-ting Gao[1†], Dan Xing[1], Man-jin Li[1], Yun-qi Dang[1,2], Heng-duan Zhang[1], Yue-e Zhao[1], Zhu Liu[2*] and Chun-xiao Li[1*]*

[1] State Key Laboratory of Pathogens and Biosecurity, Institute of Microbiology and Epidemiology, Beijing, China, [2] College of Life Science and Technology, Mudanjiang Normal University, Mudanjiang, China

OPEN ACCESS

Edited by:
Wei Wang,
Jiangsu Institute of Parasitic Diseases (JIPD), China

Reviewed by:
Steve Peper,
Anastasia Mosquito Control District, United States
Shicheng Chen,
Oakland University, United States

***Correspondence:**
Yue-e Zhao
zhaoyue126@126.com
Zhu Liu
swxlz0@126.com
Chun-xiao Li
aedes@126.com

† These authors have contributed equally to this work and share first authorship

Specialty section:
This article was submitted to Infectious Agents and Disease, a section of the journal Frontiers in Microbiology

Received: *07 March 2022*
Accepted: *12 April 2022*
Published: *11 May 2022*

Citation:
Zhao T, Li B-q, Gao H-t, Xing D, Li M-j, Dang Y-q, Zhang H-d, Zhao Y-e, Liu Z and Li C-x (2022) Metagenome Sequencing Reveals the Microbiome of Aedes albopictus and Its Possible Relationship With Dengue Virus Susceptibility. Front. Microbiol. 13:891151. doi: 10.3389/fmicb.2022.891151

Dengue fever virus (DENV) is a mosquito-borne flavivirus that poses a serious risk to human health. *Aedes albopictus* is a widely distributed vector of dengue fever in China. Based on the impact of physiological activity, the microbiome in *A. albopictus* will provide a novel environment-friendly approach to control DENV transmission. We performed metagenomic sequencing on *A. albopictus* before and after exposure to DENV blood meal to detect microbiome variation of *A. albopictus* with different susceptibilities to DENV. The dominant phyla in *A. albopictus* microbiome were *Proteobacteria* and *Ascomycota*, and the dominant genera were *Aspergillus* and *Metarhizium*. *Gammaproteobacteria bacterium*, *Lactobacillus harbinensis*, and *Neurospora crassa* differed significantly after DENV infection. There were 15 different microorganisms found to be involved in mosquito immunity and metabolism, such as *Alphaproteobacteria bacterium*, *Methyloglobulus morosus*, and *Shigella sonnei*, which might have an impact on the DENV susceptibility of *A. albopictus*. It was hypothesized that the lack of specific bacteria may lead to increased susceptibility of *A. albopictus* to DENV. Interventions in the microbiome composition or specific bacteria of *A. albopictus* may affect the susceptibility to DENV and control the mosquito-borne diseases efficiently.

Keywords: ***Aedes albopictus*, microbiome, dengue virus, metagenome, susceptibility**

INTRODUCTION

Dengue fever virus (DENV) is a mosquito-borne flavivirus that poses a serious threat to human health. In recent years, the global incidence of dengue fever has been increasing, with approximately 390 million infections per year, including nearly 20,000 deaths (Guzman et al., 2010; Guo et al., 2017). In 2013, the local outbreaks of dengue fever occurred in Guangdong and Yunnan provinces of China, resulting in thousands of infections (Luo et al., 2017; Sun et al., 2020).

Aedes albopictus, known as the "Asian tiger mosquito," is the most dominant species and is found in nearly one-third of China. Both *A. albopictus* and *Aedes aegypti* are two important vector species for dengue transmission in China (Souza-Neto et al., 2019), but *A. albopictus* is more widely distributed. *A. albopictus* is reported to be the only mosquito vector for dengue transmission in Guangdong, and *A. aegypti* has not been detected there in the last 30 years. The strong adaptability of *A. albopictus* contributed to the re-emergence and widespread spread of dengue fever in China (Ruiling et al., 2018; Wei et al., 2021).

Dengue viruses belong to the genus *Flavivirus* in the family Flaviviridae and are classified into four serotypes (Gebhard et al., 2011; Vasilakis et al., 2011), with DENV2 being the most transmissible and virulent (Guzman and Kouri, 2003; Balmaseda et al., 2006). Humans, who once infected with a specific serotype of DENV, can only produce the corresponding antibodies which cannot protect against all four serotypes simultaneously (Deng et al., 2020). Due to the lack of an effective vaccine or drug, mosquito control remains the primary means of prevention and control of DENV. There is an urgent need to find a new environmentally friendly mosquito control technology (Dimopoulos, 2019; Zheng et al., 2019).

The mosquito microbiome is extremely large and diverse, with important roles in infection, immunity, nutrition, and physiological behavior (Minard et al., 2013). Increasingly, this research is focusing on the impact of microbes on vector competence to control mosquito-borne diseases. For example, *Asaia* was a stable and dominant bacterium in mosquitoes that can compete with *Wolbachia* to negatively affect the growth and development, thereby reducing mosquito populations (Rossi et al., 2015). *Leptolegnia chapmanii Seymour* exhibited the significant pathogenicity to larvae (Pelizza et al., 2013). *Serratia marcescens* was confirmed to digest the membranous mucin of the intestine, thus facilitating virus transmission (Wu et al., 2019). In addition, mosquito symbiotic microbes ultimately influence the efficiency of pathogen transmission by regulating the full cycle of the larval development rate, pupation time, adult fecundity, and survival rate (Yee et al., 2012; Souza et al., 2019; Buxton et al., 2020).

We designed the experiment using metagenome sequencing approaches to compare the microbiomes of *A. albopictus* with different susceptibility to DENV2. By analyzing the diversity of their microbiome composition, differences in abundance, annotated gene functions, and other biological information, we also established the association between the symbiotic microbiome of *A. albopictus* and DENV2 susceptibility. Artificially interfering with the mosquito microbiome may indirectly influence the susceptibility of mosquitoes, providing a new technical means to control the DENV2 transmission by *A. albopictus*.

MATERIALS AND METHODS

Mosquito

The *A. albopictus* strain was originally collected in 2019 in Guangzhou, Guangdong Province (112°57′ to 114°3′E, 22°26′ to 23°56′N). Mosquitoes were reared at 26 ± 1°C, 75 ± 5% relative humidity and a 14:10 h light cycle, and larvae were provided with rat food. Cultures were maintained by feeding adult mosquitoes with 8% sugar water. Adult female mosquitoes used for DENV infection were 3–5 days post-emergence.

Viral and Normal Blood Meals for Mosquitoes

Dengue serotype 2 was inoculated into the brains of SPF (specific–pathogen-free) mice and cultured. Approximately 5 days after inoculation, mice were dissected to obtain DENV-infected brain suspensions. The supernatant was centrifuged at 8,000 rpm for 10 min and then filtered through 0.45 and 0.2 μm membranes. DENV2 suspension was diluted with Dulbecco's modified eagle medium (DMEM) to 1×10^6 plaque forming units (pfu)/ml and then mixed with SPF mice blood at a 1:1 concentration as DENV2 viral blood meal. The normal blood meal for the control group was DMEM to blood at a ratio of 1:1. The blood meal cups were soaked in 1% sodium heparin to avoid clotting. Blood meal cups providing the viral and normal blood meals were then sealed with film and attached to a thermostatic blood donor simulator. They were placed in cages containing approximately 500 mosquitoes that were starved 18 h in advance for 2 h. By observing the degree of abdominal expansion, virus blood-fed and normal blood-fed female mosquitoes were picked out and transferred to other cages separately. All mosquitoes were reared at 26 ± 1°C, 75 ± 5% relative humidity and a 14:10 h light cycle.

Detection and Grouping of Mosquito Infections

Approximately 7 days after blood feeding, DENV2 infection was detected in viral blood-fed and normal blood-fed female mosquitoes using an RNA extraction kit (QIAGEN Shanghai, China) and a Mylab dengue virus type II nucleic acid detection kit (Mylab Inc., Beijing, China). The PCR procedure was as follows: 50°C for 30 min, 95°C for 15 min, followed by 40 cycles of 95°C for 15 s and 60°C for 45 s. Finally, the mosquitoes were divided into three groups. Mosquitoes that fed on the viral blood meal and tested positive were defined as the infected group. Mosquitoes that fed on the viral blood meal and tested negative were defined as the uninfected group. Mosquitoes that consumed a normal blood meal were defined as the control group. Mosquitoes were randomly selected and replicated three times with 20 mosquitoes for each group.

Library Construction and Sequencing

Mosquitoes were washed three times with 75% ethanol and 1× phosphate buffer to avoid environmental bacterial contamination. Microbial genomic DNA was extracted using QIAamp DNA Microbiome Kit (Shanghai, China). Samples were tested for concentration, total amount, purity and degradation, and then sent to Biomark Technologies (Beijing, China) for metagenomic sequencing. After the genomic DNA of the samples passed quality testing, the DNA was fragmented by the mechanical shearing (ultrasonic treatment). The fragmented DNA is then purified, end-repaired, 3′-adenylated, ligated to sequencing adapters, and then electrophoresed in agarose gels for fragment size selection. The Illumina sequencing platform was used to perform the metagenomic sequencing on qualified libraries.

Bioinformatics Analysis

The raw data were filtered by the Trimmomatic software (Bolger et al., 2014), and the clean reads were compared to the reference genome to remove host using bowtie2 software

(Langmead and Salzberg, 2012), reference genome file acquired from the National Center for Biotechnology Information (NCBI)[1] (Chen et al., 2015; O'Leary et al., 2016). Metagenome assembly were conducted with megahit software (Li et al., 2016) and quality assessment of assembled contigs were conducted with QUAST software (Gurevich et al., 2013). Species annotated were using kraken2 software (Wood et al., 2019), while the bracken software was used to estimate the relative abundances within a specific sample from Kraken 2 classification results (Lu et al., 2017). Functional annotations are annotated using databases such as Kyoto Encyclopedia of Genes and Genomes (KEGG) (Kanehisa et al., 2022), non-redundant protein (Nr), Gene Ontology (GO) (Mi et al., 2019, Gene Ontology Consortium, 2021), etc. Differential species analysis was performed using the R package metagenomeSeq. The screening criteria for differentially expressed species were padj < 0.05 and $|\log2 \text{(fold change)}| \geq 1$. The random forest analysis uses the R package random Forest to calculate the optimal value of the model capacity through 10-fold cross-validation (Liaw and Wiener, 2001).

RESULTS

Sequencing Data Quality

After sample data were filtered and the host sequences were removed, the metagenomic sequencing depth of 9 samples was around 30 G. The number of valid reads ranged from 37,348,805 to 47,179,819. The Q20 values were all above 95% and N50 values were above 700 bp, suggesting a high degree of gene assembly integrity and quality (**Supplementary Table 1**). The species cumulative curve showed that the curve rose sharply as the sample size increased, indicating that a large number of species were found. The curve smoothed indicating the number of species reached saturation and the sample size was sufficient to contain most of the species at this time (**Supplementary Figure 1**).

Microbial Community Composition in *Aedes albopictus*

A total of 2,851 species were annotated in the DENV2-infected, DENV2-uninfected, and control groups. All three groups shared 2,572 (90.21%) microbiotas. Approximately 71 species (2.75%) were shared between infected and uninfected groups. The microbiota exclusive to DENV2-infected accounted for 23 species (0.81%). There were 22 (0.77%) species of microbiota exclusive to the control group and 39 (3.17%) species exclusive to the uninfected group (**Figure 1A**).

Measurements of within-sample diversity (alpha-diversity) showed differences in microbiome between the three groups. Diversity indices are usually used to judge the stability of communities. The Shannon–Wiener index reflected the diversity of community species based on the number of species: an increase in the number of species in a community represented an increase in the complexity of the community. When the value of Simpson dominance index was larger, it mean, the uninfected mosquito group had the highest Shannon and Simpson index, indicating that exposure to DENV may increase the bacterial species of *A. albopictus*. The diversity of the microbiota of DENV2-infected mosquitoes was lower than that of DENV2-uninfected mosquitoes, suggesting that the susceptibility to DENV2 may be related to the diversity of bacterial species (**Figure 1B**). Besides, Ace index and Chao index were used to estimate the species richness with the number of OTUs in the community. DENV-uninfected mosquito had a higher Ace index and Chao index (2,448.7 and 2,433.5) than infected (2,434.5 and 2,428.5) and control mosquito (2,428.3 and 2,411.4), suggesting a greater number of OTUs in the community and the greater the community richness. Species richness and diversity were consistently higher in DENV uninfected mosquito.

The principal component analysis (PCA) revealed that the microbiota of DENV2-infected, DENV2-uninfected, and control separated in the first axis and formed three distinct clusters, with overlap in both groups exposed to the virus. Microbial abundance in the infected group was more similar to the uninfected group and differed significantly from the control group, indicating that the greatest source of variation in the microbiota was proximity to DENV2 exposure (**Figure 1C**).

In **Figure 1D**, the microbiota composition of the three groups was quite similar at the phylum level. The top 10 phyla accounted for more than 90% of all phyla. In particular, Proteobacteria and Ascomycota, which accounted for about 35%, respectively, had the highest relative abundance in the infected group (38.89, 34.56%) compared to the uninfected group (38.69, 34.45%) and the control group (38.83, 34.54%). Similarly, at the genus level, the top 30 genera accounted for more than 90% of the numbers, with *Aspergillus* being the most numerous at nearly 30%, followed by *Metarhizium* at more than 15% (**Figure 1E**).

Random-Forest Model Detects Indicator Bacterial Families

The random-forest model detects bacterial families that predict DENV2-infected, uninfected, and not exposure to DENV mosquitoes. We carried out 10-fold cross-validation with five repeats to evaluate the importance of indicator bacterial families. The cross-validation error curve stabilized when the 51 most relevant families were used. Thus, we defined these 51 families as possible biomarker families. The top 51 bacterial families were identified by applying random-forest classification of the relative abundance of the microbiota. Biomarker families were ranked in descending order of importance to the accuracy of the model. Neolectaceae and Cytophagaceae were the most important microbial species for classification (**Figure 2**).

Different on High Abundance Microbiota Between Three Groups of Mosquitoes

According to the row scaled heatmap, the microbial abundance of the control group (no exposure to DENV) is significantly different from the other two groups (exposure to DENV). Based on the abundance of the microbes, it can be seen that *Wolbachia* differed significantly from the other species, occupying a separate branch in the taxonomic tree. *Anaplasma* also occupied a separate

[1] https://www.ncbi.nlm.nih.gov/

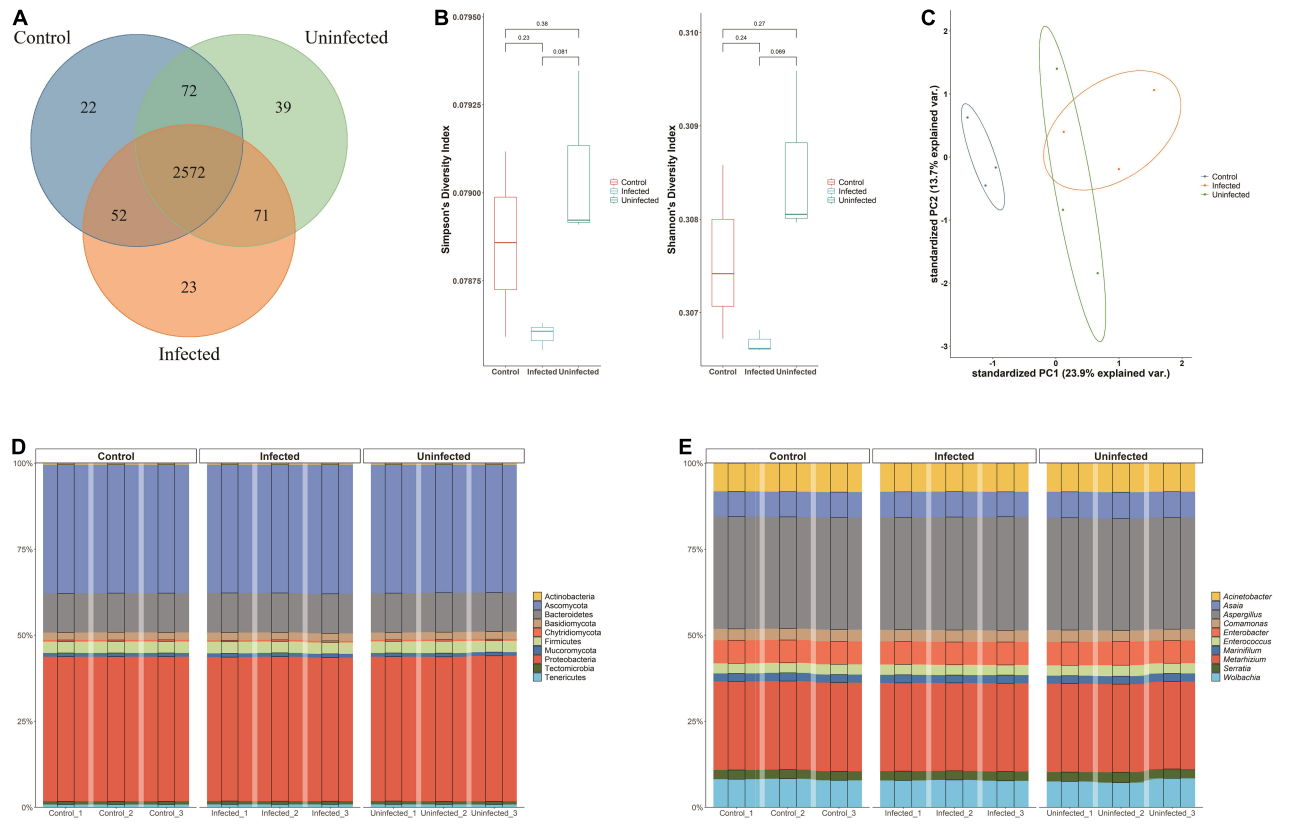

FIGURE 1 | Microbiota of *Aedes albopictus*. **(A)** Venn diagram of the overlapped species among DENV2-infected, DENV2-uninfected, and control group. **(B)** Within-sample diversity (alpha-diversity) with Shannon and Simpson index among three groups. The horizontal bars within boxes represent medians. The tops and bottoms of boxes represent the 75th and 25th percentiles, respectively. The upper and lower whiskers extend to data no more than 1.5× the interquartile range from the upper edge and lower edge of the box, respectively. **(C)** Unconstrained principle component analysis (for principal coordinates PC1 and PC2) with Bray–Curtis distance. **(D)** The microbiota composition of the three groups at the phylum level. **(E)** The microbiota composition of the three groups at the genera level.

branch of the taxonomic tree, was a microbe with a high percentage of abundance mentioned in the previous section (**Supplementary Figure 2**).

Possible Microbiota Related With Dengue Fever Virus Susceptibility

We screened for possible microbiota related to DENV susceptibility by analyzing different microbiota between DENV2-infected and uninfected mosquitoes. Using metagenomeSeq method for susceptible and non-susceptible mosquitoes, 18 microbial species with high variation were screened, namely *Pseudomonas veronii*, *Acinetobacter* spp. CIP 102129, *Gammaproteobacteria*. The LefSe method revealed 15 differential organisms between susceptible and non-susceptible mosquitoes by analyzing the difference in abundance of microbes at the species level, of which 8 showed down-regulation, i.e., lower abundance in susceptible mosquitoes, and 7 showed up-regulation, i.e., higher abundance in susceptible mosquitoes. The functional annotation of the differential microbes is shown in **Table 1**. The results showed that in infected group microbes of the Chytridiomycetes phylum, Acholeplasmataceae family, Desulfovibrionaceae family, and *Desulfovibrio* sp. DS-1, *Enterococcus gallinarum*, and *Paenibacillus* sp. IHB B 3415 regulated significantly.

Kyoto Encyclopedia of Genes and Genome Pathway Analysis

There were 22 pathways with relatively high abundance in KEGG, namely amino acid metabolism, biosynthesis of other secondary metabolites, and carbohydrate production. Among the above high abundance pathways, there were some differences in amino acid metabolism, carbohydrate metabolism, global and general overview maps, nucleotide metabolism, and translation. These differential pathways were relatively more abundant in the normal blood meal group than in the DENV2 exposed group, especially for global and overview maps with highest reabundance. Microbial metabolism in diverse environment like the citrate cycle was an important and conserved aerobic pathway for the final steps of the oxidation of carbohydrates and fatty acids. In this study, microbial metabolism like the citrate cycle was more enriched in uninfected mosquito; this implies that DENV infection may affect many biological processes, contributing to the disorder of microbiota to maintain metabolism (**Figure 3**).

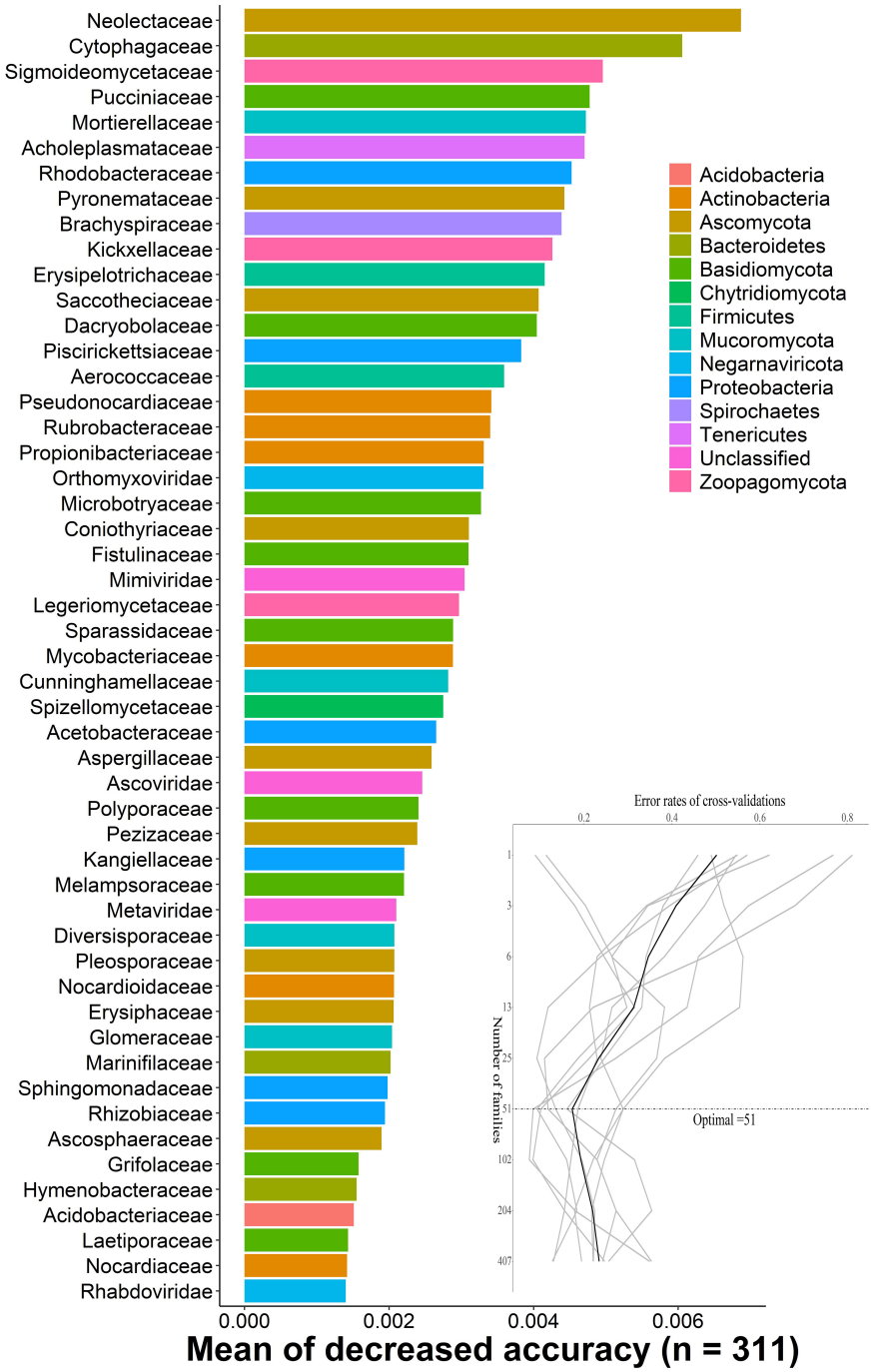

FIGURE 2 | The random-forest model detects bacterial taxa that predict DENV infection. The possible biomarker taxa were ranked in descending order of importance to the accuracy of the model. The inset represents 10-fold cross-validation error as a function of the number of input families used to differentiate microbiota in order of variable importance.

DISCUSSION

Mosquito encountered diverse assemblages of bacteria (i.e., "microbiota") and fungi from aquatic and terrestrial habitat. Individual mosquitoes in the same areas have radically different microbes, which are likely picked up from the environment. There were 158 species of fungi had been isolated from mosquito, nearly half of which could establish longer-term interactions with their hosts (Tawidian et al., 2019). The populations of symbiotic microbes changed depending on the species, period, and diet of the mosquito (Wang et al., 2011; Vogel et al., 2017). The main phyla of the *A. albopictus* microbiota were Proteobacteria,

TABLE 1 | Possible microbiota related with dengue fever virus (DENV) susceptibility to *Aedes albopictus*.

Name	Log2FC	*P*-value	Function	Regulation
Culex rhabdo-like virus	−4.38	0.0068	Unknown	Down
Pinus nigra virus 1	−2.918	0.0030	Transposon Tf2-12 polyprotein	Down
Alphaproteobacteria bacterium 65-37	−2.90	0.0154	Pyruvatedehydrogenase E1 component subunit beta mitochondrial	Down
Candidatus Dadabacteria bacterium	−2.60	0.0072	Adenosylhomocysteinase 1, non-specific lipid-transfer protein	Down
Murmansk poxvirus	−2.53	0.0042	Serine/threonine-protein kinase VRK1	Down
Methyloglobulus morosus	−2.52	0.0135	Glucosed dehydrogenase (FAD quinone)	Down
Parcubacteria group bacterium GW2011 GWA2 43 13	−2.50	0.0070	CAD protein	Down
Nocardia spp. YIM PH 21724	−2.46	0.0346	High affinity cationic amino acid transporter 1	Down
Shigella sonnei	2.46	0.0393	Uncharacterized protein ORF88	Up
Betaproteobacteria HGW-Betaproteobacteria-5	3.00	0.0446	Unknown	Up
Thielavia terrestris	3.22	0.0283	Unknown	Up
Pseudorhodoferax soli	3.25	0.0355	5-Methylthioadenosine/*S*-adenosylhomocysteine deaminase	Up
Acinetobacter spp.	3.27	0.0215	Unknown	Up
Azospira spp. I13	4.08	0.0049	Putative peptide zinc metalloprotease protein	Up
Stanieria cyanosphaera	4.26	0.0023	Apoptosis-inducing factor 3	Up

FIGURE 3 | The Kyoto Encyclopedia of Genes and Genomes (KEGG) pathway abundance map. The vertical coordinates were the KEGG metabolic pathway or secondary metabolic pathway level classification; the horizontal coordinates were the relative content of the corresponding functional gene classification.

Ascomycota, Bacteroidetes, and Firmicutes, all of which had been similarly reported in other mosquito species (Pidiyar et al., 2004; Rani et al., 2009; Boissiere et al., 2012; Lin et al., 2021). Among the Proteobacteria phylum, two genera, *Wolbachia* and *Serratia*, were most associated with mosquitoes; *Wolbachia* stimulates the production of reactive oxygen species and activates the immune system in the body, resulting in the production of antimicrobial peptides to fight viruses (Pan et al., 2012; Mains et al., 2016). *Serratia* produced hemolysin, which facilitated the digestion of food after blood absorption (Gusmao et al., 2010). *Wolbachia* was closely related to the transmission of DENV and had been confirmed to inhibit the spread of dengue fever. *Wolbachia* also affects the vector competence of mosquitoes, and has been shown to be antagonistic to certain arboviruses in mosquitoes such as *A. albopictus*, *A. aegypti*, and *Aedes polynesiensis* and other mosquitoes (Moreira et al., 2009; Walker et al., 2011; Bian et al., 2013). Nazni et al. (2019) successfully introduced *Wolbachia* into mosquitoes to prevent dengue virus transmission, which will have promising applications in the field of mosquito vector and mosquito-borne disease prevention and control.

In our study, the fungal communities identified in mosquito carcasses were dominated by fungi of the phyla Ascomycota. This paralleled previous study which reported the composition and diversity of fungal communities associated with *A. albopictus* larvae and their natural habitats. It can be explained by the ubiquity of Ascomycota in freshwater ecosystems, including larval habitats (Tawidian et al., 2021). *Aspergillus clavatus* (Ascomycota: Trichocomaceae) was previously found to be

an opportunistic pathogen of mosquitoes. Toxins secreted altered the larvae of the southern house mosquito, *Culex quinquefasciatus* larval tissues, leading to their necrosis and causing larval death (Bawin et al., 2016). There was a significant difference in the Chytridiomycetes phylum in DENV2-infected mosquito. According to previous literature, the Chytridiomycetes was found to be a host-specific parasite of mosquitoes, black flies, and ladybugs larvae (Whisler et al., 1975). By killing the mosquito and transferring to other organisms, it formed diploid methanogenic conidia through a series of proliferations, and the fertilized conidia transferred to larvae (Apperson et al., 1992). It was suspected that adult mosquitoes which infected Chytridiomycetes had a higher susceptibility to DENV2, allowing application to prevent the transmission of dengue virus by infecting adult mosquitoes with high levels of Chytridiomycetes.

It was hypothesized that the lack of a specific bacterium may lead to increase the susceptibility of mosquitoes to DENV. Approximately, 18 microbial species with high variation were screened for susceptible and non-susceptible mosquitoes, namely *P. veronii*, *Acinetobacter* spp. CIP 102129, *Gammaproteobacteria*, etc. Among them, *Gammaproteobacteria bacterium* has up to 110 corresponding functions in functional controls and most of them were associated with vital activities, which had been isolated by some scholars in mosquitoes (Wang et al., 2017; Wei et al., 2017; Wu et al., 2019), but there was still not much evidence to link it to dengue virus infection in mosquitoes. *Lactobacillus harbinensis* has been detected in the digestive system of *Anopheles culicifacies* (Sharma et al., 2014), and it was assumed that this microbe can help mosquitoes in digestion. Since the abundance of *L. harbinensis* increased after feeding on dengue virus, it is speculated that dengue virus may promote the amplification of *L. harbinensis*, which needed further experimental verification. The abundance of *Neurospora crassa* in the control group was significantly higher than that in the infected group, and it was speculated that dengue virus may inhibit its growth. It led to significant mortality in the presence of *Anopheles gambiae* defensin peptides (Vizioli et al., 2001). Several of the above microbes whose expression levels were up-regulated stimulation after DENV infection suggest their potential ability as an indicator for mosquito infection with dengue virus.

In this study, functions on possible microbiota related with DENV susceptibility to *A. albopictus* were screened. One of them was the transposon Tf2-12 polyprotein, a member of the retrotransposable (RTPs) family, whose main function was to encode a potential reverse transcriptase expressed in *A. aegypti* (Warren et al., 1997). Glucose dehydrogenase had been shown to play an important metabolic role in *Anopheles stephensi* (Mohanty et al., 2012). Other functions had not been reported in relation to mosquitoes.

CONCLUSION

The dominant phyla of the *A. albopictus* microbiome were *Proteobacteria* and *Ascomycota*, and the major genera were *Aspergillus* and *Metarhizium*. *Gammaproteobacteria*, *L. harbinensis*, and *N. crassa* might serve as biomarkers of *A. albopictus* infection with Dengue 2 virus. Screening of microbes associated with DENV2 infection in *A. albopictus* revealed 15 different microbes, such as *Alphaproteobacteria bacterium* 65-37, *Methyloglobulus morosus*, and *Shigella sonnei*. The microbial functional analysis showed that they all correspond to proteins, enzymes, and other functional substances, basically involved in circulation, protein synthesis, substance breakdown, and other life-related enzymes that may be involved in the immunity and metabolism of the mosquito itself. It was hypothesized that the lack of specific bacteria may lead to increased susceptibility of mosquitoes to DENV. Artificial intervention in the microbiome composition or special bacterium in *A. albopictus* may alter the susceptibility to the DENV.

DATA AVAILABILITY STATEMENT

The datasets presented in this study can be found in online repositories. The names of the repository/repositories and accession number(s) can be found below: https://www.ncbi.nlm.nih.gov/bioproject/PRJNA777640.

ETHICS STATEMENT

The animal study was reviewed and approved by the Institutional Ethics Committee of State Key Laboratory of Pathogens and Biosecurity/Institute of Microbiology and Epidemiology (protocol code IACUC-IME-2019-31).

AUTHOR CONTRIBUTIONS

ZL and C-XL: conceptualization. Y-QD: data curation. M-JL: formal analysis. TZ and B-QL: methodology. TZ: project administration and writing – review and editing. H-TG: software. DX: supervision. Y-EZ and ZL: validation. H-DZ: visualization. TZ, B-QL, and H-TG: writing – original draft. All authors contributed to the article and approved the submitted version.

ACKNOWLEDGMENTS

We acknowledged and appreciated their colleagues for their valuable suggestions and technical assistance for this study.

SUPPLEMENTARY MATERIAL

The Supplementary Material for this article can be found online at: https://www.frontiersin.org/articles/10.3389/fmicb.2022.891151/full#supplementary-material

Supplementary Figure 1 | The species accumulation curves assessing the quality of sequencing data.

Supplementary Figure 2 | The heatmap of different high abundance microbiota between three groups of *Aedes albopictus*.

REFERENCES

Apperson, C. S., Federici, B. A., Stewart, W., and Tarver, F. R. (1992). Evidence for the copepods Acanthocyclops robustus and Mesocyclops edax as competent intermediate hosts for Coelomomyces punctatus during an epizootic in a larval population of the mosquito Anopheles quadrimaculatus. *J. Invertebr. Pathol.* 60, 229–236. doi: 10.1016/0022-2011(92)90003-m

Balmaseda, A., Hammond, S. N., Perez, L., Tellez, Y., Saborio, S. I., Mercado, J. C., et al. (2006). Serotype-specific differences in clinical manifestations of dengue. *Am. J. Trop. Med. Hyg.* 74, 449–456.

Bawin, T., Seye, F., Boukraa, S., Zimmer, J. Y., Raharimalala, F. N., Ndiaye, M., et al. (2016). Histopathological effects of Aspergillus clavatus (Ascomycota: Trichocomaceae) on larvae of the southern house mosquito, Culex quinquefasciatus (Diptera: Culicidae). *Fung. Biol.* 120, 489–499. doi: 10.1016/j.funbio.2016.01.002

Bian, G., Zhou, G., Lu, P., and Xi, Z. (2013). Replacing a native Wolbachia with a novel strain result in an increase in endosymbiont load and resistance to dengue virus in a mosquito vector. *PLoS Negl. Trop. Dis.* 7:e2250. doi: 10.1371/journal.pntd.0002250

Boissiere, A., Tchioffo, M. T., Bachar, D., Abate, L., Marie, A., Nsango, S. E., et al. (2012). Midgut microbiota of the malaria mosquito vector Anopheles gambiae and interactions with Plasmodium falciparum infection. *PLoS Pathog.* 8:e1002742. doi: 10.1371/journal.ppat.1002742

Bolger, A. M., Lohse, M., and Usadel, B. (2014). Trimmomatic: a flexible trimmer for Illumina sequence data. *Bioinformatics* 30, 2114–2120. doi: 10.1093/bioinformatics/btu170

Buxton, M., Cuthbert, R. N., Dalu, T., Nyamukondiwa, C., and Wasserman, R. J. (2020). Cattle-induced eutrophication favours disease-vector mosquitoes. *Sci. Total Environ.* 715:136952. doi: 10.1016/j.scitotenv.2020.136952

Chen, X. G., Jiang, X., Gu, J., et al. (2015). Genome sequence of the Asian Tiger mosquito, Aedes albopictus, reveals insights into its biology, genetics, and evolution. *Proc.Natl. Acad. Sci.U.S.A.* 112, E5907–E5915.

Deng, S. Q., Yang, X., Wei, Y., Chen, J. T., Wang, X. J., and Peng, H. J. (2020). A Review on Dengue Vaccine Development. *Vaccines* 8:63. doi: 10.3390/vaccines8010063

Dimopoulos, G. (2019). Combining Sterile and Incompatible Insect Techniques for Aedes albopictus Suppression. *Trends Parasitol.* 35, 671–673. doi: 10.1016/j.pt.2019.07.006

Gebhard, L. G., Filomatori, C. V., and Gamarnik, A. V. (2011). Functional RNA elements in the dengue virus genome. *Viruses* 3, 1739–1756. doi: 10.3390/v3091739

Gene Ontology Consortium (2021). The Gene Ontology resource: enriching a GOld mine. *Nucleic Acids Res.* 49, D325–D334. doi: 10.1093/nar/gkaa1113

Guo, C., Zhou, Z., Wen, Z., Liu, Y., Zeng, C., Xiao, D., et al. (2017). Global Epidemiology of Dengue Outbreaks in 1990-2015: A Systematic Review and Meta-Analysis. *Front. Cell Infect. Microbiol.* 7:317. doi: 10.3389/fcimb.2017.00317

Gurevich, A., Saveliev, V., Vyahhi, N., and Tesler, G. (2013). QUAST: quality assessment tool for genome assemblies. *Bioinformatics* 29, 1072–1075. doi: 10.1093/bioinformatics/btt086

Gusmao, D. S., Santos, A. V., Marini, D. C., Bacci, M. Jr., Berbert-Molina, M. A., and Lemos, F. J. (2010). Culture-dependent and culture-independent characterization of microorganisms associated with Aedes aegypti (Diptera: Culicidae) (L.) and dynamics of bacterial colonization in the midgut. *Acta Trop.* 115, 275–281. doi: 10.1016/j.actatropica.2010.04.011

Guzman, M. G., Halstead, S. B., Artsob, H., Buchy, P., Farrar, J., Gubler, D. J., et al. (2010). Dengue: a continuing global threat. *Nat. Rev. Microbiol. 8* 12, S7–S16. doi: 10.1038/nrmicro2460

Guzman, M. G., and Kouri, G. (2003). Dengue and dengue hemorrhagic fever in the Americas: lessons and challenges. *J. Clin. Virol.* 27, 1–13. doi: 10.1016/s1386-6532(03)00010-6

Kanehisa, M., Sato, Y., and Kawashima, M. (2022). KEGG mapping tools for uncovering hidden features in biological data. *Protein Sci.* 31, 47–53. doi: 10.1002/pro.4172

Langmead, B., and Salzberg, S. L. (2012). Fast gapped-read alignment with Bowtie 2. *Nat. Methods* 9, 357–359. doi: 10.1038/nmeth.1923

Li, D., Luo, R., Liu, C. M., Leung, C. M., Ting, H. F., Sadakane, K., et al. (2016). MEGAHIT v1.0: A fast and scalable metagenome assembler driven by advanced methodologies and community practices. *Methods* 102, 3–11. doi: 10.1016/j.ymeth.2016.02.020

Liaw, A., and Wiener, M. (2001). Classification and Regression by RandomForest. *Forest* 23, 18–22.

Lin, D., Zheng, X., Sanogo, B., Ding, T., Sun, X., and Wu, Z. (2021). Bacterial composition of midgut and entire body of laboratory colonies of Aedes aegypti and Aedes albopictus from Southern China. *Parasit Vectors* 14:586. doi: 10.1186/s13071-021-05050-4

Lu, J., Breitwieser, F. P., Thielen, P., and Salzberg, S. L. (2017). Bracken: estimating species abundance in metagenomics data. *PeerJ. Comput. Sci.* 3:e104. doi: 10.7717/peerj-cs.104

Luo, L., Jiang, L. Y., Xiao, X. C., Di, B., Jing, Q. L., Wang, S. Y., et al. (2017). The dengue preface to endemic in mainland China: the historical largest outbreak by Aedes albopictus in Guangzhou, 2014. *Infect Dis. Poverty* 6:148. doi: 10.1186/s40249-017-0352-9

Mains, J. W., Brelsfoard, C. L., Rose, R. I., and Dobson, S. L. (2016). Female Adult Aedes albopictus Suppression by Wolbachia-Infected Male Mosquitoes. *Sci. Rep.* 6:33846. doi: 10.1038/srep33846

Mi, H., Muruganujan, A., Ebert, D., Huang, X., and Thomas, P. D. (2019). PANTHER version 14: more genomes, a new PANTHER GO-slim and improvements in enrichment analysis tools. *Nucleic Acids Res.* 47, D419–D426. doi: 10.1093/nar/gky1038

Minard, G., Mavingui, P., and Moro, C. V. (2013). Diversity and function of bacterial microbiota in the mosquito holobiont. *Parasit Vectors* 6:146. doi: 10.1186/1756-3305-6-146

Mohanty, S. S., Singh, K. V., and Bansal, S. K. (2012). Changes in glucose-6-phosphate dehydrogenase activity in Indian desert malaria vector Anopheles stephensi during aging. *Acta Trop.* 123, 132–135. doi: 10.1016/j.actatropica.2012.04.003

Moreira, L. A., Iturbe-Ormaetxe, I., Jeffery, J. A., Lu, G., Pyke, A. T., Hedges, L. M., et al. (2009). A Wolbachia symbiont in Aedes aegypti limits infection with dengue. Chikungunya, and Plasmodium. *Cell* 139, 1268–1278. doi: 10.1016/j.cell.2009.11.042

Nazni, W. A., Hoffmann, A. A., NoorAfizah, A., Cheong, Y. L., Mancini, M. V., Golding, N., et al. (2019). Establishment of Wolbachia Strain wAlbB in Malaysian Populations of Aedes aegypti for Dengue Control. *Curr. Biol.* 424:e4245. doi: 10.1016/j.cub.2019.11.007

O'Leary, N. A., Wright, M. W., Brister, J. R., et al. (2016). Reference sequence (RefSeq) database at NCBI: current status, taxonomic expansion, and functional annotation. *Nucleic Acids Res.* 44, D733–D745. doi: 10.1093/nar/gkv1189

Pan, X., Zhou, G., Wu, J., Bian, G., Lu, P., Raikhel, A. S., et al. (2012). Wolbachia induces reactive oxygen species (ROS)-dependent activation of the Toll pathway to control dengue virus in the mosquito Aedes aegypti. *Proc. Natl. Acad. Sci. U.S.A.* 109, E23–E31. doi: 10.1073/pnas.1116932108

Pelizza, S. A., Scorsetti, A. C., and Tranchida, M. C. (2013). The sublethal effects of the entomopathic fungus Leptolegnia chapmanii on some biological parameters of the dengue vector Aedes aegypti. *J. Insect. Sci.* 13:22. doi: 10.1673/031.013.2201

Pidiyar, V. J., Jangid, K., Patole, M. S., and Shouche, Y. S. (2004). Studies on cultured and uncultured microbiota of wild culex quinquefasciatus mosquito midgut based on 16s ribosomal RNA gene analysis. *Am. J. Trop. Med. Hyg.* 70, 597–603.

Rani, A., Sharma, A., Rajagopal, R., Adak, T., and Bhatnagar, R. K. (2009). Bacterial diversity analysis of larvae and adult midgut microflora using culture-dependent and culture-independent methods in lab-reared and field-collected Anopheles stephensi-an Asian malarial vector. *BMC Microbiol.* 9:96. doi: 10.1186/1471-2180-9-96

Rossi, P., Ricci, I., Cappelli, A., Damiani, C., Ulissi, U., Mancini, M. V., et al. (2015). Mutual exclusion of Asaia and Wolbachia in the reproductive organs of mosquito vectors. *Parasit Vect.* 8:278. doi: 10.1186/s13071-015-0888-0

Ruiling, Z., Peien, L., Xuejun, W., and Zhong, Z. (2018). Molecular analysis and genetic diversity of Aedes albopictus (Diptera. *Culicidae*) from China. *Mitochondrial. DNA A DNA Mapp. Seq. Anal.* 29, 594–599. doi: 10.1080/24701394.2017.1325481

Sharma, P., Sharma, S., Maurya, R. K., Das, De, T., Thomas, T., et al. (2014). Salivary glands harbor more diverse microbial communities than gut in Anopheles culicifacies. *Parasit Vectors* 7:235. doi: 10.1186/1756-3305-7-235

Souza, R. S., Virginio, F., Riback, T. I. S., Suesdek, L., Barufi, J. B., and Genta, F. A. (2019). Microorganism-Based Larval Diets Affect Mosquito Development, Size

and Nutritional Reserves in the Yellow Fever Mosquito Aedes aegypti (Diptera: Culicidae). *Front. Physiol.* 10:152. doi: 10.3389/fphys.2019.00152

Souza-Neto, J. A., Powell, J. R., and Bonizzoni, M. (2019). Aedes aegypti vector competence studies: A review. *Infect. Genet. Evol.* 67, 191–209. doi: 10.1016/j.meegid.2018.11.009

Sun, B., Zhang, X., Zhang, H., Liu, H., Sun, L., Tan, Q., et al. (2020). Genomic epidemiological characteristics of dengue fever in Guangdong province. China from 2013 to 2017. *PLoS Negl. Trop. Dis.* 14:e0008049. doi: 10.1371/journal.pntd.0008049

Tawidian, P., Coon, K. L., Jumpponen, A., Cohnstaedt, L. W., and Michel, K. (2021). Host-Environment Interplay Shapes Fungal Diversity in Mosquitoes. *mSphere* 6:e0064621. doi: 10.1128/mSphere.00646-21

Tawidian, P., Rhodes, V. L., and Michel, K. (2019). Mosquito-fungus interactions and antifungal immunity. *Insect Biochem. Mol. Biol.* 111:103182. doi: 10.1016/j.ibmb.2019.103182

Vasilakis, N., Cardosa, J., Hanley, K. A., Holmes, E. C., and Weaver, S. C. (2011). Fever from the forest: prospects for the continued emergence of sylvatic dengue virus and its impact on public health. *Nat. Rev. Microbiol.* 9, 532–541. doi: 10.1038/nrmicro2595

Vizioli, J., Richman, A. M., Uttenweiler-Joseph, S., Blass, C., and Bulet, P. (2001). The defensin peptide of the malaria vector mosquito Anopheles gambiae: antimicrobial activities and expression in adult mosquitoes. *Insect Biochem. Mol. Biol.* 31, 241–248. doi: 10.1016/s0965-1748(00)00143-0

Vogel, K. J., Valzania, L., Coon, K. L., Brown, M. R., and Strand, M. R. (2017). Transcriptome Sequencing Reveals Large-Scale Changes in Axenic Aedes aegypti Larvae. *PLoS Neglected Tropical. Dis.* 11:e0005273. doi: 10.1371/journal.pntd.0005273

Walker, T., Johnson, P. H., Moreira, L. A., Iturbe-Ormaetxe, I., Frentiu, F. D., McMeniman, C. J., et al. (2011). The wMel Wolbachia strain blocks dengue and invades caged Aedes aegypti populations. *Nature* 476, 450–453. doi: 10.1038/nature10355

Wang, S., Dos-Santos, A. L. A., Huang, W., Liu, K. C., Oshaghi, M. A., Wei, G., et al. (2017). Driving mosquito refractoriness to Plasmodium falciparum with engineered symbiotic bacteria. *Science* 357, 1399–1402. doi: 10.1126/science.aan5478

Wang, Y., Gilbreath, T. M. III, Kukutla, P., Yan, G., and Xu, J. (2011). Dynamic gut microbiome across life history of the malaria mosquito Anopheles gambiae in Kenya. *PloS One* 6:e24767. doi: 10.1371/journal.pone.0024767

Warren, A. M., Hughes, M. A., and Crampton, J. M. (1997). Zebedee: a novel copia-Ty1 family of transposable elements in the genome of the medically important mosquito Aedes aegypti. *Mol. Gen. Genet.* 254, 505–513. doi: 10.1007/s004380050445

Wei, G., Lai, Y., Wang, G., Chen, H., Li, F., and Wang, S. (2017). Insect pathogenic fungus interacts with the gut microbiota to accelerate mosquito mortality. *Proc. Natl. Acad. Sci. U.S.A.* 114, 5994–5999. doi: 10.1073/pnas.1703546114

Wei, Y., Wang, J., Wei, Y. H., Song, Z., Hu, K., Chen, Y., et al. (2021). Vector Competence for DENV-2 Among Aedes albopictus (Diptera: Culicidae) Populations in China. *Front. Cell Infect Microbiol.* 11:649975. doi: 10.3389/fcimb.2021.649975

Whisler, H. C., Zebold, S. L., and Shemanchuk, J. A. (1975). Life history of Coelomomyces psorophorae. *Proc. Natl. Acad. Sci. U.S.A.* 72, 693–696. doi: 10.1073/pnas.72.2.693

Wood, D. E., Lu, J., and Langmead, B. (2019). Improved metagenomic analysis with Kraken 2. *Gen. Biol.* 20:257. doi: 10.1186/s13059-019-1891-0

Wu, P., Sun, P., Nie, K., Zhu, Y., Shi, M., Xiao, C., et al. (2019). A Gut Commensal Bacterium Promotes Mosquito Permissiveness to Arboviruses. *Cell Host Microbe.* 10:e105. doi: 10.1016/j.chom.2018.11.004

Yee, D. A., Allgood, D., Kneitel, J. M., and Kuehn, K. A. (2012). Constitutive differences between natural and artificial container mosquito habitats: vector communities, resources, microorganisms, and habitat parameters. *J. Med. Entomol.* 49, 482–491. doi: 10.1603/me11227

Zheng, X., Zhang, D., Li, Y., Yang, C., Wu, Y., Liang, X., et al. (2019). Incompatible and sterile insect techniques combined eliminate mosquitoes. *Nature* 572, 56–61. doi: 10.1038/s41586-019-1407-9

Conflict of Interest: The authors declare that the research was conducted in the absence of any commercial or financial relationships that could be construed as a potential conflict of interest.

Publisher's Note: All claims expressed in this article are solely those of the authors and do not necessarily represent those of their affiliated organizations, or those of the publisher, the editors and the reviewers. Any product that may be evaluated in this article, or claim that may be made by its manufacturer, is not guaranteed or endorsed by the publisher.

frontiers | Frontiers in Microbiology

REVIEW
published: 09 June 2022
doi: 10.3389/fmicb.2022.925386

Multifunctional Roles of MicroRNAs in Schistosomiasis

Haoran Zhong[1,2] *and Yamei Jin*[1,2]*

[1] National Reference Laboratory for Animal Schistosomiasis, Shanghai Veterinary Research Institute, Chinese Academy of Agricultural Sciences, Shanghai, China, [2] Key Laboratory of Animal Parasitology of Ministry of Agriculture and Rural Affairs, Shanghai Veterinary Research Institute, Chinese Academy of Agricultural Sciences, Shanghai, China

Schistosomiasis is a parasitic disease that is caused by helminths of the genus *Schistosoma*. The dioecious schistosomes mate and lay eggs after undergoing a complex life cycle. Schistosome eggs are mostly responsible for the transmission of schistosomiasis and chronic fibrotic disease induced by egg antigens is the main cause of the high mortality rate. Currently, chemotherapy with praziquantel (PZQ) is the only effective treatment against schistosomiasis, although the potential of drug resistance remains a concern. Hence, there is an urgent demand for new and effective strategies to combat schistosomiasis, which is the second most prevalent parasitic disease after malaria. MicroRNAs (miRNAs) are small non-coding RNAs that play pivotal regulatory roles in many organisms, including the development and sexual maturation of schistosomes. Thus, miRNAs are potential targets for treatment of schistosomiasis. Moreover, miRNAs can serve as multifunctional "nano-tools" for cross-species delivery in order to regulate host-parasite interactions. In this review, the multifunctional roles of miRNAs in the growth and development of schistosomes are discussed. The various regulatory functions of host-derived and worm-derived miRNAs on the progression of schistosomiasis are also thoroughly addressed, especially the promotional and inhibitory effects on schistosome-induced liver fibrosis. Additionally, the potential of miRNAs as biomarkers for the diagnosis and treatment of schistosomiasis is considered.

Keywords: schistosomiasis, MicroRNA, development, liver fibrosis, biomarker, diagnosis

OPEN ACCESS

Edited by:
Wei Wang,
Jiangsu Institute of Parasitic Diseases (JIPD), China

Reviewed by:
Pengfei Cai,
QIMR Berghofer Medical Research Institute, Australia
Santiago Fontenla,
Universidad de la República, Uruguay
Adebayo James Molehin,
Texas Tech University Health Sciences Center, United States

***Correspondence:**
Yamei Jin
yameijin@shvri.ac.cn

Specialty section:
This article was submitted to Infectious Agents and Disease, a section of the journal Frontiers in Microbiology

Received: *21 April 2022*
Accepted: *20 May 2022*
Published: *09 June 2022*

Citation:
Zhong H and Jin Y (2022) Multifunctional Roles of MicroRNAs in Schistosomiasis. Front. Microbiol. 13:925386. doi: 10.3389/fmicb.2022.925386

BACKGROUND

Schistosomiasis is a momentous neglected tropical disease affecting countless numbers of people in the developing world that is caused by infection of three major species of trematode flukes, including *Schistosoma mansoni* (Africa, South America, and the Middle East), *Schistosoma haematobium* (Africa and the Middle East), and *Schistosoma japonicum* (Southeast Asia), and three locally distributed species, including *Schistosoma mekongi* (Mekong River area), *Schistosoma guineensis* (West and Central Africa), and *Schistosoma intercalatum* (West and Central Africa) (Colley et al., 2014). Schistosomes can live in human hosts for an average of 3–10 years and up to 40 years in extreme cases (Warren et al., 1974; Chabasse et al., 1985). Generally, the eggs

Abbreviations: EV, extracellular vesicles; Fox, forkhead box; HSC, hepatic stellate cells; IFN-γ, interferon-γ; IL, interleukin; LV, lentivirus vector; mRNA, messenger RNA; miRNA, microRNA; NF-κB, nuclear factor- kappa B; PPARγ, peroxisome proliferator-activated receptor gamma; PZQ, praziquantel; rAAV, recombinant adeno-associated virus; RG, reference gene; RT-PCR, reverse transcribed polymerase chain reaction; SEA, soluble egg antigens; sncRNA, small non-coding RNAs; TGF-β1, transforming growth factor β 1; Th, T helper; TLR, Toll-like receptor; TNF-α, tumor necrosis factor-α; UTR, untranslated region.

produced by mated worms rather than adult worms themselves are responsible for the pathogenesis of schistosomiasis (Gryseels et al., 2006). The schistosome life cycle is relatively complex (Nation et al., 2020). Following release from freshwater snails, the cercariae pierce the skin and enter the blood vessels of the definitive host, and then transform into schistosomula (Stirewalt, 1974), which migrate through the circulation to the lungs and then to the systemic organs *via* the pulmonary veins. Finally, the male and female worms reach the liver vasculature and mate *via* the gynacophoric canal of the male (Miller and Wilson, 1980; Colley et al., 2014). The paired worms live within either the perivascular (*S. haematobium*) or mesenteric (*S. mansoni*, *S. japonicum*, *S. mekongi*, *S. guineensis*, and *S. intercalatum*) venules, which induce urogenital or intestinal/hepatic schistosomiasis, respectively (Lewis and Tucker, 2014; Nation et al., 2020).

Each mature female worm can lay hundreds or thousands of eggs per day (depending on species), of which about one-third to one-half become trapped in the host tissues, accounting for the primary pathology of schistosomiasis (Cheever et al., 1994; Zhong et al., 2022a). Egg-induced granuloma formation and tissue fibrosis due to the host immune response are the main causes of the high morbidity and mortality of schistosomiasis (Llanwarne and Helmby, 2021). Most of the remaining eggs are excreted in urine or feces. Then, miracidia hatch from the eggs in fresh water and seek a suitable snail as an intermediate host to complete and repeat the life cycle (Nation et al., 2020; Zhong et al., 2022a). Hence, schistosome eggs are also responsible for the occurrence and spread of schistosomiasis. Human activities in infected water promotes transmission of schistosomiasis (Lam et al., 2022). More than 230 million people in 78 tropical and subtropical countries are affected annually by schistosomiasis, which is the second most prevalent parasitic disease after malaria (Li et al., 2022). Infections among travelers, migrants, and immigrants are also emerging in industrialized countries, which poses significant risks worldwide (Lu et al., 2016). The sudden re-emergence of urinary schistosomiasis on the island of Corsica has aroused great concern (De Laval et al., 2014). At present, chemotherapy with praziquantel (PZQ) is mainly used to control and treat schistosomiasis (Karanja et al., 1998). However, the continued application of PZQ may promote the evolution of drug-resistant schistosomes (Fenwick et al., 2003). Hence, inhibition of schistosome growth and host-parasite interactions could contribute to the identification of novel anti-schistosomal drugs.

Small non-coding RNAs (sncRNAs), which are enriched in many cell types, are essential modulators of various processes in animal cells, including parasite infection (Bushati and Cohen, 2007; Zhu et al., 2014). MicroRNAs (miRNAs), first discovered in the nematode *Caenorhabditis elegans* in 1993, are a class of sncRNAs (about 18–25 nucleotides in length) generated from endogenous transcripts (Lee et al., 1993) that negatively regulate the expression of target genes at the post-transcriptional level by binding to the 5′-untranslated region (5′-UTR), coding sequence (CDS) and 3′-UTR of the target gene messenger RNA in order to inhibit translation or induce degradation (Bartel, 2004; Bartel, 2009). In addition to fundamental roles in diverse biological and pathological processes, miRNAs regulate the expression of genes involved in the growth, development, differentiation, proliferation, death, metabolism, and environmental responses of many organisms (Queiroz et al., 2017; Rouas et al., 2019). To date, several research groups have conducted studies to investigate and identify miRNA in different life stages of developed and undeveloped male and female worms to gain novel insights into the maturation of schistosomes and host-parasite interactions in schistosomiasis (Lin et al., 2019; Liu et al., 2019; Yu J. et al., 2019; Gaber et al., 2020; Han et al., 2020; He et al., 2020; Wang Y. et al., 2020; Abreu et al., 2021; Jiang et al., 2022). Schistosomes have numerous naturally permissive hosts (such as 46 species for *S. japonicum*, including cattle, pigs, sheep, goats, and mice) and non-adaptive hosts (such as water buffalo, *Rattus norvegicus*, *Microtus fortis*, and immunodeficient mice). Comparative studies elucidating the miRNA expression profiles of different hosts infected different developmental stages of schistosomes were also conducted (Yu X. et al., 2019; Sun et al., 2021; Tang et al., 2021; Li et al., 2022; Liu et al., 2022). The characterization of differentially expressed worm-derived or host-derived miRNAs can also be a supplementary tool for grading and diagnosis of schistosomiasis (Cai et al., 2018; Mu et al., 2019; Cai et al., 2020).

The present review focuses on recent studies evaluating the multifunctional roles of miRNAs in the development of schistosomes and host-parasite interactions of schistosomiasis. The potential applications of miRNAs as diagnostic biomarkers for schistosomiasis and as novel therapeutic targets for treatment are also discussed. These findings provide a valuable resource set of candidate targets to further explore anti-schistosomal treatment strategies.

MicroRNAs REGULATE THE DEVELOPMENT OF SCHISTOSOMES

Identification of Schistosome MicroRNAs

The complex life cycles of schistosomes reflect the need to adapt to constantly changing environmental conditions. The schistosome life cycle consists of at least seven discrete developmental stages characterized by tremendous morphological and transcriptional changes occurring within the intermediate and definitive hosts (Nation et al., 2020). The different stages of schistosome growth and development are partially regulated by various miRNAs. Xue et al. (2008) first identified *S. japonicum* miRNAs in 2008 and Simões et al. (2011) explored the miRNA profile of *S. mansoni*, which have rapidly expanded our knowledge about miRNAs. Due to the limited methods available in 2008, the stem-loop TaqMan miRNA reverse transcribed polymerase chain reaction (RT-PCR) assay was primarily used for analysis of mammalian miRNAs. Only five novel miRNAs in *S. japonicum* have been identified by constructing and screening parasite cDNA libraries of size-fractionated RNAs, which include sja-let-7, sja-miR-71,

TABLE 1 | Summary of miRNAs upregulated in the different developmental stages or sexes of schistosome.

Species	Life stages or gender	miR-name	References
S. japonicum	Egg	sja-miR-1, sja-miR-36-3p, sja-miR-71, sja-miR-71b-5p, sja-miR-124-3p	Cai et al., 2013a
	Cercaria	sja-let-7, sja-bantam, sja-miR-1, sja-miR-2a-3p, sja-miR-2a-5p, sja-miR-2b-3p, sja-miR-2b-5p, sja-miR-7-3p, sja-miR-7-5p, sja-miR-8-3p, sja-miR-10-5p, sja-miR-31-5p, sja-miR-36-3p, sja-miR-36-5p, sja-miR-71, sja-miR-71b-3p, sja-miR-71b-5p, sja-miR-124-3p, sja-miR-125b, sja-miR-133, sja-miR-190-5p, sja-miR-219-5p, sja-miR-3479-3p, sja-miR-3479-5p, sja-miR-3485-3p, sja-miR-3487, sja-miR-3489, sja-miR-3490, sja-miR-3491, sja-miR-3492, sja-miR-3493, sja-miR-3496, sja-miR-3497, sja-miR-3499, sja-miR-3500, sja-miR-3501, sja-miR-3502, sja-miR-3503, sja-miR-3504	Xue et al., 2008; Cai et al., 2011
	Lung-stage schistosomula	sja-let-7, sja-miR-2c-3p, sja-miR-2c-5p, sja-miR-2d-3p, sja-miR-2d-5p, sja-miR-2e-3p, sja-miR-2e-5p, sja-miR-10-3p, sja-miR-61, sja-miR-124-5p, sja-miR-190-3p, sja-miR-2162-3p, sja-miR-2162-5p, sja-miR-3488, sja-miR-3494, sja-miR-3495, sja-miR-3498, sja-miR-3506	Cai et al., 2011
	16-day MM	sja-miR-2b, sja-miR-2d, sja-miR-2e, sja-miR-7, sja-miR-8, sja-miR-61, sja-miR-124, sja-miR-219, sja-miR-227, sja-miR-277b, sja-miR-2162, sja-miR-3479, sja-miR-3488	Zhu L. et al., 2016
	16-day MF	sja-miR-31	Zhu L. et al., 2016
	22-day MM	sja-miR-2b, sja-miR-2d, sja-miR-2e, sja-miR-7, sja-miR-8, sja-miR-61, sja-miR-124, sja-miR-219, sja-miR-227, sja-miR-277b, sja-miR-2162, sja-miR-3479, sja-miR-3488	Zhu L. et al., 2016
	22-day MF	sja-bantam, sja-miR-2c, sja-miR-31, sja-miR-1989	Zhu L. et al., 2016
	23-day SF	sja-miR-1, sja-miR-7, sja-miR-7-5p, sja-miR-71	Sun et al., 2014
	25-day MF	sja-bantam, sja-miR-219-3p, sja-miR-3485-5p, sja-miR-3486-5p, sja-miR-3488, sja-miR-3489, sja-miR-3490, sja-miR-3491, sja-miR-3493, sja-miR-3494, sja-miR-3495, sja-miR-3497, sja-miR-3498, sja-miR-3500, sja-miR-3501, sja-miR-3502, sja-miR-3504, sja-miR-3505, sja-miR-3506, sja-miR-3507	Han et al., 2020
	25-day SF	sja-let-7, sja-miR-1, sja-miR-2c-5p, sja-miR-7-5p, sja-miR-8-3p, sja-miR-10-5p, sja-miR-36-3p, sja-miR-36-5p, sja-miR-124-3p, sja-miR-124-5p, sja-miR-125a, sja-miR-133, sja-miR-3479-5p, sja-miR-3482-3p, sja-miR-3482-5p, sja-miR-3503	Han et al., 2020
	28-day MM	sja-miR-7, sja-miR-8, sja-miR-61, sja-miR-124, sja-miR-219, sja-miR-227, sja-miR-2162, sja-miR-3479, sja-miR-3488	Zhu L. et al., 2016
	28-day MF	sja-bantam, sja-miR-2c, sja-miR-31, sja-miR-1989	Zhu L. et al., 2016
	49-day MM	sja-let-7, sja-miR-1, sja-miR-2a-3p, sja-miR-2e-3p, sja-miR-2e-5p, sja-miR-7-5p, sja-miR-8-3p, sja-miR-10-3p, sja-miR-10-5p, sja-miR-61, sja-miR-71, sja-miR-124-3p, sja-miR-125a, sja-miR-125b, sja-miR-133, sja-miR-190-5p, sja-miR-219-3p, sja-miR-219-5p, sja-miR-227, sja-miR-307, sja-miR-2162-3p, sja-miR-3479-3p, sja-miR-3480-5p, sja-miR-3482-3p, sja-miR-3496,sja-miR-3503	Cai et al., 2011
	49-day MF	sja-bantam, sja-miR-2c-3p, sja-miR-2c-5p, sja-miR-2d-3p, sja-miR-36-3p, sja-miR-71b-5p, sja-miR-2162-5p, sja-miR-3479-5p, sja-miR-3487, sja-miR-3488, sja-miR-3489, sja-miR-3491, sja-miR-3492, sja-miR-3493, sja-miR-3494, sja-miR-3495, sja-miR-3498, sja-miR-3499, sja-miR-3505, sja-miR-3506, sja-miR-3507	Cai et al., 2011
S. mansoni	Lung-stage schistosomula	sma-bantam, sma-miR-71	Simões et al., 2011
	49-day MM	sma-miR-1, sma-miR-61, sma-miR-281	Marco et al., 2013
	49-day MF	sma-bantam, sma-miR-2c, sma-miR-2d, sma-miR-2f, sma-miR-31, sma-miR-36b, sma-miR-71b, sma-miR-755, sma-miR-8437, sma-miR-8447	Marco et al., 2013
	50-day adult worm pair	sma-miR-92a, sma-miR-125, sma-miR-250, sma-miR-new-5-5p	Abreu et al., 2021
S. haematobium	90-day MM	sha-let-7, sha-miR-1, sha-miR-7a, sha-miR-745	Stroehlein et al., 2018
	90-day MF	sha-bantam, sha-miR-71a, sha-miR-71b, sha-miR-125b, sha-miR-2162	Stroehlein et al., 2018

SF, single-sex infected female; MF, mated female; MM, mated male.

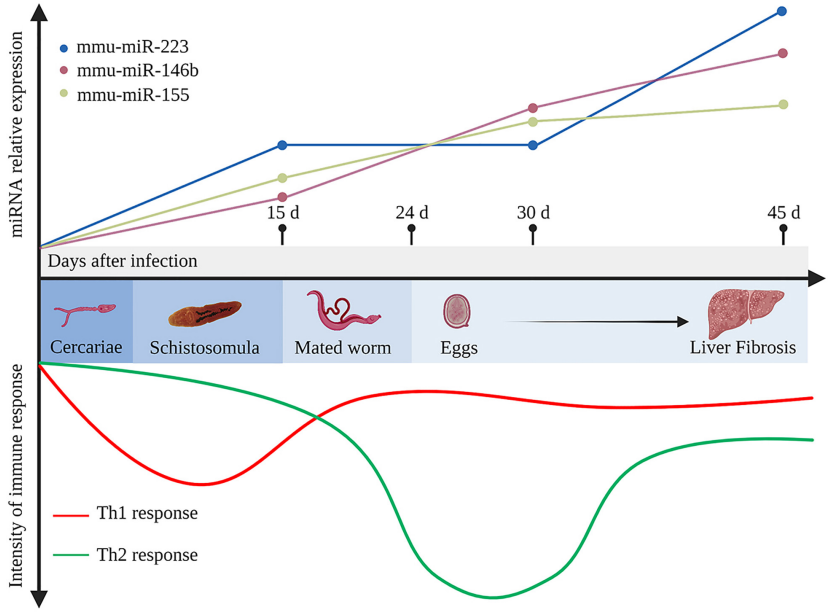

FIGURE 1 | Development of the immune response and representative differentially expressed host miRNAs during *Schistosoma japonicum* infection. In the early stage of infection, the host produces a T helper type 1 (Th1) response against the migrating immature schistosomula (about 15 days after infection). After the mated worms lay eggs (about 24 days after infection), which further secrete antigens that stimulate the body to generate a strong Th2 response. Ultimately, when the disease develops into the chronic liver fibrosis, the Th2 response is diminished but still dominant. During infection, mmu-miR-223, mmu-miR-146b, and mmu-miR-155 in the liver tissues continuously elevated at 15, 30, 45 days after infection (Cai et al., 2013b). d, days. This figure was created with Biorender.com.

sja-bantam, sja-miR-125, and sja-miR-new1 (Xue et al., 2008). Six life stages of schistosomes were selected to investigate the expression patterns of these miRNAs, which revealed that expression of sja-miR-71 and sja-bantam peaked at the cercaria stage and then decreased significantly to the lowest levels at the schistosomulum stage (Xue et al., 2008). Sja-let-7 expression was lowest in the miracidium stage, then increased during the sporocyst and cercaria stages, and gradually decreased thereafter within the mammalian host (Xue et al., 2008). In the first report of the *S. mansoni* miRNA profile, miRNA detection with probes demonstrated that Sma-miR-71, Sma-bantam, and Sma-miR-125 were evolutionarily conserved (Simões et al., 2011). Although the expression levels of sja-miR-71 and sja-bantam decreased rapidly in *S. japonicum* schistosomula in the host lung, a strong hybridization signal was observed for both miRNAs in the same stage of *S. mansoni* (Simões et al., 2011). Two other miRNAs detected in *S. japonicum* (sja-new-1 and sja-let-7) are thought to be expressed in other life cycle stages or in undetectable amounts in *S. mansoni* (Simões et al., 2011). The first genome-wide sncRNA resource for *S. haematobium* was not published until 2018. Of all 89 miRNAs (34 novel miRNAs) identified, there were 64 miRNAs presented sex-biased transcription, suggested their potential roles in sexual differentiation and reproductive processes of *S. haematobium* (Stroehlein et al., 2018). This report further expands on previous studies of schistosome miRNAs and provides additional evidence of the conservation of miRNAs among flatworms (Stroehlein et al., 2018). Most of the schistosome miRNAs studied were identified by Solexa RNA sequencing and followed by bioinformatic analysis. Differences in the expression patterns throughout the life cycle of schistosomes suggest that these miRNAs may facilitate important roles in growth and development.

An increasing number of studies have reported the miRNA profiles of *S. japonicum*, *S. mansoni*, and *S. haematobium* at various development stages, including schistosome eggs of normally developed and underdeveloped females accumulated in various host tissues and schistosomula in the host lung and liver. Adults of both sexes have been identified by transcriptome analysis and deep-sequencing technique, which provided a broader view of parasite sncRNAs (Han et al., 2020). In addition, crucial molecules associated with miRNA biogenesis, such as Dicer, Argonaute, and Drosha, are differentially expressed at different developmental stages of schistosomes (Gomes et al., 2009; Chen et al., 2010; Luo et al., 2010; Cai et al., 2012; Cardoso et al., 2020). Hence, miRNAs appear to play important roles in schistosome development. Most studies categorize schistosome-derived miRNAs based on "the stage-specific or gender-biased" principle.

Stage-Specific and Gender-Biased MicroRNAs in Schistosomes

Deep analysis of sncRNAs revealed that sja-miR-71b-5p, sja-miR-71, sja-miR-1, sja-miR-36-3p, and sja-miR-124-3p were highly expressed in purified eggs of *S. japonicum* in the host liver tissue (Cai et al., 2013a). Northern blot analysis further confirmed that members of the sja-miR-71 family were the most abundant

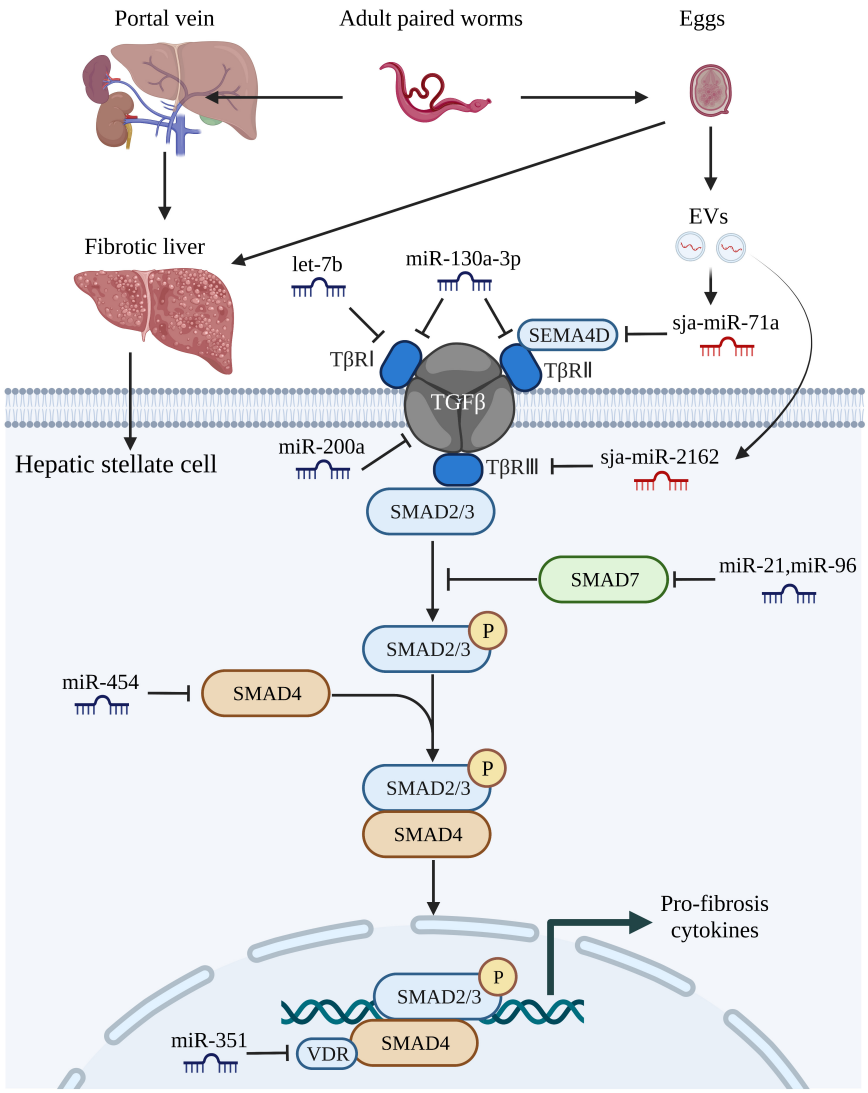

FIGURE 2 | MiRNAs regulate schistosome-induced liver fibrosis through TGF-β/SMAD signaling pathway. The adult paired worms migrate to the portal vein and lay eggs. TGF-β/SMAD signaling pathway, one of the most critical signaling pathways that associated with liver fibrosis in hepatic stellate cells, can be activated by soluble egg antigen TGF-β/SMAD signaling pathway. TGF-β binds to the receptors (TβRI, TβRII, TβRIII) leading to phosphorylation of Smad-2 and Smad-3, followed by aggregation with Smad-4 and subsequently drives the expression of Smad-7 which negatively regulates TGF-β/SMAD signaling pathway. Both host-derived miRNAs (let-7b, miR-130-3p, miR-200a, miR-21, miR-96, miR-454, and miR-351) and worm-derived miRNAs secreted from egg-derived extracellular vesicles (sja-miR-71a and sja-miR-2162) exert vital roles in the progression of schistosome-induced liver fibrosis. This figure was created with Biorender.com.

and suggested that sja-miR-71 might perform pivotal functions during development (Cai et al., 2013a). Besides, schistosome eggs, the main causative factors of schistosomiasis, release extracellular vesicles (EVs) that contain small RNAs, including parasite-specific miRNAs, that participate in host-parasite interactions (Zhu S. et al., 2016). The functions of miRNAs in EVs released by schistosome eggs are discussed later in this review.

Male-female pairing, which is essential for sexual maturation of female worms, provides an opportunity to identify miRNAs that are crucial to the reproductive biology of female schistosomes. It has been suggested that the male schistosome ensures physical transport, corrects tissue localization, aids in feeding, and provides maturation factors for the development and egg-producing ability of the female (Loverde and Chen, 1991; Rollinson et al., 1997; Colley et al., 2014). However, the underlying mechanisms remain unknown. In, Cai et al. (2011) were the first to investigate differences in miRNA profiles of male and female *S. japonicum*. The results showed that sja-miR-1, sja-miR-7-5p, sja-miR-61, sja-miR-124-3p, sja-miR-125a, sja-miR-125b, and sja-miR-219-5p were mainly dominant in males, while sja-bantam, sja-miR-71b-5p, sja-miR-3479-5p, and sja-miR-novel-23-5p were mainly found in females, suggesting possible involvement of miRNAs in sex differentiation and maintenance. A study conducted in 2013 by Marco et al. (2013)

focusing on differential expression of miRNAs in *S. mansoni* demonstrated that 10 miRNAs (sma-miR-2c, sma-miR-2d, sma-miR-2f, sma-miR-31, sma-miR-36b, sma-miR-71b, sma-miR-755, sma-miR-8437, sma-miR-8447, and sma-bantam) were more abundant in females, while expression of three miRNAs (sma-miR-1, sma-miR-61, and sma-miR-281) were higher in males. Abreu et al. (2021) recently investigated differential miRNA expression profiles in each developmental phase of *S. mansoni* and found that sma-miR-92a, sma-miR-250, and sma-miR-new-5-5p were enriched in adult worm pairs. In 90-day *S. haematobium* worms, 59 (66%) of 89 miRNAs, including sha-miR-71a, sha-miR-71b, sha-miR-2162, and sha-bantam, exhibited substantial female-biased transcription, while 5 (6%) others, including sha-let-7, sha-miR-1, sha-miR-7a, and sha-miR-125b, were sex-biased in males (Stroehlein et al., 2018). These results suggesting that changes in miRNA expression patterns might regulate sexual differentiation of schistosomes.

Mating of male and female *S. japonicum* occurs at as early as 15 or 16 days post-infection (dpi). At 20 dpi, the oogonium is differentiated from the spermatogonium and matured vitelline cells begin to appear in females, followed by eggshell formation at 22 dpi and laying of eggs at 24 dpi (Wang et al., 2017). In general, the paired worms are considered fully mature at 28 dpi (Colley et al., 2014; Wang et al., 2017). Therefore, 16, 20–24, and 24–26 dpi are crucial growth and developmental stages of *S. japonicum* (Wang et al., 2017; Yu J. et al., 2019). Due to the complex and prolonged life cycle of schistosomes, the dynamic influence of miRNAs on growth and development cannot be fully explained at a specific point in time. Zhu L. et al. (2016) identified 14 miRNAs enriched in males, including sja-miR-7, sja-miR-61, and sja-miR-219, and four in females, including sja-bantam, at 16, 22, and 28 days post-mating using a high-throughput sequencing method and further verified by RT-PCR. Among the four miRNAs enriched in females, sja-bantam and sja-miR-31 were predominantly localized to the ovary, as determined by the *in situ* hybridization, and sja-bantam was found to play regulatory roles in ovary development and oocyte maturation with the use of antisense RNA (Zhu L. et al., 2016).

The ability of a female worm to maintain egg production requires continuous stimulation by a mature male worm (Loverde and Chen, 1991; Kunz, 2001). A single-sex infected female worm is characterized by incomplete development with stunting and an immature reproductive system, as the vitelline glands that produce the eggshell precursors and nutrients for the egg are not fully developed (LoVerde et al., 2009; Zhong et al., 2022b). Hence, single-sex infected worms do not cause serious damage to the host because underdeveloped worms cannot produce normal eggs (Zhong et al., 2022a). Han et al. (2020) employed Solexa deep-sequencing technology to identify 36 differentially expressed miRNAs between normal and underdeveloped female worms at 25 dpi, of which 20 were up-regulated and 16 were down-regulated in mated females. Comparably, Sun et al. (2014) reported that sja-bantam was distinctly up-regulated in mated females at 23 dpi, while sja-miR-1, sja-miR-7, sja-miR-7-5p, and sja-miR-71 were up-regulated in single-sex infected females at 23 dpi. These findings imply a potential role of specific miRNAs in the sexual maturation of adult schistosomes.

The rationale for the choice of time points for comparison of miRNA profiles was mostly based on the schistosome life cycle (Yu J. et al., 2019). In order to gain a global view of miRNA profiles of schistosomes, Yu J. et al. (2019) quantified dynamic expression of miRNAs in *S. japonicum* at 14, 16, 18, 20, 22, 24, 26, and 28 dpi. The results showed that all 79 mature *S. japonicum* miRNAs had three similar expression clusters in male and female worms from the pairing stage, throughout development and sexual maturation, to egg production (Yu J. et al., 2019). Network analysis revealed that 15 miRNAs in cluster 1 were involved in regulating male-female and parasite-host interactions, communication, and immune responses, while 11 miRNAs in cluster 2 were associated with development and sexual maturation, and 45 miRNAs in cluster 3 might be related to metabolic regulation and synthesis of substances associated with egg laying (Yu J. et al., 2019).

The identification of related target genes would be valuable to elucidate the biological functions of miRNAs. Several groups have attempted to predict the targets of various miRNAs with the use of currently available target prediction tools, such as miRanda, TargetScanS, PicTar, RNAhybrid, and PITA (Liu et al., 2019; Du et al., 2020; Han et al., 2020; He et al., 2020; Wang L. et al., 2020). Notably, many of the putative target genes of stage-specific and gender-biased miRNAs in schistosomes are likely linked to the Wnt, transforming growth factor β (TGF-β), and chemokine signaling pathways, which reportedly are involved in the development and embryogenesis of schistosomes (Zhu L. et al., 2016; Han et al., 2020). To date, the miRBase database (version 22) (Kozomara et al., 2019) includes 79 miRNAs from mature *S. japonicum* and 225 from mature *S. mansoni*. The results of recent studies are summarized in **Table 1**.

MicroRNAs IN THE HOST-PARASITE INTERACTION

Identification of Host-Derived MicroRNAs in Schistosomiasis

The enormous number of lodged eggs in the host tissues, the major pathogenic factor of schistosomiasis, triggers granuloma formation, fibrosis, and subsequent immune responses, and even cancer (Carson et al., 2018; Schwartz and Fallon, 2018). Owing to long-term coexistence within the host, schistosomes regulate the host immune responses *via* complex molecular mechanisms. The host immune response to schistosome infection is polarized during disease progression. In the early stage of infection, the host produces a T helper type 1 (Th1) response against migrating immature and mature parasites, which involves secretion of Th1-type cytokines, such as interleukin (IL) -12, interferon-γ (IFN-γ), and tumor necrosis factor-α (TNF-α). The laid eggs of paired worms (4 and 6 weeks post infection for *S. japonicum* and *S. mansoni*, respectively) act as antigens that stimulate the host to generate a strong Th2 response, with elevated production of the Th2-type cytokines IL-4, IL-5, IL-9, and IL-13, under

the control of regulatory T-cells (Tregs) (Wynn et al., 2004). Ultimately, when disease progresses into the chronic regulatory phase, despite the fact that schistosomes live for years and continue to lay eggs, the Th2 response is diminished, but still dominant, due to the prolonged Treg environment in response to IL-10 and TGF-β (Pearce and MacDonald, 2002; Wynn et al., 2004; Mu et al., 2021b; **Figure 1**). Hyperpolarization of the Th2 immune response in the chronic phase of disease can potentially result in a lethal pathology (McManus et al., 2020). Recent observations suggest that both naïve and induced $CD4^+$ T cells (Tregs) balance the host Th1/Th2 response (Layland et al., 2007; Romano et al., 2016; Ondigo et al., 2018; Wang L. et al., 2020).

Advanced liver disease induced by *S. mansoni* and *S. japonicum*, which is often irreversible without prompt medical treatment, leads to the high morbidity and mortality rates of schistosomiasis (Zhong et al., 2022a). Elucidation of the molecular mechanisms that mediate the progression of schistosomiasis has been a primary research goal for several decades. Recent studies have demonstrated that schistosome infection also alters the miRNA expression profile of the host, suggesting that the host miRNAs might also participate in regulation of the pathogenesis of schistosomiasis (Cai et al., 2013b; Han et al., 2013b; Cabantous et al., 2017).

Cai et al. (2013b) identified more than 130 differentially expressed miRNAs in the livers of BALB/c mice infected with *S. japonicum*, including mmu-miR-15b, mmu-miR-126-5p, mmu-miR-142-3p, and mmu-miR-223, which were significantly up-regulated at 30 dpi, and mmu-miR-146b and mmu-miR-155, which were up-regulated at 30 and 45 dpi. Mmu-miR-146b and mmu-miR-155 were shown to regulate the inflammatory responses *via* the nuclear factor-kappa B (NF-κB) signaling pathway to control Toll-like receptor (TLR) and cytokine signaling through a negative feedback regulation loop (Taganov et al., 2006). Hence, upregulation of mmu-miR-146b and mmu-miR-155 at 30 dpi might be associated with the recruitment and activation of B and T lymphocytes at periphery granulomas in response to stimulation by egg antigens. Expression of mmu-miR-146b and mmu-miR-155 was consistently up-regulated at 45 dpi, suggesting that dual activation of these miRNAs subtly control the degree of liver immunopathology in schistosomiasis (Cai et al., 2013b). Notably, in a mouse model of lung injury, mmu-miR-155 attenuated the Th2 response by inhibiting expression of the transcription factor *c-Maf* (Rodriguez et al., 2007). Therefore, up-regulation of mmu-miR-155 might also control the Th1/Th2 response during immunopathological progression of schistosomiasis. As another vital component, expression of mmu-miR-223 in the liver tissue is substantially up-regulated as early as 15 dpi and is reportedly the most upregulated miRNA at 45 dpi (Cai et al., 2013b). Notably, mmu-miR-223 is mainly expressed in Kupffer cells and hepatic stellate cells (HSCs), which are the most important cell types regulating liver fibrosis during schistosomiasis (He et al., 2013). In addition, miR-223 was significantly up-regulated in both cell types after *S. japonicum*

TABLE 2 | Summary of miRNAs involved in the pathogenesis of schistosomiasis.

MiR-name	Target genes	Pathways	Function	References
Let-7b	TβRI	TGF-β/SMAD signaling pathway	Anti-fibrosis	Tang et al., 2017
MiR-21	SMAD7	TGF-β/SMAD and IL-13/STAT6 signaling pathways	Pro-fibrosis	Kong et al., 2019
MiR-27b	PPARγ	TGF-β signaling pathway	Pro-fibrosis	Zhu et al., 2018a
MiR-92a-2-5p	TLR2	Unstudied	Anti-fibrosis	Zhao et al., 2019
MiR-96	SMAD7	TGF-β/SMAD signaling pathway	Pro-fibrosis	Luo et al., 2018
MiR-130a-3p	MAPK1, TβRI, TβRII	TGF-β and MAPK signaling pathways	Anti-fibrosis	Liu et al., 2021
MiR-146a/b	STAT1	IFN-γ signaling pathway	Macrophage transformation	He et al., 2016
MiR-155	FOXO3a	ERK1 signaling pathway	Pro-fibrosis	Zhu et al., 2018b
MiR-181a	TLR4	TLR4 receptor signaling pathway	Anti-fibrosis	Tang et al., 2021
MiR-182	FOXO1	PI3K/AKT signaling pathway	Pro-fibrosis	Huang et al., 2018
MiR-200a	TGF-β2	TGF-β signaling pathway	Anti-fibrosis	Xu et al., 2021
MiR-203-3p	SMAD3	SMAD signaling pathway	Anti-fibrosis	He et al., 2018b
MiR-351	VDR	SMAD and IFN-γ signaling pathways	Pro-fibrosis	He et al., 2018a
MiR-454	SMAD4	SMAD signaling pathway	Anti-fibrosis	Zhu et al., 2014
Sja-miR-1	SFRP1	Wnt/β-catenin pathway	Pro-fibrosis	Wang Y. et al., 2020
Sja-miR-71a	SEMA4D, FZD4	TGF-β/SMAD and IL-13/STAT6 signaling pathways	Anti-fibrosis	Wang L. et al., 2020; Jiang et al., 2022
Sja-miR-125b, Sja-bantam	PROS1, FAM212B, CLMP	Unstudied	Macrophage proliferation	Liu et al., 2019
Sja-miR-2162	TβRIII	TGF-β/SMAD signaling pathway	Pro-inflammatory, Pro-fibrosis	He et al., 2020
Sja-miR-3096	PIK3C2A	Unstudied	Tumor suppressor	Lin et al., 2019

infection, thus presenting a potential molecular signature of immune cell infiltration (He et al., 2013). The expression profiles of mmu-miR-146b, mmu-miR-155, and mmu-miR-223 are presented in **Figure 1**.

Other than the liver, the miRNA expression profiles were also identified in lung and spleen tissues of BALB/c mice in the early stage of *S. japonicum* infection (10 dpi) (Han et al., 2013b). The results of miRNA microarrays showed that that 28, 8, and 8 miRNAs were up-regulated, while 28, 3, and 5 were down-regulated, in lung, liver, and spleen tissues of infected mice, respectively (Han et al., 2013b). The lung is among the most susceptible tissues to *S. japonicum* in the early stage of infection (10 dpi), as reflected by the relatively large numbers of altered host miRNAs. Bioinformatics analysis demonstrated that differentially expressed miRNAs target the MAPK, insulin, TLR, and TGF-β signaling pathways, suggesting important roles of host miRNAs in the early phase of *S. japonicum* infection (Han et al., 2013b). Comparisons of plasma miRNAs between uninfected and infected (25 dpi) BALB/c mice found that 11 (30.6%) of 36 differentially expressed miRNAs were down-regulated, particularly mmu-miR-542-3p, mmu-miR-673-3p, mmu-miR-711, and mmu-miR-5112, while 25 (69.4%) were up-regulated, especially mmu-miR-874-5p (Zhu et al., 2015). Zhu et al. (2015) also found that up-regulated expression of mmu-miR-134-5p and mmu-miR-706 in the plasma was inverse correlated with levels of *Caspase-3* and *Creb*, indicating that host miRNAs may act as important mediators of the pathology of hepatic schistosomiasis.

Schistosomes have a variety of naturally permissive hosts, thus understanding the miRNA expression profiles of permissive hosts after infection can provide an important reference for the control of schistosomiasis (Liu et al., 2022). Conversely, clarification of the changes to the miRNA expression profiles of less susceptible or semi-permissive hosts can also provide constructive insights in the biology of schistosome infection (Amiri et al., 1992). Schistosomes are not highly infectious to rats with comparatively low developmental rate of the worms, decreased egg production and increased production of immature eggs (Silva-Leitão et al., 2009). Further miRNA expression profiling confirmed that rats were semi-permissive hosts of schistosomes (Han et al., 2013a). Han et al. (2013a) used miRNA microarrays to compare miRNA expression profiles of Wistar rats before and 10 days after schistosome infection and identified 16, 61, and 10 differentially expressed miRNAs in liver, spleen, and lung tissues, respectively. In liver tissues, upregulation of mmu-miR-346* was found to induce activation of the MAPK signaling pathway and rno-miR-328*, which was down-regulated in the spleen tissues of Wistar rats, was demonstrated to play important roles in activation of the Wnt, MAPK, mTOR, and neurotrophin signaling pathways (Han et al., 2013a). Water buffalo and yellow cattle are the major mammalian hosts and transmission sources of *S. japonicum* in endemic regions of China (Liu et al., 2012), and account for the majority of all infected ruminants that graze freely near bodies of water (VAN Dorssen et al., 2017). As compared with water buffalo, yellow cattles are more susceptible to schistosome infection and, therefore, the burdens of paired worms and eggs are significantly higher (Yang et al., 2012; Zhai et al., 2018). Differences in the susceptibility of yellow cattle vs. water buffalo suggest that subtle differences in gene regulation are required for the complex biological processes involved in schistosome infection. Although five miRNAs (sja-miR-2e-3p, sja-miR-7-3p, sja-miR-124-3p, sja-miR-219-5p, and sja-miR-3490) were reportedly significantly upregulated in 56-day schistosomes from water buffalo as compared to yellow cattle, the miRNA profiles of schistosome-infected bovine species are still under investigation (Yu X. et al., 2019). Collectively, these studies suggest that differences in miRNA profiles among various hosts could provide alternative strategies for the control of schistosomiasis and offer new perspectives to elucidate the underlying pathological mechanisms.

Host MicroRNAs Mediate Schistosome-Induced Liver Fibrosis

Various stimuli can induce the differentiation of HSCs into collagen-producing myofibroblasts, which promote the progression of schistosomiasis-induced liver fibrosis (Carson et al., 2018). Recent studies have demonstrated that host miRNAs activate multiple signaling pathways that participate in the activation of HSCs during liver fibrosis (Chen et al., 2019; Sun et al., 2021; Tang et al., 2021; Xu et al., 2021). For instance, accumulating evidence suggests that miR-21 and miR-96 are involved in regulating schistosome-induced liver fibrosis through the classical TGF-β1/small mothers against decapentaplegic (SMAD) signaling pathway (He et al., 2015; Luo et al., 2018; Kong et al., 2019). Expression of miR-21 and miR-96 was inhibited in infected mice using a recombinant adeno-associated virus-8 (rAAV8) vector and further studies showed that *Smad7*, a negative regulator of the TGF-β1/SMAD signaling pathway and phosphorylation of SMAD2 and SMAD3, was the target gene of both miRNAs. Thus, miR-21 and miR-96 could activate collagen generation and stimulate liver fibrosis by targeting SMAD7 and trigger the pro-fibrotic function of the TGF-β1/SMAD signaling pathway (He et al., 2015; Kong et al., 2019). Several studies have also shown that miRNAs can target and bind to the coding regions of genes associated with the TGF-β1/SMAD signaling pathway to mediate the progression of liver fibrosis (He et al., 2020; Wang L. et al., 2020).

Let-7b, a member of the let-7 family, plays an essential role in the development of various liver diseases (Gilles and Slack, 2018). And it was reported that let-7b diminished *S. japonicum*-induced liver fibrosis by reducing expression of TGF-β receptor 1/2 in the human HSC line LX-2, while reducing expression of collagen I, suggesting that host let-7b is a potential molecular target for the treatment of schistosome-induced liver fibrosis (Tang et al., 2017; Sun et al., 2021). In a study conducted by Liu et al. (2021), the mice injected with a lentivirus vector carrying miR-130a-3p presented alleviated granuloma-induced inflammation and collagen deposition in both liver tissue and primary HSCs. In other studies (Zhu et al., 2014; He et al., 2018b), miR-203-3p played an anti-fibrotic role by targeting SMAD3, while

miR-454 exerted a similar preventive function by targeting SMAD4. Recently, miR-200a was reported to have an anti-fibrotic effect by targeting TGF-β2, although further studies are needed to determine whether miRNAs can be used to inhibit activation of the anticipated target genes (Xu et al., 2021). Liver fibrosis is a complex dynamic equilibrium, thus it is not surprising that multiple miRNAs appear to both inhibit and promote liver fibrosis. He et al. (2018a) demonstrated that miR-351 promotes schistosomiasis-related liver fibrosis by targeting the vitamin D receptor (VDR) and then they also identified a mechanism by which IFN-γ can simultaneously induce the expression of SMAD7 and VDR, which synergistically block SMAD signaling. The regulatory roles of various miRNAs associated with the TGF-β/SMAD signaling pathway in schistosome-associated liver fibrosis are summarized in **Figure 2**.

It is well documented that various miRNAs regulate schistosome-induced liver damage through different pathways depending on the cell type (Carson et al., 2018). As previously described, migrating schistosomes trigger a Th1 response in the host, which is characterized by increased expression of IFN-γ and subsequent differentiation of M1 macrophages. After eggs are released at 4–6 weeks post-infection, a swift transition from a Th1 to Th2 response occurs in the host. Up-regulation of miR-146a/b blocks IFN-γ-induced differentiation from M1 to M2 macrophages by targeting STAT1, suggesting a protective role against hepatic schistosomiasis (He et al., 2016). In both rat fibrotic liver tissues and LX-2 cells, high expression of miR-182 was correlated with down-regulation of the transcription factor forkhead box protein O1, which is a major downstream effector of the PI3K/AKT signaling pathway (Huang et al., 2018). Further studies have shown that increased expression of miR-182 promoted the proliferation of LX-2 cells, while inhibiting apoptosis, and stimulated the development of schistosome-induced liver fibrosis through feedback *via* the PI3K/AKT signaling pathway (Huang et al., 2018). Interestingly, another study found that miR-182 is an important mediator of the specialization and stability of Tregs during schistosome infections (Kelada et al., 2013). TLRs are crucial for the identification of invading pathogens and represent an essential bridge between innate and adaptive immunity (Akira and Takeda, 2004). Evidence suggests that miR-92a-2-5p and miR-181a suppress schistosome-induced liver fibrosis both *in vitro* and *in vivo* by targeting TLR2 and TLR4, respectively (Zhao et al., 2019; Tang et al., 2021). Egg antigen P40 of *S. japonicum* (SjP40), which is the main soluble egg antigen of *S. japonicum*, can suppress activation and proliferation of HSCs *via* TGF-β1 (Sun et al., 2015). Moreover, in two other studies, recombinant SjP40 treatment can make LX-2 cells activated by blocking the function of peroxisome proliferator-activated receptor gamma (PPARγ) through the expression of miR-27b, PPARγ is thought to inhibit fibrosis by maintaining HSCs in a more quiescent phenotype, while miR-155 inhibited activation of HSCs *via* FOXO3a (Zhu et al., 2018a,b). The results of these studies indicate indirect involvement of miRNAs in schistosome-induced liver fibrosis.

In summary, numerous studies have demonstrated that certain host-derived miRNAs play important roles in the pathogenesis of schistosomiasis and that the use of antisense techniques to block specific miRNAs and methods to improve the expression of certain miRNAs will likely provide a theoretical basis for reducing the pathological consequences of schistosomiasis.

MicroRNAs Mediate Cross-Species Host-Parasite Interaction Through Extracellular Vesicles

EVs are released from almost all cell types, including parasitic cells, but through different mechanisms (Hansen et al., 2019; Liu et al., 2019; Wang L. et al., 2020). The three main subtypes of EVs (50–1,000 nm in diameter and can even up to 10 μm) are microvesicles, exosomes, and apoptotic bodies (van Niel et al., 2018). Notably, among the diverse active vectors conveyed by EVs, miRNAs are regarded as regulators of various biological functions. Some studies have reported that schistosome-derived EVs mediate host-parasite interactions through miRNAs. Liu et al. (2019), who first reported EVs from adult *S. japonicum* worms and determined the miRNA profiles, found that sja-miR-125b (most enriched) and sja-bantam (helminth-specific miRNA) in SjEVs stimulated the proliferation of monocytes in infected mice and elevated expression of TNF-α by targeting the genes coding for protein S1, family with sequence similarity 212 member B, and CXADR-like membrane protein. In this study, treatment with clodronate liposomes of the infected mice resulted in remarkable reduction in worm burden, egg production, and elevated expression of TNF-α, this demonstrated the pivotal role of SjEV miRNA in mediating host-pathogen interactions. Other than worms, EVs have also been identified in schistosome eggs (Zhu S. et al., 2016). Based on the miRNA profiles of schistosome eggs, the same research group also detected sja-miR-2162 and sja-miR-1 in the HSCs of infected hosts, suggesting that EVs could deliver parasite miRNAs into HSCs (He et al., 2020; Wang Y. et al., 2020). Delivery of sja-miR-2162 and sja-miR-1 *via* the rAAV8 vector could further promote activation of HSCs and induction of liver fibrosis by targeting negative modulators of HSC activation, while inhibiting expression of the miRNAs was found to attenuate the severity of liver fibrosis both *in vivo* and *in vitro* (Chu et al., 2011; He et al., 2020; Wang Y. et al., 2020).

As previously described, miRNAs both positively and negatively regulate the progression of liver fibrosis. Previous studies identified sja-miR-71a as the most enriched miRNA in *S. japonicum* egg-derived EVs and a negative modulator of liver fibrogenesis that targets *Sema4d* and negatively regulates functions of the TGF-β1/SMAD and IL-13/signal transducer and activator of transcription 6 signaling pathways during infection (Du et al., 2016; Xu et al., 2016; Wang L. et al., 2020). Besides, the proportions of Th2 and Th17 cells were decreased, while the number of Tregs was increased in mice treated with the rAAV9 vector expressing sja-miR-71a (Wang L. et al., 2020).

Recent studies have found that the parasitic miRNAs sja-miR-7-5p, sja-miR-61, and sja-miR-3096 have significant negative

effects on the growth of hepatoma cell *in vitro* and *in vivo*, but no effect in normal non-cancerous cells (Hu et al., 2019; Lin et al., 2019; Hu et al., 2021). Although the current study does not confirm the involvement of SjEVs during liver cancer, in-depth studies of cross-species miRNA regulation may help to discover new strategies for the prevention and treatment of parasitic diseases, including schistosomiasis. Recent studies of host- and schistosome-derived miRNAs in the pathogenicity of schistosomiasis are summarized in **Table 2**.

MicroRNAs FOR GRADING SCHISTOSOME-INDUCED LIVER FIBROSIS

Unless treated in a timely manner, schistosome-induced liver fibrosis is irreversible. Hence, it is urgent to develop novel methods for early diagnosis and monitoring of schistosomiasis. Studies have shown that circulating and EV-bound miRNAs are potential diagnostic and prognostic markers of schistosomiasis. For example, the level of serum miR-223 was positively correlated with the course of schistosomiasis in mice, while treatment with PZQ reduced miR-223 expression to normal levels, indicating that miR-223 is a potential diagnostic biomarker of schistosomiasis (He et al., 2013). Host circulating let-7a-5p, let-7d-5p, miR-146a-5p, and miR-150-5p were identified in infected C57BL/6 and BALB/c mice, and miR-150-5p demonstrated the best potential for grading liver fibrosis in schistosomiasis (Cai et al., 2018). Besides, the serum level of exosomal miR-146a-5p was negatively correlated with the extent of liver fibrosis in patients, indicating that miR-146a-5p is also a potential novel marker to assess the severity of schistosomiasis (Cai et al., 2018). In another study, exosomal miR-103a-3p and miR-425-5p were determined as the most stable reference genes (RGs) in a C57BL/6 mouse model of schistosomiasis and human patients, respectively (Cai et al., 2020). The study demonstrated that the serum exosomal miR-146a-5p level was able to discriminate the schistosomiasis japonica patients with mild from severe fibrosis liver fibrosis (Cai et al., 2020).

Detection of parasite-specific miRNAs in exosomes could improve diagnostic accuracy. For returning travelers infected with schistosomiasis due to infection with *S. mansoni*, *S. haematobium*, and *S. mekongi*, the diagnostic sensitivity and specificity of parasite-specific miRNAs, including Bantam, miR-2c-3p, and miR-3488, in human serum EVs are much higher than other diagnostic methods, as the sensitivity of Bantam and miR-2c-3p combined was 91% (Meningher et al., 2017). RT-PCR analysis conducted by Mu et al. (2019) demonstrated that parasite-derived miRNAs (sja-miR-2b-5p and sja-miR-2c-5p) could detect infected patients with low infectious intensity and moderate sensitivity and specificity of 66/68% and 55/80%, respectively. Notably, in this study they also presented that the sensitivity and specificity of these two parasite miRNAs combined were 77.4 and 60.0%, respectively.

Current techniques for extraction and purification of EVs must be improved because the number of exosomes in serum is limited. Timely and rapid extraction of exosomes and efficient detection of substances contained in exosomes remains difficult (Mu et al., 2021a). Focusing on the schistosome-derived miRNAs to diagnose schistosomiasis is a promising path, but more research is needed before clinical application.

CONCLUSION

Emerging studies have indicated that miRNAs play important roles in the development of schistosomes and host-parasite interactions. Due to the complex life-cycle of schistosomes (at least seven life stages) and the variety of host species (over 40 permissive hosts for *S. japonicum*), further studies are needed to clarify the contribution of parasite-derived miRNAs in schistosome growth. Mortality associated with schistosome-induced liver disease is relatively high and recent studies suggest that miRNAs of either the host or schistosome are involved in fatal host-parasite interactions. Current studies of the miRNA expression profiles of the host liver and serum offer important insights into the pathogenesis of schistosomiasis. Interestingly, some differentially expressed miRNAs identified in these studies regulate schistosome-induced liver disease positively or negatively, suggesting that miRNAs are potential diagnostic and prognostic markers of schistosomiasis. However, miRNA-based therapy is still in the animal experimental stage and in-depth investigations are still needed. Screening of worm-specific miRNAs from schistosome-derived EVs may also be a good approach for choosing potential biomarkers of schistosomiasis. Although still in the infancy period, recent studies have focused on cross-species miRNAs. However, there still exist significant discrepancies in this concept, especially from the perspective of the basic biology of cross-species miRNAs. The extraction, purification, and substance identification of EVs still require optimization and improvement. In all, investigations of schistosomiasis-related miRNAs should be pursued to provide a theoretical basis for the growth and development of schistosomes as well as the diagnosis and treatment of schistosomiasis.

AUTHOR CONTRIBUTIONS

YJ and HZ: conceptualization, validation, investigation, resources, and writing – review and editing. HZ: writing – original draft preparation and visualization. YJ: supervision, project administration, and funding acquisition. Both authors have read and agreed to the published version of the manuscript.

FUNDING

This work was supported by the Natural Science Foundation of Shanghai (no. 20ZR1469300) and the Chinese National Natural Science Foundation (no. 31672245).

ACKNOWLEDGMENTS

We thank International Science Editing for revising the manuscript and their valuable comments.

REFERENCES

Abreu, F. C., Mota, E. A., Pereira, R. V., Oliveira, V. F., Costa, M. P., Gomes, M. S., et al. (2021). Differential expression profiles of miRNAs and their putative targets in *Schistosoma mansoni* during its life cycle. *Mem. Inst. Oswaldo Cruz.* 116:e200326. doi: 10.1590/0074-02760200326

Akira, S., and Takeda, K. (2004). Toll-like receptor signalling. *Nat. Rev. Immunol.* 4, 499–511.

Amiri, P., Locksley, R. M., Parslow, T. G., Sadick, M., Rector, E., Ritter, D., et al. (1992). Tumour necrosis factor alpha restores granulomas and induces parasite egg-laying in schistosome-infected SCID mice. *Nature* 356, 604–607. doi: 10.1038/356604a0

Bartel, D. P. (2004). MicroRNAs: genomics, biogenesis, mechanism, and function. *Cell* 116, 281–297. doi: 10.1016/s0092-8674(04)00045-5

Bartel, D. P. (2009). MicroRNAs: target recognition and regulatory functions. *Cell* 136, 215–233.

Bushati, N., and Cohen, S. M. (2007). microRNA functions. *Annu. Rev. Cell Dev. Biol.* 23, 175–205.

Cabantous, S., Hou, X., Louis, L., He, H., Mariani, O., Sastre, X., et al. (2017). Evidence for an important role of host microRNAs in regulating hepatic fibrosis in humans infected with *Schistosoma japonicum*. *Int J Parasitol* 47, 823–830. doi: 10.1016/j.ijpara.2017.05.007

Cai, P., Hou, N., Piao, X., Liu, S., Liu, H., Yang, F., et al. (2011). Profiles of small non-coding RNAs in *Schistosoma japonicum* during development. *PLoS Negl. Trop. Dis.* 5:e1256. doi: 10.1371/journal.pntd.0001256

Cai, P., Mu, Y., Olveda, R. M., Ross, A. G., Olveda, D. U., and Mcmanus, D. P. (2018). Circulating miRNAs as footprints for liver fibrosis grading in schistosomiasis. *EBioMedicine* 37, 334–343. doi: 10.1016/j.ebiom.2018.10.048

Cai, P., Mu, Y., Olveda, R. M., Ross, A. G., Olveda, D. U., and Mcmanus, D. P. (2020). Serum Exosomal miRNAs for grading hepatic fibrosis due to schistosomiasis. *Int. J. Mol. Sci.* 21:3560. doi: 10.3390/ijms21103560

Cai, P., Piao, X., Hao, L., Liu, S., Hou, N., Wang, H., et al. (2013a). A deep analysis of the small non-coding RNA population in *Schistosoma japonicum* eggs. *PLoS One* 8:e64003. doi: 10.1371/journal.pone.0064003

Cai, P., Piao, X., Liu, S., Hou, N., Wang, H., and Chen, Q. (2013b). MicroRNA-gene expression network in murine liver during *Schistosoma japonicum* infection. *PLoS One* 8:e67037. doi: 10.1371/journal.pone.0067037

Cai, P., Piao, X., Hou, N., Liu, S., Wang, H., and Chen, Q. (2012). Identification and characterization of argonaute protein, Ago2 and its associated small RNAs in *Schistosoma japonicum*. *PLoS Negl. Trop. Dis.* 6:e1745. doi: 10.1371/journal.pntd.0001745

Cardoso, T. C. S., De Araujo, C. B., Portilho, L. G., Mendes, L. G. A., Alves, T. C., Silva, G. C., et al. (2020). Computational prediction and characterisation of miRNAs and their pathway genes in human schistosomiasis caused by *Schistosoma haematobium*. *Mem. Inst. Oswaldo Cruz.* 115:e190378. doi: 10.1590/0074-02760190378

Carson, J. P., Ramm, G. A., Robinson, M. W., Mcmanus, D. P., and Gobert, G. N. (2018). Schistosome-induced fibrotic disease: the role of hepatic stellate cells. *Trends Parasitol.* 34, 524–540. doi: 10.1016/j.pt.2018.02.005

Chabasse, D., Bertrand, G., Leroux, J. P., Gauthey, N., and Hocquet, P. (1985). [Developmental bilharziasis caused by *Schistosoma mansoni* discovered 37 years after infestation]. *Bull. Soc. Pathol. Exot. Filiales* 78, 643–647.

Cheever, A. W., Macedonia, J. G., Mosimann, J. E., and Cheever, E. A. (1994). Kinetics of egg production and egg excretion by *Schistosoma mansoni* and *S. japonicum* in mice infected with a single pair of worms. *Am. J. Trop. Med. Hyg.* 50, 281–295. doi: 10.4269/ajtmh.1994.50.281

Chen, J., Yang, Y., Guo, S., Peng, J., Liu, Z., Li, J., et al. (2010). Molecular cloning and expression profiles of Argonaute proteins in *Schistosoma japonicum*. *Parasitol. Res.* 107, 889–899. doi: 10.1007/s00436-010-1946-3

Chen, Q., Zhang, J., Zheng, T., Chen, H., Nie, H., Zheng, B., et al. (2019). The role of microRNAs in the pathogenesis, grading and treatment of hepatic fibrosis in schistosomiasis. *Parasit. Vectors* 12:611.

Chu, W., Li, X., Li, C., Wan, L., Shi, H., Song, X., et al. (2011). TGFBR3, a potential negative regulator of TGF-β signaling, protects cardiac fibroblasts from hypoxia-induced apoptosis. *J. Cell Physiol.* 226, 2586–2594. doi: 10.1002/jcp.22604

Colley, D. G., Bustinduy, A. L., Secor, W. E., and King, C. H. (2014). Human schistosomiasis. *Lancet* 383, 2253–2264.

De Laval, F., Savini, H., Biance-Valero, E., and Simon, F. (2014). Human schistosomiasis: an emerging threat for Europe. *Lancet* 384, 1094–1095. doi: 10.1016/S0140-6736(14)61669-X

Du, P., Giri, B. R., Liu, J., Xia, T., Grevelding, C. G., and Cheng, G. (2020). Proteomic and deep sequencing analysis of extracellular vesicles isolated from adult male and female *Schistosoma japonicum*. *PLoS Negl. Trop. Dis.* 14:e0008618. doi: 10.1371/journal.pntd.0000861

Du, P., Ma, Q., Zhu, Z. D., Li, G., Wang, Y., Li, Q. Q., et al. (2016). Mechanism of Corilagin interference with IL-13/STAT6 signaling pathways in hepatic alternative activation macrophages in schistosomiasis-induced liver fibrosis in mouse model. *Eur. J. Pharmacol.* 793, 119–126. doi: 10.1016/j.ejphar.2016.11.018

Fenwick, A., Savioli, L., Engels, D., Robert Bergquist, N., and Todd, M. H. (2003). Drugs for the control of parasitic diseases: current status and development in schistosomiasis. *Trends Parasitol.* 19, 509–515. doi: 10.1016/j.pt.2003.09.005

Gaber, D. A., Wassef, R. M., El-Ayat, W. M., El-Moazen, M. I., Montasser, K. A., Swar, S. A., et al. (2020). Role of a schistosoma haematobium specific microRNA as a predictive and prognostic tool for bilharzial bladder cancer in Egypt. *Sci. Rep.* 10:18844. doi: 10.1038/s41598-020-74807-1

Gilles, M. E., and Slack, F. J. (2018). Let-7 microRNA as a potential therapeutic target with implications for immunotherapy. *Expert Opin. Ther. Targets* 22, 929–939. doi: 10.1080/14728222.2018.1535594

Gomes, M. S., Cabral, F. J., Jannotti-Passos, L. K., Carvalho, O., Rodrigues, V., Baba, E. H., et al. (2009). Preliminary analysis of miRNA pathway in *Schistosoma mansoni*. *Parasitol. Int.* 58, 61–68.

Gryseels, B., Polman, K., Clerinx, J., and Kestens, L. (2006). Human schistosomiasis. *Lancet* 368, 1106–1118.

Han, H., Peng, J., Hong, Y., Zhang, M., Han, Y., Liu, D., et al. (2013b). MicroRNA expression profile in different tissues of BALB/c mice in the early phase of *Schistosoma japonicum* infection. *Mol. Biochem. Parasitol.* 188, 1–9. doi: 10.1016/j.molbiopara.2013.02.001

Han, H., Peng, J., Hong, Y., Zhang, M., Han, Y., Fu, Z., et al. (2013a). Comparison of the differential expression miRNAs in Wistar rats before and 10 days after *S.japonicum* infection. *Parasit. Vectors* 6:120. doi: 10.1186/1756-3305-6-120

Han, Y., Feng, J., Ren, Y., Wu, L., Li, H., Liu, J., et al. (2020). Differential expression of microRNA between normally developed and underdeveloped female worms of *Schistosoma japonicum*. *Vet. Res.* 51:126. doi: 10.1186/s13567-020-00851-4

Hansen, E. P., Fromm, B., Andersen, S. D., Marcilla, A., Andersen, K. L., Borup, A., et al. (2019). Exploration of extracellular vesicles from *Ascaris suum* provides evidence of parasite-host cross talk. *J. Extracell. Vesicles* 8:1578116.

He, X., Sai, X., Chen, C., Zhang, Y., Xu, X., Zhang, D., et al. (2013). Host serum miR-223 is a potential new biomarker for *Schistosoma japonicum* infection and the response to chemotherapy. *Parasit. Vectors* 6:272. doi: 10.1186/1756-3305-6-272

He, X., Xie, J., Wang, Y., Fan, X., Su, Q., Sun, Y., et al. (2018b). Down-regulation of microRNA-203-3p initiates type 2 pathology during schistosome infection *via* elevation of interleukin-33. *PLoS Pathog.* 14:e1006957. doi: 10.1371/journal.ppat.1006957

He, X., Sun, Y., Lei, N., Fan, X., Zhang, C., Wang, Y., et al. (2018a). MicroRNA-351 promotes schistosomiasis-induced hepatic fibrosis by targeting the vitamin D receptor. *Proc. Natl. Acad. Sci. U.S.A.* 115, 180–185. doi: 10.1073/pnas.1715965115

He, X., Tang, R., Sun, Y., Wang, Y. G., Zhen, K. Y., Zhang, D. M., et al. (2016). MicroR-146 blocks the activation of M1 macrophage by targeting signal transducer and activator of transcription 1 in hepatic schistosomiasis. *EBioMedicine* 13, 339–347. doi: 10.1016/j.ebiom.2016.10.024

He, X., Wang, Y., Fan, X., Lei, N., Tian, Y., Zhang, D., et al. (2020). A schistosome miRNA promotes host hepatic fibrosis by targeting transforming growth factor beta receptor III. *J. Hepatol.* 72, 519–527. doi: 10.1016/j.jhep.2019.10.029

He, X., Xie, J., Zhang, D., Su, Q., Sai, X., Bai, R., et al. (2015). Recombinant adeno-associated virus-mediated inhibition of microRNA-21 protects mice against the lethal schistosome infection by repressing both IL-13 and transforming growth factor beta 1 pathways. *Hepatology* 61, 2008–2017. doi: 10.1002/hep.27671

Hu, C., Li, Y., Pan, D., Wang, J., Zhu, L., Lin, Y., et al. (2021). A *Schistosoma japonicum* MicroRNA exerts antitumor effects through inhibition of both cell

migration and angiogenesis by targeting PGAM1. *Front. Oncol.* 11:652395. doi: 10.3389/fonc.2021.652395

Hu, C., Zhu, S., Wang, J., Lin, Y., Ma, L., Zhu, L., et al. (2019). *Schistosoma japonicum* MiRNA-7-5p inhibits the growth and migration of hepatoma cells *via* cross-species regulation of S-phase kinase-associated protein 2. *Front Oncol* 9:175.

Huang, Y., Fan, X., Tao, R., Song, Q., Wang, L., Zhang, H., et al. (2018). Effect of miR-182 on hepatic fibrosis induced by *Schistosomiasis japonica* by targeting FOXO1 through PI3K/AKT signaling pathway. *J. Cell Physiol.* 233, 6693–6704. doi: 10.1002/jcp.26469

Jiang, P., Wang, J., Zhu, S., Hu, C., Lin, Y., and Pan, W. (2022). Identification of a *Schistosoma japonicum* MicroRNA that suppresses hepatoma cell growth and migration by targeting host FZD4 gene. *Front. Cell Infect. Microbiol.* 12:786543. doi: 10.3389/fcimb.2022.786543

Karanja, D. M., Boyer, A. E., Strand, M., Colley, D. G., Nahlen, B. L., Ouma, J. H., et al. (1998). Studies on schistosomiasis in western Kenya: II. Efficacy of praziquantel for treatment of schistosomiasis in persons coinfected with human immunodeficiency virus-1. *Am. J. Trop. Med. Hyg.* 59, 307–311. doi: 10.4269/ajtmh.1998.59.307

Kelada, S., Sethupathy, P., Okoye, I. S., Kistasis, E., Czieso, S., White, S. D., et al. (2013). miR-182 and miR-10a are key regulators of Treg specialisation and stability during Schistosome and Leishmania-associated inflammation. *PLoS Pathog.* 9:e1003451. doi: 10.1371/journal.ppat.1003451

Kong, D., Guo, H., Lu, Z., and Cui, J. (2019). MicroRNA-21 mediates the inhibiting effect of praziquantel on NLRP3 inflammasome in *Schistosoma japonicum* infection. *Front. Vet. Sci.* 6:517. doi: 10.3389/fvets.2019.00517

Kozomara, A., Birgaoanu, M., and Griffiths-Jones, S. (2019). miRBase: from microRNA sequences to function. *Nucleic Acids Res.* 47, D155–D162. doi: 10.1093/nar/gky1141

Kunz, W. (2001). Schistosome male-female interaction: induction of germ-cell differentiation. *Trends Parasitol.* 17, 227–231. doi: 10.1016/s1471-4922(01)01893-1

Lam, H. Y. P., Huang, S. P., Liang, T. R., Wu, W. J., Cheng, P. C., Chang, K. C., et al. (2022). Increased immunogenicity and protection of recombinant Sm14 antigens by heat-killed *Cutibacterium acnes* in BALB/c mice infected with *Schistosoma mansoni*. *Parasitol. Int.* 86:102446. doi: 10.1016/j.parint.2021.102446

Layland, L. E., Rad, R., Wagner, H., and Da Costa, C. U. (2007). Immunopathology in schistosomiasis is controlled by antigen-specific regulatory T cells primed in the presence of TLR2. *Eur. J. Immunol.* 37, 2174–2184. doi: 10.1002/eji.200737063

Lee, R. C., Feinbaum, R. L., and Ambros, V. (1993). The *C. elegans* heterochronic gene lin-4 encodes small RNAs with antisense complementarity to lin-14. *Cell* 75, 843–854. doi: 10.1016/0092-8674(93)90529-y

Lewis, F. A., and Tucker, M. S. (2014). Schistosomiasis. *Adv. Exp. Med. Biol.* 766, 47–75.

Li, S., Giri, B. R., Liu, J., He, X., Cai, P., Jing, Z., et al. (2022). Characterization of MicroRNA cargo of extracellular vesicles isolated from the plasma of *Schistosoma japonicum*-infected mice. *Front. Cell Infect. Microbiol.* 12:803242. doi: 10.3389/fcimb.2022.803242

Lin, Y., Zhu, S., Hu, C., Wang, J., Jiang, P., Zhu, L., et al. (2019). Cross-species suppression of hepatoma cell growth and migration by a *Schistosoma japonicum* MicroRNA. *Mol. Ther. Nucleic Acids* 18, 400–412. doi: 10.1016/j.omtn.2019.09.006

Liu, J., Zhu, C., Shi, Y., Li, H., Wang, L., Qin, S., et al. (2012). Surveillance of *Schistosoma japonicum* infection in domestic ruminants in the Dongting Lake region, Hunan province, China. *PLoS One* 7:e31876. doi: 10.1371/journal.pone.0031876

Liu, J., Zhu, L., Wang, J., Qiu, L., Chen, Y., Davis, R. E., et al. (2019). *Schistosoma japonicum* extracellular vesicle miRNA cargo regulates host macrophage functions facilitating parasitism. *PLoS Pathog.* 15:e1007817. doi: 10.1371/journal.ppat.1007817

Liu, L., Wang, P., Wang, Y. S., Zhang, Y. N., Li, C., Yang, Z. Y., et al. (2021). MiR-130a-3p alleviates liver fibrosis by suppressing HSCs activation and skewing macrophage to Ly6C^{lo} phenotype. *Front Immunol* 12:696069. doi: 10.3389/fimmu.2021.696069

Liu, R., Zhong, Q. P., Tang, H. B., and Dong, H. F. (2022). Comparative characterization of microRNAs of *Schistosoma japonicum* from SCID mice and BALB/c mice: clues to the regulation of parasite growth and development. *Acta Trop.* 225:106200. doi: 10.1016/j.actatropica.2021.106200

Llanwarne, F., and Helmby, H. (2021). Granuloma formation and tissue pathology in *Schistosoma japonicum* versus *Schistosoma mansoni* infections. *Parasite Immunol.* 43:e12778. doi: 10.1111/pim.12778

Loverde, P. T., and Chen, L. (1991). Schistosome female reproductive development. *Parasitol. Today* 7, 303–308. doi: 10.1016/0169-4758(91)90263-n

LoVerde, P. T., Andrade, L. F., and Oliveira, G. (2009). Signal transduction regulates schistosome reproductive biology. *Curr. Opin. Microbiol.* 12, 422–428. doi: 10.1016/j.mib.2009.06.005

Lu, Z., Sessler, F., Holroyd, N., Hahnel, S., Quack, T., Berriman, M., et al. (2016). Schistosome sex matters: a deep view into gonad-specific and pairing-dependent transcriptomes reveals a complex gender interplay. *Sci. Rep.* 6:31150. doi: 10.1038/srep31150

Luo, R., Xue, X., Wang, Z., Sun, J., Zou, Y., and Pan, W. (2010). Analysis and characterization of the genes encoding the Dicer and Argonaute proteins of *Schistosoma japonicum*. *Parasit. Vectors* 3:90. doi: 10.1186/1756-3305-3-90

Luo, X., Zhang, D., Xie, J., Su, Q., He, X., Bai, R., et al. (2018). MicroRNA-96 promotes schistosomiasis hepatic fibrosis in mice by suppressing Smad7. *Mol. Ther. Methods Clin. Dev.* 11, 73–82. doi: 10.1016/j.omtm.2018.10.002

Marco, A., Kozomara, A., Hui, J. H., Emery, A. M., Rollinson, D., Griffiths-Jones, S., et al. (2013). Sex-biased expression of microRNAs in *Schistosoma mansoni*. *PLoS Negl. Trop. Dis.* 7:e2402.

McManus, D. P., Bergquist, R., Cai, P., Ranasinghe, S., Tebeje, B. M., and You, H. (2020). Schistosomiasis-from immunopathology to vaccines. *Semin. Immunopathol.* 42, 355–371.

Meningher, T., Lerman, G., Regev-Rudzki, N., Gold, D., Ben-Dov, I. Z., Sidi, Y., et al. (2017). Schistosomal MicroRNAs isolated from extracellular vesicles in sera of infected patients: a new tool for diagnosis and follow-up of human schistosomiasis. *J. Infect. Dis.* 215, 378–386. doi: 10.1093/infdis/jiw539

Miller, P., and Wilson, R. A. (1980). Migration of the schistosomula of *Schistosoma mansoni* from the lungs to the hepatic portal system. *Parasitology* 80, 267–288. doi: 10.1017/s0031182000000743

Mu, Y., Cai, P., Olveda, R. M., Ross, A. G., Olveda, D. U., and Mcmanus, D. P. (2019). Parasite-derived circulating microRNAs as biomarkers for the detection of human *Schistosoma japonicum* infection. *Parasitology* 147, 889–896. doi: 10.1017/S0031182019001690

Mu, Y., Mcmanus, D. P., Hou, N., and Cai, P. (2021b). Schistosome infection and schistosome-derived products as modulators for the prevention and alleviation of immunological disorders. *Front. Immunol.* 12:619776. doi: 10.3389/fimmu.2021.619776

Mu, Y., Mcmanus, D. P., Gordon, C. A., and Cai, P. (2021a). Parasitic helminth-derived microRNAs and extracellular vesicle cargos as biomarkers for helminthic infections. *Front. Cell Infect. Microbiol.* 11:708952. doi: 10.3389/fcimb.2021.708952

Nation, C. S., Da'dara, A. A., Marchant, J. K., and Skelly, P. J. (2020). Schistosome migration in the definitive host. *PLoS Negl. Trop. Dis.* 14:e0007951. doi: 10.1371/journal.pntd.0007951

Ondigo, B. N., Ndombi, E. M., Nicholson, S. C., Oguso, J. K., Carter, J. M., Kittur, N., et al. (2018). Functional studies of T regulatory lymphocytes in human schistosomiasis in Western Kenya. *Am. J. Trop. Med. Hyg.* 98, 1770–1781. doi: 10.4269/ajtmh.17-0966

Pearce, E. J., and MacDonald, A. S. (2002). The immunobiology of schistosomiasis. *Nat. Rev. Immunol.* 2, 499–511.

Queiroz, F. R., Silva, L. M., Jeremias, W. J., Babá, ÉH., Caldeira, R. L., Coelho, P. M. Z., et al. (2017). Differential expression of small RNA pathway genes associated with the *Biomphalaria glabrata*/*Schistosoma mansoni* interaction. *PLoS One* 12:e0181483. doi: 10.1371/journal.pone.0181483

Rodriguez, A., Vigorito, E., Clare, S., Warren, M. V., Couttet, P., Soond, D. R., et al. (2007). Requirement of bic/microRNA-155 for normal immune function. *Science* 316, 608–611. doi: 10.1126/science.1139253

Rollinson, D., Kaukas, A., Johnston, D. A., Simpson, A. J., and Tanaka, M. (1997). Some molecular insights into schistosome evolution. *Int. J. Parasitol.* 27, 11–28. doi: 10.1016/s0020-7519(96)00169-5

Romano, A., Hou, X., Sertorio, M., Dessein, H., Cabantous, S., Oliveira, P., et al. (2016). FOXP3^{+} regulatory T cells in hepatic fibrosis and splenomegaly caused by *Schistosoma japonicum*: the spleen may be a major source of tregs in subjects with splenomegaly. *PLoS Negl. Trop. Dis.* 10:e0004306.

Rouas, R., Merimi, M., Najar, M., El Zein, N., Fayyad-Kazan, M., Berehab, M., et al. (2019). Human $CD8^+$ $CD25^+$ $CD127^{low}$ regulatory T cells: microRNA signature and impact on TGF-β and IL-10 expression. *J. Cell Physiol.* 234, 17459–17472.

Schwartz, C., and Fallon, P. G. (2018). Schistosoma "Eggs-Iting" the host: granuloma formation and egg excretion. *Front. Immunol.* 9:2492. doi: 10.3389/fimmu.2018.02492

Silva-Leitão, F. W., Biolchini, C. L., Neves, R. H., and Machado-Silva, J. R. (2009). Development of *Schistosoma mansoni* in the laboratory rat analyzed by light and confocal laser scanning microscopy. *Exp. Parasitol.* 123, 292–295. doi: 10.1016/j.exppara.2009.07.016

Simões, M. C., Lee, J., Djikeng, A., Cerqueira, G. C., Zerlotini, A., Da Silva-Pereira, R. A., et al. (2011). Identification of *Schistosoma mansoni* microRNAs. *BMC Genomics* 12:47.

Stirewalt, M. A. (1974). *Schistosoma mansoni*: cercaria to schistosomule. *Adv. Parasitol.* 12, 115–182. doi: 10.1016/s0065-308x(08)60388-7

Stroehlein, A. J., Young, N. D., Korhonen, P. K., Hall, R. S., Jex, A. R., Webster, B. L., et al. (2018). The small RNA complement of adult *Schistosoma haematobium*. *PLoS Negl. Trop. Dis.* 12:e0006535. doi: 10.1371/journal.pntd.0006535

Sun, J., Wang, S., Li, C., Ren, Y., and Wang, J. (2014). Novel expression profiles of microRNAs suggest that specific miRNAs regulate gene expression for the sexual maturation of female *Schistosoma japonicum* after pairing. *Parasit. Vectors* 7:177. doi: 10.1186/1756-3305-7-177

Sun, X., Zhang, L., Jiang, Y., Li, A., Zhu, D., Wu, J., et al. (2021). The role of let-7b in the inhibition of hepatic stellate cell activation by rSjP40. *PLoS Negl. Trop. Dis.* 15:e0009472. doi: 10.1371/journal.pntd.0009472

Sun, X., Zhang, L., Wang, J., Chen, J., Zhu, D., Shen, P., et al. (2015). *Schistosoma japonicum* protein SjP40 inhibits TGF-β1-induced activation of hepatic stellate cells. *Parasitol. Res.* 114, 4251–4257. doi: 10.1007/s00436-015-4663-0

Taganov, K. D., Boldin, M. P., Chang, K. J., and Baltimore, D. (2006). NF-kappaB-dependent induction of microRNA miR-146, an inhibitor targeted to signaling proteins of innate immune responses. *Proc. Natl. Acad. Sci. U.S.A.* 103, 12481–12486. doi: 10.1073/pnas.0605298103

Tang, N., Wu, Y., Cao, W., Liang, Y., Gao, Y., Hu, L., et al. (2017). Lentivirus-mediated over-expression of let-7b microRNA suppresses hepatic fibrosis in the mouse infected with *Schistosoma japonicum*. *Exp. Parasitol.* 182, 45–53. doi: 10.1016/j.exppara.2017.09.024

Tang, Y., Shen, Y., Hong, Y., Zhang, Z., Zhai, Q., Fu, Z., et al. (2021). miR-181a regulates the host immune response against *Schistosoma japonicum* infection through the TLR4 receptor pathway. *Parasit. Vectors* 14:548. doi: 10.1186/s13071-021-05063-z

VAN Dorssen, C. F., Gordon, C. A., Li, Y., Williams, G. M., Wang, Y., Luo, Z., et al. (2017). Rodents, goats and dogs–their potential roles in the transmission of schistosomiasis in China. *Parasitology* 144, 1633–1642. doi: 10.1017/S0031182017000907

van Niel, G., D'angelo, G., and Raposo, G. (2018). Shedding light on the cell biology of extracellular vesicles. *Nat. Rev. Mol. Cell Biol.* 19, 213–228. doi: 10.1038/nrm.2017.125

Wang, J., Yu, Y., Shen, H., Qing, T., Zheng, Y., Li, Q., et al. (2017). Dynamic transcriptomes identify biogenic amines and insect-like hormonal regulation for mediating reproduction in *Schistosoma japonicum*. *Nat. Commun.* 8:14693. doi: 10.1038/ncomms14693

Wang, L., Liao, Y., Yang, R., Yu, Z., Zhang, L., Zhu, Z., et al. (2020). Sja-miR-71a in Schistosome egg-derived extracellular vesicles suppresses liver fibrosis caused by schistosomiasis *via* targeting semaphorin 4D. *J. Extracell. Vesicles* 9:1785738. doi: 10.1080/20013078.2020.1785738

Wang, Y., Fan, X., Lei, N., He, X., Wang, X., Luo, X., et al. (2020). A MicroRNA derived from *Schistosoma japonicum* promotes schistosomiasis hepatic fibrosis by targeting host secreted frizzled-related protein 1. *Front. Cell Infect. Microbiol.* 10:101. doi: 10.3389/fcimb.2020.00101

Warren, K. S., Mahmoud, A. A., Cummings, P., Murphy, D. J., and Houser, H. B. (1974). *Schistosomiasis mansoni* in Yemeni in California: duration of infection, presence of disease, therapeutic management. *Am. J. Trop. Med. Hyg.* 23, 902–909. doi: 10.4269/ajtmh.1974.23.902

Wynn, T. A., Thompson, R. W., Cheever, A. W., and Mentink-Kane, M. M. (2004). Immunopathogenesis of schistosomiasis. *Immunol. Rev.* 201, 156–167.

Xu, A., Zhong, G., Wang, J., Liu, C., Liu, Y., and Wang, W. (2021). MicroRNA 200a inhibits liver fibrosis of schistosoma. *Bioengineered* 12, 4736–4746. doi: 10.1080/21655979.2021.1950441

Xu, F., Liu, C., Zhou, D., and Zhang, L. (2016). TGF-beta/SMAD pathway and its regulation in hepatic fibrosis. *J. Histochem. Cytochem.* 64, 157–167.

Xue, X., Sun, J., Zhang, Q., Wang, Z., Huang, Y., and Pan, W. (2008). Identification and characterization of novel microRNAs from *Schistosoma japonicum*. *PLoS One* 3:e4034. doi: 10.1371/journal.pone.0004034

Yang, J., Feng, X., Fu, Z., Yuan, C., Hong, Y., Shi, Y., et al. (2012). Ultrastructural observation and gene expression profiling of *Schistosoma japonicum* derived from two natural reservoir hosts, water buffalo and yellow cattle. *PLoS One* 7:e47660. doi: 10.1371/journal.pone.0047660

Yu, J., Yu, Y., Li, Q., Chen, M., Shen, H., Zhang, R., et al. (2019). Comprehensive analysis of miRNA profiles reveals the role of *Schistosoma japonicum* miRNAs at different developmental stages. *Vet. Res.* 50:23.

Yu, X., Zhai, Q., Fu, Z., Hong, Y., Liu, J., Li, H., et al. (2019). Comparative analysis of microRNA expression profiles of adult *Schistosoma japonicum* isolated from water buffalo and yellow cattle. *Parasit. Vectors* 12:196. doi: 10.1186/s13071-019-3450-7

Zhai, Q., Fu, Z., Hong, Y., Yu, X., Han, Q., Lu, K., et al. (2018). iTRAQ-based comparative proteomic analysis of adult *Schistosoma japonicum* from water buffalo and yellow cattle. *Front. Microbiol.* 9:99. doi: 10.3389/fmicb.2018.00099

Zhao, Y., Dang, Z., and Chong, S. (2019). Mmu-miR-92a-2-5p targets TLR2 to relieve *Schistosoma japonicum*-induced liver fibrosis. *Int. Immunopharmacol.* 69, 126–135.

Zhong, H., Gui, X., Hou, L., Lv, R., and Jin, Y. (2022a). From inflammation to fibrosis: novel insights into the roles of high mobility group protein box 1 in schistosome-induced liver damage. *Pathogens* 11:289. doi: 10.3390/pathogens11030289

Zhong, H., Ren, Y., Qin, F., Li, X., Hou, L., Gu, S., et al. (2022b). *Schistosoma japonicum* translationally controlled tumor protein, which is associated with the development of female worms, as a target for control of schistosomiasis. *Int. J. Parasitol.* doi: 10.1016/j.ijpara.2022.01.005 [Epub ahead of print].

Zhu, D., He, X., Duan, Y., Chen, J., Wang, J., Sun, X., et al. (2014). Expression of microRNA-454 in TGF-β1-stimulated hepatic stellate cells and in mouse livers infected with *Schistosoma japonicum*. *Parasit. Vectors* 7:148. doi: 10.1186/1756-3305-7-148

Zhu, D., Yang, C., Shen, P., Chen, L., Chen, J., Sun, X., et al. (2018b). rSjP40 suppresses hepatic stellate cell activation by promoting microRNA-155 expression and inhibiting STAT5 and FOXO3a expression. *J. Cell Mol. Med.* 22, 5486–5493. doi: 10.1111/jcmm.13819

Zhu, D., Lyu, L., Shen, P., Wang, J., Chen, J., Sun, X., et al. (2018a). rSjP40 protein promotes PPARγ expression in LX-2 cells through microRNA-27b. *Faseb J.* 32, 4798–4803. doi: 10.1096/fj.201700520RR

Zhu, L., Dao, J., Du, X., Li, H., Lu, K., Liu, J., et al. (2015). Altered levels of circulating miRNAs are associated *Schistosoma japonicum* infection in mice. *Parasit. Vectors* 8:196. doi: 10.1186/s13071-015-0806-5

Zhu, L., Zhao, J., Wang, J., Hu, C., Peng, J., Luo, R., et al. (2016). MicroRNAs are involved in the regulation of ovary development in the pathogenic blood fluke *Schistosoma japonicum*. *PLoS Pathog.* 12:e1005423.

Zhu, S., Wang, S., Lin, Y., Jiang, P., Cui, X., Wang, X., et al. (2016). Release of extracellular vesicles containing small RNAs from the eggs of *Schistosoma japonicum*. *Parasit. Vectors* 9:574. doi: 10.1186/s13071-016-1845-2

Conflict of Interest: The authors declare that the research was conducted in the absence of any commercial or financial relationships that could be construed as a potential conflict of interest.

frontiers | Frontiers in Microbiology

ORIGINAL RESEARCH
published: 10 June 2022
doi: 10.3389/fmicb.2022.913650

Co-existence of Multiple *Anaplasma* Species and Variants in Ticks Feeding on Hedgehogs or Cattle Poses Potential Threats of Anaplasmosis to Humans and Livestock in Eastern China

Yong Qi[1,2†], *Lele Ai*[1,2†], *Changqiang Zhu*[1,2,3], *Yongfeng Lu*[4], *Ruichen Lv*[1,2], *Yingqing Mao*[1,2], *Nianhong Lu*[1,2] *and Weilong Tan*[1,2*]

[1] *Huadong Research Institute for Medicine and Biotechniques, Nanjing, China,* [2] *Nanjing Bioengineering (Gene) Technology Center for Medicines, Nanjing, China,* [3] *Institute of Rocket Force Medicine, State Key Laboratory of Trauma, Burns and Combined Injury, Army Medical University, Chongqing, China,* [4] *Administration for Drug and Instrument Supervision and Inspection of PLAJLSF, Beijing, China*

Background: *Anaplasma* spp., causative agents of anaplasmosis, pose significant a threat to public health and economic losses in livestock farming. Co-infections/co-existence of various *Anaplasma* spp. may facilitate pathogen interactions and the emergence of novel variants, represent potential dangers to public health and economic losses from livestock farming, and raise challenges of detection and diagnosis. The information regarding co-infection/co-existence of *Anaplasma* in their vector ticks and wild animals is limited and needs urgent investigation.

Methods: Wild hedgehogs and ticks from hedgehogs and cattle were collected from Jiangsu province, Eastern China, and DNA was extracted from hedgehog organs and tick homogenates. Various genera of species-specific polymerase chain reaction (PCR) or nested PCR amplifications targeting 16S ribosomal RNA (*rrs*), *msp4*, or *groEL* gene coupled with sequencing were conducted to identify *Anaplasma* spp.

Results: *Anaplasma phagocytophilum* (1, 0.6%), *A. marginale* (2, 1.2%), *A. platys* variants xyn10pt-1 (13, 7.7%), xyn21pt-2 (3, 1.8%), and xyn3pt-3 (3, 1.8%), *A. bovis* variant cwp72bo-1 (12, 7.1%), and a novel *Candidatus* Cryptoplasma sp. (1, 0.6%) were identified in 168 *Haemaphysalis longicornis* ticks from cattle. *A. platys* variant xyn10pt-1 (20, 11.4%) and *A. bovis* variants cwp72bo-1 (12, 6.9%) and cwp55-36bo-2 (1, 0.6%) were detected in 173 *H. flava* ticks from hedgehogs. However, only *A. bovis* variant cwp72bo-1 (15, 46.7%) was identified in 32 *Erinaceus amurensis* hedgehogs. Various co-existence combinations were found only in ticks.

Conclusion: The co-existence of various *Anaplasma* spp. and variants in *H. flava* and *H. longicornis* was detected for the first time in the world. The high infection rate of *A. bovis* in hedgehogs and its moderate infection rate in their parasitic ticks suggest that *Er. amurensis* hedgehog could be an important reservoir of *A. bovis*, rather than *A. platys*.

OPEN ACCESS

Edited by:
Wei Wang,
Jiangsu Institute of Parasitic Diseases (JIPD), China

Reviewed by:
Jun Jiao,
Beijing Institute of Microbiology and Epidemiology, China
Algimantas Paulauskas,
Vytautas Magnus University, Lithuania
Sun Tee Tay,
University of Malaya, Malaysia
Bohai Wen,
Beijing Institute of Microbiology and Epidemiology, China

***Correspondence:**
Weilong Tan
mosquito_2008@126.com

[†] These authors have contributed equally to this work

Specialty section:
This article was submitted to Infectious Agents and Disease, a section of the journal Frontiers in Microbiology

Received: *06 April 2022*
Accepted: *02 May 2022*
Published: *10 June 2022*

Citation:
Qi Y, Ai L, Zhu C, Lu Y, Lv R, Mao Y, Lu N and Tan W (2022) Co-existence of Multiple Anaplasma Species and Variants in Ticks Feeding on Hedgehogs or Cattle Poses Potential Threats of Anaplasmosis to Humans and Livestock in Eastern China. Front. Microbiol. 13:913650. doi: 10.3389/fmicb.2022.913650

Horizontal transmission of *Anaplasma* spp. may exist among different tick species *via* their shared hosts in the investigated area. This study provided epidemiological data that could be crucial for strategy development for early warning, prevention, and control of potential *Anaplasma* infections.

Keywords: *Anaplasma*, co-infection, co-existence, hedgehogs, ticks, *Erinaceus amurensis*

INTRODUCTION

Anaplasma spp. are causative agents of anaplasmosis, with a significant impact on the health of a number of animals and human species, as well as economic losses in livestock farming systems (Battilani et al., 2017). Traditionally, the genus *Anaplasma* includes pathogenic *Anaplasma phagocytophilum*, *A. bovis*, *A. ovis*, *A. platys*, *A. marginale*, and *A. centrale*, in which the first four species can infect both humans and animals, while the remaining two are of veterinary importance, according to published evidence (Battilani et al., 2017; Lu et al., 2019). Tick-borne pathogens (TBPs) have attracted scholars' attention in molecular epidemiology, genetics, and pathobiology, leading to the discovery of novel species, such as *A. capra* and *A. odocoilei* (Tate et al., 2013; Li et al., 2015).

To date, ticks have been found to acquire various pathogenic species, such as parasites (*Babesia* spp.), bacteria (*Borrelia* spp., *Coxiella* spp., *Anaplasma* spp., *Ehrlichia* spp., and *Francisella* spp.), or viruses (tick-borne encephalitis virus and other tick-borne flaviviruses/phleboviruses), and multiple TBPs have been reported to co-exist within the same tick, which is not very surprising considering their great varieties (Cutler et al., 2021). Co-infections/co-existence of various TBPs may pose more potential health risks to humans and animals, raise the challenge of target pathogen detection and disease diagnosis, and facilitate pathogen interactions, resulting in potential recombination and novel mutant emergence. Previous studies aimed to provide valuable insights into co-infection (Cutler et al., 2021), and they mainly concentrated on the co-infection of TBPs with different genera. Co-infection of different *Anaplasma* spp. in domestic animals has been reported in several studies (Liu et al., 2012; Koh et al., 2018; Yang et al., 2020; Miranda et al., 2021), while there is a lack of information regarding *Anaplasma* co-infection/co-existence in their vector ticks and wild hedgehogs. Therefore, in the present study, we aimed to assess the prevalence and co-existence of various *Anaplasma* spp. or variants circulating in ticks feeding on cattle or wild hedgehogs, as well as their hedgehog hosts in Eastern China to provide epidemiological data to develop strategies for prevention and control of anaplasmosis.

MATERIALS AND METHODS

Tick and Hedgehog Samples

Thirty-two hedgehogs were collected from several villages near Tieshan Temple (E 118°29' 6", N 32°43' 55") in Xuyi County, Jiangsu province, China, from May 2019 to October 2020. All of the hedgehog samples were road-killed or killed by domestic or stray dogs within 24 h of our obtaining them. After the collection of the ticks, the hedgehogs were immediately dissected for their hearts, livers, spleens, lungs, kidneys, brains, and intestines, and the specimens were stored at −80°C. In addition, ticks were also collected from 30 cattle from a farm located near the same sampling site.

In total, 341 ticks, including 173 adults from the hedgehogs and 168 adults from cattle, were collected and stored in tubes containing 70% ethanol. All the ticks were collected if the animal carried no more than 10 ticks; otherwise, 10 ticks were randomly collected from different parts of their bodies. The collected hedgehogs and ticks were first identified by their morphological features, as described previously (Feng, 1983), with an additional classification using a molecular method, as described below.

The Ethics Committee approved the animal experiments of the Huadong Research Institute for Medicine and Biotechniques. The animal care and treatment met the standards of the committee, with all efforts made to minimize the suffering of animals. Written informed consent was obtained from the cattle owners for the participation of their animals in the present study.

DNA Purification

After twice washing with sterile phosphate-buffered saline (PBS), the ticks were individually homogenized in 1,000 μL of PBS using glass homogenizers. DNA from 200 μL of each tick homogenate or 10–30 mg of each hedgehog organ sample was extracted with a commercial DNeasy Blood & Tissue kit (Qiagen, Hilden, Germany), according to the manufacturer's instructions. The purified DNA was subsequently stored at −20°C before use.

PCR Amplification and Sequencing

The Premix Ex Taq Version 2.0 kit (Takara, Beijing, China) was employed for the polymerase chain reaction (PCR) amplification, with 1 μL of the template and 1 μL of each primer (10 nM) used in each reaction. Molecular identification of each hedgehog or tick species was performed by amplifying the sequences of the mitochondrial 16S ribosomal RNA gene, as described previously (Sarri et al., 2014; Liu et al., 2016).

For screening *Anaplasma*-positive samples, a set of nested PCR primers (**Table 1**) targeting a short sequence of the 16S ribosomal RNA (*rrs*) gene with a length of about 280 bp was used, as previously described (Wen et al., 2003; Jiao et al., 2021). The amplified products were analyzed with 1.5% agarose gel electrophoresis and detected with GelStain Dye (Transgene, Beijing, China) under ultraviolet (UV) light. PCR products with expected sizes were excised from gels, extracted with a Gel Extraction kit (Sangon, Shanghai, China), and sequenced by Sangon Biotech Co., Ltd. (Shanghai, China). All the sequencing data were analyzed using SnapGene software (from Insightful Science; available at SnapGene.com). The obtained sequences

TABLE 1 | Primers used for PCR amplification in the present study.

Target	Primer names	Nucleotide sequence (5′-3′)	Expected length (bp)	Annealing temperatures (°C)
Anaplasma genus (*rrs* gene)	Eh-out1	TTGAGAGTTTGATCCTGGCTCAGAACG	660	55
	Eh-out2	CACCTCTACACTAGGAATTCCGCTATC		
	Eh-gs1	GTAATAACTGTATAATCCCTG	280	55
	Eh-gs2	GTACCGTCATTATCTTCCCTA		
Anaplasma spp. (*rrs* gene)	An16S1	GTCACTGACCCAACCTTAAATGGCTGC	1,432	51
	An16S2	ATCCTGGCTCAGAACGAACGCTGG		
	An16S3	GCGCCCTTCCGTTAAGAAGGATCTA	930	54
	An16S4	AGCTTAACACATGCAAGTCGAACGGA		
Four *Anaplasma* spp. (*rrs* gene, 1st)	AnU1F	AAGCTTAACACATGCAAGTCGAA	1,400	56
	AnU1R	AGTCACTGACCCAACCTTAAATG		
A. phagocytophilum (*rrs* gene, 2nd)	Anph2F	GTCGAACGGATTATTCTTTATAGCTTGC	926	56
	Anph2R	CCCTTCCGTTAAGAAGGATCTAATCTCC		
A. platys (*rrs* gene, 2nd)	Anpt2F	GATTTTTGTCGTAGCTTGCTATG	680	55
	Anpt2R	TAGCACTCATCGTTTACAGC		
A. centrale (*rrs* gene, 2nd)	Anct2F	CTGCTTTTAATACTGCAGGACTA	426	55
	Anct2R	ATGCAGCACCTGTGYGAGG		
A. bovis (*rrs* gene, 2nd)	Anbo2F	CTCGTAGCTTGCTATGAGAAC	551	55
	Anbo2R	TCTCCCGGACTCCAGTCTG		
A. ovis (*msp4* gene)	AnovMSP45	GGGAGCTCCTATGAATTACAGAGAATTGTTTAC	852	60
	AnovMSP43	CCGGATCCTTAGCTGAACAGGAATCTTGC		
A. centrale and *A. marginale* discrimination (*groEL* gene)	ACM1F	GCGCATTCTGGAGGCTG	1,479	55
	ACM1R	GACACAGCCAAGTCAAACGC		
	ACM2F	AATGAAGCGTGAAGTGGC	848	55
	ACM2R	GTACCACGCCTTCCTCAA		
Ticks (large subunit ribosomal RNA gene)	TickHF	GGTATTTTGACTATACAAAGGTATTG	278	54
	TickHR	TTATTACGCTGTTATCCCTAGAGTATT		

First, the primer pair used in the first round for the amplification of the 16S rRNA gene shared by all the four Anaplasma spp., including A. phagocytophilum, A. platys, A. centrale, and A. bovis. Second, species-specific primer sets were used in the second round for the amplification of the 16S rRNA gene of the four Anaplasma spp.

were aligned using the BLAST search engine (https://blast.ncbi.nlm.nih.gov) to confirm the *Anaplasma*-positive samples.

All the *Anaplasma*-positive samples were submitted for amplification for species identification using nested PCR targeting a longer sequence of the *rrs* gene about 930 bp as described previously (Barlough et al., 1996), with primers modified and optimized for the samples according to the former alignment results (**Table 1**). Moreover, to confirm the presence of multiple *Anaplasma* spp. in each sample, four different nested PCRs targeting the *rrs* gene of *A. phagocytophilum*, *A. platys*, *A. centrale*, and *A. bovis* were conducted for each sample, as previously described (Miranda et al., 2021). The same primer pairs were shared in the first round, and species-specific primer pairs were used in the second round (**Table 1**). In addition, the major surface protein 4 (*msp4*) gene was amplified to detect the presence of *A. ovis*, th and the *groEL* gene was amplified to distinguish *A. centrale* and *A. marginale*, as previously described with some modifications in primers (**Table 1**) (Byaruhanga et al., 2018; Miranda et al., 2021). In each PCR experiment, sterile distilled water and corresponding pathogen DNA samples were used as negative and positive control templates, respectively. The amplified products were sequenced on both strands by Sangon Biotech Co., Ltd. The PCR amplification for the samples to be sequenced was conducted in duplicate.

Phylogenetic Analysis

The sequencing data were first analyzed using SnapGene software for quality evaluation and nucleotide sequence acquisition. The primer sequences were removed from both ends of the obtained sequences for subsequent alignment searches in GenBank using the BLAST search engine (https://blast.ncbi.nlm.nih.gov/Blast.cgi). Sequences, especially from available whole genomes in the GenBank database, with high homology, were selected for multiple sequence alignment using the ClustalW multiple alignment tool in MEGA 7.0 software. Phylogenetic analysis was conducted using MEGA 7.0 software, according to the maximum likelihood method with the Kimura two-parameter distance model and a bootstrap value of 1,000.

Statistical Analysis

The positive rates of *Anaplasma* or the co-existence of various species/variants in different species of ticks feeding on hedgehogs or cattle were statistically analyzed using the Chi-square test,

the continuity-adjusted Chi-square test, or Fisher's exact test according to the number of samples (n) and theoretical frequencies (T) using an online tool (available at http://quantpsy.org). $P < 0.05$ was considered statistically significant.

Nucleotide Sequence Accession Numbers

The generated nucleotide sequences obtained in the present study were presented in **Supplementary Table 1** and deposited into the GenBank database under accession numbers ranging from ON152887 to ON152896 and ON016525 to ON016529.

RESULTS

Tick and Animal Taxonomic Classification

The hedgehogs were identified as *Erinaceus amurensis* by showing the highest nucleotide similarity (96.98%) of the amplified partial mitochondrial 16S ribosomal RNA gene sequences (Accession no. ON016529) with *Er. amurensis* in the GenBank database (Accession no. KX964606).

Similarly, the obtained mitochondrial 16S ribosomal RNA gene sequences from all the tick samples were aligned by the BLAST search engine, and tick species were identified. Among the 173 adult ticks collected from hedgehogs, 167 were determined to be *Haemaphysalis flava* (Accession nos. ON016525 to ON016528), and the other six were *H. longicornis* (Accession no. ON152895), while in the 168 ticks collected from cattle, one adult tick was identified to be *H. flava*, 15 adults were determined to be *Rhipicephalus microplus*, and the remaining 152 adults were *H. longicornis*. The predominant species of ticks harbored by hedgehogs and cattle were statistically different ($\chi 2 = 295$, $P < 0.001$).

Identification of *Anaplasma* spp. or Variants

The original sequencing data of each sample were analyzed with SnapGene software, and overlapping peaks were found in a few ticks (**Figure 1**), indicating the co-existence of various *Anaplsama* species in these samples. Thus, for each sample, various primer sets targeting the *rrs* gene were used to identify its containing *Anaplasma* spp. or variants.

Overall, 3, 2, 1, 1, and 1 representative partial *rrs* gene sequences of *A. platys* (Accession nos. ON152888 to ON152890), *A. bovis* (Accession nos. ON152887 and ON152893), *A. phagocytophilum* (Accession no. ON152891), *A. marginale* (Accession no. ON152892), and *Candidatus* Cryptoplasma sp. (Accession no. ON152894) were identified, respectively (**Figure 2**), of which six covered the similar position of the *rrs* gene and were phylogenetically analyzed together, as shown in **Figure 2**. The other two sequences, covering a relatively shorter part of *rrs*, were individually analyzed (**Supplementary Figures 1, 2**).

Analysis based on the partial 16S rRNA gene fragments revealed the presence of two distinct strains of *A. bovis*, namely variants cwp72bo-1 and cwp55-36bo-2, and three distinct strains of *A. platys*, including variants xyn10pt-1, xyn21pt-2, and xyn3pt-3. *A. bovis* variant cwp72bo-1 shared an identity rate of 100%, with the *A. bovis* (formerly named *Ehrlichia bovis*) sequence (Accession no. U03775) submitted by an institute from South Africa, while variant cwp55-36bo-2 (**Supplementary Figure 1**) shared an identity rate of 98.68% with this sequence. *A. platys* variants xyn10pt-1 and xyn21pt-2 showed the highest homology (identity rates of 100 and 99.87%, respectively) with the corresponding sequences (Accession nos. KU586031 and KU586168) identified in mosquitos in Wuhan, China, while the variant xyn3pt-3 sequence shared an identity rate of 100% with that of dozens of *A. platys* isolates or strains in the GenBank database. The identified *A. phagocytophilum* (xyn32ph-1 in **Figure 1**) sequence showed identity rates of 98.04–99.88% with those of various *A. phagocytophilum* strains or isolates in the GenBank database, indicating that it is a novel variant. The sequence xyn10ma-1 showed identity rates of 98.58–100% with *A. marginale* and 99.61–100% with its former subspecies, *A. centrale*. Therefore, a partial sequence of the *groEL* gene was amplified for further genotyping of this isolate. As a result, the sequence (Accession no. ON152896) shared an identity rate of 100% with various strains or isolates of *A. marginale*. The maximum identity rate was 98.89% with *A. centrale* strains or isolates, indicating that it belongs to *A. marginale*.

The short partial *rrs* gene sequence xyn113cr-1 revealed that this species was different from other *Anaplasma* spp. based on the highest identity rate of 97.08% with any variant of *Anaplasma* spp. (*A. phagocytophilum* strain Shandong JN59, Accession no. KY242454), while it showed a higher identity rate of 98.33% with 4 *Candidatus* Cryptoplasma sp. isolates (Accession nos. MG924904, KP276587, KP276585, and MW900167). The phylogenetic analysis (**Supplementary Figure 2**) showed that the sequence xyn113cr-1 and the *Candidatus* Cryptoplasma sp. isolates formed a separate clade on the phylogenetic tree with *Anaplasma* spp., which was distinct from the clade formed by *Ehrlichia* spp. and *Candidatus* Neoehrlichia spp., indicating that it belongs to the novel genus described previously by Eshoo et al. (2015). However, it was not clustered with these *Candidatus* Cryptoplasma sp. isolates (bootstrap support of 97%, **Supplementary Figure 2**), and the divergence between the sequence xyn113cr-1 and these *Candidatus* Cryptoplasma sp. isolates was greater than most of the variations between species within the genus *Anaplasma*, *Ehrlichia*, or '*Candidatus* Neoehrlichia', thereby providing strong phylogenetic evidence for the recognition of a novel *Candidatus* Cryptoplasma sp.

Prevalence of *Anaplasma* spp. or Variants in Individual Ticks and Hedgehogs

The presence of *Anaplasma* spp. in each sample was detected by nested PCR combined with sequencing. As a result, 15.0% (26/173) of ticks from hedgehogs and 7.7% (13/168) of ticks from cattle were positive, with a statistically significant difference ($\chi 2=4.3$, $P<0.05$). In the present study, all the *Anaplasma*-positive ticks from hedgehogs were *H. flava*, and those from cattle were *H. longicornis*. In contrast, the differences in positive rates between *H. flava* and *H. longicornis* from hedgehogs or between *H. longicornis* and non-*H. longicornis* from cattle were not statistically significant ($P > 0.05$). In hedgehogs, 43.8%

FIGURE 1 | Typical co-infection with various *Anaplasma* spp. are indicated by overlapping in the sequencing analysis with SnapGene software. The overlapping peaks are indicated by black arrows.

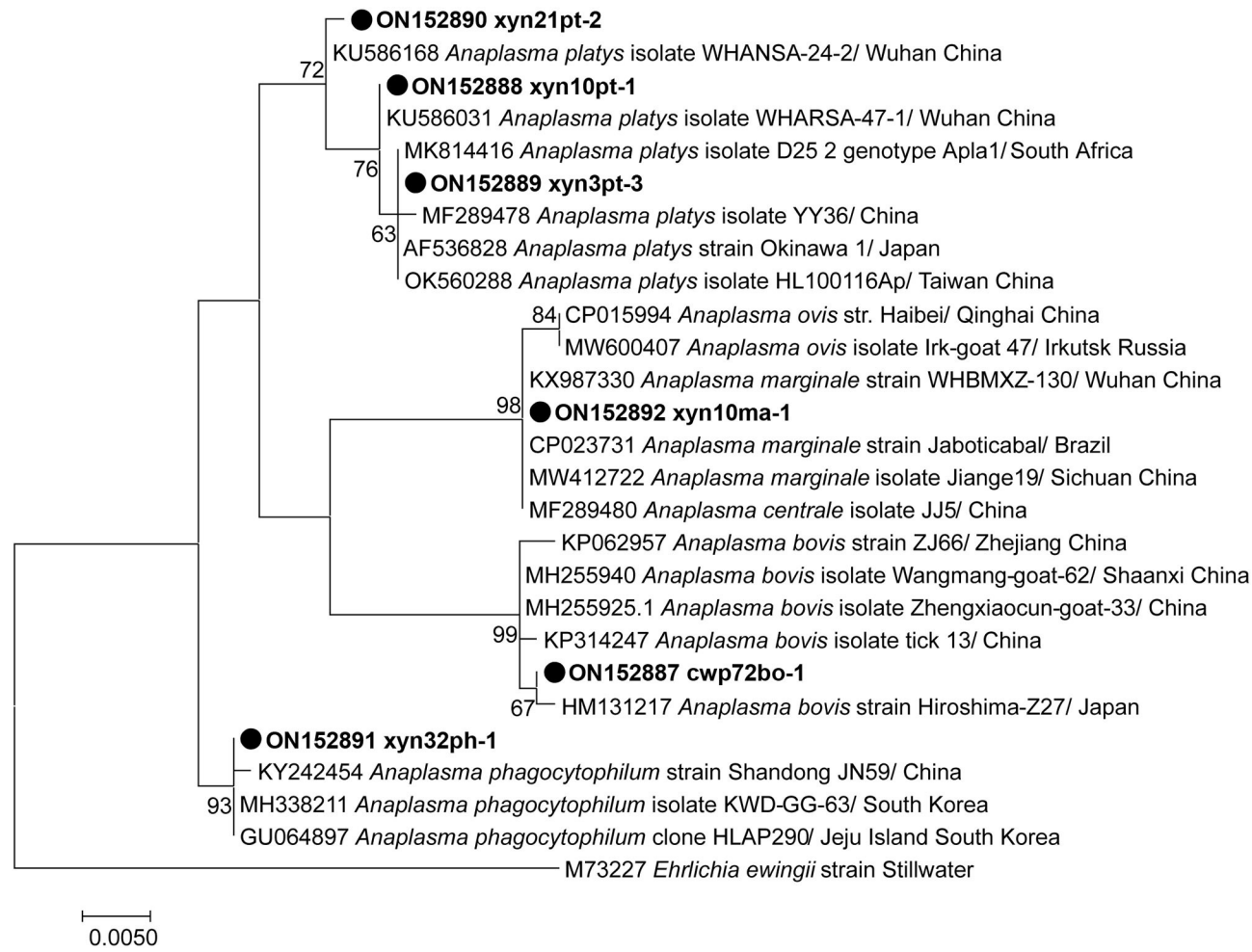

FIGURE 2 | Phylogenetic tree of *Anaplasma* species based on partial *rrs* gene sequence. The sequences obtained in this study are indicated with black dots. The phylogenetic tree was generated using the maximum likelihood method with 1,000 replicates for bootstrap testing in MEGA 7.0 software. Only bootstrap values > 50% are shown. The scale bar indicates nucleotide substitutions per site. The species, locations, and GenBank accession numbers of the reference sequences are shown in each line.

(14/32) were *Anaplasma*-positive, which was significantly higher than that in their parasitic ticks ($\chi 2 = 14.2$, $P < 0.001$). Different positive rates were found in different organs. Briefly, *Anaplasma* spp. was detected in 0% (0/32) of the brain samples, 25% (8/32) of the spleen samples, 25% (8/32) of the lung samples, 18.8% (6/32) of the liver samples, 15.6% (5/32) of the heart samples,

12.5% (4/32) of the intestine samples, and 9.4% (3/32) of the kidney samples.

The predominant *Anaplasma* spp. variants were *A. bovis* variant cwp72bo-1 (both in ticks and hedgehogs) and *A. platys* variant xyn10pt-1 (in ticks). In general, the *A. bovis* variant cwp72bo-1-positive samples accounted for 100% (14/14), 76.9% (20/26), and 92.3% (12/13) of the total *Anaplasma*-positive hedgehogs, ticks feeding on hedgehogs, and ticks feeding on cattle, respectively; the *A. platys* variant xyn10pt-1-positive samples accounted for 46.2% (12/26) and 100% (13/13) of the total *Anaplasma*-positive ticks feeding on hedgehogs and cattle, respectively. The *A. bovis* variant cwp55-36bo-2 was only found in one tick from hedgehogs, while *A. platys* variants xyn21pt-2 and xyn3pt-3, *A. marginale*, *A. phagocytophilum*, and *Candidatus* Cryptoplasma sp., were found in 3, 3, 4, 1, and 1 tick from cattle, respectively.

Co-existence of *Anaplasma* spp. or Variants in Individual Ticks and Hedgehogs

In hedgehogs, co-infection/co-existence of various *Anaplasma* spp. or variants was not observed, and only *A. bovis* variant cwp72bo-1 was identified (**Table 2**). However, in the hedgehog-attached ticks, *A. platys* variant xyn10pt-1 and the 2 *A. bovis* variants were detected, in which co-existence of these 3 *Anaplasma* spp. or variants was found in one tick, and co-existence of *A. platys* variant xyn10pt-1 and *A. bovis* variant cwp72bo-1 was observed in five ticks.

In ticks from cattle, the co-existence of various *Anaplasma* spp. or variants was more complicated. As indicated in **Table 2**, single existence or quintuple co-existence of *Anaplasma* spp. or variants was rarely observed (in one tick individually), while triple and dual-existences were frequently detected (in five and four ticks, respectively). Surprisingly, the co-existence of up to three different *A. platys* variants in one tick was also observed.

In all the ticks with co-existence, whether from hedgehogs or cattle, *A. bovis* variant cwp72bo-1 and *A. platys* variant xyn10pt-1 were identified. In *Anaplasma*-positive samples, significantly more co-existence was found in ticks from cattle than in those from hedgehogs ($\chi 2 = 14.0$, $P < 0.001$).

TABLE 2 | Co-existence/co-infections of various *Anaplasma* spp. or variants in various samples.

***Anaplasma* spp. or variants**	**Number of individuals positive for single and co-infections/co-existence**		
	Ticks from hedgehogs ($n = 175$)	**Hedgehogs ($n = 30$)**	**Ticks from cattle ($n = 168$)**
Quintuple	0	0	1
A. bovis cwp72bo-1, *A. platys* xyn10pt-1, *A. platys* xyn21pt-2, *A. marginale*, and *A. phagocytophilum*	0	0	1
Quadruple	0	0	2
A. bovis cwp72bo-1, *A. platys* xyn10pt-1, *A. platys* xyn21pt-2, and *A. platys* xyn3pt-3	0	0	2
Triple	1	0	5
A. bovis cwp72bo-1, *A. platys* xyn10pt-1, and *A. marginale*	0	0	3
A. bovis cwp72bo-1, *A. platys* xyn10pt-1, and *A. platys* xyn3pt-3	0	0	1
A. bovis cwp72bo-1, *A. platys* xyn10pt-1, and *Candidatus* Cryptoplasma sp.	0	0	1
A. bovis cwp72bo-1, *A. bovis* cwp55-36bo-2, and *A. platys* xyn10pt-1	1	0	0
Double	5	0	4
A. bovis cwp72bo-1, and *A. platys* xyn10pt-1,	5	0	4
Single	20	0	1
A. platys xyn10pt-1	6	0	1
A. bovis cwp72bo-1	14	14	0
None	149	16	155

DISCUSSION

In this study, the main parasitic ticks of hedgehogs and cattle were *H. flava* and *H. longicornis*, respectively, while only 0.6% of the cattle-attached ticks were *H. flava*, and 3.5% of the hedgehog-attached ticks were *H. longicornis* (**Figure 3**). The predominance of *H. flava* in hedgehogs was also observed in Central China, where all the 125 ticks collected from hedgehogs were *H. flava* (Fang et al., 2021). Several genera of ticks have their own set of preferred hosts, and the associations of ticks with their hosts indicate their roles in TBP circulation (Islam et al., 2006; Spengler and Estrada-Peña, 2018). Therefore, to some extent, the acquisition of epidemiological information on hosts and their predominantly parasitic tick species, as well as the fact that TBPs that harbor and transmit, may be advantageous for the development of prevention and control strategies for tick-borne diseases (Chisu et al., 2020; Song et al., 2021).

With increasing awareness about TBPs, the co-infections/co-existence of multiple pathogens in ticks or their hosts have greatly attracted scholars' attention (Cutler et al., 2021; Fang et al., 2021; Jiao et al., 2021; Soong and Dong, 2021). *Anaplasma* spp. are tick-transmitted obligate intracellular bacteria that may infect numerous wild and domestic animals and humans through tick biting. Hedgehogs have been suggested to be an appropriate reservoir for some *Anaplasma* spp. (Silaghi et al., 2012; Jahfari et al., 2017; Khodadadi et al., 2021), and their harboring TBPs are more easily transmitted to domestic animals

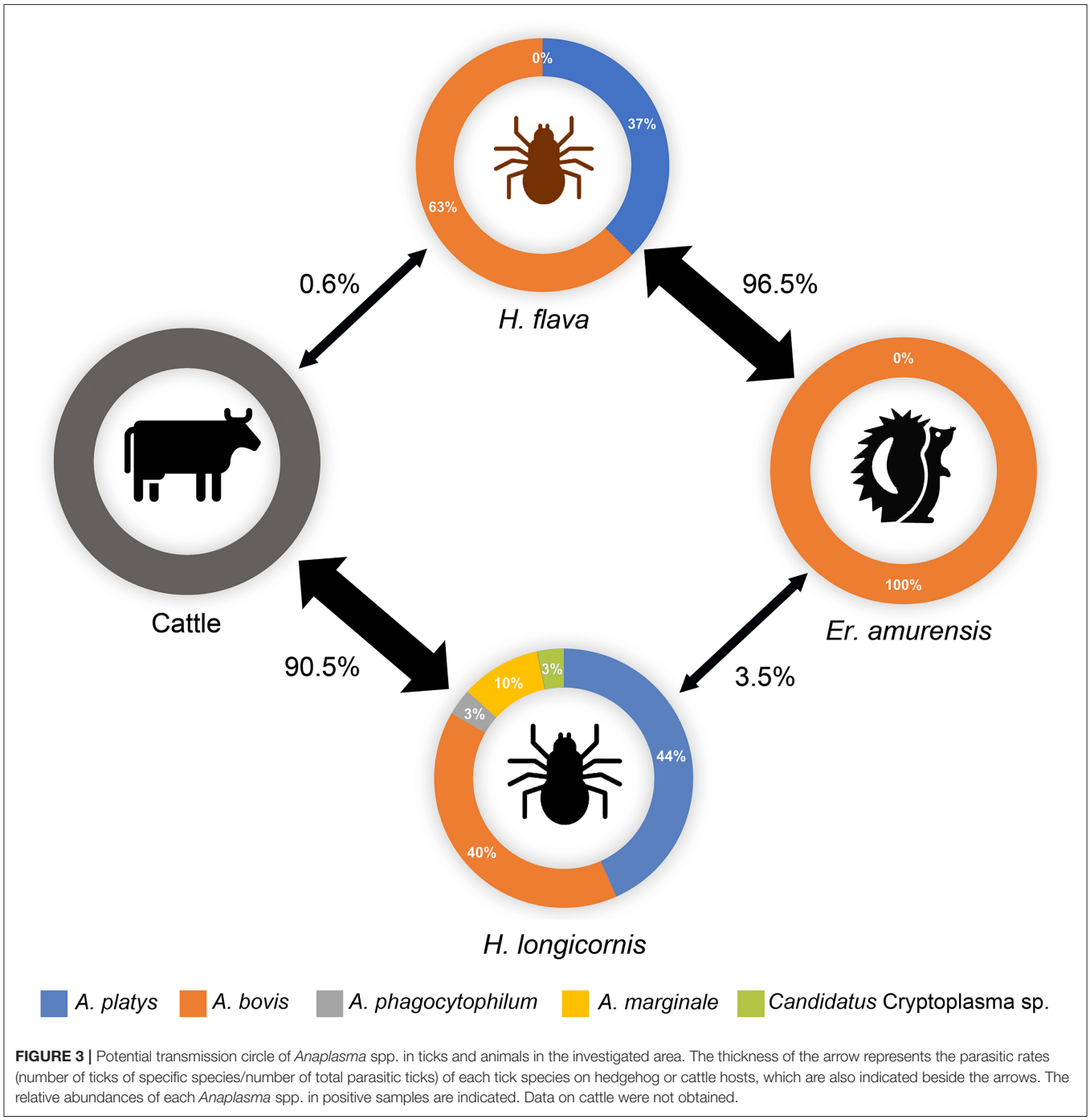

FIGURE 3 | Potential transmission circle of *Anaplasma* spp. in ticks and animals in the investigated area. The thickness of the arrow represents the parasitic rates (number of ticks of specific species/number of total parasitic ticks) of each tick species on hedgehog or cattle hosts, which are also indicated beside the arrows. The relative abundances of each *Anaplasma* spp. in positive samples are indicated. Data on cattle were not obtained.

and humans (Chisu et al., 2020). On the one hand, the activity area of hedgehogs for searching for food and shelter typically intersects with that of humans in (sub) urban areas, such as parks, gardens, urban green areas, farmlands, livestock farms, etc.; on the other hand, people mainly take hedgehogs into their homes as pets or to rescue injured ones. These possible contacts with hedgehogs or their contaminated environment will expose people to various zoonotic pathogens that hedgehogs harbor (Ruszkowski et al., 2021). Hence, it seems equally important to investigate the prevalence and co-infections/co-existence of *Anaplasma* spp. in wild hedgehogs and ticks to assess their transmission risks. Several spirochete species have been reported to co-exist in ticks (Herrmann et al., 2013), while co-existence/co-infections of various *Anaplasma* spp. or variants have only been reported in domestic animals (e.g., goats, sheep, cattle, and dogs), rather than in ticks or wild hedgehogs (Liu et al., 2012; Yang et al., 2015, 2020; Seo et al., 2018; Miranda et al., 2021). To our knowledge, this is the first study that investigated the

co-infections/co-existence of various *Anaplasma* spp. or variants in wild hedgehogs and ticks and confirmed their co-existence in *H. flava* and *H. longicornis* ticks.

Although significantly varied in species, ticks from hedgehogs or cattle, *Anaplasma* spp. prevalence or co-infection/co-existence rates were always found to contain *A. bovis* variant cwp72bo-1 coupled with *A. platys* variant xyn10pt-1 in the co-existence. These two variants were both predominant in the ticks from hedgehogs or cattle, indicating that they are the main endemic *Anaplasma* spp. variants in this region, and there may be a horizontal transmission of *Anaplasma* spp. between *H. flava* and *H. longicornis via* their shared hosts (**Figure 3**).

A. bovis was detected in *Er. amurensis* hedgehogs with a high positive rate (43.8%), while *A. platys* was found in none of the hedgehogs in the present study. *A. bovis* was reported to infect small mammals and ruminants monocytes and cause anaplasmosis (Liu et al., 2012; Ben Said et al., 2018), while *A. platys*, as the etiological agent of the infectious canine cyclic thrombocytopenia by infecting the platelets of dogs, can cause human infections (Harvey et al., 1978; Maggi et al., 2013; Arraga-Alvarado et al., 2014). To our knowledge, no previous study has reported that *A. platys* could infect hedgehogs. Thus, *Er. amurensis* may be an important reservoir for certain *Anaplasma* spp., like *A. bovis* in the present study and *A. phagocytophilum* in the previous study (Silaghi et al., 2012), rather than *A. platys*. However, more hedgehogs should be further investigated, considering the small size of animals included in the present study. In the infected hedgehogs, *Anaplasma*-positive or negative might be found in the same organs from different individuals, resulting in different positive rates in different organs. This phenomenon, which was also observed in a sheep model (Almazán et al., 2020), may be due to individual variations, including their immune status, pathogen loads, and co-existence of other bacteria. However, in general, higher rates were observed in the spleens, livers, and lungs of the hedgehogs in the present study, which is consistent with results obtained from another model using C3H/HeJ mice (Blas-Machado et al., 2007), in which scholars found splenomegaly and microscopical lesions in the lungs, spleens, and livers, rather than in other organs or tissues of the *A. phagocytophilum*-infected mice.

The co-existence of various *Anaplasma* spp. or variants in ticks may be due to transstadial transmission or their blood meal from the present host. For instance, in the present study, the *A. bovis* carried by *H. flava* could have come from tick biting hedgehogs or from transstadial transmission, while *A. platys* most likely came from transstadial transmission. Nevertheless, a previous study reported that hosts harboring diverse *A. phagocytophilum* strains may enable the emergence of new variants or types *via* bacterial recombination (Tegtmeyer et al., 2019), indicating that the co-existence of various *Anaplasma* spp. or variants in the present study has the potential to lead to the emergence of novel variants and cause pathogenic risks in the investigated area. The observations of various variants of *A. platys* or *A. bovis* in this area, and these minority variants (*A. bovis* variant cwp55-36bo-2 or *A. platys* variants xyn21pt-2 and xyn3pt-3) were always detected together in ticks containing their corresponding majority variants (*A. bovis* variant cwp72bo-1 or *A. platys* variant xyn10pt-1), supporting the hypothesis mentioned above.

A. phagocytophilum and *A. marginale* are the most significant disease-causing pathogens in the genus *Anaplasma* (Battilani et al., 2017). *A. phagocytophilum*, the agent of human granulocytic anaplasmosis (HGA), also causes tick-borne fever in sheep and goats and pasture fever in cattle (Battilani et al., 2017). *A. marginale* causes bovine anaplasmosis, a crucial rickettsial disease in cattle worldwide, which is characterized by severe anemia, abortions, loss of weight and milk production, and high morbidity and mortality (Quiroz-Castañeda et al., 2016). Both agents were detected in ticks feeding on cattle, indicating their potential threat to both humans and livestock in this area. However, the prevalence of these pathogens in humans or livestock needs further investigation.

Moreover, a novel *Candidatus* Cryptoplasma sp. was also identified in a tick from cattle. Similar sequences were found in China and South Korea (Accession nos. JN715833, KT596737, and GU075699-GU075704) and are classified as uncultured *Anaplasma* spp. Compared with *Anaplasma* spp., the sequences shared higher identity rates than those from *Candidatus* Cryptoplasma spp., which were recently characterized and named in 2015 (Eshoo et al., 2015). However, whether this bacterium could cause human infections requires further investigation.

Several studies have investigated the prevalence of *Anaplasma* spp. in animal and tick hosts in the Northeastern, Northwestern, Southern, and Central China (Jiang et al., 2011; Liu et al., 2012; Zhang et al., 2012; Li et al., 2015; Yang et al., 2015; Wei et al., 2016; Fang et al., 2021; Jiao et al., 2021; Yan et al., 2021), while few studies have been carried out in Eastern China (Lu et al., 2019; Yang et al., 2020). The *Anaplasma* species, their distribution, and prevalence in Eastern China have remained elusive. The present study filled the gaps by providing useful epidemiological data related to the pathogen species and their presence in the ticks or animal hosts in Jiangsu province, Eastern China.

Some limitations exist in the present study. First, although various PCR amplifications toward the *rrs* gene were used to detect different *Anaplasma* spp., there is still the possibility of missed detection of other possible *Anaplasma* spp. or variants due to the diversity of pathogens in the samples. Second, the detection limit of the typically used nested PCR may influence the positive rates, and a more sensitive real-time PCR method may overcome the bias. Third, the co-infections/co-existence make it potentially difficult to achieve precise detection or typing of *Anaplasma* spp. or variants. For instance, when a sample contains several variants with only a few nucleotide distinctions in their conserved genes (e.g., *rrs* or *groEL*), it will be challenging to indicate which *rrs* and *groEL* genes sequenced belong to the same strain. Hence, for further characterization, pathogen isolation should be conducted. Finally, the co-infection agents in the cattle remain to be defined.

In conclusion, we investigated the co-infections/co-existence of various *Anaplasma* spp. and variants in hedgehogs and ticks

feeding on hedgehogs and cattle for the first time. Important pathogenic *Anaplasma* spp., including *A. phagocytophilum*, *A. marginale*, 3 *A. platys* variants, and 2 *A. bovis* variants, as well as a novel *Candidatus* Cryptoplasma sp. were identified, with various prevalence rates in ticks and hedgehogs, and different co-existence combinations were observed only in ticks, rather than in hedgehogs. Hedgehogs may be important reservoirs for *A. bovis*, rather than for *A. platys*. Horizontal transmission of *Anaplasma* spp. may exist between different tick species *via* their shared hosts. Co-existence of various *Anaplasma* spp. or variants in the present study may facilitate the emergence of novel variants, pose potential threats to public health as well as economic losses from livestock farming, and raise challenges for detection and diagnosis in the investigated area. The present study, with the identification of important pathogenic *Anaplasma* spp. and their co-infections/co-existence in the ticks, provided epidemiological data that could be crucial for strategy development in early warning, prevention, and control of potential *Anaplasma* infections.

DATA AVAILABILITY STATEMENT

The data presented in the study are deposited in the GenBank database, accession numbers ON152887 to ON152896 and ON016525 to ON016529.

ETHICS STATEMENT

The animal study was reviewed and approved by Ethics Committee of Huadong Research Institute for Medicine and Biotechniques. Written informed consent was obtained from the owners for the participation of their animals in this study.

AUTHOR CONTRIBUTIONS

YQ, LA, and WT conceptualized the study. YQ and LA curated the data and formal analysis was performed by CZ and YM. WT and YQ provided the funding. The methodology was designed by RL and NL. The software was designed by YL. The original draft was prepared by YQ, while WT and YQ were involved in writing, reviewing, and editing. All authors contributed to the article and approved the submitted version.

FUNDING

This work was supported by Medical Science and Technology Projects (19SWAQ04 and 2020QN06357), a Jiangsu Social Development Project (BE2017620), and the National Natural Science Foundation of China (U1602223).

SUPPLEMENTARY MATERIAL

The Supplementary Material for this article can be found online at: https://www.frontiersin.org/articles/10.3389/fmicb.2022.913650/full#supplementary-material

REFERENCES

Almazán, C., Fourniol, L., Rouxel, C., Alberdi, P., Gandoin, C., Lagrée, A. C., et al. (2020). Experimental *Ixodes ricinus*-Sheep Cycle of *Anaplasma phagocytophilum* NV2Os Propagated in Tick Cell Cultures. *Front. Vet. Sci.* 7, 40. doi: 10.3389/fvets.2020.00040

Arraga-Alvarado, C. M., Qurollo, B. A., Parra, O. C., Berrueta, M. A., Hegarty, B. C., and Breitschwerdt, E. B. (2014). Case report: molecular evidence of *Anaplasma platys* infection in two women from Venezuela. *Am. J. Trop. Med. Hyg.* 91, 1161. doi: 10.4269/ajtmh.14-0372

Barlough, J. E., Madigan, J. E., Derock, E., and Bigornia, L. (1996). Nested polymerase chain reaction for detection of *Ehrlichia equi* genomic DNA in horses and ticks (*Ixodes pacificus*). *Vet. Parasitol.* 63, 319–329. doi: 10.1016/0304-4017(95)00904-3

Battilani, M., De Arcangeli, S., Balboni, A., and Dondi, F. (2017). Genetic diversity and molecular epidemiology of *Anaplasma*. *Infect. Genet. Evol.* 49, 195–211. doi: 10.1016/j.meegid.2017.01.021

Ben Said, M., Belkahia, H., and Messadi, L. (2018). *Anaplasma* spp. in North Africa: a review on molecular epidemiology, associated risk factors and genetic characteristics. *Ticks Tick Borne Dis.* 9, 543–555. doi: 10.1016/j.ttbdis.2018.01.003

Blas-Machado, U., De La Fuente, J., Blouin, E. F., Almazan, C., Kocan, K. M., and Mysore, J. V. (2007). Experimental Infection of C3H/HeJ Mice with the NY18 Isolate of *Anaplasma phagocytophilum*. *Vet. Pathol.* 44, 64–73. doi: 10.1354/vp.44-1-64

Byaruhanga, C., Collins, N. E., Knobel, D. L., Khumalo, Z. T. H., Chaisi, M. E., and Oosthuizen, M. C. (2018). Molecular detection and phylogenetic analysis of *Anaplasma marginale* and *Anaplasma centrale* amongst transhumant cattle in north-eastern Uganda. *Ticks Tick Borne Dis.* 9, 580–588. doi: 10.1016/j.ttbdis.2018.01.012

Chisu, V., Loi, F., Foxi, C., Chessa, G., Masu, G., Rolesu, S., et al. (2020). Coexistence of tick-borne pathogens in ticks collected from their hosts in Sardinia: an update. *Acta Parasitol.* 65, 999–1004. doi: 10.1007/s11686-020-00240-z

Cutler, S. J., Vayssier-Taussat, M., Estrada-Peña, A., Potkonjak, A., Mihalca, A. D., and Zeller, H. (2021). Tick-borne diseases and co-infection: Current considerations. *Ticks Tick Borne Dis.* 12, 101607. doi: 10.1016/j.ttbdis.2020.101607

Eshoo, M. W., Carolan, H. E., Massire, C., Chou, D. M., Crowder, C. D., Rounds, M. A., et al. (2015). Survey of *Ixodes pacificus* ticks in California reveals a diversity of microorganisms and a novel and widespread anaplasmataceae species. *PLoS ONE* 10, e0135828. doi: 10.1371/journal.pone.0135828

Fang, L. Z., Lei, S. C., Yan, Z. J., Xiao, X., Liu, J. W., Gong, X. Q., et al. (2021). Detection of multiple intracellular bacterial pathogens in *Haemaphysalis flava* ticks collected from hedgehogs in central China. *Pathogens* 10, 115. doi: 10.3390/pathogens10020115

Feng, L. (1983). *Medical Entomology*. Beijing: Science Press.

Harvey, J. W., Simpson, C. F., and Gaskin, J. M. (1978). Cyclic thrombocytopenia induced by a *Rickettsia*-like agent in dogs. *J. Infect. Dis.* 137, 182–188. doi: 10.1093/infdis/137.2.182

Herrmann, C., Gern, L., and Voordouw, M. J. (2013). Species co-occurrence patterns among Lyme borreliosis pathogens in the tick vector *Ixodes ricinus*. *Appl. Environ. Microbiol.* 79, 7273–7280. doi: 10.1128/AEM.02158-13

Islam, M. K., Alim, M. A., Tsuji, N., and Mondal, M. M. (2006). An investigation into the distribution, host-preference and population density of ixodid ticks

affecting domestic animals in Bangladesh. *Trop. Anim. Health Prod.* 38, 485–490. doi: 10.1007/s11250-006-4381-9

Jahfari, S., Ruyts, S. C., Frazer-Mendelewska, E., Jaarsma, R., Verheyen, K., and Sprong, H. (2017). Melting pot of tick-borne zoonoses: the European hedgehog contributes to the maintenance of various tick-borne diseases in natural cycles urban and suburban areas. *Parasit. Vectors* 10, 134. doi: 10.1186/s13071-017-2065-0

Jiang, J. F., Jiang, B. G., Yu, J. H., Zhang, W. Y., Gao, H. W., Zhan, L., et al. (2011). *Anaplasma phagocytophilum* infection in ticks, China-Russia border. *Emerg. Infect. Dis.* 17, 932–934. doi: 10.3201/eid1705.101630

Jiao, J., Lu, Z., Yu, Y., Ou, Y., Fu, M., Zhao, Y., et al. (2021). Identification of tick-borne pathogens by metagenomic next-generation sequencing in *Dermacentor nuttalli* and *Ixodes persulcatus* in Inner Mongolia, China. *Parasit. Vectors* 14, 287. doi: 10.1186/s13071-021-04740-3

Khodadadi, N., Nabavi, R., Sarani, A., Saadati, D., Ganjali, M., Mihalca, A. D., et al. (2021). Identification of *Anaplasma marginale* in long-eared hedgehogs (*Hemiechinus auritus*) and their *Rhipicephalus turanicus* ticks in Iran. *Ticks Tick Borne Dis.* 12, 101641. doi: 10.1016/j.ttbdis.2020.101641

Koh, F. X., Panchadcharam, C., Sitam, F. T., and Tay, S. T. (2018). Molecular investigation of *Anaplasma* spp. in domestic and wildlife animals in Peninsular Malaysia. *Vet. Parasitol. Reg. Stud. Rep.* 13, 141–147. doi: 10.1016/j.vprsr.2018.05.006

Li, Y., Yang, J., Chen, Z., Qin, G., Li, Y., Li, Q., et al. (2015). *Anaplasma* infection of Bactrian camels (*Camelus bactrianus*) and ticks in Xinjiang, China. *Parasit. Vectors* 8, 313. doi: 10.1186/s13071-015-0931-1

Liu, H., Li, Q., Zhang, X., Li, Z., Wang, Z., Song, M., et al. (2016). Characterization of rickettsiae in ticks in northeastern China. *Parasit. Vectors* 9, 498. doi: 10.1186/s13071-016-1764-2

Liu, Z., Ma, M., Wang, Z., Wang, J., Peng, Y., Li, Y., et al. (2012). Molecular survey and genetic identification of *Anaplasma* species in goats from central and southern China. *Appl. Environ. Microbiol.* 78, 464–470. doi: 10.1128/AEM.06848-11

Lu, M., Li, F., Liao, Y., Shen, J. J., Xu, J. M., Chen, Y. Z., et al. (2019). Epidemiology and diversity of rickettsiales bacteria in humans and animals in Jiangsu and Jiangxi provinces, China. *Sci. Rep.* 9, 13176. doi: 10.1038/s41598-019-49059-3

Maggi, R. G., Mascarelli, P. E., Havenga, L. N., Naidoo, V., and Breitschwerdt, E. B. (2013). Co-infection with *Anaplasma platys*, *Bartonella henselae* and *Candidatus* Mycoplasma haematoparvum in a veterinarian. *Parasit. Vectors* 6, 103. doi: 10.1186/1756-3305-6-103

Miranda, E. A., Han, S. W., Cho, Y. K., Choi, K. S., and Chae, J. S. (2021). Co-infection with *anaplasma* species and novel genetic variants detected in cattle and goats in the Republic of Korea. *Pathogens* 10, 28. doi: 10.3390/pathogens10010028

Quiroz-Castañeda, R. E., Amaro-Estrada, I., and Rodríguez-Camarillo, S. D. (2016). *Anaplasma marginale*: diversity, virulence, and vaccine landscape through a genomics approach. *Biomed. Res. Int.* 2016, 9032085. doi: 10.1155/2016/9032085

Ruszkowski, J. J., Hetman, M., Turlewicz-Podbielska, H., and Pomorska-Mól, M. (2021). Hedgehogs as a potential source of zoonotic pathogens-a review and an update of knowledge. *Animals (Basel)* 11, 1754. doi: 10.3390/ani11061754

Sarri, C., Stamatis, C., Sarafidou, T., Galara, I., and Mamuris, Z. (2014). A new set of 16S rRNA universal primers for identification of animal species. *Food Control.* 43, 35–41. doi: 10.1016/j.foodcont.2014.02.036

Seo, M. G., Ouh, I. O., Kwon, O. D., and Kwak, D. (2018). Molecular detection of *Anaplasma phagocytophilum*-like *Anaplasma* spp. and pathogenic *A. Phagocytophilum* in cattle from South Korea. *Mol. Phylogenet. Evol.* 126, 23–30. doi: 10.1016/j.ympev.2018.04.012

Silaghi, C., Skuballa, J., Thiel, C., Pfister, K., Petney, T., Pfäffle, M., et al. (2012). The European hedgehog (*Erinaceus europaeus*)–a suitable reservoir for variants of *Anaplasma phagocytophilum*? *Ticks Tick Borne Dis.* 3, 49–54. doi: 10.1016/j.ttbdis.2011.11.005

Song, K., Ji, Y., Sun, S., Yue, X., Wang, C., Luo, T., et al. (2021). Bacterial Microbiota in Unfed Ticks (Dermacentor nuttalli) From Xinjiang Detected Through 16S rDNA Amplicon Sequencing and Culturomics. *Zoonoses* 1. doi: 10.15212/ZOONOSES-2021-0007

Soong, L., and Dong, X. (2021). Emerging and Re-emerging Zoonoses are Major and Global Challenges for Public Health. *Zoonoses* 1, 1–2. doi: 10.15212/ZOONOSES-2021-00011

Spengler, J. R., and Estrada-Peña, A. (2018). Host preferences support the prominent role of Hyalomma ticks in the ecology of Crimean-Congo hemorrhagic fever. *PLoS Negl. Trop. Dis.* 12, e0006248. doi: 10.1371/journal.pntd.0006248

Tate, C. M., Howerth, E. W., Mead, D. G., Dugan, V. G., Luttrell, M. P., Sahora, A. I., et al. (2013). *Anaplasma odocoilei* sp. nov. (family Anaplasmataceae) from white-tailed deer (*Odocoileus virginianus*). *Ticks Tick Borne Dis.* 4, 110–119. doi: 10.1016/j.ttbdis.2012.09.005

Tegtmeyer, P., Ganter, M., and Von Loewenich, F. D. (2019). Simultaneous infection of cattle with different *Anaplasma phagocytophilum* variants. *Ticks Tick Borne Dis.* 10, 1051–1056. doi: 10.1016/j.ttbdis.2019.05.011

Wei, F., Song, M., Liu, H., Wang, B., Wang, S., Wang, Z., et al. (2016). Molecular Detection and Characterization of Zoonotic and Veterinary Pathogens in Ticks from Northeastern China. *Front. Microbiol.* 7, 1913. doi: 10.3389/fmicb.2016.01913

Wen, B., Cao, W., and Pan, H. (2003). *Ehrlichiae* and ehrlichial diseases in china. *Ann. N. Y. Acad. Sci.* 990, 45–53. doi: 10.1111/j.1749-6632.2003.tb07335.x

Yan, Y., Wang, K., Cui, Y., Zhou, Y., Zhao, S., Zhang, Y., et al. (2021). Molecular detection and phylogenetic analyses of *Anaplasma* spp. in *Haemaphysalis longicornis* from goats in four provinces of China. *Sci. Rep.* 11, 14155. doi: 10.1038/s41598-021-93629-3

Yang, B., Ye, C., Sun, E., Wen, Y., Qian, D., and Sun, H. (2020). First molecular evidence of *Anaplasma* spp. co-infection in stray dogs from Anhui, China. *Acta Trop* 206, 105453. doi: 10.1016/j.actatropica.2020.105453

Yang, J., Li, Y., Liu, Z., Liu, J., Niu, Q., Ren, Q., et al. (2015). Molecular detection and characterization of *Anaplasma* spp. in sheep and cattle from Xinjiang, northwest China. *Parasit. Vectors* 8, 108. doi: 10.1186/s13071-015-0727-3

Zhang, L., Liu, H., Xu, B., Lu, Q., Li, L., Chang, L., et al. (2012). *Anaplasma phagocytophilum* infection in domestic animals in ten provinces/cities of China. *Am. J. Trop. Med. Hyg.* 87, 185. doi: 10.4269/ajtmh.2012.12-0005

Conflict of Interest: The authors declare that the research was conducted in the absence of any commercial or financial relationships that could be construed as a potential conflict of interest.

Publisher's Note: All claims expressed in this article are solely those of the authors and do not necessarily represent those of their affiliated organizations, or those of the publisher, the editors and the reviewers. Any product that may be evaluated in this article, or claim that may be made by its manufacturer, is not guaranteed or endorsed by the publisher.

frontiers | Frontiers in Microbiology

ORIGINAL RESEARCH
published: 13 June 2022
doi: 10.3389/fmicb.2022.928025

Development of a Lateral Flow Strip-Based Recombinase-Aided Amplification for Active *Chlamydia psittaci* Infection

Jun Jiao[1†], Yong Qi[2†], Peisheng He[1], Weiqiang Wan[1], Xuan OuYang[1], Yonghui Yu[1], Bohai Wen[1] and Xiaolu Xiong[1]*

[1]State Key Laboratory of Pathogen and Biosecurity, Beijing Institute of Microbiology and Epidemiology, Beijing, China, [2]Huadong Research Institute for Medicine and Biotechniques, Nanjing, China

Chlamydia psittaci is the causative agent of psittacosis, a worldwide zoonotic disease. A rapid, specific, and sensitive diagnostic assay would be benefit for *C. psittaci* infection control. In this study, an assay combining recombinase-aided amplification and a lateral flow strip (RAA-LF) for the detection of active *C. psittaci* infection was developed. The RAA-LF assay targeted the *CPSIT_RS02830* gene of *C. psittaci* and could be accomplished in 15 min at a single temperature (39°C). The analytical sensitivity of the assay was as low as 1×10^0 copies/μl and no cross-reaction with some other intracellular pathogens was observed. Moreover, all feces samples from mice infected with *C. psittaci* at day-1 post-infection were positive in the RAA-LF assay. In conclusion, the RAA-LF assay provides a convenient, rapid, specific and sensitive method for detection of active *C. psittaci* infection and it is also suitable for *C. psittaci* detection in field.

Keywords: *Chlamydia psittaci*, detection, recombinase-aided amplification, lateral flow strip, infection

OPEN ACCESS

Edited by:
Wei Wang,
Jiangsu Institute of Parasitic Diseases (JIPD), China

Reviewed by:
Valentina A. Feodorova, Federal Research Center for Virology and Microbiology, Russia
Tian Qin, Chinese Center for Disease Control and Prevention, China

***Correspondence:**
Xiaolu Xiong
xiongxiaolu624@sohu.com

†These authors have contributed equally to this work

Specialty section:
This article was submitted to Infectious Agents and Disease, a section of the journal Frontiers in Microbiology

Received: *25 April 2022*
Accepted: *27 May 2022*
Published: *13 June 2022*

Citation:
Jiao J, Qi Y, He P, Wan W, OuYang X, Yu Y, Wen B and Xiong X (2022) Development of a Lateral Flow Strip-Based Recombinase-Aided Amplification for Active Chlamydia psittaci Infection. Front. Microbiol. 13:928025. doi: 10.3389/fmicb.2022.928025

INTRODUCTION

Zoonoses are major and global challenges for public health (Xiaoping and Lynn, 2021). *Chlamydia psittaci*, an obligate intracellular Gram-negative bacterium with a unique developmental cycle, is the causative agent of psittacosis, a worldwide zoonotic disease. More than 467 bird species and many nonavian domestic animals, including swine, dogs, horses, cattle, sheep, goats, and cats, as well as rodents are susceptible to *C. psittaci* (Pantchev et al., 2010; Lenzko et al., 2011; Knittler and Sachse, 2015; Gu et al., 2020). *C. psittaci* infection in humans could occasionally occur after inhalation of *C. psittaci*-contaminated aerosols from infected birds/nonavian animals (Wolff et al., 2018). Due to low awareness of the disease and atypical clinical presentation in majority of the cases, psittacosis in humans is underestimated (Gu et al., 2020).

The burden of *C. psittaci* infection is also likely underestimated due to diagnostic challenges: the bacterium requires intracellular growth and is a zoonotic human pathogen responsible for atypical pneumonias that may be caused by various pathogens such as *Mycoplasma pneumonia*, *Legionella pneumophila and Coxiella burnetii* (Cunha, 2006; Jiao et al., 2014). To date, several assays have been developed for *C. psittaci* detection. Conventional methods including pathogen isolation, indirect immunofluorescence, enzyme linked immunosorbent assay (ELISA), complement fixation, outer membrane protein A (ompA) sequencing and restriction fragment length polymorphism

analysis have been used (Souriau and Rodolakis, 1986; Sanderson et al., 1994; Mitchell et al., 2009a,b; Opota et al., 2015), but these methods are laborious, low sensitive, time-consuming and also require a trained personnel. The PCR-based diagnostic methods such as conventional PCR, multi-PCR, and real-time PCR have been developed to detect *C. psittaci* (Hewinson et al., 1997; Messmer et al., 1997; Wolff et al., 2018). Although these PCR-based methods are highly sensitive, the requirement of expensive instruments and skilled operators make the use of these methods difficult in resource-limited settings.

Recombinase-aided amplification (RAA) assay is a new isothermal amplification technology for pathogens detection with the advantages of rapidity, simplicity, and low cost (Chen et al., 2018; Duan et al., 2018; Yan et al., 2018; Wang et al., 2020; Ruichen Lv et al., 2022). This amplification process only requires approximately 15–30 min at 39°C and has been successfully applied for detection of African Swine Fever Virus (Fan et al., 2020), *Klebsiella pneumoniae* (Hou et al., 2021), human norovirus GII.4 (Qin et al., 2021), duck circovirus (Li et al., 2021), *Trypanosoma evansi* (Li et al., 2020), etc. Additionally, the result of RAA assay can be observed on the lateral flow strip (LF) by naked eyes, providing a convenient and rapid diagnostic assay for the detection of the target pathogens, and thus it is suitable for clinical application and/or testing in field.

For *Chlamydia* spp. detection, urethral swabs, choanal cleft swabs, pharyngeal swab, and cloacal swabs from animals or human are often used for DNA extraction and testing (Holland et al., 1990; Dumke et al., 2015; Mina et al., 2019; Feodorova et al., 2022). One route of transmission of *C. psittaci* is a inhalation of aerosolized bird feces from the environment (Szeredi et al., 2005), and fresh feces samples from animals are also used for detection of *C. psittaci* (Takashima et al., 1996; Sachse et al., 2012; McGovern et al., 2021). Another advantage for the choice of fresh feces as a key specimen for detection of *C. psittaci* maybe that a feces collection is more convenient than a blood collection: rapid, harmless, and suitable for detection in filed. In the present study, a convenient and rapid recombinase-aided amplification and a lateral flow strip (RAA-LF) assay was developed for the detection of active *C. psittaci* infection, and its sensitivity and specificity were investigated. In addition, the effectiveness of the RAA-LF assay was evaluated with feces samples from mice experimentally infected with *C. psittaci*.

MATERIALS AND METHODS

Bacteria and DNA Samples

Chlamydia psittaci strain 6BC was cultured in buffalo green monkey kidney (BGMK) cells, and then the whole DNA were extracted from the cells infected with the strain using a QIAamp Blood and Tissue Mini DNA kit (Qiagen, Hilden, Germany) according to the manufacturer's instructions. The DNA sample was eluted in 100 µl of nuclease-free water and determined by quantitative PCR (qPCR) as described previously (Menard et al., 2006).

DNA samples of *Anaplasma phagocytophilum*, *Rickettsia heilongjiangensis, Rickettsia rickettsii*, *Rickettsia sibirica, Rickettsia canada*, *Rickettsia australis*, *Rickettsia typhi*, *Rickettsia prowazekii*, *Ehrlichia chaffeensis*, *C. burnetii* (strain Henzerling and QIYI), *L. pneumophila*, *Listeria monocytogenes*, *Salmonella typhimurium*, *Staphylococcus aureus*, *Vibrio cholera*, *Bartonella henselae*, *Bartonella quintana*, *Streptococcus suis*, *Shigella sonnei* and *Chlamydia trachomatis* were preserved in our laboratory.

Deoxyribonucleic acid samples extracted from fresh feces of *C. psittaci*-infected mice were also provided. Briefly, specific-pathogen free (SPF) BALB/c mice (female, 6–8 weeks old) were divided into two groups with four mice per group and each mouse was infected with 1×10^5 *C. psittaci* organisms suspended in 50 µl phosphate buffer saline (PBS) *via* intranasal administration. All individuals in Group 2 were intraperitoneally administered with tetracycline (40 mg per kg) at day 7 post-infection. Fresh feces samples from mice in both groups were collected at days 1, 3, 7, 10, 14, 17 and/or 20 post-infection, and DNA was extracted from each feces sample using a QIAamp Blood and Tissue Mini DNA kit (Qiagen, Hilden, Germany). The purified DNA was eluted in 100 µl of nuclease-free water.

Primers and Probes

The nucleotide sequences of the *CPSIT_RS02830* gene of several *C. psittaci* strains were aligned and their conserved regions were selected to design the primers and probes. The designed primers and probe were blasted against nucleotide database (GenBank) in the National Center for Biotechnology Information[1] to confirm their specificity. The primers and probe were synthesized by GenScript Biotech (Nanjing, China).

RAA Assay and Lateral Flow Reading

The RAA assays were performed in 50-µl reaction volumes using a commercial RAA kit (ZC Biosicence, Hangzhou, China). The reaction mixture contained 4 µl of extracted DNA template, 2.5 µl of distilled water, 37.9 µl of reaction buffer A, 2 µl of primer F (2.5 µm), 2 µl of primer R (2.5 µm), and 0.6 µl of probe (2.5 µm). The reaction mixture was added to a tube containing the RAA enzyme mix, and then 1 µl of reaction buffer B was added to initiate the reaction. The tubes were transferred to a metal bath (Coyote, Beijing, China) at 39°C for 15 min. A negative control (blank) was included in each run. After the reaction, 10 µl of the amplified product was diluted in 90 µl PBS, and then 50 µl of the diluted sample was transferred to the sample pad of a Milenia GenLine HybriDetect strip (Milenia Biotec, Gieben, Germany) and incubated 3 min at room temperature. Results were judged visually by naked eyes, and a positive result was determined when both the low line of test (T) and the upper line of control (C) developed. Only C line occurrence indicated a negative result, and if the C line did not develop, the strip should be replaced. The assays were performed in triplicate.

Evaluation of the RAA-LF Conditions

The optimal RAA-LF reaction time and temperature were determined by examining different time settings ranging from 5 to 30 min and various temperature settings ranging from 37 to 42°C. For evaluation of the specificity, 1×10^5 copies/µl of

[1]https://www.ncbi.nlm.nih.gov/

C. psittaci DNA and at least 1×10^4 copies/μl of DNA templates from other bacteria were utilized in a 50 μl RAA reaction mixture. For evaluation of the sensitivity, the RAA-LF reaction was evaluated using 10-fold serial dilutions of *C. psittaci* DNA, ranging from 1×10^0 copy to 1×10^5 copies/μl.

Evaluation of the RAA-LF Assay Using Experimental Samples

To evaluate the performance of the RAA-LF assays for the detection of active *C. psittaci* infection, specific-pathogen free (SPF) BALB/c mice ($n=8$, female, 6–8 weeks old) were divided into two groups with four mice per group, and each mouse was infected with 1×10^5 *C. psittaci* strain 6BC suspended in 50 μl phosphate buffer saline (PBS) *via* intranasal administration. Fresh feces samples from mice in both the groups were collected at days 1, 3, 7, 10, 14, 17, and/or 20 post-infection and DNA extracted from fresh feces obtained from experimentally infected mice was subjected to RAA-LF or qPCR. Fresh feces collected from naïve mice ($n=4$, female, 6–8 weeks old) were used as negative control. RAA-LF amplification was performed as mentioned above, and qPCR was performed as previously described (Menard et al., 2006).

RESULTS

Designing of Primers and Probes for RAA

Screening of specific primer pairs and probes is the critical step for RAA assay. In the present study, the conservation of *CPSIT_RS02830* gene sequence among 20 *C. psittaci* strains was evaluated by alignment (**Figure 1A**). As a result, the sequence between primers F and R was aligned with the corresponding sequence in all 20 *C. psittaci* strains but without that of another *Chlamydia* species such as *C. trachomatis* or *C. abortus*, and only one base in the probe mismatched with that of several strains, indicating the target sequence was conserved and suitable for the detection for *C. psittaci* (**Figure 1B** and **Table 1**).

Evaluation of the RAA-LF Reaction Time and Temperature

The RAA-LF reaction temperature was tested at a wide range of temperatures from 37 to 42°C. The results showed that the reaction performs well at 38–42°C after 3 min incubation on the lateral flow strip (**Figure 2A**). Then the RAA-LF amplification was achieved at times ranging from 5 to 30 min at 39°C. The results showed that a bright T line could be detected when the amplification time was 10 min, and it became brighter as the amplified time increased to 30 min (**Figure 2B**).

Analytical Specificity and Sensitivity of the RAA-LF Assay

To evaluate the specificity of the developed RAA-LF assay, DNA samples belong to *Rickettsia*, *Legionella*, and several other pathogenic bacteria were assessed. Our results showed that a clearly T line could be observed by the naked eyes only for DNA sample of *C. psittaci*, and there was no cross-reactivity with DNA samples of *A. phagocytophilum*, *R. heilongjiangensis*, *R. rickettsia*, *R. sibirica*, *R. Canada*, *R. australis*, *R. typhi*, *R. prowazekii*, *E. chaffeensis*, *C. burnetii* (Henzerling and QIYI), *L. pneumophila*, *L. monocytogenes*, *S. typhimurium*, *S. aureus*, *V. cholera*, *B. henselae*, *B. quintana*, *S. suis*, *S. sonnei* and *C. trachomatis* (**Figure 3**).

To evaluate the sensitivity of the developed RAA-LF assay, 10-fold serial dilutions of *C. psittaci* DNA, ranging from 1×10^0 copy to 1×10^5 copies/μl were used. Results showed that the developed RAA-LF assay was highly sensitive with a detection limit as low as 1×10^0 copies/μl of *C. psittaci* (**Figure 4**).

The RAA-LF Assay Can Detect Active *Chlamydia psittaci* Infection in an Experimental Mouse Model

In the experiment, BALB/c mice infected with *C. psittaci* were divided into two groups. Mice in group 1 were left untreated, while mice in group 2 were treated with tetracycline at day-7 post-infection. Fresh feces samples from mice of both the groups were collected at days 1, 3, 7, 10, 14, 17, and/or 20 post-infection, and DNA extracted from feces samples were detected by the developed RAA-LF assay.

As shown in **Figure 5**, the two techniques did not yield identical results for all of the feces samples. All of the feces samples were detected positive in the RAA-LF assay. However, none of the feces samples from the infected mice at day 1 post-infection was detected positive in *C. psittaci*-specific qPCR (**Figure 5; Supplementary Table S1** and **Supplementary Figure S1**), suggesting that the RAA-LF assay is more sensitive for detection of an early *C. psittaci* infection compared with qPCR. All of the feces samples in group 1, which contained around 10^3–10^4 copies/μl of genomic DNA as determined in qPCR at days 3, 7, 10, and 14 post-infection (**Supplementary Table S1**), were also detected positive in the RAA-LF assay. Unfortunately, all mice in group 1 died at day 15 post-infection.

In group 2, all mice were survival and their feces samples were detected with decreasing levels of *C. psittaci* from day 7 post-infection (**Supplementary Table S1**). All of the feces samples from day 3 post-infection were detected positive in *C. psittaci*-specific qPCR and RAA-LF assay, indicating that the RAA-LF is a suitable assay for visual detection of active *C. psittaci* infection under the experimental condition. The feces samples from naïve mice were also detected and there was no positive result in the RAA-LF assay (**Supplementary Figure S1**).

DISCUSSION

Chlamydia psittaci is a zoonotic agent of systemic wasting disease in birds and atypical pneumonia in mammalians including humans, constituting a public health risk (Knittler and Sachse, 2015). Human infections caused by *C. psittaci* are underestimated, which is mainly due to the difficulty in diagnosing this disease. A convenient, rapid, specific and sensitive method for the detection of *C. psittaci* infection is needed in order to achieve an effective psittacosis control. In the present study, we have developed a convenient and rapid RAA-LF assay for detection of active *C. psittaci* infection.

Evaluation of specificity of a detection assay using unrelated bacteria DNA is of equal importance as using related bacteria

A

select all *20 sequences selected* GenBank Graphics Distance tree of results New MSA Viewer

Description	Scientific Name	Max Score	Total Score	Query Cover	E value	Per. Ident	Acc. Len	Accession
Chlamydia psittaci strain Horse_pl chromosome	Chlamydia psittaci	425	425	100%	6e-115	100.00%	1169652	CP025423.1
Chlamydia psittaci strain GIMC 2005:CpsCP1 chromosome, complete genome	Chlamydia psittaci	425	425	100%	6e-115	100.00%	1172381	CP024451.1
Chlamydia psittaci strain GIMC 2004:CpsAP23 chromosome, complete genome	Chlamydia psittaci	425	425	100%	6e-115	100.00%	1172364	CP024455.1
Chlamydia psittaci strain GIMC 2003:Cps25SM chromosome, complete genome	Chlamydia psittaci	425	425	100%	6e-115	100.00%	1166857	CP024453.1
Chlamydia psittaci VS225, complete genome	Chlamydia psittaci VS225	425	425	100%	6e-115	100.00%	1157385	CP003793.1
Chlamydia psittaci 84/55, complete genome	Chlamydia psittaci 84/55	425	425	100%	6e-115	100.00%	1172064	CP003790.1
Chlamydia psittaci 08DC60, complete genome	Chlamydia psittaci 08DC60	425	425	100%	6e-115	100.00%	1172032	CP002807.1
Chlamydia psittaci 02DC15, complete genome	Chlamydia psittaci 02DC15	425	425	100%	6e-115	100.00%	1172182	CP002806.1
Chlamydia psittaci 01DC11, complete genome	Chlamydia psittaci 01DC11	425	425	100%	6e-115	100.00%	1172197	CP002805.1
Chlamydia psittaci C19/98, complete genome	Chlamydia psittaci C19/98	425	425	100%	6e-115	100.00%	1169374	CP002804.1
Chlamydia psittaci 6BC chromosome, complete genome	Chlamydia psittaci 6BC	425	425	100%	6e-115	100.00%	1171667	CP002586.1
Chlamydia psittaci 6BC, complete genome	Chlamydia psittaci 6BC	425	425	100%	6e-115	100.00%	1171660	CP002549.1
Chlamydophila psittaci RD1 genome	Chlamydia psittaci RD1	425	425	100%	6e-115	100.00%	1164076	FQ482149.1
Chlamydia psittaci Mat116 chromosome, complete genome	Chlamydia psittaci Mat116	420	420	100%	3e-113	99.57%	1163362	CP002744.1
Chlamydia psittaci strain Ful127 chromosome, complete genome	Chlamydia psittaci	403	403	100%	3e-108	98.26%	1171317	CP033059.1
Chlamydia psittaci 01DC12 complete genome	Chlamydia psittaci 01DC12	403	403	100%	3e-108	98.26%	1171011	HF545614.1
Chlamydia psittaci CP3, complete genome	Chlamydia psittaci CP3	403	403	100%	3e-108	98.26%	1168150	CP003797.1
Chlamydia psittaci WC, complete genome	Chlamydia psittaci WC	403	403	100%	3e-108	98.26%	1172265	CP003796.1
Chlamydia psittaci MN, complete genome	Chlamydia psittaci MN	403	403	100%	3e-108	98.26%	1168490	CP003792.1
Chlamydia psittaci NJ1, complete genome	Chlamydia psittaci NJ1	398	398	100%	1e-106	97.83%	1161434	CP003798.1

B

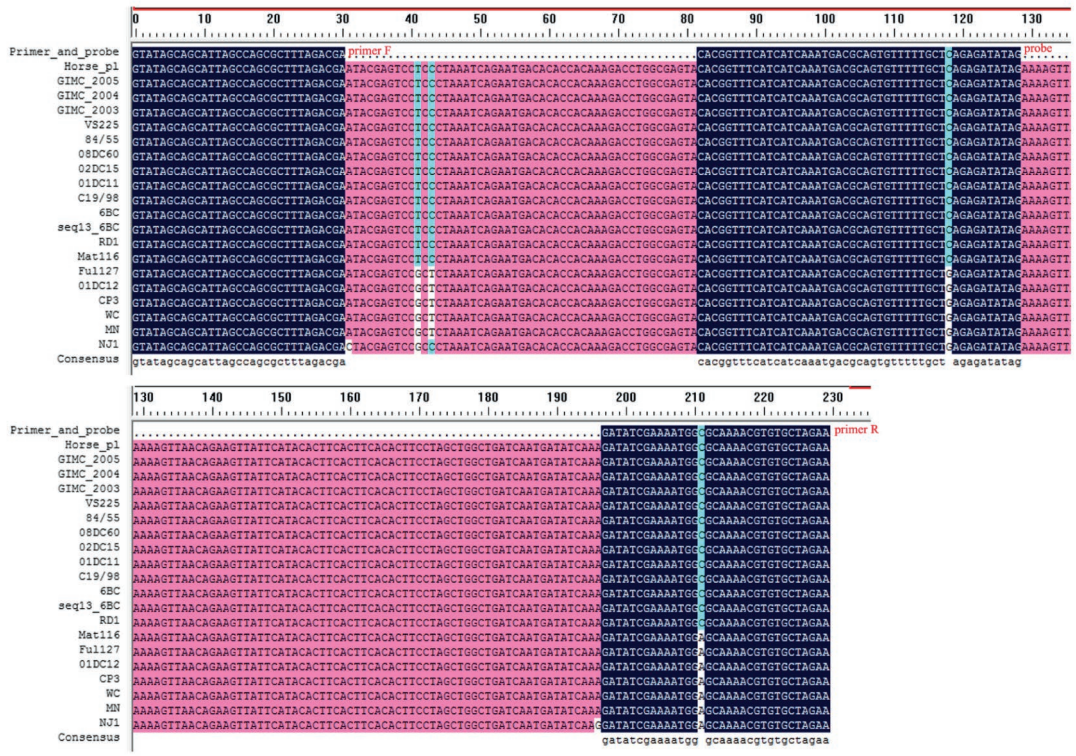

FIGURE 1 | Alignment of the conservation of the *CPSIT_RS02830* gene. The conservative sequence of the *CPSIT_RS02830* gene in *Chlamydia psittaci* was blasted against the National Center for Biotechnology Information nucleotide database **(A)**. The target sequences of the *CPSIT_RS02830* gene was aligned between the forward and reverse primers among various *C. psittaci* strains **(B)**.

DNA (Sails et al., 2003; Gumaa et al., 2019). The RAA-LF assay was evaluated using the whole DNA samples of *C. psittaci* or another intracellular pathogenic bacteria which are typically neglected in causing fever of unknown origin (*Rickettsia* spp. or *Legionella* spp.), or another unrelated pathogenic bacterium (*S. typhimurium*, *S. aureus* etc.). Specially, DNA of *V. cholera*, a pathogenic bacterium which is commonly transmitted by drinking water contaminated by the patients' feces, was also used as an unrelated sample in the present study. As a result, only DNA samples of *C. psittaci* were detected positive in the RAA-LF assay, suggesting that this RAA-LF assay performs a good specificity. Further studies should focus on verifying

TABLE 1 | Sequences of the primers and probes used for the RAA amplification.

Primer/probe	Sequence (5′–3′)	Source of the primer/probe	Sequence of product
F	GTATAGCAGCATTAGCCAGCGCTTTAGACGA	This study	GTATAGCAGCATTAGCCAGCGCTTTAGACGAATACGAGTCCTCCCTAAAT
R	Biotin-TTCTAGCACACGTTTTGCGCCATTTTCGATATC	This study	CAGAATGACACACCACAAAGACCTGGCGAGTACACGGTTTCATCATCAAA TGACGCAGTGTTTTTGCTCAGAGATATAGAAAAGTTAACAGAAGTTATTC
Probe	Fam-CACGGTTTCATCATCAAATGACGCAGTGTT[THF]TTTGCTCAGAGATATAG-Phosphate	This study	ATACACTTCACTTCACACTTCCTAGCTGGCTGATCAATGATATCAAAGAT ATCGAAAATGGCGCAAAACGTGTGCTAGAA

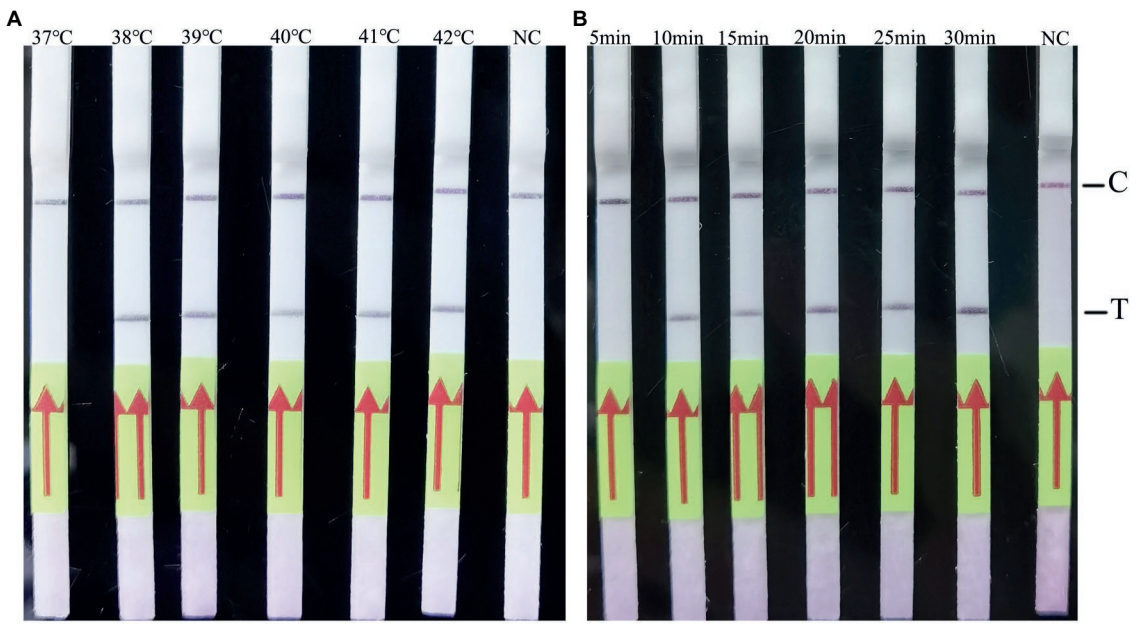

FIGURE 2 | Evaluation of the amplification temperatures and amplification times on the RAA-LF assay. 1×10^5 copies/μl of *C. psittaci* DNA was utilized in a 50 μl RAA reaction mixture and deionized water was provide as negative control. A positive result was determined when both the low line of test (T) and the upper line of control (C) developed. Only C line occurrence indicated a negative result. The RAA-LF worked well in a wide range of amplification temperature from 37 to 42°C **(A)**. After 5–30 min of isothermal amplification reaction, the positive reaction was visible on the test strip **(B)**.

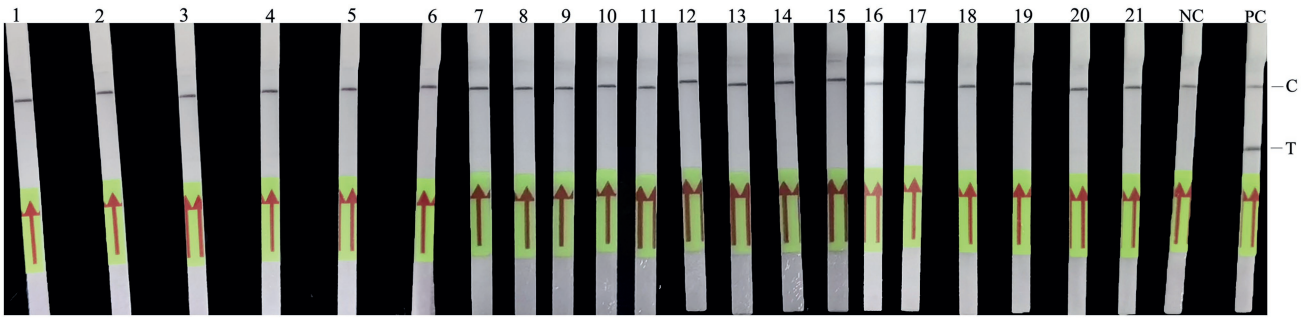

FIGURE 3 | Analytical specificity of the RAA-LF assay. Line 1: *Anaplasma phagocytophilum*; Line 2: *Rickettsia heilongjiangensis*; Line 3: *R. rickettsia*; Line 4: *R. sibirica*; Line 5: *R. Canada*; Line 6: *R. australis*; Line 7: *R. typhi*; Line 8: *R. prowazekii*; Line 9: *Ehrlichia chaffeensis*; Line 10: *Coxiella burnetii* (Henzerling); Line 11: *C. burnetii* (QIYI); Line 12: *Legionella pneumophila*; Line 13: *Listeria monocytogenes*; Line 14: *Salmonella typhimurium*; Line 15: *Staphylococcus aureus*; Line 16: *Vibrio cholera*; Line 17: *Bartonella henselae*; Line 18: *Bartonella quintana*; Line 19: *Streptococcus suis*; Line 20: *Shigella sonnei*; Line 21: *Chlamydia trachomatis*; NC: negative control; PC: *C. psittaci*. A positive result was determined when both the low line of test (T) and the upper line of control (C) developed. Only C line occurrence indicated a negative result.

potential cross-reactivity with DNA from other species belong to *chlamydia* spp., like *C. abortus*.

The developed RAA-LF assay is also highly sensitive and the detected limitation is as low as 1×10^0 copies/μl of *C. psittaci* genomic

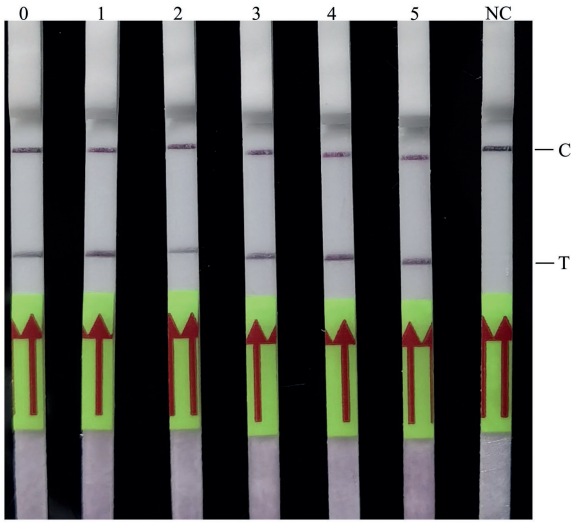

FIGURE 4 | Analytical sensitivity of the RAA-LF assay. Ten-fold serial dilutions of *C. psittaci* genomic DNA were evaluated by the RAA-LF assay, and deionized water was provided as negative control. A positive result was determined when both the low line of test (T) and the upper line of control (C) developed. Only C line occurrence indicated a negative result. Lines 0–5: 1×10^0 copy to 1×10^5 copies/μl. NC: negative control.

DNA, which is almost 20-fold more sensitive compared with that of the recombinant polymerase amplification (RPA/RAA) assay developed by Pang et al. (2021), making it useful for assessing the samples from the patients in the early acute phase of *C. psittaci* infection. Actually, three forward primers, three reverse primers, and two probes targeting the conservation of *CPSIT_RS02830* gene sequence have been designed and combined to generate 18 different combinations, and then these combinations have been screened for the RAA-LF assay (data not shown). The best combination is the one that descried in **Table 1**. This may be one explanation of the high sensitivity of the developed RAA-LF assay. In addition, compared with conventional PCR and real-time PCR requiring more than 1 h to complete in a well-equipped laboratory (Herring, 1991; Rasmussen et al., 1992; Sykes et al., 2001; Angen et al., 2021), the time required of the RAA-LF assay is also shorter and could be completed in less than 20 min. Moreover, the RAA-LF assay works well in a wide range of temperature (38–42°C) which is lower than the ones required in loop-mediated isothermal amplification (LAMP) assay (Njiru, 2012). Therefore, this RAA-LF assay does not require any expensive instrument and can be performed in minimally equipped laboratories and even in field.

The RAA-LF assay was evaluated for its potential to detect active *C. psittaci* infection at various time points in an experimental mouse model. The results showed that the RAA-LF assay exhibits

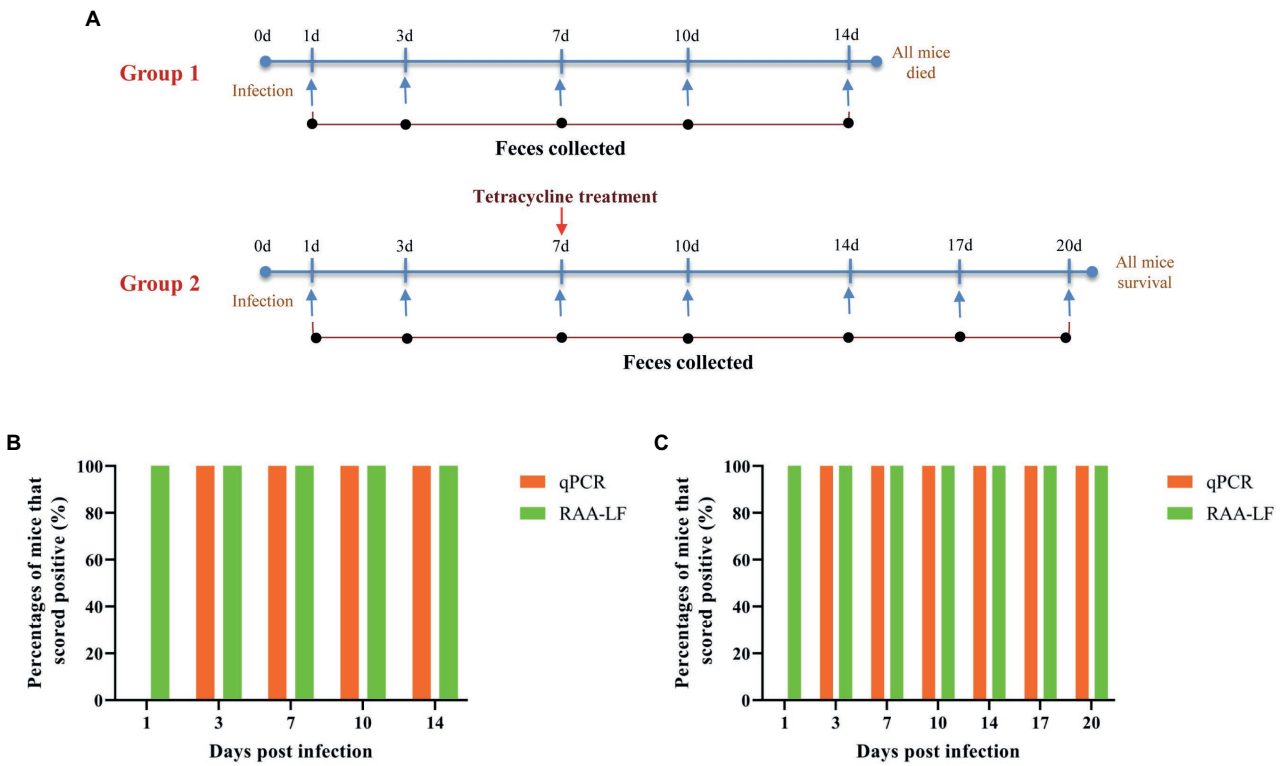

FIGURE 5 | Results of the evaluation of qPCR and the RAA-LF assay for experimentally infected samples. BALB/c mice infected with *Chlamydia psittaci* were divided into two groups of four individuals. Group 1 was left untreated, while Group 2 was treated with tetracycline at 7 days post-infection. All mice in group 1 died at day 15 post-infection and all mice in group 2 were survival **(A)**. Fresh feces samples from group 1 **(B)** and group 2 **(C)** were collected at days 1, 3, 7, 10, 14, 17 and/or 20 post-infection, and the extracted DNA from fresh feces samples were evaluated by qPCR and the RAA-LF assay. The results were displayed as the percentages of mice that scored positive (orange) or negative (green).

a potential suitable for direct detection of early *C. psittaci* infection. Feces, as the primary test sample, has potential for PCR inhibition and ultimately reduced analytical and diagnostic sensitivity (Acharya et al., 2017), what's important is that the complex compositions of feces seems to have not much effects on the test results in the present study. The *C. psittaci* could be detected from fresh feces samples of infected mice at day 1 post-infection, also indicating the available for assessing patient samples in the acute phase. Moreover, an important feature of the method is the results can also be visualized with naked eyes. Therefore, the RAA-LF assay is more suitable for usage under field conditions.

However, there are several limitations in evaluation of the developed RAA-LF assay. Firstly, for lacking of genomic DNA, no various strains of *C. psittaci* or other *Chlamydia* spp. strains except *C. trachomatis* were tested in the present study. Secondly, no clinical samples of patients with psittacosis were used to verify the developed RAA-LF assay. And the addressing of these limitations will contribute to the further preciseness of this study.

CONCLUSION

A method for the detection of active *C. psittaci* infection based on a RAA-LF was developed in the present study. The RAA-LF assay can be performed within 20 min using a portable device and positively detect as low as 1×10^0 copies/μl of DNA. In addition, the assay results can be visualized with naked eyes. Therefore, it is a convenient, rapid, sensitive and specific assay for detection of active *C. psittaci* infection, and it is suitable for use in minimally equipped laboratories even field settings.

DATA AVAILABILITY STATEMENT

The original contributions presented in the study are included in the article/**Supplementary Material**, further inquiries can be directed to the corresponding author.

ETHICS STATEMENT

The animal study was reviewed and approved by the Institutional Animal Care and Use Committee (IACUC) of the Academy of Military Medical Science.

AUTHOR CONTRIBUTIONS

This study was conceived and designed by JJ and XX. Samples collection and laboratory work were performed by PH, XO, and YY. Experimental data analysis was performed by YQ and WW. The manuscript was drafted by JJ and XX, and edited by BW. All authors contributed to the article and approved the submitted version.

FUNDING

This work was supported by the National Natural Science Foundation of China [grant numbers 32000139 and 31970178] and the National Key Research and Development Program of China [grant numbers 2019YFC1200500 and 2019YFC1200602].

SUPPLEMENTARY MATERIAL

The Supplementary Material for this article can be found online at: https://www.frontiersin.org/articles/10.3389/fmicb.2022.928025/full#supplementary-material

Supplementary Figure S1 | Evaluation of the RAA-LF assay for detection of active *Chlamydia psittaci* infection in mice. Fresh feces samples from group 1 **(A)**, group 2 **(B)** and naïve mice **(C)** were tested by the developed RAA-LF assay. 1, 3 7, 10, 14, 17, 20: days at post-infection. N: negative control. N1–N4: naïve mice. A positive result was determined when both the low line of test (T) and the upper line of control (C) developed. Only C line occurrence indicated a negative result.

REFERENCES

Acharya, K. R., Dhand, N. K., Whittington, R. J., and Plain, K. M. (2017). PCR inhibition of a quantitative PCR for detection of *Mycobacterium avium* subspecies Paratuberculosis DNA in feces: diagnostic implications and potential solutions. *Front. Microbiol.* 8:115. doi: 10.3389/fmicb.2017.00115

Angen, O., Johannesen, T. B., Petersen, R. F., Uldum, S. A., and Schnee, C. (2021). Development of a species-specific real-time PCR test for *Chlamydia psittaci* and its employment in the investigation of zoonotic transmission from racing pigeons in Denmark. *Diagn. Microbiol. Infect. Dis.* 100:115341. doi: 10.1016/j.diagmicrobio.2021.115341

Chen, C., Li, X. N., Li, G. X., Zhao, L., Duan, S. X., Yan, T. F., et al. (2018). Use of a rapid reverse-transcription recombinase aided amplification assay for respiratory syncytial virus detection. *Diagn. Microbiol. Infect. Dis.* 90, 90–95. doi: 10.1016/j.diagmicrobio.2017.10.005

Cunha, B. A. (2006). The atypical pneumonias: clinical diagnosis and importance. *Clin. Microbiol. Infect.* 12, 12–24. doi: 10.1111/j.1469-0691.2006.01393.x

Duan, S., Li, G., Li, X., Chen, C., Yan, T., Qiu, F., et al. (2018). A probe directed recombinase amplification assay for detection of MTHFR A1298C polymorphism associated with congenital heart disease. *BioTechniques* 64, 211–217. doi: 10.2144/btn-2018-2010

Dumke, R., Schnee, C., Pletz, M. W., Rupp, J., Jacobs, E., Sachse, K., et al. (2015). *Mycoplasma pneumoniae* and *Chlamydia* spp. infection in community-acquired pneumonia, Germany, 2011-2012. *Emerg. Infect. Dis.* 21, 426–434. doi: 10.3201/eid2103.140927

Fan, X., Li, L., Zhao, Y., Liu, Y., Liu, C., Wang, Q., et al. (2020). Clinical validation of two Recombinase-based isothermal amplification assays (RPA/RAA) for the rapid detection of African swine fever virus. *Front. Microbiol.* 11:1696. doi: 10.3389/fmicb.2020.01696

Feodorova, V. A., Saltykov, Y. V., Kolosova, A. A., Rubanik, L. V., Poleshchuk, N. N., and Motin, V. L. (2022). Emergence of novel *Chlamydia trachomatis* sequence types among *Chlamydia* patients in the Republic of Belarus. *Microorganisms* 10:478. doi: 10.3390/microorganisms10020478

Gu, L., Liu, W., Ru, M., Lin, J., Yu, G., Ye, J., et al. (2020). The application of metagenomic next-generation sequencing in diagnosing *Chlamydia psittaci* pneumonia: a report of five cases. *BMC Pulm. Med.* 20:65. doi: 10.1186/s12890-020-1098-x

Gumaa, M. M., Cao, X., Li, Z., Lou, Z., Zhang, N., Zhang, Z., et al. (2019). Establishment of a recombinase polymerase amplification (RPA) assay for

the detection of *Brucella* spp. *Infection. Mol Cell Probes.* 47:101434. doi: 10.1016/j.mcp.2019.101434

Herring, A. J. (1991). PCR test for *Chlamydia psittaci*. *Vet. Rec.* 128:555. doi: 10.1136/vr.128.23.555-b

Hewinson, R. G., Griffiths, P. C., Bevan, B. J., Kirwan, S. E., Field, M. E., Woodward, M. J., et al. (1997). Detection of *Chlamydia psittaci* DNA in avian clinical samples by polymerase chain reaction. *Vet. Microbiol.* 54, 155–166. doi: 10.1016/S0378-1135(96)01268-0

Holland, S. M., Gaydos, C. A., and Quinn, T. C. (1990). Detection and differentiation of *Chlamydia trachomatis*, *Chlamydia psittaci*, and *Chlamydia pneumoniae* by DNA amplification. *J. Infect. Dis.* 162, 984–987. doi: 10.1093/infdis/162.4.984

Hou, L., Li, D., Zhang, N., Zhao, J., Zhao, Y., and Sun, X. (2021). Development of an isothermal recombinase aided amplification assay for the rapid and visualized detection of *Klebsiella pneumoniae*. *J. Sci. Food Agric.* doi: 10.1002/jsfa.11737 [Epub ahead of print]

Jiao, J., Xiong, X., Qi, Y., Gong, W., Duan, C., Yang, X., et al. (2014). Serological characterization of surface-exposed proteins of *Coxiella burnetii*. *Microbiology (Reading)* 160, 2718–2731. doi: 10.1099/mic.0.082131-0

Knittler, M. R., and Sachse, K. (2015). *Chlamydia psittaci*: update on an underestimated zoonotic agent. *Pathog. Dis.* 73, 1–15. doi: 10.1093/femspd/ftu007

Lenzko, H., Moog, U., Henning, K., Lederbach, R., Diller, R., Menge, C., et al. (2011). High frequency of chlamydial co-infections in clinically healthy sheep flocks. *BMC Vet. Res.* 7:29. doi: 10.1186/1746-6148-7-29

Li, Z., Pinto Torres, J. E., Goossens, J., Stijlemans, B., Sterckx, Y. G., and Magez, S. (2020). Development of a recombinase polymerase amplification lateral flow assay for the detection of active *Trypanosoma evansi* infections. *PLoS Negl. Trop. Dis.* 14:e0008044. doi: 10.1371/journal.pntd.0008044

Li, X., Wang, C., Wang, W., Zhang, Z., Zhang, Z., Wang, C., et al. (2021). Research note: development of rapid isothermal amplification assay for detection of duck circovirus. *Poult. Sci.* 100:101339. doi: 10.1016/j.psj.2021.101339

McGovern, O. L., Kobayashi, M., Shaw, K. A., Szablewski, C., Gabel, J., Holsinger, C., et al. (2021). Use of real-time PCR for *Chlamydia psittaci* detection in human specimens During an outbreak of psittacosis–Georgia and Virginia, 2018. *MMWR Morb. Mortal. Wkly Rep.* 70, 505–509. doi: 10.15585/mmwr.mm7014a1

Menard, A., Clerc, M., Subtil, A., Megraud, F., Bebear, C., and De Barbeyrac, B. (2006). Development of a real-time PCR for the detection of *Chlamydia psittaci*. *J. Med. Microbiol.* 55, 471–473. doi: 10.1099/jmm.0.46335-0

Messmer, T. O., Skelton, S. K., Moroney, J. F., Daugharty, H., and Fields, B. S. (1997). Application of a nested, multiplex PCR to psittacosis outbreaks. *J. Clin. Microbiol.* 35, 2043–2046. doi: 10.1128/jcm.35.8.2043-2046.1997

Mina, A., Fatemeh, A., and Jamshid, R. (2019). Detection of *Chlamydia psittaci* genotypes among birds in Northeast Iran. *J. Avian Med. Surg.* 33, 22–28. doi: 10.1647/2017-334

Mitchell, S. L., Budhiraja, S., Thurman, K. A., Lanier Thacker, W., and Winchell, J. M. (2009a). Evaluation of two real-time PCR chemistries for the detection of *Chlamydophila pneumoniae* in clinical specimens. *Mol. Cell. Probes* 23, 309–311. doi: 10.1016/j.mcp.2009.07.005

Mitchell, S. L., Wolff, B. J., Thacker, W. L., Ciembor, P. G., Gregory, C. R., Everett, K. D., et al. (2009b). Genotyping of *Chlamydophila psittaci* by real-time PCR and high-resolution melt analysis. *J. Clin. Microbiol.* 47, 175–181. doi: 10.1128/JCM.01851-08

Njiru, Z. K. (2012). Loop-mediated isothermal amplification technology: towards point of care diagnostics. *PLoS Negl. Trop. Dis.* 6:e1572. doi: 10.1371/journal.pntd.0001572

Opota, O., Jaton, K., Branley, J., Vanrompay, D., Erard, V., Borel, N., et al. (2015). Improving the molecular diagnosis of *Chlamydia psittaci* and *Chlamydia abortus* infection with a species-specific duplex real-time PCR. *J. Med. Microbiol.* 64, 1174–1185. doi: 10.1099/jmm.0.000139

Pang, Y., Cong, F., Zhang, X., Li, H., Chang, Y. F., Xie, Q., et al. (2021). A recombinase polymerase amplification-based assay for rapid detection of *Chlamydia psittaci*. *Poult. Sci.* 100, 585–591. doi: 10.1016/j.psj.2020.11.031

Pantchev, A., Sting, R., Bauerfeind, R., Tyczka, J., and Sachse, K. (2010). Detection of all *Chlamydophila* and *Chlamydia* spp. of veterinary interest using species-specific real-time PCR assays. *Comp. Immunol. Microbiol. Infect. Dis.* 33, 473–484. doi: 10.1016/j.cimid.2009.08.002

Qin, Z., Xue, L., Cai, W., Gao, J., Jiang, Y., Yang, J., et al. (2021). Development of a recombinase-aided amplification assay for rapid detection of human norovirus GII.4. *BMC Infect. Dis.* 21:248. doi: 10.1186/s12879-021-05942-x

Rasmussen, S. J., Douglas, F. P., and Timms, P. (1992). PCR detection and differentiation of *Chlamydia pneumoniae*, *Chlamydia psittaci* and *Chlamydia trachomatis*. *Mol. Cell. Probes* 6, 389–394. doi: 10.1016/0890-8508(92)90032-S

Ruichen Lv, N. L., Wang, J., Li, Y., and Qi, Y. (2022). Recombinase polymerase amplification for rapid detection of zoonotic pathogens: an overview. *Zoonoses* 2, 1–12. doi: 10.15212/ZOONOSES-2022-0002

Sachse, K., Kuehlewind, S., Ruettger, A., Schubert, E., and Rohde, G. (2012). More than classical *Chlamydia psittaci* in urban pigeons. *Vet. Microbiol.* 157, 476–480. doi: 10.1016/j.vetmic.2012.01.002

Sails, A. D., Fox, A. J., Bolton, F. J., Wareing, D. R., and Greenway, D. L. (2003). A real-time PCR assay for the detection of *Campylobacter jejuni* in foods after enrichment culture. *Appl. Environ. Microbiol.* 69, 1383–1390. doi: 10.1128/AEM.69.3.1383-1390.2003

Sanderson, T. P., Andersen, A. A., Miller, L. D., Andrews, J. J., Janke, B. H., Larson, D. L., et al. (1994). An indirect microimmunofluorescence test for detection of chlamydial antibodies in ovine fetal fluids. *J. Vet. Diagn. Investig.* 6, 315–320. doi: 10.1177/104063879400600306

Souriau, A., and Rodolakis, A. (1986). Rapid detection of *Chlamydia psittaci* in vaginal swabs of aborted ewes and goats by enzyme linked immunosorbent assay (ELISA). *Vet. Microbiol.* 11, 251–259. doi: 10.1016/0378-1135(86)90027-1

Sykes, J. E., Allen, J. L., Studdert, V. P., and Browning, G. F. (2001). Detection of feline calicivirus, feline herpesvirus 1 and *Chlamydia psittaci* mucosal swabs by multiplex RT-PCR/PCR. *Vet. Microbiol.* 81, 95–108. doi: 10.1016/S0378-1135(01)00340-6

Szeredi, L., Hotzel, H., and Sachse, K. (2005). High prevalence of *chlamydial* (*Chlamydophila psittaci*) infection in fetal membranes of aborted equine fetuses. *Vet. Res. Commun.* 29, 37–49. doi: 10.1007/s11259-005-0835-1

Takashima, I., Imai, Y., Itoh, N., Kariwa, H., and Hashimoto, N. (1996). Polymerase chain reaction for the detection of *Chlamydia psittaci* in the feces of budgerigars. *Microbiol. Immunol.* 40, 21–26. doi: 10.1111/j.1348-0421.1996.tb03312.x

Wang, Y., Cui, Y., Yu, Z., Li, Y., Bai, C., Sun, P., et al. (2020). Development of a recombinase-aided amplification assay for detection of orf virus. *J. Virol. Methods* 280:113861. doi: 10.1016/j.jviromet.2020.113861

Wolff, B. J., Morrison, S. S., and Winchell, J. M. (2018). Development of a multiplex TaqMan real-time PCR assay for the detection of *Chlamydia psittaci* and *Chlamydia pneumoniae* in human clinical specimens. *Diagn. Microbiol. Infect. Dis.* 90, 167–170. doi: 10.1016/j.diagmicrobio.2017.11.014

Xiaoping, D., and Lynn, S. (2021). Emerging and re-emerging zoonoses are major and global challenges for public health. *Zoonoses* 1, 1–2. doi: 10.15212/ZOONOSES-2021-0001

Yan, T. F., Li, X. N., Wang, L., Chen, C., Duan, S. X., Qi, J. J., et al. (2018). Development of a reverse transcription recombinase-aided amplification assay for the detection of coxsackievirus A10 and coxsackievirus A6 RNA. *Arch. Virol.* 163, 1455–1461. doi: 10.1007/s00705-018-3734-9

Conflict of Interest: The authors declare that the research was conducted in the absence of any commercial or financial relationships that could be construed as a potential conflict of interest.

Publisher's Note: All claims expressed in this article are solely those of the authors and do not necessarily represent those of their affiliated organizations, or those of the publisher, the editors and the reviewers. Any product that may be evaluated in this article, or claim that may be made by its manufacturer, is not guaranteed or endorsed by the publisher.

frontiers | Frontiers in Microbiology

ORIGINAL RESEARCH
published: 28 June 2022
doi: 10.3389/fmicb.2022.947852

In silico Analysis of Peptide-Based Biomarkers for the Diagnosis and Prevention of Latent Tuberculosis Infection

Peng Cheng[1,2], Liang Wang[3] and Wenping Gong[1]**

[1] *Tuberculosis Prevention and Control Key Laboratory/Beijing Key Laboratory of New Techniques of Tuberculosis Diagnosis and Treatment, Senior Department of Tuberculosis, The 8th Medical Center of PLA General Hospital, Beijing, China,* [2] *Hebei North University, Zhangjiakou, China,* [3] *Department of Geriatrics, The 8th Medical Center of PLA General Hospital, Beijing, China*

Background: Latent tuberculosis infection (LTBI) is the primary source of active tuberculosis (ATB), but there are no specific methods for diagnosing and preventing LTBI.

Methods: Dominant T and B cell epitopes predicted from five antigens related to LTBI and *Mycobacterium tuberculosis* region of difference (LTBI-RD) were used to construct a novel polypeptide molecule (PPM). Then, the physicochemical properties, secondary structure, tertiary structure of the PPM, and its binding ability to toll-like receptor 2 (TLR2) and TLR4 were analyzed by bioinformatics tools. Finally, immune stimulation and expression optimization of the PPM were carried out.

Results: Four helper T lymphocytes (HTL) epitopes, five cytotoxic T lymphocytes (CTL) epitopes, and three B cell epitopes were predicted and screened from five LTBI-RD related antigens. These epitopes were connected in series with linkers and adjuvants to construct a novel PPM termed C543P. The results indicated that antigenicity and immunogenicity scores of the C543P candidate were 0.936399 and 1.36469, respectively. The structural analysis results showed that the C543P candidate had good stability. Its secondary structure contained 43.6% α-helix, the Z-score after tertiary structure optimization was −7.9, and the Ramachandran diagram showed that 88.77% amino acid residues of the C543P candidate were in the allowable region. Furthermore, the C543P candidate showed an excellent affinity to TLR2 (−1091.7kcal/mol) and TLR4 (−1102.7kcal/mol). In addition, we also analyzed the immunological characteristics of the C543P candidate. Immune stimulation prediction showed that the C543P candidate could effectively activate T and B lymphocytes and produce high levels of Th1 cytokines such as IFN-γ and IL-2.

Conclusion: We constructed a novel PPM with acceptable antigenicity, immunogenicity, stability, and ability to induce robust immune responses. This study provides a new diagnostic biomarker or peptides-based vaccine for LTBI diagnosis and prevention.

Keywords: tuberculosis (TB), latent tuberculosis infection (LTBI), biomarker, vaccine, diagnosis

OPEN ACCESS

Edited by:
Wei Wang,
Jiangsu Institute of Parasitic Diseases (JIPD), China

Reviewed by:
Chuan Wang,
Sichuan University, China
Mohammad Tahir Waheed,
Quaid-i-Azam University, Pakistan

****Correspondence:***
Wenping Gong
gwp891015@whu.edu.cn
Liang Wang
Wangl309@sina.com

Specialty section:
This article was submitted to Infectious Agents and Disease, a section of the journal Frontiers in Microbiology

Received: *19 May 2022*
Accepted: *08 June 2022*
Published: *28 June 2022*

Citation:
Cheng P, Wang L and Gong W (2022) In silico Analysis of Peptide-Based Biomarkers for the Diagnosis and Prevention of Latent Tuberculosis Infection. Front. Microbiol. 13:947852. doi: 10.3389/fmicb.2022.947852

INTRODUCTION

Tuberculosis (TB), a respiratory infectious disease caused by *Mycobacterium tuberculosis* (MTB) infection, is the second leading cause of death from a single infectious agent after coronavirus disease 2019 (COVID-19). The Global Tuberculosis Report released by the World Health Organization (WHO) pointed out that there were 10 million new TB cases and 1.3 million deaths globally in 2020 (WHO, 2021). TB prevention and control are facing severe challenges, such as latent TB infection (LTBI), multidrug-resistant TB (MDR-TB), rifampicin-resistant TB (RR-TB), and co-infection with SARS-CoV-2 or human immunodeficiency virus (HIV) (WHO, 2021). Previous studies have shown that more than 85% of ATB patients originate from LTBI (Gong and Wu, 2021). LTBI is a subclinical mycobacterial infection defined on the basis of cellular immune response to mycobacterial antigens without clinical manifestations in patients with ATB (Carranza et al., 2020). Previous studies reported that about 23% of the global population had been infected with MTB, but only 10% developed ATB, and nearly 90% of these people are LTBI (Houben and Dodd, 2016; Gong et al., 2018). However, there are no specific diagnostic methods for LTBI and ATB differential diagnosis. Only two methods were approved by the WHO for auxiliary diagnosis of LTBI, including tuberculin skin test (TST) and interferon-gamma (IFN-γ) release assay (IGRA) (Zellweger et al., 2020; Mosavari et al., 2021).

Traditional TST uses purified protein derivative (PPD) as an antigen stimulant. Although this method has the advantages of low price, simplicity, and no need for special equipment, it can not eliminate the interference caused by Bacillus Calmette–Guérin (BCG) vaccination. Therefore, some new TST and IGRAs diagnosis methods have been developed in recent years, including Diaskintest, C-Tb skin test, EC-Test, T-cell spot of TB assay (T-SPOT.TB), QuantiFERON-TB Gold In-Tube (QFT-GIT), QuantiFERON-TB Gold-Plus (QFT-Plus), LIAISON QFT-Plus, and LIOFeron TB/LTBI (Gong and Wu, 2021). These new technologies coincidentally replace the PPD antigen used in the traditional TST with early secreted antigenic target 6 (EAST-6) and culture filtrate protein 10 (CFP-10) antigens. EAST-6 and CFP10 are encoded by Rv3874 and Rv3875 genes, located in the MTB Region of Difference 1 (RD1) (Tang et al., 2014). Both antigens can eliminate BCG vaccination's interference in LTBI diagnosis and reduce the false-positive diagnosis rate. Unfortunately, EAST-6 and CFP10 antigens are not expressed in the latent period of MTB, so it is still not possible to distinguish the LTBI population from ATB patients.

Our previous study found that antigens related to LTBI and RD (LTBI-RD) were promising candidates for LTBI differential diagnosis (Gong and Wu, 2021). Among these 21 LTBI-RD related antigens, five antigens (Rv1737c, Rv2659c, Rv2660c, Rv1981c, and Rv3879c) have been widely reported to be candidate biomarkers for discriminating diagnosis of LTBI. It has been reported that, compared with patients with ATB, the Rv1737c antigen located in the DosR region of MTB could induce significantly higher levels of IFN-γ and TNF-α and promote the expression of $CD4^+$ T cells and $CD8^+$ T cells with $CD45RO^+CD27^+$ phenotype in peripheral blood in individuals with LTBI (Arroyo et al., 2016, 2018). Furthermore, Bai et al. (2015) compared the ability of Rv2659c to stimulate the release of IFN-γ in TB patients, non-TB patients, and LTBI individuals, and they found that the IFN-γ level in LTBI individuals was significantly higher than that in ATB patients. In addition, a study in China using Rv2659c to screen LTBI in recruits also proved that Rv2659c can identify individuals with LTBI with an accuracy rate of 70%, so this antigen may be one of the candidate antigens for discriminating LTBI (Bai et al., 2017). He and colleagues used recombinant protein Rv2660c to evaluate its diagnostic value by enzyme-linked immunosorbent assay (ELISA) (He et al., 2015). The results showed that the number of plaques formed in the LTBI individuals stimulated by the Rv2660c antigen was significantly higher than in ATB patients and healthy populations (He et al., 2015). Furthermore, cytokines such as IL-2, IL-10, IFN-γ, and MIP-1a induced by Rv2660c antigen in LTBI individuals were significantly higher than those in TB patients. These results indicated that Rv2660 could induce more robust immune responses in individuals with LTBI (He et al., 2015).

Based on the evidence mentioned above, in this study, we predicted and screened helper T lymphocytes (HTL), cytotoxic T lymphocytes (CTL), and B cell epitopes from five antigens related to LTBI-RD to construct a polypeptide molecule (PPM) for diagnosing and preventing LTBI. We predicted the antigenicity, immunity, sensitization, physicochemical properties, and secondary structure of the PPM. We also performed the tertiary structure modeling and model validation of the PPM and docked the model with the human toll-like receptor (TLR) to understand its binding affinity. Subsequently, the thermodynamic stability of the PPM was analyzed, and the immune response process of immune cells *in vivo* after antigen injection was predicted by the C-ImmSim server. Finally, electronic cloning and codon optimization were carried out to better express this PPM. This study aimed to design a PPM covering HTL, CTL and B cell epitopes simultaneously, which could provide a novel candidate target for the diagnosis and prevention of LTBI.

Abbreviations: ACC, auto-cross-covariance; ATB, active tuberculosis; ANN, Artificial Neural Network; BCG, Bacillus Calmette–Guérin; CTL, cytotoxic T lymphocytes; CFP10, culture filtrate protein 10; CAI, codon adaptation index; DCs, Dendritic cells; E. coli, Escherichia coli; EAST-6, early secreted antigenic target 6; ELISpot, enzyme-linked immunosorbent spot; ELISA, enzyme-linked immunosorbent assay; GRAVY, grand average of hydrophilicity; HIV, human immunodeficiency virus; HLA, Human leukocyte antigen; HTL, helper T lymphocytes; IFN-γ, interferon gamma; IGRA, interferon gamma release assays; IEDB, Immune Epitope Database; JACT, Java Adaptation Tool; kNN, k nearest neighbors; LTBI, latent tuberculosis infection; MTB, *Mycobacterium tuberculosis*; MDR-TB, multidrug-resistant TB; MHC, major histocompatibility complex; NIAID, National Institute of Allergy and Infectious Diseases; NMA, normal mode analysis; PopAvrSol, population average for the experimental dataset; PBMCs, peripheral blood mononuclear cells; PPD, purified protein derivative; QFT-Plus, QuantiFERON-TB Gold-Plus; QFT-GIT, QuantiFERON-TB Gold In-Tube; RR-TB, rifampicin-resistant TB; RMSD, root mean square deviation; RD1, Region of Difference 1; T-SPOT.TB, T-cell spot of TB assay; TST, tuberculin skin test; TB, Tuberculosis; TLR, toll-like receptor; VdW, van der Waals energy; WHO, World Health Organization.

TABLE 1 | Characteristics of five selected LTBI-RD-associated antigens.

Antigen name	Gene	Product	Length (aa)	Functions	References
Rv1737c	*narK2*	Possible nitrate/nitrite transporter NarK2	395	(1) Higher TNF-α^+ CD4$^+$ T cells and IFN-γ^+ TNF-α^+ CD4$^+$ T cells in LTBI vs. PTB. (2) Higher IFN-γ^+ TNF-α^+ CD8$^+$ T cells in LTBI vs. HC	Arroyo et al., 2016; Chegou et al., 2012
Rv2659c	*Rv2659c*	Probable PhiRv2 prophage integrase	375	higher IFN-γ producing T cells in LTBI vs. aTB & HC	Bai, 2015
Rv2660c	*Rv2660c*	Hypothetical protein	75	(1) Induces stronger immune response in LTBI vs aTB (2) A component of vaccine H56:IC31 and will affect the diagnosis of Rv2660c once the vaccine is available	He et al., 2015; Luabeya et al., 2015
Rv1981c	*nrdF1*	Ribonucleoside-diphosphate reductase (beta chain) NrdF1	322	ELISPOT of Rv1981c achieved sensitivities of 60% in aTB and specificities of 90% in BCG-vaccinated HC.	Chen et al., 2009
Rv3879c	*espK*	ESX-1 secretion-associated protein EspK	729	The immunodominance of Rv3879c is higher than that of Rv3878 and Rv3873 in aTB and LTBI subjects.	Hinks et al., 2009

MATERIALS AND METHODS

Antigens Selection

In our previous study, we screened 21 most potential LTBI-RD related antigens from 133 RD antigens and 124 latency-associated antigens, including Rv1736c, Rv1737c, Rv2031c, Rv2626c, Rv2653c, Rv2654c, Rv2656c, Rv2657c, Rv2658c, Rv2659c, Rv2660c, Rv1511, Rv1978, Rv1980c, Rv1981c, Rv3872, Rv3873, Rv3878, Rv3879c, Rv3425, and Rv3429 (Gong and Wu, 2021). Through extensive literature reading, we found that five antigens have great potential in identifying LTBI, including Rv1737c (NarK2), Rv2659c, Rv2660c, Rv1981c (nrdf1), and Rv3879c (espk) (**Table 1**). The amino acid sequences of these candidate antigens were downloaded through the Mycobrowser server[1] (Kapopoulou et al., 2011).

Prediction of HTL Epitopes

Immune Epitope Database (IEDB) is a free resource funded by the National Institute of Allergy and Infectious Diseases (NIAID). This database documents experimental data on antibodies and T-cell epitopes studied in humans, non-human primates, and other animal species in infectious diseases, allergy, autoimmunity, and transplantation. This study used IEDB's major histocompatibility complex (MHC) II server[2] to predict HTL epitopes (Zhang et al., 2008). Parameter settings are as follows: Prediction Method = IEDB recommended 2.22, MHC source species = Human, MHC allele(s) = total human leukocyte antigen (HLA) reference set (HLA-DR, HLA-DP, HLA-DQ), epitope length = 15. Potential HTL epitopes were selected using the percentile rank method. The percentile rank is obtained by comparing the peptide score with five million 15-mers in the SWISSPROT database. The lower the percentile rank score represents the higher binding of the epitope to MHC II. We choose the epitopes whose percentile rank is less than 0.5 for further exploration in this study. Then, the VaxiJen v2.0[3] was used to predict the antigenicity of the epitopes, and the threshold was 0.5 (Doytchinova and Flower, 2007). VaxJen v2.0 lists selected targets by auto-cross-covariance (ACC) transformation and gives predicted probabilities and protective antigen or non-protective claims. Next, the IFN-gamma epitope server[4] was used to predict the IFN-γ inducibility of epitopes (Dhanda et al., 2013). The prediction method was Motif and SVM hybrid, and the model was IFN-γ versus Non-IFN-gamma. Then, epitopes with positive predictions were selected. Finally, the epitopes that passed the above screening were determined as the immunodominant HTL epitopes for constructing the PPM.

Prediction of CTL Epitopes

Cytotoxic T lymphocytes plays a vital role in controlling the occurrence and development of TB. Therefore, we predicted the CTL epitopes of five LTBI-RD related antigens using the IEDB MHC I server.[5] This server predicts epitopes that bind to MHC I molecules and uses Artificial Neural Network (ANN) 4.0 for 36 HLA-A alleles, 34 HLA-B alleles, and 10 HLA-C alleles (Kim et al., 2012). Parameter settings: Prediction Method = IEDB recommended 2020.09 (NetMHCpan EL4.1), MHC source species = Human, MHC allele(s) = HLA allele reference set, and epitope length(s) = All lengths. We selected CTL epitopes with a percentile rank of <0.5 for subsequent analysis. Subsequently, the Class I Immunogenicity server[6] was selected to analyze the immunogenicity of these epitopes. The CTL epitopes with a percentile rank of <0.5 and immune scores >0 were selected for further analysis. Finally, the VaxiJen v2.0 server was used to predict the antigenicity of the above epitopes, and the selection threshold was set at 0.5 (Doytchinova and Flower, 2007). The epitopes that passed the above screening were determined as the immunodominant CTL epitopes for constructing PPM.

Prediction of Linear B-cell Epitopes

Recent studies have shown that B cells play an essential role in antigen presentation and killing MTB, but they

[1]https://mycobrowser.epfl.ch/

[2]http://tools.iedb.org/mhcii/

[3]http://www.ddg-pharmfac.net/vaxijen/VaxiJen/VaxiJen.html

[4]http://crdd.osdd.net/raghava/ifnepitope/index.php

[5]http://tools.iedb.org/mhci/

[6]http://tools.iedb.org/immunogenicity/

are often overlooked. Herein, the ABCpred server[7] was used to predict linear B-cell epitopes of the five LTBI-RD antigens. The ABCpred server uses artificial neural networks to predict linear B-cell epitope regions in antigen sequences and is widely used in candidate diagnostic antigen and vaccine research (Saha and Raghava, 2006). The server predicted epitopes with an accuracy of 65.93%. Parameter setting: epitope length = 20, the screening threshold = 0.51. Thresholds range from +0.1 to +1.0, and an increased threshold will enhance the specificity but decrease the sensitivity. Finally, the epitopes that passed the above screening were determined to be the immunodominant B cell epitopes for constructing the PPM.

Construction of PPM for LTBI Diagnosis and Prevention

We linked the predicted and screened immunodominant HTL, CTL, and B cell epitopes by using linkers to construct a novel PPM for LTBI diagnosis and prevention. Adjuvant and pan HLA DR-binding epitope (PADRE) were added at the amino terminal of PPM. Besides, adjuvant and 6 × His tag (HHHHHH) were added at the carboxyl-terminal of PPM. The adjuvants used in the PPM included TLR4 receptor agonist CTB (AIE88420.1) (Meza et al., 2017) and TLR2 receptor agonist Pam2Cys (Jackson et al., 2004), and the linkers chosen in this study included GGPPG, AAY, and KK.

Immunogenicity, Antigenicity, Allergenicity, and Toxicity Prediction of PPM

The immunogenicity of the PPM was predicted by using the IEDB Immunogenicity server (see footnote 6). The antigenicity of PPM was predicted by using VaxiJen v2.0 (see footnote 3) and ANTIGENpro server,[8] respectively. The parameters in both servers were set as default values. The ANTIGENpro server is based on cross-validation experiments with 76% accuracy on the combined dataset (Magnan et al., 2010). Identifying allergens is of great significance to developing diagnostic candidates and vaccines. Herein, two servers, AllerTOP v.2.0 server[9] and Allergen FP v.1.0 server,[10] were used to predict the sensitization of the PPM. AllerTOP v.2.0 develops the k nearest neighbors (kNN), ACC transformation, and amino acid E-descriptors machine learning techniques for classifying allergens by exploring the physiochemical properties of proteins. The accuracy of the AllerTOP v.2.0 was stated as 85.3% at fivefold cross-validation (Dimitrov et al., 2014a). AllerFP v.1.0 uses an alignment-free, descriptor-based fingerprint method to identify known allergens and non-allergens. AllerFP v.1.0 correctly recognized 88% of them with a Matthews correlation coefficient of 0.75945 (Dimitrov et al., 2014b). Finally, the ToxinPred server (http://crdd.osdd.net/raghava/toxinpred/) was used to predict the toxicity of the PPM.

Physiochemical Properties and Solubility Prediction

The physicochemical properties of the PPM were predicted using the Expasy Protparam server.[11] This server can indicate molecular protein weight, theoretical isoelectric point (pI), amino acid composition, *in vitro* and *in vivo* half-life, instability, aliphatic index, and grand average of hydrophilicity (GRAVY) (Gasteiger, 2005). Then, the Protein-Sol server[12] was used to predict the solubility of the PPM. The population average for the experimental dataset (PopAvrSol) is 0.45. Therefore, if the prediction result is >0.45, the candidate protein shows a higher solubility than the average soluble *Escherichia coli* (*E. coli*) protein from the experimental solubility dataset (Hebditch et al., 2017).

Secondary Structure and Three-Dimensional Structure Prediction and Refinement

The PSIPRED[13] and Prabi servers[14] were used to predict the secondary structure of the PPM. PSIPRED is a secondary structure generation tool that provides an excellent prediction of transmembrane topology, transmembrane helix, folds, domain recognition, etc. (McGuffin et al., 2000). Prabi severs use GOR4 to predict the secondary structure of peptide molecules, and the average accuracy of this method is 64.4% (Garnier et al., 1996). In addition, the I-TASSER server[15] was used to predict the three-dimensional (3D) spatial structure of polypeptide molecules. The I-TASSER server is a platform for computerized protein structure and function prediction based on sequence-to-structure-to-function paradigms (Yang et al., 2015). At the same time, the I-TASSER server generates 3D atomic models through several thread alignments and iterative structural assembly simulations, and the estimated accuracy of the predictions is based on the modeled confidence score (C-score) of the modeling. In general, the value of the C-score is between −5 and 2. Therefore, the higher the value, the higher the accuracy (Roy et al., 2010). Then, the 3D model of the PPM model was optimized using the GalaxyRefine web server[16] to improve the quality of its partial or complete structure (Heo et al., 2013).

Validation of 3D Structure

The ProSA-web server[17] and the ERRAT-web server[18] were used to evaluate the possible errors in the 3D structure of the PPM. The ProSA-web server accurately enters the frame by estimating the total quality score exact input

[7]https://webs.iiitd.edu.in/raghava/abcpred/ABC_submission.html

[8]http://scratch.proteomics.ics.uci.edu/

[9]http://www.ddg-pharmfac.net/AllerTOP/

[10]http://ddg-pharmfac.net/AllergenFP/

[11]https://web.expasy.org/protparam/

[12]https://protein-sol.manchester.ac.uk/

[13]http://bioinf.cs.ucl.ac.uk/psipred/

[14]https://npsa-prabi.ibcp.fr/cgi-bin/npsa_automat.pl?page=/NPSA/npsa_gor4.html

[15]https://zhanggroup.org//I-TASSER/

[16]https://galaxy.seoklab.org/cgi-bin/submit.cgi?type=REFINE

[17]https://prosa.services.came.sbg.ac.at/prosa.php

[18]https://saves.mbi.ucla.edu/

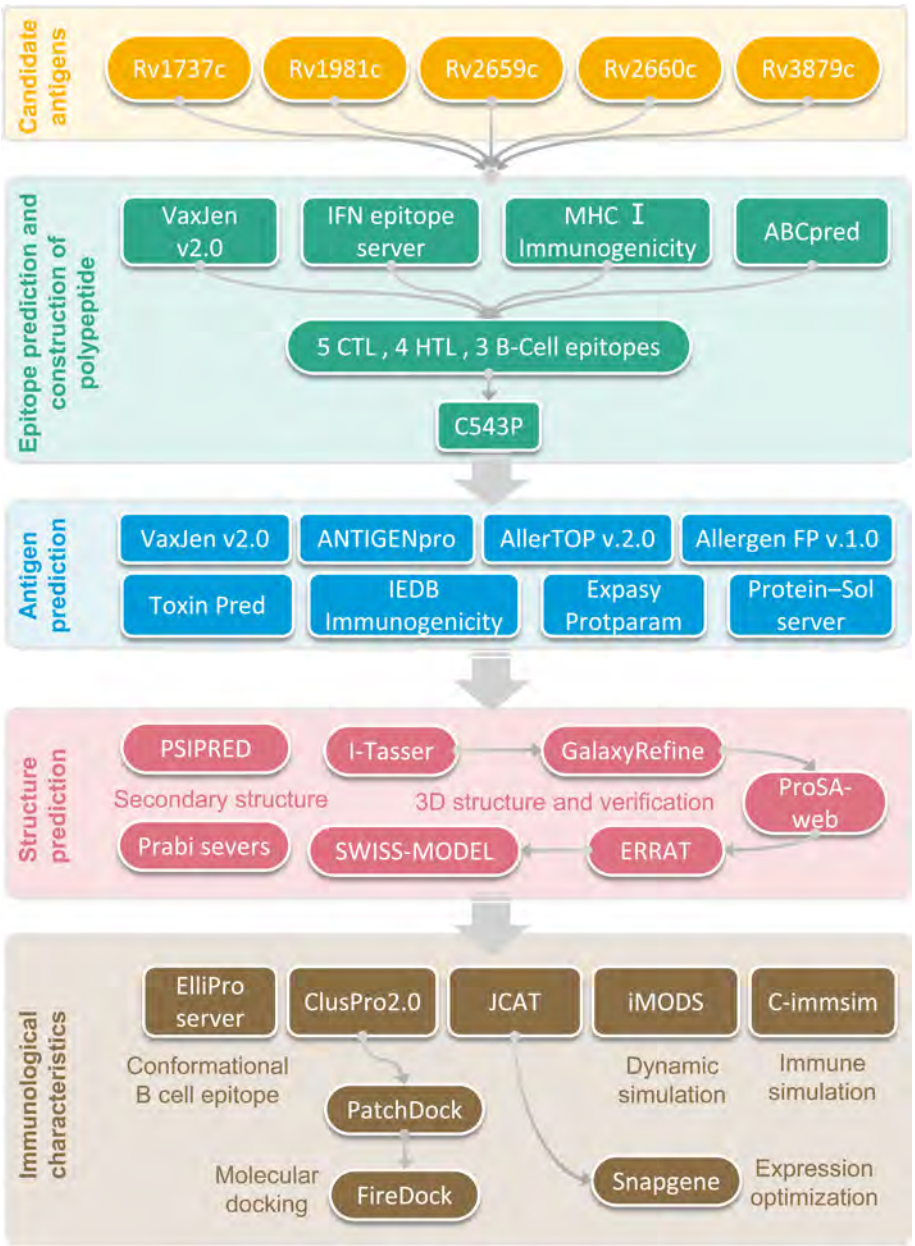

FIGURE 1 | Flow chart of epitope prediction, screening, construction, and PPM analysis.

structure and displays it in the form of a Z score. When the Z score exceeds the properties of the native protein, it indicates that the structure contains errors (Wiederstein and Sippl, 2007). The ERRAT-web server predicts the high-resolution crystallography structure of the PPM from non-bonded atom–atom interactions (Colovos and Yeates, 1993). Then, the SWISS-MODEL server[19] was used to draw a Ramachandran diagram for the PPM (Waterhouse et al., 2018). The Ramachandran diagram shows the favorable region of the dihedral angle of the main chain relative to the amino acid residues in the protein structure (Waterhouse et al., 2018). The structure evaluation page shows the most relevant scores provided by MolProbity and helps us quickly identify the location of low-quality residues in its model or structure (Waterhouse et al., 2018).

Prediction of Discontinuous B-cell Epitopes

Most B cell epitopes are discontinuous, and the constructed proteins are folded in different ways to form discontinuous B cell epitopes. So we predict their discontinuous epitopes

[19]https://swissmodel.expasy.org/assess

by using the ElliPro server[20] following a previous study (Ponomarenko et al., 2008).

Molecular Docking With Immune Receptors

Molecular docking is the most basic and promising method to describe the interaction and binding affinity between peptides and human TLR2 and TLR4. We obtained PDB files for TLR2 (PDB ID: 6NIG) and TLR4 (PDB ID: 4G8A) from the NCBI Molecular Modeling Database (MMDB).[21] Firstly, the ClusPro 2.0 online server[22] was used for ligand-receptor docking analysis (Kozakov et al., 2017). Secondly, the protein-protein docking complexes were refined and re-scored using the PatchDock server[23] and FireDock server[24] (Schneidman-Duhovny et al., 2005; Andrusier et al., 2007; Mashiach et al., 2008). Finally, the HawDOCK server[25] was used to measure the Molecular Mechanics/Generalized Born Surface Area (MM-GBSA) score. The lower the prediction score, the better the prediction result (Weng et al., 2019).

Molecular Dynamics Simulation and Immune Simulation

Molecular dynamics simulation of the PPM was explored using the iMODS web-server,[26] through which the flexibility of the PPM can be defined and calculated (Lopéz-Blanco et al., 2011). Then, the C-ImmSim server[27] was used to predict the PPM's ability to induce immune cells to produce specific antibodies and various cytokines. In addition, this server can also estimate the immune response of B lymphocytes and T lymphocytes (including Th1 and Th2 lymphocytes) (Rapin et al., 2010). The parameters are set as follows: random seed, simulation volume, and simulation steps were selected default values; HLA selection: A0101, A0201, B0702, B0801, DRB10101, and DRB1501. Finally, one injection of the PPM was conducted in the human host.

Codon Optimization and *in silico* Cloning

Codon optimization can improve the expression of recombinant proteins. We used the Java Codon Adaptation Tool (JCAT) server[28] to provide a feasible method for constructing a multi-epitopes-based recombinant plasmid. This server offers a codon-optimized version of the interest DNA sequence based on a chosen organism (Grote et al., 2005). The expression vector *E. coli* (K12) was selected. The output includes two parameters: codon adaptation index (CAI) and GC content percentage. In general, the ideal value of CAI is 1, and the GC content is 30–70%. The PPM sequence was inserted between *EcoR I* and *Xbn I* restriction sites of the pET30a (+) plasmid. SnapGene software was used to finalize *in silico* cloning.

[20]http://tools.iedb.org/ellipro/

[21]https://www.ncbi.nlm.nih.gov/structure/

[22]https://cluspro.bu.edu/home.php

[23]https://bioinfo3d.cs.tau.ac.il/PatchDock/php.php

[24]http://bioinfo3d.cs.tau.ac.il/FireDock/

[25]http://cadd.zju.edu.cn/hawkdock/

[26]https://imods.iqfr.csic.es/

[27]https://150.146.2.1/C-IMMSIM/index.php

[28]http://www.jcat.de/Result.jsp

RESULTS

Selection of Immunodominant Epitopes and Construction of the PPM

The flow chart of prediction, screening, construction, and physicochemical properties of immunodominant epitopes was shown in **Figure 1**. One hundred and fifty-seven HTL epitopes (**Supplementary Table 1**) and 1184 CTL epitopes (**Supplementary Table 2**) with a percentile rank score of <0.5 were identified by using IEDB MHC II and MHC I web servers, respectively. Then, 18 epitopes with antigenicity score >0.7 and positive IFN-γ inducibility were screened from 157 HTL epitopes. In addition, 60 epitopes with immunogenicity > 0 and antigenicity > 1 were screened from 1184 CTL epitopes (**Supplementary Table 3**). Finally, we selected 8 epitopes with a truncated binding score > 0.9 from 154 B cell epitopes using the ABCpred server (**Supplementary Table 4**).

The potential immunodominant epitopes were selected following the below principles: (1) HTL epitopes with antigenicity > 0.7 and the highest IFN prediction score in each antigen were selected; (2) CTL epitopes with the highest immunogenicity score in each antigen were selected; (3) B cell epitopes with the highest ABCpred prediction score (>0.9) were selected. Thus, four HTL, five CTL, and three B cell epitopes were finally selected to construct a new PPM (**Table 2**). The GGPPG, AAY, or KK linker was chosen to connect HTL, CTL, or B cell epitopes, respectively. Adjuvant or agonist CTB (MTPQNITDLCAEYHNTQIYTLNDKIFSYTESLAGKREMAII TFKNGAIFQVEVPGSQHIDSQKKAIERMKDTLRIAYLTEAKV EKLCVWNNKTPHAIAAISMAN), PADRE (AGLFQRHGEGT KATVGEPV), and Pam2Cys (FNNFTVSFWLRVPKVSASHLE) were linked with EAAAK linkers. The above-constructed PPM was named C543P, and its construction pattern and amino acid sequence were shown in **Figures 2A,B**, respectively.

Antigenicity, Immunogenicity, Sensitization, and Toxicity of the C543P Candidate

An ideal LTBI diagnostic and prophylactic candidate should be immunogenic, antigenic, non-toxic, and non-allergenic. Herein, to clarify these characteristics of the C543P candidate, we used multiple servers or databases for analysis. The results showed that the antigenicity predicted by VaxiJen v2.0 and ANTIGENpro were 0.7501 and 0.936399, respectively. The immunogenicity of the C543P candidate predicted by the IEDB Immunogenicity server was 1.36469. These data suggested that the C543P candidate had excellent antigenicity and immunogenicity, and showed a potential ability to induce strong immune responses. Furthermore, the prediction results of AllerTOP v.2.0 and AllergenFP v.1.0 servers showed that the C543P candidate was non-allergenic, and the prediction results of Toxin Pred sever revealed that the C543P candidate was non-toxic. These results

TABLE 2 | Overall the HTL, CTL, and B-cell epitopes selected to construct the C543P candidate.

Protein	Peptide sequence	Length	Alleles	Percentile rank	Antigenicity score	IFN-γ score	Immunogenicity score	ABC pred score
HTL epitopes								
Rv1981c	SFLFYSGFYLPMYWS	15	HLA-DPA1*01:03/DPB1*04:01	0.01	0.8327	1	–	–
	FFSGSGSSYVMGTHQ	15	HLA-DRB1*09:01	0.3	0.7221	0.23620419	–	–
Rv2659c	AFVLMAAWLAMRYGE	15	HLA-DRB1*01:01	0.16	0.7809	0.301353	–	–
Rv3879c	AAASGVPGARAAAAA	15	HLA-DQA1*05:01/DQB1*03:01	0.09	0.9853	0.787876	–	–
CTL epitopes								
Rv1737c	VVNFWAWNL	9	HLA-A*32:01	0.36	2.3392	–	0.55139	–
Rv1981c	DTAQATVGA	9	HLA-A*68:02	0.07	1.3115	–	0.02542	–
Rv2659c	RPDLRVHDL	9	HLA-B*07:02	0.03	2.4462	–	0.12556	–
Rv2660c	ASGGVTVGV	9	HLA-A*68:02	0.47	1.8481	–	0.17684	–
Rv3879c	TATHGANVSL	10	HLA-A*68:02	0.43	1.8613	–	0.04834	–
B cellular epitopes								
Rv1981c	RGDDALKRKASSVMLESFLF	20	–	–	–	–	–	0.95
Rv2659c	RRKFGRIRQFNSGRWQASYT	20	–	–	–	–	–	0.92
Rv3879c	AASVTPAAASGVPGARAAAA	20	–	–	–	–	–	0.93

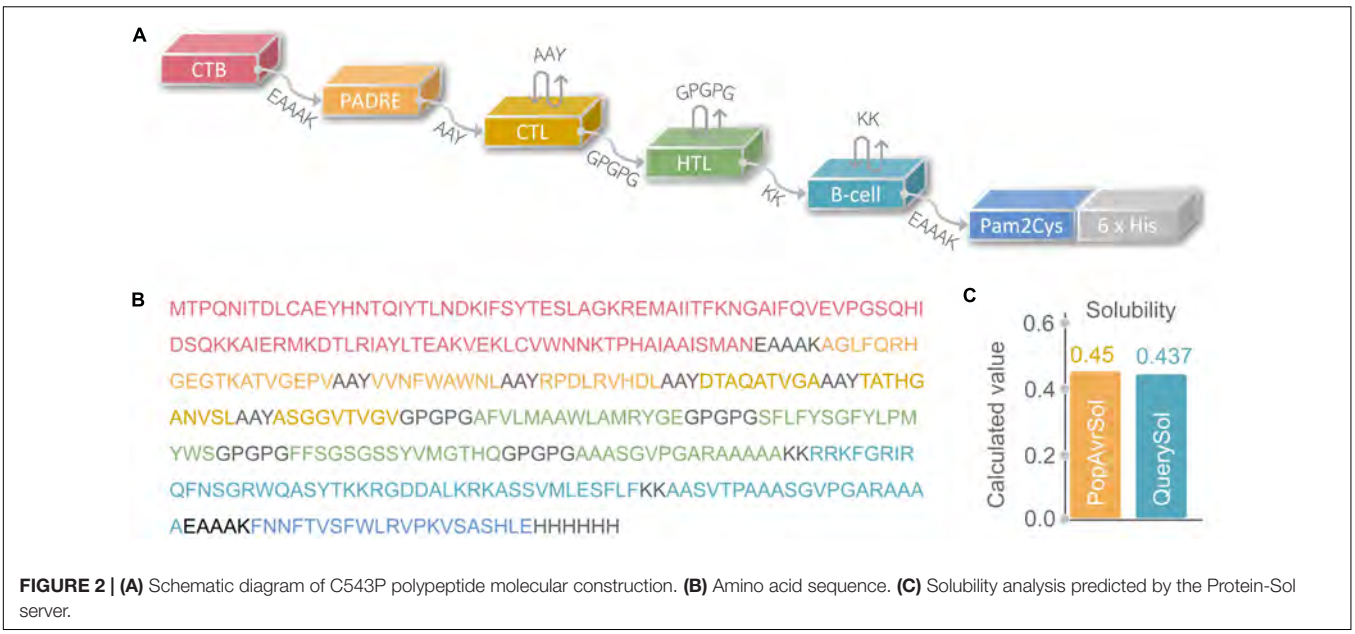

FIGURE 2 | (A) Schematic diagram of C543P polypeptide molecular construction. **(B)** Amino acid sequence. **(C)** Solubility analysis predicted by the Protein-Sol server.

indicate that the C543P candidate is immunogenic, antigenic, non-toxic, and non-allergenic, highlighting that the C543P candidate may be a promising biomarker or vaccine for LTBI diagnosis and prevention.

Physicochemical Properties and Solubility of C543P Candidate

The physicochemical properties of a diagnostic biomarker or a vaccine significantly impact their immunological functions (Ikai, 1980). Therefore, various physical and chemical properties of the C543P candidate were analyzed by the Expasy Protparam server, and the results showed that the C543P candidate is a protein with 367 amino acids, the weight of 39188.54 Da, the theoretical PI value of 9.74, instability index of 27.36, and fat index of 69.35 (**Table 3**). In addition, we also found that the estimated half-life of the C543P candidate in mammalian reticulocytes (*in vitro*), yeast (*in vivo*), and *E. coli* (*in vivo*) were 30 hours, > 20 hours, and > 10 hours, respectively (**Table 3**). These data suggest that the C543P candidate is very stable and has thermal stability (**Table 3**). Furthermore, the solubility of C543P predicted by Protein-Sol server was 0.437 (**Figure 2C**), which indicates that the C543P candidate had an acceptable solubility.

Secondary Structure, Tertiary Structure, and Tertiary Structure Validation of C543P Candidate

Based on the PSIPRED server and Prabi server, we presented the secondary structure of the C543P candidate (**Figure 3A**). The

TABLE 3 | Physicochemical property of C543P predicted by the Expasy Protparam.

Number of amino acids	Weight	Theoretical pI	Estimated half-life:	Instability index:	Aliphatic index	GRAVY
367 aa	39,188.54	9.74	30 h (mammalian reticulocytes, *in vitro*). > 20 hours (yeast, *in vivo*). > 10 hours (Escherichia coli, *in vivo*).	27.36	69.35	−0.16

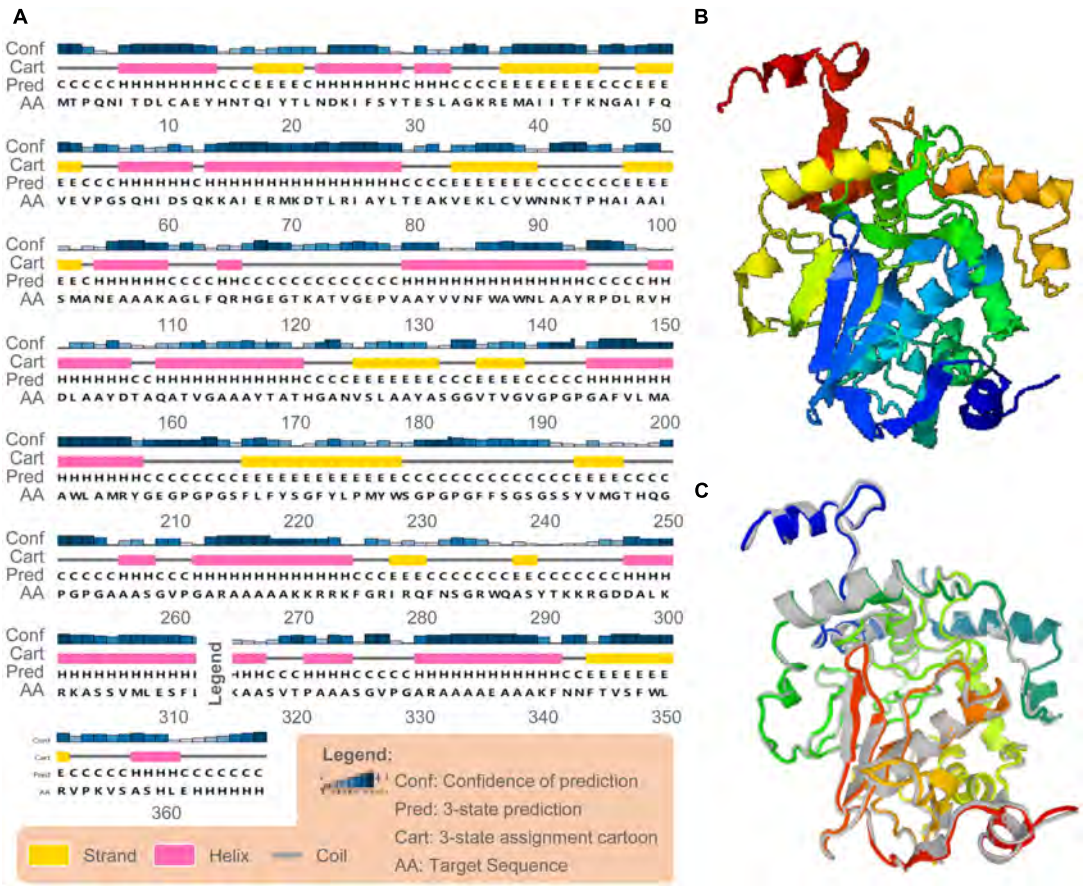

FIGURE 3 | Secondary and tertiary structure prediction of the C543P candidate. **(A)** The C543P candidate was predicted to contain 43.6% α-helices, 15.8% β-strand, and 40.6% random coils by the PSIPRED server. **(B)** The 3D model of the C543P candidate was obtained on the I-TASSER server. **(C)** The 3D model of the peptide molecule after optimization by the Galaxy refining server, and the colored structure was superimposed on the rough gray model.

C543P candidate contains 43.6% α-helix, 15.8% β-strand, and 40.6% random coil. Subsequently, we predicted the 3D structures of the five 3D models designed by the I-TASSER server. The results showed that the Z scores of the five 3D models were between 0.82 and 9.12. Their confidence scores (C-score) were −1.55, −2.36, −2.33, −2.30, and −2.42, respectively. We selected the optimal 3D model with C-score = −2.36 to simulate the 3D structure of the C543P candidate (**Figure 3B**). We found that under this 3D model, the TM score of the C543P candidate was 0.52 ± 0.15, and the expected root-mean-square deviation (RMSD) was 10.2 ± 4.6A. The TM-value has been recommended as a calculating scale for the structural resemblance among the structures. The TM-value was suggested to address the issue of RMSD, which is delicate to native errors. Then, the GalaxyRefine web server was used to optimize the 3D model of the C543P candidate. GalaxyRefine web server can improve the consistency of modeled proteins to obtain higher quality prediction results. Through loop refinement and energy minimization on the rough model, we again obtained five optimized 3D models, from which model 2 was selected for further study (**Figure 3C**). The GDT-HA value of this model was 0.9469, RMSD value was 0.429, MolProbity value was 2.13, Clash score was 10.7, low Rotamers was 0.7, and Rama favored was 88.8.

ProSA-web server and ERRAT-web server were used to verify the quality and potential errors in the 3D model of the C543P candidate. The results showed that the Z score of the optimized C543P candidate was −7.9 (**Figure 4A**), and the energy map was shown in **Figure 4B**. The Overall Quality Factor of the C543P candidate was improved from 86.9436 to 91% after being optimized by the ERRAT-web server. The Ramachandran

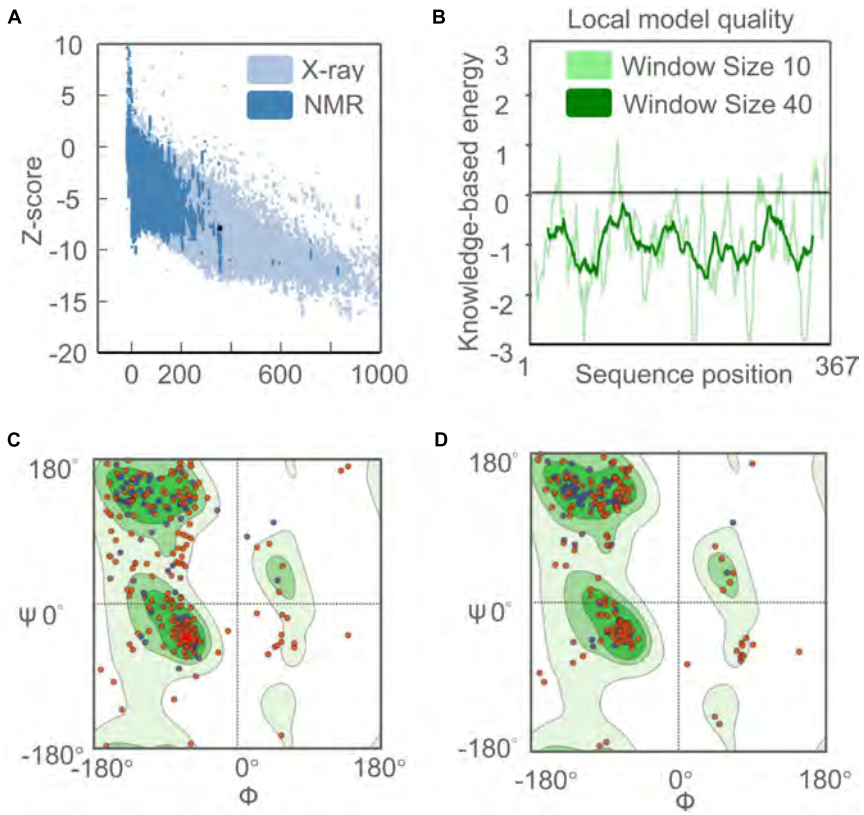

FIGURE 4 | Evaluation and validation of the tertiary structure model of the C543P candidate. **(A)** Z-score predicted by ProSA-web server: −7.9. **(B)** Energy map of C543P peptide molecule validation. **(C)** Ramachandran diagram analysis of C543P peptide molecule before optimization shows Favored region: 75.39%, outliers region: 7.85%, rotamer region: 9.70%. **(D)** Ramachandran diagram of C543P peptide molecule optimization: Favored region: 88.77%, outliers region: 1.92%, rotamer region: 0.37%.

diagram showed that, before optimizing the C543P candidate, the Favored region was 75.39%, the outliers region was 7.85%, and the rotamer region was 9.70% (**Figure 4C**). After optimization, the Favored region was 88.77%, the outliers region was 1.92%, and the rotamer region was 0.37% (**Figure 4D**). Therefore, the Favored region of the C543P candidate was increased from 75.39 to 88.77%.

Conformational B-cell Epitopes

According to data obtained from the ElliPro server, 193 residues were distributed on 10 putative B-cell epitopes with values ranging from 0.501 to 0.992 (**Supplementary Table 5**). For discontinuous epitopes predicted by the ElliPro server, epitopes with a score > 0.69 are usually selected. The conformational B-cell epitopes of the C543P candidate were estimated to have 74 residues with scores ranging from 0.709 to 0.992 (**Figure 5** and **Table 4**).

Molecular Docking

This study used several servers to predict protein-protein docking to improve prediction accuracy. Firstly, the docking exploration of TLR2 and TLR4 was performed using the ClusPro 2.0 server, which generated 30 predicted complexes. Secondly, two models (1091.7 and 1102.7 kcal/mol models) with lower complex binding energies were selected for further optimization. Then, the C543P candidate was evaluated using the PatchDock server, which generated different score sheets by identifying different models. Finally, the top 10 complexes identified by the above methods were refined through the FireDock server, from which the model with the lowest required binding energy was selected. The optimization results of the TLR2-C543P complex showed that the global energy was 1.34, the attractive van der Waals energy (VdW) was −5.62, the repulsive (VdW) was 2.38, and the atomic contact energy was 6.04 (**Figure 6A**). The optimization results of the TLR4-C543P complex showed that the global energy was −0.35, the attractive (VdW) was −3.49, the repulsive (VdW) was 1.66, and the atomic contact energy was −1.96 (**Figure 6B**). The HawDock server predicted the relative binding free energies of the C543P candidate to TLR2 and TLR4 in the MM-GBSA were −4.86 and −22.58 kcal/mol, respectively.

Molecular Dynamics Simulation Between C543P Candidate and TLRs

The molecular dynamics simulation and normal mode analysis (NMA) of the docking complex of the C543P candidate

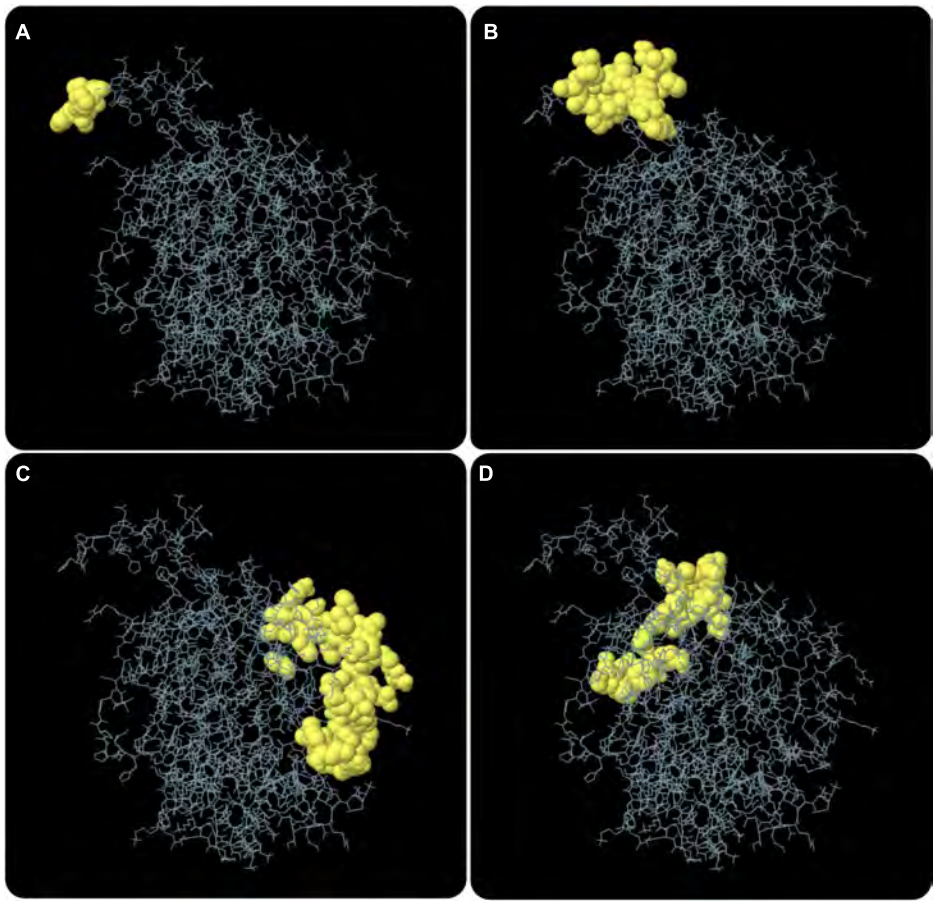

FIGURE 5 | The conformation or discontinuous B cell epitope of the C543P candidate. The yellow balls in panels **(A–D)** represented 4 conformations or discontinuous B cell epitopes, respectively, and the rest were shown in gray.

TABLE 4 | The conformational B cell epitopes residues of the C543P candidate predicted by the ElliPro.

No	Residues	Number of residues	Score
1	A:H365, A:H366, A:H367	3	0.992
2	A:W349, A:L350, A:R351, A:V352, A:P353, A:K354, A:V355, A:S356, A:A357, A:S358, A:H359, A:L360, A:E361, A:H362, A:H363, A:H364	16	0.918
3	A:R144, A:P145, A:D146, A:L147, A:R148, A:D151, A:L152, A:G163, A:S289, A:Y290, A:T291, A:K292, A:R294, A:G295, A:D296, A:D297, A:A298, A:L299, A:K300, A:R301, A:K302, A:A303, A:S304, A:S305, A:V306, A:M307, A:L308, A:S310, A:F311, A:L312, A:K314, A:K315	32	0.712
4	A:R206, A:G238, A:S239, A:G240, A:S241, A:S242, A:Y243, A:S318, A:V319, A:T320, A:P321, A:A322, A:A323, A:A324, A:S325, A:G326, A:V327, A:P328, A:G329, A:A330, A:R331, A:A332, A:E336	23	0.709

with TLR2 and TLR4 were shown in **Figures 7A**, **8A**, respectively. Simulation prediction was performed to determine the movement of molecules and atoms in the antigenic structure. The deformability of TLR2-C543P (**Figure 7B**) or TLR4-C543P (**Figure 8B**) complex was shown with peaks in the deformable regions of the C543P candidate. The simulation results showed that the TLR2-C543P complex and TLR4-C543P complex eigenvalues were 8.659505e-06 (**Figure 7C**) and 9.469126e-06 (**Figure 8C**), respectively. Variance plots showed a cumulative or individual variance of TLR2-C543P complex (**Figure 7D**) and TLR4-C543P complex (**Figure 8D**) with green or purple, respectively. The relation of the docked TLR2-C543P complex (**Figure 7E**) and TLR4-C543P complex (**Figure 8E**) between the NMA and the PDB sector was shown by the B-factor graph. The co-variance map of the complex where the correlated motion between a pair of residues was indicated by red color, uncorrelated by white color, and anti-correlated by blue color (**Figures 7F**, **8F**). The elastic network model showed that the docked protein molecule (C-α) atoms were interconnected with some degree

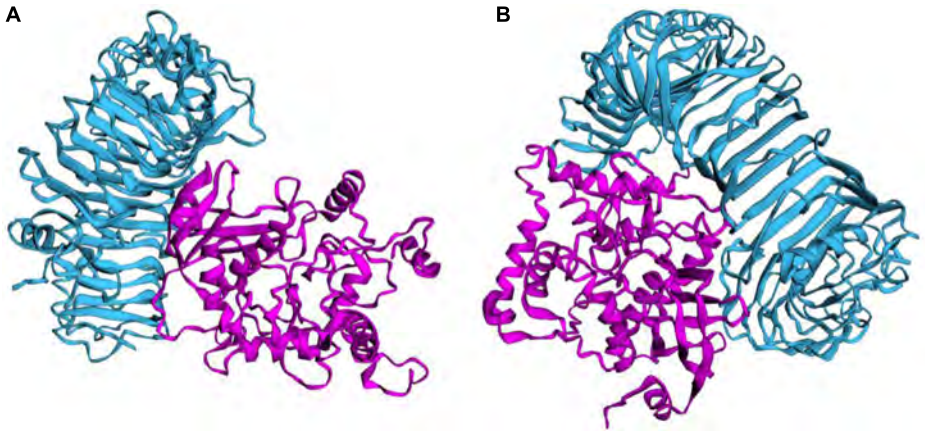

FIGURE 6 | Ligand–receptor interaction. C543P was shown in purple and TLR2 **(A)** and TLR4 **(B)** were shown in blue.

of "spring" (harder springs were shown in darker gray) (**Figures 7G**, **8G**).

Immune Responses Induced by the Candidate C543P

Mycobacterium tuberculosis is an intracellular pathogen, and cellular and humoral immunity play essential roles in killing and eliminating MTB. We found that the C543P candidate could effectively stimulate the innate immune system to induce immune responses in the immune simulation prediction. The results showed that after C543P stimulation, the population per state of NK cells increased in a staged and fluctuating manner, reaching a peak on day 9 (**Figure 9A**). The population per state of dendritic cells (DCs) reached a peak on day 23, mainly resting DCs. Interestingly, we found that presenting-2 DCs populations per state peaked on day 2 after C543P stimulation and gradually decreased (**Figure 9B**). In addition to DCs, macrophages can clear infected cells. Our study showed that the presenting-2 macrophages population per state started to proliferate after stimulation with C543P, peaked on day 2, and gradually decreased (**Figure 9C**). When presenting-2 macrophages reached their peak, the active macrophages population per state began to proliferate rapidly, reaching a peak on day 7 and maintaining a high level of activation (**Figure 9C**). Finally, considering that MTB first interacts with alveolar epithelial cells after entering the lungs, we also analyzed the effect of C543P on epithelial cells. The results showed that the population per state of epithelial cells would maintain a significantly high secretion level after being stimulated by C543P (**Figure 9D**).

Innate immunity plays a vital role in the initial stage of MTB infection, but the clearance and killing of MTB mainly depend on the adaptive immune responses. Recent studies suggested that B lymphocyte-mediated humoral immune responses also play a role in MTB clearance (Gong et al., 2021, 2022). C-ImmSim server prediction showed that after the C543P candidate stimulation, B lymphocytes mainly performed an antigen-presenting function in the initial stage. The presenting-2 B lymphocytes population per state reached 450 cells/mm^3 on day 2 after C543P stimulation. Then, the active B lymphocytes population per state proliferated in large numbers, reaching a peak on day 7 after C543P stimulation (**Figure 10A**). C543P also induced B lymphocytes to produce high levels of IgG and IgM antibodies, peaking on day 6 (**Figure 10B**). CD4$^+$ T lymphocytes are the central effector cells that kill and clear MTB. The C-ImmSim server showed that C543P could stimulate the proliferation of memory and non-memory CD4$^+$ T lymphocytes significantly, reaching a peak on day 10 (>3,500 cells/mm^3) and then decreasing slowly (**Figure 10C**). The population per state of active and resting HTL peaked on day 7 and then gradually declined (**Figure 10D**). Regulatory T cells can regulate the immune response of helper T cells to avoid the overreaction of Th1 and Th2 cells. The results showed that the regulatory T cell population per state reached as high as 140 cells/mm^3 on day 5 after C543P stimulation, followed by a decrease (**Figure 10E**). Furthermore, it is reported that CTL plays an essential role in killing the host cells infected by MTB via producing granular enzymes and nitric oxide. Herein, we found that the population per state of non-memory cytotoxic T cells gradually increased and peaked (1,150 cells/mm^3) on day 13, and that of memory cytotoxic T cells remained at the level of 1,125 cells/mm^3 (**Figure 10F**). Moreover, we also found that the population per state of active cytotoxic T lymphocytes gradually increased and reached a peak on the 30th day after stimulation. In contrast, resting cytotoxic T lymphocytes showed an opposite trend (**Figure 10G**). Interestingly, our results indicated that C543P could induce significantly high levels of IFN-γ and IL-2 (**Figure 10H**).

Codon Optimization and *in-silico* Cloning

To predict the molecular cloning and expression levels of the C543P candidate *in vitro*, we used the Java Adaptation Tool (JACT) server to predict maximum protein expression in *E. coli* (K12). The data showed that the CAI value of the C543P candidate was 1, and the average GC content of the adapted sequence was 52.6%, indicating that the C543P candidate could be highly expressed in *E. coli*. Finally, using SnapGene software,

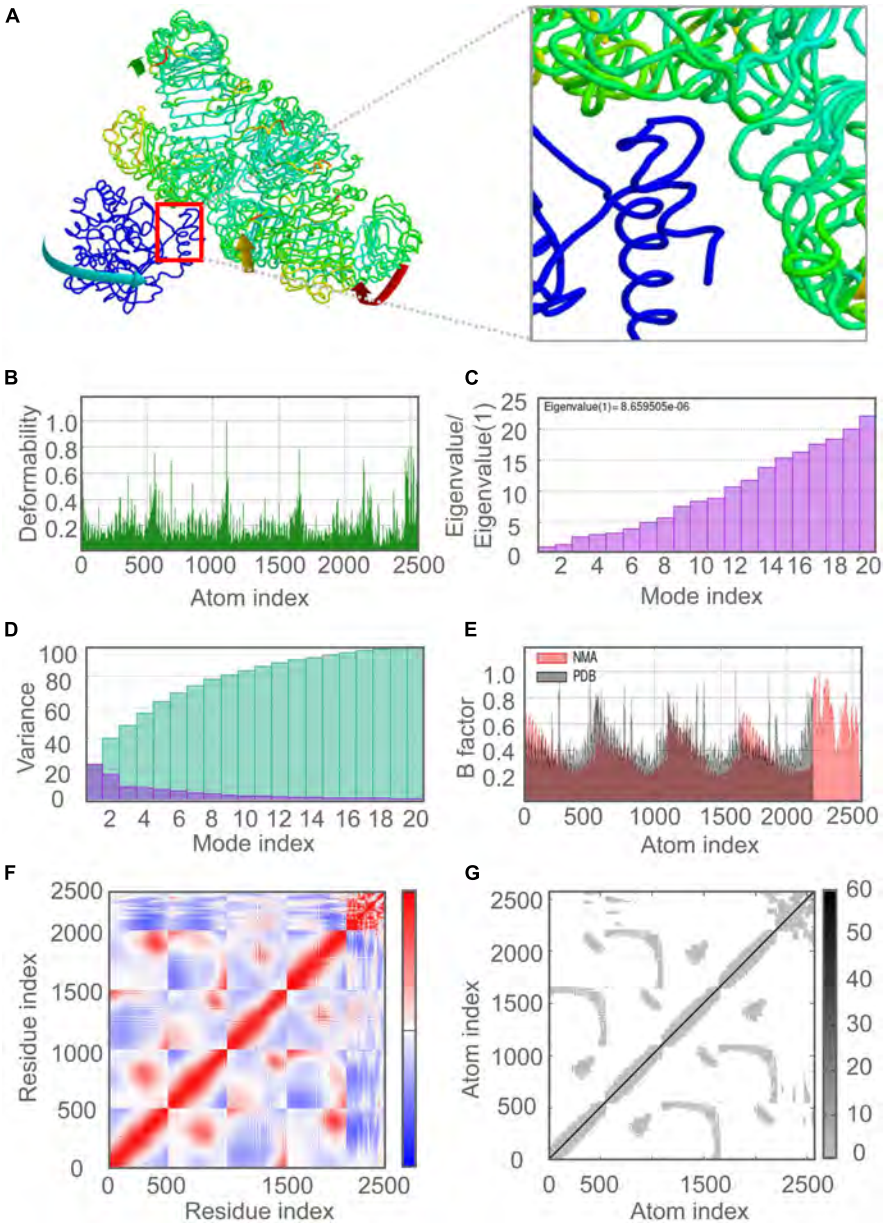

FIGURE 7 | Molecular dynamics simulation of the C543P candidate and TLR2. **(A)** NMA mobility. The direction of the arrow indicates the direction of molecular motion. Blue represents the C543P molecule and green expresses the TLR2 receptor. **(B)** variability; **(C)** eigenvalues; **(D)** variance (Purple for individual variance, green for cumulative variance); **(E)** B-factor; **(F)** covariance plot (red for correlated motion, white for uncorrelated motion, the blue color indicates anti-correlated motion); **(G)** elastic network (dark gray areas indicate harder areas).

the gene sequence of the optimized C543P candidate was inserted into the pET30a(+) plasmid to construct a recombinant plasmid (**Supplementary Figure 1**).

DISCUSSION

Rapid advances in bioinformatics, structural biology, and computational tools have revolutionized the development of diagnostic biomarkers and vaccines. The use of these tools has greatly aided in the processing and analyzing basic data on microorganisms (Kardani et al., 2020). The methods for predicting and designing diagnostic biomarkers and vaccines *in-silico* have greatly improved, and they have been applied to bacteria, viruses, fungi, and even cancers (Raoufi et al., 2020). Previous studies have designed several peptides-based vaccine candidates against MTB infection (Bibi et al., 2021; Sharma et al., 2021; Shiraz et al., 2021). The bioinformatics technologies used in these studies promote the development of TB vaccines and reduce cost and save time. However, the

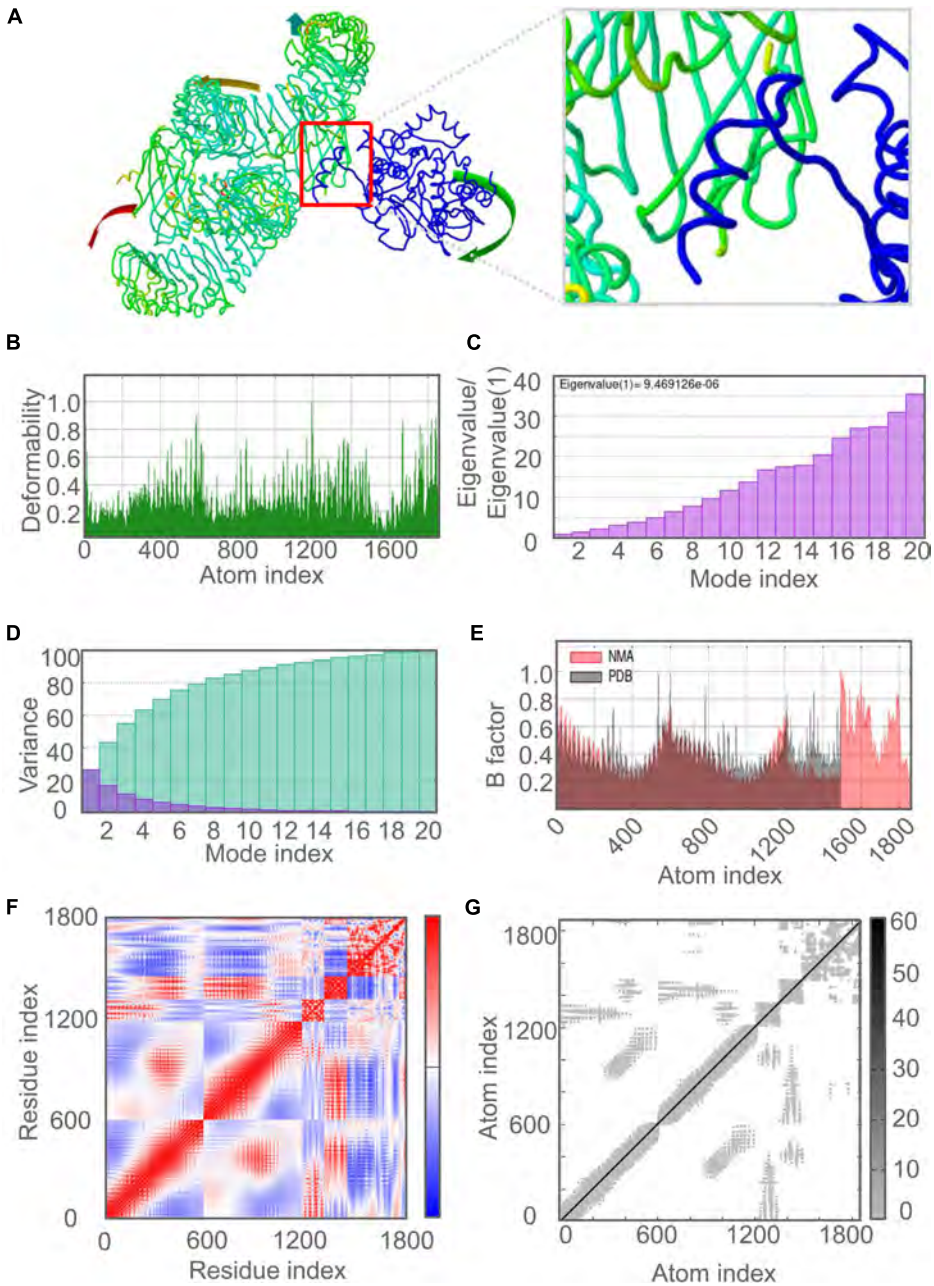

FIGURE 8 | Molecular dynamics simulation of the C543P candidate and TLR4. **(A)** NMA mobility. The direction of the arrow indicates the direction of molecular motion. Blue represents the C543P molecule and green expresses the TLR2 receptor. **(B)** variability; **(C)** eigenvalues; **(D)** variance (Purple for individual variance, green for cumulative variance); **(E)** B-factor; (F) covariance plot (red for correlated motion, white for uncorrelated motion, the blue color indicates anti-correlated motion); **(G)** elastic network (dark gray areas indicate harder areas).

epitopes of these TB vaccines were predicted and selected from antigens secreted by MTB during proliferation, which means that these TB vaccines may not fight against LTBI. Thus, we designed a PPM named C543P based on epitopes selected from five LTBI-RD-associated antigens, including Rv1737c, Rv1981c, Rv2659c, Rv2660c, and Rv3879c. The C543P candidate might be a promising candidate biomarker for the diagnosis and prevention of LTBI.

LTBI is a dynamic equilibrium state achieved by mutual antagonism between host immune function and invasiveness of MTB (Gong and Wu, 2021). The activation of $CD4^+$ T cells and $CD8^+$ T cells depends on recognizing the MHC-II and MHC-I molecules on the surface of antigen-presenting cells. Therefore, the C543P candidate has the following advantages: (1) As a preventive vaccine for LTBI, the C543P can activate $CD4^+$ T cells and $CD8^+$ T cells to produce high levels of cytokines such as

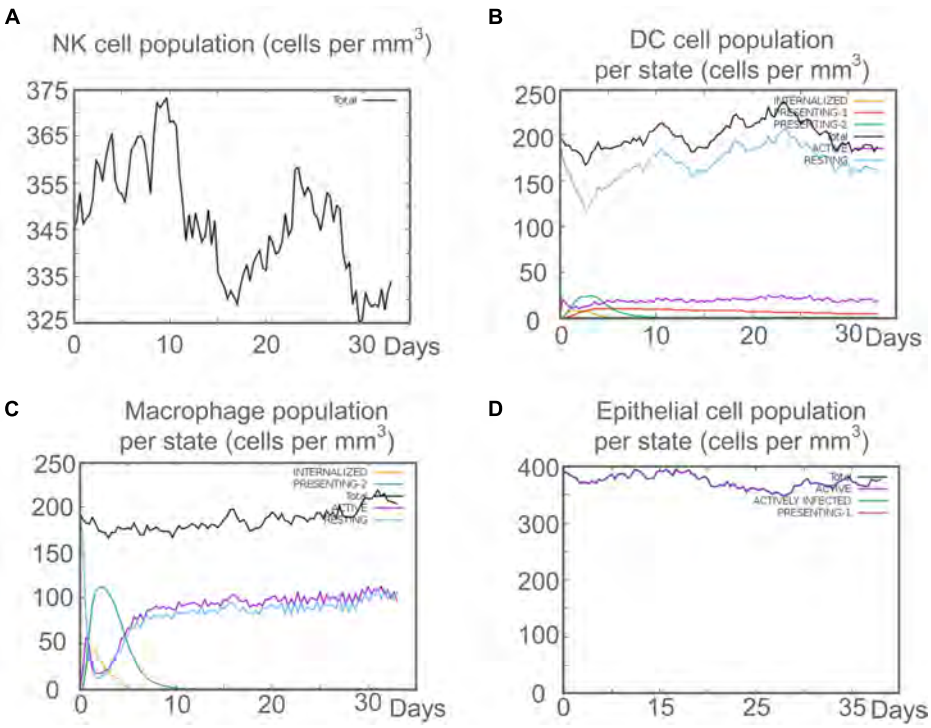

FIGURE 9 | The innate immune responses induced by C543P in C-ImmSim server. **(A)** Expression of NK cells after antigen stimulation. **(B)** Expression of DC cells (black) after antigen stimulation. **(C)** Expression in macrophages (black) after antigen stimulation. **(D)** Secretion from active epithelial cells (purple) after antigen stimulation.

IFN-γ and IL-2, enhancing the anti-MTB activity of macrophages (Bertholet et al., 1950), and inhibit the transformation of LTBI to ATB. (2) As a biomarker for the differential diagnosis of LTBI, C543P could stimulate the peripheral blood mononuclear cells (PBMCs) of the LTBI population to produce significantly high levels of IFN-γ in a short time, thereby separating the LTBI population from ATB patients.

The enzyme-linked immunosorbent spot (ELISpot) assay is a commonly used method to detect human-specific T cells, accurately assessing the number of T cells with IFN-γ releasing ability. Therefore, the C543P was constructed based on immunodominant epitopes inducing a high level of IFN-γ in individuals with LTBI. However, differences in racial genetic background constitute a significant obstacle to developing epitope-based diagnostic markers and vaccines. HLA is highly polymorphic, thus, selecting immunodominant epitopes that can be recognized by numerous HLAs is beneficial to improving the coverage of the C543P candidate and avoiding racial bias (Bui et al., 2006). Therefore, when predicting HTL and CTL epitopes, we choose the default HLA-I and HLA-II alleles most frequently distributed in the population from the IEDB database. On this basis, the immunodominant epitopes with better antigenicity and immunogenicity were selected. In addition, the addition of B cell epitopes allows C543P to activate B lymphocytes more efficiently to induce humoral immunity.

The C543P candidate also contains several vital adjuvants and TLR agonists to enhance its ability to induce immune responses. These TLR agonists used in C543P can be recognized by cognate TLRs on different immune cells and polarize naive $CD4^+$ T cells through the Th1 pathway to induce an immune response (Kawai and Akira, 2010). Our prediction data showed that the antigenicity of C543P was 0.7501, and the immunogenicity was 1.36469. These data indicate that the C543P has a good antigenicity and can induce a high level of immune response. Furthermore, we found that C543P was a non-toxic, non-allergenic, and stable candidate for LTBI diagnosis and prevention. The limitation of the C543P is that the solubility of C543P was 0.437, so it is necessary to improve its solubility in the subsequent optimization for better cloning and expression in *E. coli*.

The secondary structure of C543P mainly contains 43.6% α-helix, 15.8% β-strand, and 40.6% random coil. Naturally unfolded protein regions and α-helices are considered essential types of "structural antigens." Thus, the increase of these two structures contributes to the recognition of antibodies induced after infection (Corradin et al., 2007). It was found that 88.77% of the amino acid residues of C543P were in the Favored region, indicating that the entire model's prediction quality was acceptable. The main targets of host recognition of MTB are TLR2 and TLR4, so adding TLR2 and TLR4 agonists as adjuvants in the design of C543P can significantly improve the presentation efficiency of C543P. We tested the binding ability of C543P to TLR2 and TLR4, and the results showed that the C543P has a high binding affinity, suggesting that the C543P can be

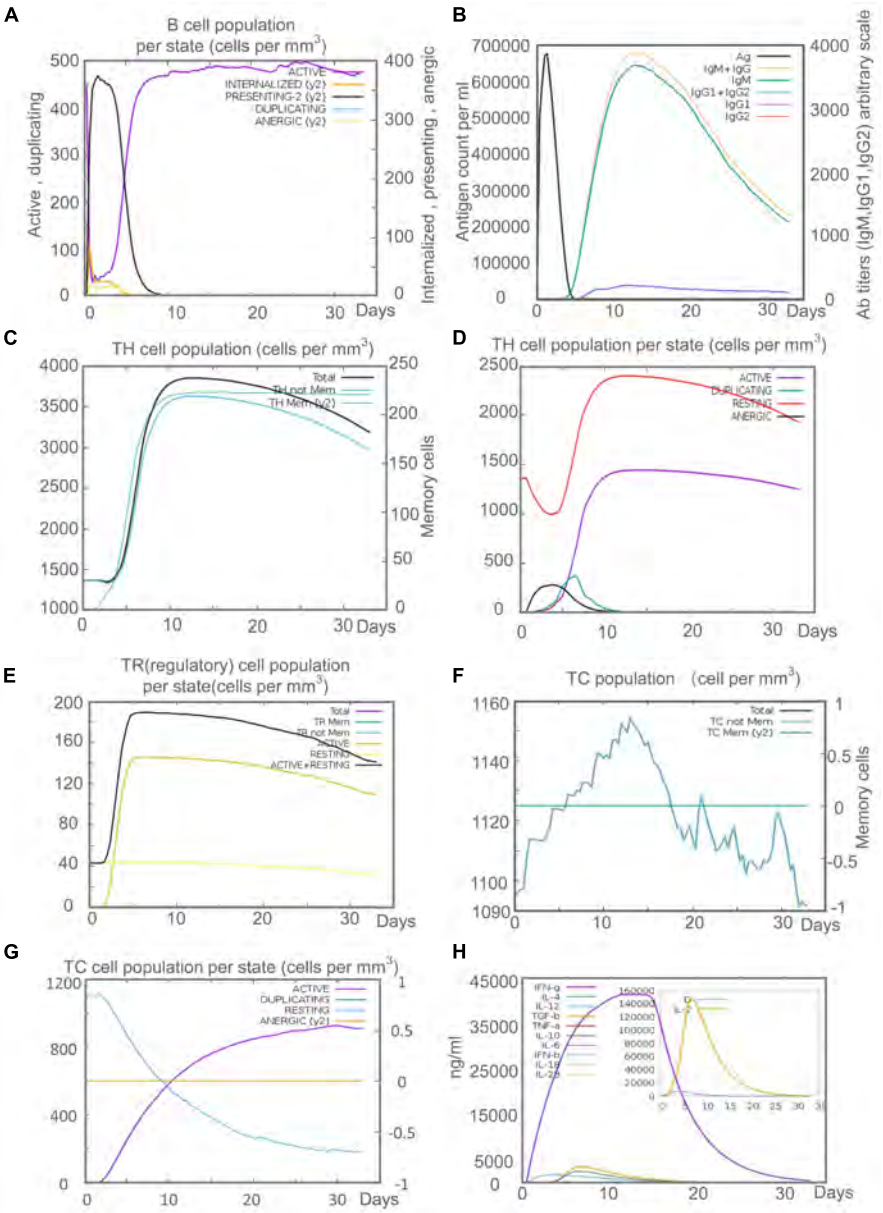

FIGURE 10 | The adaptive immune responses induced by C543P in C-ImmSim server. **(A)** Active B cell (purple) secretion after antigen stimulation. **(B)** The primary B cell antibody produced after antigen stimulation is IgM + IgG (yellow) changes over time. **(C,D)** Changes in the secretion level of helper T lymphocytes and the secretion levels of helper T lymphocytes of different memory types. **(E)** Changes in Treg T cell secretion after antigen stimulation. **(F,G)** Changes in the level of $CD8^+$ T secretion after antigen stimulation and the secretion of different types of $CD8^+$ T cells. **(H)**. Changes in secretion levels of cytokines, mainly IFN-γ (purple) and IL-2 (yellow).

efficiently recognized by TLR2 and TLR4 and induce a more robust immune response.

Whether as a biomarker for differential diagnosis of LTBI or as a vaccine for LTBI prevention, the ability of C543P to induce immune responses in T and B lymphocytes determines its potential value. Previous studies have shown that macrophages clear MTB through oxygen, chloride, cytokine production, phagosome acidification, and intracellular MTB autophagy (Liu et al., 2017). In addition, some macrophages phagocytose MTB present antigens or epitopes to T cells for recognition and activate adaptive immune responses (Gong et al., 2022). Our immune prediction found that the C543P could induce effective innate and adaptive immune responses in humans. As the first line of defense against MTB infection, alveolar epithelial cells can use MHC-II molecules to influence the lungs' immune system. Furthermore, the high level of alveolar epithelial cells can promote the secretion of cytokines by HTL to kill MTB (Shenoy, 2021). Our study found that macrophages play an essential role in C543P antigen

presentation. The population per state of macrophages exceeded 100 cells/mm^3 on the second day after C543P stimulation. The Th1 subset of CD4$^+$ T lymphocytes plays a central role in the host killing of MTB infection, mainly secreting IFN-γ, IL-2, IL-12, and TNF-α (Boom et al., 2003). The results of C-ImmSim server prediction found that the C543P induced T lymphocytes to secrete high levels of Th1-type cytokines such as IFN-γ and IL-2, indicating that the C543P mainly induced the secretion of Th1-type cytokines. Apart from this, the C543P can also effectively activate CD8$^+$ T lymphocytes, and the population per state of CD8$^+$ T cells reached 1155 cells/mm^3 on the 13th day after stimulation. These massively proliferated and activated CD8$^+$ T cells can effectively lyse and kill cells infected with MTB by secreting a large amount of granzyme B, perforin, and other cytotoxic factors (Kumar and Babu, 2017).

CONCLUSION

In summary, a novel diagnostic biomarker or vaccine candidate named C543P was designed in this study. The C543P candidate consists of four HTL, five CTL, and three B cell epitopes as well as adjuvant or agonists. Our results showed that C543P was highly antigenic and immunogenic while non-sensitizing and non-toxic. Furthermore, it was found that the C543P candidate had a good affinity with both TLR2 and TLR4, and the kinetic simulation showed that C543P had good stability and could promote its interaction with TLRs. In addition, the C543P candidate can induce high levels of innate and adaptive immune responses in humans, characterized by markedly higher levels of the Th1-type cytokines such as IFN-γ and IL-2. This study provides a promising diagnostic biomarker and a vaccine candidate for diagnosing and preventing LTBI.

DATA AVAILABILITY STATEMENT

The original contributions presented in the study are included in the article/**Supplementary Material**, further inquiries can be directed to the corresponding authors.

AUTHOR CONTRIBUTIONS

WG and LW: conceptualization and writing—review and editing. PC: data curation, formal analysis and writing—original draft. WG: funding acquisition. PC and WG: methodology and software. All authors contributed to the article and approved the submitted version.

FUNDING

This study was funded by the Beijing Municipal Science & Technology Commission (Grant No. 19L2065, 7212103, and Z181100001718005) and the Chinese PLA General Hospital (Grant No. QNC19047).

SUPPLEMENTARY MATERIAL

The Supplementary Material for this article can be found online at: https://www.frontiersin.org/articles/10.3389/fmicb.2022.947852/full#supplementary-material

Supplementary Figure 1 | The polypeptide molecular sequence was electronically cloned into the pET30a expression vector by SnapGene software. The diagnostic antigen is the gene coding for the insertion of antigen molecules, and the rest is the expression vector.

Supplementary Table 1 | The detailed information of the whole HTL epitopes predicted by IEDB database. The potential HTL epitopes were identified by adjusted rank, antigenicity score, and IFN score, and marked with yellow color.

Supplementary Table 2 | The detailed information of the whole CTL epitopes predicted by IEDB database.

Supplementary Table 3 | The potential CTL epitopes identified by immunogenicity and antigenicity.

Supplementary Table 4 | The detailed information of linear B-cell epitopes predicted by the ABCpred. The epitopes selected for further study were marked with yellow color.

Supplementary Table 5 | The detailed information of conformational B cell epitopes residues of C543P predicted by the ElliPro.

REFERENCES

Andrusier, N., Nussinov, R., and Wolfson, H. J. (2007). FireDock: fast interaction refinement in molecular docking. *Proteins* 69, 139–159.

Arroyo, L., Marín, D., Franken, K., Ottenhoff, T. H. M., and Barrera, L. F. (2018). Potential of DosR and Rpf antigens from Mycobacterium tuberculosis to discriminate between latent and active tuberculosis in a tuberculosis endemic population of Medellin Colombia. *BMC Infect. Dis.* 18:26. doi: 10.1186/s12879-017-2929-0

Arroyo, L., Rojas, M., Franken, K. L., Ottenhoff, T. H., and Barrera, L. F. (2016). Multifunctional T Cell Response to DosR and Rpf Antigens Is Associated with Protection in Long-Term Mycobacterium tuberculosis-Infected Individuals in Colombia. *Clin. Vaccine Immunol.* 23, 813–824. doi: 10.1128/CVI.00217-16

Bai, X. (2015). *Preparation of Four Tuberculosis Latent Proteins and the Evaluation of Their Immunological Characteristic*. Beijing: Medical School of Chinese PLA.

Bai, X., Liang, Y., Yang, Y., Zhang, J., and Wu, X. (2017). A new method of screening for latent tuberculosis infection: results from army recruits in Beijing in 2014. *Immunol. Lett.* 186, 28–32. doi: 10.1016/j.imlet.2017.03.014

Bai, X. J., Liang, Y., Yang, Y. R., Li, N., Zhang, X. Y., An, H. R., et al. (2015). Immune responses to latent tuberculosis antigen Rv2659c in Chinese populations. *J. Microbiol. Immunol. Infect.* 48, 381–389. doi: 10.1016/j.jmii.2014.02.006

Bertholet, S., Ireton, G. C., Kahn, M., Guderian, J., Mohamath, R., Stride, N., et al. (1950). Identification of human T cell antigens for the development of vaccines against Mycobacterium tuberculosis. *J. Immunol.* 2008, 7948–7957. doi: 10.4049/jimmunol.181.11.7948

Bibi, S., Ullah, I., Zhu, B., Adnan, M., Liaqat, R., Kong, W. B., et al. (2021). In silico analysis of epitope-based vaccine candidate against tuberculosis using reverse vaccinology. *Sci. Rep.* 11:1249. doi: 10.1038/s41598-020-80899-6

Boom, W. H., Canaday, D. H., Fulton, S. A., Gehring, A. J., Rojas, R. E., and Torres, M. (2003). Human immunity to M. tuberculosis: t cell subsets and antigen processing. *Tuberculosis* 83, 98–106. doi: 10.1016/s1472-9792(02)00054-9

Bui, H. H., Sidney, J., Dinh, K., Southwood, S., Newman, M. J., and Sette, A. (2006). Predicting population coverage of T-cell epitope-based diagnostics and vaccines. *BMC Bioinform.* 7:153. doi: 10.1186/1471-2105-7-153

Carranza, C., Pedraza-Sanchez, S., de Oyarzabal-Mendez, E., and Torres, M. (2020). Diagnosis for Latent Tuberculosis Infection: new Alternatives. *Front. Immunol.* 11:2006. doi: 10.3389/fimmu.2020.02006

Chegou, N. N., Essone, P. N., Loxton, A. G., Stanley, K., Black, G. F., van der Spuy, G. D., et al. (2012). Potential of host markers produced by infection phase-dependent antigen-stimulated cells for the diagnosis of tuberculosis in a highly endemic area. *PLoS One* 7:e38501. doi: 10.1371/journal.pone.0038501

Chen, J., Su, X., Zhang, Y., Wang, S., Shao, L., Wu, J., et al. (2009). Novel recombinant RD2- and RD11-encoded Mycobacterium tuberculosis antigens are potential candidates for diagnosis of tuberculosis infections in BCG-vaccinated individuals. *Microbes infect.* 11, 876–885. doi: 10.1016/j.micinf.2009.05.008

Colovos, C., and Yeates, T. O. (1993). Verification of protein structures: patterns of nonbonded atomic interactions. *Protein Sci.* 2, 1511–1519. doi: 10.1002/pro.5560020916

Corradin, G., Villard, V., and Kajava, A. V. (2007). Protein structure based strategies for antigen discovery and vaccine development against malaria and other pathogens. *Endocr. Metab. Immune. Disord. Drug Targets* 7, 259–265. doi: 10.2174/187153007782794371

Dhanda, S. K., Vir, P., and Raghava, G. P. (2013). Designing of interferon-gamma inducing MHC class-II binders. *Biol. Direct.* 8:30. doi: 10.1186/1745-6150-8-30

Dimitrov, I., Bangov, I., Flower, D. R., and Doytchinova, I. (2014a). AllerTOP v.2–a server for in silico prediction of allergens. *J. Mol. Model.* 20:2278. doi: 10.1007/s00894-014-2278-5

Dimitrov, I., Naneva, L., Doytchinova, I., and Bangov, I. (2014b). AllergenFP: allergenicity prediction by descriptor fingerprints. *Bioinformatics* 30, 846–851. doi: 10.1093/bioinformatics/btt619

Doytchinova, I. A., and Flower, D. R. (2007). VaxiJen: a server for prediction of protective antigens, tumour antigens and subunit vaccines. *BMC Bioinform.* 8:4. doi: 10.1186/1471-2105-8-4

Garnier, J., Gibrat, J. F., and Robson, B. (1996). GOR method for predicting protein secondary structure from amino acid sequence. *Meth. Enzymol.* 266, 540–553. doi: 10.1016/s0076-6879(96)66034-0

Gasteiger, E. (2005). *The Proteomics Protocols Handbook*. Berlin: Springer, 571–607.

Gong, W., Liang, Y., Mi, J., Jia, Z., Xue, Y., Wang, J., et al. (2021). Peptides-Based Vaccine MP3RT Induced Protective Immunity Against Mycobacterium Tuberculosis Infection in a Humanized Mouse Model. *Front. Immunol.* 12:666290. doi: 10.3389/fimmu.2021.666290

Gong, W., Liang, Y., and Wu, X. (2018). The current status, challenges, and future developments of new tuberculosis vaccines. *Hum. Vaccin Immunother.* 14, 1697–1716. doi: 10.1080/21645515.2018.1458806

Gong, W., Pan, C., Cheng, P., Wang, J., Zhao, G., and Wu, X. (2022). Peptide-Based Vaccines for Tuberculosis. *Front. Immunol.* 13:830497. doi: 10.3389/fimmu.2022.830497

Gong, W., and Wu, X. (2021). Differential Diagnosis of Latent Tuberculosis Infection and Active Tuberculosis: a Key to a Successful Tuberculosis Control Strategy. *Front. Microbiol.* 12:745592. doi: 10.3389/fmicb.2021.745592

Grote, A., Hiller, K., Scheer, M., Münch, R., Nörtemann, B., Hempel, D. C., et al. (2005). JCat: a novel tool to adapt codon usage of a target gene to its potential expression host. *Nucleic Acids Res.* 33, W526–W531. doi: 10.1093/nar/gki376

He, H., Yang, H., and Deng, Y. (2015). Mycobacterium tuberculosis dormancy-associated antigen of Rv2660c induces stronger immune response in latent Mycobacterium tuberculosis infection than that in active tuberculosis in a Chinese population. *Eur. J. Clin. Microbiol. Infect. Dis.* 34, 1103–1109. doi: 10.1007/s10096-015-2335-8

Hebditch, M., Carballo-Amador, M. A., Charonis, S., Curtis, R., and Warwicker, J. (2017). Protein-Sol: a web tool for predicting protein solubility from sequence. *Bioinformatics* 33, 3098–3100. doi: 10.1093/bioinformatics/btx345

Heo, L., Park, H., and Seok, C. (2013). GalaxyRefine: protein structure refinement driven by side-chain repacking. *Nucleic Acids Res.* 41, W384–W388. doi: 10.1093/nar/gkt458

Hinks, T. S., Dosanjh, D. P., Innes, J. A., Pasvol, G., Hackforth, S., Varia, H., et al. (2009). Frequencies of region of difference 1 antigen-specific but not purified protein derivative-specific gamma interferon-secreting T cells correlate with the presence of tuberculosis disease but do not distinguish recent from remote latent infections. *Infect. Immun.* 77, 5486–5495. doi: 10.1128/IAI.01436-08

Houben, R. M., and Dodd, P. J. (2016). The Global Burden of Latent Tuberculosis Infection: a Re-estimation Using Mathematical Modelling. *PLoS Med.* 13:e1002152. doi: 10.1371/journal.pmed.1002152

Ikai, A. (1980). Thermostability and aliphatic index of globular proteins. *J. Biochem.* 88, 1895–1898.

Jackson, D. C., Lau, Y. F., Le, T., Suhrbier, A., Deliyannis, G., Cheers, C., et al. (2004). A totally synthetic vaccine of generic structure that targets Toll-like receptor 2 on dendritic cells and promotes antibody or cytotoxic T cell responses. *Proc. Natl. Acad. Sci. U.S.A.* 101, 15440–15445. doi: 10.1073/pnas.0406740101

Kapopoulou, A., Lew, J. M., and Cole, S. T. (2011). The MycoBrowser portal: a comprehensive and manually annotated resource for mycobacterial genomes. *Tuberculosis* 91, 8–13. doi: 10.1016/j.tube.2010.09.006

Kardani, K., Bolhassani, A., and Namvar, A. (2020). An overview of in silico vaccine design against different pathogens and cancer. *Expert Rev. Vaccines.* 19, 699–726. doi: 10.1080/14760584.2020.1794832

Kawai, T., and Akira, S. (2010). The role of pattern-recognition receptors in innate immunity: update on Toll-like receptors. *Nat. Immunol.* 11, 373–384. doi: 10.1038/ni.1863

Kim, Y., Ponomarenko, J., Zhu, Z., Tamang, D., Wang, P., Greenbaum, J., et al. (2012). Immune epitope database analysis resource. *Nucleic Acids Res.* 40, W525–W530.

Kozakov, D., Hall, D. R., Xia, B., Porter, K. A., Padhorny, D., Yueh, C., et al. (2017). The ClusPro web server for protein-protein docking. *Nat. Protoc.* 12, 255–278. doi: 10.1038/nprot.2016.169

Kumar, N. P., and Babu, S. (2017). Influence of diabetes mellitus on immunity to human tuberculosis. *Immunology* 152, 13–24. doi: 10.1111/imm.12762

Liu, C. H., Liu, H., and Ge, B. (2017). Innate immunity in tuberculosis: host defense vs pathogen evasion. *Cell. Mol. Immunol.* 14, 963–975. doi: 10.1038/cmi.2017.88

Lopéz-Blanco, J. R., Garzón, J. I., and Chacón, P. (2011). iMod: multipurpose normal mode analysis in internal coordinates. *Bioinformatics* 27, 2843–2850. doi: 10.1093/bioinformatics/btr497

Luabeya, A. K., Kagina, B. M., Tameris, M. D., Geldenhuys, H., Hoff, S. T., Shi, Z., et al. (2015). First-in-human trial of the post-exposure tuberculosis vaccine H56:IC31 in Mycobacterium tuberculosis infected and non-infected healthy adults. *Vaccine* 33, 4130–4140. doi: 10.1016/j.vaccine.2015.06.051

Magnan, C. N., Zeller, M., Kayala, M. A., Vigil, A., Randall, A., Felgner, P. L., et al. (2010). High-throughput prediction of protein antigenicity using protein microarray data. *Bioinformatics* 26, 2936–2943. doi: 10.1093/bioinformatics/btq551

Mashiach, E., Schneidman-Duhovny, D., Andrusier, N., Nussinov, R., and Wolfson, H. J. (2008). FireDock: a web server for fast interaction refinement in molecular docking. *Nucleic Acids Res.* 36, W229–W232. doi: 10.1093/nar/gkn186

McGuffin, L. J., Bryson, K., and Jones, D. T. (2000). The PSIPRED protein structure prediction server. *Bioinformatics* 16, 404–405.

Meza, B., Ascencio, F., Sierra-Beltrán, A. P., Torres, J., and Angulo, C. (2017). A novel design of a multi-antigenic, multistage and multi-epitope vaccine against *Helicobacter* pylori: an in silico approach. *Infect. Genet. Evol.* 49, 309–317. doi: 10.1016/j.meegid.2017.02.007

Mosavari, N., Karimi, A., Tadayon, K., Shahhosseini, G., Zavaran Hosseini, A., and Babaie, M. (2021). Evaluation of Heating and Irradiation Methods for Production of Purified Protein Derivative (PPD) of Mycobacterium Tuberculosis. *Arch. Razi Inst.* 75, 439–449. doi: 10.22092/ari.2019.123082.1238

Ponomarenko, J., Bui, H. H., Li, W., Fusseder, N., Bourne, P. E., Sette, A., et al. (2008). ElliPro: a new structure-based tool for the prediction of antibody epitopes. *BMC Bioinform.* 9:514. doi: 10.1186/1471-2105-9-514

Raoufi, E., Hemmati, M., Eftekhari, S., Khaksaran, K., Mahmodi, Z., Farajollahi, M. M., et al. (2020). Epitope Prediction by Novel Immunoinformatics Approach: a State-of-the-art Review. *Int. J. Pept. Res. Ther.* 26, 1155–1163. doi: 10.1007/s10989-019-09918-z

Rapin, N., Lund, O., Bernaschi, M., and Castiglione, F. (2010). Computational immunology meets bioinformatics: the use of prediction tools for molecular binding in the simulation of the immune system. *PLoS One* 5:e9862. doi: 10.1371/journal.pone.0009862

Roy, A., Kucukural, A., and Zhang, Y. (2010). I-TASSER: a unified platform for automated protein structure and function prediction. *Nat. Protoc.* 5, 725–738. doi: 10.1038/nprot.2010.5

Saha, S., and Raghava, G. P. (2006). Prediction of continuous B-cell epitopes in an antigen using recurrent neural network. *Proteins* 65, 40–48. doi: 10.1002/prot.21078

Schneidman-Duhovny, D., Inbar, Y., Nussinov, R., and Wolfson, H. J. (2005). PatchDock and SymmDock: servers for rigid and symmetric docking. *Nucleic Acids Res.* 33, W363–W367. doi: 10.1093/nar/gki481

Sharma, R., Rajput, V. S., Jamal, S., Grover, A., and Grover, S. (2021). An immunoinformatics approach to design a multi-epitope vaccine against Mycobacterium tuberculosis exploiting secreted exosome proteins. *Sci. Rep.* 11:13836.

Shenoy, A. T. (2021). Lyon De Ana C, Arafa EI, Salwig I, Barker KA, Korkmaz FT, et al. Antigen presentation by lung epithelial cells directs CD4(+) T(RM) cell function and regulates barrier immunity. *Nat. Commun.* 12:5834. doi: 10.1038/s41467-021-26045-w

Shiraz, M., Lata, S., Kumar, P., Shankar, U. N., and Akif, M. (2021). Immunoinformatics analysis of antigenic epitopes and designing of a multi-epitope peptide vaccine from putative nitro-reductases of Mycobacterium tuberculosis DosR. *Infect Genet. Evol.* 94:105017. doi: 10.1016/j.meegid.2021.105017

Tang, X. L., Zhou, Y. X., Wu, S. M., Pan, Q., Xia, B., and Zhang, X. L. (2014). CFP10 and ESAT6 aptamers as effective Mycobacterial antigen diagnostic reagents. *J. Infect.* 69, 569–580. doi: 10.1016/j.jinf.2014.05.015

Waterhouse, A., Bertoni, M., Bienert, S., Studer, G., Tauriello, G., Gumienny, R., et al. (2018). SWISS-MODEL: homology modelling of protein structures and complexes. *Nucleic Acids Res.* 46, W296–W303. doi: 10.1093/nar/gky427

Weng, G., Wang, E., Wang, Z., Liu, H., Zhu, F., Li, D., et al. (2019). HawkDock: a web server to predict and analyze the protein-protein complex based on computational docking and MM/GBSA. *Nucleic Acids Res.* 47, W322–W330. doi: 10.1093/nar/gkz397

WHO (2021). *Global Tuberculosis Report 2021*. Genevapp: World Health Organization.

Wiederstein, M., and Sippl, M. J. (2007). ProSA-web: interactive web service for the recognition of errors in three-dimensional structures of proteins. *Nucleic Acids Res.* 35, W407–W410. doi: 10.1093/nar/gkm290

Yang, J., Yan, R., Roy, A., Xu, D., Poisson, J., and Zhang, Y. (2015). The I-TASSER Suite: protein structure and function prediction. *Nat. Methods* 12, 7–8.

Zellweger, J. P., Sotgiu, G., Corradi, M., and Durando, P. (2020). The diagnosis of latent tuberculosis infection (LTBI): currently available tests, future developments, and perspectives to eliminate tuberculosis (TB). *Med. Lav.* 111, 170–183. doi: 10.23749/mdl.v111i3.9983

Zhang, Q., Wang, P., Kim, Y., Haste-Andersen, P., Beaver, J., Bourne, P. E., et al. (2008). Immune epitope database analysis resource (IEDB-AR). *Nucleic Acids Res.* 36, W513–W518.

Conflict of Interest: The authors declare that the research was conducted in the absence of any commercial or financial relationships that could be construed as a potential conflict of interest.

Publisher's Note: All claims expressed in this article are solely those of the authors and do not necessarily represent those of their affiliated organizations, or those of the publisher, the editors and the reviewers. Any product that may be evaluated in this article, or claim that may be made by its manufacturer, is not guaranteed or endorsed by the publisher.

frontiers | Frontiers in Microbiology

ORIGINAL RESEARCH
published: 04 July 2022
doi: 10.3389/fmicb.2022.942587

Epidemiology and Genetic Diversity of *Bartonella* in Rodents in Urban Areas of Guangzhou, Southern China

*Xin-Yan Yao†, Hong Liu†, Jing Sun†, Yu-Qian Zhang, Zhi-Hang Lv, Xue-Lian Zhang and Jian-Wei Shao**

School of Life Science and Engineering, Foshan University, Foshan, China

Bartonella spp. are gram-negative bacteria that can infect a wide spectrum of mammals. Rodents are considered to be the natural reservoir of many *Bartonella* species that are transmitted by various blood-sucking arthropods. The close contact between rodents and humans in urban areas increased the chance of transmitting rodent-borne *Bartonella* to humans. Investigation of the epidemiological characteristics of *Bartonella* infection in rodents is of great significance for the prevention and control of human Bartonellosis. In this study, rodents were captured to monitor the prevalence of *Bartonella* in urban areas of Guangzhou city. Six official or candidate species of *Bartonella,* including two confirmed zoonotic species, were detected with an overall prevalence of 6.4% in rodents captured herein. In addition, *Rattus norvegicus* was the predominant host species for *Bartonella* infection, and *B. queenslandensis* was the dominant species circulating in rodents in these areas. These results provide insights into the prevalence and genetic diversity of *Bartonella* species circulating in rodents in the urban areas of Guangzhou, and also urged the surveillance of rodent-associated *Bartonella* species in these areas.

Keywords: *Bartonella*, epidemiology, genetic diversity, rodents, urban areas

OPEN ACCESS

Edited by:
Wei Wang,
Jiangsu Institute of Parasitic Diseases (JIPD), China

Reviewed by:
Wen-Ping Guo,
Northwest A&F University, China
Xia Zhou,
Soochow University, China

***Correspondence:**
Jian-Wei Shao
jwshao1988@163.com

†These authors have contributed equally to this work

Specialty section:
This article was submitted to Infectious Agents and Disease, a section of the journal Frontiers in Microbiology

Received: *12 May 2022*
Accepted: *13 June 2022*
Published: *04 July 2022*

Citation:
Yao X-Y, Liu H, Sun J, Zhang Y-Q, Lv Z-H, Zhang X-L and Shao J-W (2022) Epidemiology and Genetic Diversity of Bartonella in Rodents in Urban Areas of Guangzhou, Southern China. Front. Microbiol. 13:942587. doi: 10.3389/fmicb.2022.942587

INTRODUCTION

Bartonella spp. are gram-negative bacteria that belong to the genus of α-proteobacteria within the family *Bartonellaceae* (Anderson and Neuman, 1997). They can infect a wide range of mammals and are mainly transmitted by blood-sucking arthropods, such as fleas, lice, sandflies, biting flies, and ticks (Álvarez-Fernández et al., 2018). More than 50 validated species of *Bartonella* have been identified from domestic and wild animals, including horses, cattle, deer, sheep, rodents, and bats (Chang et al., 2000; Valentine et al., 2007; Okaro et al., 2017). As far as we know, at least 18 species of *Bartonella*, including *Bartonella alsatica*, *B. ancashensis*, *B. bacilliformis*, *B. clarridgeiae*, *B. doshiae*, *B. elizabethae*, *B. grahamii*, *B. henselae*, *B. koehlerae*, *B. kosoyi*, *B. mayotimonensis*, *B. quintana*, *B. rattimassiliensis*, *B. rochalimae*, *B. tamiae*, *B. tribocorum*, *B. vinsonii*, and *B. washoensis*, have been recognized to be associated with human diseases (Gundi et al., 2004; Kosoy et al., 2010; Kandelaki et al., 2016; Vayssier-Taussat et al., 2016; Okaro et al., 2017; Von Loewenich et al., 2019). Infection of different species of *Bartonella* can cause human diseases with different clinical manifestations, sometimes even fatal in immunocompromised patients (Mosepele et al., 2012).

Rodents represent the most abundant taxonomic order with some special ecological traits, such as wide geographic distribution and intimate interactions with humans and livestock. Thus, rodents play key roles in the transmission of a large variety of pathogenic agents of infectious diseases, including *Bartonella* (Meerburg et al., 2009). Among all known reservoir hosts of *Bartonella* species, rodents are considered the primary host, and *Bartonella* spp. in rodents have been reported in Asia (Li et al., 2015; Saengsawang et al., 2021; Liu et al., 2022), Africa (Hatyoka et al., 2019), Europe (Divari et al., 2020; Szewczyk et al., 2021), Americas (De Sousa et al., 2018; Müller et al., 2020), and Australia (Dybing et al., 2016; Egan et al., 2021). Approximately 90 species of rodents are known to be associated with more than 22 different species of *Bartonella*, ten of which have been confirmed to cause human infection (Daly et al., 1993; Welch et al., 1999; Birtles et al., 2002; Kosoy et al., 2003, 2008, 2010; Lin et al., 2008; Kandelaki et al., 2016; Vayssier-Taussat et al., 2016). Interestingly, many different rodent species have been reported to be infected with different *Bartonella* spp. in high prevalence globally (Gutiérrez et al., 2015). The high genetic diversity and infection rate of *Bartonella* in rodents emphasized the important roles that rodents played in the maintenance and transmission of *Bartonella*.

A previous study showed high infection rates, ranging from 4 to 50%, of *Bartonella* in rodents in China (Gutiérrez et al., 2015). Importantly, several studies reported the high prevalence of *Bartonella* species in rodents in the western (Rao et al., 2021), eastern (Qin et al., 2019), southern (Su et al., 2020), southeastern (Liu et al., 2022), southwest (Li et al., 2007), and northeastern China (Li et al., 2015), indicating the wide geographical distribution of *Bartonella* in rodents. However, most of the previous studies were conducted in the field environment. Information about the epidemiology of *Bartonella* spp. in urban areas where rodents have more chance of contact with humans is limited. Guangzhou, the provincial capital city of Guangdong province and the largest city in southern China, is located in the tropical and subtropical regions with a warm and moist climate (Wei et al., 2018), an ideal habitat for rodents. However, little information about the epidemiology of *Bartonella* in rodents in urban areas of Guangzhou is available. Therefore, in this study, we collected rodent samples in urban areas of Guangzhou to investigate the epidemiology of *Bartonella* spp. in rodents. The results of this study will provide insights into the genetic diversity and prevalence of *Bartonella* in Guangzhou, and also formulate the prevention and control strategies for *Bartonella* infections in this city.

MATERIALS AND METHODS

Rodent Samples: Collection and Processing

Rodents were captured using live-capture traps baited with cooked food in the urban areas of six districts (Liwan, Huadu, Tianhe, Huangpu, Baiyun, and Conghua) in Guangzhou city in 2020 (**Figure 1**). All rodents were euthanized, and the species, age, and sex were identified by trained field biologists, and the species were further confirmed by the sequence analysis of the mt-*cyt* b gene (Guo et al., 2013). Spleen samples were aseptically obtained immediately after euthanasia and stored at −80 °C until further use.

Approximately 20 mg of spleen samples were homogenized and further subjected to extract the total DNA using a DNA extraction kit (OMEGA, Doraville, CA, USA) as per the manufacturer's instructions. Then, all extracted DNA samples were used to detect the presence of *Bartonella*.

Detection and Molecular Characterization of *Bartonella*

Bartonella spp. were detected by nested-PCR using the primers targeting the conserved region of 16S rRNA (*rrs*) gene of *Bartonella* species as previously described (Zhang et al., 2019). The targeted region, about 1,100 bp fragment, was suspected to be a *Bartonella*-positive sample and was further confirmed by sequencing. To better determine and characterize the species of detected *Bartonella* strains, the citrate synthase gene (*gltA*) and the RNA polymerase beta-subunit gene (*rpoB*) were also amplified from the positive samples. All primer sequences used in the present study are listed in **Table 1**.

The PCR products with the expected size of each primer set were purified using a gel extraction kit (TaKaRa, Dalian, China) after electrophoresis. The purified DNA was cloned into a pMD19-T vector (TaKaRa, China), and the resulting plasmid was used to transform into competent *E. coli* cells. Positive inserts were confirmed by PCR, and five positive clones were sequenced by the Sangon Biotechnology Company (Shanghai, China). To prevent contamination, the procedures including extraction of total DNA, preparation of PCR mix, adding the template DNA, and agarose gel electrophoresis were performed in separate rooms using dedicated pipets and filtered tips. Distilled water was used as the negative control in all the PCR amplifications.

Sequence Comparison and Phylogenetic Analysis

Sequence assembly and manual editing were performed using the SeqMan program (DNASTAR, Madison, WI). The nucleotide (nt) sequence identities were calculated by the MegAlign program available within the Lasergene software package (version 7.1, DNAstar). All the sequences obtained in this study have been submitted to GenBank under the accession numbers ON413697–ON413715 for *rrs* gene and ON394008–ON394045 for *gltA* and *rpoB* genes, respectively.

The maximum-likelihood (ML) trees were constructed based on the general time-reversible (GTR) nucleotide substitution model and the optimized parameters of gamma (Γ)-distribution and proportion of invariable sites (i.e., GTR + Γ + I) with bootstrap support values calculated from 100 replicates implemented in MEGA X (Kumar et al., 2018).

Statistical Analysis

Statistical Package for Social Sciences (SPSS) Version 21.0 software was used in the statistical analyses of this study, and Fisher exact test was used to calculate the *P*-value to determine the differences in *Bartonella* positive rates between

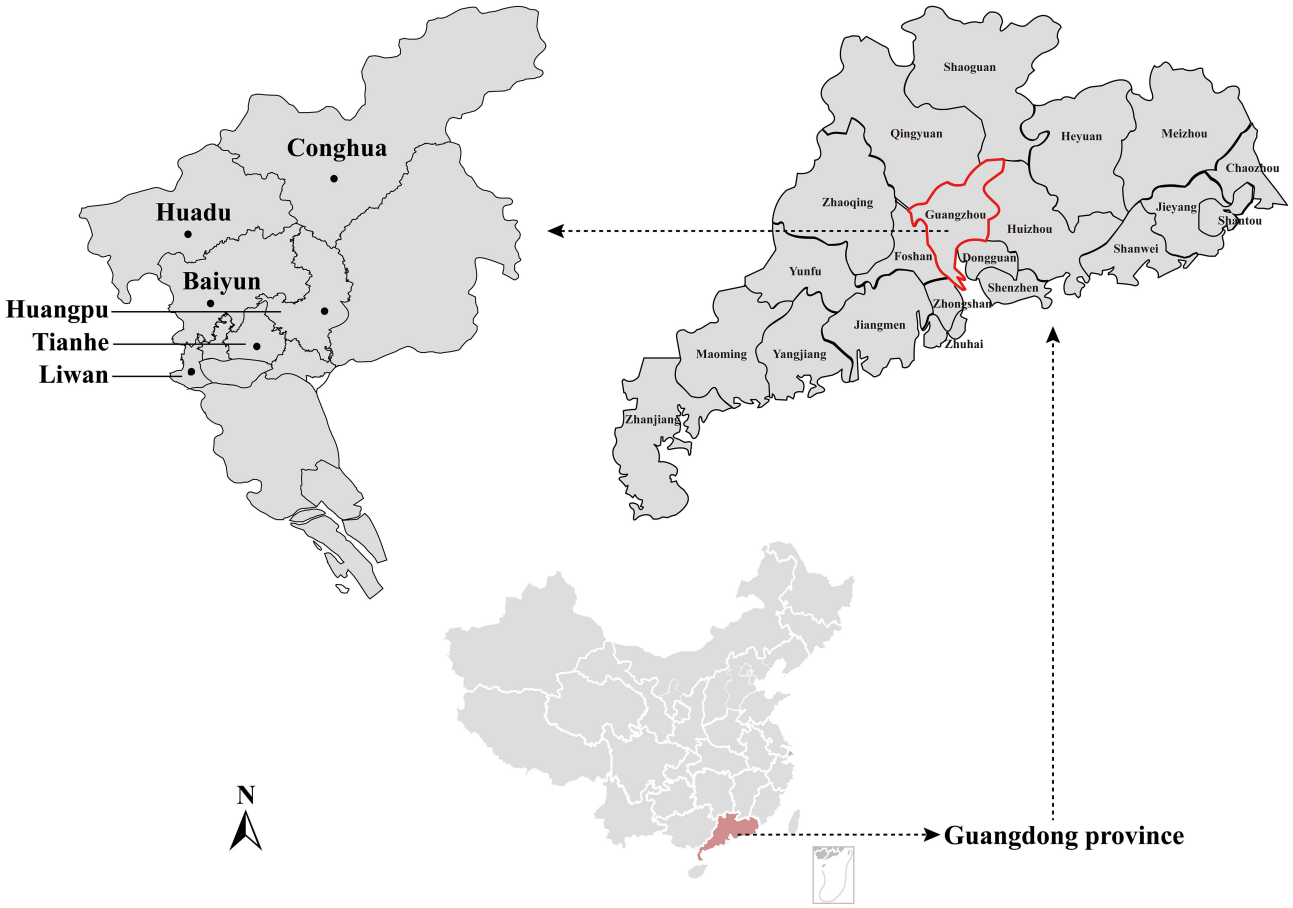

FIGURE 1 | Geographic maps showing the location of sampling sites from where the rodents were captured in this study. This map was plotted by combination of Surfer software version-4 (Golden Software, USA) and Adobe illustrator version CC2017 (Adobe, USA). The black dots indicate the sampling regions in this study.

TABLE 1 | Primers used in this study.

gene	Primers	Sequences (5′ → 3′)	Tm	Amplicon (bp)
rrs	Bar1	AGAGTTTGATCMTGGCTCAGA	62 °C	1100
	Bar2	GTAGCACGTGTGTAGCCCA		
	Bar3	CACTCTTTTAGAGTGAGCGGCAA	65 °C	1000
	Bar4	CCCCCTAGAGTGCCCAACCA		
gltA	gltA-1F	GCTTCTTGTGAATCRAAAATYAC	48 °C	1100
	gltA-1R	GATCYTCAATCATTTCTTTCCA		
	gltA-2F	TTTAYCGYGGTTATCCTATYG	55 °C	1000
	gltA-2R	AATGCAAAAAGAACAGTAAACA		
rpoB	rpoB-F	ACAGTKATGCCGCAGGATTT	54 °C	747
	rpoB-R1	GAATAACAATACGGGTMGCAT		
	rpoB-F	ACAGTKATGCCGCAGGATTT	54 °C	742
	rpoB-R2	ACAATACGGGTHGCATCAAC		

TABLE 2 | Prevalence of Bartonella in rodents collected in urban areas of Guangzhou.

Parameters	Location						Sub-total (%)	95% CI (%)	χ^2-value	*P*-value
	Liwan	Huadu	Tianhe	Huangpu	Baiyun	Conghua				
Species									3.736	0.291
R.norvegicus	0/46	11/50	5/50	–/48	2/46	1/10	19/250 (7.6)	4.3–10.9		
R. losea	–	–	–	–	–	40	0/40	0		
R. tanezumi	0/2	–	–	–	–	–	0/2	0		
Mus musculus	0/2	–	–	0/2	–	–	0/4	0		
Gender									0.003	0.571
Female	0/22	6/24	2/19	0/19	0/18	0/21	8/123 (6.5)	2.1–10.9		
Male	0/28	5/26	3/31	0/31	2/28	1/29	11/173 (6.4)	2.8–10.0		
Age										
Juvenile	0/44	6/21	5/38	0/29	1/40	1/36	13/208 (6.3)	3.0–9.5	0.033	0.518
Adult	0/6	5/29	0/12	0/21	1/6	0/14	6/88 (6.8)	1.5–12.1		

Bartonella spp. DNA positive specimens/total specimens; "–" indicates that no animals were captured.

sampling sites and animal hosts. A $P < 0.05$ was considered statistically significant.

Ethics Statement

The authors confirmed that this study complies with the ethical policies of the journal, as specified in the journal's guidelines. All rodents were trapped by experienced field workers, and the sampling procedures and sample processing have been approved by the ethics committee of Foshan University.

RESULTS

Rodent Trapping

A total of 296 rodents were captured in six districts of Guangzhou city in 2020 (**Table 2**). The captured rodents were identified into four species, including 250 *Rattus norvegicus*, 40 *R. losea*, 2 *R. tanezumi*, and 4 *Mus musculus*. *R. norvegicus* (250/296, 84.5%) was the most abundant species in urban environment in Guangzhou city. Among all rodents, the female and male were 123 and 173, respectively. In addition, the juvenile and adult rodents were 208 and 88, respectively.

Prevalence of *Bartonella* in Rodents

The total DNAs extracted from the rodents' spleen were subjected to PCR targeting the *rrs* gene of *Bartonella* spp., and PCR products with expected sizes were detected in 19 samples (**Table 2**). Sequencing and blast analysis of the PCR products confirmed that these 19 samples were *Bartonella* positive. Overall, the prevalence of *Bartonella* spp. in this study was 6.4% (19/296, 95% CI: 3.6–9.2%). Specifically, all *Bartonella*-positive samples were exclusively detected from *R. norvegicus* (7.6%, 95% CI: 4.3–10.9%). In addition, the infection rates of *Bartonella* in female and male rodents were 6.5% (95% CI: 2.1–10.9%) and 6.4% (95% CI: 2.8–10.0%), respectively. Moreover, 6.3% (95% CI: 3.0–9.5%) of the juvenile rodents and 6.8% (95% CI: 1.5–12.1%) of adult rodents were determined as *Bartonella*-positive. Notably, no significant difference was observed associated either with the rodent species or with the gender or age of the rodents.

Molecular Characterization of *Bartonella*

The *rrs*, *gltA*, and *rpoB* genes were recovered from positive samples to better characterize the species of detected *Bartonella* strains. Sequencing and blast analyses based on the *rrs* gene sequences (1,100 bp) revealed that *Bartonella* strains detected in this study were *B. queenslandensis* ($n = 7$), *B. mastomydis* ($n = 5$), *B. tribocorum* ($n = 2$), *B. rattimassiliensis* ($n = 1$), *Bartonella* sp. AA86HXZ ($n = 3$), and *Bartonella* sp. Fuji 12-1 ($n = 1$).

Sequence comparison analysis showed that all *rrs* gene sequences generated herein shared 98.2–100% nucleotide sequences identity with each other. The seven *rrs* gene sequences of *B. queenslandensis* obtained in the present study shared the highest sequence similarity with *B. queenslandensis* strain AUST/NH8 (EU111756), with 99.3–100% nucleotide sequences identity. Similarly, the *rrs* gene sequences of *B. mastomydis*, *B. tribocorum*, *B. rattimassiliensis*, *Bartonella* sp. AA86HXZ, and *Bartonella* sp. Fuji 12-1 obtained in the present study exhibited 99.5–99.9%, 99.8–100%, 100%, 99.3–99.6%, and 99.7% nucleotide sequences identical with the sequences of the corresponding species of *Batonella* under the GenBank accession number KY555064, NR074354, NR115255, KJ361602, and AB242293, respectively. Phylogenetic trees reconstructed based on the *rrs* gene sequences and the concatenated sequence of *rrs*, *gltA*, and *rpoB* genes showed a similar topology that these sequences determined in this study clustered together with the corresponding reference sequences, respectively (**Figures 2**, **3**).

DISCUSSION

A wide range of emerging and re-emerging infectious diseases have become major global threats to human health (Dong and Soong, 2021). *Bartonella* spp. are emerging vector-borne pathogens distributed worldwide and cause global public health concerns (Mogollon-Pasapera et al., 2009). Rodents are considered the major reservoirs that harbor the largest number and the greatest diversity of *Bartonella* species (Gutiérrez et al., 2015), and the presence of many pathogenic *Bartonella*

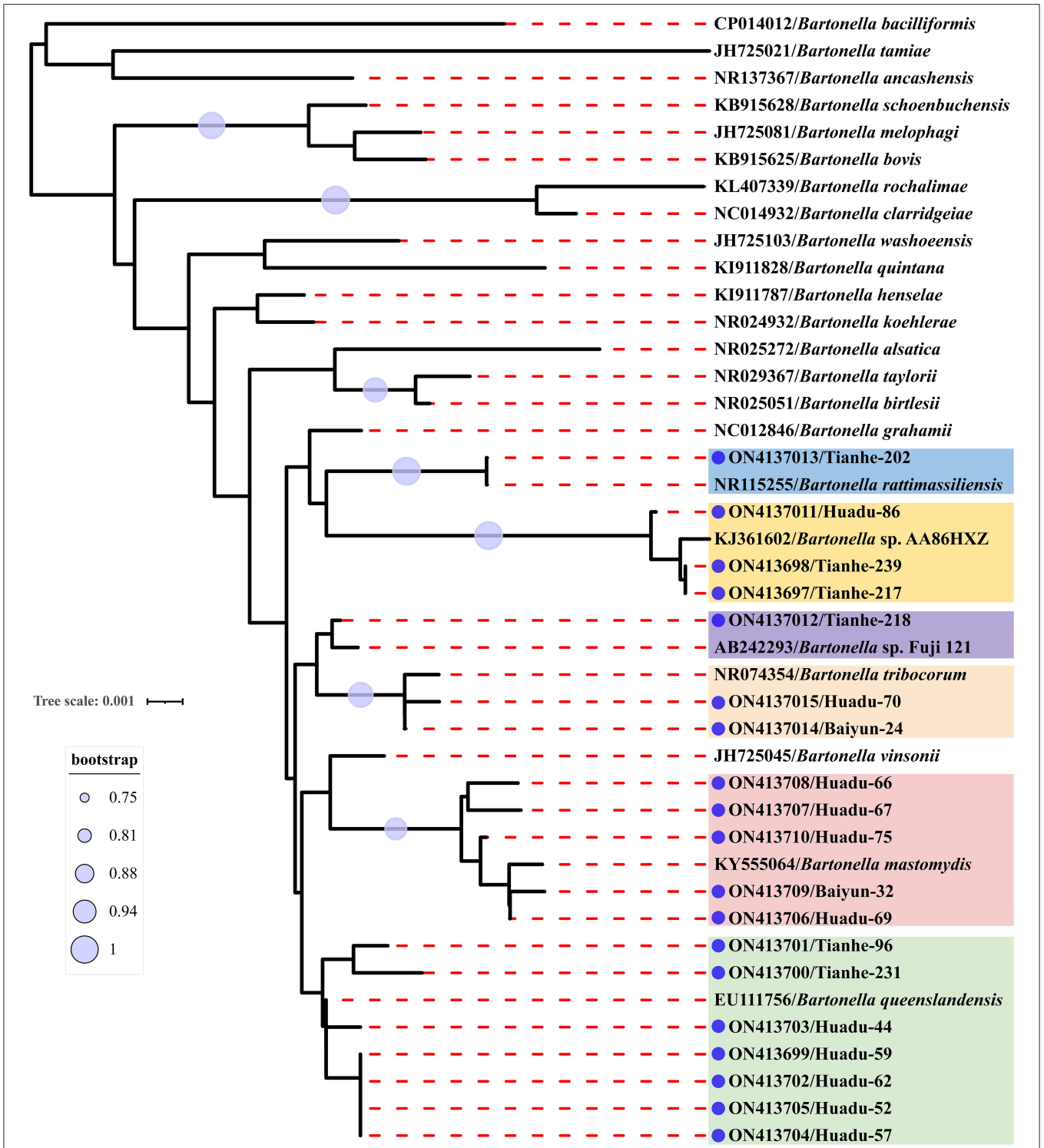

FIGURE 2 | Maximum-likelihood phylogenetic tree reconstructed based on the nucleotide sequences of *rrs* gene of *Bartonella*. Bootstrap values were calculated with 100 replicates of the alignment, and only bootstrap values >70% are shown at appropriate nodes. Sequences of *Bartonella* determined in this study are marked with blue dot.

species have been confirmed (Okaro et al., 2017). Therefore, investigation of the epidemiological characteristics of *Bartonella* infection in rodents is of great significance for the prevention and control of human Bartonellosis.

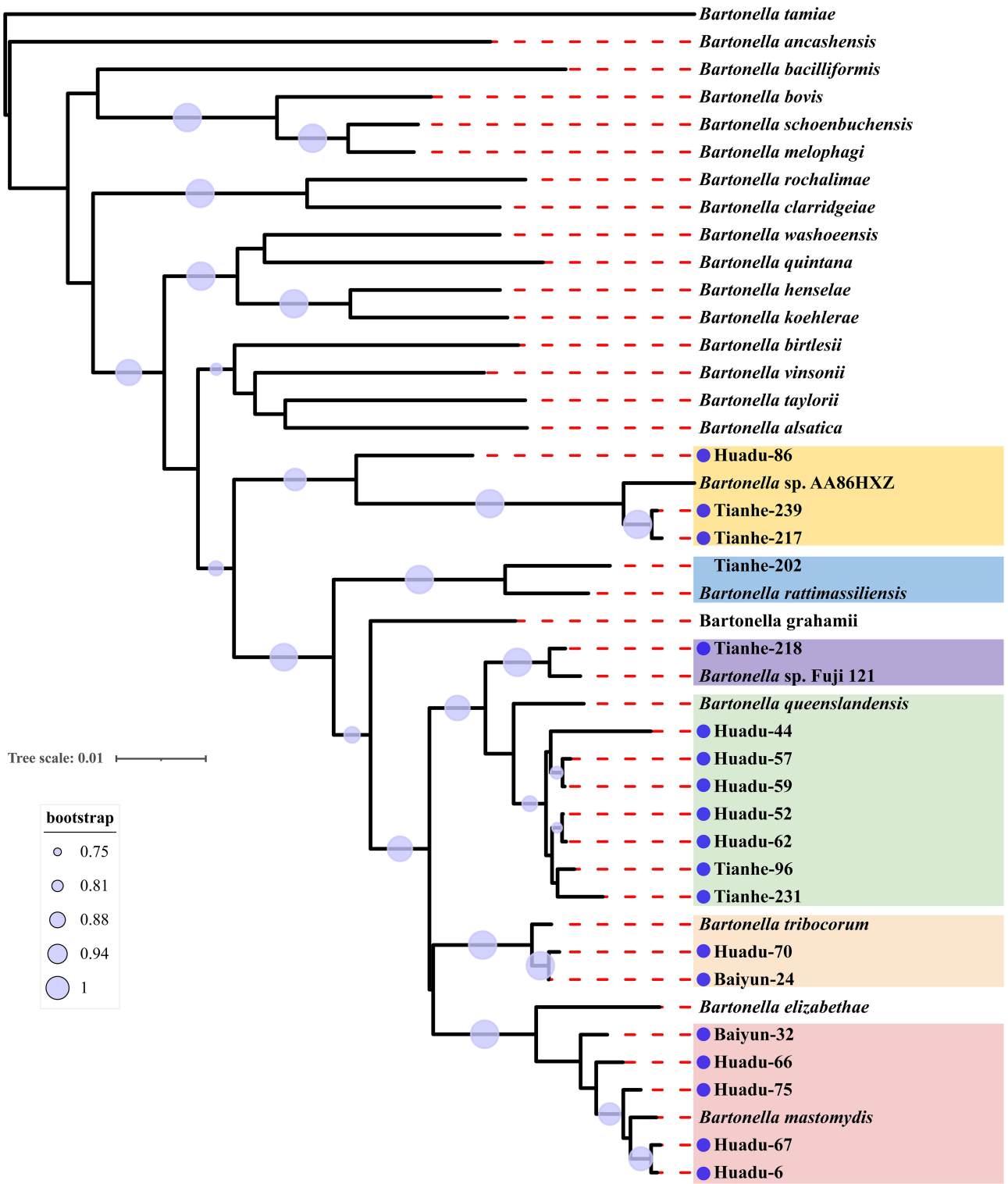

FIGURE 3 | Maximum-likelihood phylogenetic tree reconstructed based on the concatenated nucleotide sequences of *rrs*, *gltA*, and *rpoB* genes of *Bartonella*. Bootstrap values were calculated with 100 replicates of the alignment, and only bootstrap values >70% are shown at appropriate nodes. Sequences of *Bartonella* determined in this study are marked with blue dot.

In the present study, rodents were captured in urban areas of Guangzhou city, and *Bartonella* was detected with an overall prevalence of 6.4%, which was lower than the results reported previously in the urban environments in Thailand (Saengsawang et al., 2021), Argentina (De Salvo et al., 2020), and Malaysia (Blasdell et al., 2019). In addition, the prevalence of *Bartonella* in our study was lower than those in other areas in China (Li et al., 2015; An et al., 2020; Rao et al., 2021; Liu et al., 2022). The observed differences in the prevalence of *Bartonella* in rodents may be related to rodent species, habitats, and arthropod vector populations (Meheretu et al., 2013). Herein, all *Bartonella*-positive were detected from *R. norvegicus*, which is the predominant species of rodents captured in our study and also a synanthropic rodent species mostly found in the urban environments (Gardner-Santana et al., 2009; Kosoy and Bai, 2019). Particularly, fleas have been shown to play an extremely important role in the transmission and acquisition of *Bartonella* species in rodents (Silaghi et al., 2016). Rodents inhabiting urban environments have less chance of flea-parasitic infestation, thus reducing the possibility of *Bartonella* infection. However, *R. norvegicus* closely cohabitates with humans living inside buildings and enhances the likelihood of human contact with rodents, suggesting that *R. norvegicus* may be an important source of zoonotic pathogens (Firth et al., 2014). *Bartonella* species detected in this study also suggest that much more attention should be focused on the increased risk of *Bartonella* transmission to humans in urban environments.

revious data indicated that the majority of known *Bartonella* spp. are carried by rodents, some of which have been implicated as the causative agents of human diseases (Gutiérrez et al., 2015; Okaro et al., 2017). In this study, six official or candidate species of *Bartonella*, including *B. queenslandensis*, *B. mastomydis*, *B. tribocorum*, *B. rattimassiliensis*, *Bartonella* sp. AA86HXZ, and *Bartonella* sp. Fuji 12-1 were detected in rodents, indicating the genetic diversity of *Bartonella* circulating in the rodent population in the urban areas of Guangzhou city. Notably, two confirmed human-pathogenic *Bartonella* species, i.e., *B. tribocorum* and *B. rattimassiliensis,* were detected in this study, indicating that infection risks exist in human populations in urban areas that originated from rodent-associated *Bartonella*, and also highlighting the importance of the surveillance of *Bartonella* infection in rodents.

In conclusion, genetically diversified *Bartonella,* including two confirmed zoonotic species, were detected in rodents in the urban areas of Guangzhou city with an overall prevalence of 6.4%. Moreover, *R. norvegicus* was the predominant host species for *Bartonella* infection, and *B. queenslandensis* was the dominant species circulating in rodents in these areas. These results provide a better understanding of the prevalence and genetic diversity of *Bartonella* species circulating in rodents in the urban areas of Guangzhou and also urged the necessity of the surveillance of rodent-associated *Bartonella* species in these areas.

DATA AVAILABILITY STATEMENT

The datasets presented in this study can be found in online repositories. The names of the repository/repositories and accession number(s) can be found in the article/**Supplementary Material**.

ETHICS STATEMENT

The animal study was reviewed and approved by Ethics Committee of Foshan University.

AUTHOR CONTRIBUTIONS

J-WS conceived and designed the experiments and writing—review and editing. X-YY, HL, and JS performed the experiments and analyzed the data. Y-QZ, Z-HL, and X-LZ help to collect the samples. X-YY writing—original draft preparation. All authors contributed to the article and approved the submitted version.

FUNDING

This work was funded by the Key Project of Agricultural and Social Development Science and Technology Projects of Guangzhou (No. 202103000008). The funder had no role in study design, data collection and interpretation, or the decision to submit the work for publication.

ACKNOWLEDGMENTS

We wish to thank all the people who had collected samples in the field.

SUPPLEMENTARY MATERIAL

The Supplementary Material for this article can be found online at: https://www.frontiersin.org/articles/10.3389/fmicb.2022.942587/full#supplementary-material

REFERENCES

Álvarez-Fernández, A., Breitschwerdt, E. B., and Solano-Gallego, L. (2018). *Bartonella* infections in cats and dogs including zoonotic aspects. *Parasit Vectors* 11, 624. doi: 10.1186/s13071-018-3152-6

An, C. H., Chen, B. B., Lyu, W., Nie, S. M., Li, S. Z., Fan, S. P., et al. (2020). *Bartonella* species investigated among rodents from Shaanxi Province of China. *Biomed. Environ. Sci.* 33, 201–205.

Anderson, B. E., and Neuman, M. A. (1997). *Bartonella* spp. as emerging human pathogens. *Clin. Microbiol. Rev.* 10, 203–219. doi: 10.1128/CMR.10.2.203

Birtles, R. J., Laycock, G., Kenny, M. J., Shaw, S. E., and Day, M. J. (2002). Prevalence of *Bartonella* species causing bacteraemia in domesticated and companion animals in the United Kingdom. *Vet. Rec.* 151, 225–229. doi: 10.1136/vr.151.8.225

Blasdell, K. R., Perera, D., and Firth, C. (2019). High prevalence of rodent-borne *Bartonella* spp. in urbanizing environments in sarawak, malaysian

Borneo. *Am. J. Trop. Med. Hyg.* 100, 506–509. doi: 10.4269/ajtmh.18-0616

Chang, C. C., Chomel, B. B., Kasten, R. W., Heller, R. M., Kocan, K. M., Ueno, H., et al. (2000). *Bartonella* spp. isolated from wild and domestic ruminants in North America. *Emerg. Infect. Dis.* 6, 306–311. doi: 10.3201/eid0603.000313

Daly, J. S., Worthington, M. G., Brenner, D. J., Moss, C. W., Hollis, D. G., Weyant, R. S., et al. (1993). *Rochalimaea elizabethae* sp. nov. isolated from a patient with endocarditis. *J. Clin. Microbiol.* 31, 872–881. doi: 10.1128/jcm.31.4.872-881.1993

De Salvo, M. N., Hercolini, C., Arístegui, E., Bruno, A., Brambati, D. F., and Cicuttin, G. L. (2020). *Bartonella* spp. associated with rodents in an urban protected area, Buenos Aires (Argentina). *Comp. Immunol. Microbiol. Infect. Dis.* 72, 101515. doi: 10.1016/j.cimid.2020.101515

De Sousa, K. C. M., Do Amaral, R. B., Herrera, H. M., Santos, F. M., Macedo, G. C., De Andrade Pinto, P. C. E., et al. (2018). Genetic diversity of *Bartonella* spp. in wild mammals and ectoparasites in Brazilian Pantanal. *Microb. Ecol.* 76, 544–554. doi: 10.1007/s00248-017-1138-0

Divari, S., Pregel, P., Zanet, S., Ferroglio, E., Giannini, F., Scaglione, F. E., et al. (2020). Molecular evidence of *Bartonella* spp. in rodents: a study in Pianosa Island, Italy. *Animals.* 10, 2070. doi: 10.3390/ani10112070

Dong, X., and Soong, L. (2021). Emerging and re-emerging zoonoses are major and global challenges for public health. *Zoonoses* 1, 1. doi: 10.15212/ZOONOSES-2021-0001

Dybing, N. A., Jacobson, C., Irwin, P., Algar, D., and Adams, P. J. (2016). *Bartonella* species identified in rodent and feline hosts from island and mainland western Australia. *Vector Borne. Zoonotic. Dis.* 16, 238–244. doi: 10.1089/vbz.2015.1902

Egan, S. L., Taylor, C. L., Banks, P. B., Northover, A. S., Ahlstrom, L. A., Ryan, U. M., et al. (2021). The bacterial biome of ticks and their wildlife hosts at the urban-wildland interface. *Microb. Genom.* 7, 000730. doi: 10.1099/mgen.0.000730

Firth, C., Bhat, M., Firth, M. A., Williams, S. H., Frye, M. J., Simmonds, P., et al. (2014). Detection of zoonotic pathogens and characterization of novel viruses carried by commensal *Rattus norvegicus* in New York City. *mBio* 5, e01933–e01914. doi: 10.1128/mBio.01933-14

Gardner-Santana, L. C., Norris, D. E., Fornadel, C. M., Hinson, E. R., Klein, S. L., and Glass, G. E. (2009). Commensal ecology, urban landscapes, and their influence on the genetic characteristics of city-dwelling Norway rats (*Rattus norvegicus*). *Mol. Ecol.* 18, 2766–2778. doi: 10.1111/j.1365-294X.2009.04232.x

Gundi, V. A., Davoust, B., Khamis, A., Boni, M., Raoult, D., and La Scola, B. (2004). Isolation of *Bartonella rattimassiliensis* sp. nov. and *Bartonella phoceensis* sp. nov. from European *Rattus norvegicus*. *J. Clin. Microbiol.* 42, 3816–3818. doi: 10.1128/JCM.42.8.3816-3818.2004

Guo, W. P., Lin, X. D., Wang, W., Tian, J. H., Cong, M. L., Zhang, H. L., et al. (2013). Phylogeny and origins of hantaviruses harbored by bats, insectivores, and rodents. *PLoS Pathog.* 9, e1003159. doi: 10.1371/journal.ppat.1003159

Gutiérrez, R., Krasnov, B., Morick, D., Gottlieb, Y., Khokhlova, I. S., and Harrus, S. (2015). *Bartonella* infection in rodents and their flea ectoparasites: an overview. *Vector Borne. Zoonotic. Dis.* 15, 27–39. doi: 10.1089/vbz.2014.1606

Hatyoka, L. M., Brettschneider, H., Bennett, N. C., Kleynhans, D. J., Muteka, S. P., and Bastos, A. D. S. (2019). *Bartonella* diversity and zoonotic potential in indigenous Tete Veld rats (*Aethomys ineptus*) from south Africa. *Infect. Genet. Evol.* 73, 44–48. doi: 10.1016/j.meegid.2019.04.012

Kandelaki, G., Malania, L., Bai, Y., Chakvetadze, N., Katsitadze, G., Imnadze, P., et al. (2016). Human Lymphadenopathy Caused by Ratborne *Bartonella*, Tbilisi, Georgia. *Emerg. Infect. Dis.* 22, 544–546. doi: 10.3201/eid2203.151823

Kosoy, M., and Bai, Y. (2019). *Bartonella* bacteria in urban rats: a movement from the jungles of southeast Asia to metropoles around the globe. *Front. Ecol. Evol.* 7, 88. doi: 10.3389/fevo.2019.00088

Kosoy, M., Bai, Y., Sheff, K., Morway, C., Baggett, H., Maloney, S. A., et al. (2010). Identification of *Bartonella* infections in febrile human patients from Thailand and their potential animal reservoirs. *Am. J. Trop. Med. Hyg.* 82, 1140–1145. doi: 10.4269/ajtmh.2010.09-0778

Kosoy, M., Morway, C., Sheff, K. W., Bai, Y., Colborn, J., Chalcraft, L., et al. (2008). *Bartonella tamiae* sp. nov., a newly recognized pathogen isolated from three human patients from Thailand. *J. Clin. Microbiol.* 46, 772–775. doi: 10.1128/JCM.02120-07

Kosoy, M., Murray, M., Gilmore, R. D. Jr., Bai, Y., and Gage, K. L. (2003). *Bartonella* strains from ground squirrels are identical to *Bartonella washoensis* isolated from a human patient. *J. Clin. Microbiol.* 41, 645–650. doi: 10.1128/JCM.41.2.645-650.2003

Kumar, S., Stecher, G., Li, M., Knyaz, C., and Tamura, K. (2018). MEGA X: molecular evolutionary genetics analysis across computing platforms. *Mol. Biol. Evol.* 35, 1547–1549. doi: 10.1093/molbev/msy096

Li, D. M., Hou, Y., Song, X. P., Fu, Y. Q., Li, G. C., Li, M., et al. (2015). High prevalence and genetic heterogeneity of rodent-borne *Bartonella* species on Heixiazi Island, China. *Appl. Environ. Microbiol.* 81, 7981–7992. doi: 10.1128/AEM.02041-15

Li, D. M., Liu, Q. Y., Yu, D. Z., Zhang, J. Z., Gong, Z. D., and Song, X. P. (2007). Phylogenetic analysis of *Bartonella* detected in rodent fleas in Yunnan, China. *J. Wildl. Dis.* 43, 609–617. doi: 10.7589/0090-3558-43.4.609

Lin, J. W., Chen, C. Y., Chen, W. C., Chomel, B. B., and Chang, C. C. (2008). Isolation of *Bartonella* species from rodents in Taiwan including a strain closely related to '*Bartonella rochalimae*' from *Rattus norvegicus*. *J. Med. Microbiol.* 57, 1496–1501. doi: 10.1099/jmm.0.2008/004671-0

Liu, H., Han, T., Liu, W., Xu, G., Zheng, K., and Xiao, F. (2022). Epidemiological characteristics and genetic diversity of *Bartonella* species in rodents from southeastern China. *Zoonoses Public Health* 69, 224–234. doi: 10.1111/zph.12912

Meerburg, B. G., Singleton, G. R., and Kijlstra, A. (2009). Rodent-borne diseases and their risks for public health. *Crit. Rev. Microbiol.* 35, 221–270. doi: 10.1080/10408410902989837

Meheretu, Y., Leirs, H., Welegerima, K., Breno, M., Tomas, Z., Kidane, D., et al. (2013). *Bartonella* prevalence and genetic diversity in small mammals from Ethiopia. *Vector Borne Zoonotic. Dis.* 13, 164–175. doi: 10.1089/vbz.2012.1004

Mogollon-Pasapera, E., Otvos, L. Jr., Giordano, A., and Cassone, M. (2009). *Bartonella*: emerging pathogen or emerging awareness? *Int. J. Infect. Dis.* 13, 3–8. doi: 10.1016/j.ijid.2008.04.002

Mosepele, M., Mazo, D., and Cohn, J. (2012). *Bartonella* infection in immunocompromised hosts: immunology of vascular infection and vasoproliferation. *Clin. Dev. Immunol.* 2012, 612809. doi: 10.1155/2012/612809

Müller, A., Gutiérrez, R., Seguel, M., Monti, G., Otth, C., Bittencourt, P., et al. (2020). Molecular survey of *Bartonella* spp. in rodents and fleas from Chile. *Acta Trop* 212, 105672. doi: 10.1016/j.actatropica.2020.105672

Okaro, U., Addisu, A., Casanas, B., and Anderson, B. (2017). *Bartonella* species, an emerging cause of blood-culture-negative endocarditis. *Clin. Microbiol. Rev.* 30, 709–746. doi: 10.1128/CMR.00013-17

Qin, X. R., Liu, J. W., Yu, H., and Yu, X. J. (2019). *Bartonella* species detected in rodents from eastern China. *Vector Borne Zoonotic Dis.* 19, 810–814. doi: 10.1089/vbz.2018.2410

Rao, H., Li, S., Lu, L., Wang, R., Song, X., Sun, K., et al. (2021). Genetic diversity of *Bartonella* species in small mammals in the Qaidam Basin, western China. *Sci. Rep.* 11, 1735. doi: 10.1038/s41598-021-81508-w

Saengsawang, P., Morand, S., Desquesnes, M., Yangtara, S., and Inpankaew, T. (2021). Molecular detection of *Bartonella* Species in rodents residing in urban and suburban areas of central Thailand. *Microorganisms* 9, 2588. doi: 10.3390/microorganisms9122588

Silaghi, C., Pfeffer, M., Kiefer, D., Kiefer, M., and Obiegala, A. (2016). *Bartonella*, rodents, fleas and ticks: a molecular field study on host-vector-pathogen associations in Saxony, Eastern Germany. *Microb. Ecol.* 72, 965–974. doi: 10.1007/s00248-016-0787-8

Su, Q., Chen, Y., Wang, B., Huang, C., Han, S., Yuan, G., et al. (2020). Epidemiology and genetic diversity of zoonotic pathogens in urban rats (*Rattus* spp.) from a subtropical city, Guangzhou, southern China. *Zoonoses Public Health* 67, 534–545. doi: 10.1111/zph.12717

Szewczyk, T., Werszko, J., Slivinska, K., Laskowski, Z., and Karbowiak, G. (2021). Molecular detection of *Bartonella* spp. in rodents in Chernobyl Exclusion Zone, Ukraine. *Acta Parasitol.* 66, 222–227. doi: 10.1007/s11686-020-00276-1

Valentine, K. H., Harms, C. A., Cadenas, M. B., Birkenheuer, A. J., Marr, H. S., Braun-Mcneill, J., et al. (2007). *Bartonella* DNA in loggerhead sea turtles. *Emerg. Infect. Dis.* 13, 949–950. doi: 10.3201/eid1306.061551

Vayssier-Taussat, M., Moutailler, S., Féménia, F., Raymond, P., Croce, O., La Scola, B., et al. (2016). Identification of novel zoonotic activity of *Bartonella* spp., France. *Emerg. Infect. Dis.* 22, 457–462. doi: 10.3201/eid2203.150269

Von Loewenich, F. D., Seckert, C., Dauber, E., Kik, M. J. L., De Vries, A., Sprong, H., et al. (2019). Prosthetic valve endocarditis with *Bartonella washoensis* in a human european patient and its detection in red squirrels (Sciurus vulgaris). *J. Clin. Microbiol.* 58, e01404–e01419. doi: 10.1128/JCM.01404-19

Wei, Y., Wang, Y., Li, X., Qin, P., Lu, Y., Xu, J., et al. (2018). Meteorological factors and risk of hemorrhagic fever with renal syndrome in Guangzhou, southern China, 2006-2015. *PLoS Negl. Trop. Dis.* 12, e0006604. doi: 10.1371/journal.pntd.0006604

Welch, D. F., Carroll, K. C., Hofmeister, E. K., Persing, D. H., Robison, D. A., Steigerwalt, A. G., et al. (1999). Isolation of a new subspecies, *Bartonella vinsonii* subsp. arupensis, from a cattle rancher: identity with isolates found in conjunction with Borrelia burgdorferi and *Babesia microti* among naturally infected mice. *J. Clin. Microbiol.* 37, 2598–2601. doi: 10.1128/JCM.37.8.2598-2601.1999

Zhang, X. L., Li, X. W., Li, W. F., Huang, S. J., and Shao, J. W. (2019). Molecular detection and characterization of *Bartonella* spp. in pet cats and dogs in Shenzhen, China. *Acta Trop.* 197, 105056. doi: 10.1016/j.actatropica.2019.105056

Conflict of Interest: The authors declare that the research was conducted in the absence of any commercial or financial relationships that could be construed as a potential conflict of interest.

frontiers | Frontiers in Microbiology

TYPE Original Research
PUBLISHED 22 July 2022
DOI 10.3389/fmicb.2022.962326

OPEN ACCESS

EDITED BY
Wei Wang,
Jiangsu Institute of Parasitic Diseases (JIPD), China

REVIEWED BY
Jintao Li,
Army Medical University, China
Yuelan Yin,
Yangzhou University, China

*CORRESPONDENCE
Zhaobin Chen
chenzb.md@vip.163.com
Chuan Wang
wangchuan@scu.edu.cn

†These authors share first authorship

SPECIALTY SECTION
This article was submitted to Infectious Agents and Disease, a section of the journal Frontiers in Microbiology

RECEIVED 06 June 2022
ACCEPTED 30 June 2022
PUBLISHED 22 July 2022

CITATION
Liang Q, Li R, Liu S, Zhang Y, Tian S, Ou Q, Chen Z and Wang C (2022) Recombinant *Listeria ivanovii* strain expressing listeriolysin O in place of ivanolysin O might be a potential antigen carrier for vaccine construction.
Front. Microbiol. 13:962326.
doi: 10.3389/fmicb.2022.962326

Recombinant *Listeria ivanovii* strain expressing listeriolysin O in place of ivanolysin O might be a potential antigen carrier for vaccine construction

Qian Liang[1,2†], Ruidan Li[1,2†], Sijing Liu[1†], Yunwen Zhang[1], Sicheng Tian[1], Qian Ou[1], Zhaobin Chen[2*] and Chuan Wang[1*]

[1]Department of Public Health Laboratory Sciences, West China School of Public Health and West China Fourth Hospital, Sichuan University, Chengdu, China, [2]Shen Zhen Biomed Alliance Biotech Group Co., Ltd., Shenzhen, China

Listeria monocytogenes (LM) induces efficient and specific T-cell immune responses in the host. Listeriolysin O (LLO) is the main virulence protein of LM. LLO helps LM escape from the lysosome. However, the pronounced pathogenicity of LM limits its practical application as a live bacterial vector. *Listeria ivanovii* (LI) also displays intracellular parasitic abilities, cell to cell transfer, and other LM properties, with an elevated biosafety relative to LM. We have confirmed that LI can be used as a viable bacterial vaccine vector. However, we have also observed *in vivo* that LI vector vaccine candidates survive in the immune organ (spleen) for a shorter time compared with the survival time of LM and elicit weaker immune responses compared with LM. Studies have confirmed that hemolysin correlates with some important biological properties of *Listeria*, including cell invasion, intracellular proliferation, and the ability to induce immune responses. We speculated that the weaker immunogenicity of LI compared to LM may be related to the function of ivanolysin O (ILO). Here, we established a hemolysin gene deletion strain, LIΔ*ilo*, and a modified strain, LIΔ*ilo*:*hly*, whose *ilo* was replaced by *hly*. The hemolysin-modified strain was attenuated; however, it led to significantly improved invasive and proliferative activities of antigen-presenting cells, including those of RAW 264.7 macrophages, compared with the effects of LI. Mice immunized twice with LIΔ*ilo*:*hly* showed higher cytokine levels and better challenge protection rates than LI-immunized mice. This is the first description in *Listeria* carrier vaccine research of the modification of LI hemolysin to obtain a better vaccine carrier than LI. The recombinant strain LIΔ*ilo*:*hly* showed good biosafety and immunogenicity, and thus appears to be a good vector strain for vaccine development.

KEYWORDS

***Listeria monocytogenes*, *Listeria ivanovii*, listeriolysin O, ivanolysin O, immune effect**

Introduction

Listeria monocytogenes (LM) is a gram-positive food-borne pathogen that is widely distributed in nature. LM can cause listeriosis, which mainly manifests as mild gastroenteritis, but which can be severe and cause meningitis, gastroenteritis, and sepsis (Farber and Peterkin, 1991; Wallecha et al., 2009). LM can proliferate intracellularly. This process is generally considered to be related to listeriolysin O (LLO). LLO is encoded by *hly*, which is located on LM pathogenicity island 1 (LPI-1). LLO is a major virulence factor of LM (Vázquez-Boland et al., 2001). LLO degrades lysosomal membranes to help bacteria escape phagocytic vesicles and enter host cytoplasm for growth. LLO also has an immunomodulatory role and is thus a potential adjuvant for cancer immunotherapy. A previous study showed that fusing LLO protein to human papillomavirus E7 protein improved the tumoricidal function of E7-specific $CD8^+$ T cells and increased the number of antigen-specific $CD8^+$ T cells in the tumor (Lamikanra et al., 2001), resulting in an improved antitumor therapeutic effect. The unique intracellular lifecycle of LM allows antigens present in or expressed by LM to elicit antigen-specific cellular immune responses through both MHC class I and MHC class II molecular pathways (Harty et al., 1996; Ruan et al., 2016). Therefore, LM is considered to be a promising vector for constructing vaccines that mainly induce cellular immune responses. However, since LM is pathogenic to humans, it must be attenuated before it can be used as a vaccine vector. Many reports have described preventive and therapeutic vaccines that utilize attenuated LM strains as carriers. For example, Yang et al. (2014) described an attenuated LM strain, deleting the *dal* and *dat* genes and carrying the human CD24 gene, led to Hepa1-6-CD24-induced tumor regression and increased tumor-free survival in mice. Tumor therapeutic vaccines based on LM have also shown expected results in clinical trials (Le et al., 2019). Vaccine vectors must have reliable biological safety. However, whether the virulence of LM strains remains attenuated after knocking out virulence or metabolic genes is a major safety issue that remains to be investigated.

Listeria ivanovii (LI) was first isolated from a lamb with congenital listeriosis in Bulgaria in 1955. LI rarely infects humans. Thus it displays better biosafety than LM in humans. LI has properties similar to those of LM, such as intracellular growth and cell-to-cell spread, and can enter antigen-presenting cells and proliferate intracellularly (Frehel et al., 2003). We immunized mice with a recombinant LI strain carrying *Mycobacterium tuberculosis* antigen in its genome. We found that the recombinant strain induced antigen-specific $CD8^+$ T cell immune responses, confirming that it can be used as a vaccine carrier. However, the immune responses were not very strong (Lin et al., 2015). Ivanolysin O (ILO) differs from LLO in some respects. One study demonstrated that the recombinant strain LIΔ*ilo*:*hly*, constructed by replacing *hly* with ILO coding gene *ilo*, proliferated in mouse livers, but not spleens (Zhou et al., 2016). Since LLO is important for intracellular parasitism and induction of cellular immune responses by LM, we speculated that the weak immunogenicity of LI may be related to the function of ILO. We assumed that the immunogenicity of LI can be improved by replacing its hemolysin with LLO. Improved immunogenicity combined with LI's increased biosafety may render the modified strain a safe and effective vaccine carrier.

In this study, we constructed a hemolysin gene deletion strain LIΔ*ilo* by knocking out *ilo*. From this strain, we constructed a modified strain, LIΔ*ilo*:*hly* whose *ilo* has been replaced by *hly*. We studied the *in vitro* growth rate, hemolytic titer, and changes in biochemical characteristics of the strain after hemolysin replacement. Next, we studied the adhesion, invasion, and proliferative ability of cells *in vitro*, and the biosafety, immune effect, and immune protection rate *in vivo* of LIΔ*ilo*:*hly*. Replacement of the hemolysin gene did not significantly affect bacterial growth, and LIΔ*ilo*:*hly* maintained biological properties similar to LI. Compared with LI, the *in vitro* proliferation ability of LIΔ*ilo*:*hly* in RAW 264.7 macrophages was significantly improved, but *in vivo* virulence was attenuated; after immunizing animals twice, LIΔ*ilo*:*hly* induced higher cytokine levels and improved the challenge protection rate. The recombinant strain LIΔ*ilo*:*hly* displays good biosafety and immunogenicity, and appears to be a good vector strain for vaccine construction.

Materials and methods

Bacteria, plasmids, cells, and animals

Bacteria strains LM 10403s and LI PAM55 were provided by Dr. Hao Shen (Department of Microbiology, Perelman School of Medicine, University of Pennsylvania, Philadelphia, PA, United States), and plasmid pCW-107 was constructed for this study (Wang et al., 2014; Zhou et al., 2016; Mahdy et al., 2019). RAW 264.7, and Hepa1-6 cells were maintained in DMEM (Gibco, New York, NY, United States). Specific-pathogen-free, female C57BL/6 mice (6–8 weeks old) were purchased from Vital River Laboratory Animal Technology Co., Ltd., (Zhejiang, China) and housed at the Animal Center of the School of Public Health in Sichuan University. Animal experiments were approved by the Animal Care and Use Committee of Sichuan University.

Construction of recombinant strains

Plasmid pCW107 was extracted and digested with *Xba* I and *Not* I restriction enzymes to obtain a linear fragment of the targeting plasmid vector. The LI genome was used as a template to amplify the upstream and downstream homologous

sequences of *ilo*. The upstream homologous sequence was inserted into the pCW107 *Xba* I and *Not* I sites to generate plasmid pCW618. This plasmid was digested with *Spe* I and *Not* I, and the downstream homologous sequence was inserted to obtain pCW619. Plasmid pCW619 was cut with *Not* I, then inserted into *lacZ* or *hly* fragments to obtain pCW620 carrying *lacZ* or pCW621 carrying *hly*, respectively. Plasmid pCW620 was electroporated into LI, and strain LIΔ*ilo*:*lacZ* was constructed by homologous recombination (Liu et al., 2020). Plasmids pCW619 and pCW621 were electroporated into LIΔ*ilo*:*lacZ* to construct strains LIΔ*ilo* and LIΔ*ilo*:*hly*, respectively. The strategy used for recombinant bacterial strain construction is shown in **Supplementary Figure 1**. The primers used are listed in **Supplementary Table 1**.

Basic characteristics

In vitro growth characteristics

Single colonies of LM, LI, LIΔ*ilo*, and LIΔ*ilo*:*hly* were inoculated into 5 mL BHI broth and cultured at 37°C for 18∼24 h. A portion of each culture was inoculated into 40 mL of BHI broth. The inoculum volume that was used resulted in an initial absorbance at 600 nm (A_{600}) of each resulting suspension of 0.05. Each culture was incubated in a constant-temperature shaker at 200 rpm and at 37°C. Three milliliters were withdrawn every 1 h for 10 h to measure and record the A_{600} value. These measurements were used to plot growth curves.

Recombinant strain protein expression

LIΔ*ilo*:*hly* was inoculated into BHI broth medium and cultured to the logarithmic phase of growth. The culture supernatant and bacterial precipitate were respectively collected after centrifugation. The total protein from the culture supernatant was extracted by TCA-acetone precipitation, and the total protein from the bacterial precipitate was extracted by ultrasonic breaking and TCA-acetone precipitation. The protein samples were subjected to SDS-PAGE electrophoresis and then transferred onto a PVDF membrane. The membrane was incubated with rabbit anti-listeriolysin O antibody (1:1000) (Abcam, Cambridge, United Kingdom) as the primary antibody, and horseradish peroxidase (HRP)-labeled goat anti-rabbit IgG (H + L) (1:1,000) (Beyotime Biotechnology Co., Ltd., Shanghai, China) as the secondary antibody. The HRP chemiluminescence substrate was applied for color development and the results were analysis after incubation.

Bacterial biochemical identification test

Fresh single colonies of LM, LI, LIΔ*ilo*, and LIΔ*ilo*:*hly* were collected and individually added to a tube filled with 4 mL of sterile water. A bacterial suspension was prepared with a McFarland turbidity ranging from 0.4 to 0.6. A bacterial biochemical identification reagent card was placed in the bacterial suspension to sample the bacteria. After removing the bacterial liquid, the reagent card was placed in an automatic microbial identification and drug susceptibility analyzer (Merier Biotechnology Co., Lyon, France) to culture and biochemically identify bacteria.

Determination of hemolytic titer

Five milliliters of each logarithmic phase bacterial culture was centrifuged at 13,000 rpm for 5 min. Supernatants were pipetted after centrifugation into wells of a U-shaped 96-well plate and diluted two-fold to 2^{-8}. PBS was used instead of culture supernatants to prepare the same dilution for use as a negative control. Thirty microliters of 1% sheep erythrocyte suspension was added to both sample and control wells, and then mixed, and incubated at 37°C for 2 h. The hemolytic titer of each strain was recorded.

Intracellular proliferation, adhesion and invasion to the cells

Proliferation in RAW 264.7 cells

RAW264.7 macrophages were seeded in wells of a 24-well plate at a density of 1×10^6 cells/well and cultured to 70–80% confluency. Next, 100 μL of LM, LI, LIΔ*ilo*, or LIΔ*ilo*:*hly* bacterial suspensions were added to each well at a multiplicity of infection (MOI) of 20:1 and incubated at 37°C for 1 h. Culture medium was discarded, cells were washed with PBS, 1 mL of DMEM medium containing 200 μg/mL gentamicin and 10% fetal bovine serum was added to each well, and cells were cultured at 37°C for 1 h to kill extracellular bacteria. Culture medium was then discarded, cells were washed with PBS, and 0.1% Triton X-100 was added to 2 wells to lyse the cells. After a 1:10 dilution, 20 μL of the suspension was dropped onto the surface of a BHI plate and cultured at 37°C for 48 h. The colony forming unit (CFU) was defined as the total number of bacteria that invaded the cells. The remaining wells were added to DMEM containing 100 μg/mL gentamicin and 10% fetal bovine serum, and incubation was continued. Cells were lysed 2, 4, and 6 h later, and the number of viable bacteria was counted using the above method. Fold changes = (total number of bacteria at each time point)/(total number of bacteria invading cells at 2 h); Multiplication factor (%) = (total number of bacteria at each time point)/(total number of bacteria initially added).

Laser scanning confocal microscopy observation of bacteria growth in RAW 264.7 cells

The pCW-*gfp* plasmid expressing green fluorescent protein was electroporated into LM, LI, and LIΔ*ilo*:*hly* to obtain LM-*gfp*, LI-*gfp*, and LIΔ*ilo*:*hly*-*gfp*. RAW264.7 cells were plated on a 24-well plate with slides. After the cells had grown to 70–80% confluency, fresh bacterial suspension was added at an MOI of approximately 10:1. After culturing for 1 h, the culture medium was replaced with DMEM containing 30 μg/mL

gentamicin. A 24-well plate was removed after 1 and 7 h, and 200 μL immunostaining fixative was added to each well. Cells were fixed at room temperature for 15 min. Supernatants were discarded, and cells were washed with PBS, followed by addition of 200 μL of PBS containing 0.1% Triton X-100 to each well to lyse cell membranes for 10 min at room temperature. After washing, 200 μL PBS-Tween buffer containing 1% BSA and 22.52 mg/ml glycine was added to each well and cells were blocked at room temperature for 30 min. Supernatants were discarded, and pellets were washed. Phagosome staining (Beuzón et al., 2000) was performed using rabbit anti-lysosomal-associated membrane protein 1 (LAMP-1) antibody (Abcam, Cambridge, United Kingdom) and Alexa Fluor 647-conjugated AffiniPure donkey anti-rabbit secondary antibody (Jackson ImmunoResearch, Pennsylvania, United States). After washing, staining solution containing 10 μg/mL 4',6-diamidino-2-phenylindol (DAPI; Solarbio, Beijing, China) was added to each well in the dark and incubated at room temperature for 5 min. The staining solution was discarded followed by thorough washing, LSCM observation, and photography.

Adhesion and invasion rate of the strains to Hepa1-6 cells

Hepa1-6 cells were seeded in 24-well plates at a density of 1×10^6 cells/well and cultured to 70–80% confluency. One hundred microliters of LM, LI, LIΔ*ilo*, or LIΔ*ilo*:*hly* bacterial suspensions were added to each well at an MOI of approximately 20:1.

To determine the adhesion rate, after culturing for 1 h, the 24-well plate was washed with PBS, and 0.1% Triton X-100 solution was added to lyse the cells. Suspensions were then diluted 1:10. Twenty microliters of the diluted suspension was spread onto the surface of a BHI plate and cultured at 37°C for 48 h. CFU was defined as the number of adherent bacteria. The bacterial adhesion rate (%) was calculated as [(number of adherent bacteria)/(total number of bacteria added to cells)] × 100.

To calculate the invasion rate, after culturing for 1 h, the 24-well plate was removed and washed with PBS. DMEM containing 200 μg/mL gentamicin and 10% fetal bovine serum was added to each well and cultured for 1 h. The subsequent operations were the same as described above. CFU is considered to represent the number of invading bacteria. The bacterial invasion rate (%) was calculated as = [(number of invading bacteria)/(total number of bacteria added to cells)] × 100.

In vivo safety and immunogenicity

LD_{50} of each strain in C57BL/6 mice

The 50% lethal dose (LD_{50}) of LI was previously determined to be 6.3×10^6 CFU per mouse (Lin et al., 2015). To determine LD_{50} for each of the other strains, C57BL/6 mice were injected with 100 μL of the bacterial suspension through the tail vein. The dose groups and inoculation volumes for each strain are shown in **Supplementary Table 4**. Deaths among the mice were recorded for 10 days. LD_{50} values were determined using an improved Karber method.

Determination of bacterial load in organs

C57BL/6 mice were intravenously inoculated with LM, LI, LIΔ*ilo*, or LIΔ*ilo*:*hly* at a dose of $0.1 \times LD_{50}$ of each strain. The mice were observed daily, and their body weights were recorded. Mice were sacrificed 1, 3, 5, 7, 9, and 14 days post-injection. The liver, spleen, and lungs were collected aseptically and homogenized in PBS containing 0.1% Triton X-100. The homogenate (50 μL) was diluted 1:10, and 20 μL was dropped onto the surface of a BHI plate. Plates were incubated at 37°C for 48 h. Colonies were counted to determine CFU values.

Determination of serum alanine aminotransferase and aspartate aminotransferase levels

At 1, 3, 5, 7, 9, and 14 days after injection, blood was collected from the mice. The serum was separated to detect the levels of alanine aminotransferase (ALT) and aspartate aminotransferase (AST).

Tissue sections and pathological observation

Liver, spleen, and lungs were aseptically dissected on days 3 and 4 after injection. Tissues were perfused with 4% paraformaldehyde solution and sent to Sewell Biotechnology Co., Ltd., (Wuhan, China) for section preparation and observation/pathological grading.

Determination of cytokine levels

Mice were randomly divided into four groups. Each mouse was intravenously inoculated twice at an interval of 7 days with LM, LI, or LIΔ*ilo*:*hly* at a dose of $0.1 \times LD_{50}$ of each strain, or with PBS as a blank control. The mice were sacrificed 9 and 40 days after the second immunization. Splenocyte suspensions were added to 24-well plates. Mixed LLO peptides (LLO318-329 AFDAAVSGKSVS; LLO297-304 AYGRQVYL; LLO253-264 QIYYNVNVNEPT; LLO91-99 GYKDGNEYI; LLO190-201 NEKYAQAYPNVS) were used as stimulants to stimulate LM and LIΔ*ilo*:*hly* groups for 48 h. ILO protein was used for the LI group. Plates were centrifuged at 1,200 rpm for 20 min and supernatants were collected. Levels of tumor necrosis factor-alpha (TNF-α), interleukin (IL)-12, IL-6, IL-4, and interferon-gamma (IFN-γ) were determined according to ELISA kit (Elabscience, China) instructions.

Determination of immune protection rate

The LM, LI, LIΔ*ilo*, and LIΔ*ilo*:*hly* groups were immunized with the corresponding strains, as described above. Challenges were conducted 7 days after the second immunization with 5 × LD_{50} of LM for the LM group and 5 × LD_{50} of LI for the LI, LIΔ*ilo*, LIΔ*ilo*:*hly*, and PBS groups *via* the tail vein. Mice were observed for 14 days, deaths were recorded, and protection rates were calculated.

Statistical analysis

Data were analyzed using SPSS 21.0 (IBM, United States). The data with a normal distribution are expressed as means ± standard deviation. One-way ANOVA was used for parametric tests, and the LSD test was used for pairwise comparisons between groups. Non-parametric data were analyzed using the Kruskal-Wallis non-parametric test. Count data were analyzed using Fisher's probability method. $P < 0.05$ indicated statistical significance.

Results

Targeting plasmid and recombinant strain construction

Four recombinant plasmids (pCW618, pCW619, pCW620, and pCW621) were obtained by amplifying target fragments using PCR, followed by enzyme digestion, ligation, and transformation. The *lacZ* gene fragment carried by the pCW620 plasmid was integrated into LI by electrotransformation and homologous recombination. LIΔ*ilo*:*lacZ* was obtained, and pCW619 and pCW621 were electro-transformed into LIΔ*ilo*:*lacZ*. After homologous recombination, blue-spot and white-spot screening, antibiotic screening, genome PCR, and sequencing were conducted to verify the successful construction of LIΔ*ilo* and LIΔ*ilo*:*hly* (**Supplementary Figure 2**).

Growth of the strains

The growth of LM, LI, LIΔ*ilo*, and LIΔ*ilo*:*hly* reached the logarithmic phase after 2 h of culture. Growth plateaued 9 h after inoculation. After 3 h, the growth rate of LM was higher than that of LI, LIΔ*ilo*, and LIΔ*ilo*:*hly*. The growth rate differences between LM and the other three strains were statistically significant. The rate and trend of the growth of LIΔ*ilo*:*hly* and LIΔ*ilo* were consistent with those observed for LI at each time point (**Figure 1**). The growth difference was not statistically significant, indicating that *ilo* knockout and *hly* complementation did not affect the *in vitro* growth of the recombinant strains.

Analysis of protein expression of recombinant strain

The culture supernatant and bacterial pellet of LIΔ*ilo*:*hly* were collected, and the total protein was extracted from culture supernatant and bacterial pellet, respectively. The obtained protein samples were denatured and subjected to SDS-PAGE electrophoresis and western blot. The specific-band with expected length (58 KD) was obviously visible in both the medium supernatant and the cell lysate protein samples, indicating that the recombinant bacteria successfully expressed and secreted the LLO protein (**Figure 2**).

Biochemical properties of strains

Most of the biochemical properties of the hemolysin-deletion strain LIΔ*ilo* and hemolysin-modified strain LIΔ*ilo*:*hly* were consistent with those of LI (**Supplementary Table 1**). The hemolytic titer of LIΔ*ilo*:*hly* was higher than that of LM, but lower than that of LI (**Supplementary Figure 3**).

Intracellular proliferation, cell adhesion, invasion, and lysosome escape

RAW264.7 macrophages were infected with LM, LI, LIΔ*ilo*:*hly*, and LIΔ*ilo*, and intracellular bacterial numbers were determined at 2, 4, 6, and 8 h post-infection. All strains except LIΔ*ilo* proliferated in macrophages. LIΔ*ilo*:*hly* showed the same proliferation trend as that of LI. Its intracellular proliferation ability was weaker than that of LM but stronger than that of LI, indicating that the intracellular proliferation ability of the modified strain was improved to a certain extent (**Figures 3A,B**).

The adhesion rates of LM, LI, LIΔ*ilo*, and LIΔ*ilo*:*hly* to Hepa1-6 cells were 0.54, 0.56, 0.57, and 0.48%, respectively (**Figure 3C**). Knockout of *ilo* did not affect the ability to adhere to mouse hepatocellular carcinoma cells. The invasion rates of LM, LI, LIΔ*ilo*:*hly*, and LIΔ*ilo* into Hepa1-6 cells were 0.076, 0.062, 0.075, and 0.024%, respectively (**Figure 3D**). LIΔ*ilo* had the lowest invasion rate, indicating that knockout of *ilo* affected invasiveness, and that replacement with *hly* restored the strain's invasiveness.

Laser scanning confocal microscopy (LSCM) of the infected macrophages (**Figure 3E**) showed that the bacterial numbers at 8 h were significantly higher than those at 2 h. LM-*gfp* showed the strongest proliferative ability, followed by LIΔ*ilo*:*hly*-*gfp* and LI-*gfp*. At 2 h post-infection, there were more green fluorescent

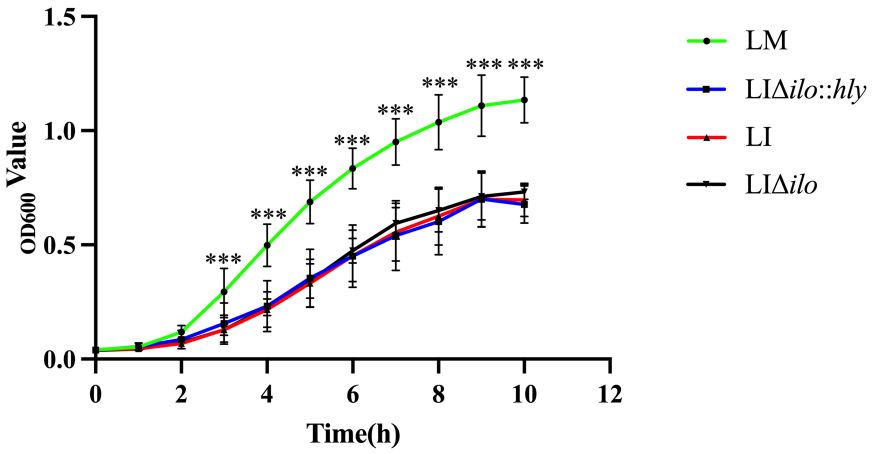

FIGURE 1
The growth curves of the strains. ***$P < 0.001$ vs. *Listeria monocytogenes* (LM). Experiments were carried out at least three times.

bacteria in the lysosome. At 8 h post-infection, there were almost no bacteria in the lysosome and many bacteria appeared in the cytoplasm, indicating that the bacteria had escaped from the lysosomes. Because the total number of bacteria at 8 h was different between the groups, the escape ability of the strains could not be accurately compared.

In vivo biosafety evaluation

Determination of LD_{50}, bacterial load in organs, and levels of alanine aminotransferase and aspartate aminotransferase

To evaluate the virulence of each strain *in vivo*, the LD_{50} of LM, LIΔ*ilo:hly* and LIΔ*ilo* in C57BL/6 mice was determined. LD_{50} results were 4.3×10^4 CFU/mouse for LM, 1.1×10^7 CFU/mouse for LIΔ*ilo:hly*, and 4.3×10^7 CFU/mouse for LIΔ*ilo*. The LD_{50} of LI was 6.3×10^6 CFU/mouse (determined in our laboratory) (Lin et al., 2015). Virulence *in vivo* was significantly attenuated by *ilo* knockout. Although virulence was restored after *hly* compensation, the strain still had reduced virulence compared with LI, confirming the increased biosafety of LIΔ*ilo:hly* (**Figures 4A–C**).

C57BL/6 mice were inoculated with $0.1 \times LD_{50}$ of each strain as the immunizing dose. The growth of the strains in the main organs of the mice is shown in **Figures 4D–F**. Bacterial numbers in the liver, spleen, and lung of the LM immunized mice group reached a peak on day 3, while peak bacterial numbers in the liver, spleen, and lung of the LI, LIΔ*ilo:hly*, and LIΔ*ilo* immunized mice groups were observed on day 1. Bacterial numbers gradually decreased thereafter, indicating that the body quickly began to clear bacteria. Notably, the mice required two more days to completely remove LIΔ*ilo:hly* from the spleen than to clear LI from the spleen.

Serum ALT and AST levels reflect the status of the liver. As shown in **Figures 4G–N**, the ALT and AST levels in the serum of mice after LIΔ*ilo* inoculation did not change significantly, indicating that LIΔ*ilo* inoculation caused no obvious damage to the liver. At day 1 after inoculation, the levels of ALT and AST in the serum of LM-, LI-, and LIΔ*ilo:hly* inoculated mice were significantly higher than those before inoculation ($P < 0.001$). Afterward, they began to decrease and returned to the level of the control group on day 5 in the LM group or on day 3 in the LIΔ*ilo:hly* group. This trend is consistent with the above bacterial organ load trend.

Organ pathological examination

After tail vein inoculation, the pathological changes in the liver, spleen, and lung showed a consistent trend in each

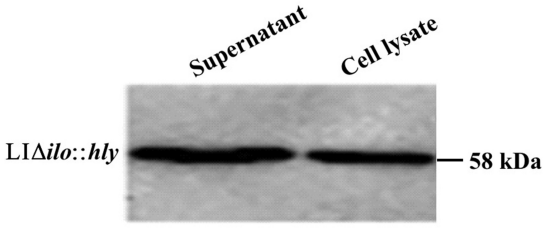

FIGURE 2
Western blot detection results of hemolysin-modified strain LIΔ*ilo:hly*. Supernant: the sample was the protein extracted from 35 mL medium supernatant; Cell lysate: the sample was the protein extracted from the bacterial pellet collected from 6 mL bacteria culture.

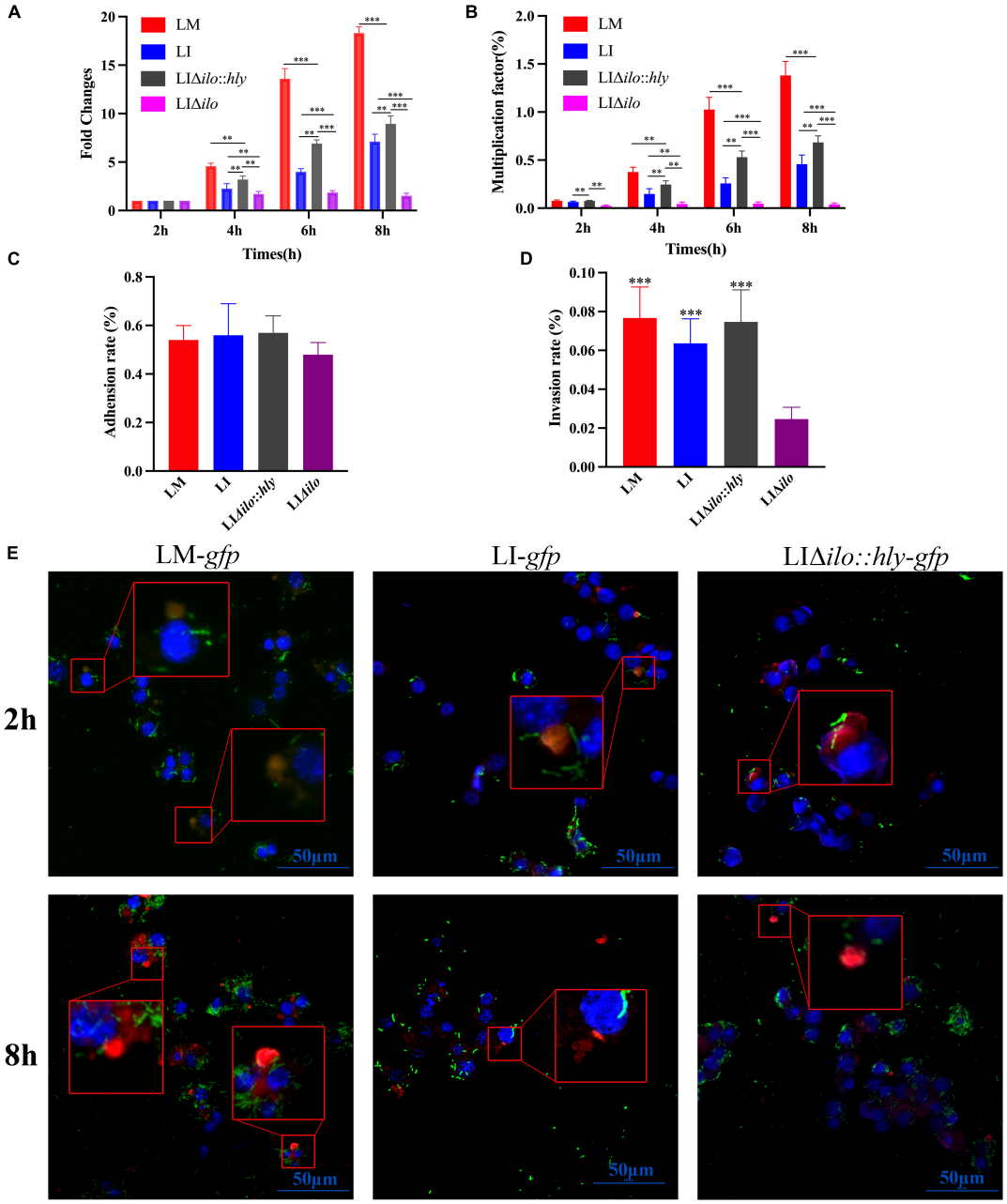

FIGURE 3
Intracellular proliferation, cell adhesion and invasion and lysosome escape ability. The fold changes **(A)** and multiplication factor **(B)** of each strain in mouse macrophage RAW 264.7, $^{**}P < 0.01$, $^{***}P < 0.001$; The adhesion **(C)** and invasion **(D)** ability of each strain to Hepa1-6 cells, the experiments were performed with biological triplicates, and results are expressed as means ± SEM per group, $^{***}P < 0.001$, vs. LIΔ*ilo*. Experiments were carried out at least three times. The proliferation of each strain at 2 and 8 h post infection in RAW 264.7 observed by Laser scanning confocal microscopy (LSCM) **(E)**, blue, green, and red were labeled the nucleus, bacteria and lysosomes respectively. The lysosomes in Figure 3D were orange or pink at 2 h (bacteria have not escaped), but were red at 8 h (bacteria had escaped). The scale bar in Figure 3D is 50 μm.

group. A visible pathological change occurred on day 3, but the pathological status was restored to normal by day 14 (Figures 5A–C). The pathological status of the LIΔ*ilo*:*hly* group at day 3 was better than that of the LM and LI groups. In the liver, a small amount of inflammatory cell focal infiltration in the hepatic lobule (black arrow) was accompanied by inflammatory cell punctate infiltration (red arrow). In the spleen, there was occasional pyknosis and fragmentation accompanied by a small amount of inflammatory cell infiltration. The pathological degree of the spleen was weaker than that of the LM group

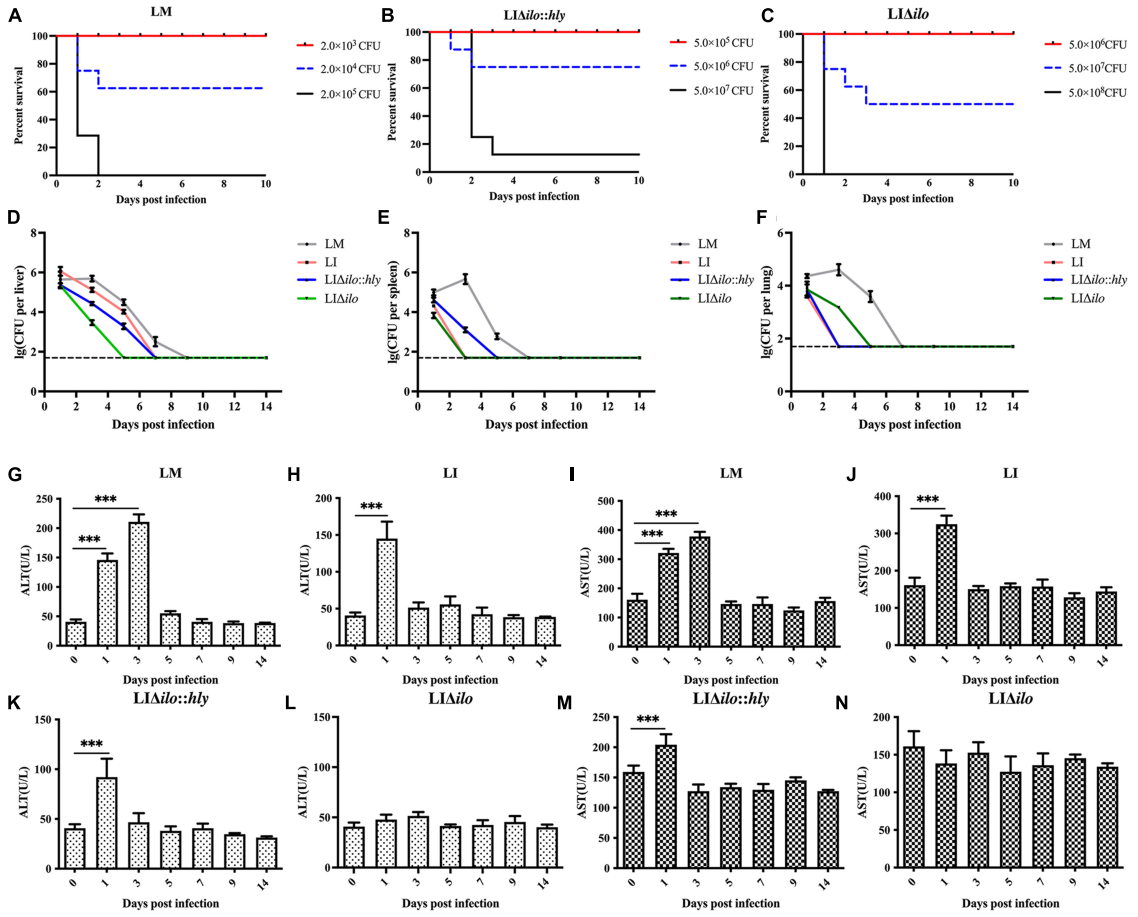

FIGURE 4
In vivo biosafety evaluation of each strain. Survival curves of C57BL/6 mice intravenously inoculated of *Listeria monocytogenes* (LM) **(A)**, LIΔ*ilo*:*hly* **(B)**, and LIΔ*ilo* **(C)**; Eight mice per group in this experiment. The bacteria load in liver **(D)**, spleen **(E)**, and lung **(F)** of mice intravenously inoculated of each strain; each point represents the mean ± SEM for a group of three mice from one independent experiment. Mice serum ALT levels after inoculation of LM **(G)**, LI **(H)**, LIΔ*ilo*:*hly* **(K)**, and LIΔ*ilo* **(L)**, and mice serum AST levels after inoculation of LI **(J)**, LM **(I)**, LIΔ*ilo*:*hly* **(M)**, and LIΔ*ilo* **(N)**. Results are expressed as means ± SEM per group, $^{***}P < 0.005$. The experiments were performed with biological triplicates.

and the LI group. In the lung, a small amount of alveolar wall around the airway of the lung tissue was slightly thickened (black arrow), the alveolar space was narrow, and inflammatory cell infiltration was scattered. Pathological scores for each organ are shown in **Supplementary Table 3**. The overall pathological severity of the LIΔ*ilo*:*hly* group was lower than that of the LM and LI groups, indicating that *hly* supplementation improved the biosafety of the strain.

In vivo immunogenicity and immune protection

The mice in each group were immunized twice by tail vein injection. Spleens were collected aseptically at on days 9 and 40 after the second immunization to prepare splenocyte suspensions for cytokine determination. TNF-α, IL-4, IL-12, IL-6, and IFN-γ levels in the LM, LI, and LIΔ*ilo*:*hly* groups were higher than those in the PBS control group. The levels of TNF-α, IL-6, and IFN-γ at day 9 and the levels of IL-6 and IFN-γ at day 40 in the LIΔ*ilo*:*hly* group were higher than those in the LI group (**Figures 6A–E**). Mice were challenged 1 week after the second immunization. The protection rates of the LM, LI, LIΔ*ilo*:*hly*, LIΔ*ilo*, and PBS groups were 60, 30, 40, 0, and 0%, respectively. There was a statistically significant difference in the protection rate between LIΔ*ilo*:*hly* and PBS groups. The protection rate of the LIΔ*ilo*:*hly* group was 10% higher than that of the LI group. However, the difference was not significant (**Figure 6F**).

Discussion

A qualified live bacterial vaccine carrier should be safe for the host, and should simultaneously stimulate the host immune system to generate a corresponding immune response. Improving the biosafety of LM as a vaccine carrier is an

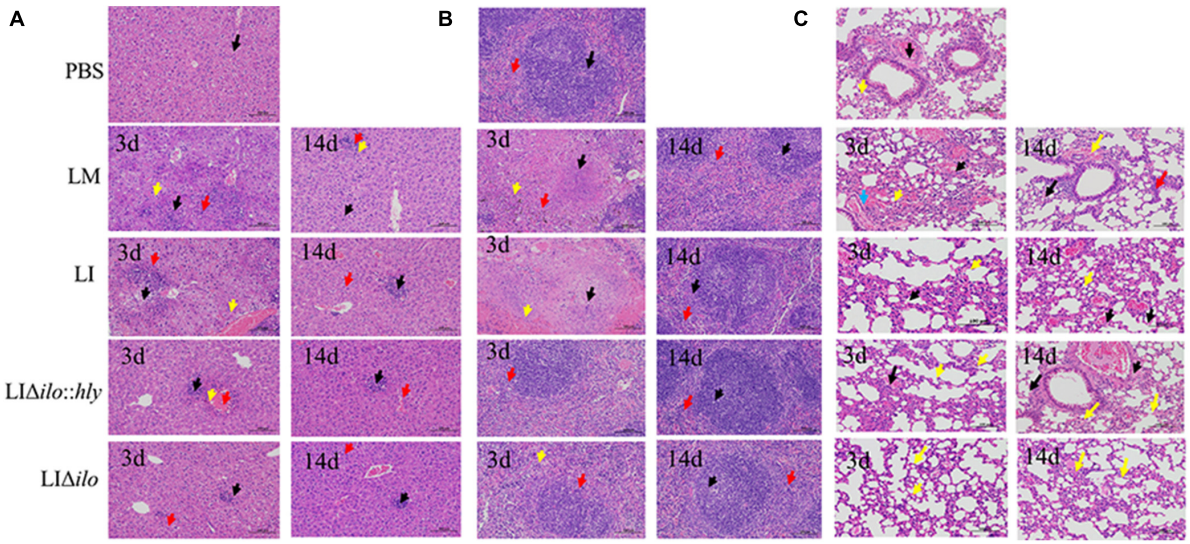

FIGURE 5
Pathological changes of mouse organs. Pathological changes of Liver **(A)**, spleen **(B)**, and lung **(C)** after inoculation of each strain (200×). The arrows in panel **(A)** indicated the lesions as below: ballooning or cytoplasmic vacuolation (black arrows); small foci of necrosis (yellow arrows), and inflammatory cell infiltration (red arrows); The arrows in panel **(B)** indicated the lesions as below: central expansion of the white pulp or pyknotic fragmentation (black arrows); extensive hemorrhage or multinucleated giant cells (yellow arrows), and inflammatory cell infiltration (red arrows); The arrows in panel **(C)** indicated the lesions as below: minor hemorrhage in the alveolar space (blue arrow); central dilation of the white pulp or pyknosis and fragmentation (black arrow); small hemorrhage (red arrow), and inflammatory cell infiltration (yellow arrow).

important goal for researchers. Most attenuation strategies adopted for LM are based on inactivating virulence. Although virulence has been greatly reduced, potential biosafety problems remain. Sometimes, deletion of the key virulence genes of *Listeria* will affect its ability to grow and proliferate *in vitro* and *in vivo*, and also affect its ability to stimulate cellular immune responses and the efficiency of antigen presentation (Maciag et al., 2009; Shahabi et al., 2011; Fares et al., 2019). Insufficient attenuation of LM may lead to potential safety problems. Conversely, excess attenuation of LM may lead to low immunogenicity. Therefore, we used a different approach by selecting LI, which displays good biosafety, as the vaccine carrier. To improve the immunogenicity of LI, we replaced the *ilo* gene with *hly*. LLO is an important virulence protein in LM that triggers innate and adaptive immune responses (Mandal and Lee, 2002; Radford et al., 2002). LLO is also utilized as an adjuvant when constructing subunit vaccines to improve the immunogenicity of the antigen. LLO can stimulate the innate immune system and induce the expression of IL-1, IL-12, and IL-18 in macrophages, and the production of IFN-γ by natural killer cells (Kohda, 2002; Carrero et al., 2012). A previous study constructed a recombinant *Escherichia coli* strain expressing LLO and ovalbumin (OVA) and found that it could kill OVA-expressing melanoma cells (B16-OVA) and effectively inhibit tumor growth in mice. Additionally, LLO can mediate bacterial escape from phagosomes and promote bacterial proliferation during infection. LLO plays a crucial role in the control and specific regulation of immune responses. Therefore, in this study, we modified the hemolysin gene of LI with the expectation of full use of the unique advantages of LLO to obtain an excellent vaccine vector.

In this study, *hly* was complemented by *ilo* deletion in the LI strain. The cell invasion and proliferation abilities, biosafety, and immunogenicity of the modified strain LIΔ*ilo*:*hly* were evaluated. The modified strain grew stably *in vitro* and maintained a growth trend similar to that of wild type LI, and it successfully expressed and secreted LLO protein. It could proliferate in phagocytic cells, and its proliferative capacity was stronger than that of LI, confirming that the intracellular proliferative capacity is closely related to hemolysin, and LLO is more helpful in phagocytic vesicle escape and intra-cytoplasm proliferation. Knockout of *ilo* significantly reduced cell invasion ability, and replacement with *hly* restored invasion, indicating that hemolysin is also related to cell invasion. In addition to hemolysin, the internalins of *Listeria* are also closely related to its adhesion and invasion properties. Internalins A (*InlA*) and Internalins B (*InlB*) play their respective roles by binding to specific receptors through leucine rich repeats (LRRs), of which *InlA* mainly binds Cadherin mediates the passage of bacteria across epithelial cells, and *InlB* mainly binds to the hepatocyte growth factor receptor (HGFR) and mediates the entry of bacteria into fibroblasts, hepatocytes and epithelial cells (Vázquez-Boland et al., 2001; Domínguez-Bernal et al., 2006; Hamon et al., 2006). The LD_{50} of LIΔ*ilo*:*hly* was higher than that of LI, and the overall pathological status of the liver, spleen, and lungs was better than that of LI, suggesting that it is

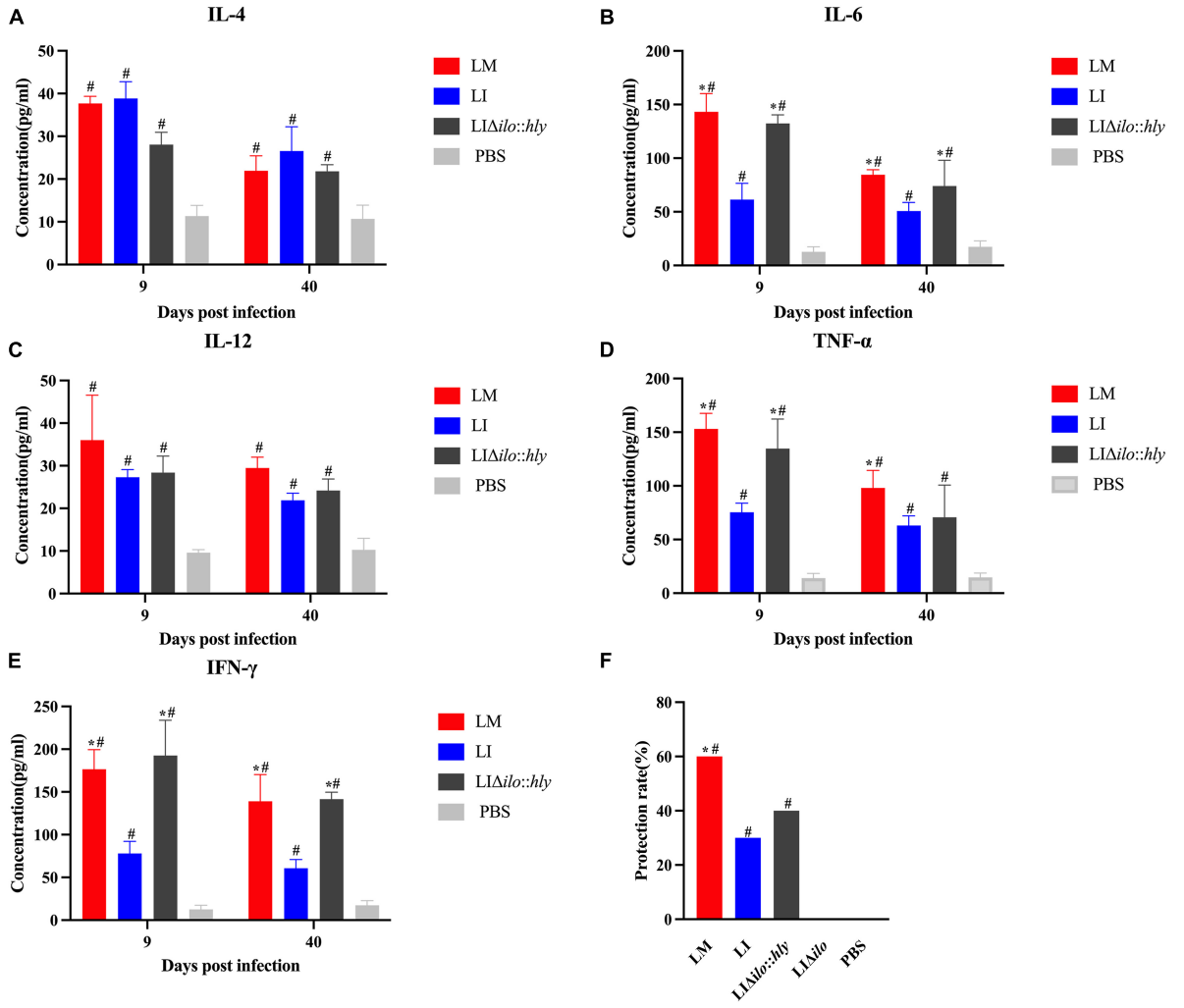

FIGURE 6
Immunogenicity and immune protection of each strain. Cytokines IL-4 **(A)**, IL-6 **(B)**, IL-12 **(C)**, TNF-α **(D)**, and IFN-γ **(E)** at the 9th and 40th day after the secondary immunization of each strain, $^{*}P < 0.05$, vs. *Listeria ivanovii* (LI); $^{\#}P < 0.05$, vs. PBS, the experiments were performed with biological triplicates. Each bar represents the mean ± SEM for a group of three mice from one independent experiment; Challenge protection rate after twice immunizations **(F)**, $^{*}P < 0.05$, vs. LI; $^{\#}P < 0.05$, vs. PBS. Ten mice per group in this experiment.

less virulent and safer than LI. We speculate that replacement of *ilo* by *hly* may affect the expression levels of virulence genes encoded by *Listeria* pathogenicity islands (LIPI). LIPI is recognized as unstable chromosomal regions, carrying genes related to specific metabolic activities, antibiotic resistance, or pathogenesis, which can be horizontally transferred between bacteria, and contains the essential virulence genes (*prfA*, *hly*, *plcA*, *mpl*, *actA*, and *plcB*) and internalin genes of *Listeria* (Hacker and Kaper, 2000; Vázquez-Boland et al., 2001). We also speculate that the synergy effect of *hly* gene with other virulence genes is weakened within the genome environment of LI. After LIΔ*ilo*:*hly* infection, it was maintained in the liver of mice with a higher bacterial number and a longer duration than in other organs, indicating its superiority in colonizing the liver. This is mainly because the internalin inlB of *Listeria* can bind to specific receptors on the surface of liver cells, resulting in the targeted invasion of the liver by Listeria (Khelef et al., 2006; Pentecost et al., 2010). The clearance time for LIΔ*ilo*:*hly* from the spleen was two more days than that for LI, indicating that LLO has better spleen cell adaptability than ILO. This result also confirmed a previous report that LMΔ*hly*:*ilo* cannot proliferate in the spleen (Frehel et al., 2003). We speculate that the longer survival time of LIΔ*ilo*:*hly* in the spleen may elicit stronger immune responses. After mice were immunized twice with each strain, we detected levels of IFN-γ, TNF-α, IL-4, IL-6, and IL-12. These cytokines coordinate an effective immune response during *Listeria* infection, and are closely related to the establishment of protection. Their interactions promote the proliferation and activation of immune cells, resulting in

a stronger and longer-lasting cellular immune response. The results showed that on days 9 and 40 after the secondary immunization of mice with LIΔ*ilo*:*hly*, these cytokines were significantly higher than those in the PBS group, and were comparable to those in the LM group. Especially, the levels of IFN-γ, IL-6, and TNF-α (at day 9) were higher than those of LI group. In addition, the challenge results showed that the immune protection rate of LIΔ*ilo*:*hly* was higher than that of LI. These results are consistent with our hypotheses. A longer survival time in the spleen can result in a more durable, specific immune response. LIΔ*ilo*:*hly* has comparable potency to LM in causing a T helper 1 (Th1) cell-mediated immunity response and inducing various cytokines and chemokines.

The recombinant strain LIΔ*ilo*:*hly* was successfully constructed. Through evaluations at both the cellular and animal levels, we confirmed its safety and immunogenicity. Thus, it can be used as a vaccine carrier. In the future, the heterologous antigen genes can be introduced into the recombinant LI strain by genome recombination technique described previously (Wang et al., 2014) or by recombinant plasmid that carrying heterologous antigen genes, thus to acquire the potential vaccine candidates. Subsequently, it is necessary to explore whether the vaccine candidates can stably express and secret foreign genes by western blot, and through animal experiments to determine antibody titers and measure T/B cell immune responses, to evaluate the safety and efficacy of vaccine candidate strains (Xiao et al., 2021; Clint et al., 2022). Thus to prove that LIΔ*ilo*:*hly* is an excellent antigen carrier for vaccine development, contributing to cancer immunotherapy and infectious diseases prevention.

Data availability statement

The original contributions presented in this study are included in the article/**Supplementary Material**, further inquiries can be directed to the corresponding authors.

Ethics statement

The animal study was reviewed and approved by the Animal Care and Use Committee of Sichuan University.

Author contributions

CW and ZC conceived and designed the research. QL, RL, SL, YZ, ST, and QO performed the experiments and acquired, interpreted, and analyzed the data. QL, RL, SL, and CW wrote the manuscript. All the authors read and critically reviewed the manuscript and approved the submitted version.

Funding

This work was supported by the National Natural Science Foundation of China (grant number: 31570924) and the Key Program of Sichuan Science and Technology Department (Nos. 2021YFQ0060 and 2021YFS0005).

Conflict of interest

QL, RL, and ZC were employed by Shen Zhen Biomed Alliance Biotech Group Co., Ltd.

The remaining authors declare that the research was conducted in the absence of any commercial or financial relationships that could be construed as a potential conflict of interest.

Publisher's note

All claims expressed in this article are solely those of the authors and do not necessarily represent those of their affiliated organizations, or those of the publisher, the editors and the reviewers. Any product that may be evaluated in this article, or claim that may be made by its manufacturer, is not guaranteed or endorsed by the publisher.

Supplementary material

The Supplementary Material for this article can be found online at: https://www.frontiersin.org/articles/10.3389/fmicb.2022.962326/full#supplementary-material

References

Beuzón, C. R., Méresse, S., Unsworth, K. E., Ruíz-Albert, J., Garvis, S., Waterman, S. R., et al. (2000). *Salmonella* maintains the integrity of its intracellular vacuole through the action of SifA. *EMBO J.* 19, 3235–3249.

Carrero, J. A., Vivanco-Cid, H., and Unanue, E. R. (2012). Listeriolysin O Is Strongly Immunogenic Independently of Its Cytotoxic Activity. *PLoS One* 7:e32310. doi: 10.1371/journal.pone.0032310

Clint, A. H., Rafael, K. C., Sasha, R. A., Tiffany, F. K., Naomi, L. F., et al. (2022). Venezuelan equine encephalitis virus V3526 vaccine RNA-Dependent RNA polymerase mutants increase vaccine safety through restricted tissue tropism in a murine model. *Zoonoses* 2:2. doi: 10.15212/zoonoses-2021-0016

Domínguez-Bernal, G., Müller-Altrock, S., González-Zorn, B., Scortti, M., Herrmann, P., Monzó, H. J., et al. (2006). A spontaneous genomic deletion in *Listeria ivanovii* identifies LIPI-2, a species-specific pathogenicity island encoding sphingomyelinase and numerous internalins. *Mole. Microb.* 59, 415–432. doi: 10.1111/j.1365-2958.2005.04955.x

Farber, J. M., and Peterkin, P. (1991). *Listeria monocytogenes*, a food-borne pathogen. *Microbiolog. Rev.* 55, 476–511.

Fares, E., Mccloskey, C. B., Gutierrez, A., Princiotta, M., and Drevets, D. A. (2019). Vaccine strain *Listeria monocytogenes* bacteremia occurring 31 months after immunization. *Infection* 47, 489–492. doi: 10.1007/s15010-018-1249-7

Frehel, C., Lety, M. A., Autret, N., Beretti, J. L., Berche, P., Charbit, A., et al. (2003). Capacity of ivanolysin O to replace listeriolysin in phagosomal escape and *in vivo* survival of *Listeria monocytogenes*. *Microbiology* 149, 611–620. doi: 10.1099/mic.0.25986-0

Hacker, J., and Kaper, J. B. (2000). Pathogenicity islands and the evolution of microbes. *Rev. Microbiol.* 54, 641–679. doi: 10.1146/annurev.micro.54.1.641

Hamon, M., Bierne, H., and Cossart, P. (2006). *Listeria monocytogenes*: a multifaceted model. *Nat. Rev. Microbiol.* 4, 423–434. doi: 10.1038/nrmicro1413

Harty, J. T., Lenz, L. L., and Bevan, M. J. (1996). Primary and secondary immune responses to *Listeria monocytogenes*. *Curr. Opin. Immunol.* 8, 526–530.

Khelef, N., Lecuit, M., Bierne, H., and Cossart, P. (2006). Species specificity of the *Listeria monocytogenes* InlB protein. *Cell Microbiol.* 8, 457–470. doi: 10.1111/j.1462-5822.2005.00634.x

Kohda, C. (2002). Dissociated Linkage of Cytokine-Inducing Activity and Cytotoxicity to Different Domains of Listeriolysin O from *Listeria monocytogenes*. *Infect. Immun.* 70, 1334–1341. doi: 10.1128/IAI.70.3.1334-1341.2002

Lamikanra, A., Pan, Z.-K., Isaacs, S. N., Wu, T.-C., and Paterson, Y. (2001). Regression of established *Human papillomavirus* type 16 (HPV-16) immortalized tumors in vivo by vaccinia viruses expressing different forms of HPV-16 E7 correlates with enhanced CD8+ T-cell responses that home to the tumor site. *J. Virol.* 75, 9654–9664. doi: 10.1128/JVI.75.20.9654-9664.2001

Le, D. T., Picozzi, V. J., Ko, A. H., Wainberg, Z. A., Kindler, H., Wang-Gillam, A., et al. (2019). Results from a phase IIb, randomized, multicenter study of GVAX pancreas and CRS-207 compared with chemotherapy in adults with previously treated metastatic pancreatic adenocarcinoma (ECLIPSE study). *Clin. Can. Res.* 25, 5493–5502. doi: 10.1158/1078-0432.CCR-18-2992

Lin, Q., Zhou, M., Xu, Z., Khanniche, A., Shen, H., Wang, C., et al. (2015). Construction of two *Listeria ivanovii* attenuated strains expressing *Mycobacterium tuberculosis* antigens for TB vaccine purposes. *J. Biotechnol.* 196, 20–26. doi: 10.1016/j.jbiotec.2015.01.008

Liu, S.-J., Tian, S.-C., Zhang, Y.-W., Tang, T., Zeng, J.-M., Fan, X.-Y., et al. (2020). Heterologous Boosting With *Listeria*-Based Recombinant Strains in BCG-Primed Mice Improved Protection Against Pulmonary Mycobacterial Infection. *Front. Immunol.* 11:2036. doi: 10.3389/fimmu.2020.02036

Maciag, P. C., Radulovic, S., and Rothman, J. (2009). The first clinical use of a live-attenuated *Listeria monocytogenes* vaccine: a Phase I safety study of Lm-LLO-E7 in patients with advanced carcinoma of the cervix. *Vaccine* 27, 3975–3983. doi: 10.1016/j.vaccine.2009.04.041

Mahdy, S. E., Liu, S., Su, L., Zhang, X., Chen, H., Pei, X., et al. (2019). Expression of the VP1 protein of FMDV integrated chromosomally with mutant *Listeria monocytogenes* strain induced both humoral and cellular immune responses. *Appl. Microbiol. Biotechnol.* 103, 1919–1929. doi: 10.1007/s00253-018-09605-x

Mandal, M., and Lee, K. D. (2002). Listeriolysin O-Liposome-Mediated cytosolic delivery of macromolecule antigen *in vivo*: enhancement of antigen-specific cytotoxic T lymphocyte frequency, activity, and tumor protection. *Biochimica et Biophysica Acta* 1563, 7–17. doi: 10.1016/s0005-2736(02)00368-1

Pentecost, M., Kumaran, J., Ghosh, P., and Amieva, M. R. (2010). *Listeria monocytogenes* internalin B activates junctional endocytosis to accelerate intestinal invasion. *PLoS Pathog.* 6:e1000900. doi: 10.1371/journal.ppat.1000900

Radford, K. J., Higgins, D. E., Pasquini, S., Cheadle, E. J., Carta, L., Jackson, A. M., et al. (2002). A recombinant *E. coli* vaccine to promote MHC class I-dependent antigen presentation: application to cancer immunotherapy. *Gene Therapy* 9, 1455–1463. doi: 10.1038/sj.gt.3301812

Ruan, Y., Rezelj, S., Bedina Zavec, A., Anderluh, G., and Scheuring, S. (2016). Listeriolysin O membrane damaging activity involves arc formation and lineaction–implication for *Listeria monocytogenes* escape from phagocytic vacuole. *PLoS Pathog.* 12:e1005597. doi: 10.1371/journal.ppat.1005597

Shahabi, V., Seavey, M. M., Maciag, P. C., Rivera, S., and Wallecha, A. (2011). Development of a live and highly attenuated *Listeria monocytogenes*-based vaccine for the treatment of Her2/neu-overexpressing cancers in human. *Cancer Gene Ther.* 18, 43–62. doi: 10.1038/cgt.2010.48

Vázquez-Boland, J. A., Kuhn, M., Berche, P., Chakraborty, T., Domınguez-Bernal, G., Goebel, W., et al. (2001). *Listeria* pathogenesis and molecular virulence determinants. *Clin. Microbiol. Rev.* 14, 584–640. doi: 10.1128/CMR.14.3.584-640.2001

Wallecha, A., Carroll, K. D., Maciag, P. C., Rivera, S., Shahabi, V., and Paterson, Y. (2009). Multiple effector mechanisms induced by recombinant *Listeria monocytogenes* anticancer immunotherapeutics. *Adv. Appl. Microbiol.* 66, 1–27. doi: 10.1016/S0065-2164(08)00801-0

Wang, C., Zhang, F., Yang, J., Khanniche, A., and Shen, H. (2014). Expression of Porcine Respiratory and Reproductive Syndrome Virus Membrane-Associated Proteins in *Listeria ivanovii* via a Genome Site-Specific Integration and Expression System. *J. Mole. Microbiol. Biotechnol.* 24, 191–195. doi: 10.1159/000363450

Xiao, X., Zhou, K., Gu, M., Li, G., Li, Y., Liao, et al. (2021). The immungenicity and Cross-Neutralizing Activity of Enterovirus 71 Vaccine Candidate Strains. *Zoonoses* 1:9. doi: 10.15212/ZOONOSES-2021-0008

Yang, Y., Hou, J., Lin, Z., Zhuo, H., Chen, D., Zhang, X., et al. (2014). Attenuated *Listeria monocytogenes* as a cancer vaccine vector for the delivery of CD24, a biomarker for hepatic cancer stem cells. *Cell. Mole. Immunol.* 11, 184–196. doi: 10.1038/cmi.2013.64

Zhou, M., Jiang, M., Ren, C., Liu, S., Pu, Q., Howard, G., et al. (2016). *Listeria ivanovii* Infection in Mice: restricted to the Liver and Lung with Limited Replication in the Spleen. *Front. Microbiol.* 7:790. doi: 10.3389/fmicb.2016.00790

frontiers | Frontiers in Microbiology

TYPE Original Research
PUBLISHED 04 August 2022
DOI 10.3389/fmicb.2022.968872

OPEN ACCESS

EDITED BY
Wei Wang,
Jiangsu Institute of Parasitic Diseases (JIPD), China

REVIEWED BY
Xiaola Guo,
Lanzhou Veterinary Research Institute (CAAS), China
Klaus Rüdiger Brehm,
Julius Maximilian University of Würzburg, Germany
Yujuan Shen,
National Institute of Parasitic Diseases, China

*CORRESPONDENCE
Yanhai Wang
wangyh@xmu.edu.cn
Zhe Cheng
chengzhe@xmu.edu.cn

†These authors have contributed equally to this work and share first authorship

SPECIALTY SECTION
This article was submitted to Infectious Agents and Disease, a section of the journal Frontiers in Microbiology

RECEIVED 14 June 2022
ACCEPTED 11 July 2022
PUBLISHED 04 August 2022

CITATION
Feng C, Cheng Z, Xu Z, Tian Y, Tian H, Liu F, Luo D and Wang Y (2022) EmCyclinD-EmCDK4/6 complex is involved in the host EGF-mediated proliferation of *Echinococcus multilocularis* germinative cells *via* the EGFR-ERK pathway. *Front. Microbiol.* 13:968872. doi: 10.3389/fmicb.2022.968872

EmCyclinD-EmCDK4/6 complex is involved in the host EGF-mediated proliferation of *Echinococcus multilocularis* germinative cells *via* the EGFR-ERK pathway

Chonglv Feng[1,2†], Zhe Cheng[1,2*†], Zhijian Xu[1,2], Ye Tian[1,2], Huimin Tian[3], Fan Liu[3], Damin Luo[1,2] and Yanhai Wang[1,2*]

[1]State Key Laboratory of Cellular Stress Biology, Faculty of Medicine and Life Sciences, School of Life Sciences, Xiamen University, Xiamen, Fujian, China, [2]Parasitology Research Laboratory, School of Life Sciences, Xiamen University, Xiamen, Fujian, China, [3]Medical College, Xiamen University, Xiamen, Fujian, China

The larval stage of the tapeworm *Echinococcus multilocularis* causes alveolar echinococcosis (AE), one of the most lethal helminthic infections in humans. The tumor-like growth and development of the metacestode larvae within host organs are driven by a population of somatic stem cells, the germinative cells, which represent the only proliferative cells in the parasite. Host-derived factors have been shown to promote germinative cell proliferation. Since cells sense the external signal mainly in G1 phase of the cell cycle, host factors are expected to exert impacts on the machinery regulating G1/S phase of the germinative cells, which still remains largely unknown in *E. multilocularis*. In this study, we described the characterization of two key members of the G1/S phase cell-cycle regulation, EmCyclinD and EmCDK4/6. Our data show that EmCyclinD and EmCDK4/6 display significant sequence similarity to their respective mammalian homologs, and that EmCyclinD interacts with EmCDK4/6, forming a kinase-active complex to activate its substrate Rb1. EmCyclinD was actively expressed in the germinative cells. Addition of human EGF caused an elevated expression of EmCyclinD while inhibition of the EGFR-ERK signaling pathway in the parasite reduced the expression of EmCyclinD and downstream transcriptional factors. Treatment with Palbociclib, a specific CDK4/6 inhibitor, downregulated the expression of cell cycle-related factors and impeded germinative cell proliferation and vesicle formation from protoscoleces. Our data demonstrated that the

EmCyclinD-EmCDK4/6 complex participates in the cell cycle regulation of germinative cells which is mediated by host EGF via the EGFR-ERK-EmCyclinD pathway in *E. multilocularis*.

KEYWORDS

***Echinococcus multilocularis*, germinative cells, cyclin-dependent kinases, cyclin, proliferation**

Introduction

Alveolar echinococcosis (AE) is the most lethal helminthic infection caused by *Echinococcus multilocularis*. AE poses a serious threat to human health (Eckert and Deplazes, 2004) and lacks effective methods of prevention as with other zoonotic diseases (Vazquez-Chagoyan et al., 2011; Tang et al., 2022; Yin et al., 2022). From a public health perspective, AE infection is usually caused by pathogens spillover events from domestic or wild animal species, especially exposed to the larval stage parasites (Dharmarajan et al., 2022). The larval stage of *E. multilocularis* grows as diffuse infiltration in the liver of patients, and eventually affects the entire liver, and may metastasizes to the brain, lungs and other important organs. The neoblasts of the free-living flatworm planarian are a population of pluripotent somatic stem cells with unlimited capacity for self-renewal and differentiation potential and are fundamental to planarian growth and development, as well as tissue renewal and regeneration (Pellettieri and Sanchez, 2007; Eisenhoffer et al., 2008; Rink, 2013). Cells with similar functions and renewal mechanisms have also been found in parasitic flatworms, the trematode and tapeworm (Koziol et al., 2010, 2014; Collins et al., 2013; Wang et al., 2013). In *E. multilocularis*, these cells are called germinative cells and are the only cells with proliferative capacity and differentiation potential in the larvae (Koziol et al., 2014). The germinative cells are the basis for the continuous growth and development of the alveolar hydatid in the host (Brehm, 2010a; Koziol et al., 2014).

Host factors are considered to interact with the corresponding receptors in *E. multilocularis* and activate the associated highly conserved signaling pathways, thereby affecting the growth and development of the parasite (Brehm and Spiliotis, 2008; Brehm, 2010b). Recent studies reported that host insulin and FGF (fibroblast growth factor) can stimulate the proliferation of germinative cells and the growth of metacestode vesicles (Hemer et al., 2014; Forster et al., 2019). We also demonstrated that host EGF can promote germinative cell proliferation and vesicle development by activating the EGFR/ERK signaling pathway in alveolar hydatid (Cheng et al., 2017). Since cell proliferation requires the accurate control of cell cycle, it is expected that the machinery implicated in regulation of the cell cycle of germinative cells is influenced by host-derived factors.

The cell cycle regulatory network, comprising the cyclin-dependent kinases (CDKs), Cyclin, and cyclin-dependent kinase inhibitors (CDIs), is a key mechanism determining the progression of cell proliferation, differentiation, senescence and death. This network precisely regulates the cell cycle by activating or inhibiting downstream signaling molecules of Cyclin-CDK complexes. In addition, negative regulation of CDIs are also essential for maintaining network precision. The control of the cell cycle initiation generally occurs in the G_1 phase (Duronio and Xiong, 2013). When cells receive the mitogenic signals, they initiate the synthesis of Cyclin D, which in turn forms active complexes with CDK4 or CDK6. The complexes phosphorylate members of the retinoblastoma (Rb) protein family. Rb proteins inhibit the transcription of cell cycle-related factors by binding and modulating transcription factors such as E2F family members. One of the most crucial targets of Rb–E2F complexes is Cyclin E. Cyclin E-CDK2 complexes have been proposed to irreversibly inactivate Rb, so an event considered to be the passage of the cell to the restriction point (R-point) during G1 in which cells no longer require mitogenic stimuli to undergo cell division (Malumbres and Barbacid, 2005). It is assumed that the level of CyclinD determines the onset of cell cycle functioning (Lim and Kaldis, 2013). The protein families of Cyclin and CDK as well as related signaling pathways are conserved in evolution and have been shown to play a key role in regulating somatic stem cells in *Drosophila*, nematodes, and planarian (Fernandez-Taboada et al., 2010; Zhu and Pearson, 2013; Hetie et al., 2014; Ishidate et al., 2014).

In this study, we identified two key cell cycle regulators, EmCyclinD and EmCDK4/6 in *E. multilocularis*. Our data demonstrated that EmCyclinD forms an active complex with EmCDK4/6. Targeting the EGFR-ERK-EmCyclinD pathway can inhibits host EGF-stimulated germinative cell proliferation, suggesting EmCyclinD and EmCDK4/6 as druggable targets for the development of chemotherapeutics against AE.

Materials and methods

Ethics statement

All animal experiments were conducted in strict accordance with China regulations on the protection of experimental

animals (Regulations for the Administration of Affairs Concerning Experimental Animals, version from 18 July, 2013) and specifically approved by the Institutional Animal Care and Use Committee of Xiamen University (Permit Number: 2013–0053).

Identification and cloning of CyclinD and CDK4/6 gene of *Echinococcus multilocularis*

Published sequences of CDK4, CDK6, and CyclinD of human, mouse, *Drosophila*, zebrafish, *Xenopus,* and *C. elegans* (**Supplementary Table 1**) were used as queries to BLAST the *E. multilocularis* genome database (Tsai et al., 2013) available at Wormbase database.[1] EmuJ_000456500 and EmuJ_001021000 were then identified as the homologs of CyclinD and CDK4/6, respectively, and their full coding sequences were amplified from the cDNA preparations as described previously (Brehm et al., 2000). Kinase domain and cyclin characteristic domain were determined using the online software SMART.[2] The phylogenetic tree was generated by the neighbor-joining method (bootstrap = 1,000) using MEGA 7.0. Primers for amplification of the full coding sequences of EmCyclinD and EmCDK4/6 were used as shown in **Supplementary Table 2**.

Parasite *in vitro* cultivation and drug treatment

In vitro cultivation and drug treatment of *E. multilocularis* metacestode vesicles were performed as previously described (Cheng et al., 2017). Briefly, for the growth assay, vesicles were cultured in the host cell conditioned medium supplemented with drug and the growth of vesicles was analyzed at indicated time. For the vesicle formation assay, protoscoleces were collected from parasite material and *in vitro* cultured in conditioned medium supplemented with drugs. The initial process of vesicle formation, in which protoscoleces dilate and vacuolate, were examined after 21 days of culture. The CDK4/6 inhibitor Palbociclib, EGFR inhibitor CI-1033, MEK inhibitor U0126 and hydroxyurea were supplied by Selleck Chemicals. Recombinant human EGF was supplied by PeproTech. Drugs were added into the culture medium at a final concentration as required. The vesicles were then used for RNA isolation, whole protein extraction, or EdU labeling at the indicated time.

1 https://parasite.wormbase.org/Echinococcus_multilocularis_prjeb122/Info/Index/

2 http://smart.embl-heidelberg.de/

Co-immunoprecipitation and western blot

HEK-293T cell was conserved by the State Key Laboratory of Cellular Stress Biology, Xiamen University, China. EmCyclinD and EmCDK4/6, tagged at their C-terminus with Myc-tag or HA-tag, respectively, were sub-cloned into pcDNA3.3 plasmid (gifts from Prof. Han Jiahuai, Xiamen University, China). The expression plasmids were co-transfected into the HEK-293T cells with the aid of Turbofect Transfection Reagent (Thermo Scientific). Cell lysates were harvested at 36 h post-transfection using RIPA lysis buffer (Beyotime, China). Co-immunoprecipitation experiments were performed using anti-Myc or anti-HA antibodies conjugated Sepharose Beads (#3,400 and #3,956, Cell Signaling Technology). The lysates from experiments were subjected to 10% SDS-PAGE and transferred electrically to PVDF membranes. Detection of tagged proteins was performed using anti-Myc and anti-HA antibodies (#2,278 and #3,724, Cell Signaling Technology). The membranes then reacted in an enzyme-linked immunoassay with anti-rabbit IgG conjugated with HRP (Invitrogen) and subsequently detected using ECL according to the manufacturer's instructions.

In vitro kinase assay

In vitro kinase activity was determined by measuring the rate of ADP production in the *in vitro* kinase reaction using the ADP-Glo Kinase Assay Kit (Promega). Briefly, the EmCDK4/6-EmCyclinD complex was purified by Co-immunoprecipitation as the kinase (Fry et al., 2004) and then incubated with 3 μg of recombination human Rb1 protein (Proteintech) as the substrate in the experiment. The kinase reactions were performed with 1X Kinase Reaction Buffer A [40 mM Tris (pH 7.5), 20 mM $MgCl_2$, 0.1 mg/mL BSA], 25 μM ATP, 1 mM DTT and incubated at RT, 20 min. The reactions were terminated by ADP-Glo reagent and then detected according to the manufacturer's instructions. Each data point was collected in duplicate.

mRNA expression analysis of EmCyclinD and downstream factors

Total RNA was extracted from metacestode vesicles treated with different drugs and then reverse transcribed into cDNA as previously described (Cheng et al., 2017). cDNAs were processed for real-time quantitative (qPCR) analysis using the primers as listed in **Supplementary Table S2**. The constitutively expressed gene *elp* was used as the internal control (Brehm et al., 2003).

EmCyclinD polyclonal antibody preparation and western blot assay

The polyclonal antibody against EmCyclinD was prepared by immunizing New Zealand Rabbit with the synthetic peptide "CASAPNGSSNSRKHS" of EmCyclinD (Genscript, China). Purification of the EmCyclinD antibody from the antiserum was performed further by protein A and peptide affinity chromatography. Western blot was performed using the EmCyclinD antibody with a dilution of 1:200.

Molecular docking

The EmCDK4/6 and Palbociclib docking analysis was performed by AutoDock (version 4.2). The Palbociclib three-dimensional structure was retrieved by the Pubchem website[3] and the EmCDK4/6 three-dimensional structure was built with online tool Swiss-model.[4] The AutoDock software was adopted for EmCDK4/6 protein hydrogenation processing, calculating charge, and setting the receptor proteins docking lattice parameter. We eventually obtained 10 conformations about the interaction between EmCDK4/6 and Palbociclib. The three-dimensional diagram of the interaction between EmCDK4/6 and Palbociclib was displayed by PyMOL (version 2.4.0a0).

5-ethynyl-2′-deoxyuridine labeling

In vitro cultivated metacestode vesicles were treated with different drugs as required and then incubated with 50 μM of EdU for 4 h and whole-mount prepared as described before (Cheng et al., 2015). The detection of EdU was using Click-iT EdU Alexa Fluor 555 or Alexa Fluor 488 Imaging KIT (Life Technologies). DNA was counterstained with 4′,6-diamidino-2-phenylindole (DAPI) after EdU detection. For the quantification of EdU^+ cells, at least four random microscopic fields from at least five vesicles were captured and the positive cells were counted manually. The labeling experiments were repeated at least two times and analyzed for each control and treatment group.

Data analyses and statistics

Data was shown as mean ± *SD* as indicated in the respective figure legend. Data from the control and experimental groups were compared, and the significance was determined using two-tailed Student's *t*-test.

3 https://pubchem.ncbi.nlm.nih.gov

4 https://swissmodel.expasy.org

Results

Identification of EmCyclinD and EmCDK4/6

We excavated the genome information of *E. multilocularis* by BLAST analyses using human and mouse CyclinD1, D2, D3, or CDK4, 6 as the queries and procured as best hit proteins encoded by locus EmuJ_000456500 (annotated as G1: S specific cyclin D1) and EmuJ_001021000 (annotated as Cyclin-dependent kinase 6). Phylogenetic analysis revealed that EmuJ_000456500 could be classified as *D*-type cyclin group (**Figures 1A,C**) and EmuJ_001021000 is closely related to the CDK4 and CDK6 group (**Figures 1B,D**). Then EmuJ_000456500 was named *EmCyclinD* and EmuJ_001021000 was named *EmCDK4/6*.

The inferential EmCyclinD protein is comprised of 386 amino acids with a predicted molecular weight of 43.2 kDa. *EmCyclinD* locus consists of 4 exons and 3 introns distributed in the genome region of 1,334 bps with a coding sequence length of 1,161 bps. A conserved cyclin characteristic domain Cyc_N (or cyclin box) which contains the CDK-binding site is located between residues 72 and 156 (marked "C" in **Figure 1A**) (Nugent et al., 1991). The Cyc-C domain, which is typical for mammalian CyclinD, is absent in *E. multilocularis*, similar to the *C. elegans* ortholog (Kitagawa et al., 1996).

EmCDK4/6 which occupies the genome region of 2,884 bps is made up of 6 exons and 5 introns. The coding sequence comprised 2,136 bps. *EmCDK4/6* has over 1,000 bps additional C-terminal extension compared to *CDK4* or *CDK6* of human or other model species. To investigate possible alternative splicing events, we performed 3' RACE on cDNA from metacestode vesicles but detected only one single transcript. The EmCDK4/6 protein contains 711 amino acids with a calculated molecular weight of 77.0 kDa. Structural analysis showed that EmCDK4/6 possesses the conserved CDK domains and functional amino acid sites of CDK4 and CDK6 proteins, including the Serine/Threonine kinase catalytic domain (S_TKc, positions 24–311, **Figure 1B**) and the phosphorylation motif Ser/Thr-Pro-X (positions 187–189, marked "M" in **Figure 1B**), so it is equiped with the typical features of CDK4 or 6 proteins (Matsushime et al., 1992; Kitagawa et al., 1996; Park and Krause, 1999).

The analysis of three-dimensional structure revealed that EmCyclinD Cyc_N domain has similar α-helix structures as human CyclinD (**Figure 1E**). EmCDK4/6 has a bilobed flap shape in S_Tkc domain which contains the amino end (bottom of the model) rich in β-folds and the carboxyl end (top of the model) rich in α-helices. The ATP binding site is located in the cleft between the domains, showing a pocket-like structure (**Figure 1F**; Day et al., 2009).

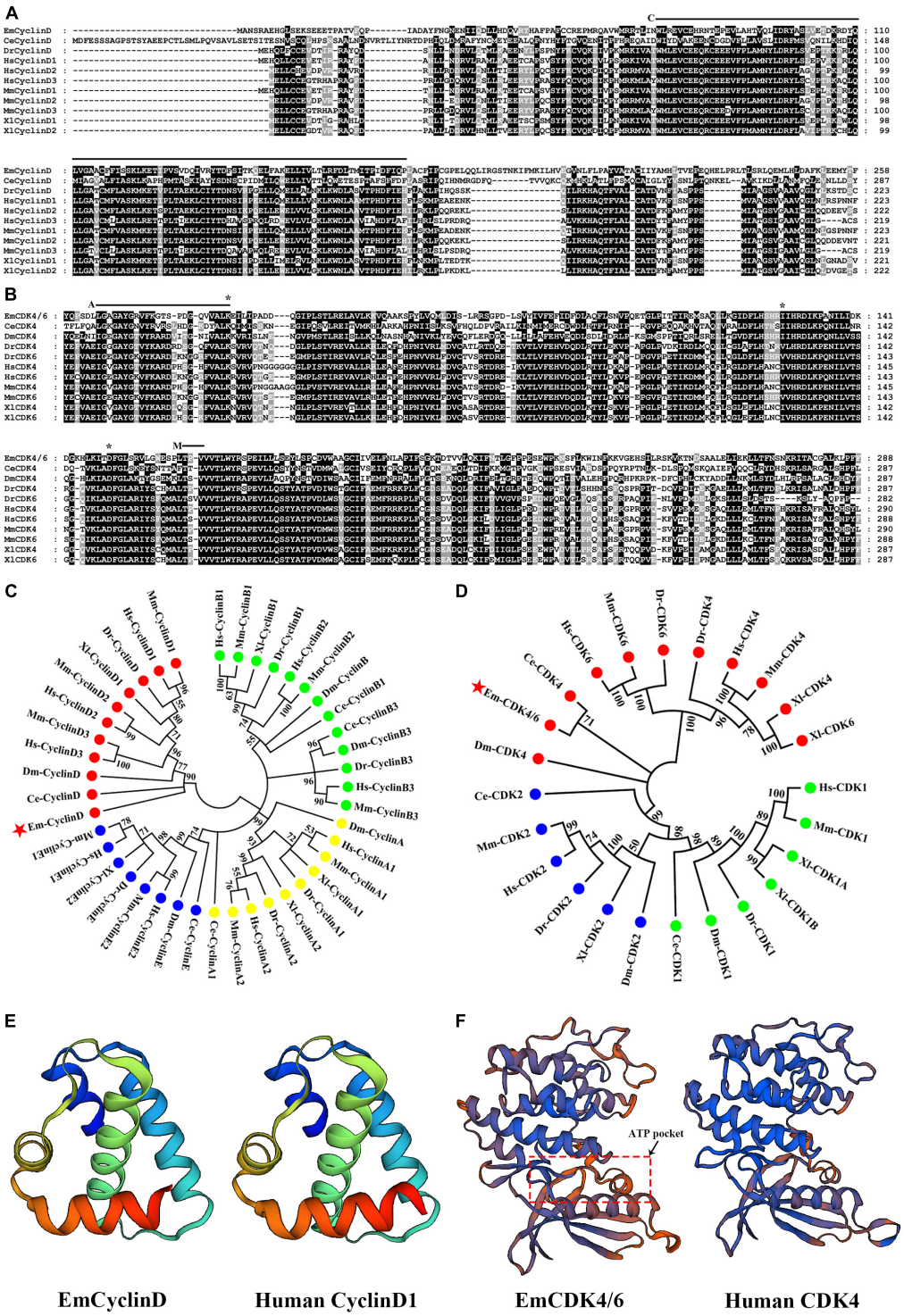

FIGURE 1
Identification of CyclinD and CDK4/6 homologs in *E. multilocularis*. **(A)** Alignment of EmCyclinD with other established CyclinD members. The Cyclin box domain is marked with "C." **(B)** Alignment of the S_Tkc domain of EmCDK4/6 with that of other CDK4 or 6 members. The ATP binding site is marked with "A," the phosphorylation motif is marked with "M" and predicted Palbociclib binding sites are marked with "*." **(C,D)** Phylogenetic analysis of EmCyclinD and EmCDK4/6 (marked with red stars). The full-length sequence of CyclinD members and the S_Tkc domain of CDK4/6 members were used for phylogenetic tree construction. Em, *Echinococcus multilocularis*; Ce, *Caenorhabditis elegans*; Hs, *Homo sapiens*; Mm, *Mus musculus*; Dm, *Drosophila melanogaster*; Dr, *Danio rerio*; Xl, *Xenopus laevis*. **(E)** Comparison of the predicted three-dimensional structures of the Cyclin box of human CyclinD (UniprotKB code P24385) and EmCyclinD. **(F)** Comparison of the predicted three-dimensional structures of the S_Tkc domain of human CDK4 (UniprotKB code P11802) and EmCDK4/6.

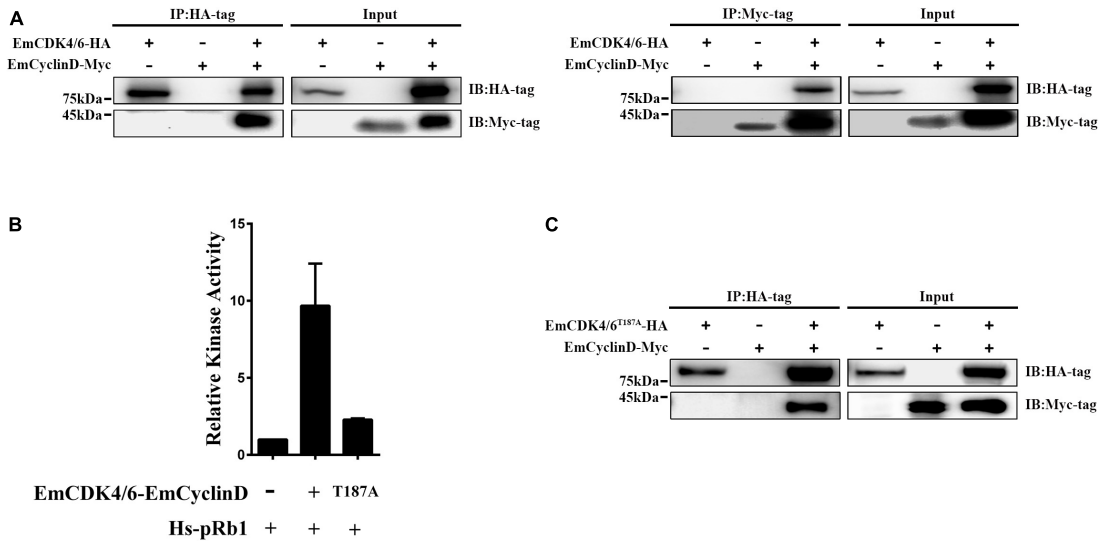

FIGURE 2
EmCDK4/6 interacts with EmCyclinD and displays *in vitro* kinase activity. **(A)** Co-Immunoprecipitation of HA-tagged EmCDK4/6 with Myc-tagged EmCyclinD. The left shows the results using the anti-HA tag antibody for immunoprecipitation and the right using the anti-Myc tag antibody. **(B)** *In vitro* kinase assay of the EmCyclinD-EmCDK4/6 complex or EmCyclinD-EmCDK4/6^{T187A} complex. Data are shown as mean ± *SD* of duplicate. **(C)** Co-Immunoprecipitation of EmCyclinD with EmCDK4/6^{T187A} mutant. Note that the mutation T187A does not affect the binding of EmCyclinD to EmCDK4/6.

EmCDK4/6 interacts with EmCyclinD and activates Rb1 *In vitro*

In mammals, cyclin D generally binds to CDK4 or 6 during G1/S phase and then the CyclinD-CDK4/6 complex phosphorylates downstream Rb1 proteins to release transcriptional factors such as E2F (Sherr and Roberts, 1999; Choi and Anders, 2014). Our data revealed that EmCyclinD co-immunoprecipitates with EmCDK4/6 *in vitro* (**Figure 2A**), suggesting an interaction between EmCyclinD and EmCDK4/6. By mining the genome database, we found that *E. multilocularis* also possesses a CDK2 homolog (EmuJ_000258800, referred to as *EmCDK2* in this study) and that EmCyclinD could not interact with EmCDK2 (**Supplementary Figure 1**). These results suggest that EmCyclinD may specifically form a complex with EmCDK4/6 but not with other CDKs in *E. multilocularis*, in line with the previous findings in other species (Wianny et al., 1998).

To further investigate whether the EmCDK4/6-EmCyclinD complex possesses enzymatic activities, we performed *in vitro* kinase assays using human Rb1 as the substrate. As shown in **Figure 2B**, the EmCDK4/6-EmCyclinD complex displayed kinase activity against human Rb1. In mammalian cells, the activity of CDK4/6 depends on the Ser/Thr-Pro-X motif within the Serine/Threonine kinase catalytic domain, whereas mutations of the Ser/Thr residue in this motif do not affect the binding of CDK4/6 to CyclinD (Kato et al., 1994). We then generated an inactive form of EmCDK4/6 by substituting alanine for threonine (T187A). The results show that EmCDK4/6^{T187A} could complex with EmCyclinD but the kinase activity was greatly reduced (**Figures 2B,C**), suggesting the necessity of Thr187 for EmCDK4/6's kinase function. Together, these results demonstrated that EmCDK4/6 interacts with EmCyclinD and possesses enzymatic activities.

Expression of EmCyclinD in *Echinococcus multilocularis* larvae

Given that the germinative cells are the only proliferative cells in *E. multilocularis*, we speculated that EmCyclinD would be highly expressed in the actively proliferating germinative cells. We then analyzed EmCyclinD expression in metacestode vesicles which have a large population of proliferating germinative cells and in the mature protoscoleces in which the germinative cells maintain slow cell cycle kinetics or remain in a quiescent state (Koziol et al., 2014). As shown in **Figure 3A**, we found that the mRNA level of *EmCyclinD* was much higher in the metacestode vesicles than in the mature protoscoleces (**Figure 3A**).

We also generated a polyclonal antibody against EmCyclinD, which effectively detected the recombinant His-tagged EmCyclinD protein as well as the endogenous EmCyclinD in the *in vitro*-cultivated vesicles (**Figure 3B**). We then explored the protein expression of EmCyclinD in the vesicles treated with hydroxyurea (HU). HU is a DNA synthesis inhibitor and has been shown to arrest the cell cycle at G1/S phase (Timson, 1975) and specifically to deplete the

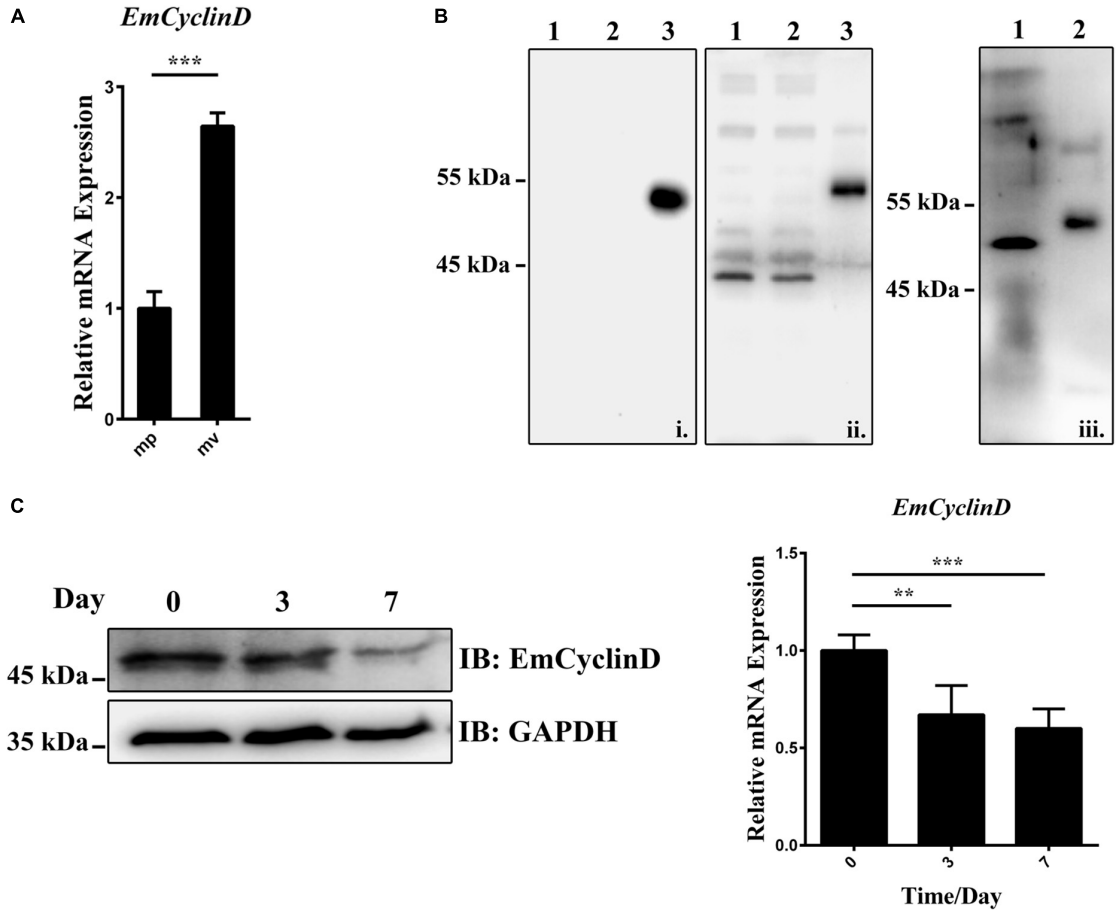

FIGURE 3
Expression of EmCyclinD in *E. multilocularis* germinative cells. **(A)** Relative mRNA levels of EmCyclinD in the mature protoscoleces (mp) and metacestode vesicles (mv). **(B)** Lysates of bacteria expressing His-tagged EmCyclinD were analyzed by western blotting using the anti-His tag antibody (i) or the anti-EmCyclinD antibody (ii). Line 1 and 4: empty vector control; line 2 and 5: IPTG uninduced; line 3 and 6: IPTG induced. Total protein of *in vitro*-cultured vesicles (iii, line 7) was analyzed with the anti-EmCyclinD antibody. His-tagged recombinant EmCyclinD was used as a control (iii, line 8). **(C)** mRNA and protein expressions of EmCyclinD in the metacestode vesicles treated with 40 mM of hydroxyurea for 3 or 7 days. Data in **(A,C)** are shown as mean ± *SD*. $^{**}P < 0.01$, $^{***}P < 0.001$.

germinative cell populations in *E. multilocularis* (Koziol et al., 2014). As shown in **Figure 3C**, we found that both of the mRNA and protein levels of EmCyclinD were lower after HU treatment. Taken together, these results suggest that EmCyclinD is actively expressed in the proliferating germinative cells of *E. multilocularis*.

EmCyclinD-EmCDK4/6 complex participates in the *Echinococcus multilocularis* germinative cell proliferation *via* EGFR-ERK pathway

It has been shown that Palbociclib, a highly selective inhibitor of human CDK4/6, can bind to the ATP-binding pocket of CDK4/6. Consequently, it induces G1 arrest and a concomitant reduction of Rb1 phosphorylation (Fry et al., 2004; Chen et al., 2016). Considering the similarities between human CDK4 and EmCDK4/6 three-dimensional structures, we inferred that Palbociclib might also inhibit the activities of EmCDK4/6. The result of docking predictions demonstrated that Palbociclib exhibits the potential ability to bind to EmCDK4/6 (**Figure 4A**). Palbociclib integrated into the ATP binding pocket of EmCDK4/6 and involves 4 hydrogen bonds in 3 amino acids (i.e., Lys52, Ile151, and Asp173.), which are all conserved in human CDK6 (corresponding to Lys43, Val101 and Asp163, respectively, **Figure 1B**). These three amino acids are involved in the binding of Palbociclib to human CDK6 and the last two among them are considered to contribute mostly to the binding energy (Hernandez et al., 2017). The *in vitro* kinase assay also revealed that Palbociclib attenuated the kinase activity of EmCyclinD-EmCDK4/6 complex (**Figure 4B**).

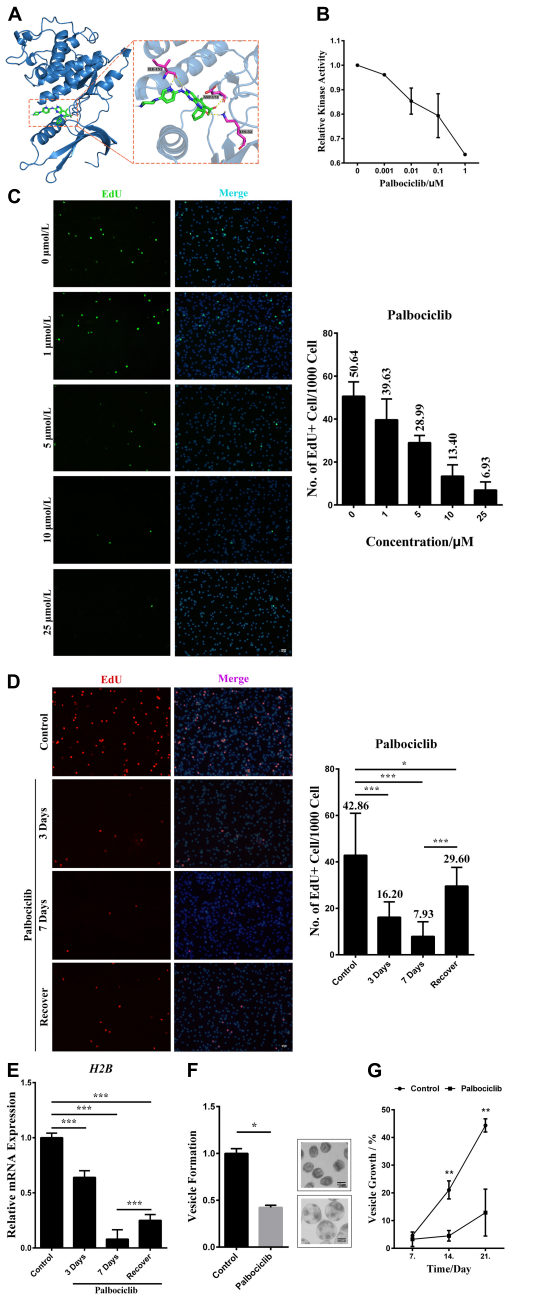

FIGURE 4
EmCyclinD-EmCDK4/6 complex participates in regulating germinative cell proliferation in *E. multilocularis*. **(A)** Docking structure and interactions between EmCDK4/6 and Palbociclib. The left shows that Palbociclib binds to the ATP binding pocket of EmCDK4/6. The right shows the details of the EmCDK4/6-Palbociclib interaction. **(B)** *In vitro* kinase assay of EmCyclinD-EmCDK4/6 complex with Palbociclib. Data are shown as mean ± *SD* of duplicate. **(C)** 3 days effects of different concentrations of Palbociclib on germinative cell proliferation. Representative images are shown in the left panel, Bar = 50 μm. Quantification of EdU + cells is shown in the right panel. Data are shown as mean ± *SD* of 2 separate labeling experiments. EdU detection was performed using green fluorophore (Alexa Fluor 488). **(D)** Proliferation recovery after 7 days of 10 μM

(Continued)

FIGURE 4
Palbociclib treatment. Metacestode vesicles were allowed for recovery in the absence of drugs for 1 day. Representative images are shown in the left panel, Bar = 50 μm. Quantification of EdU + cells is shown in the right panel. $^{*}P < 0.05$, $^{***}P < 0.001$. Data are shown as mean ± *SD* of 12 vesicles. EdU detection was performed using red fluorophore (Alexa Fluor 555). **(E)** mRNA expression of downstream H2B factor upon Palbociclib treatment. Data are shown as mean ± *SD*. $^{***}P < 0.001$. **(F)** 10 μM Palbociclib inhibits the process of vesicle formation from protoscoleces after 21 days treatment. Control was set to 1 and results were normalized against the control. Representative images of vesicle formation are shown on the right. Upper: protoscoleces collected from parasite material. Lower: protoscoleces undergoing vesicle formation **(G)** 10 μM Palbociclib inhibits the growth of metacestode vesicles. Metacestode vesicles growth is shown as the increase of vesicle diameter as compared to day 0. Comparison between the Palbociclib treatment and the control at the same timepoint was performed using two-tailed Student's *t*-test. $^{**}P < 0.01$.

We then treated metacestode vesicles with Palbociclib and labeled the proliferating germinative cells with EdU, an analog of thymidine. The results show that Palbociclib greatly reduced the number of EdU^{+} cells in a dose-dependent manner (**Figure 4C**). The number of proliferating germinative cells was decreased by ∼80% after 7 days of treatment with 10 μM of Palbociclib. With the consideration of Palbociclib as a reversible CDK inhibitor, we removed the drug after 7 days of treatment and found that the proliferation of germinative cells was mostly restored (**Figure 4D**). Furthermore, Palbociclib treatment inhibited the mRNA expression of *EmH2B*, a S-phase marker of the proliferating germinative cells (**Figure 4E**). These results suggest that Palbociclib may cause cell cycle arrest of the germinative cells. *Echinococcus* protoscoleces have a unique feature that they can mature into adult tapeworms in the definitive host (canids), or can undergo reverse development into metacestode vesicles if distributed in the intermediate host (Eckert et al., 1983; Mehlhorn et al., 1983; Koziol et al., 2014). When cultured in the conditioned medium, protoscoleces would tend to develop into vesicles (Hemer et al., 2014; Cheng et al., 2017). Our data show that the initial process of vesicle formation from protoscoleces and the growth of vesicles were also greatly inhibited by Palbociclib (**Figures 4F,G**). Taken together, these data suggest that Palbociclib inhibits the activity of the EmCyclinD-EmCDK4/6 complex, leading to impeded germinative cell proliferation and parasite growth.

The expression and accumulation of Cyclin D are induced by growth factors such as EGF (Musgrove, 2006). In this study, we found that EmCyclinD expression was up-regulated upon host EGF stimulation (**Figure 5A** and **Supplementary Figure 2**), suggesting that host EGF affects the cell cycle of germinative cells. It has been shown that the EGFR/ERK signaling pathway in *E. multilocularis* responds to host EGF and promotes germinative cell proliferation (Cheng et al., 2017). We then treated vesicles with the EGFR inhibitor

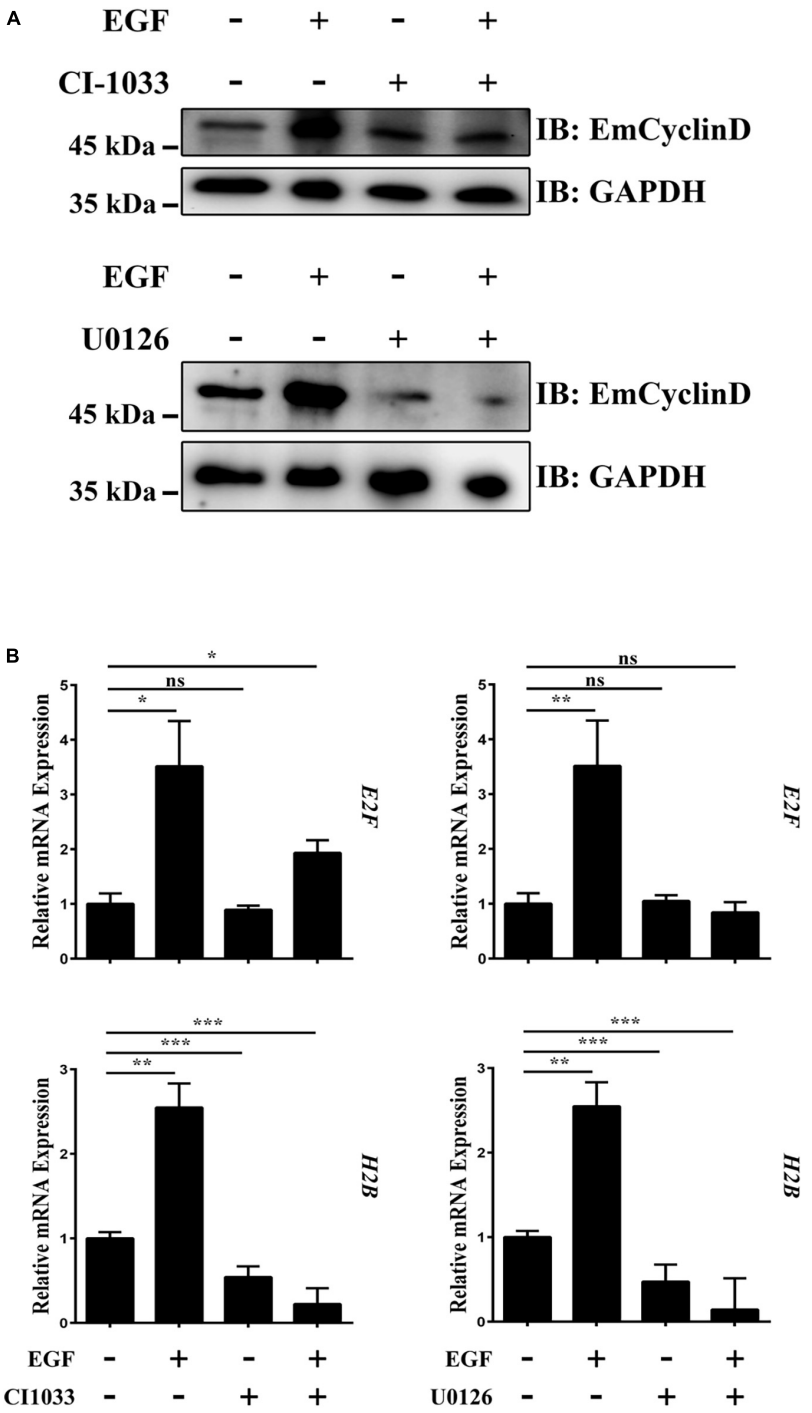

FIGURE 5
The EGFR-ERK pathway regulates EmCyclinD and downstream factors expression in *E. multilocularis*. **(A)** CI-1033 and U0126 inhibit EGF-stimulated EmCyclinD expression in *E. multilocularis*. Metacestode vesicles were treated with 10 μM CI-1033 or 40 μM U0126 for 3 h and then stimulated with EGF for 45 min. **(B)** mRNA expressions of EmCyclinD and S-phase related factors after CI-1033 or U0126 treatment. Data are shown as mean ± *SD*. **P* < 0.05, ***P* < 0.01, ****P* < 0.001. ns, *P* > 0.05.

CI-1033 or the MEK/ERK inhibitor U0126 in the presence or absence of EGF. The results showed that CI-1033 and U0126 not only reduced the basal levels of EmCyclinD in the vesicles but also greatly inhibited the EGF-induced upregulation of EmCyclinD (Figure 5A). E2F and Histone H2B (H2B) are known as the CyclinD downstream and

S phase-related factor in mammalian cells (Whitfield et al., 2006). Orthologs to these factors are also present in the *E. multilocularis* genome: E2F (EmuJ_000535700, annotated as transcription factor E2F4), H2B (EmuJ_000387800, annotated as histone H2B). We found that, along with the downregulation of EmCyclinD, inhibition of EGFR and MEK also decreased the transcriptional levels of E2F and H2B (**Figure 5B**). Meanwhile, the proliferation of germinative cells in the vesicles was promoted upon EGF stimulation while inhibited upon the treatment with CI-1033 or U0126 (**Supplementary Figure 3**), consistent with our earlier research. Taken together, these results suggest that EmCyclinD and downstream cell cycle-related factors expression levels could be regulated by the host EGF-mediated EGFR-ERK signaling pathway.

Discussion

Cyclin-CDK complex play a key role in orchestrating the complex events of cell cycle. In the matter of the G1 phase, as long as the cells sense the mitogenic signals from external cues, Cyclin D accumulates, associates with and activates CDK4/6 to initiate the cell cycle. This mechanism of cell-cycle regulation has been extensively documented in various free-living animals and is considered conserved across metazoans; however, the situation is somewhat different for the metacestode larvae of *E. multilocularis*. In the light of the intimate contact with host tissues and the long-term co-evolutionary process, the parasite is believed, and indeed proved by multiple lines of evidence, capable of sensing the host-derived signals that in turn exert an influence on the germinative cells (Vicogne et al., 2004; Hemer et al., 2014; Cheng et al., 2017; Forster et al., 2019). Since the germinative cells are the only cells that undergo cell division cycle in *E. multilocularis*, this information therefore provides clues regarding the possibility that host factors have been implicated in regulating Cyclin-CDK complex and cell cycle in the parasite.

In this study, we describe two important molecules, EmCyclinD and EmCDK4/6, which are involved in the G1/S-phase regulation in *E. multilocularis*. In comparison with their mammalian homologs, EmCyclinD and EmCDK4/6 are highly conserved in terms of functionally relevant domains (**Figure 1**). While EmCyclinD lacks the CYC_C domain like *C. elegans* CyclinD (Kitagawa et al., 1996). Moreover, EmCDK4/6 has a functional unknown sequence at its carboxyl terminus which was predicted to be randomly coiled. Similar sequences have not been identified in other species and the role remains to be investigated.

Our data show that EmCyclinD is actively expressed in the proliferating germinative cells and could interact with EmCDK4/6 to form a complex which displayed the kinase activity of phosphorylating human Rb1 protein *in vitro* (**Figures 2**, **3**). During the G1 phase of mammalian cells, Rb1 is the most crucial downstream effector of the CyclinD-CDK4/6 complexes, phosphorylated by the complexes at Ser780, Ser795, Ser807, and Ser811, and then allows progression of the cell cycle from G1 to S phase (Rubin, 2013). *E. multilocularis* possesses a single Rb1 homolog (encoded by EmuJ_000159800, referred to as EmRb1 in this study) and 3 of the phosphorylation sites (T910, T922 and T926, corresponding to S795, S807 and S811 of Human Rb1, respectively) related to CyclinD-CDK4/6 were well conserved (**Supplementary Figure 4**). We could also identify a single E2F member in *E. multilocularis* (encoded by EmuJ_000535700, referred to as EmE2F), indicating that the conserved CyclinD-CDK4/6-Rb1-E2F signaling cascade may also exist in the parasite. Interestingly, we found that EmCyclinD could not complex with EmCDK2, suggesting a specific interaction between the Cyclins and their corresponding CDKs in *E. multilocularis* (**Supplementary Figure 1**). An investigation identifying the Cyclin that associates with EmCDK2 is currently being carried out in our laboratory.

We have previously defined that the EGFR/ERK signaling pathway in *E. multilocularis* responds to host EGF and promotes germinative cell proliferation (Cheng et al., 2017). We herein deepen our understanding of this mechanism. Despite failing to detect the changes in the phosphorylation of the downstream effector EmRb1 due to unavailable antibodies, we show that the transcriptional levels of the S-phase related factor were elevated upon host EGF stimulation, accompanied by the promoted EmCyclinD expression and germinative cell proliferation (**Figure 5** and **Supplementary Figure 3**). Since EmCyclinD could form a complex with EmCDK4/6 and inhibition of either the complex or the EGFR/ERK signaling resulted in attenuated effects of EGF on EmCyclinD expression (**Figures 4**, **5**), our data suggest that host EGF is implicated in regulating the activity of EmCyclinD-EmCDK4/6 complex through the EGFR/ERK signaling, which in turn influences the cell cycle progression and the proliferation of germinative cells. Although these findings are mainly based on *in vitro* experiments, our data also demonstrated that the physiologically relevant concentrations of EGF (1–10 ng/mL) could apparently induce the expression of EmCyclinD in the cultivated metacestode vesicles (**Supplementary Figure 2**), and therefore it is conceivable that a similar situation may occur in the growing and developing parasite within the host.

Increasing evidence has shown that a number of kinase inhibitors originally designed for the treatment of human tumors also display effects on parasitic helminths including *E. multilocularis*, owing to the structural similarities between the parasite's kinases and their mammalian homologs (Graeser et al., 1996; Santori et al., 2002; Augusto et al., 2018). Palbociclib has been proved as a potent inhibitor of human CDK4/6 and few reports have demonstrated its activity against other kinases. Generally, 0.1–1 μM of Palbociclib reduces Rb1 phosphorylation, inhibits cell proliferation and even causes cell

death in a variety of cell lines (Menu et al., 2008; Finn et al., 2009; Katsumi et al., 2011; Kwong et al., 2012; Salvador-Barbero et al., 2020). While there are a little research concerning the effects of Palbociclib on non-mammalian animals, the considerable concentration for the CDK4/6-inhibition phenotype in zebrafish is 50 μM (Liu et al., 2011). In the present study, we showed that Palbociclib inhibited the activity of EmCyclinD-EmCDK4/6 complex *in vitro* and 5 μM or higher concentrations of drugs significantly inhibited the proliferation of germinative cells (**Figure 4**). It was reported that Palbociclib, in spite of being considered a reversible CDK inhibitor, causes cytotoxic effects and tumor regression with long-term treatment (Leonard et al., 2012; Dickson et al., 2013; Altenburg and Farag, 2015; Goel et al., 2016). Our data show that long-term treatment of Palbociclib could effectively reduce the metacestode vesicle formation and growth (**Figure 4**), suggesting EmCDK4/6 as a druggable target for new drug development against AE.

In conclusion, we described the characterization of EmCyclinD and EmCDK4/6 and showed that host EGF activates EmCyclinD-EmCDK4/6 complex via the EGFR/ERK signaling in *E. multilocularis*, which in turn regulates germinative cell proliferation and parasite growth. These findings will deepen our understanding of the stem cell biology of *E. multilocularis* and the complex host-parasite interaction, and it will be helpful for the development of novel chemotherapeutics against AE.

Data availability statement

The datasets presented in this study can be found in online repositories. The names of the repository/repositories and accession number(s) can be found below: https://www.uniprot.org/uniprotkb/A0A068Y4X2/entry, EmCDK4/6 (EmuJ_000456500): A0A068Y4X2 and https://www.uniprot.org/uniprotkb/A0A068YJR9/entry, EmCyclinD (EmuJ_001021000): A0A068YJR9.

Ethics statement

The animal study was reviewed and approved by the Institutional Animal Care and Use Committee of Xiamen University.

Author contributions

CF, ZC, and YW conceived and designed the experiments. CF and ZX performed the experiments. CF and ZC analyzed the data and wrote the manuscript. YT, HT, and FL offered writing proposals. All authors contributed to the article and approved the submitted version.

Funding

This study was supported by the National Natural Science Foundation of China (81772211 and 81871679), the National Sharing Service Platform for Parasite Resources (TDRC-22), and the Natural Science Foundation of Fujian Province, China (2020J01019).

Conflict of interest

The authors declare that the research was conducted in the absence of any commercial or financial relationships that could be construed as a potential conflict of interest.

Publisher's note

All claims expressed in this article are solely those of the authors and do not necessarily represent those of their affiliated organizations, or those of the publisher, the editors and the reviewers. Any product that may be evaluated in this article, or claim that may be made by its manufacturer, is not guaranteed or endorsed by the publisher.

Supplementary material

The Supplementary Material for this article can be found online at: https://www.frontiersin.org/articles/10.3389/fmicb.2022.968872/full#supplementary-material

SUPPLEMENTARY FIGURE 1
Analysis of the CDK2 homolog of *E. multilocularis* amino acid sequence and the interaction with EmCyclinD. **(A)** Alignment of the S_Tkc domain of EmCDK2 with multiple species CDK2. **(B)** Phylogenetic analysis of EmCDK2 (marked with red star). The BLAST analyses of the S_Tkc domain of EmCDK2 were used for phylogenetic tree construction. **(C)** The Co-Immunoprecipitation of EmCyclinD and EmCDK2. Using an Anti-HA tag antibody for Immunoprecipitation.

SUPPLEMENTARY FIGURE 2
Effects of EGF on EmCyclinD expression. Metacestode vesicles were cultured in DMEM without serum for 5 days, and then stimulated with 0 (Control) to 100 ng/mL recombinant human EGF for 45 min.

SUPPLEMENTARY FIGURE 3
The inhibition of EGFR-ERK inhibits the proliferation of germinative cells. **(A)** Host EGF stimulates the proliferation of germinative cells. Metacestode vesicles were pretreated with 40 mM of hydroxyurea for 3 days and allowed for a 4 days' recovery in conditioned medium (control) supplemented with EGF. **(B)** CI-1033 and U0126 treatment inhibit germinative cell proliferation. Metacestode vesicles were treated with 10 μM CI-1033 or 40 μM U0126 for 4 days, Representative images are shown in the left panel, Bar = 50 μm. Quantification of EdU + cells is shown in the right panel. $^{*}P < 0.05$, $^{**}P < 0.01$. Data are shown as mean ± *SD* of at least three vesicles.

SUPPLEMENTARY FIGURE 4
Analysis of amino acid sequence of EmRb1. Alignment of the full length of EmRb1 with Human Rb1. Three CyclinD-CDK4/6 complex-related phosphorylation sites are conserved (Orange box).

References

Altenburg, J. D., and Farag, S. S. (2015). The potential role of PD0332991 (Palbociclib) in the treatment of multiple myeloma. *Expert Opin. Investig. Drugs* 24, 261–271. doi: 10.1517/13543784.2015.993753

Augusto, L., Martynowicz, J., Staschke, K. A., Wek, R. C., and Sullivan, W. J. (2018). Effects of PERK eIF2alpha Kinase Inhibitor against *Toxoplasma gondii*. *Antimicrob. Agents Chemother.* 62:e01442-18. doi: 10.1128/AAC.01442-18

Brehm, K. (2010a). *Echinococcus multilocularis* as an experimental model in stem cell research and molecular host-parasite interaction. *Parasitology* 137, 537–555. doi: 10.1017/S0031182009991727

Brehm, K. (2010b). The role of evolutionarily conserved signalling systems in *Echinococcus multilocularis* development and host-parasite interaction. *Med. Microbiol. Immunol.* 199, 247–259. doi: 10.1007/s00430-010-0154-1

Brehm, K., and Spiliotis, M. (2008). The influence of host hormones and cytokines on *Echinococcus multilocularis* signalling and development. *Parasite* 15, 286–290. doi: 10.1051/parasite/2008153286

Brehm, K., Jensen, K., and Frosch, M. (2000). MRNA trans-splicing in the human parasitic cestode *Echinococcus multilocularis*. *J. Biol. Chem.* 275, 38311–38318. doi: 10.1074/jbc.M006091200

Brehm, K., Wolf, M., Beland, H., Kroner, A., and Frosch, M. (2003). Analysis of differential gene expression in *Echinococcus multilocularis* larval stages by means of spliced leader differential display. *Int. J. Parasitol.* 33, 1145–1159. doi: 10.1016/s0020-7519(03)00169-3

Chen, P., Lee, N. V., Hu, W., Xu, M., Ferre, R. A., Lam, H., et al. (2016). Spectrum and degree of CDK drug interactions predicts clinical performance. *Mol. Cancer Ther.* 15, 2273–2281. doi: 10.1158/1535-7163.MCT-16-0300

Cheng, Z., Liu, F., Li, X., Dai, M., Wu, J., Guo, X., et al. (2017). EGF-mediated EGFR/ERK signaling pathway promotes germinative cell proliferation in *Echinococcus multilocularis* that contributes to larval growth and development. *PLoS Negl. Trop. Dis.* 11:e5418. doi: 10.1371/journal.pntd.0005418

Cheng, Z., Liu, F., Zhu, S., Tian, H., Wang, L., Wang, Y., et al. (2015). A rapid and convenient method for fluorescence analysis of *in vitro* cultivated metacestode vesicles from *Echinococcus multilocularis*. *PLoS One* 10:e118215. doi: 10.1371/journal.pone.0118215

Choi, Y. J., and Anders, L. (2014). Signaling through cyclin D-dependent kinases. *Oncogene* 33, 1890–1903. doi: 10.1038/onc.2013.137

Collins, J. R., Wang, B., Lambrus, B. G., Tharp, M. E., Iyer, H., Newmark, P. A., et al. (2013). Adult somatic stem cells in the human parasite *Schistosoma mansoni*. *Nature* 494, 476–479. doi: 10.1038/nature11924

Day, P. J., Cleasby, A., Tickle, I. J., O'Reilly, M., Coyle, J. E., Holding, F. P., et al. (2009). Crystal structure of human CDK4 in complex with a D-type cyclin. *Proc. Natl. Acad. Sci. U.S.A.* 106, 4166–4170. doi: 10.1073/pnas.0809645106

Dharmarajan, G., Li, R., Chanda, E., Dean, K. R., Dirzo, R., Jakobsen, K. S., et al. (2022). The animal origin of major human infectious diseases: what can past epidemics teach us about preventing the next pandemic? *Zoonoses* 2:11. doi: 10.15212/ZOONOSES-2021-0028

Dickson, M. A., Tap, W. D., Keohan, M. L., D'Angelo, S. P., Gounder, M. M., Antonescu, C. R., et al. (2013). Phase II trial of the CDK4 inhibitor PD0332991 in patients with advanced CDK4-amplified well-differentiated or dedifferentiated liposarcoma. *J. Clin. Oncol.* 31, 2024–2028. doi: 10.1200/JCO.2012.46.5476

Duronio, R. J., and Xiong, Y. (2013). Signaling pathways that control cell proliferation. *Cold Spring Harb. Perspect. Biol.* 5:a008904. doi: 10.1101/cshperspect.a008904

Eckert, J., and Deplazes, P. (2004). Biological, epidemiological, and clinical aspects of echinococcosis, a zoonosis of increasing concern. *Clin. Microbiol. Rev.* 17, 107–135. doi: 10.1128/CMR.17.1.107-135.2004

Eckert, J., Thompson, R. C., and Mehlhorn, H. (1983). Proliferation and metastases formation of larval *Echinococcus multilocularis*. I. Animal model, macroscopical and histological findings. *Z. Parasitenkd.* 69, 737–748. doi: 10.1007/BF00927423

Eisenhoffer, G. T., Kang, H., and Sanchez, A. A. (2008). Molecular analysis of stem cells and their descendants during cell turnover and regeneration in the planarian *Schmidtea mediterranea*. *Cell Stem Cell* 3, 327–339. doi: 10.1016/j.stem.2008.07.002

Fernandez-Taboada, E., Moritz, S., Zeuschner, D., Stehling, M., Scholer, H. R., Saló, E., et al. (2010). Smed-SmB, a member of the LSm protein superfamily, is essential for chromatoid body organization and planarian stem cell proliferation. *Development* 137, 1055–1065. doi: 10.1242/dev.042564

Finn, R. S., Dering, J., Conklin, D., Kalous, O., Cohen, D. J., Desai, A. J., et al. (2009). PD 0332991, a selective cyclin D kinase 4/6 inhibitor, preferentially inhibits proliferation of luminal estrogen receptor-positive human breast cancer cell lines *in vitro*. *Breast Cancer Res.* 11:R77. doi: 10.1186/bcr2419

Forster, S., Koziol, U., Schafer, T., Duvoisin, R., Cailliau, K., Vanderstraete, M., et al. (2019). The role of fibroblast growth factor signalling in *Echinococcus multilocularis* development and host-parasite interaction. *PLoS Negl. Trop. Dis.* 13:e0006959. doi: 10.1371/journal.pntd.0006959

Fry, D. W., Harvey, P. J., Keller, P. R., Elliott, W. L., Meade, M., Trachet, E., et al. (2004). Specific inhibition of cyclin-dependent kinase 4/6 by PD 0332991 and associated antitumor activity in human tumor xenografts. *Mol. Cancer Ther.* 3, 1427–1438.

Goel, S., Wang, Q., Watt, A. C., Tolaney, S. M., Dillon, D. A., Li, W., et al. (2016). Overcoming therapeutic resistance in HER2-Positive breast cancers with CDK4/6 inhibitors. *Cancer Cell* 29, 255–269. doi: 10.1016/j.ccell.2016.02.006

Graeser, R., Wernli, B., Franklin, R. M., and Kappes, B. (1996). Plasmodium falciparum protein kinase 5 and the malarial nuclear division cycles. *Mol. Biochem. Parasitol.* 82, 37–49. doi: 10.1016/0166-6851(96)02716-8

Hemer, S., Konrad, C., Spiliotis, M., Koziol, U., Schaack, D., Förster, S., et al. (2014). Host insulin stimulates *Echinococcus multilocularis* insulin signalling pathways and larval development. *BMC Biol.* 12:5. doi: 10.1186/1741-7007-12-5

Hernandez, M. S., Jensen, P., Caracelli, I., Zukerman, S. J., Frohling, S., Friedman, R., et al. (2017). Palbociclib can overcome mutations in cyclin dependent kinase 6 that break hydrogen bonds between the drug and the protein. *Protein Sci.* 26, 870–879. doi: 10.1002/pro.3135

Hetie, P., de Cuevas, M., and Matunis, E. (2014). Conversion of quiescent niche cells to somatic stem cells causes ectopic niche formation in the *Drosophila testis*. *Cell Rep.* 7, 715–721. doi: 10.1016/j.celrep.2014.03.058

Ishidate, T., Elewa, A., Kim, S., Mello, C. C., and Shirayama, M. (2014). Divide and differentiate: cDK/Cyclins and the art of development. *Cell Cycle* 13, 1384–1391. doi: 10.4161/cc.28656

Kato, J. Y., Matsuoka, M., Strom, D. K., and Sherr, C. J. (1994). Regulation of cyclin D-dependent kinase 4 (cdk4) by cdk4-activating kinase. *Mol. Cell. Biol.* 14, 2713–2721. doi: 10.1128/mcb.14.4.2713-2721.1994

Katsumi, Y., Iehara, T., Miyachi, M., Yagyu, S., Tsubai-Shimizu, S., Kikuchi, K., et al. (2011). Sensitivity of malignant rhabdoid tumor cell lines to PD 0332991 is inversely correlated with p16 expression. *Biochem. Biophys. Res. Commun.* 413, 62–68. doi: 10.1016/j.bbrc.2011.08.047

Kitagawa, M., Higashi, H., Jung, H. K., Suzuki-Takahashi, I., Ikeda, M., Tamai, K., et al. (1996). The consensus motif for phosphorylation by cyclin D1-Cdk4 is different from that for phosphorylation by cyclin A/E-Cdk2. *EMBO J.* 15, 7060–7069.

Koziol, U., Dominguez, M. F., Marin, M., Kun, A., and Castillo, E. (2010). Stem cell proliferation during *in vitro* development of the model cestode *Mesocestoides corti* from larva to adult worm. *Front. Zool.* 7:22. doi: 10.1186/1742-9994-7-22

Koziol, U., Rauschendorfer, T., Zanon, R. L., Krohne, G., and Brehm, K. (2014). The unique stem cell system of the immortal larva of the human parasite *Echinococcus multilocularis*. *Evodevo* 5:10. doi: 10.1186/2041-9139-5-10

Kwong, L. N., Costello, J. C., Liu, H., Jiang, S., Helms, T. L., Langsdorf, A. E., et al. (2012). Oncogenic NRAS signaling differentially regulates survival and proliferation in melanoma. *Nat. Med.* 18, 1503–1510. doi: 10.1038/nm.2941

Leonard, J. P., LaCasce, A. S., Smith, M. R., Noy, A., Chirieac, L. R., Rodig, S. J., et al. (2012). Selective CDK4/6 inhibition with tumor responses by PD0332991 in patients with mantle cell lymphoma. *Blood* 119, 4597–4607. doi: 10.1182/blood-2011-10-388298

Lim, S., and Kaldis, P. (2013). Cdks, cyclins and CKIs: roles beyond cell cycle regulation. *Development* 140, 3079–3093. doi: 10.1242/dev.091744

Liu, N. A., Jiang, H., Ben-Shlomo, A., Wawrowsky, K., Fan, X. M., Lin, S., et al. (2011). Targeting zebrafish and murine pituitary corticotroph tumors with a cyclin-dependent kinase (CDK) inhibitor. *Proc. Natl. Acad. Sci. U.S.A.* 108, 8414–8419. doi: 10.1073/pnas.1018091108

Malumbres, M., and Barbacid, M. (2005). Mammalian cyclin-dependent kinases. *Trends Biochem. Sci.* 30, 630–641. doi: 10.1016/j.tibs.2005.09.005

Matsushime, H., Ewen, M. E., Strom, D. K., Kato, J. Y., Hanks, S. K., Roussel, M. F., et al. (1992). Identification and properties of an atypical catalytic subunit (p34PSK-J3/cdk4) for mammalian D type G1 cyclins. *Cell* 71, 323–334. doi: 10.1016/0092-8674(92)90360-o

Mehlhorn, H., Eckert, J., and Thompson, R. C. (1983). Proliferation and metastases formation of larval *Echinococcus multilocularis*. II. Ultrastructural investigations. *Z. Parasitenkd.* 69, 749–763. doi: 10.1007/BF00927424

Menu, E., Garcia, J., Huang, X., Di Liberto, M., Toogood, P. L., Chen, I., et al. (2008). A novel therapeutic combination using PD 0332991 and bortezomib: study in the 5T33MM myeloma model. *Cancer Res.* 68, 5519–5523. doi: 10.1158/0008-5472.CAN-07-6404

Musgrove, E. A. (2006). Cyclins: roles in mitogenic signaling and oncogenic transformation. *Growth Factors* 24, 13–19. doi: 10.1080/08977190500361812

Nugent, J. H., Alfa, C. E., Young, T., and Hyams, J. S. (1991). Conserved structural motifs in cyclins identified by sequence analysis. *J. Cell Sci.* 99, 669–674.

Park, M., and Krause, M. W. (1999). Regulation of postembryonic G(1) cell cycle progression in Caenorhabditis elegans by a cyclin D/CDK-like complex. *Development* 126, 4849–4860. doi: 10.1242/dev.126.21.4849

Pellettieri, J., and Sanchez, A. A. (2007). Cell turnover and adult tissue homeostasis: from humans to planarians. *Annu. Rev. Genet.* 41, 83–105. doi: 10.1146/annurev.genet.41.110306.130244

Rink, J. C. (2013). Stem cell systems and regeneration in planaria. *Dev. Genes Evol.* 223, 67–84. doi: 10.1007/s00427-012-0426-4

Rubin, S. M. (2013). Deciphering the retinoblastoma protein phosphorylation code. *Trends Biochem. Sci.* 38, 12–19. doi: 10.1016/j.tibs.2012.10.007

Salvador-Barbero, B., Alvarez-Fernandez, M., Zapatero-Solana, E., El, B. A., Menendez, M., López-Casas, P. P., et al. (2020). CDK4/6 Inhibitors Impair Recovery from Cytotoxic Chemotherapy in Pancreatic Adenocarcinoma. *Cancer Cell* 37, 340–353. doi: 10.1016/j.ccell.2020.01.007

Santori, M. I., Laria, S., Gomez, E. B., Espinosa, I., Galanti, N., Téllez-Iñón, M. T., et al. (2002). Evidence for CRK3 participation in the cell division cycle of *Trypanosoma cruzi*. *Mol. Biochem. Parasitol.* 121, 225–232. doi: 10.1016/s0166-6851(02)00039-7

Sherr, C. J., and Roberts, J. M. (1999). CDK inhibitors: positive and negative regulators of G1-phase progression. *Genes Dev.* 13, 1501–1512. doi: 10.1101/gad.13.12.1501

Tang, B., Li, J., Li, T., Xie, Y., Guan, W., Zhao, Y., et al. (2022). Vaccines as a strategy to control trichinellosis. *Front. Microbiol.* 13:857786. doi: 10.3389/fmicb.2022.857786

Timson, J. (1975). Hydroxyurea. *Mutat. Res.* 32, 115–132. doi: 10.1016/0165-1110(75)90002-0

Tsai, I. J., Zarowiecki, M., Holroyd, N., Garciarrubio, A., Sanchez-Flores, A., Brooks, K. L., et al. (2013). The genomes of four tapeworm species reveal adaptations to parasitism. *Nature* 496, 57–63. doi: 10.1038/nature12031

Vazquez-Chagoyan, J. C., Gupta, S., and Garg, N. J. (2011). Vaccine development against *Trypanosoma cruzi* and Chagas disease. *Adv. Parasitol.* 75, 121–146. doi: 10.1016/B978-0-12-385863-4.00006-X

Vicogne, J., Cailliau, K., Tulasne, D., Browaeys, E., Yan, Y. T., Fafeur, V., et al. (2004). Conservation of epidermal growth factor receptor function in the human parasitic helminth *Schistosoma mansoni*. *J. Biol. Chem.* 279, 37407–37414. doi: 10.1074/jbc.M313738200

Wang, B., Collins, J. R., and Newmark, P. A. (2013). Functional genomic characterization of neoblast-like stem cells in larval *Schistosoma mansoni*. *Elife* 2:e00768. doi: 10.7554/eLife.00768

Whitfield, M. L., George, L. K., Grant, G. D., and Perou, C. M. (2006). Common markers of proliferation. *Nat. Rev. Cancer* 6, 99–106. doi: 10.1038/nrc1802

Wianny, F., Real, F. X., Mummery, C. L., Van Rooijen, M., Lahti, J., Samarut, J., et al. (1998). G1-phase regulators, cyclin D1, cyclin D2, and cyclin D3: up-regulation at gastrulation and dynamic expression during neurulation. *Dev. Dyn.* 212, 49–62. doi: 10.1002/(SICI)1097-0177(199805)212:1<49::AID-AJA5<3.0.CO;2-2

Yin, J., Shen, Y., and Cao, J. (2022). Burden of cryptosporidium infections in the yangtze river delta in china in the 21st century: a one health perspective. *Zoonoses* 2:7. doi: 10.15212/ZOONOSES-2021-0025

Zhu, S. J., and Pearson, B. J. (2013). The Retinoblastoma pathway regulates stem cell proliferation in freshwater planarians. *Dev. Biol.* 373, 442–452. doi: 10.1016/j.ydbio.2012.10.025

frontiers | Frontiers in Microbiology

TYPE Original Research
PUBLISHED 25 August 2022
DOI 10.3389/fmicb.2022.977405

OPEN ACCESS

EDITED BY
Wei Wang,
Jiangsu Institute of Parasitic Diseases (JIPD), China

REVIEWED BY
Sabri Hacioglu,
Veterinary Control Central Research Institute, Turkey
Wen-Ping Guo,
Northwest A&F University, China
Jia-Fu Jiang,
Beijing Institute of Microbiology and Epidemiology, China
Katsunori Okazaki,
Health Sciences University of Hokkaido, Japan

*CORRESPONDENCE
Fu-Qiang Huang
qxhuangfuqiang@fosu.edu.cn
Ming-Fei Sun
smf7810@126.com

†These authors have contributed equally to this work

SPECIALTY SECTION
This article was submitted to Infectious Agents and Disease, a section of the journal Frontiers in Microbiology

RECEIVED 24 June 2022
ACCEPTED 10 August 2022
PUBLISHED 25 August 2022

CITATION
Zhang X, Li H-Y, Shao J-W, Pei M-C, Cao C, Huang F-Q and Sun M-F (2022) Genomic characterization and phylogenetic analysis of a novel Nairobi sheep disease genogroup Orthonairovirus from ticks, Southeastern China.
Front. Microbiol. 13:977405.
doi: 10.3389/fmicb.2022.977405

Genomic characterization and phylogenetic analysis of a novel Nairobi sheep disease genogroup Orthonairovirus from ticks, Southeastern China

Xu Zhang[1†], Hang-Yuan Li[1†], Jian-Wei Shao[1], Ming-Chao Pei[1], Chong Cao[2,3], Fu-Qiang Huang[1*] and Ming-Fei Sun[4,5,6,7*]

[1]School of Life Science and Engineering, Foshan University, Foshan, China, [2]Fujian Provincial Key Laboratory for the Prevention and Control of Animal Infectious Diseases and Biotechnology, Longyan, China, [3]Key Laboratory of Preventive Veterinary Medicine and Biotechnology, Longyan University, Longyan, China, [4]Zhaoqing/Maoming Branch Center of Guangdong Laboratory for Lingnan Modern Agricultural Science and Technology, Zhaoqing, China, [5]Key Laboratory of Livestock Disease Prevention of Guangdong Province, Guangzhou, China, [6]Key Laboratory of Avian Influenza and Other Major Poultry Diseases Prevention and Control, Ministry of Agriculture and Rural Affairs, Guangzhou, China, [7]Institute of Animal Health, Guangdong Academy of Agricultural Sciences, Guangzhou, China

The increasing prevalence and transmission of tick-borne diseases, especially those emerging ones, have posed a significant threat to public health. Thus, the discovery of neglected pathogenic agents carried and transmitted by ticks is urgently needed. Using unbiased high-throughput sequencing, a novel Orthonairovirus designated as Meihua Mountain virus (MHMV), was identified in bloodsucking ticks collected from cattle and wild boars in Fujian province, Southeastern China. The full-length genome was determined by RT-PCR and RACE. Genomic architecture of MHMV shares typical features with orthonairoviruses. Phylogenetic analyses suggested that MHMV is clustered into the Nairobi sheep disease (NSD) genogroup of the genus *Orthonairovirus* and is closely related to the Hazara virus. The RdRp, GPC, and N protein of MHMV shares 62.3%–83.5%, 37.1%–66.1%, and 53.4%–77.3% amino acid identity with other NSD genogroup viruses, respectively, representing a novel species. The overall pooled prevalence of MHMV in ticks was 2.53% (95% CI: 1.62%–3.73%, 22 positives of 134 tick pools), with 7.38% (95% CI: 3.84%–12.59%, 11 positives of 18 pools) in *Haemaphysalis hystricis*, 6.02% (95% CI: 1.85%–14.22%, four positives of eight pools) in *H. formosensis*, 25.03% (95% CI: 9.23%–54.59%, six positive of eight pools) in *Dermacentor taiwanensis*, and 0.16% (95% CI: 0.01%–0.72%, one positive of 100 pools) in *Rhipicephalus microplus*. This study presented the first report of tick-carried Orthonairovirus in Fujian province and highlighted the broad geographic distribution and high genetic diversity of orthonairoviruses in China.

KEYWORDS

Meihua Mountain virus, novel Orthonairovirus, NSD genogroup, metatranscriptomics, China

Introduction

Ticks are one of the main vectors transmitting viral, bacterial, and parasitic pathogens that cause severe illnesses to animals and humans. The increasing prevalence and transmission of tick-borne diseases, especially those emerging ones such as severe fever with thrombocytopenia syndrome and Heartland virus diseases, are keeping challenging our preparedness and have posed a significant threat to public health (Madison-Antenucci et al., 2020). Thus, unbiased discovery and detection of emerging human-pathogenic agents carried and transmitted by ticks are urgently needed.

Members of the genus *Orthonairovirus* are all transmitted by ticks, distinguishing themselves from most of the other members of the family *Nairoviridae* (Lasecka and Baron, 2014). Based on the phylogenetic relationships, tick-associated orthonairoviruses were classified into nine genogroups, of which the most important is the Nairobi sheep disease (NSD) genogroup (Walker et al., 2016). The NSD genogroup includes Crimean-Congo hemorrhagic fever virus (CCHFV), Nairobi sheep disease virus (NSDV), Hazara virus (HAZV), Dugbe virus (DUGV), and Kupe virus (KUPV; Walker et al., 2016). The recently identified Tofla virus (TFLV) also belongs to this genogroup (Shimada et al., 2016). Among these, the fatal human pathogen CCHFV can cause hemorrhagic fever with mortality up to 30% (Shahhosseini et al., 2021), and the NSDV causes severe hemorrhagic gastroenteritis in sheep and goats with mortality up to 90% (Krasteva et al., 2020). Both CCHFV and NSDV endemic foci can be found in Africa, Asia, and the Middle East, suggesting the wide geographic distribution of orthonairoviruses. Except for CCHFV and NSDV, the vertebrate host has not been established for other members of the NSD genogroup. Meanwhile, human infection has not been reported, thus their relevance to public health remains unclear. However, infection with these viruses can be lethal to immunocompromised mice, emphasizing their pathogenic potential (Dowall et al., 2012; Shimada et al., 2016). Importantly, several recently discovered tick-borne orthonairoviruses in Eastern Asia, such as the Yezo virus (Kodama et al., 2021), Songling virus (Ma et al., 2021), and Tacheng tick virus 1 (Liu et al., 2019), were associated with human febrile illness with different severity, suggesting the high diversity of orthonairoviruses in nature and their potential risk to public health.

With the expansion of tick habitats, it is necessary to monitor the agents they carried (Dong and Soong, 2021). Fujian, a coastal mountainous province, locates in Southeastern China and possesses a middle subtropical climate. The suitable climatic conditions and abundant wildlife in mountains shaped a perfect environment for several tick species, such as *Ixodes granulatus*, *Rhipicephalus microplus*, and *Dermacentor auratus* (Zhang et al., 2019). The Meihua Mountain Nature Reserve in Fujian province is an ecological forest area, in which a variety of wild animals provide abundant host resources for ectoparasitic ticks. However, little is known about the background information of tick-carried pathogenic agents. In this study, we performed unbiased high-throughput meta-transcriptomic sequencing to profile RNA virus in ticks. A novel member of NSD genogroup Orthonairovirus, designated as Meihua Mountain virus (MHMV), was identified in bloodsucking ticks collected from cattle and wild boar. The complete genome sequence, genomic characteristics, phylogenetic relationship, and molecular prevalence of MHMV were analyzed. This study presented the first report of tick-borne Orthonairovirus in Fujian province and highlighted the broad geographic distribution and genetic diversity of orthonairoviruses in China.

Materials and methods

Tick collection and RNA extraction

From 2019 to 2020, 988 bloodsucking ticks were collected from cattle and wild boar in seven villages of Meihua Mountain Nature Reserve, Fujian province, Southeastern China. The tick species were morphologically identified by microscopy, and were further confirmed by 16S ribosomal RNA gene sequencing as described (The primers used are listed in Supplementary Table S1; Sameroff et al., 2019). Subsequently, the same species of ticks were pooled and stored at −80°C until further processing.

Before extracting nucleic acid, pooled samples were washed in 1 ml of 70% ethanol followed by three washes with nuclease-free water and then dried. Each pool was homogenized in 400 μl Dulbecco's Modified Eagle Medium (DMEM; Thermo Fisher Scientific, Waltham, MA, United States) using TissueLyser II (Qiagen, Hilden, Germany). Homogenates were then centrifuged at 12,000 rpm for 1 min to precipitate debris. To extract RNA, 100 μl supernatant was mixed with 300 μl TRIzol LS reagent (Invitrogen, Carlsbad, CA, United States) and purified according to the manufacturer's instructions. For meta-transcriptomic sequencing, a total of 34 pools were selected based on tick species and host animals (Supplementary Table S2). The total RNA was extracted using the homogenate mixture from 34 pools according to tick numbers in the pools to make sure that the RNA from each tick is equal. All purified RNA was quantified using Qubit 3.0 fluorometer (Thermo Fisher Scientific) and stored at −80°C until further use.

Meta-transcriptome sequencing

RNA library preparation was conducted following the library preparation protocol provided by Illumina, with slight modification. Briefly, ribosomal RNA in total RNA was removed by a Ribo-Zero Plus rRNA Depletion Kit (Illumina, San Diego, CA, United States). The remaining RNA was then fragmented, reverse-transcribed, adapted, purified, and analyzed with the Agilent 2100 Bioanalyzer. Paired-end (150 bp) sequencing was conducted on the Illumina HiSeq 2500 platform (Illumina). The

library preparation and sequencing were performed at Novogene (Tianjin, China).

Bioinformatics analysis and full-length genome determination

The sequencing reads (raw data) were quality-controlled with SOAPnuke (v2.0.5) software to generate clean reads (Chen et al., 2018). The rRNA and host reads were then filtered by BWA (v0.7.17) with default settings (Li and Durbin, 2009). *De novo* assembly was performed with Megahit (v1.1.2; Li et al., 2015b) and the resulting contigs were blasted against reference virus nucleotides and proteins by BLASTN as well as Diamond BLASTX, respectively (Buchfink et al., 2015). The viral contigs mapped to the same segment were further assembled using ContigExpress, and subsequently mapped to a Hazara virus reference genome (GenBank accession numbers are listed in Supplementary Table S3) using Geneious (Biomatters, Ltd., New Zealand).

To fill the gaps between contigs, primers were designed according to corresponding contigs. Then nested reverse transcription polymerase chain reaction (RT-PCR) was done and followed by Sanger sequencing. For the genome termini, rapid amplification of cDNA ends (RACE) was performed using a SMARTer RACE 5′/3′ Kit (Takara, Beijing, China), as described previously (Li et al., 2015a).

Molecular screening of MHMV in individual tick pools

Primer pairs targeting the coding region of the L segment were designed. Primers are listed in Supplementary Table S1. Total RNA extracted from individual tick pools (134) was subjected to the screening of MHMV using nested RT-PCR and confirmed by sequencing. The nested PCR was performed according to the manufacturer's instructions. Briefly, RT-PCR was performed with the PrimeScript One Step RT-PCR kit (TaKaRa). The 50 μl reaction contained 18 μl RNase-Free ddH_2O, 25 μl 2× buffer, 2 μl PrimeScript Enzyme, 2 μl of forward and reverse primers, and 2 μg total RNA. The cycling program was set at 50°C for 30 min and 94°C for 2 min, followed by 35 cycles of standard PCR and a final extension step at 72°C for 5 min. The second round PCR was performed with ExTaq Premix (TaKaRa). The reaction was assembled by combining 19 μl RNase-Free ddH_2O, 25 μl Taq Premix, 2 μl of forward and reverse primers each, and 2 μl PCR product from RT-PCR reaction. The following cycles were set as 98°C for 1 min, 35 cycles of standard PCR, and 72°C for 5 min. The annealing temperature of both RT-PCR and the second round PCR was set as 55°C.

Prevalence of MHMV was estimated assuming perfect sensitivity and specificity of molecular detection using the EPITOOLS online statistical program "Pooled prevalence for variable pool size and perfect tests"[1] that based on the model established by Williams and Moffitt (2001). The input data were prepared as instructed by the EPITOOLS user guide.

Virus isolation

The homogenate from positive tick samples was centrifuged at 6,000 *g* for 10 min and the supernatant was collected. The 100 μl of undiluted and diluted (1:5 and 1:10) supernatant was inoculated onto monolayers of Vero E6, SW-13, and BHK-21 cell in 6-well plate. After 2 h of inoculation, the supernatant was aspirated out and replaced with medium containing 2% fetal bovine serum. The cytopathic effect (CPE) was examined daily and each passage was tested for the presence of MHMV RNA using RT-PCR as described in section 2.4. Unfortunately, neither apparent CPE nor the existence of viral RNA was observed throughout eight blind passages, indicating that MHMV may not be able to propagate in the above cell lines.

Genomic characterization and phylogenetic analysis

The potential open reading frames (ORFs) were predicted in ORFfinder and compared with other Orthonairovirus sequences (GenBank accession numbers are listed in Supplementary Table S2). Analysis of the glycoprotein precursor (GPC) domains and post-translational modification features was conducted with TMHMM (for transmembrane protein prediction; Krogh et al., 2001), ProP−1.0 (for signal peptidase cleavage site prediction; Petersen et al., 2011), NetNGlyc−1.0 (for *N*-linked glycosylation site prediction), and NetOGlyc (for mucin-type *O*-glycosylation site prediction; Steentoft et al., 2013).

To determine the phylogenetic relationship among orthonairoviruses, amino acid alignments were conducted using the E-INS-i algorithm in MAFFT 7.0 (Katoh et al., 2019). TrimAI 1.2 was used to trim off ambiguous positions and sequences were re-aligned in MEGA X (MUSCLE; Capella-Gutiérrez et al., 2009; Kumar et al., 2018). Phylogenetic trees were constructed using the maximum likelihood (ML) method (LG substitution model, Gamma-distributed rate variation) with 100 bootstrap replications (Le and Gascuel, 2008).

The amino acid and nucleotide sequence identity was determined with Clustal Omega (Sievers and Higgins, 2018). Both the putative Gn and Gc protein amino acid sequence alignment of NSD genogroup viruses were performed with MAFFT version 7.0 online server[2] (Katoh et al., 2019). G-INS-i algorithm was used

1 https://epitools.ausvet.com.au/ppvariablepoolsize

2 https://mafft.cbrc.jp/alignment/server/

and the Unaligned level value was set as 0.4 with other parameters that were set as default. Visualization of the resulting alignments was done with the ESpriPt 3.0[3] (Robert and Gouet, 2014) and edited in Adobe Illustrator CC.

Ethical approval

This study did not involve the purposeful killing of animals. All samples were collected by passive surveillance under Chinese legislation. No ethical approval was necessary.

Results

Identification of MHMV in ticks

From 2019 to 2020, a total of 988 bloodsucking ticks were collected from cattle and wild boar in seven villages of the Meihua Mountain Nature Reserve, Fujian province, Southeastern China. The tick species were determined as *Dermacentor taiwanensis* (59, 8 pools), *Haemaphysalis hystricis* (214, 18 pools), *Haemaphysalis formosensis* (103, 8 pools), and *Rhipicephalus microplus* (612, 100 pools). The 988 ticks were divided into 134 individual pools based on tick species and host animals (Figure 1).

RNA from 34 pools was selected based on tick species and host animals, mixed, and subjected to meta-transcriptomic sequencing. A total of 41,271,206 paired-end clean reads were generated. After removing the ribosomal and tick host reads, 14,569,764 reads were obtained and assembled. The resulting contigs were blasted against virus nucleotides and proteins, which identified 706,102 viral reads, accounting for 1.71% of total clean reads. Among the assembled contigs, 59 viral contigs were annotated as the Large (L) (32), Middle (M) (21), and Small (S) (6) segments of orthonairoviruses within the family *Nairoviridae*. The novel virus was tentatively designated as MHMV. The full-length genome was determined by RT-PCR to fill the gaps between assembled contigs and RACE to obtain the genome termini. Thereafter, a total of 94,802 reads were re-mapped to the determined MHMV genome, revealing an overall >99% genome coverage with a mean depth of >350 × (Figure 2). MHMV has a tripartite negative-sense RNA genome that comprises three segments, including an L segment encoding an RNA-dependent RNA polymerase (RdRp), an M segment encoding a GPC, and an S segment encoding a nucleocapsid protein. The nucleotide sequences of L, M, and S segments of MHMV have been deposited in GenBank under accession numbers ON184084—ON184086, respectively.

3 https://espript.ibcp.fr/ESPript/cgi-bin/ESPript.cgi

Phylogenetic analysis of MHMV

The virus sequence was preliminarily compared against Viruses reference sequences with blastn suite. The nucleotide sequences of L segment, M segment, and S segment of MHMV have the highest sequence similarity with HAZV with identities of 71.9%, 64.4%, and 69.4%, respectively (Table 1). These results support that MHMV is a novel species in genus *Orthonairovirus* according to the criteria suggested (He et al., 2022). ML phylogenetic trees reconstructed based on the amino acid sequences from L, M, and S segments of orthonairoviruses confirmed that members of the genus *Orthonairovirus* have been assigned into nine genogroups (Figure 3; Walker et al., 2016). The RdRp, GPC, and N protein trees all showed that MHMV was closely clustered with HAZV and a recently identified Orthonairovirus, TFLV (Figure 3). These three viruses formed a well-supported (100% bootstrap value at the node) small clade in the NSD genogroup, indicating MHMV is a novel member of the NSD genogroup.

Genome characteristics of the novel MHMV

The MHMV has a tripartite negative-sense RNA genome that comprises three segments as other orthonairoviruses. The L segment is 11,897 nt in length encoding an RdRp (3,923 aa). The M segment (4,853 nt) encodes a GPC (1,482 aa), and an S segment (1,682 nt) encodes an N protein (485 aa). The RdRp ORF is flanked by an 85 bp 5′-non-coding region (NCR) and a 40 bp 3′-NCR in the L segment. The M segment is flanked by a 337 bp 5′-NCR and a 67 bp 3′-NCR, while the S segment has a 143 bp 5′-NCR and an 81 bp 3′-NCR. All three segments shared the conserved terminal sequences with 3′-AGAGUUUCU and a reverse complementary 5′-AGAAACUCU, the typical feature of the genus *Orthonairovirus* (Kuhn et al., 2016).

The RdRp of nairoviruses contains several presumed regions and domains, including ovarian tumor-like (OTU-like) protease domain, polymerase module (pre-Motif A, motif A-E), and the Region I, Region II (a recently identified N-terminal localized Influenza-Like endonuclease domain which had a cap-snatching activity) and Region IV (Honig et al., 2004; Kinsella et al., 2004; Reguera et al., 2010). Amino acid sequence alignment of these regions confirmed that the RdRp of MHMV contains all the aforementioned highly conserved regions as other NSD genogroup members (Supplementary Figure S1).

Moreover, protein domain and post-translational modification analysis of MHMV GPC showed typical organizational characteristics in terms of three predicted signal peptidase cleavage sites, three subtilisin/kexin-isozyme-1 (SKI-1) protease cleavage sites (RRKL^{51}, RRLM^{310}, and RKLL^{837}), 5 transmembrane domains, presumable

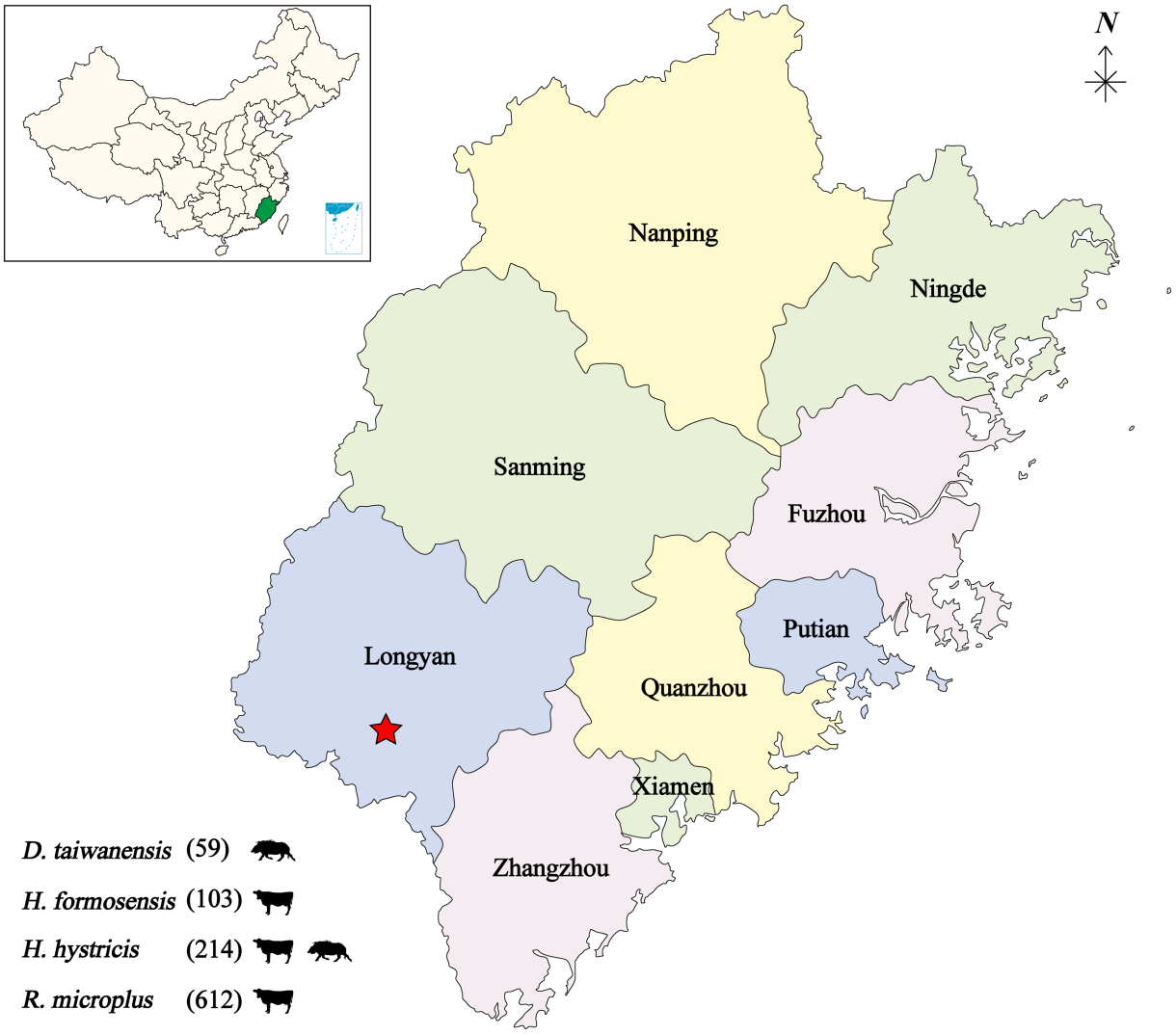

FIGURE 1
Geographic map showing the tick sampling information. The tick collection site is indicated by a red star, annotated with tick species and infesting animals. *D, Dermacentor; H, Haemaphysalis; R, Rhipicephalus*.

mucin-like domain located at the N-terminus, glycoprotein (Gn), a non-structural protein (NSm), and glycoprotein (Gc; Figure 4). Notably, MHMV has similar Gn and Gc structure and protein size, although a relatively lower amino acid identity with other NSD genogroup viruses (Figure 4; Table 1). Interestingly, MHMV, HAZV, and TFLV contain much shorter mucin-like domains and fewer *O*-glycosylation sites in comparison with NSDV, KUPV, DUGV, and CCHFV (Figure 4). The Gn protein of MHMV contains two *N*-glycosylation sites, two transmembrane domains, and a pair of conserved zinc-finger domains that have also been found in CCHFV (Supplementary Figure S2; Estrada and De Guzman, 2011). Similarly, three conserved *N*-glycosylation sites have been found in Gc of MHMV and other NSD group viruses (Supplementary Figure S3). A C-terminus localized transmembrane domain and two conserved *N*-glycosylation sites were also predicted in other NSD genogroup members (Supplementary Figure S3). Moreover, MHMV possesses conserved fusion loop regions as other Orthonairovirus (Supplementary Figure S3; Li et al., 2022).

Structural biology studies of N protein of nairoviruses identified two major domains, a globular head and an extended stalk, with RNA/DNA binding-associated sites. The head domains of the MHMV and other NSD genogroup viruses showed high conservation while apparent high flexibility can be seen in the stalk domain as previously reported (Supplementary Figure S4; Wang et al., 2015). In addition, the DEVD caspase-3 cleavage site motif that has been identified in CCHFV is not present in MHMV N protein (Wang et al., 2012). These results showed that MHMV shares conserved genome organization and protein structures with other NSD genogroup orthonairoviruses.

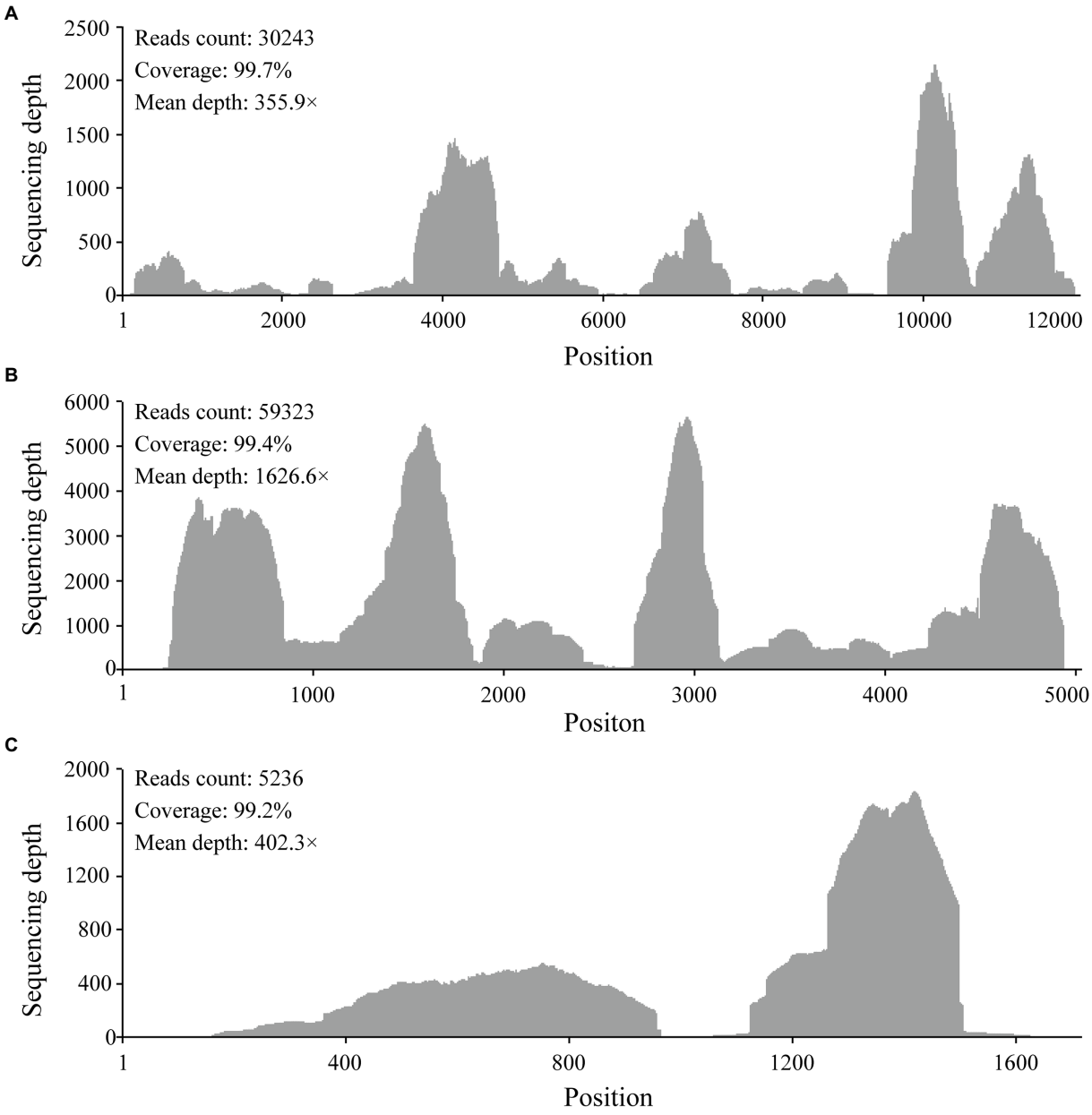

FIGURE 2
Mapped reads count plot of the MHMV genome. **(A)** L segment; **(B)** M segment; **(C)** S segment. The histograms show the depth at a given base position.

Sequence comparison of MHMV with other NSD genogroup members

The NSD genogroup now consists of six representative species, including HAZV, TFLV, NSDV, KUPV, DUGV, and CCHFV. The pairwise alignment showed that the RdRp, GPC, and N protein of MHMV share 62.3%–83.5%, 37.1%–66.1%, and 53.4%–77.3% amino acid identity with other NSD genogroup viruses, respectively (Table 1). The RdRp amino acid sequence of MHMV has the highest identity (83.5%) with TFLV, while GPC and N both showed the highest identity to HAZV with the identity of 66.1 and 77.3%, respectively (Table 1).

Notably, the Gn protein of the NSD genogroup viruses has a similar percent identity (38.4%–66.5%) with GPC polyprotein (35.8%–66.1%; Table 2). However, the Gc part showed a significantly higher percent identity range from 44.8% to 78.0% within the genogroup (Table 2). To date, an objective species demarcation criterion of *Orthonairovirus* stays unestablished. The species demarcation criteria for *Nairoviridae* are recently proposed to be <93% identity in L protein, considering that available CCHFV strains possess a maximum amino acid distance of 6.8%

(Walker et al., 2016). Thus, we tentatively designated the newly identified virus, MHMV, as a novel species of the NSD genogroup in the genus *Orthonairovirus*.

Prevalence of MHMV in ticks

To estimate the prevalence of MHMV in ticks, the collected 134 individual tick pools were subjected to molecular screening of MHMV. The amplicon of RT-PCR was sequenced and two variant sequences have been deposited to Genbank under accession numbers of OP056094 and OP056095, respectively. The positive rate was 7.38% (95% CI: 3.84%–12.59%, 18 pools) in *H. hystricis*, 6.02% (95% CI: 1.85%–14.22%, eight pools) in *H. formosensis*, and 25.03% (95% CI: 9.23%–54.59%, eight pools) in *D. taiwanensis*, while only one pool of *R. microplus* was tested positive out of 100 (Table 3), suggesting that the hard ticks, *Haemaphysalis* spp. and *Dermacentor* spp., might be the predominant vectors of MHMV. However, isolation of MHMV with commonly used cell lines for NSD genogroup virus isolation was not successful.

TABLE 1 Amino acid sequence and nucleotide identity of MHMV RdRp (L segment), GPC (M segment), and N protein (S segment) with the NSD genogroup orthonairoviruses.

	Amino acid sequence identity (%)			Nucleotide sequence identity (%)		
	RdRp	GPC	N	L	M	S
HAZV	82.4	66.1	77.3	71.9	64.4	69.4
TFLV	83.5	64.5	75.3	71.1	63.2	69.4
NSDV	68.9	45.4	61.1	65.1	51.2	61.8
KUPV	65.6	43.2	54.7	62.5	50.3	58.5
DUGV	65.9	38.9	53.4	62.6	48.0	56.0
CCHFV	62.3	37.1	59.1	61.5	47.3	58.0

Discussion

Tick-transmitted viral pathogens can cause deadly illnesses in animals and humans, which has posed a significant threat to public health (Madison-Antenucci et al., 2020). With the expansion of tick habitats, it is necessary to survey the pathogenic agents they carried. In this study, we took unbiased high throughput meta-transcriptomic sequencing to profile viruses carried by ticks collected from Fujian, a coastal mountainous province, Southeastern China. A novel

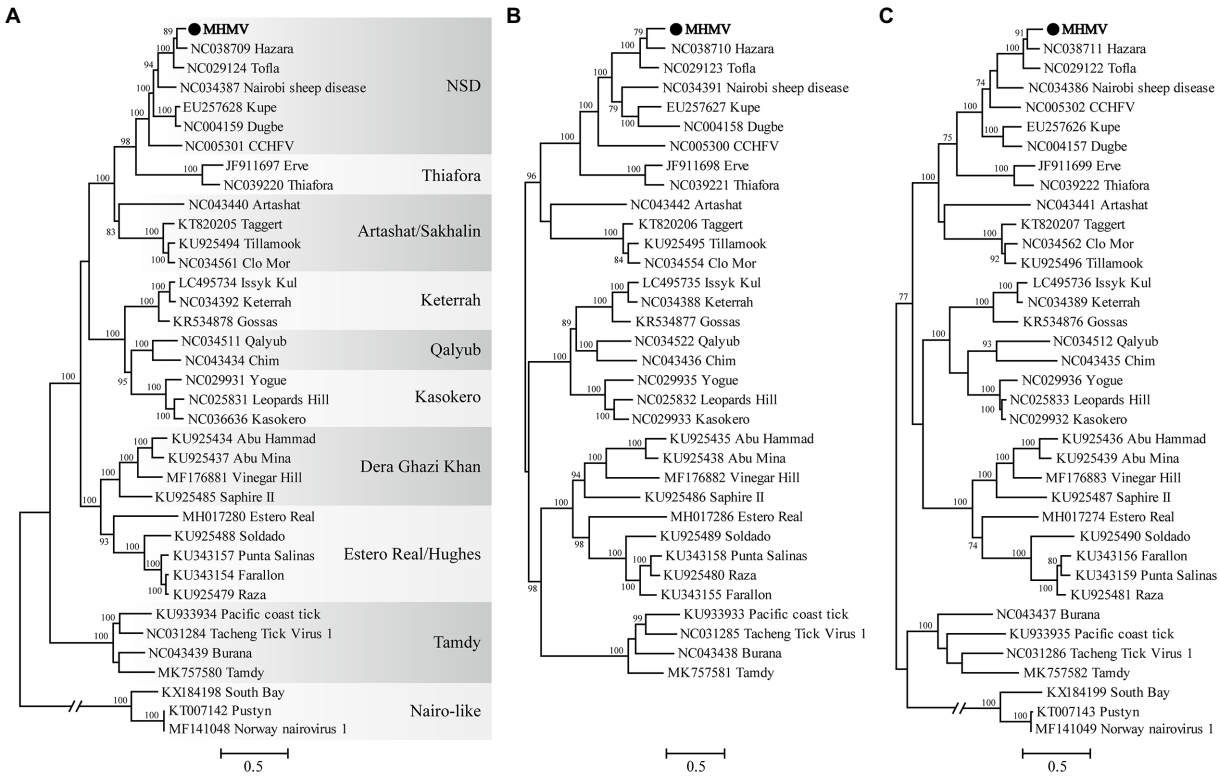

FIGURE 3
ML phylogenetic trees based on the amino acid sequences deduced from L, M, and S segments of Meihua Mountain Virus (Black dots) and other representative orthonairoviruses. **(A)** Tree inferred from the RdRp amino acid sequences. **(B)** Tree inferred from the GPC amino acid sequences. **(C)** Tree inferred from the N protein amino acid sequences. Genogroup assignments are indicated with differential shading patterns. Bootstrap support values ≥70% are indicated. Sequences are identified by their GenBank accession numbers, followed by the virus name. GenBank accession numbers of sequences used in the alignments are listed in Supplementary Table S2.

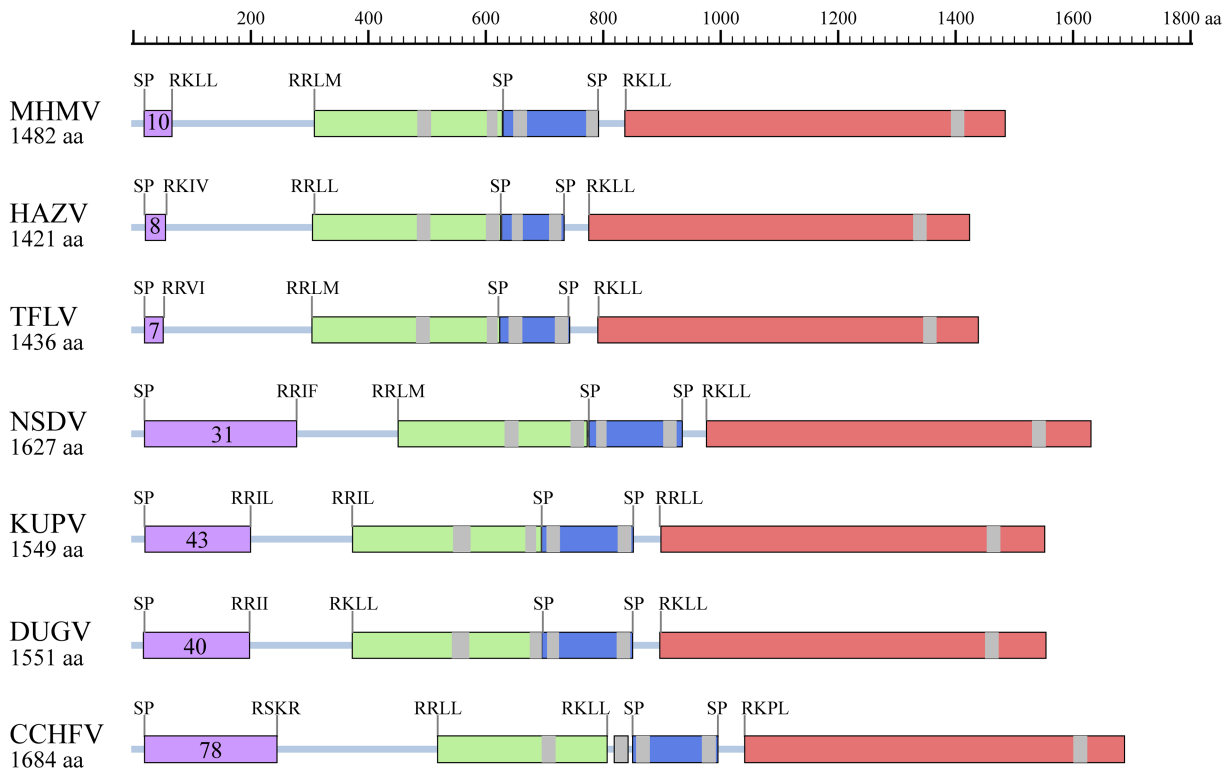

FIGURE 4
Illustration of GPC structures of the NSD genogroup viruses. Mucin-like domain (purple), Gn (light green), NSm (dark blue), and Gc (pink) are shaded correspondingly. Predicted signal peptidase (SP) cleavage sites and putative furin-like and subtilisin/kexin-isozyme-1 (SKI-I) cleavage sites are labeled. The number of predicted *O*-linked glycosylation sites in the mucin-like domain is also shown in the purple shaded box. The transmembrane domains are shaded with grey. The protein length is scaled. HAZV, Hazara virus; TFLV, Tofla virus; NSDV, Nairobi sheep disease virus; KUPV, Kupe virus; DUGV, Dugbe virus; CCHFV, Crimean-Congo hemorrhagic fever virus.

Orthonairovirus, MHMV, was identified in bloodsucking ticks collected from cattle and wild boar. Since the viral structural proteins possess relatively low identity (<83.5% in L, <66.1% in GPC, and <77.3% in N) to its closest Orthonairovirus relatives, we herein suggest MHMV as a novel species of genus *Orthonairovirus*. Phylogenetic analysis suggested that MHMV is closely related to HAZV and belongs to the NSD genogroup in the genus *Orthonairovirus*. It shares typical genomic characteristics with other orthonairoviruses. Molecular surveillance showed that MHMV is mainly carried by the ticks of *Haemaphysalis* spp. and *Dermacentor* spp.

The expanding genus *Orthonairovirus* is now a large group with 15 highly divergent species and several unclassified nairoviruses (Garrison et al., 2020). Among them, CCHFV, the most pathogenic one, has been found in China by molecular and serological detection in ticks and humans, respectively (Sun et al., 2009; Moming et al., 2018). Recently, some novel Orthonairovirus, such as Songling virus (Ma et al., 2021), Tacheng tick virus 1(Liu et al., 2019), and Tamdy virus (strain XJ01/TAMV/China/2018; Zhou et al., 2019) have been identified in ticks collected in Northeastern and Northwestern China, respectively. The identification of MHMV in Fujian province, Southeastern China, suggested the genetic diversity and wide geographic distribution of orthonairoviruses in China. More importantly, songling virus and Tacheng tick virus 1 have been confirmed associated with human febrile illness (Liu et al., 2019; Ma et al., 2021), indicating the public health significance of Orthonairovirus. Although the pathogenicity of MHMV needs further investigation, the close phylogenetic relationship with other pathogenic Orthonairovirus still indicates its pathogenic potential to human or animal.

Previously, it has been established that the classification of the genus *Orthonairovirus* was well supported by phylogenetic relationships and structural features of GPC (Walker et al., 2016). In this study, we compared the sequence conservativity and protein structure of the NSD genogroup members. Both sequence alignment and protein structure analysis supported the genogroup classification proposed by Walker et al. (2016). Notably, we showed that the Gn amino acid sequence has a similar level of identity with the whole GPC polyprotein, while the Gc part shared an apparently higher identity. If these observations infer functional consequences in terms of pathogenesis and viral biology of the NSD genogroup members remains unclear.

We have attempted to isolate MHMV with Vero E6, SW-13, and BHK-21 cell lines that have been used for isolation of NSD

TABLE 2 Pairwise comparisons of GPC, Gn, and Gc amino acid sequences among the NSD genogroup orthonairoviruses.

	Amino acid sequence identity (%)					
	MHMV	**HAZV**	**TFLV**	**NSDV**	**KUPV**	**DUGV**
GPC						
MHMV	100					
HAZV	66.1	100				
TFLV	64.5	62.0	100			
NSDV	45.4	48.6	46.3	100		
KUPV	43.2	46.0	43.8	49.6	100	
DUGV	38.4	42.1	40.0	45.5	56.3	100
CCHFV	37.1	38.7	38.9	40.5	40.3	35.8
Gn						
MHMV	100					
HAZV	66.5	100				
TFLV	66.1	64.3	100			
NSDV	46.4	45.5	45.8	100		
KUPV	45.8	45.8	47.3	53.9	100	
DUGV	42.1	44.0	43.4	51.6	60.4	100
CCHFV	38.4	40.9	41.5	43.7	44.6	41.0
Gc						
MHMV	100					
HAZV	78.0	100				
TFLV	75.5	74.6	100			
NSDV	59.7	62.3	58.1	100		
KUPV	56.5	58.1	55.6	61.9	100	
DUGV	57.1	59.4	56.7	63.1	72.2	100
CCHFV	48.8	49.1	49.1	52.0	51.3	52.0

TABLE 3 Prevalence of MHMV in tick pools screened by RT-PCR.

	No. of MHMV positive/tested pools (positive rate, 95% CI)			
	H. hystricis	***D. taiwanensis***	***H. formosensis***	***R. microplus***
Wild boar	8/12 (8.89, 4.04%–16.63%)	6/- (25.03, 9.23%–54.59%)	—	—
Cattle	3/6 (5.16, 1.3%–13.06%)	—	4/8 (6.02, 1.85%–14.22%)	1/100 (0.16, 0.01%–0.72%)

D, Dermacentor; H, Haemaphysalis; R, Rhipicephalus.

genogroup viruses (CCHFV, HAZV, and TFLV; Shimada et al., 2016; Fuller et al., 2020; Dai et al., 2021). However, neither CPE nor viral RNA has been detected across several passages in cell cultures. This could be explained by that MHMV is a novel virus with low identity with known NSD genogroup viruses. Tick cell line may be a better alternative for MHMV isolation in the future since it has been successfully applied in the isolation of several novel viruses from ticks (Jia et al., 2019; Kholodilov et al., 2020).

Taken together, a novel Orthonairovirus was identified in ticks collected in the Fujian province of China through unbiased RNA sequencing, which expands the knowledge about the genetic diversity of orthonairoviruses in China.

Data availability statement

The datasets presented in this study can be found in online repositories. The names of the repository/repositories and accession number(s) can be found at: https://www.ncbi.nlm.nih.gov/genbank/, ON184084, ON184085, and ON184086.

Author contributions

XZ and CC sampled the ticks. XZ, H-YL, and M-CP prepared the nucleic acid samples and gathered the molecular data. XZ, J-WS, and F-QH performed the bioinformatics analyses and drafted the manuscript. F-QH and M-FS conceived the study and revised the manuscript. All authors contributed to the article and approved the submitted version.

Funding

This research was funded by the Guangdong Basic and Applied Basic Research Foundation (2020A1515011575, 2021A1515110450) and the Natural Science Foundation of Fujian Province (2021J05235).

Conflict of interest

The authors declare that the research was conducted in the absence of any commercial or financial relationships that could be construed as a potential conflict of interest.

Publisher's note

Supplementary material

The Supplementary material for this article can be found online at: https://www.frontiersin.org/articles/10.3389/fmicb.2022.977405/full#supplementary-material

References

Buchfink, B., Xie, C., and Huson, D. H. (2015). Fast and sensitive protein alignment using DIAMOND. *Nat. Methods* 12, 59–60. doi: 10.1038/nmeth.3176

Capella-Gutiérrez, S., Silla-Martínez, J. M., and Gabaldón, T. (2009). trimAl: a tool for automated alignment trimming in large-scale phylogenetic analyses. *Bioinformatics* 25, 1972–1973. doi: 10.1093/bioinformatics/btp348

Chen, Y., Chen, Y., Shi, C., Huang, Z., Zhang, Y., Li, S., et al. (2018). SOAPnuke: a MapReduce acceleration-supported software for integrated quality control and preprocessing of high-throughput sequencing data. *GigaScience* 7, 1–6. doi: 10.1093/gigascience/gix120

Dai, S., Wu, Q., Wu, X., Peng, C., Liu, J., Tang, S., et al. (2021). Differential cell line susceptibility to Crimean-Congo hemorrhagic fever virus. *Front. Cell. Infect. Microbiol.* 11:648077. doi: 10.3389/fcimb.2021.648077

Dong, X. P., and Soong, L. (2021). Emerging and re-emerging zoonoses are major and global challenges for public health. *Zoonoses* 1, 1–2. doi: 10.15212/ZOONOSES-2021-0001

Dowall, S. D., Findlay-Wilson, S., Rayner, E., Pearson, G., Pickersgill, J., Rule, A., et al. (2012). Hazara virus infection is lethal for adult type I interferon receptor-knockout mice and may act as a surrogate for infection with the human-pathogenic Crimean–Congo hemorrhagic fever virus. *J. Gen. Virol.* 93, 560–564. doi: 10.1099/vir.0.038455-0

Estrada, D. F., and De Guzman, R. N. (2011). Structural characterization of the Crimean-Congo hemorrhagic fever virus Gn tail provides insight into virus assembly. *J. Biol. Chem.* 286, 21678–21686. doi: 10.1074/jbc.M110.216515

Fuller, J., Álvarez-Rodríguez, B., Todd, E., Mankouri, J., Hewson, R., and Barr, J. N. (2020). *Hazara nairovirus* requires COPI components in both Arf1-dependent and Arf1-independent stages of its replication cycle. *J. Virol.* 94:e00766-20. doi: 10.1128/jvi.00766-20

Garrison, A. R., Alkhovsky, S. V., Avsic-Zupanc, T., Bente, D. A., Bergeron, E., Burt, F., et al. (2020). ICTV virus taxonomy profile: nairoviridae. *J. Gen. Virol.* 101, 798–799. doi: 10.1099/jgv.0.001485

He, W. T., Hou, X., Zhao, J., Sun, J., He, H., Si, W., et al. (2022). Virome characterization of game animals in China reveals a spectrum of emerging pathogens. *Cell* 185, 1117.e8–1129.e8. doi: 10.1016/j.cell.2022.02.014

Honig, J. E., Osborne, J. C., and Nichol, S. T. (2004). Crimean-Congo hemorrhagic fever virus genome L RNA segment and encoded protein. *Virology* 321, 29–35. doi: 10.1016/j.virol.2003.09.042

Jia, N., Liu, H. B., Ni, X. B., Bell-Sakyi, L., Zheng, Y. C., Song, J. L., et al. (2019). Emergence of human infection with Jingmen tick virus in China: a retrospective study. *EBioMedicine* 43, 317–324. doi: 10.1016/j.ebiom.2019.04.004

Katoh, K., Rozewicki, J., and Yamada, K. D. (2019). MAFFT online service: multiple sequence alignment, interactive sequence choice and visualization. *Brief. Bioinform.* 20, 1160–1166. doi: 10.1093/bib/bbx108

Kholodilov, I. S., Litov, A. G., Klimentov, A. S., Belova, O. A., Polienko, A. E., Nikitin, N. A., et al. (2020). Isolation and characterisation of Alongshan virus in Russia. *Viruses* 12:362. doi: 10.3390/v12040362

Kinsella, E., Martin, S. G., Grolla, A., Czub, M., Feldmann, H., and Flick, R. (2004). Sequence determination of the Crimean-Congo hemorrhagic fever virus L segment. *Virology* 321, 23–28. doi: 10.1016/j.virol.2003.09.046

Kodama, F., Yamaguchi, H., Park, E., Tatemoto, K., Sashika, M., Nakao, R., et al. (2021). A novel nairovirus associated with acute febrile illness in Hokkaido. *Japan. Nat. Commun.* 12:5539. doi: 10.1038/s41467-021-25857-0

Krasteva, S., Jara, M., Frias-De-Diego, A., and Machado, G. (2020). Nairobi sheep disease virus: a historical and epidemiological perspective. *Front. Vet. Sci.* 7:419. doi: 10.3389/fvets.2020.00419

Krogh, A., Larsson, B., von Heijne, G., and Sonnhammer, E. L. (2001). Predicting transmembrane protein topology with a hidden Markov model: application to complete genomes. *J. Mol. Biol.* 305, 567–580. doi: 10.1006/jmbi.2000.4315

Kuhn, J. H., Wiley, M. R., Rodriguez, S. E., Bào, Y., Prieto, K., Travassos da Rosa, A. P. A., et al. (2016). Genomic characterization of the genus Nairovirus (family Bunyaviridae). *Viruses* 8:164. doi: 10.3390/v8060164

Kumar, S., Stecher, G., Li, M., Knyaz, C., and Tamura, K. (2018). MEGA X: molecular evolutionary genetics analysis across computing platforms. *Mol. Biol. Evol.* 35, 1547–1549. doi: 10.1093/molbev/msy096

Lasecka, L., and Baron, M. D. (2014). The molecular biology of nairoviruses, an emerging group of tick-borne arboviruses. *Arch. Virol.* 159, 1249–1265. doi: 10.1007/s00705-013-1940-z

Le, S. Q., and Gascuel, O. (2008). An improved general amino acid replacement matrix. *Mol. Biol. Evol.* 25, 1307–1320. doi: 10.1093/molbev/msn067

Li, H., and Durbin, R. (2009). Fast and accurate short read alignment with burrows-wheeler transform. *Bioinformatics* 25, 1754–1760. doi: 10.1093/bioinformatics/btp324

Li, D., Liu, C. M., Luo, R., Sadakane, K., and Lam, T. W. (2015b). MEGAHIT: an ultra-fast single-node solution for large and complex metagenomics assembly *via* succinct de Bruijn graph. *Bioinformatics* 31, 1674–1676. doi: 10.1093/bioinformatics/btv033

Li, N., Rao, G., Li, Z., Yin, J., Chong, T., Tian, K., et al. (2022). Cryo-EM structure of glycoprotein C from Crimean-Congo hemorrhagic fever virus. *Virol. Sin.* 37, 127–137. doi: 10.1016/j.virs.2022.01.015

Li, C. X., Shi, M., Tian, J. H., Lin, X. D., Kang, Y. J., Chen, L. J., et al. (2015a). Unprecedented genomic diversity of RNA viruses in arthropods reveals the ancestry of negative-sense RNA viruses. *elife* 4:e05378. doi: 10.7554/eLife.05378

Liu, X., Zhang, X., Wang, Z., Dong, Z., Xie, S., Jiang, M., et al. (2019). A tentative Tamdy Orthonairovirus related to febrile illness in northwestern China. *Clin. Infect. Dis.* 70, 2155–2160. doi: 10.1093/cid/ciz602

Ma, J., Lv, X. L., Zhang, X., Han, S. Z., Wang, Z. D., Li, L., et al. (2021). Identification of a new orthonairovirus associated with human febrile illness in China. *Nat. Med.* 27, 434–439. doi: 10.1038/s41591-020-01228-y

Madison-Antenucci, S., Kramer, L. D., Gebhardt, L. L., and Kauffman, E. (2020). Emerging tick-borne diseases. *Clin. Microbiol. Rev.* 33, e00083–e00018. doi: 10.1128/cmr.00083-18

Moming, A., Yue, X., Shen, S., Chang, C., Wang, C., Luo, T., et al. (2018). Prevalence and phylogenetic analysis of Crimean-Congo hemorrhagic fever virus in ticks from different ecosystems in Xinjiang. *China. Virol. Sin.* 33, 67–73. doi: 10.1007/s12250-018-0016-3

Petersen, T. N., Brunak, S., von Heijne, G., and Nielsen, H. (2011). SignalP 4.0: discriminating signal peptides from transmembrane regions. *Nat. Methods* 8, 785–786. doi: 10.1038/nmeth.1701

Reguera, J., Weber, F., and Cusack, S. (2010). Bunyaviridae RNA polymerases (L-protein) have an N-terminal, influenza-like endonuclease domain, essential for viral cap-dependent transcription. *PLoS Pathog.* 6:e1001101. doi: 10.1371/journal.ppat.1001101

Robert, X., and Gouet, P. (2014). Deciphering key features in protein structures with the new ENDscript server. *Nucleic Acids Res.* 42, W320–W324. doi: 10.1093/nar/gku316

Sameroff, S., Tokarz, R., Charles, R. A., Jain, K., Oleynik, A., Che, X., et al. (2019). Viral diversity of tick species parasitizing cattle and dogs in Trinidad and Tobago. *Sci. Rep.* 9:10421. doi: 10.1038/s41598-019-46914-1

Shahhosseini, N., Wong, G., Babuadze, G., Camp, J. V., Ergonul, O., Kobinger, G. P., et al. (2021). Crimean-Congo hemorrhagic fever virus in Asia, Africa and Europe. *Microorganisms* 9:1907. doi: 10.3390/microorganisms9091907

Shimada, S., Aoki, K., Nabeshima, T., Fuxun, Y., Kurosaki, Y., Shiogama, K., et al. (2016). Tofla virus: a newly identified Nairovirus of the Crimean-Congo hemorrhagic fever group isolated from ticks in Japan. *Sci. Rep.* 6:20213. doi: 10.1038/srep20213

Sievers, F., and Higgins, D. G. (2018). Clustal omega for making accurate alignments of many protein sequences. *Protein Sci.* 27, 135–145. doi: 10.1002/pro.3290

Steentoft, C., Vakhrushev, S. Y., Joshi, H. J., Kong, Y., Vester-Christensen, M. B., Schjoldager, K. T., et al. (2013). Precision mapping of the human O-GalNAc glycoproteome through SimpleCell technology. *EMBO J.* 32, 1478–1488. doi: 10.1038/emboj.2013.79

Sun, S., Dai, X., Aishan, M., Wang, X., Meng, W., Feng, C., et al. (2009). Epidemiology and phylogenetic analysis of crimean-Congo hemorrhagic fever viruses in Xinjiang, China. *J. Clin. Microbiol.* 47, 2536–2543. doi: 10.1128/JCM.00265-09

Walker, P. J., Widen, S. G., Wood, T. G., Guzman, H., Tesh, R. B., and Vasilakis, N. (2016). A global genomic characterization of Nairoviruses identifies nine discrete Genogroups with distinctive structural characteristics and host-vector associations. *Am. J. Trop. Med. Hyg.* 94, 1107–1122. doi: 10.4269/ajtmh.15-0917

Wang, Y., Dutta, S., Karlberg, H., Devignot, S., Weber, F., Hao, Q., et al. (2012). Structure of Crimean-Congo hemorrhagic fever virus nucleoprotein: superhelical homo-oligomers and the role of caspase-3 cleavage. *J. Virol.* 86, 12294–12303. doi: 10.1128/jvi.01627-12

Wang, W., Liu, X., Wang, X., Dong, H., Ma, C., Wang, J., et al. (2015). Structural and functional diversity of Nairovirus-encoded nucleoproteins. *J. Virol.* 89, 11740–11749. doi: 10.1128/jvi.01680-15

Williams, C. J., and Moffitt, C. M. (2001). A critique of methods of sampling and reporting pathogens in populations of fish. *J. Aquat. Anim. Health* 13, 300–309. doi: 10.1577/1548-8667(2001)013<0300:ACOMOS>2.0.CO;2

Zhang, G., Zheng, D., Tian, Y., and Li, S. (2019). A dataset of distribution and diversity of ticks in China. *Sci. Data* 6:105. doi: 10.1038/s41597-019-0115-5

Zhou, H., Ma, Z., Hu, T., Bi, Y., Mamuti, A., Yu, R., et al. (2019). Tamdy virus in Ixodid ticks infesting Bactrian camels, Xinjiang, China, 2018. *Emerg. Infect. Dis.* 25, 2136–2138. doi: 10.3201/eid2511.190512

frontiers | Frontiers in Microbiology

TYPE Original Research
PUBLISHED 29 August 2022
DOI 10.3389/fmicb.2022.959901

OPEN ACCESS

EDITED BY
Wei Wang,
Jiangsu Institute of Parasitic Diseases (JIPD), China

REVIEWED BY
Malini Sen,
Indian Institute of Chemical Biology (CSIR), India
Prasad Liyanage,
National Institute of Health Sciences, Sri Lanka

*CORRESPONDENCE
Zhengbin Zhou
zhouzb@nipd.chinacdc.cn
Shizhu Li
lisz@chinacdc.cn

†These authors have contributed equally to this work

SPECIALTY SECTION
This article was submitted to Infectious Agents and Disease, a section of the journal Frontiers in Microbiology

RECEIVED 02 June 2022
ACCEPTED 05 August 2022
PUBLISHED 29 August 2022

CITATION
Li Y, Luo Z, Hao Y, Zhang Y, Yang L, Li Z, Zhou Z and Li S (2022) Epidemiological features and spatial-temporal clustering of visceral leishmaniasis in mainland China from 2019 to 2021. *Front. Microbiol.* 13:959901. doi: 10.3389/fmicb.2022.959901

Epidemiological features and spatial-temporal clustering of visceral leishmaniasis in mainland China from 2019 to 2021

Yuanyuan Li[1†], Zhuowei Luo[1†], Yuwan Hao[1], Yi Zhang[1,2], Limin Yang[1], Zhongqiu Li[1], Zhengbin Zhou[1*] and Shizhu Li[1,2*]

[1]National Institute of Parasitic Diseases, Chinese Center for Disease Control and Prevention (Chinese Center for Tropical Diseases Research), NHC Key Laboratory of Parasite and Vector Biology, WHO Collaborating Centre for Tropical Diseases, National Center for International Research on Tropical Diseases, Shanghai, China, [2]School of Global Health, Chinese Center for Tropical Diseases Research, Shanghai Jiao Tong University School of Medicine, Shanghai, China

Background: Visceral leishmaniasis (VL) is a serious vector-borne disease in central and western China. In recent years, the number of VL cases increased gradually, particularly the mountain-type zoonotic visceral leishmaniasis (MT-ZVL). This study clarified the epidemiological features and spatial-temporal clustering of VL in China between 2019 and 2021, identified the risk areas for VL transmission, and provided scientific evidence for the prevention and control of VL.

Materials and methods: The information on VL cases in 2019–2021 was collected from the Infectious Disease Reporting Information Management System of the Chinese Center for Disease Control and Prevention. The epidemiological characteristics of VL cases were analyzed. The global *Moran's I* and Getis-ORD Gi* statistical data were processed for spatial autocorrelation and hotspot analysis in ESRI ArcGIS software. Also, spatial-temporal clustering analysis was conducted with the retrospective space–time permutation scan statistics.

Results: A total of 608 VL cases were reported from 2019 to 2021, with 158, 213, and 237 cases reported each year, respectively. Of the 608 cases, there were 10 cases of anthroponotic visceral leishmaniasis (AVL), 20 cases of desert-type zoonotic visceral leishmaniasis (DT-ZVL), and 578 cases of MT-ZVL. The age of VL cases was mainly distributed in the group of subjects aged ≥ 15 years. Peasants and infants were the dominant high-risk population. The incidence peak season of VL occurred between March and May. The cases were mainly distributed in Shanxi (299 cases), Shaanxi (118 cases), and Gansu (106 cases) Provinces, accounting for 86.02% (523/608) of the total reported cases in China. Spatial analysis revealed that clustering of infection is mainly located in eastern Shanxi Province and Shaanxi–Shanxi border areas, as well as southern Gansu and northern Sichuan Province. In

addition, new reemergence hotspots in Shanxi, Henan, and Hebei Provinces have been detected since 2020. Spatio-temporal clustering analysis revealed an increase in the degree of infection aggregation in eastern Shanxi Province and Shaanxi–Shanxi border areas.

Conclusion: The AVL and DT-ZVL were endemic at a lower level in western China, whereas MT-ZVL rebounded rapidly and showed a resurgence in historically endemic counties. The spatial-temporal clustering analysis displayed that the high-incidence areas of VL have shifted to central China, particularly in Shanxi and Shaanxi Provinces. Integrated mitigation strategies targeting high-risk populations are needed to control VL transmission in high-risk areas.

KEYWORDS

visceral leishmaniasis, epidemiology, China, spatial-temporal clustering, hotspot

Introduction

Visceral leishmaniasis (VL), also known as Kala-azar, is a serious infectious disease caused by Leishmania spp. that is transmitted by the bite of phlebotomine sand flies (Alvar et al., 2006; Bates, 2007; World Health Organization [WHO], 2010), the hosts of which include animals like canids, rodents, marsupials, hyraxes, and human beings (Akhoundi et al., 2016), because VL can be fatal if left untreated in over 95% of the cases (World Health Organization [WHO], 2022). In many countries, more male than female cases are reported. The incubation period ranges from 10 days to over 1 year, and the onset of the disease is usually gradual (World Health Organization [WHO], 2010). The main clinical manifestations of this disease are usually chronic irregular fever, weight loss, hepatosplenomegaly,anemia,leukopenia, and increased serum globulin levels (World Health Organization [WHO], 2010). In 2018, a total of 83 countries or territories were considered endemic for or had previously reported cases of VL (World Health Organization [WHO], 2020), mainly distributed in South Asia, East Africa, South America, the Mediterranean Region, and Central Asia (Killick-Kendrick, 1990). VL is considered as the second most deadly parasitic disease following malaria, with 200,000–400,000 cases reported and approximately 60,000 fatalities annually (Alvar et al., 2012). In 2021, World Health Organization (WHO) listed VL as a public health problem that must be eliminated (Casulli, 2021).

In the early 1950s, VL was one of the five most serious parasitic diseases endangering human health in the People's Republic of China. It was prevalent in 16 provinces (autonomous regions and municipalities) located north of the Yangtze River, with about 530,000 patients (Wang and Wu, 1956; He et al., 1959). In 1956, the Chinese government put the elimination of VL within a specified time limit as the top priority of public health work. Through active efforts by the government, VL was brought under control by 1960 in most areas of the country (Wang et al., 2000). In the 1980s, only a few sporadic cases remained in southern Xinjiang, Gansu, Sichuan, Shaanxi, and Shanxi Provinces (Guan et al., 2000). Since the 21st century, the epidemic situation of VL has changed with the evolvement of natural ecology and the social environment. A large number of historically endemic counties have experienced the resurgence of VL, leading to the gradual expansion of endemic scope (Han et al., 2019; Zhou et al., 2020c). During the historical period, three epidemiological types of VL, namely, AVL, DT-ZVL, and MT-ZVL, were identified in mainland China (Xiong et al., 1976; Guan and Shen, 1991).

The AVL, whose transmission cycle is from human to human, is caused by *Leishmania donovani* (Guan and Wu, 2014). This type was once seriously endemic in the plain areas of eastern and central China, including the south-eastern suburbs of Beijing, southern Hebei, Shandong, eastern Henan, northern Jiangsu, northern Anhui, Shaanxi plains, the northern Jianghan plain of Hubei, and the ancient oasis area of southern Xinjiang, where the majority of the cases were juveniles (Zhou et al., 2020d). Because the patients were the primary reservoir hosts of AVL, concurrent or consecutive cases often occurred in one household with spatial clusters, sometimes leading to outbreaks (Zhou et al., 2020d). After the control program was established, the disease was remarkably controlled in the above-mentioned regions, and is currently distributed in the oases of the plains of Kashi Prefecture, Xinjiang (Zheng et al., 2020).

The MT-ZVL, caused by *Leishmania infantum*, is currently distributed in the northern suburbs of Beijing, northern Hebei, western Henan, Shanxi, northern and southern Shaanxi, southern Gansu, and northwestern Sichuan, where a sub-type

of *Ph. Chinensis* (a semiwild species) was the vector and dogs were the reservoirs with high infection rates. MT-ZVL was hypoendemic in humans and affected mainly infants under 5 years of age. The incidence rate in humans is much lower than the rate in canines, and no obvious correlation was found between the cases (Guan and Shen, 1991).

The most prominent epidemic area of DT-ZVL is located in the desert regions of southern Xinjiang, western Inner Mongolia, and northern Gansu Province, where Phlebotomus Wui (an exophilic species) was the primary vector (Guan, 1991). The incidence of the infection was sporadic and affected mainly infants under 2 years of age (Han et al., 2019). The DT-ZVL region was considered to be a natural nidus of VL, with wild animals presumed to be the source of infection (Wang et al., 2010). It had been an uncultivated desert for a considerable period of time before it was populated by immigrants who introduced agriculture cultivation and other activities. Consequently, autochthonous infantile VL occurs after immigration.

These three types of VL exhibit substantial differences in epidemiological characteristics, i.e., geographical and landscape features, ecosystem, vector species, and infectious sources (Guan et al., 2016), and therefore require targeted and timely control measures to efficiently allocate the relatively scarce resources.

In recent years, a rapid reemergence of VL has been seen in counties that had previously achieved elimination in China. It presented a significant challenge for the control of the disease. From the year 2019, public health agencies have been recruited by the government to perform epidemiological investigations on each VL case, to trace it back to their original infection place. This detailed information will facilitate more accurate risk identification than before, and analysis of epidemiological features and spatial-temporal clustering of VL.

Scholars have carried out some studies on the spatial-temporal clustering of VL. Zheng et al. (2020) executed a spatio-temporal analysis of VL in northwest China from 2004 to 2018, showing that VL is still seriously prevalent in Kashi Prefecture, Xinjiang Uygur Autonomous Region. Hao et al. (2021) conducted a spatio-temporal clustering analysis of MT-ZVL in central China. Guan et al. (2021) detected the shifting of high-incidence areas of VL through spatial-temporal distribution analysis in mainland China. However, these studies were either limited to the spatio-temporal analysis in localized provinces, or to a single epidemic type of VL, failing to elucidate the whole epidemiological features and spatial-temporal clustering of all three kinds of VL in China, so they are not conducive to guiding the prevention and control of the disease.

In this study, large-scale epidemiological investigations on each case were conducted for the first time to determine their specific infected counties. We classified VL cases into MT-ZVL, AVL, and DT-ZVL, and elucidated their epidemiological features and spatial-temporal clustering of all three different epidemic types of VL, which will be helpful for guiding the accurate prevention and control of VL.

Materials and methods

Data sources

In 2004, the web-based National Diseases Reporting Information System (NDRIS) was established in China. It is a network covering all the medical and health institutions at or above the township level. According to the Law of the Infectious Disease Control and Prevention, each medical and health institution in the country has to notify the cases of VL online within 24 h after the clinical cases are confirmed with the diagnostic criteria of VL in China (WS258-2006). Then the county CDC, where the cases are reported, will take responsibility to conduct the epidemiological investigation of individual cases in 7 days to determine whether the patient is an autochthonic case or not, and subsequently take countermeasures onsite according to relevant guidance. The information of the cases reported through NDRIS includes age, gender, occupation, current residential address, symptom onset date, diagnosis date, and therapeutic outcome, based on which demographic distribution, geographic distribution, temporal distribution, and the lag time between symptom onset and diagnosis can be analyzed.

In this study, VL case data, reported in mainland China from 2019 to 2021, were obtained from the National Notifiable Communicable Disease Reporting System (Zhang et al., 2017). Suspected cases of VL were excluded, and the revised final audit data of the cases were taken as the statistical data. The county with each case of contracted VL was selected as the sampling point for latitude and longitude coordinates.

Analysis of changes in epidemic trend of visceral leishmaniasis

All VL-related epidemiological data from 2019 to 2021 were integrated into Microsoft Excel 2016, to analyze the demographic, temporal, and geographic distribution characteristics of VL cases through descriptive epidemiological methods. Joinpoint Regression (JPR) used mathematical statistical analysis to search for turning points and divided the trend of disease incidence over a long period into several statistically significant sections for analysis. In this study, the number of VL cases in 2015–2018 was obtained from the National Notifiable Communicable Disease Reporting System (Zhou et al., 2020a). We analyzed the trends in crude rates per 100,000 people of three epidemic types of VL using the JPR Program (version 4.3.1). A *t*-test was used to judge the significant difference in the incidence trend of VL during a

certain period (Weir et al., 2016). The long-term trend of the linear segment is depicted in accordance with the best-fit result, and the annual percentage change (APC) values were calculated (Hou and Huo, 2013). The "crude rate" means crude incidence rate which refers to the frequency of new cases of a disease in a specific range of people over a period of time. It is a measurement that reflects the impact of disease on the health of the population and describes the disease distribution status.

Spatial autocorrelation analysis

Spatial autocorrelation is defined as the correlation between values of a single variable at different geographical locations using a measurement of spatial clustering based on feature locations and attribute values (Kirby et al., 2017), and the closer the things or phenomena are in spatial locations, the more similar they are. ArcGIS software is mainly used to analyze the spatial clustering of diseases. In ESRI ArcGIS software (version 10.3), global Moran's I and Getis-ORD Gi* statistical data were used for spatial autocorrelation and hotspot analysis, respectively (Bhunia et al., 2013). The Global Moran's I statistic estimates the overall degree of spatial correlation for a dataset and is calculated using the following formula (Lun et al., 2015; Engels and Zhou, 2020).

$$I = \frac{n\sum_{i=1}^{n}\sum_{j=1}^{n} w_{ij}(x_i-\bar{x})(x_j-\bar{x})}{\sum_{i=1}^{n}\sum_{j=1}^{n} w_{ij}\sum_{j=1}^{n}(x_i-\bar{x})^2}$$

where I is indicative of the Moran's I statistic, with values ranging from -1 (perfect dispersion) to 1 (perfect correlation). Negative values indicate dispersion, positive values mean clustering, and a value of zero indicates no spatial correlation (Blazquez et al., 2018).

The Getis-ord Gi* statistic is a spatial autocorrelation index, based on a weighted distance matrix, and it determines spatial clustering of locations using high (hot spot) or low values (cold spot) with statistical significance judged by Z-scores and P-values (World Health Organization [WHO], 2010; Alvar et al., 2012; Abdullah et al., 2017). It is calculated using the following formula:

$$G_i^* = \frac{\sum_{j=1}^{n} w_{ij}x_j - \bar{x}\sum_{j=1}^{n} w_{ij}}{\sqrt{\frac{[n\sum_{j=1}^{n} w_{ij}^2-(\sum_{j=1}^{n} w_{ij})^2]}{n-1}}}$$

Gi* statistics is an indicator of local aggregation. If the value of Gi* is greater than 0, it indicates that the neighbor attribute value of its spatial unit i is high; otherwise, the neighbor attribute value is low. Local spatial autocorrelation at the county level is reflected by the local indicators of spatial association (LISA). The LISA clustering map involves four patterns: high-high, high-low, low-high, and low-low.

Spatio-temporal clustering analysis

Spatio-temporal statistics were employed to describe the temporal and spatial distribution, and to detect the geographic and temporal clusters of VL during 2019–2021. A Poisson model using a retrospective space–time permutation scan statistic was used to identify spatio-temporal clusters of VL using SatScan software version 9.4.2 (Satscan). Space–time scanning, defined as a dynamic scan using a cylindrical window in dimensions of time scales and geographical locations, was also used in the identification of spatio-temporal disease clusters. The log-likelihood ratio (LLR) is used as a measure of change in the time and space in a cylindrical window (Kulldorff et al., 1998), and the relative risk (RR) was also calculated. All incidence data were processed separately for each year for which data were available, and potential spatial clusters were detected using a restricted log-likelihood ratio (RLLR). A Monte Carlo simulation was used for permutation testing with statistical significance judged by p-value. A p-$value < 0.05$ was indicative of a statistically significant cluster. The grade is based on the value of the log-likelihood ratio (LLR) to generate Grade I, Grade II, Grade III, and Grade IV cluster areas. According to the P-value and LLR value, it is determined whether there is clustering in the study area, and its exact location and risk size are also analyzed. Finally, the result was visualized through ESRI ArcGIS software (version 10.3).

Results

General status

Between 2019 and 2021, a total of 612 VL cases were reported in China, including one fatality. The annual incidence increased year by year, with 161, 214, and 237 cases reported each year, respectively. After the epidemiological investigation of individual cases, the origin of 608 cases, including 10 cases of AVL, 20 cases of DT-ZVL, and 578 cases of MT-ZVL, can be traced to the county level. However,

TABLE 1 Number of visceral leishmaniasis cases reported in China between 2019 and 2021.

Year	Endemic areas			Total	*n*/%
	AVL	DT-ZVL	MT-ZVL		
2019	0	8	150	158	25.99
2020	5	4	204	213	35.03
2021	5	8	224	237	38.98
Total	10	20	578	608	100

AVL, anthroponotic visceral leishmaniasis; MT-ZVL, mountain-type zoonotic visceral leishmaniasis; DT-ZVL, desert-type zoonotic visceral leishmaniasis.

TABLE 2 Demographic distribution of visceral leishmaniasis cases in China between 2019 and 2021.

Characters	Endemic area						Total	
	AVL		DT-ZVL		MT-ZVL			
	No. of case	*n*/%	No. of case	*n*/%	No. of case	*n*/%	No. of case	*n*/%
Age group/year								
0–2	1	10.00	7	35.00	118	20.42	126	20.72
3–6	1	10.00	0	0.00	39	6.75	40	6.57
7–14	2	20.00	0	0.00	17	2.94	19	3.13
≥15	6	60.00	13	65.00	404	69.90	423	69.57
Occupation								
Infants and young children	2	20.00	7	35.00	156	26.99	165	27.14
Students	3	30.00	0	0.00	25	4.33	28	4.61
Peasants	4	40.00	10	50.00	271	46.89	285	46.88
Workers	0	0.00	0	0.00	31	5.36	31	5.10
Officials	0	0.00	0	0.00	7	1.21	7	1.15
Housewives	0	0.00	0	0.00	39	6.75	39	6.41
Others	1	10.00	3	15.00	49	8.48	53	8.72
Gender								
Male	5	50.00	16	80.00	396	68.51	417	68.59
Female	5	50.00	4	20.00	182	31.49	191	31.41
Total	10	100.0	20	100.0	578	100.0	608	100.0

AVL, anthroponotic visceral leishmaniasis; MT-ZVL, mountain-type zoonotic visceral leishmaniasis; DT-ZVL, desert-type zoonotic visceral leishmaniasis.

the other four cases could not be traced to the source of infection and were not included in the epidemiological analysis (Table 1).

Demographic distribution

The VL cases were mainly distributed in the age group ≥ 15 years old, accounting for 69.57% (423/608) of the total cases. AVL, DT-ZVL, and MT-ZVL cases were mainly distributed in the age group ≥ 15 years old, accounting for 60.00, 65.00, and 69.90% of the total cases of each type, respectively (Table 2).

In terms of occupation, peasants are the highest risk population for VL (285/608), followed by infants and young children (165/608). For AVL, the predominant cases (4/10) were peasants. For DT-ZVL, most of the cases were peasants (10/20). For MT-ZVL, the majority of cases were also peasants (271/578) followed by infants and young children (156/578; Table 2).

In addition, the male/female ratio of VL cases in China was 421:191, and the male cases were significantly higher than the female cases. The ratio of males to females was 1:1, 1:0.25, and 1:0.46 for AVL, DT-ZVL, and MT-ZVL, respectively (Table 2).

Temporal distribution

The incidence peak varied in different types of VL. For MT-ZVL, it appeared in the period from March to May. However, no obvious peak of AVL and DT-ZVL was observed due to the low number of cases (Figure 1).

Epidemic trend of visceral leishmaniasis from 2015 to 2021

JoinPoint regression analysis showed different incidence trends in three types of VL between 2015 and 2021. The incidence of MT-ZVL increased significantly (APC = 18.94, $P < 0.05$). On the contrary, the incidence of DT-ZVL decreased rapidly (APC = -58.37, $P < 0.05$; Figure 2).

Analysis of spatial-temporal characteristics geographic distribution

During the study period, the areas with a high incidence of VL were mainly concentrated in southern Gansu, eastern Shaanxi (Huazhou, Linwei District), the Shaanxi–Shanxi border areas (Hancheng city, Hejin City, and Xiangning County), eastern Shanxi (Yangquan City), and northern Henan Province (Linzhou City). In addition, a total of 54 VL cases were detected

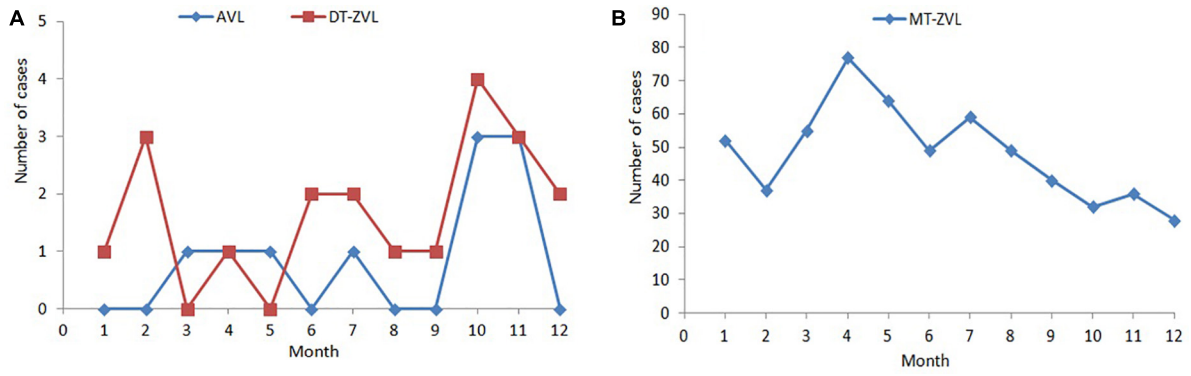

FIGURE 1
Monthly distribution of visceral leishmaniasis cases in China between 2019 and 2021. **(A)** Monthly distribution of anthroponotic visceral leishmaniasis and desert-type zoonotic visceral leishmaniasis cases. **(B)** Monthly distribution of mountain-type zoonotic visceral leishmaniasis.

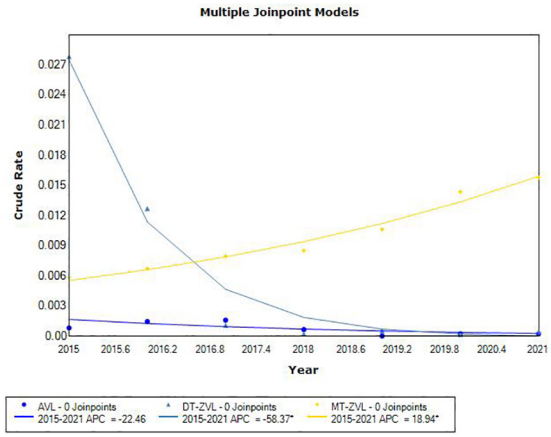

FIGURE 2
The joinpoint regression analysis for determining changes in the trend of visceral leishmaniasis incidence in China from 2015 to 2021.

in 24 resurgence counties which were mainly located in Henan (8), Shanxi (6), Hebei (5), Shaanxi (4), and Gansu (3) Provinces, and Beijing Municipality (1) (Figure 3).

Spatial autocorrelation analysis

In the last 3 years, the high-high clusters were mainly observed in the eastern Shanxi (Yangquan), the border areas of Shaanxi–Shanxi (Hancheng, Hejin, and Linfen), southern Gansu and northern Sichuan (Wudu, Zhouqu, and Jiuzhaigou), and southeast Shanxi Province (Changzhi). Since 2020, new high-high clusters began to occur in the northwestern Henan Province (Zhengzhou) and southern Xinjiang (Kashi Prefecture). In 2019, high-low clustering appeared in western Inner Mongolia (Ejina Banner) and eastern Xinjiang (Hami City), since sporadic cases were reported in these sparsely populated areas (Table 3 and Figure 4).

Hotspots analysis

Consistent with the result of spatial autocorrelation analysis, hotspots were predominantly identified in eastern Shanxi, the border areas of Shaanxi–Shanxi, southern Gansu, and northern Sichuan, as well as southeast Shanxi Province (Changzhi), from 2019 to 2021. In addition, new hotspots were identified in northwestern Henan Province and southern Xinjiang from 2020 to 2021 (Figure 5).

Spatio-temporal clustering analysis

A p-value < 0.05 was indicative of a statistically significant cluster.The result, using LLR to estimate the degree of infection clustering (Table 4), showed that 3, 4, and 3 statistically significant spatio-temporal clusters were detected at the county level each year of 2019–2021, respectively. The clusters detected in southern Gansu and northern Sichuan Province degraded from Grade I in 2019 to Grade III in 2020 and 2021. However, the clusters identified in eastern Shanxi Province (Yangquan City) upgraded from Grade II in 2019 to Grade I in 2020 and 2021. In addition, the cluster located in Shaanxi–Shanxi border areas upgraded from Grade III in 2020 to Grade II in 2021 (Figures 6–8).

Discussion

As a momentous parasitic disease, VL has been brought under control in China (Wang et al., 2000). However, with the development of society and the improvement in the ecological

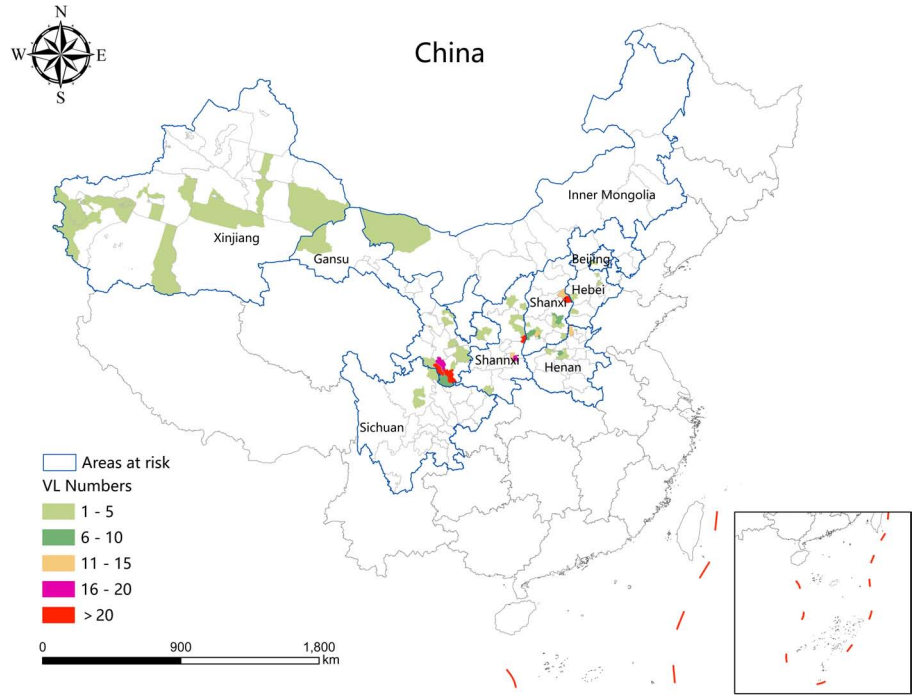

FIGURE 3
Cumulative number of visceral leishmaniasis cases between 2019 and 2021.

TABLE 3 Spatial autocorrelation analysis of visceral leishmaniasis incidence in mainland China from 2019 to 2021.

Year	Moran's *I*	Variance	*Z* value	*P*-value	Distributed
2019	0.014934	0.000002	11.017085	<0.05	Clustered
2020	0.016131	0.000001	13.618712	<0.05	Clustered
2021	0.017449	0.000002	12.151884	<0.05	Clustered

environment, the incidence of MT-ZVL rocketed rapidly and generated new hotspots in central China recently (Zhou et al., 2020a,b; Guan et al., 2021; Hao et al., 2021). Therefore, the objective of this study was to retrospectively analyze the epidemiology and spatiotemporal distribution characteristics of VL in China from 2019 to 2021, aiming to provide insights into the prevention and control of VL.

Between 2019 and 2021, a total of 612 VL cases were reported in endemic areas of China, mostly in Shanxi (48.86%), Shaanxi (19.28%), and Gansu (17.32%), rather than Xinjiang Uygur Autonomous Region which was the predominant former endemic area. It indicates that the main endemic areas shifted from the Xinjiang Uygur Autonomous Region in western China to Shanxi, Shaanxi, and Gansu Province in central China (Han et al., 2019; Zhou et al., 2020c; Guan et al., 2021). During the study period, the cases of AVL, DT-ZVL, and MT-ZVL accounted for 1.63, 3.27, and 94.44% of the total number of reported cases in the country, respectively, indicating that the predominant epidemic type of VL has changed from DT-ZVL to MT-ZVL (Han et al., 2019; Zhou et al., 2020c; Guan et al., 2021). Joinpoint regression analysis showed an upward trend (APC = 18.94, $P < 0.05$) in the incidence of MT-ZVL in China from 2015 to 2021, most notably in Shanxi and Shaanxi Provinces, revealing an observable increase in the incidence of MT-ZVL in these areas. On the contrary, the incidence of DT-ZVL decreased rapidly (APC = -58.37, $P < 0.05$). It may be due to the large-scale renovations of old housing constructions supported by poverty alleviation campaigns in rural areas, particularly in southern Xinjiang which was the most affected area in China. The greatly improved housing conditions of residents destroyed the breeding sites of peridomestic sand flies, and reduced the frequency of contact between the population and sand flies (Zhou et al., 2020c).

Three types of VL exhibit substantially different epidemiological characteristics in China (Wang et al., 2012; Zheng et al., 2017). AVL is mostly endemic in the oasis area of southern Xinjiang, and DT-ZVL is primarily located in the desert area of southern Xinjiang (Zhou et al., 2007; Wang et al., 2012). In this study, the cases of AVL and DT-ZVL were not sufficient to perform a demographic distribution analysis. For MT-ZVL, it mainly occurred in the mountainous regions of western and central China (Zheng et al., 2017; Han et al., 2019; Zhou et al., 2020b), and the principal patients were farmers, followed by infants and young children aged 6 years and below,

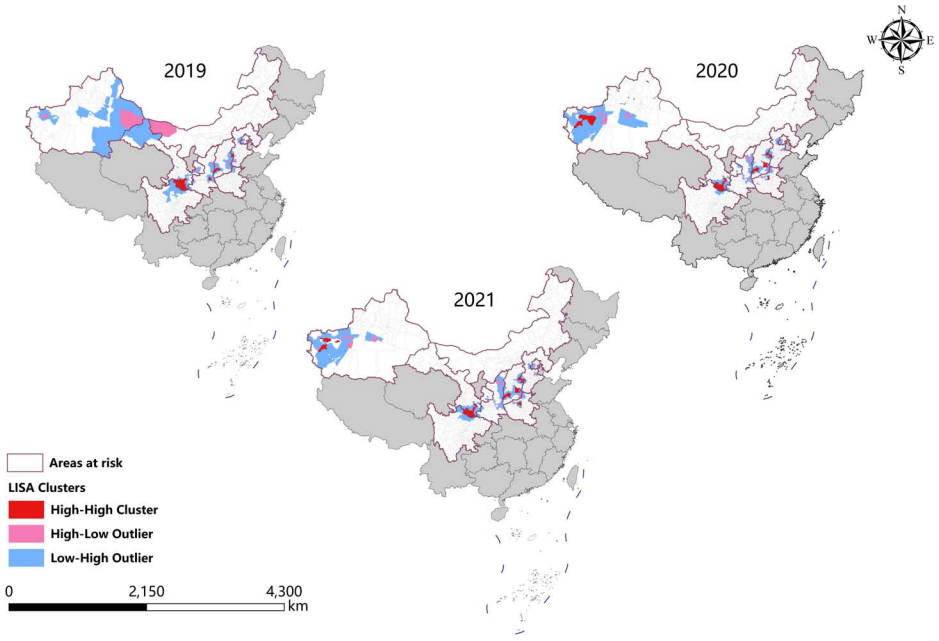

FIGURE 4
Spatial autocorrelation analysis of visceral leishmaniasis incidence in mainland China from 2019 to 2021.

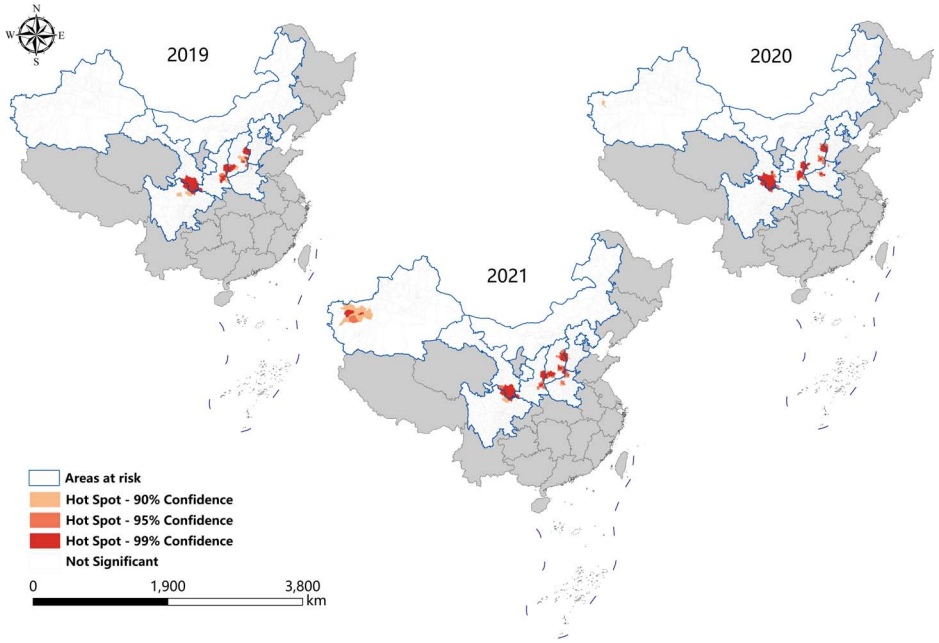

FIGURE 5
Hotspot analysis of visceral leishmaniasis incidence in mainland China from 2019 to 2021.

who constituted high-risk population who need to be targeted with prevention and control measures.

The substantial increase in the incidence of MT-ZVL in China may be related to the emergence of VL in the historically endemic areas and the formation of some new hotspot areas of MT-ZVL (Zhou et al., 2020c; Guan et al., 2021; Hao et al., 2021). Between 2019 and 2021, a total of 27 new reemerged historically endemic counties were identified that were mainly located in Shanxi, Shaanxi, Henan, and Hebei Provinces and Beijing municipality, where 54 VL cases were

TABLE 4 Spatio-temporal clustering analysis of visceral leishmaniasis incidence in mainland China from 2019 to 2021.

Year	Cluster center		Radius(km)	No. of clustered countries	No. of cases	No. of expected Cases	Relative risk	LLR	*P*-value
	Latitude	Longitude							
2019	33.628442	104.319255	83.79	5	31	0.22	174.32	125.48	<0.05
	37.851191	113.591199	14.60	4	24	0.21	137.98	92.30	<0.05
	35.574249	110.381627	0.00	1	16	0.07	234.34	70.46	<0.05
2020	37.851191	113.591199	14.60	4	56	0.28	279.77	250.25	<0.05
	35.574249	110.381627	0.00	1	19	0.10	203.22	81.12	<0.05
	33.628442	104.319255	87.13	7	22	0.49	50.65	63.54	<0.05
	33.891805	109.861779	78.36	10	9	0.80	11.71	13.74	<0.05
2021	37.925958	113.524286	36.34	5	59	0.39	207.11	246.57	<0.05
	35.591589	110.951950	52.16	10	34	0.95	42.16	91.28	<0.05
	32.942840	104.774279	50.31	2	9	0.20	47.31	25.72	<0.05

FIGURE 6
Spatio-temporal clustering analysis of visceral leishmaniasis incidence in mainland China in 2019.

notified. Several factors contributed to the reemergence of MT-ZVL. First, the number of roaming dogs increased the spread of VL from the natural nidus, where the circulation of VL was maintained in the wild animals, to the residential areas. Second, imported dogs with leishmaniasis facilitated the reestablishment of VL, while sandflies widely infested mountainous areas (Zhou et al., 2020c).

Spatial analysis showed highly consistent hotspots and clustering regions by different methods (spatial autocorrelation and hotspot analysis), particularly for the high-risk region (Grade I), revealing spatial clustering of VL in the whole country for each year of the study period. In the past 3 years, the high-incidence clusters were maintained mainly in the eastern and southeast Shanxi Province, the border of Shanxi Province, and Shaanxi Province, as well as the border of southern Gansu and northern Sichuan regions, demonstrating that although southern Gansu and northern Sichuan were still traditionally the high-incidence regions, two new higher-incidence regions have formed in Yangquan City and Hancheng City in recent years, where they have become the most predominant endemic areas of VL in China. The spatio-temporal cluster analysis also showed similar results that the clusters located in eastern Shanxi

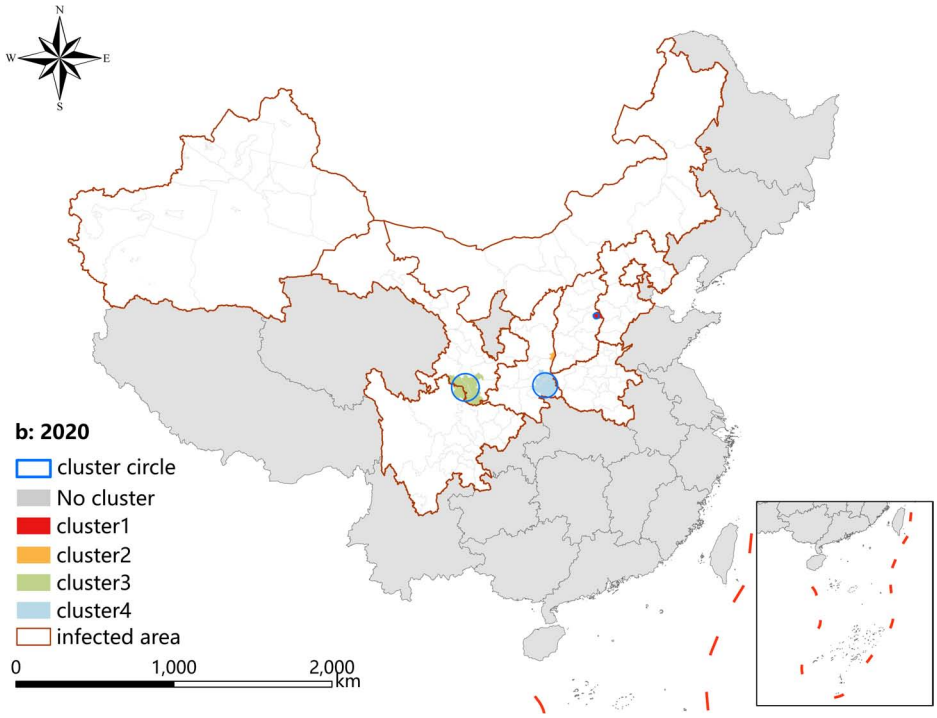

FIGURE 7
Spatio-temporal clustering analysis of visceral leishmaniasis incidence in mainland China in 2020.

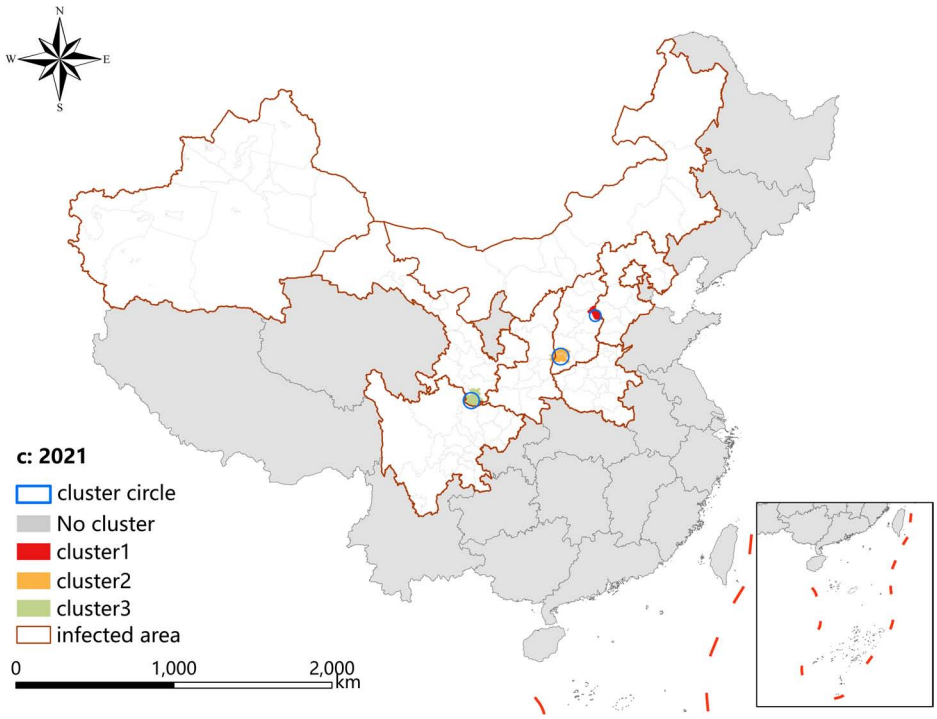

FIGURE 8
Spatio-temporal clustering analysis of visceral leishmaniasis incidence in mainland China in 2021.

Province (Yangquan City) and Shaanxi–Shanxi border areas have surpassed those located in southern Gansu and northern Sichuan, and became the top grade clusters. These areas are extension regions of the Loess Plateau and are mainly hilly settings, where the Yanshan-Taihangshan mountain deciduous broad-leaved forest ecological zone and Fenwei Basin Agro-ecological zone are located (Gong et al., 2021). The hilly and frondent environments provide a favorable habitat for a large number of wild animals and sandflies, making it a suitable natural endemic focus of MT-ZVL. Since the 1990s, with the rapid development of urbanization in China, the rural population has decreased dramatically, and the vigorous promotion of ecological protection measures in China, such as returning farmland to forests, has provided a suitable ecological environment in the countryside of these areas for the reproduction of *Phlebotomus sinensis*(*Ph. sinensis*), to the extent that the density of *Ph. sinensis* in Yangquan City has reached as high as 103 sandflies / per person per hour recently (Luo et al., 2022). At the same time, a huge number of dogs are kept in these areas as watchdogs, sheeplings, and pets, abundant of which are stray dogs with infection rates of canine visceral leishmaniasis as high as 30% (Li et al., 2021a,b). In comparison with the region of southern Gansu and northern Sichuan, these areas possess a better breeding condition for *Ph. sinensis,* such as lower elevation, higher temperature, longer active season, and more moist and loose soil, so they have higher vector capacity for the transmission of VL. Given all this, it is no surprise that Yangquan City and Hancheng City developed into the highest incidence regions of VL in China.

Since 2020, small clusters located in southern Xinjiang indicated that risks of DT-ZVL still existed in the desert areas of southern Xinjiang, so we still need to pay close attention to these areas in case of their cyclical outbreaks. Scattered small clusters that appeared in northwestern Henan, southeast Shanxi, western Hebei, and northern Beijing showed that MT-ZVL is reemerging in the Yanshan-Taihangshan mountain regions. Therefore, there is an urgent need for better cooperation among multi-sectors of government for the prevention and control of further extension of MT-ZVL in the surrounding regions.

Several phenomena discovered recently have made the prevention and control of VL more complicated. The first is that autochthonic cases, canine leishmaniasis, and *Ph. sinensis* have been detected in the densely populated main city of Yangquan, indicating that there is a trend of urbanization of MT-ZVL, which has been reported in Europe and South America (Dujardin, 2006; World Health Organization [WHO], 2002). The second is that MT-ZVL is spreading from lower latitudes to higher latitude areas in China due to global warming, and this trend has been seen in Germany and Italy (Ferroglio et al., 2005; Naucke et al., 2008), indicating further expansion of the suitable area for VL transmission. The third is that a large amount of reemerged historically endemic counties have been detected in the mountain areas of central and Western China, indicating that the ecological and geographical environment is favorable for the resurgence and even the outbreak of MT-ZVL. Therefore, control efforts should be strengthened to prevent further growth of MT-ZVL cases. Prevention of infection can be achieved by utilizing insecticide-impregnated collars, the effectiveness of which directly depends on the coverage and loss rate. Stray dogs may function as infection reservoirs if not targeted, so stray dog population management should be an important part of VL control programs (Zhou et al., 2020c). Strictly, MSZ-VL is a zoonotic disease with both dogs and wild animals serving as reservoir hosts, so it is a big challenge to completely eliminate the disease. The government must establish a collaboration mechanism with multisectors involved, such as the Centers for Disease Control and Prevention, hospitals, and Veterinary Department and Public Security Department. It is also necessary to provide long-term necessary policy and financial support for routine surveillance and control programs.

Conclusion

This study showed that the number of DT-ZVL and AVL cases decreased, while MT-ZVL cases increased quickly. Therefore, it is urgent to strengthen organizational leadership and systematically carry out necessary interventions to prevent further growth of MT-ZVL cases in hotspots and clustering areas, especially in Shanxi and Shaanxi Provinces.

Data availability statement

The raw data supporting the conclusions of this article will be made available by the authors, without undue reservation.

Author contributions

YL, ZZ, and SL: conceptualization. YL, ZWL, YH, ZZ, and SL: data curation. YL, ZWL, ZZ, and SL: formal analysis and methodology. YL, ZWL, YH, YZ, ZZ, and SL: funding acquisition. YL, LY, ZQL, and ZZ: investigation. YZ and SL: project administration and supervision. ZWL: software. YL, ZWL, and ZZ: writing of the original draft. ZZ, YZ, and SL: reviewing and editing. All authors contributed to the article and approved the submitted version.

Funding

This research was funded by the National Key Research and Development Program of China (Nos. 2021YFC2300800 and 2021YFC2300804) and the National Natural Science Foundation of China (No.32161143036).

Acknowledgments

We thank the staff of the Centers for Disease Control and Prevention and Institutes of Parasitic Diseases at different levels in China for their assistance.

Conflict of interest

The authors declare that the research was conducted in the absence of any commercial or financial relationships that could be construed as a potential conflict of interest.

Publisher's note

All claims expressed in this article are solely those of the authors and do not necessarily represent those of their affiliated organizations, or those of the publisher, the editors and the reviewers. Any product that may be evaluated in this article, or claim that may be made by its manufacturer, is not guaranteed or endorsed by the publisher.

References

Abdullah, A. Y. M., Dewan, A., Shogib, M. R. I., Rahman, M. M., and Hossain, M. F. (2017). Environmental factors associated with the distribution of visceral leishmaniasis in endemic areas of Bangladesh: Modeling the ecological niche. *Trop. Med. Health* 45:13. doi: 10.1186/s41182-017-0054-9

Akhoundi, M., Kuhls, K., Cannet, A., Votрpka, J., Marty, P., Delaunay, P., et al. (2016). A historical overview of the classification, evolution, and dispersion of *Leishmania* Parasites and Sandflies. *PLoS Negl. Trop. Dis.* 10:e0004349. doi: 10.1371/journal.pntd.0004349

Alvar, J., Velez, I. D., Bern, C., Herrero, M., Desjeux, P., Cano, J., et al. (2012). Leishmaniasis worldwide and global estimates of its incidence. *PLoS One* 7:e35671. doi: 10.1371/journal.pone.0035671

Alvar, J., Yactayo, S., and Bern, C. (2006). Leishmaniasis and poverty. *Trends Parasitol.* 22, 552–557. doi: 10.1016/j.pt.2006.09.004

Bates, P. A. (2007). Transmission of *Leishmania* metacyclic promastigotes by phlebotomine sand flies. *Int. J. Parasitol.* 37, 1097–1106. doi: 10.1016/j.ijpara

Bhunia, G. S., Kesari, S., Chatterjee, N., Kumar, V., and Das, P. (2013). Spatial and temporal variation and hotspot detection of kala-azar disease in Vaishali district (Bihar), India. *BMC Infect. Dis.* 13:64. doi: 10.1186/1471-2334-13-64

Blazquez, C. A., Picarte, B., Calderón, J. F., and Losada, F. (2018). Spatial autocorrelation analysis of cargo trucks on highway crashes in Chile. *Accid. Anal. Prev.* 120, 195–210. doi: 10.1016/j.aap.2018.08.022

Casulli, A. (2021). New global targets for NTDs in the WHO roadmap 2021-2030. *PLoS Negl. Trop. Dis.* 15:e0009373. doi: 10.1371/journal.pntd.0009373

Dujardin, J. C. (2006). Risk factors in the spread of leishmaniases: Towards integrated monitoring? *Trends Parasitol.* 22, 4–6. doi: 10.1016/j.pt.2005.11.004

Engels, D., and Zhou, X. (2020). Neglected tropical diseases: An effective global response to local poverty-related disease priorities. *Infect. Dis. Poverty* 9:10. doi: 10.1186/s40249-020-0630-9

Ferroglio, E., Maroli, M., Gastaldo, S., Mignone, W., and Rossi, L. (2005). Canine leishmaniasis, Italy. *Emerg. Infect. Dis.* 11, 1618–1620. doi: 10.3201/eid1110.040966

Gong, Y. F., Hu, X. K., Zhou, Z. B., Zhu, H. H., Hao, Y. W., Wang, Q., et al. (2021). Ecological niche modeling-based prediction on transmission risk of visceral leishmaniasis in the extension region of Loess Plateau, China. *Chin. J. Parasitol. Parasit. Dis.* 39, 1–8. doi: 10.12140/j.issn.1000-7423.2021.02.015

Guan, L. R. (1991). Current status of kala-azar and vector control in China. *Bull. World Health Organ.* 69, 595–601.

Guan, L. R., and Shen, W. X. (1991). Recent advances in visceral leishmaniasis in China. *Southeast Asian J. Trop. Med. Pub. Health* 22, 291–298.

Guan, L. R., and Wu, Z. X. (2014). Historical experience in the elimination of visceral leishmaniasis in the plain region of eastern and central China. *Infect. Dis. Poverty* 3:10. doi: 10.1186/2049-9957-3-10

Guan, L. R., Qu, J. Q., and Chai, J. J. (2000). Leishmaniasis in China-present status of prevalence and some suggestions on its contro. *Endem. Dis. Bull.* 15, 49–52.

Guan, L. R., Zhou, Z. B., Jin, C. F., Fu, Q., and Chai, J. J. (2016). Phlebotomine sand flies (Diptera: Psychodidae) transmitting visceral leishmaniasis and their geographical distribution in China: A review. *Infect. Dis. Poverty* 5:15. doi: 10.1186/s40249-016-0107-z

Guan, Z., Chen, C., Huang, C. Y., Zhang, H. W., Zhou, Y. Y., Zhou, Y. Q., et al. (2021). Epidemiological features and spatial–temporal distribution of visceral leishmaniasis in mainland China: A population-based surveillance study from 2004 to 2019. *Parasit. Vectors* 14:517. doi: 10.1186/s13071-021-05002-y

Han, S., Wu, W. P., Xue, C. Z., Ding, W., Hou, Y. Y., Feng, Y., et al. (2019). Endemic status of visceral leishmaniasis in China from 2004 to 2016. *Chin. J. Parasitol. Parasit. Dis.* 37, 189–195. doi: 10.12140/j.issn.1000-7423.2019.02.013

Hao, Y. W., Hu, X. K., Gong, Y. F., Xue, J. B., Zhou, Z. B., Li, Y. Y., et al. (2021). Spatio-temporal clustering of Mountain-type zoonotic visceral leishmaniasis in China between 2015 and 2019. *PLoS Negl. Trop. Dis.* 15:e0009152. doi: 10.1371/journal.pntd.0009152

He, K. Z., Wang, J., and Huang, C. M. (1959). *Compilation of investigation data of Kala-azar [M]*. Shanghai: Shanghai Science and Technology Press, 34–42.

Hou, N., and Huo, D. (2013). A trend analysis of breast cancer incidence rates in the United States from 2000 to 2009 shows a recent increase. *Breast Cancer Res. Treat.* 138, 633–641. doi: 10.1007/s10549-013-2434-0

Killick-Kendrick, R. (1990). Phlebotomine vectors of the leishmaniases: A review. *Med. Vet. Entomol.* 4, 1–24. doi: 10.1111/j.1365-2915.1990.tb00255.x

Kirby, R. S., Delmelle, E., and Eberth, J. M. (2017). Advances in spatial epidemiology and geographic information systems. *Ann. Epidemiol.* 27, 1–9. doi: 10.1016/j.annepidem.2016.12.001

Kulldorff, M., Athas, W., Feuer, E., Miller, B. A., and Key, C. R. (1998). Evaluating cluster alarms: A space-time scan statistic and brain cancer in Los Alamos, New Mexico. *Am. J. Public Health* 88, 1377–1380. doi: 10.2105/ajph.88.9.1377

Li, F., Feng, Y., Yu, D. W., Yang, C. M., Yang, J. K., Liu, L. L., et al. (2021a). Survey on *Leishmania* infection in dogs in Wenxian county and Diebu county of Gansu Province in 2019. *Chin. J. Endem.* 40, 460–463. doi: 10.3760/cma.j.cn231583-20200806-00216

Li, F., Yu, D. W., Yang, C. M., Feng, Y., Yang, J. K., Liu, L. L., et al. (2021b). Analysis of the environment factors affecting *Leishmania* infection in dogs in two counties of Gansu Province. *Chin. J. Zoonoses* 37, 763–766. doi: 10.3969/j.issn.1002-2694.2021.00.079

Lun, Z. R., Wu, M. S., Chen, Y. F., Wang, J. Y., Zhou, X. N., Liao, L. F., et al. (2015). Visceral leishmaniasis in China: An endemic disease under control. *Clin. Microbiol. Rev.* 28, 987–1004. doi: 10.1128/CMR.00080-14

Luo, Z. W., Zhou, Z. B., Gong, Y. F., Feng, J. X., Li, Y. Y., Zhang, Y., et al. (2022). Current status and challenges of visceral leishmaniasis in China. *Chin. J. Parasitol. Parasit. Dis.* 40, 146–152. doi: 10.12140/j.issn.1000-7423.2022.02.003

Naucke, T. J., Menn, B., Massberg, D., and Lorentz, S. (2008). Sandflies and leishmaniasis in Germany. *Parasitol. Res.* 1, S65–S68. doi: 10.1007/s00436-008-1052-y

Satscan. *A Poisson model using a retrospective space–time permutation scan statistic was used to identify spatio-temporal clusters of VL using SatScan software version 9.4.2 (Satscan)*. Available online at: http://www.satscan.org/ [Google Scholar].

Wang, C. J., Xiong, G. H., and Guan, L. R. (2000). Achievement on the epidemiology and control of kala-azar in China. *Chin. J. Epidemiol.* 21, 51–54. doi: 10.3760/j.issn:0254-6450.2000.01.017

Wang, J. Y., Cui, G., Chen, H. T., Zhou, X. N., Gao, C. H., and Yang, Y. T. (2012). Current epidemiological profile and features of visceral leishmaniasis in people's republic of China. *Parasit. Vectors* 5:31. doi: 10.1186/1756-3305-5-31

Wang, J. Y., Gao, C. H., Yang, Y. T., Chen, H. T., Zhu, X. H., Lv, S., et al. (2010). An outbreak of the desert sub-type of zoonotic visceral leishmaniasis in Jiashi. Xinjiang Uygur Autonomous Region, People's Republic of China. *Parasitol. Int.* 59, 331–337. doi: 10.1016/j.parint.2010.04.002

Wang, Z. J., and Wu, Z. J. (1956). *Kala-azar [M]*. Beijing: People's Health Publisher, 433–609.

Weir, H. K., Johnson, C. J., Ward, K. C., and Coleman, M. P. (2016). The effect of multiple primary rules on cancer incidence rates and trends. *Cancer Causes Control* 27, 377–390. doi: 10.1007/s10552-016-0714-9

World Health Organization [WHO] (2002). Urbanization: An increasing risk factor for leishmaniasis. *Wkly. Epidemiol. Rec.* 44, 365–370.

World Health Organization [WHO] (2010). *Control of the Leishmaniasis*. Geneva: WHO, 5–12.

World Health Organization [WHO] (2020). *Leishmaniasis*. Geneva: World Health Organization.

World Health Organization [WHO] (2022). *Leishmaniasis*. Geneva: World Health Organization.

Xiong, G. H., Hu, Y. D., and Guan, L. R. (1976). The natural nidus of kala-azar in northwest China. *J. Control Res. Epidemiol. Dis.* 1, 63–68.

Zhang, H., Wang, L., Lai, S., Li, Z., Sun, Q., and Zhang, P. (2017). Surveillance and early warning systems of infectious disease in China: From 2012 to 2014. *Int. J. Health Plann. Manage.* 32, 329–338. doi: 10.1002/hpm.2434

Zheng, C. J., Wang, L. P., Li, N., and Zhou, X. N. (2020). Visceral leishmaniasis in northwest China from 2004 to 2018: A spatio-temporal analysis. *Infect. Dis. Poverty* 9:165. doi: 10.1186/s40249-020-00782-4

Zheng, C. J., Xue, C. Z., Wu, W. P., and Zhou, X. N. (2017). Epidemiological characteristics of kala-azar disease in China, during 2005–2015. *Chin. J. Epidemiol.* 38, 431–434. doi: 10.3760/cma.j.issn.0254-6450.2017.04.004

Zhou, X. N., Lv, S., Yang, G. J., Kristensen, T. K., Bergquist, N. R., Utzinger, J., et al. (2007). Spatial epidemiology in zoonotic parasitic diseases: Insights gained at the 1st international symposium on geospatial health in Lijiang. China, 2007. *Parasit. Vectors* 2:10. doi: 10.1186/1756-3305-2-10

Zhou, Z. B., Lyu, S., Zhang, Y., Li, Y. Y., Li, S. Z., and Zhou, X. N. (2020c). Visceral leishmaniasis—China, 2015-2019. *CCDC Wkly.* 2, 625–628. doi: 10.46234/ccdcw2020.173

Zhou, Z. B., Wang, J. Y., Gao, C. H., Han, S., Li, Y. Y., Zhang, Y., et al. (2020d). Contributions of the national institute of parasitic diseases to the control of visceral leishmaniasis in China. *Adv. Parasitol.* 110, 185–216. doi: 10.1016/bs.apar.2020.04.003

Zhou, Z. B., Li, Y. Y., Zhang, Y., and Li, S. Z. (2020a). Prevalence of visceral leishmaniasis in China during 2015–2018. *Chin. J. Parasitol. Parasit. Dis.* 38, 339–345. doi: 10.12140/j.issn.1000-7423.2020.03.013

Zhou, Z. B., Li, Y. Y., Zhang, Y., and Li, S. Z. (2020b). Prevalence of visceral leishmaniasis in China in 2019. *Chin. J. Parasitol. Parasit. Dis.* 38, 602–607. doi: 10.12140/j.issn.1000-7423.2020.05.012

frontiers | Frontiers in Microbiology

TYPE Review
PUBLISHED 25 January 2023
DOI 10.3389/fmicb.2023.1076947

OPEN ACCESS

EDITED BY
Jian Li,
Hubei University of Medicine, China

REVIEWED BY
Paul R. Gilson,
Burnet Institute,
Australia
Karine Gaelle Le Roch,
University of California,
Riverside, United States

*CORRESPONDENCE
Li Yu
✉ lilyyu33@126.com
Chao Zhang
✉ happy2008con@aliyun.com

†These authors have contributed equally to this work

SPECIALTY SECTION
This article was submitted to Infectious Agents and Disease, a section of the journal Frontiers in Microbiology

RECEIVED 24 October 2022
ACCEPTED 03 January 2023
PUBLISHED 25 January 2023

CITATION
Quansah E, Chen Y, Yang S, Wang J, Sun D, Zhao Y, Chen M, Yu L and Zhang C (2023) CRISPR-Cas13 in malaria parasite: Diagnosis and prospective gene function identification. *Front. Microbiol.* 14:1076947. doi: 10.3389/fmicb.2023.1076947

CRISPR-Cas13 in malaria parasite: Diagnosis and prospective gene function identification

Elvis Quansah[1†], Yihuan Chen[2†], Shijie Yang[2†], Junyan Wang[2], Danhong Sun[2], Yangxi Zhao[3], Ming Chen[2], Li Yu[1*] and Chao Zhang[1*]

[1]Anhui Provincial Laboratory of Microbiology and Parasitology, Anhui Key Laboratory of Zoonoses, Department of Microbiology and Parasitology, School of Basic Medical Sciences, Anhui Medical University, Hefei, China, [2]The Second Clinical Medical College, Anhui Medical University, Hefei, China, [3]The First Clinical Medical College, Anhui Medical University, Hefei, China

Malaria caused by *Plasmodium* is still a serious public health problem. Genomic editing is essential to understand parasite biology, elucidate mechanical pathways, uncover gene functions, identify novel therapeutic targets, and develop clinical diagnostic tools. Recent advances have seen the development of genomic diagnostic technologies and the emergence of genetic manipulation toolbox comprising a host of several systems for editing the genome of *Plasmodium* at the DNA, RNA, and protein level. Genomic manipulation at the RNA level is critical as it allows for the functional characterization of several transcripts. Of notice, some developed artificial RNA genome editing tools hinge on the endogenous RNA interference system of *Plasmodium*. However, *Plasmodium* lacks a robust RNAi machinery, hampering the progress of these editing tools. CRISPR-Cas13, which belongs to the VI type of the CRISPR system, can specifically bind and cut RNA under the guidance of crRNA, with no or minimal permanent genetic scar on genes. This review summarizes CRISPR-Cas13 system from its discovery, classification, principle of action, and diagnostic platforms. Further, it discusses the application prospects of Cas13-based systems in *Plasmodium* and highlights its advantages and drawbacks.

KEYWORDS

malaria, *Plasmodium*, CRISPR-Cas system, CRISPR-Cas13 diagnosis, CRISPR-Cas13 RNA editing

1. Introduction

Malaria has been a major global health problem for humans throughout their history and is a leading cause of mortality across many tropical and subtropical countries (Hemingway and Bates, 2003; Cowman et al., 2016; Monroe et al., 2022). Malaria control efforts have been undermined by the decline in the effectiveness of the primary malaria-figurehting tools, increasing resistance to treated-insecticide nets and anti-malarial drugs, and no effective vaccine (Olotu et al., 2013; Haldar et al., 2018; Memvanga and Nkanga, 2021). Spotlights from the 2022 world malaria report by WHO showed that cases of malaria increased from 245 million in 2020 to 247 million in 2021, although malaria-related deaths slightly decreased from 625,000 to 619,000 (World Health Organization, 2022). The etiological agent of malaria, *Plasmodium,* mainly thrives in human and mosquito hosts. Of all *Plasmodium* parasites, five species are responsible for global malaria infections in humans: *Plasmodium falciparum*, *Plasmodium vivax*, *Plasmodium malariae*, *Plasmodium ovale*, and *Plasmodium knowlesi* (Lalremruata et al., 2017; Memvanga and Nkanga, 2021; Sato, 2021).

Microscopic examination of Giemsa-stained peripheral blood smears has over the years been the "gold standard" for the diagnosis of malaria (Oboh et al., 2021; Fitri et al., 2022). However, its

usefulness has been confronted with a host of challenges as results generated from microscopy are dependent on the technical know-how of the microscopist, the quality of blood sample, the parasite density, and the subjectivity of results interpretation (Barber et al., 2013; Berzosa et al., 2018; Ospina-Villa et al., 2018), indicating a void in diagnosis and the need to develop new effective tools. The *Plasmodium falciparum* genome encompasses 22.8 mega-bases with an average gene density of 1 gene per 4,338 base pairs—distributed among a total of 14 chromosomes (Gardner et al., 2002). Almost two-thirds of the proteins coded by these genes are unique to *Plasmodium* (Gardner et al., 2002) providing peculiar targets for molecular detection. In an attempt to fill the gaps in malaria diagnosis, several molecular diagnostic tools have been established to target various unique genes in *Plasmodium*. Molecular diagnosis notwithstanding remains a big huddle as the performance of these tools varies depending on the epidemiological setting (Oboh et al., 2018).

Interestingly, 74% of the total genes in *Plasmodium* remain functionally uncharacterized despite the availability of the parasite's genome (Tan and Mutwil, 2020). To address this paucity, forward and reverse functional genomic tools have been developed to manipulate the parasites' genomes to functionally characterize these genes (Zhang et al., 2014; Walker and Lindner, 2019; Cárdenas et al., 2022; Thiam et al., 2022). In particular, RNA-targeting tools hold great potential to understand the biological functions of genes and identify novel anti-malarial targets and effective vaccines (Nisbet et al., 2016; Liu et al., 2019). RNA level manipulation/editing affects the timing and/or level of transcription and alters the stability of gene expression, thereby offering scientists the platform to study the basic cellular functions of mRNAs, and non-coding RNAs (ncRNA) such as small nuclear RNA (snRNA), ribosomal RNA (rRNA), microRNA (miRNA), and piwi interaction RNA (piRNA; Briquet et al., 2022).

CRISPR (Clustered Regularly Interspaced Short Palindromic Repeats)-Cas (CRISPR-associated protein) system is found in archaea and bacteria—responsible for coordinating defense against foreign genetic elements (Mojica et al., 2000; Marraffini, 2015; Moon et al., 2019). The CRISPR-Cas system is a powerful biological tool whose usefulness scientists have been unlocking in the last few decades. It is a double-edged tool that scientists have applied for both diagnosis and gene editing to unravel the function of many genes at the DNA and RNA levels in several organisms (Graham and Root, 2015; Hartenian and Doench, 2015; Zhang D. et al., 2021). Currently, the CRISPR-Cas system is structurally and functionally diverse and divided into 2 classes, 6 types, and more than 30 subtypes. The first class includes type I, type III, and type IV, and the second class includes type II, type V, and type VI (O'Connell, 2019). The small size, atypical hypercompact architecture, and high efficiency of class 2 multi-domain Cas proteins have made them a prime focus of many researchers compared to class I proteins (Cao et al., 2022; Liu and Pei, 2022). Of these, the majority of research in the past decade has focused on CRISPR-Cas9 belonging to the type II category (Atkins et al., 2021), and its properties have been harnessed for gene knockdown, gene editing, epitranscriptomics modification, and sensing of RNA targets (Zhang H. et al., 2021). CRISPR-Cas13 systems—which constitute the type VI group—have been demonstrated to generally lack DNase (Deoxyribonuclease) activity, but are fixated on RNA cleaving, and could offer distinct targeting advantages to RNA. Thus they represent a clinically promising platform capable of efficiently characterizing genes at the RNA level (Gaj, 2021).

In this review, we have summarized the CRISPR-Cas13 system from its discovery, classification, principle of action, and its application in malaria diagnosis. Given that malaria parasites lack relevant interference systems (Baum et al., 2009) thereby limiting the use of endogenous interference-dependent RNA editing systems, we will further discuss the application prospects of Cas13 in *Plasmodium* at the RNA level.

2. Discovery of CRISPR-Cas systems, especially for Casl3

In 1987, Yoshizumi Ishino of Osaka University in Japan detected regularly spaced direct palindromic repeats downstream of the stop codon of the iap (isoenzymes of alkaline phosphate) genes of *E. coli* K-12 cells (Ishino et al., 1987). This event provided the blueprint for the discovery of new CRISPR-Cas systems, ushering scientists into a new era of gene editing and genomic engineering. At the time, the relevance of these repeat sequences remained obscure. Mojica and his team detected a similar sequence in phylogenetically distinct organisms: *Haloferax mediterranei* and *Haloferax volcanii* of the Archaea domain (Mojica et al., 1993). They later postulated that these repeats are involved in replicon partitioning (Mojica et al., 1995). In 2002, substantial progress was made by Jansen and collaborators resulting in the official naming of this mysterious repeat as CRISPR which is now commonly accepted by the scientific community (Jansen et al., 2002). Soon after, spurred on by his previous findings, a major leap toward the understanding of the function of CRISPR was made by Mojica and his team (Mojica et al., 2005). They pointed out that the spacer sequence in CRISPR had homology with foreign phages or plasmids, and that the virus could not infect cells carrying homologous spacer sequences, but was easy to invade cells without spacer sequences. Against this background, it was posited that CRISPR might participate in the immune function of bacteria and it requires a precise sequence match between the spacer and the target sequence of the virus (Mojica et al., 2005; Lander, 2016). The functionality of the second component of the CRISPR-Cas complex, CRISPR-associated protein (Cas), was computationally demonstrated later by Marakova and collaborators as a composite of the DNA repair machinery (Makarova et al., 2006). In a later study by Horvath, he noticed a palindromic repeat that coded for an endonuclease protein, Cas9, and intimated that the protein cleaves viral DNA and thus grants immunity to the host bacteria (Horvath and Barrangou, 2010). A few years later, in 2012, Doudna and Charpentier's team discovered the third component of the CRISPR system—the trans-acting crRNA (tracrRNA) which oversees the maturation of precursor crRNA into crRNA and also directs Cas9 cleavage of dsDNA (Jinek et al., 2012). Subsequent development saw the exploitation of the CRISPR-Cas system as a genomic editing tool. In 2013, the gene-editing tool CRISPR-Cas9 was applied in mammalian cells and became popular all over the world, because of its novelty, efficiency, and versatility (Shmakov et al., 2015).

Different from CRISPR-Cas9, which binds and cuts at the DNA level, as shown in Figure 1, in 2016, deeply searching for microbial genome data, it was found that a new CRISPR-Cas system effector protein, named c2c2 (now referred to as Casl3a), could specifically bind and cut RNA under the guidance of crRNA, and regulate the activity of genes at the RNA level (Abudayyeh et al., 2016). This opened up a new avenue for editing targeted RNA. In 2017, through rigorous biochemical experiments and genetic computations, Zhang Feng's team identified two new Cas13 subtypes, Cas13b and Cas13c

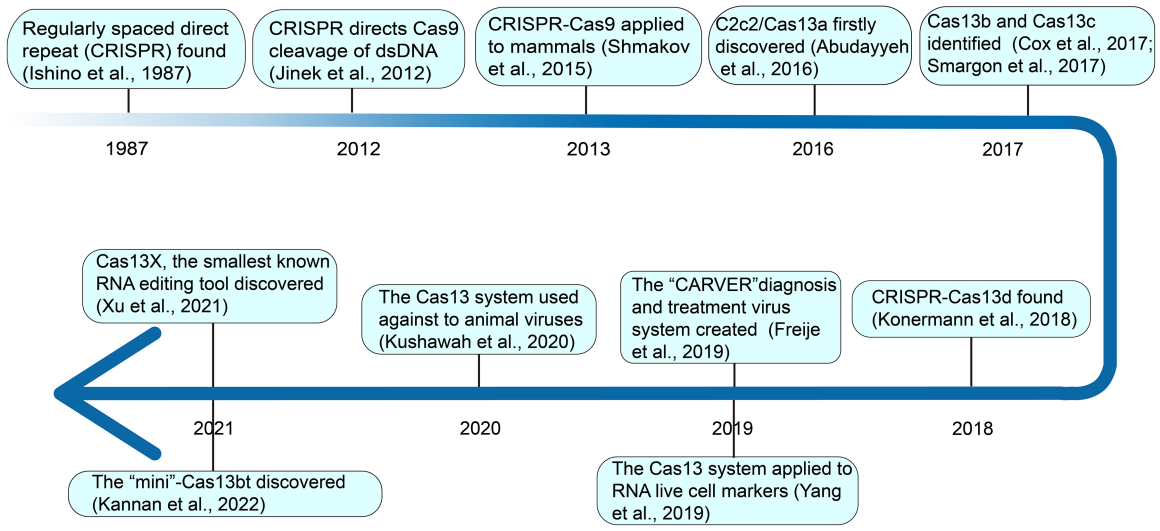

FIGURE 1
The discovery and application timeline of CRISPR-Cas13 system.

(Cox et al., 2017; Smargon et al., 2017). Subsequent investigation revealed that CRISPR-Cas13 systems uniquely lack the third component, tracrRNA (Yan et al., 2019). Going further, they demonstrated that Cas13b could be applied to precisely edit the full length of transcript harboring deleterious mutations in mammalian cells (Cox et al., 2017). In 2018, Konermarm et al. analyzed a prokaryote genome and discovered the CRISPR-Casl3d system, which has the smallest molecular weight of all CRISPR-Casl3 effectors, and was suitable for virus vectors, and had great application potential *in vivo* (Konermann et al., 2018). Through the exploration of bulk metagenomic data, Hu et al. (2022) identified novel hypercompact Cas13 systems and therein named them Cas13e, Cas13f, Cas13g, Cas13h, and Cas13i. However, their functional relevance remains to be described in future studies.

Since its advent, Cas13 has been widely used in various fields. For example, in 2019, Zhang Feng's team created a new CRISPR-Cas13 system called CARVER (Cas13-assisted Restriction of Viral Expression and Readout) antiviral, which combines the antiviral activity of Cas13 and its diagnostic capabilities, as a promising system for the diagnosis and treatment of viral infections (Freije et al., 2019). In the same year, Chen Lingling's group used the CRISPR-Casl3d system for RNA live cell labeling (Yang et al., 2019). In 2020, Gopal Kushawah and others used CRISPR-Cas13d to induce high-efficiency nucleoprotein degradation in animal embryos, providing new conditions for animal antiviral research (Kushawah et al., 2020). More recently, in 2021, Yang Hui's team identified Cas13X and Cas13Y from high-salinity samples and designed an RNA interference experiment for Cas13X.1 in a mammalian cell line (Xu et al., 2021). During the same period, Zhang Feng's team discovered "Mini"-Cas13bt, functionalizing Cas13bt through the use of adenosine and cytosine deaminase (Kannan et al., 2022).

Collectively, the catalog of CRISPR-Cas13 systems keeps expanding as novel types and orthologs are being described in current studies. At present, based on phylogeny, this important class of effector proteins is categorized into VI-A (Cas13a), VI-B (Cas13b), VI-C (Cas13c), VI-D (Cas13d; Zhang H. et al., 2021), VI-E to I (Cas13e-Cas13i; Hu et al., 2022), and the latest CRISPR-Cas13 system like Cas13X, Cas13Y (Xu et al., 2021) and Cas13bt (Kannan et al., 2022). Here, the classification and average size of Cas13 proteins, which have been widely used in various fields, were summarized (Figure 2).

3. The components of the CRISPR-Cas13 system

As shown in Figure 3, using Cas13a as an example, the CRISPR-Cas13 system mainly consists of crRNA (CRISPR RNA) and CRISPR-related nucleases (Cas1, Cas2, and Cas13). The biology of these components is briefly discussed below.

3.1. CRISPR-related nuclease (Cas13)

Cas13a has a bi-lobed structure comprising a 'Nuclease' (NUC) lobe and a 'Recognition' (REC) lobe. These two domains form a cavity that accommodates the crRNA. NUC Lobe contains two distinct but functionally linked endonuclease sites—Higher Eukaryotes and Prokaryotes Nucleotide-binding Domain 1 and 2 (HEPN-1 and HEPN-2) separated by a basic linker/Helical-3 domain, and a Helical-2 domain (Zhu and Huang, 2018; O'Connell, 2019; Figure 3A). The REC lobe encompasses the N-terminal domain (NTD) and the Helical-1 domain (Liu and Pei, 2022). The HEPN-1 acts as a scaffold that links NUC and REC lobes (Zhang et al., 2018). The formation of the spacer-protospacer binary complex is driving the recognition of the stem-loop (5'handle) of crRNA by NTD. In Cas13d effectors, the α1 component of the HEPN1 and the C-terminal of HEPN-2 domains form a catalytic site that primes the spacer-protospacer binary complex for both targeted and collateral cleavage (Zhang et al., 2018). The 5′ end repeat region of crRNA binds to the REC leaf so that the guide region sequence of crRNA is guided into the cavity, formed in the NUC area (nuclease lobe). The NUC leaf has two different domains, NUC1 and NUC2. The function of these two domains is to "sandwich" the guide region of crRNA, thereby forming a plane, allowing the complementary sequence of the target ssRNA (single-stranded RNA) to bind for cleavage.

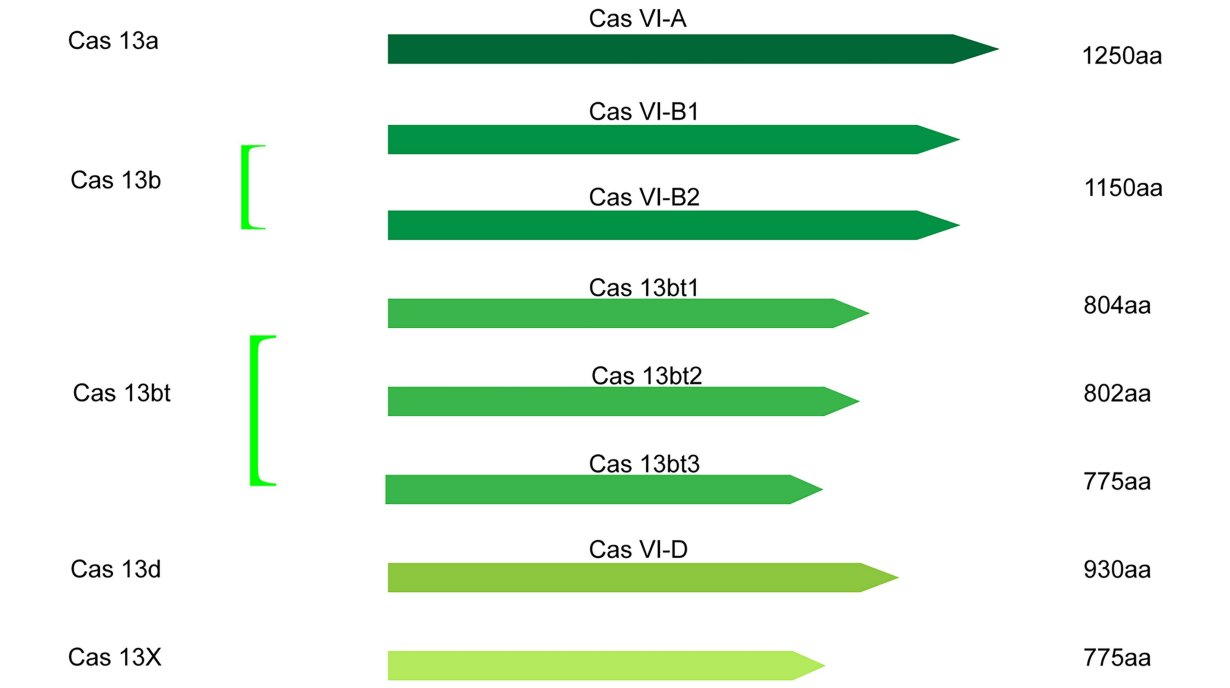

FIGURE 2
The classification and average size of Cas13 proteins with having been widely used in various fields.

3.2. CRISPR RNA

A typical crRNA landscape includes a promoter within an AT-rich leader sequence adjacent to the first CRISPR repeat (Jiang and Doudna, 2015). CRISPR RNA (crRNA) is synthesized from the transcriptions of the CRISPR array into a long precursor crRNA (pre-crRNA) and subsequently processed enzymatically by removing the repeat region and part of the spacer sequence into a smaller matured crRNA (Kenchappa et al., 2013; Jiang and Doudna, 2015). The crRNA is composed of a single variable spacer flanked by short direct CRISPR repeat sequences at the 5′ and 3′ ends. The 5′ end direct repeat (5′ handle) morphs into a short hairpin loop (handle) with a guide segment which when in complex with Cas13 proteins is sandwiched by the HEPN2 of the Nuclease domain and NTD of the Recognition domain (Zhu and Huang, 2018). Downstream, the hairpin loop is a 3–5 nucleotide sequence which promotes firm binding and Cas13 catalytic activities (O'Connell, 2019). The spacer region of crRNA is clamped between the Helical-1 and Helical-2 domains (Zhang et al., 2018). Embedded at the center of the 3′ end of the guide sequence is a "seed" region that directs the scanning-for-target process and ensures firm hybridization with the protospacer of target RNA (Zhu and Huang, 2018; Bandaru et al., 2020). Mismatch at the middle of the seed region of Cas13a maximally reduces the binding affinity, while mismatches elsewhere result in a subtle reduction in binding affinity (Tambe et al., 2018). Thus precise complementarity, particularly in the middle of the seed region, is key for target binding and subsequent cleavage. Of importance, a single base-pair mismatch is sufficient to attenuate Cas13a HEPN activation despite the firm binding affinity between crRNA and target RNA (Tambe et al., 2018).

4. The mechanism of action of the CRISPR-Cas13 system

During bacteria immune surveillance and cleavage of exogenous RNA, CRISPR-Cas13 requires a guide from a matured crRNA (Bayoumi and Munir, 2021; Krohannon et al., 2022). At a glance, this seems a challenge since CRISPR type V1 lacks Cas6 or Cas5d endonuclease activity for processing pre-crRNA into matured crRNA (crRNA biogenesis). Now, it has been shown that Cas13 performs both crRNA biogenesis and RNA cleavage employing two chemically and mechanistically distinct mechanisms for both tasks (East-Seletsky et al., 2016). Using three purified recombinant Cas13 proteins, it was revealed that Cas13 cut at two to five nucleotides upstream of the target pre-crRNA to produce a 60–66 nucleotide-long matured crRNA (Huynh et al., 2020). The resulting matured crRNA contains a single spacer sequence (20–30 nucleotide long) that is complementary to the target RNA sequence and a direct repeat region (Ai et al., 2022).

A generalized molecular action of CRISPR-Cas13 is briefly described in Figures 3B,C. CRISPR-Cas13-mediated cleavage is initiated as pre-crRNA recognizes and binds to the REC leaves of Cas13 to form an intermediate transition state complex. This event induces a conformational change in the conserved residues between Helical-1 and HEPN2 in the NUC region (Zhang et al., 2019). HEPN-2 provides an acid–base catalytic site that catalyzes the processing of pre-crRNA into a matured crRNA (Zhang et al., 2019). Upon complementary pairing between the matured crRNA and target ssRNA, a conformational rearrangement is triggered, as the catalytic HEPN domain of HEPN-2 moves close to the catalytic HEPN domain of HEPN-1 (Zhang et al., 2019). The two HEPN domains combine to form a single catalytically competent active site—which subsequently cleaves the RNA target sequence (Makarova et al., 2017; O'Connell, 2019).

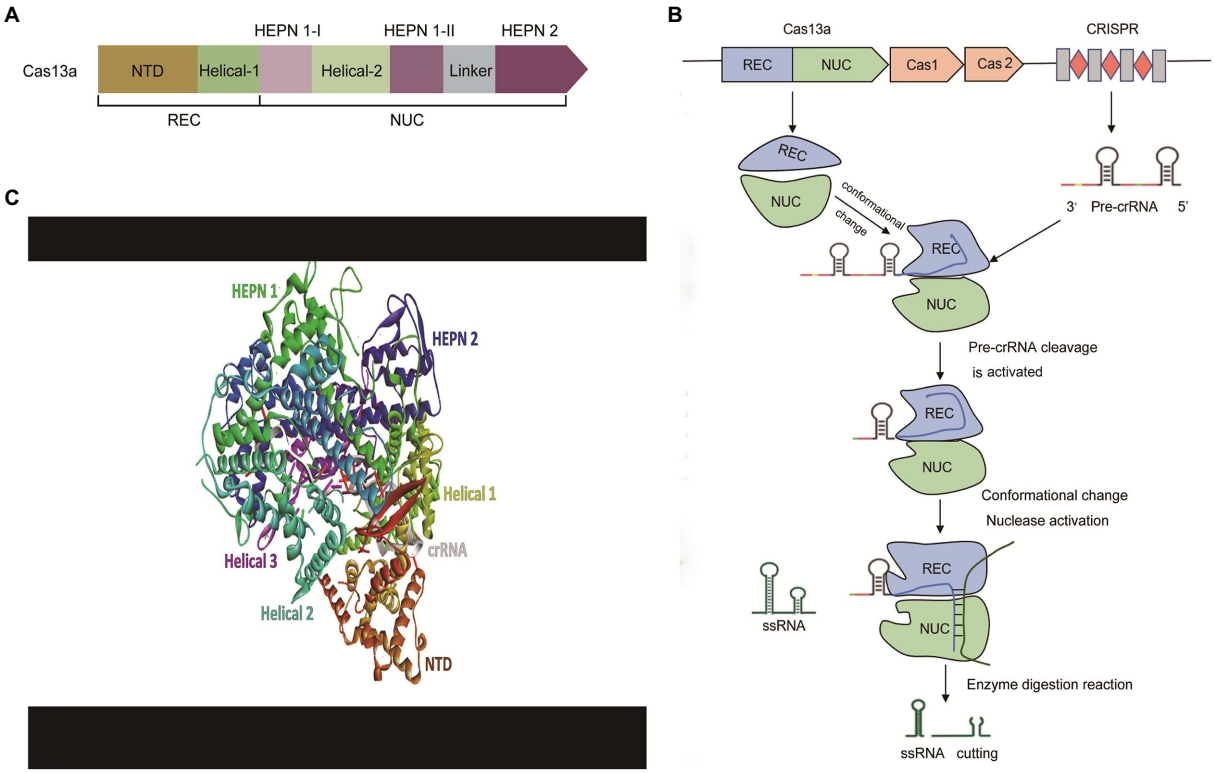

FIGURE 3
The effector modules and mechanism of action of the CRISPR-Cas13a. **(A)** The architecture of effector modules of Cas13a. Cas13a has a bi-lobed structure comprising a 'Nuclease' (NUC) lobe and a 'Recognition' (REC) lobe. NUC Lobe contains two distinct but functionally linked endonuclease sites—Higher Eukaryotes and Prokaryotes Nucleotide-binding Domain 1 and 2 (HEPN-1 and HEPN-2) separated by a basic linker/Helical-3 domain, and a Helical-2 domain. The REC lobe encompasses the N-terminal domain (NTD) and the Helical-1 domain, **(B)** The mechanism of action of the CRISPR-Cas13a. The pre-crRNA recognizes and binds to the REC leaves of Cas13a. Next, Cas13a processes its pre-crRNA to form a stable crRNA-Cas13a complex. Subsequently, the target ssRNA is recruited to the crRNA-Cas13a complex to undergo base-complementary pairing with the matured crRNA resulting in the activation of the Cas13a endonuclease enzyme. Finally, the activated catalytic domain of Cas13cleaves the target sequence, and **(C)** Crystal structure of Cas13a complex with crRNA. REC, Recognition lobe; NUC, Nuclease lobe; CRISPR, Clustered Regularly Interspaced Short Palindromic Repeats; Pre-crRNA, Precursor CRISPR RNA; ssRNA, Single-stranded RNA.

4.1. The collateral damage pitfall of Cas13 system

The utility of CRISPR-Cas13 has been hampered by its promiscuous degradation of unintended RNA targets by the active HEPN domain resulting in collateral damage (Abudayyeh et al., 2016; Smargon et al., 2017; Yan et al., 2018; Ai et al., 2022). This setback seems not typical of all Cas13 systems, but it has been observed in Cas13a of *Leptotrichia shahii* (Shmakov et al., 2015) and *Leptotrichia buccalis* (East-Seletsky et al., 2016). It is expected that any efficient Cas13-based editing platform should invariably eliminate the Cas13 off-target activity to increase specificity. To avert this undesirable property, different engineering strategies have been adopted. In one recent study, the truncation of the crRNA spacer length led to the loss of off-target catalytic activities but maintained target binding specificity, and this property was harnessed to effectively knock down multiple transcripts with reduced collateral damage (Abudayyeh et al., 2017). In a different study, transgenic constructs of cas13 (a-d) variants with altered codons were shown to be specific with very low tolerance to off-RNA targets but high fidelity in Drosophila SG4_CD cells (Huynh et al., 2020). Interestingly, Lin et al. have discovered and described novel anti-CRISPR-Cas13a inhibitors (arcVI-A) capable of attenuating RNA targeting and editing in human cells. The application of these molecules could modulate precise RNA editing and also inhibit unintended cleavage (Lin et al., 2020). Altogether, it appears that the off-target property of Cas13 effector proteins is amendable and thus could be efficiently used to edit RNA targets.

5. CRISPR-Cas13 system as a diagnostic tool

As described earlier, the promiscuous nuclease activity of some Cas13 systems possess a central challenge in their application. This challenge is not essentially negative but opens up new ways for nucleic acid detection if it is carefully harnessed and appropriately applied. This is what the recently developed SHERLOCK platform does. As shown in Figure 4, the SHERLOCK CRISPR tool combines an isothermal nucleic acid amplification technique, and recombinant polymerase amplification technique (RPA), and leverages the indiscriminate endonuclease activity of Cas13 effector protein for clinical diagnosis of diseases (Kellner et al., 2019; Mahas et al., 2021; Mustafa and Makhawi, 2021). While many Cas13 orthologs have been identified and functionally characterized in different bacteria, LwCas13a is the most widely used type in the SHERLOCK applications (Patchsung et al., 2020). Recent advances have

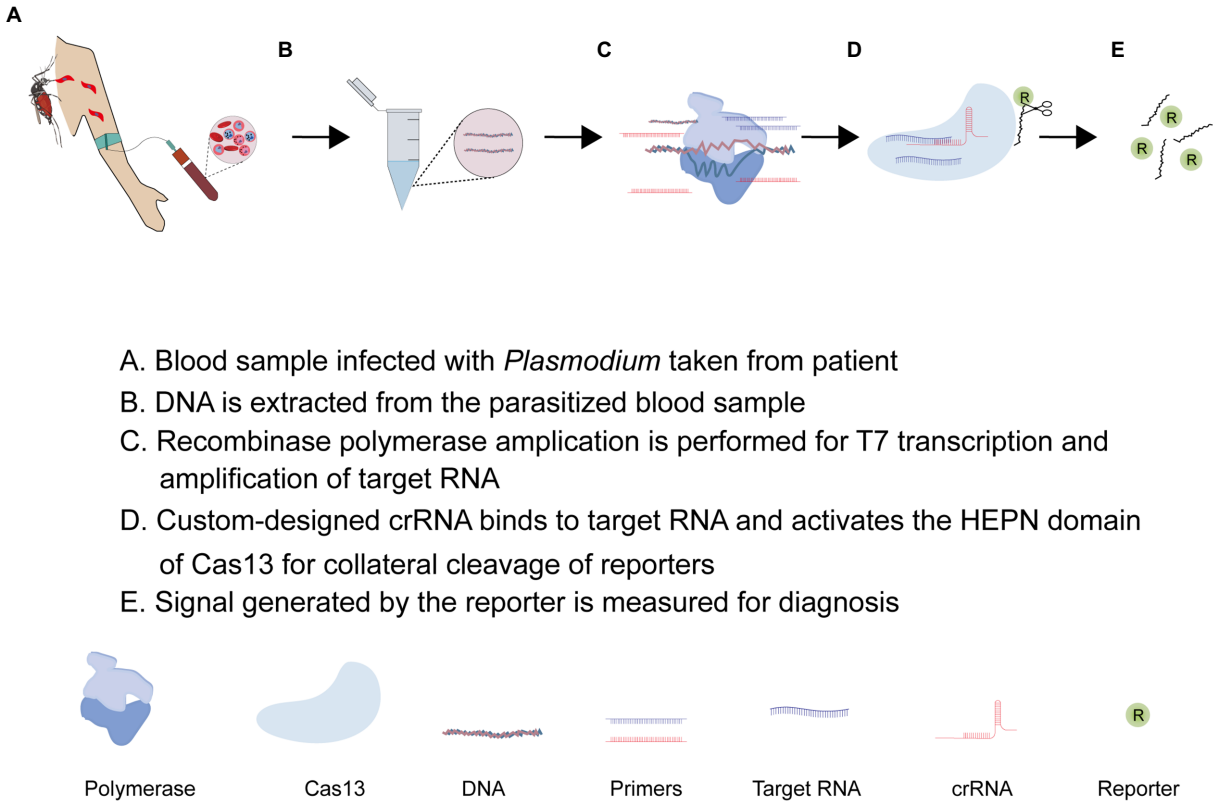

FIGURE 4
The flow chart of CRISPR-Cas13 genetic testing tool "SHERLOCK."

seen LwCas13a-based SHERLOCK adopted in different ways (Patchsung et al., 2020). Regardless of the approach, the Cas13-based SHERLOCK platform essentially makes use of: (1) target sequence found in the test sample; (2) T7 RNA polymerase promoter and T7 RNA polymerase for RPA; (3) RNA reporters or sensors sensitive to Cas13 collateral activities; and (4) custom-designed crRNA linked to a programmed Cas13 effector protein for guided detection of target RNA and collateral cleavage of reporters, respectively. The SHERLOCK protocol usually starts with the pre-amplification of the DNA/RNA using RPA primers and the conversion of target dsDNA into ssRNA using the T7 transcriptase enzyme. This is followed by the detection of RNA targets with custom Cas13-crRNA. The custom-designed crRNA is generally composed of a variable spacer region complementary to the target RNA, a constant region that recruits Cas13a, and a T7 promoter sequence that enhances *in vitro* transcription (Gootenberg et al., 2017; Kellner et al., 2019). Once the spacer of the crRNA aligns with the target RNA, the constant region binds to the Cas13 effector protein resulting in the activation of the off-target HEPN endonuclease activity of Cas13 which consequently cleaves an RNA-tagged reporter to generate a signal for detection (Rajan et al., 2022). To improve signal generation, Yang et al. (2022) engineered a LwCas13a with improved collateral activity by inserting different RNA-binding domains into a unique site within the HEPN domain. The SHERLOCK application has been developed into a cheap and convenient paper-based CRISPR-Cas13-base diagnosing assay capable of detecting and differentiating RNAs of viruses (Zika virus and Dengue virus) and genotyping DNA of bacteria (*Escherichia coli* and *Pseudomonas aeruginosa*; Gootenberg et al., 2017; Myhrvold et al., 2018; Manning et al., 2021).

5.1. CRISPR-Cas13-based diagnosis of *Plasmodium* infection

Besides Cas13a, Class II type V CRISPR-Cas12a (cpf1) has been described to possess a weak collateral activity making it useful in detecting target ssDNA or dsDNA (Nguyen et al., 2020; Kim et al., 2021; Lv et al., 2021; Wei et al., 2021). A Cas12-based SHERLOCK platform has been employed in detecting and differentiating *Plasmodium* species. In 2020, Lee and his team adopted this application to detect and distinguish *P. falciparum* (Pfr364 gene)-, *P. vivax* (18s rRNA)-, *P. ovale* (18s rRNA)-, and *P. malaria* (18s rRNA)-specific dsDNA using programmed Cas12a (cpf1) effector proteins (Lee et al., 2020). Noteworthy, the T7 transcription step is skipped, allowing for the direct detection of amplified targeted DNA instead of RNA. This assay could detect less than two parasites per microliter of blood and showed high sensitivity and specificity in differentiating clinical samples of *P. falciparum* and *P. vivax* with 100% accuracy. Based on these data, a field-applied diagnostic method for asymptomatic carriers was established for a rapid clinical diagnosis of non-*falciparum* malaria and low-density *P. falciparum* infections (Lee et al., 2020). Of notice, their fluorescence read-out assay demonstrated a relatively low fluorescence signal at 50 attomolar (30 parasites per microliter) possibly due to the weak collateral activity of Cas12a. Against this backdrop, the strong collateral activity of Cas13a provides an appropriate alternative to efficiently detect *Plasmodium* infections using the Cas13-based SHERLOCK platform. An additional advantage of Cas13 is its auto-catalytic ability to process its pre-cRNA without the involvement of tracrRNA and thus allows for the use of multiple guide crRNA in a single streamlined multiplex assay. Accordingly, these

properties have been leveraged for a triple-purpose assay involving *Plasmodium* detection, species differentiation, and drug resistance genotyping using custom-designed crRNA with spacers specific to *P. falciparum*, *P. vivax,* and *dhps* (dihydropteroate synthetase) variants in a single multiplex assay (Cunningham et al., 2021). In briefly, 30–35 nucleotide-long RPA primers tagged with T7 promoter sequences were used to amplify *a dhps* sequence and/or *Plasmodium* 18S ribosomal RNA sequence conserved across human-infecting *Plasmodium* species to generate a short dsDNA. The assay utilized a custom-designed 67 nucleotide-long crRNA composed of a variable spacer region complementary to the target RNA, a constant region that recruits LwCas13a, and a T7 promoter sequence to enhance *in vitro* transcription. Using T7 polymerase, the resulting short dsDNA of the target sequence is transcribed into ssRNAs *in vitro*. Once the spacer of the crRNA aligns with the target RNA, the constant region binds to LwCas13a resulting in the activation of the off-target endonuclease activity of LwCas13a which consequently cleaves a fluorescent or colorimetric reporter RNA to generate a signal. Predefined nucleotide variations in *dhps* are known to confer resistance to sulfadoxine or sulfadoxine-pyrimethamine (SP; Okell et al., 2017), which are the main anti-malarial drug for intermittent preventive treatment in pregnant women. Thus, when the Cas13a-based SHERLOCK platform is improved to a point-of-care diagnostic tool, it will inevitably benefit the quest to track the continuous evolution of anti-malarial drug resistance in endemic areas.

6. Gene manipulating tools at the RNA level in *Plasmodium*

Most eukaryotic organisms possess an evolutionarily conserved mechanism—RNAi, which regulates genes post-transcriptionally and guards against intrinsic and extrinsic threats by degrading the coding regions of target genes. Typical RNAi-related genes such as Dicer and Argonaute have been identified in *Plasmodium*, but they lack endogenous RNAi machinery, which hinders gene annotation (Mueller et al., 2014). In this regard, non-canonical RNAi systems have been designed to target RNAs in *Plasmodium*. In 2020, Franziska Hentzschel's team designed the rodent *Plasmodium berghei* to express a minimal, unconventional RNAi mechanism that only requires Ago2 (argonaute 2) and a modified short loop RNA, AgoshRNA. The non-canonical AgoshRNA for target genes structurally encompasses a 5 bp hairpin loop (CTTCA) with a sense sequence (having G-U and G-C mismatches initial and terminal codons, respectively) and an antisense sequence attached to either end of the construct. By integrating an AgoshRNA episomally maintained in plasmid into an RNAi-competent *Plasmodium*, they achieved an efficient gradient gene-knockout of several genes although its application is currently limited to the erythrocytic-stage parasites (Hentzschel et al., 2020).

To circumvent the occurrence of cell death when essential genes are detected for editing/manipulation, conditional manipulating tools such as glms ribozyme system and the Tet operating system have been designed to manipulate the RNA of *Plasmodium* (Prommana et al., 2013; Briquet et al., 2022). In Tet systems, the promoter of the target gene is replaced with unstable multiple tetracycline operating sites that bind to a transactivator domain for transcription. This system can be turned off or on depending on the presence or absence of anhydrotetracycline (de Koning-Ward et al., 2015). The glms/riboswitch system is designed to integrate an auto-cleaving ribozyme gene into the target gene sequence which upon expression cleaves the UTR region of the target mRNA to induce degradation (Prommana et al., 2013; de Koning-Ward et al., 2015).

6.1. RNA editing advantages of Cas13

In the last decade, steady progress has been made in the use of CRISPR-Cas13 systems to systematically interrogate the genome of several different organisms. For instance, Cas13 (Cas13a, Cas13d, cas13X, and cas13Y) RNAi systems have been applied for functional characterization of various genes in zebrafish embryos, medaka embryos, mouse embryos, and other mammalian cells demonstrating their practicability in varied cell lines (Cox et al., 2017; Konermann et al., 2018; Kushawah et al., 2020; Xu et al., 2021). Although the CRISPR-Cas13-based system has not been widely applied to RNAs of *Plasmodium* it would be of great importance if adapted to *Plasmodium* owing to the advantages discussed below.

The CRISPR-Cas9 system is by far the most established CRISPR-Cas system for interrogating *Plasmodium*'s genome at the DNA level (Crawford et al., 2017; Nishi et al., 2021). Based on the observation that the HNH catalytic domain of Cas9 is homologous to RNA-cleaving HNH, Cas9 has been repurposed to cleave RNA targets (O'Connell et al., 2014) adding to its already known DNA cleaving property. It has however been shown that the binding affinity and programmable cleaving of target RNA by Cas9 require the presence of sequence-specific PAM-presenting oligonucleotide as a separate DNA, an additional component that is not needed when using Cas13 (O'Connell et al., 2014). In the absence of PAM-presenting oligonucleotides, Cas9 only exhibits steric inhibition of protein translation with no obvious effect on mRNA architecture or levels indicating a limitation to its transcript editing prospects (Liu et al., 2016). Like Cas13, Cas9 is also limited by its unexpected off-target effects (Fu et al., 2013, 2014; Yang et al., 2014) although there have been attempts to experimentally avert this undesirable catalytic property (Fu et al., 2014; Kleinstiver et al., 2016; Slaymaker et al., 2016). Due to the affinity of HNH and RuvC domains of Cas9 to DNA, off-target mutagenesis by Cas9 could imprint unwanted permanent genomic scars on genomic DNA sites having corresponding RNA PAMs or any proximal endogenous locus (Haeussler et al., 2016; Ayabe et al., 2019), which may hinder attempts to associate intended genetic edits to observed experimental results. Cas13 is not constrained by PAM sequence at the target locus (Cox et al., 2017; Tang et al., 2021), making it a flexible tool to use compared to Cas9. Another impediment to the use of Cas9 is that, for DNA targets, edits cannot be made distal (50–100 bp away from) to the point of cut (Elison and Acar, 2018). It is however unknown if this limitation also exists during RNA editing with Cas9. Another peculiar RNA editing advantage of Cas13 is its auto-catalytic ability of Cas13 to process its pre-crRNA, which allows for streamlined delivery of targeting crRNAs for large-scale mRNA transcript editing without loss of specificity and efficiency (Gootenberg et al., 2018; Ackerman et al., 2020; Li et al., 2022; Thakku et al., 2022). This property has already been applied to manipulate a host of genes in live cells (East-Seletsky et al., 2016).

Although the already discussed RNAi systems (Dicer, Argonaute, Tet, and glms ribozyme systems) have great potential, Cas13-based RNA systems have advantages: (1) it does not depend on the cellular RNAi machinery; (2) it is not prone to toxicity from exogenous additives (as in the case of the use of glucosamine-6-phosphate in the glms system); and (3) it can be used in strains the lacks inducible expression systems.

Cas13-based systems however have drawbacks. Firstly, many investigators have shown that the effectiveness of Cas13a, Cas13b, and Cas13d is dependent on the length of crRNA (Abudayyeh et al., 2017; Bandaru et al., 2020; Huynh et al., 2020). It has been demonstrated that the ideal crRNA length is 23–30 nucleotides and any guide shorter or longer may have compromised effectiveness (Abudayyeh et al., 2017; Bandaru et al., 2020; Huynh et al., 2020). Secondly, it has been revealed that crRNA designed to target intronic splice sites or 3' UTR regions activates lower cleavage activity relative to crRNAs targeting coding regions (Wessels et al., 2020). Thus, an improvement on the combined HEPN catalytic activity of HEPN-1 and HEPN-2 may be required when targeting splice sites or 3' UTR regions. Thirdly, effective cleavage of mRNAs of essential genes may be toxic to the host cell (Abudayyeh et al., 2016). Lastly, the delivery of less compact Cas13 effectors is derailed by the size of the RNA editors as they exceed the loading capacity of the adeno-associated virus vectors (Hu et al., 2022). Thus, the size of Cas13 effectors is a critical factor to consider in future applications of the CRISPR-Cas13 genomic tool in *Plasmodium*.

6.2. Prospects of Cas13 for manipulating RNAs in *Plasmodium*

As earlier mentioned, >70% of *Plasmodium*'s genome remains functionally uncharacterized. It has indeed been posited that the sparse application of functionally characterizing genetic tools in *Plasmodium* forecasts that this proportion is unlikely to change if no new methods are developed (Le Roch et al., 2003). In light of this, the addition of the promising CRISPR-Cas13-based tools to the existing tool set for investigating the parasites' genome will be immensely useful (Figure 5). Below we discuss the prospects of emerging Cas13 systems in alternative RNA editing and identify "hotspots" in *Plasmodium* research where they could be adapted.

6.2.1. Hybrid Cas13-based systems as prospective tools for single-base editing in *Plasmodium*

Recent advances have seen the design of hybrid Cas13-based editing platforms capable of performing single-nucleotide editing in target locus. Generally, as shown in Figures 5A,B, these platforms make use of genetically engineered (mutated) Cas13 effectors (Cas13b or Cas13x.1) fused or tethered to other catalytic domains. One such application is RNA Editing for Programmable A-to-I Replacement version 1/2 (REPAIRv1 and REPAIRv2). The REPAIR systems introduce dead Cas13 effectors (Cas13 with a mutation in HEPN lacking RNase activity) fused with either endogenous exogenous adenosine deaminase acting on RNAs (ADARs) catalytic domain, which substitute adenosine for inosine into target transcripts and thereby stalls translation (Cox et al., 2017). Following the advent of the REPAIR systems, a new platform, RNA Editing for Specific C-to-U Exchange (RESCUE) system and its variants which performs both A-to-I and C-to-U RNA editing have been designed and applied to several genes (Abudayyeh et al., 2019; Li et al., 2021). These systems utilize the fusion of Cas13b with ADR2dd to create synergistic effectors with precise single-base editing capabilities (Abudayyeh et al., 2019; Li et al., 2021).

Although the development of these platforms is still at the embryonic stage (Li et al., 2021; Tang et al., 2021), they may be useful for the study of single-nucleotide polymorphism (SNP) variants and point mutations in *Plasmodium* if expanded and their efficiencies are improved. In *Plasmodium* parasites, there is a wealth of SNPs that could be used as proxies for genomic surveillance of drug resistance, and tracking the movement of *Plasmodium* strains on a global scale (Campino et al., 2011). For instance, a genome-wide integrated analysis of just three parasite strains from the Netherlands, Honduras, and Indochina unraveled 27,000 SNP of which many were uncharacterized (Miles et al., 2016). While few SNPs have been used to genotypically distinguish between parasites originating from different geographical locations, their phenotypic relevance is unknown (Campino et al., 2011; Bankole et al., 2018), suggesting the need to apply novel tools like REPAIR and RESCUE for characterization.

6.2.2. Cas13, a prospective tool for characterizing alternative polyadenylation in *Plasmodium*

Alternative polyadenylation (APA) is conserved post-transcriptional machinery that promotes transcriptome and proteome diversity through the cleaving of alternative polyadenylation sites, followed by the adding of poly (A) tail to generate isoforms differing at the 3′ ends (Arora et al., 2022). APA shields mRNA from enzymatic degradation and regulates nuclear exports and translation (Zhang Y. et al., 2021). Depending on the site of cleavage, APA events could result in the inclusion or exclusion of exon (exon skipping) and intron retention (Yang et al., 2021) which consequently contributes to a diverse protein repertoire. Employing long-read sequencing techniques, Yang et al. (2021) identified 1,555 alternative polyadenylation sites in transcripts of asexual blood stages of *Plasmodium* parasites. Further results from this team indicated that 369 (23.7%) of the total transcripts harbored more than five (5) poly (A) sites. A different study showed the presence of AT-rich hexamer, AAUAUU, which putatively serves as a positive signal for polyadenylation in *Plasmodium falciparum* (Stevens et al., 2018). Nonetheless, the relevance of these APA sites and their corresponding isoforms remains largely unexplored in *Plasmodium* perhaps due to the unavailability of suitable tools for APA perturbation. Further, the types of APA (tandem 3' UTR APA, alternative terminal exon APA, intronic APA, internal exon APA) events in *Plasmodium* remains largely unclassified. Recently, as shown in Figure 5C, Tian et al. (2022) developed a CRISPR-dCas13 system (CRISPR iPAS) that can be used to functionally characterize APA sites. They achieved this by combining EGFP-tagged dCasf13b from *Porphyromonas gulae* with crRNA-targeting upstream UGUA element or AAUAAA polyadenylation sites core regulation region to block access by the polyadenylation machinery. They demonstrated that, in HEK293T cells, CRISPR iPAS could regulate tandem 3'UTR, alternative terminal exon, and intronic polyadenylation site APA types with high specificity and efficiency. This system could be harnessed to study isoforms of genes that modulate drug resistance, transcriptional and post-transcriptional modification, and cellular differentiation in *Plasmodium* parasites.

6.2.3. Cas13, a prospective tool for characterizing alternative splicing in *Plasmodium*

As established, alternative splicing plays an essential role in stage-specific cellular differentiation and the transition of the *Plasmodium* parasite from the sexual stage to the asexual stage and vice versa (Yeoh et al., 2019; Yang et al., 2021). It has been demonstrated to be a common phenomenon that usually controls sexual dimorphisms in *Plasmodium* species. Alternative splicing results in the generation of many different matured mRNA transcripts from a single pre-mRNA transcript; creating an important layer of regulation at the RNA level (Iriko et al., 2009). Indeed, a myriad of investigators had sought to quantify and explore the role of alternative splicing in essential genes of *Plasmodium* using RNA

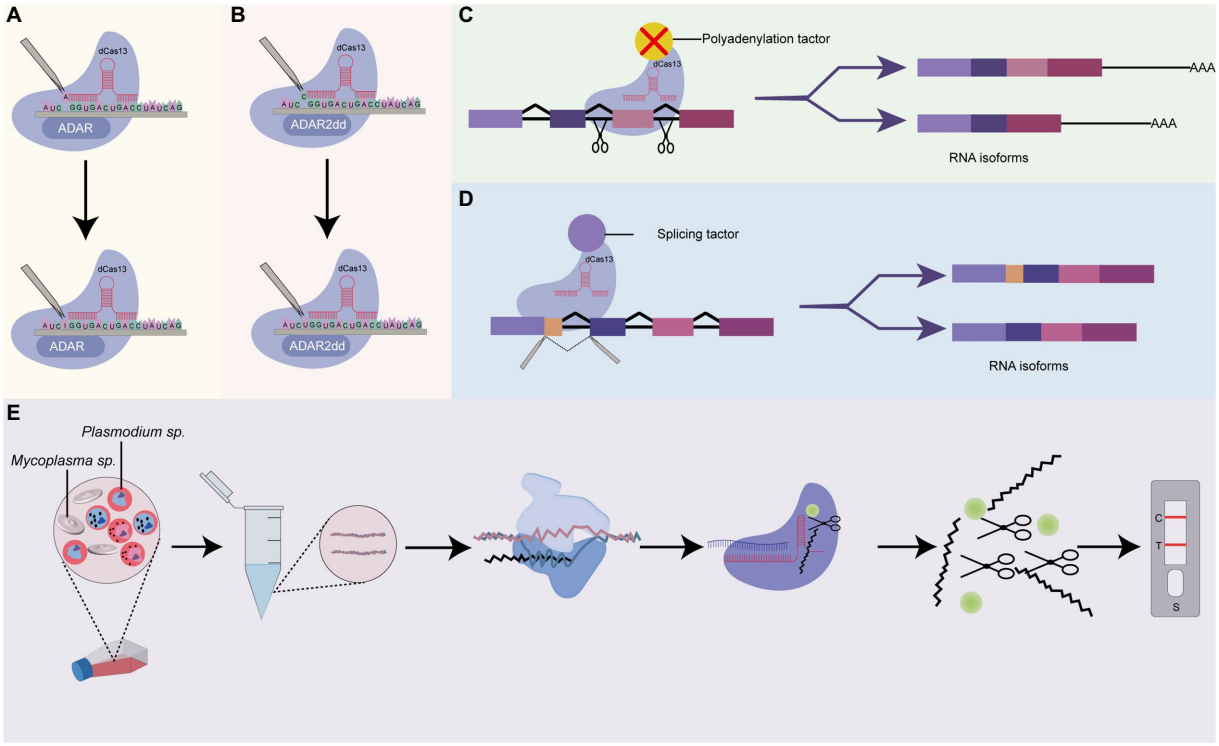

FIGURE 5
Prospects of Cas13-base systems for RNA editing in *Plasmodium*. **(A)** dCas13 tethered to ADARs for a single-nucleotide base editing in RNA. This system uses dCas13 effector-deaminase acting on RNAs (ADARs) domains fusion, for crRNA-guided programmable adenosine to inosine RNA editing, **(B)** dCas13 tethered to ADAR2dds for a single-nucleotide base editing in RNA. The dCas13 effector is fused with deaminase acting on RNA2 (ADAR2dd) for programmable Cytosine to Uracil RNA editing, **(C)** dCas13 tethered to a polyadenylation site or a polyadenylation factor. This system uses a dCas13 effector fused with an alternative splicing factor or AAUAAA polyadenylation sites to block access by the polyadenylation machinery. Depending on the positions of the polyadenylation site, it could be used to include or exclude specific exons during pre-mRNA processing, **(D)** dCas13 tethered to a splicing factor. This system could be used to characterize the functions of RNA isoforms of a specific gene, and **(E)** Cas13 system for rapid detection of *Mycoplasma* sp. as a contaminant in *Plasmodium* culture. CRISPR-Cas13 can be used to target *Mycoplasma* sp. AfterT7 transcription and amplification of target *Mycoplasma* sp. RNA, the transcript is subjected to CRISPR-Cas13 detection. The binding of crRNA to the target RNA activates the solvent-exposed HEPN site for non-specific cleavage of nearby RNA-linked reporters to emit a signal. The resulting signal could be measured using lateral flow detection with antigen-labeled reporters.

sequencing techniques (Sorber et al., 2011; Gabriel et al., 2015; Turnbull et al., 2017; Yeoh et al., 2019). Excitingly, recent advances in Cas13-based systems have seen the development of programmable mRNA splicing tools that can be used to efficiently characterize splicing events in *Plasmodium*. Generally, these Cas13-based splicing systems are designed to fuse dCas13 effectors with distinct splice elements for isoform perturbation (Figure 5D). *Via* this approach, *Konermann* and co-workers achieved >80% exon exclusion efficiency in human cells using multiple crRNAs targeting intronic branch point, splice acceptor site, exonic splice enhancer, and splice donor (Konermann et al., 2018). Interestingly, this system was adopted differently by Du et al. (2020). In their study, they successfully engineered a CRISPR artificial splicing factor by fusing dCas13 orthologs with splicing regulatory domains. They designed two crRNA that simultaneously target different positions on the sequence element which efficiently excludes or includes exons of interest during the processing of pre-mRNA. These programmable systems could be adapted to interrogate the role of alternative splicing in ApiAP2 transcriptional factors and how they contribute to the stage-dependent functions of ApiAP2 members in *Plasmodium* species (Quansah et al., 2022). Conceptually, these systems could be adapted for a bulk interrogation of alternative splicing targeting many isoforms of ApiAP2 genes in a single assay.

6.2.4. Cas13, a prospective tool for detecting contaminants in cell cultures

Contaminants such as *Mycoplasma* usually remain inconspicuous in continuous *Plasmodium* cultures but substantially alter the property and behavior of infected cells making them potential significant confounders in experimental studies (Malave-Ramos et al., 2022). There is the prospect of repurposing the off-target property of Cas13 for detecting contaminants in long-term *in vitro Plasmodium* cell cultures (Figure 5E). Cas12a system has already been applied in *Mycoplasma* as a diagnostic tool proving the applicability of the CRISPR-Cas system in *Mycoplasma*. The relatively robust collateral activity of Cas13 over Cas12 makes it a more robust tool for the detection of *Mycoplasma* contaminants in *in vitro Plasmodium* cultures.

7. Conclusion

This review has summarized the discovery, classification, principle of action, and diagnostic platforms of CRISPR-Cas13 system. Further, it has shown that Cas13-based systems could be prospectively used for single-base editing, and characterizing

alternative polyadenylation or alternative splicing in *Plasmodium* and detecting contaminants in *in vitro Plasmodium* cultures. The promising CRISPR-Cas13-based tools will be immensely useful for investigating the parasites' genome.

Author contributions

CZ: conceptualization. YC, EQ, CZ, and LY: writing–original draft. CZ, LY, DS, YC, EQ, SY, JW, YZ, and MC: writing– review and editing. All authors contributed to the article and approved the submitted version.

Funding

This work was supported by the National Natural Science Foundation of China (82072304 and 81871671 to LY), grants from Scientific Research of BSKY from Anhui Medical University (XJ201807 to CZ), and the Foundation of Education Department of Anhui province (KJ2021A0213 to CZ).

Conflict of interest

The authors declare that the research was conducted in the absence of any commercial or financial relationships that could be construed as a potential conflict of interest.

Publisher's note

All claims expressed in this article are solely those of the authors and do not necessarily represent those of their affiliated organizations, or those of the publisher, the editors and the reviewers. Any product that may be evaluated in this article, or claim that may be made by its manufacturer, is not guaranteed or endorsed by the publisher.

References

Abudayyeh, O. O., Gootenberg, J. S., Essletzbichler, P., Han, S., Joung, J., Belanto, J. J., et al. (2017). RNA targeting with CRISPR–Cas13. *Nature* 550, 280–284. doi: 10.1038/nature24049

Abudayyeh, O. O., Gootenberg, J. S., Franklin, B., Koob, J., Kellner, M. J., Ladha, A., et al. (2019). A cytosine deaminase for programmable single-base RNA editing. *Science* 365, 382–386. doi: 10.1126/science.aax7063

Abudayyeh, O. O., Gootenberg, J. S., Konermann, S., Joung, J., Slaymaker, I. M., Cox, D. B., et al. (2016). C2c2 is a single-component programmable RNA-guided RNA-targeting CRISPR effector. *Science* 353:aaf5573. doi: 10.1126/science.aaf5573

Ackerman, C. M., Myhrvold, C., Thakku, S. G., Freije, C. A., Metsky, H. C., Yang, D. K., et al. (2020). Massively multiplexed nucleic acid detection with Cas13. *Nature* 582, 277–282. doi: 10.1038/s41586-020-2279-8

Ai, Y., Liang, D., and Wilusz, J. E. (2022). CRISPR/Cas13 effectors have differing extents of off-target effects that limit their utility in eukaryotic cells. *Nucleic Acids Res.* 50:e65. doi: 10.1093/nar/gkac159

Arora, A., Goering, R., Lo, H. Y. G., Lo, J., Moffatt, C., and Taliaferro, J. M. (2022). The role of alternative polyadenylation in the regulation of subcellular RNA localization. *Front. Genet.* 12:818668. doi: 10.3389/fgene.2021.818668

Atkins, A., Chung, C. H., Allen, A. G., Dampier, W., Gurrola, T. E., Sariyer, I. K., et al. (2021). Off-target analysis in gene editing and applications for clinical translation of CRISPR/Cas9 in HIV-1 therapy. *Front. Genome Ed.* 3:673022. doi: 10.3389/fgeed.2021.673022

Ayabe, S., Nakashima, K., and Yoshiki, A. (2019). Off- and on-target effects of genome editing in mouse embryos. *J. Reprod. Dev.* 65, 1–5. doi: 10.1262/jrd.2018-128

Bandaru, S., Tsuji, M. H., Shimizu, Y., Usami, K., Lee, S., Takei, N. K., et al. (2020). Structure-based design of gRNA for Cas13. *Sci. Rep.* 10:11610. doi: 10.1038/s41598-020-68459-4

Bankole, B. E., Kayode, A. T., Nosamiefan, I. O., Eromon, P., Baniecki, M. L., Daniels, R. F., et al. (2018). Characterization of plasmodium falciparum structure in Nigeria with malaria SNPs barcode. *Malar. J.* 17:472. doi: 10.1186/s12936-018-2623-8

Barber, B. E., William, T., Grigg, M. J., Yeo, T. W., and Anstey, N. M. (2013). Limitations of microscopy to differentiate plasmodium species in a region co-endemic for plasmodium falciparum, plasmodium vivax and plasmodium knowlesi. *Malar. J.* 12:8. doi: 10.1186/1475-2875-12-8

Baum, J., Papenfuss, A. T., Mair, G. R., Janse, C. J., Vlachou, D., Waters, A. P., et al. (2009). Molecular genetics and comparative genomics reveal RNAi is not functional in malaria parasites. *Nucleic Acids Res.* 37, 3788–3798. doi: 10.1093/nar/gkp239

Bayoumi, M., and Munir, M. (2021). Potential use of CRISPR/Cas13 machinery in understanding virus–host interaction. *Front. Microbiol.* 12:743580. doi: 10.3389/fmicb.2021.743580

Berzosa, P., de Lucio, A., Romay-Barja, M., Herrador, Z., González, V., García, L., et al. (2018). Comparison of three diagnostic methods (microscopy, RDT, and PCR) for the detection of malaria parasites in representative samples from Equatorial Guinea. *Malar. J.* 17:333. doi: 10.1186/s12936-018-2481-4

Briquet, S., Gissot, M., and Silvie, O. J. M. M. (2022). A toolbox for conditional control of gene expression in apicomplexan parasites. *Mol. Microbiol.* 117, 618–631. doi: 10.1111/mmi.14821

Campino, S., Auburn, S., Kivinen, K., Zongo, I., Ouedraogo, J. B., Mangano, V., et al. (2011). Population genetic analysis of plasmodium falciparum parasites using a customized Illumina GoldenGate genotyping assay. *PLoS One* 6:e20251. doi: 10.1371/journal.pone.0020251

Cao, H., Wang, Y., Zhang, N., Xia, S., Tian, P., Lu, L., et al. (2022). Progress of CRISPR-Cas13 mediated live-cell RNA imaging and detection of RNA-protein interactions. *Front. Cell Dev. Biol.* 10:866820. doi: 10.3389/fcell.2022.866820

Cárdenas, P., Esherick, L. Y., Chambonnier, G., Dey, S., Turlo, C. V., Nasamu, A. S., et al. (2022). GeneTargeter: automated in silico Design for Genome Editing in the malaria parasite, Plasmodium falciparum. *CRISPR J.* 5, 155–164. doi: 10.1089/crispr.2021.0069

Cowman, A. F., Healer, J., Marapana, D., and Marsh, K. (2016). Malaria: biology and disease. *Cells* 167, 610–624. doi: 10.1016/j.cell.2016.07.055

Cox, D. B. T., Gootenberg, J. S., Abudayyeh, O. O., Franklin, B., Kellner, M. J., Joung, J., et al. (2017). RNA editing with CRISPR-Cas13. *Science* 358, 1019–1027. doi: 10.1126/science.aaq0180

Crawford, E. D., Quan, J., Horst, J. A., Ebert, D., Wu, W., and DeRisi, J. L. (2017). Plasmid-free CRISPR/Cas9 genome editing in plasmodium falciparum confirms mutations conferring resistance to the dihydroisoquinolone clinical candidate SJ733. *PLoS One* 12:e0178163. doi: 10.1371/journal.pone.0178163

Cunningham, C. H., Hennelly, C. M., Lin, J. T., Ubalee, R., Boyce, R. M., Mulogo, E. M., et al. (2021). A novel CRISPR-based malaria diagnostic capable of plasmodium detection, species differentiation, and drug-resistance genotyping. *EBioMedicine* 68:103415. doi: 10.1016/j.ebiom.2021.103415

de Koning-Ward, T. F., Gilson, P. R., and Crabb, B. S. (2015). Advances in molecular genetic systems in malaria. *Nat. Rev. Microbiol.* 13, 373–387. doi: 10.1038/nrmicro3450

Du, M., Jillette, N., Zhu, J. J., Li, S., and Cheng, A. W. (2020). CRISPR artificial splicing factors. *Nat. Commun.* 11:2973. doi: 10.1038/s41467-020-16806-4

East-Seletsky, A., O' Connell, M. R., Knight, S. C., Burstein, D., Cate, J. H. D., Tjian, R., et al. (2016). Two distinct RNase activities of CRISPR-C2c2 enable guide-RNA processing and RNA detection. *Nature* 538, 270–273. doi: 10.1038/nature19802

Elison, G. L., and Acar, M. (2018). Scarless genome editing: progress towards understanding genotype-phenotype relationships. *Curr. Genet.* 64, 1229–1238. doi: 10.1007/s00294-018-0850-8

Fitri, L. E., Widaningrum, T., Endharti, A. T., Prabowo, M. H., Winaris, N., and Nugraha, R. Y. B. (2022). Malaria diagnostic update: from conventional to advanced method. *J. Clin. Lab. Anal.* 36:e24314. doi: 10.1002/jcla.24314

Freije, C. A., Myhrvold, C., Boehm, C. K., Lin, A. E., Welch, N. L., Carter, A., et al. (2019). Programmable inhibition and detection of RNA viruses using Cas13. *Mol. Cell* 76, 826–837.e11. doi: 10.1016/j.molcel.2019.09.013

Fu, Y., Foden, J. A., Khayter, C., Maeder, M. L., Reyon, D., Joung, J. K., et al. (2013). High-frequency off-target mutagenesis induced by CRISPR-Cas nucleases in human cells. *Nat. Biotechnol.* 31, 822–826. doi: 10.1038/nbt.2623

Fu, Y., Sander, J. D., Reyon, D., Cascio, V. M., and Joung, J. K. (2014). Improving CRISPR-Cas nuclease specificity using truncated guide RNAs. *Nat. Biotechnol.* 32, 279–284. doi: 10.1038/nbt.2808

Gabriel, H. B., De Azevedo, M. F., Palmisano, G., Wunderlich, G., Kimura, E. A., Katzin, A. M., et al. (2015). Single-target high-throughput transcription analyses reveal high levels of alternative splicing present in the FPPS/GGPPS from plasmodium falciparum. *Sci. Rep.* 5:18429. doi: 10.1038/srep18429

Gaj, T. (2021). Next-generation CRISPR technologies and their applications in gene and cell therapy. *Trends Biotechnol.* 39, 692–705. doi: 10.1016/j.tibtech.2020.10.010

Gardner, M. J., Hall, N., Fung, E., White, O., Berriman, M., Hyman, R. W., et al. (2002). Genome sequence of the human malaria parasite plasmodium falciparum. *Nature* 419, 498–511. doi: 10.1038/nature01097

Gootenberg, J. S., Abudayyeh, O. O., Kellner, M. J., Joung, J., Collins, J. J., and Zhang, F. (2018). Multiplexed and portable nucleic acid detection platform with Cas13, Cas12a, and Csm6. *Science* 360, 439–444. doi: 10.1126/science.aaq0179

Gootenberg, J. S., Abudayyeh, O. O., Lee, J. W., Essletzbichler, P., Dy, A. J., Joung, J., et al. (2017). Nucleic acid detection with CRISPR-Cas13a/C2c2. *Science* 356, 438–442. doi: 10.1126/science.aam9321

Graham, D. B., and Root, D. E. (2015). Resources for the design of CRISPR gene editing experiments. *Genome Biol.* 16:260. doi: 10.1186/s13059-015-0823-x

Haeussler, M., Schönig, K., Eckert, H., Eschstruth, A., Mianné, J., Renaud, J. B., et al. (2016). Evaluation of off-target and on-target scoring algorithms and integration into the guide RNA selection tool CRISPOR. *Genome Biol.* 17:148. doi: 10.1186/s13059-016-1012-2

Haldar, K., Bhattacharjee, S., and Safeukui, I. (2018). Drug resistance in plasmodium. *Nat. Rev. Microbiol.* 16, 156–170. doi: 10.1038/nrmicro.2017.161

Hartenian, E., and Doench, J. G. (2015). Genetic screens and functional genomics using CRISPR/Cas9 technology. *FEBS J.* 282, 1383–1393. doi: 10.1111/febs.13248

Hemingway, J., and Bates, I. (2003). Malaria: past problems and future prospects. After more than a decade of neglect, malaria is finally black on the agenda for both biomedical research and public health politics. *EMBO Rep.* 4, S29–S31. doi: 10.1038/sj.embor.embor841

Hentzschel, F., Mitesser, V., Fraschka, S. A., Krzikalla, D., Carrillo, E. H., Berkhout, B., et al. (2020). Gene knockdown in malaria parasites via non-canonical RNAi. *Nucleic Acids Res.* 48:e2. doi: 10.1093/nar/gkz927

Horvath, P., and Barrangou, R. (2010). CRISPR/Cas, the immune system of bacteria and archaea. *Science* 327, 167–170. doi: 10.1126/science.1179555

Hu, Y., Chen, Y., Xu, J., Wang, X., Luo, S., Mao, B., et al. (2022). Metagenomic discovery of novel CRISPR-Cas13 systems. *Cell Discov.* 8:107. doi: 10.1038/s41421-022-00464-5

Huynh, N., Depner, N., Larson, R., and King-Jones, K. (2020). A versatile toolkit for CRISPR-Cas13-based RNA manipulation in drosophila. *Genome Biol.* 21:279. doi: 10.1186/s13059-020-02193-y

Iriko, H., Jin, L., Kaneko, O., Takeo, S., Han, E. T., Tachibana, M., et al. (2009). A small-scale systematic analysis of alternative splicing in plasmodium falciparum. *Parasitol. Int.* 58, 196–199. doi: 10.1016/j.parint.2009.02.002

Ishino, Y., Shinagawa, H., Makino, K., Amemura, M., and Nakata, A. (1987). Nucleotide sequence of the iap gene, responsible for alkaline phosphatase isozyme conversion in Escherichia coli, and identification of the gene product. *J. Bacteriol.* 169, 5429–5433. doi: 10.1128/jb.169.12.5429-5433.1987

Jansen, R., Embden, J. D. A., Gaastra, W., and Schouls, L. M. (2002). Identification of genes that are associated with DNA repeats in prokaryotes. *Mol. Microbiol.* 43, 1565–1575. doi: 10.1046/j.1365-2958.2002.02839.x

Jiang, F., and Doudna, J. A. (2015). The structural biology of CRISPR-Cas systems. *Curr. Opin. Struct. Biol.* 30, 100–111. doi: 10.1016/j.sbi.2015.02.002

Jinek, M., Chylinski, K., Fonfara, I., Hauer, M., Doudna, J. A., and Charpentier, E. (2012). A programmable dual-RNA–guided DNA endonuclease in adaptive bacterial immunity. *Science* 337, 816–821. doi: 10.1126/science.1225829

Kannan, S., Altae-Tran, H., Jin, X., Madigan, V. J., Oshiro, R., Makarova, K. S., et al. (2022). Compact RNA editors with small Cas13 proteins. *Nat. Biotechnol.* 40, 194–197. doi: 10.1038/s41587-021-01030-2

Kellner, M. J., Koob, J. G., Gootenberg, J. S., Abudayyeh, O. O., and Zhang, F. (2019). SHERLOCK: nucleic acid detection with CRISPR nucleases. *Nat. Protoc.* 14, 2986–3012. doi: 10.1038/s41596-019-0210-2

Kenchappa, C. S., Heidarsson, P. O., Kragelund, B. B., Garrett, R. A., and Poulsen, F. M. (2013). Solution properties of the archaeal CRISPR DNA repeat-binding homeodomain protein Cbp2. *Nucleic Acids Res.* 41, 3424–3435. doi: 10.1093/nar/gks1465

Kim, H., Lee, S., Yoon, J., Song, J., and Park, H. G. (2021). CRISPR/Cas12a collateral cleavage activity for simple and rapid detection of protein/small molecule interaction. *Biosens. Bioelectron.* 194:113587. doi: 10.1016/j.bios.2021.113587

Kleinstiver, B. P., Pattanayak, V., Prew, M. S., Tsai, S. Q., Nguyen, N. T., Zheng, Z., et al. (2016). High-fidelity CRISPR–Cas9 nucleases with no detectable genome-wide off-target effects. *Nature* 529, 490–495. doi: 10.1038/nature16526

Konermann, S., Lotfy, P., Brideau, N. J., Oki, J., Shokhirev, M. N., and Hsu, P. D. (2018). Transcriptome engineering with RNA-targeting type VI-D CRISPR effectors. *Cells* 173, 665–676.e14. doi: 10.1016/j.cell.2018.02.033

Krohannon, A., Srivastava, M., Rauch, S., Srivastava, R., Dickinson, B. C., and Janga, S. C. (2022). CASowary: CRISPR-Cas13 guide RNA predictor for transcript depletion. *BMC Genomics* 23:172. doi: 10.1186/s12864-022-08366-2

Kushawah, G., Hernandez-Huertas, L., Del Prado, J. A. N., Martinez-Morales, J. R., DeVore, M. L., Hassan, H., et al. (2020). CRISPR-Cas13d induces efficient mRNA knockdown in animal embryos. *Dev. Cell* 54, 805–817. doi: 10.1016/j.devcel.2020.07.013

Lalremruata, A., Jeyaraj, S., Engleitner, T., Joanny, F., Lang, A., Bélard, S., et al. (2017). Species and genotype diversity of plasmodium in malaria patients from Gabon analysed by next generation sequencing. *Malar. J.* 16:398. doi: 10.1186/s12936-017-2044-0

Lander, E. (2016). The heroes of CRISPR. *Cells* 164, 18–28. doi: 10.1016/j.cell.2015.12.041

Le Roch, K. G., Zhou, Y., Blair, P. L., Grainger, M., Moch, J. K., Haynes, J. D., et al. (2003). Discovery of gene function by expression profiling of the malaria parasite life cycle. *Science* 301, 1503–1508. doi: 10.1126/science.1087025

Lee, R. A., Puig, H. D., Nguyen, P. Q., Angenent-Mari, N. M., Donghia, N. M., McGee, J. P., et al. (2020). Ultrasensitive CRISPR-based diagnostic for field-applicable detection of plasmodium species in symptomatic and asymptomatic malaria. *Proc. Natl. Acad. Sci. U. S. A.* 117, 25722–25731. doi: 10.1073/pnas.2010196117

Li, L., Duan, C., Weng, J., Qi, X., Liu, C., Li, X., et al. (2022). A field-deployable method for single and multiplex detection of DNA or RNA from pathogens using Cas12 and Cas13. *Sci. China Life Sci.* 65, 1456–1465. doi: 10.1007/s11427-021-2028-x

Li, G., Wang, Y., Li, X., Wang, Y., Huang, X., Gao, J., et al. (2021). Developing PspCas13b-based enhanced RESCUE system, eRESCUE, with efficient RNA base editing. *Cell Commun. Signal.* 19:84. doi: 10.1186/s12964-021-00716-z

Lin, P., Qin, S., Pu, Q., Wang, Z., Wu, Q., Gao, P., et al. (2020). CRISPR-Cas13 inhibitors block RNA editing in bacteria and mammalian cells. *Mol. Cell* 78, 850–861.e5. doi: 10.1016/j.molcel.2020.03.033

Liu, Y., Chen, Z., He, A., Zhan, Y., Li, J., Liu, L., et al. (2016). Targeting cellular mRNAs translation by CRISPR-Cas9. *Sci. Rep.* 6:29652. doi: 10.1038/srep29652

Liu, M., Lu, B., Fan, Y., He, X., Shen, S., Jiang, C., et al. (2019). TRIBE uncovers the role of Dis3 in shaping the dynamic transcriptome in malaria parasites. *Front. Cell Dev. Biol.* 7:264. doi: 10.3389/fcell.2019.00264

Liu, L., and Pei, D. S. (2022). Insights gained from RNA editing targeted by the CRISPR-Cas13 family. *Int. J. Mol. Sci.* 23:11400. doi: 10.3390/ijms231911400

Lv, H., Wang, J., Zhang, J., Chen, Y., Yin, L., Jin, D., et al. (2021). Definition of CRISPR Cas12a trans-cleavage units to facilitate CRISPR diagnostics. *Front. Microbiol.* 12:766464. doi: 10.3389/fmicb.2021.766464

Mahas, A., Wang, Q., Marsic, T., and Mahfouz, M. M. (2021). A novel miniature CRISPR-Cas13 system for SARS-CoV-2 diagnostics. *ACS Synth. Biol.* 10, 2541–2551. doi: 10.1021/acssynbio.1c00181

Makarova, K. S., Grishin, N. V., Shabalina, S. A., Wolf, Y. I., and Koonin, E. V. (2006). A putative RNA-interference-based immune system in prokaryotes: computational analysis of the predicted enzymatic machinery, functional analogies with eukaryotic RNAi, and hypothetical mechanisms of action. *Biol. Direct.* 1:7. doi: 10.1186/1745-6150-1-7

Makarova, K. S., Zhang, F., and Koonin, E. V. J. C. (2017). SnapShot: class 2 CRISPR-Cas systems. *Cells* 168, 328–328.e1. doi: 10.1016/j.cell.2016.12.038

Malave-Ramos, D. R., Kennedy, K., Key, M. N., Dou, Z., and Kafsack, B. F. (2022). Safe, effective, and inexpensive clearance of mycoplasma contamination from cultures of apicomplexan parasites with Sparfloxacin. *Microbiol. Spectr.* 10:e03497-22. doi: 10.1128/spectrum.03497-22

Manning, B. J., Khan, W. A., Peña, J. M., Fiore, E. S., Boisvert, H., Tudino, M. C., et al. (2021). High-throughput CRISPR-Cas13 SARS-CoV-2 test. *Clin. Chem.* 68, 172–180. doi: 10.1093/clinchem/hvab238

Marraffini, L. A. (2015). CRISPR-Cas immunity in prokaryotes. *Nature* 526, 55–61. doi: 10.1038/nature15386

Memvanga, P. B., and Nkanga, C. I. J. M. J. (2021). Liposomes for malaria management: the evolution from 1980 to 2020. *Malar. J.* 20:327. doi: 10.1186/s12936-021-03858-0

Miles, A., Iqbal, Z., Vauterin, P., Pearson, R., Campino, S., Theron, M., et al. (2016). Indels, structural variation, and recombination drive genomic diversity in plasmodium falciparum. *Genome Res.* 26, 1288–1299. doi: 10.1101/gr.203711.115

Mojica, F. J., Díez-Villaseñor, C., García-Martínez, J., and Soria, E. (2005). Intervening sequences of regularly spaced prokaryotic repeats derive from foreign genetic elements. *J. Mol. Evol.* 60, 174–182. doi: 10.1007/s00239-004-0046-3

Mojica, F. J., Díez-Villaseñor, C., Soria, E., and Juez, G. (2000). Biological significance of a family of regularly spaced repeats in the genomes of Archaea, Bacteria and mitochondria. *Mol. Microbiol.* 36, 244–246. doi: 10.1046/j.1365-2958.2000.01838.x

Mojica, F. J. M., Ferrer, C., Juez, G., and Rodríguez-Valera, F. (1995). Long stretches of short tandem repeats are present in the largest replicons of the archaea *Haloferax mediterranei* and *Haloferax volcanii* and could be involved in replicon partitioning. *Mol. Microbiol.* 17, 85–93. doi: 10.1111/j.1365-2958.1995.mmi_17010085.x

Mojica, F. J., Juez, G., and Rodríguez-Valera, F. (1993). Transcription at different salinities of *Haloferax mediterranei* sequences adjacent to partially modified PstI sites. *Mol. Microbiol.* 9, 613–621. doi: 10.1111/j.1365-2958.1993.tb01721.x

Monroe, A., Williams, N. A., Ogoma, S., Karema, C., and Okumu, F. (2022). Reflections on the 2021 world malaria report and the future of malaria control. *Malar. J.* 21:154. doi: 10.1186/s12936-022-04178-7

Moon, S. B., Kim, D. Y., Ko, J. H., and Kim, Y. S. (2019). Recent advances in the CRISPR genome editing tool set. *Exp. Mol. Med.* 51, 1–11. doi: 10.1038/s12276-019-0339-7

Mueller, A. K., Hammerschmidt-Kamper, C., and Kaiser, A. (2014). RNAi in Plasmodium. *Curr. Pharm. Des.* 20, 278–283. doi: 10.2174/13816128113199990027

Mustafa, M. I., and Makhawi, A. M. (2021). SHERLOCK and DETECTR: CRISPR-Cas systems as potential rapid diagnostic tools for emerging infectious diseases. *J. Clin. Microbiol.* 59:e00745-20. doi: 10.1128/JCM.00745-20

Myhrvold, C., Freije, C. A., Gootenberg, J. S., Abudayyeh, O. O., Metsky, H. C., Durbin, A. F., et al. (2018). Field-deployable viral diagnostics using CRISPR-Cas13. *Science* 360, 444–448. doi: 10.1126/science.aas8836

Nguyen, L. T., Smith, B. M., and Jain, P. K. (2020). Enhancement of trans-cleavage activity of Cas12a with engineered crRNA enables amplified nucleic acid detection. *Nat. Commun.* 11:4906. doi: 10.1038/s41467-020-18615-1

Nisbet, R. E. R., Kurniawan, D. P., Bowers, H. D., and Howe, C. J. (2016). Transcripts in the plasmodium Apicoplast undergo cleavage at tRNAs and editing, and include antisense sequences. *Protist* 167, 377–388. doi: 10.1016/j.protis.2016.06.003

Nishi, T., Shinzawa, N., Yuda, M., and Iwanaga, S. (2021). Highly efficient CRISPR/Cas9 system in plasmodium falciparum using Cas9-expressing parasites and a linear donor template. *Sci. Rep.* 11:18501. doi: 10.1038/s41598-021-97984-z

O'Connell, M. R., Oakes, B. L., Sternberg, S. H., East-Seletsky, A., Kaplan, M., and Doudna, J. A. (2014). Programmable RNA recognition and cleavage by CRISPR/Cas9. *Nature* 516, 263–266. doi: 10.1038/nature13769

Oboh, M. A., Badiane, A. S., Ntadom, G., Ndiaye, Y. D., Diongue, K., Diallo, M. A., et al. (2018). Molecular identification of plasmodium species responsible for malaria reveals plasmodium vivax isolates in Duffy negative individuals from southwestern Nigeria. *Malar. J.* 17:439. doi: 10.1186/s12936-018-2588-7

Oboh, M. A., Oriero, E. C., Ndiaye, T., Badiane, A. S., Ndiaye, D., and Amambua-Ngwa, A. (2021). Comparative analysis of four malaria diagnostic tools and implications for malaria treatment in southwestern Nigeria. *Int. J. Infect. Dis.* 108, 377–381. doi: 10.1016/j.ijid.2021.05.049

O'Connell, M. R. J. J. O. M. B. (2019). Molecular mechanisms of RNA targeting by Cas13-containing type VI CRISPR–Cas systems. *J. Mol. Biol.* 431, 66–87. doi: 10.1016/j.jmb.2018.06.029

Okell, L. C., Griffin, J. T., and Roper, C. (2017). Mapping sulphadoxine-pyrimethamine-resistant plasmodium falciparum malaria in infected humans and in parasite populations in Africa. *Sci. Rep.* 7:7389. doi: 10.1038/s41598-017-06708-9

Olotu, A., Fegan, G., Wambua, J., Nyangweso, G., Awuondo, K. O., Leach, A., et al. (2013). Four-year efficacy of RTS, S/AS01E and its interaction with malaria exposure. *N. Engl. J. Med.* 368, 1111–1120. doi: 10.1056/NEJMoa1207564

Ospina-Villa, J. D., López-Camarillo, C., Castañón-Sánchez, C. A., Soto-Sánchez, J., Ramírez-Moreno, E., and Marchat, L. A. (2018). Advances on aptamers against protozoan parasites. *Genes (Basel)* 9:584. doi: 10.3390/genes9120584

Patchsung, M., Jantarug, K., Pattama, A., Aphicho, K., Suraritdechachai, S., Meesawat, P., et al. (2020). Clinical validation of a Cas13-based assay for the detection of SARS-CoV-2 RNA. *Nat. Biomed. Eng.* 4, 1140–1149. doi: 10.1038/s41551-020-00603-x

Prommana, P., Uthaipibull, C., Wongsombat, C., Kamchonwongpaisan, S., Yuthavong, Y., Knuepfer, E., et al. (2013). Inducible knockdown of plasmodium gene expression using the glmS ribozyme. *PLoS One* 8:e73783. doi: 10.1371/journal.pone.0073783

Quansah, E., Pappoe, F., Shen, J., Liu, M., Yang, S., Yu, L., et al. (2022). ApiAP2 gene-network regulates Gametocytogenesis in plasmodium parasites. *Cell. Microbiol.* 2022:5796578. doi: 10.1155/2022/5796578

Rajan, A., Shrivastava, S., Kumar, A., Singh, A. K., and Arora, P. K. (2022). CRISPR-Cas system: from diagnostic tool to potential antiviral treatment. *Appl. Microbiol. Biotechnol.* 106, 5863–5877. doi: 10.1007/s00253-022-12135-2

Sato, S. (2021). Plasmodium—a brief introduction to the parasites causing human malaria and their basic biology. *J. Physiol. Anthropol.* 40:1. doi: 10.1186/s40101-020-00251-9

Shmakov, S., Abudayyeh, O. O., Makarova, K. S., Wolf, Y. I., Gootenberg, J. S., Semenova, E., et al. (2015). Discovery and functional characterization of diverse class 2 CRISPR-Cas systems. *Mol. Cell* 60, 385–397. doi: 10.1016/j.molcel.2015.10.008

Slaymaker, I. M., Gao, L., Zetsche, B., Scott, D. A., Yan, W. X., and Zhang, F. (2016). Rationally engineered Cas9 nucleases with improved specificity. *Science* 351, 84–88. doi: 10.1126/science.aad5227

Smargon, A. A., Cox, D. B. T., Pyzocha, N. K., Zheng, K., Slaymaker, I. M., Gootenberg, J. S., et al. (2017). Cas13b is a type VI-B CRISPR-associated RNA-guided RNase differentially regulated by accessory proteins Csx27 and Csx28. *Mol. Cell* 65, 618–630.e7. e7. doi: 10.1016/j.molcel.2016.12.023

Sorber, K., Dimon, M. T., and DeRisi, J. L. (2011). RNA-Seq analysis of splicing in plasmodium falciparum uncovers new splice junctions, alternative splicing and splicing of antisense transcripts. *Nucleic Acids Res.* 39, 3820–3835. doi: 10.1093/nar/gkq1223

Stevens, A. T., Howe, D. K., and Hunt, A. G. (2018). Characterization of mRNA polyadenylation in the apicomplexa. *PLoS One* 13:e0203317. doi: 10.1371/journal.pone.0203317

Tambe, A., East-Seletsky, A., Knott, G. J., Doudna, J. A., and O'Connell, M. R. (2018). RNA binding and HEPN-nuclease activation are decoupled in CRISPR-Cas13a. *Cell Rep.* 24, 1025–1036. doi: 10.1016/j.celrep.2018.06.105

Tan, Q. W., and Mutwil, M. (2020). Malaria.Tools-comparative genomic and transcriptomic database for plasmodium species. *Nucleic Acids Res.* 48, D768–d775. doi: 10.1093/nar/gkz662

Tang, T., Han, Y., Wang, Y., Huang, H., and Qian, P. (2021). Programmable system of Cas13-mediated RNA modification and its biological and biomedical applications. *Front. Cell Dev. Biol.* 9:677587. doi: 10.3389/fcell.2021.677587

Thakku, S. G., Ackerman, C. M., Myhrvold, C., Bhattacharyya, R. P., Livny, J., Ma, P., et al. (2022). Multiplexed detection of bacterial nucleic acids using Cas13 in droplet microarrays. *PNAS Nexus.* 1:pgac021. doi: 10.1093/pnasnexus/pgac021

Thiam, L. G., Mangou, K., Ba, A., Mbengue, A., and Bei, A. K. (2022). Leveraging genome editing to functionally evaluate plasmodium diversity. *Trends Parasitol.* 38, 558–571. doi: 10.1016/j.pt.2022.03.005

Tian, S., Zhang, B., He, Y., Sun, Z., Li, J., Li, Y., et al. (2022). CRISPR-iPAS: a novel dCAS13-based method for alternative polyadenylation interference. *Nucleic Acids Res.* 50:e26. doi: 10.1093/nar/gkac108

Turnbull, L. B., Siwo, G. H., Button-Simons, K. A., Tan, A., Checkley, L. A., Painter, H. J., et al. (2017). Simultaneous genome-wide gene expression and transcript isoform profiling in the human malaria parasite. *PLoS One* 12:e0187595. doi: 10.1371/journal.pone.0187595

Walker, M. P., and Lindner, S. E. (2019). Ribozyme-mediated, multiplex CRISPR gene editing and CRISPR interference (CRISPRi) in rodent-infectious plasmodium yoelii. *J. Biol. Chem.* 294, 9555–9566. doi: 10.1074/jbc.RA118.007121

Wei, Y., Zhou, Y., Liu, Y., Ying, W., Lv, R., Zhao, Q., et al. (2021). Indiscriminate ssDNA cleavage activity of CRISPR-Cas12a induces no detectable off-target effects in mouse embryos. *Protein Cell* 12, 741–745. doi: 10.1007/s13238-021-00824-z

Wessels, H.-H., Méndez-Mancilla, A., Guo, X., Legut, M., Daniloski, Z., and Sanjana, N. E. (2020). Massively parallel Cas13 screens reveal principles for guide RNA design. *Nat. Biotechnol.* 38, 722–727. doi: 10.1038/s41587-020-0456-9

World Health Organization (2022). Available at: https://www.who.int/teams/global-malaria-programme/reports/world-malaria-report-2022#:~:text=Despite%20continued%20impact%20of%20COVID,further%20setbacks%20to%20malaria%20control

Xu, C., Zhou, Y., Xiao, Q., He, B., Geng, G., Wang, Z., et al. (2021). Programmable RNA editing with compact CRISPR–Cas13 systems from uncultivated microbes. *Nat. Methods* 18, 499–506. doi: 10.1038/s41592-021-01124-4

Yan, W. X., Chong, S., Zhang, H., Makarova, K. S., Koonin, E. V., Cheng, D. R., et al. (2018). Cas13d is a compact RNA-targeting type VI CRISPR effector positively modulated by a WYL-domain-containing accessory protein. *Mol. Cell* 70, 327–339.e5. doi: 10.1016/j.molcel.2018.02.028

Yan, F., Wang, W., and Zhang, J. (2019). CRISPR-Cas12 and Cas13: the lesser known siblings of CRISPR-Cas9. *Cell Biol. Toxicol.* 35, 489–492. doi: 10.1007/s10565-019-09489-1

Yang, L., Grishin, D., Wang, G., Aach, J., Zhang, C. Z., Chari, R., et al. (2014). Targeted and genome-wide sequencing reveal single nucleotide variations impacting specificity of Cas9 in human stem cells. *Nat. Commun.* 5:5507. doi: 10.1038/ncomms6507

Yang, M., Shang, X., Zhou, Y., Wang, C., Wei, G., Tang, J., et al. (2021). Full-length transcriptome analysis of plasmodium falciparum by single-molecule long-read sequencing. *Front. Cell. Infect. Microbiol.* 11:631545. doi: 10.3389/fcimb.2021.631545

Yang, J., Song, Y., Deng, X., Vanegas, J. A., You, Z., Zhang, Y., et al. (2022). (Online ahead of print)). Engineered LwaCas13a with enhanced collateral activity for nucleic acid detection. *Nat. Chem. Biol.* 19, 45–54. doi: 10.1038/s41589-022-01135-y

Yang, L. Z., Wang, Y., Li, S. Q., Yao, R. W., Luan, P. F., Wu, H., et al. (2019). Dynamic imaging of RNA in living cells by CRISPR-Cas13 systems. *Mol. Cell* 76, 981–997. doi: 10.1016/j.molcel.2019.10.024

Yeoh, L. M., Goodman, C. D., Mollard, V., McHugh, E., Lee, V. V., Sturm, A., et al. (2019). Alternative splicing is required for stage differentiation in malaria parasites. *Genome Biol.* 20:151. doi: 10.1186/s13059-019-1756-6

Zhang, C., Konermann, S., Brideau, N. J., Lotfy, P., Wu, X., Novick, S. J., et al. (2018). Structural basis for the RNA-guided ribonuclease activity of CRISPR-Cas13d. *Cells* 175, 212–223.e17. doi: 10.1016/j.cell.2018.09.001

Zhang, Y., Liu, L., Qiu, Q., Zhou, Q., Ding, J., Lu, Y., et al. (2021). Alternative polyadenylation: methods, mechanism, function, and role in cancer. *J. Exp. Clin. Cancer Res.* 40:51. doi: 10.1186/s13046-021-01852-7

Zhang, H., Qin, C., An, C., Zheng, X., Wen, S., Chen, W., et al. (2021). Application of the CRISPR/Cas9-based gene editing technique in basic research, diagnosis, and therapy of cancer. *Mol. Cancer* 20:126. doi: 10.1186/s12943-021-01431-6

Zhang, C., Xiao, B., Jiang, Y., Zhao, Y., Li, Z., Gao, H., et al. (2014). Efficient editing of malaria parasite genome using the CRISPR/Cas9 system. *MBio* 5:e01414. doi: 10.1128/mBio.01414-14

Zhang, B., Ye, Y., Ye, W., Perčulija, V., Jiang, H., Chen, Y., et al. (2019). Two HEPN domains dictate CRISPR RNA maturation and target cleavage in Cas13d. *Nat. Commun.* 10:2544. doi: 10.1038/s41467-019-10507-3

Zhang, D., Zhang, Z., Unver, T., and Zhang, B. (2021). CRISPR/Cas: a powerful tool for gene function study and crop improvement. *J. Adv. Res.* 29, 207–221. doi: 10.1016/j.jare.2020.10.003

Zhu, Y., and Huang, Z. (2018). Recent advances in structural studies of the CRISPR-Cas-mediated genome editing tools. *Natl. Sci. Rev.* 6, 438–451. doi: 10.1093/nsr/nwy150

Frontiers in Microbiology

Explores the habitable world and the potential of microbial life

The largest and most cited microbiology journal which advances our understanding of the role microbes play in addressing global challenges such as healthcare, food security, and climate change.

Discover the latest Research Topics

See more →

Frontiers

Avenue du Tribunal-Fédéral 34
1005 Lausanne, Switzerland
frontiersin.org

Contact us

+41 (0)21 510 17 00
frontiersin.org/about/contact